



The Design, Synthesis and Optimisation of Epigenetic Mechanism Inhibitors

Matthew Campbell

A report submitted for a Degree of Doctor of Philosophy

DEPARTMENT OF PURE AND APPLIED CHEMISTRY
UNIVERSITY OF STRATHCLYDE AND GLAXOSMITHKLINE

2016

Declaration of Authenticity and Author's Rights

This thesis is the result of the author's original research. It has been composed by the author and has not been previously submitted for examination which has led to the award of a degree.

The copyright of this thesis belongs to GSK in accordance with the author's contract of engagement with GSK under the terms of the United Kingdom Copyright Acts. Due acknowledgement must always be made of the use of any material contained in, or derived from, this thesis.

Signed: Matt Campbell

Date: 10th August 2016

Table of Contents

Please note: chapter one and chapter two of this thesis each has self-contained abstract, introduction, aims, results and discussion, chemistry, conclusions, future work, general methods, experimentals and references sections.

Acknowledgements.....	iv
Acronyms and Definitions	v
Chapter 1: The Design, Synthesis and Optimisation of PAD4 Inhibitors.....	1
1.1. Abstract.....	2
1.2. Introduction.....	3
1.2.1. Epigenetics.....	3
1.2.2. What is a Chemical Probe?	16
1.2.3. The Biological Significance of Arginine	19
1.2.4. Protein Arginine Deiminase (PAD) Regulation of Histone Methylation.....	22
1.2.5. PAD4 as a Drug Target.....	25
1.2.6. PAD4 X-ray Crystal Structure	26
1.2.7. PAD4 Fluorescence Intensity Assay.....	30
1.3. Aims.....	32
1.4. Results and Discussion	33
1.4.1. Discovery of Novel Lead-like PAD4 Hits using an HTS	33
1.4.2. Fluorescence Polarisation Binding Assay.....	34
1.4.3. Prioritisation of the HTS PAD4 Hits	35
1.4.4. Identification of Isoquinoline Hit, 4b	43
1.4.5. Identification of Further PAD4 Hits	45
1.4.6. Lead Optimisation of Triazolopyridazine Hit, 6	46
1.4.7. Lead Optimisation of Hydroxypyridinone Hit, 7	47
1.4.8. Lead Optimisation of the Pyridazine Hit 8	55
1.5. Chemistry.....	75
1.5.1. Resynthesis of Isoquinoline Hit 4b	75
1.5.2. Hydroxypyridinone Chemistry	77
1.5.3. Pyridazine Chemistry	88
1.6. Conclusions.....	98
1.7. Future Work.....	103
1.8. General Methods.....	105

1.8.1.	Analytical Methods.....	105
1.8.2.	Assay Methods.....	107
1.9.	Experimental.....	110
1.10.	References.....	151
Chapter 2: The Design, Synthesis and Optimisation of BET BD1 Inhibitors.....		160
2.1.	Abstract.....	161
2.2.	Introduction.....	164
2.2.1.	Bromodomains.....	164
2.2.2.	Discovery of a BET BD1 Selective Lead Series and First Generation <i>in vivo</i> Probe.....	172
2.2.3.	Discovery of the FP Template.....	178
2.2.4.	Identification of the First Generation Probe, 10	180
2.3.	Aims.....	187
2.4.	Results and Discussion.....	188
2.4.1.	Reducing Clearance in the FP and TP Series.....	188
2.4.2.	Optimisation of the Piperazine Methylsulfonamide Headgroup.....	202
2.4.3.	Investigating the Optimum Position of the Pyridine Nitrogen.....	210
2.4.4.	Optimisation of the Pyridyl Amide Substituent.....	213
2.4.5.	Improving Selectivity for BRD4 BD1 <i>versus</i> BRD9: <i>ortho</i> -substitution on the Aryl Tail Group.....	216
2.4.6.	Improving <i>In Vitro</i> Clearance of the FP Series.....	220
2.4.7.	Selection of the BRD4 BD1 Selective <i>in vivo</i> Probe.....	228
2.4.8.	Dog Toxicity Study Using the BET BRD BD1 Selective Inhibitor, 89	233
2.5.	Chemistry.....	236
2.5.1.	Synthesis of Mono-methyl Substituted Analogues 20, 21, 23 and 24	236
2.5.2.	Synthesis of Dimethyl Analogue, 25	243
2.5.3.	Synthesis of Des-methyl Headgroup Analogue 26	244
2.5.4.	Synthesis of Array of Headgroup Analogues 27-55	245
2.5.5.	Synthesis of Pyridine Regioisomers 56 to 58	249
2.5.6.	Synthesis of Pyridyl Amide Analogues 59-64	256
2.5.7.	Synthesis of Cyclic Amide, 65	259
2.5.8.	Synthesis of <i>ortho</i> -substituted Tail-group Compounds 67 and 68	260
2.5.9.	Chemistry Towards <i>ortho</i> -substituted Pyridine Regioisomers 69 and 71	261
2.5.10.	Synthesis of <i>ortho</i> -Cyclopropylmethyl <i>N</i> -linked Pyridyl Ring FP Analogues, 72 and 73	264

2.5.11.	Synthesis of <i>ortho</i> -Hydroxy Pyridyl Ring FP Analogue, 77	265
2.5.12.	Synthesis of <i>ortho</i> -Pyridyl Substituted FP Analogues, 74-75, 76, 78-82, 84, 86-88, 89 and 90	266
2.5.13.	Scaled-up Synthesis of 89	275
2.6.	Conclusions.....	286
2.7.	Future Work.....	299
2.8.	General Methods.....	301
2.8.1.	Analytical Methods.....	301
2.8.2.	Assay Methods.....	305
2.9.	Experimental.....	309
2.9.1.	Synthesis of Intermediates and Final Compounds	309
2.9.2.	Large Scale Preparation of BET BD1 Selective Chemical Probe, 89 ¹⁹	364
2.10.	References.....	371
Chapter 3:	Future Work and Overall Conclusions.....	380
3.1.	Future Considerations for Epigenetic Therapies.....	381
3.2.	Thesis Conclusions	383
Appendix:	Experimental for Compounds Prepared by Colleagues	384

Acknowledgements

I would like to thank my academic supervisor, Professor Jonathan Percy, and my industrial supervisor, Dr. Vipul Patel, for their invaluable guidance, advice and seemingly limitless patience that helped me to get this far in the GSK/University of Strathclyde DPhil program. I would also like to thank GSK colleagues who were involved with the PAD4 and BET BD1 Inhibitor programs, particularly program leaders Matt Lindon, and Drs. John Liddle, Sue Westaway and Huw Lewis who provided invaluable input into the direction of this research, and the head of Epinova Dr. Rab Prinjha, who had the vision to pursue this research. Fellow colleagues Dr. Stephen Atkinson and Alex Preston contributed to SAR expansion of early PAD4 HTS hits, and Heather Barnett, Neil Garton, Darren Mitchell and Dr. Bob Watson contributed to the synthesis of BET BD1 inhibitors. Rino Bit and Drs. Dominique Amans, and Chris Wellaway formed part of the original BET BD1 Inhibitor program team and enabled the discovery of the original lead compounds, on which the BET BD1 work is based. Biology colleagues Kelly Locke, Rob Davis, Laurie Gordon and Melanie Leveridge were instrumental in providing efficient assay development and screening support, and DMPK scientists Rob Willis and Simon Taylor provided DMPK support, while Probash Chowdhury and Cerys Lovatt provided safety assessment support for the BET BD1 program. Professor Jonathan Percy and Dr. Pam Thomas contributed computational modelling and analytical support, while Dr. Richard Upton helped to decipher some of the trickier NMR spectra. I would like to acknowledge the efforts and tenacity of Dr. Ben Bax who somehow managed to resolve an X-ray crystal structure of PAD4 bound to one of the HTS hits where others had failed before him, and also the efforts of Dr. Chun-wa Chung who helped generate so many BET BD1 X-ray crystal structures so efficiently. I would like to profoundly thank Professors Harry Kelly and William Kerr for providing me with the opportunity to further my education, and also Drs. Nicole Hamblin, Edith Hessel, Dave Allen and Professor Patrick Vallance for their support of my studies. Finally, I would like to acknowledge my other half Jay for her support and understanding during all the weekends and evenings that inevitably needed to be sacrificed to write up this research, and also my dear old dad who I lost during this long journey; I wish he could still be here with us.

Acronyms and Definitions

[M - <i>t</i> Bu] ⁺	Detected electrospray molecular cation, minus <i>tert</i> -butyl group
[M + H] ⁺	Detected electrospray molecular cation
Acetyl-CoA	Acetyl Coenzyme A
ADEPT	A Daylight Enumeration and Profiling Tool
ADMA	Asymmetric dimethylarginine
ADME	Adsorption-distribution-metabolism and excretion
AML	Acute myeloid leukemia
AMP	Artificial membrane permeability
ANCA	Anti-neutrophil cytoplasmic Autoantibody
ASL	Argininosuccinate lyase
ASS	Argininosuccinate synthetase
ATP	Adenosine triphosphate
BAA	<i>N</i> - α -benzoyl-L-arginine amide
BAEE	<i>N</i> - α -Benzoyl-L-arginine ethyl ester
BD1	Binding Domain 1
BD2	Binding Domain 2
BEH	Ethylene bridged hybrid
BET	Bromodomain Extra-terminal
Boc	<i>tert</i> -Butyloxycarbonyl
br. s	Broad singlet
BRD	Bromodomain
BSA	Bovine serum albumin
C18	A retentive, non-polar sorbent for extraction of compounds from solution using a non-polar retention mechanism
cAMP	Cyclic adenosine monophosphate
CARM1	Co-activator-associated arginine methyltransferase 1
CHAPS	3-[(3-Cholamidopropyl)dimethylammonio]-1-propanesulfonate
ChIP	Chromatin immunoprecipitation
ChIP-seq	ChIP sequencing
ChromLogD _{7.4}	Chromatographic LogD at pH 7.4
CIA	Collagen induced arthritis
Cl _b	Clearance from the blood
CLND	Chemiluminescent nitrogen detection solubility
cLogP	Calculated LogP
CNS	Central nervous system
COMT	Catechol <i>O</i> -methyl transferase
COSY	Correlation spectroscopy
cPFI	Calculated Property Forecast Index
CpG	Cytosine-phosphate-Guanine
cpK _a	Calculated pK _a
CREBBP	cAMP response element-binding protein binding protein
CRO	Contract research organisation
CSD	Cambridge Structural Database
CTCL	Cutaneous T cell lymphoma
δ	NMR chemical shift, ppm

d	Doublet
DCE	1,2-Dichloroethane
DCM	Dichloromethane
dd	Double doublet
DDAH	Dimethylarginine dimethylaminohydrolase
DIPEA	<i>N,N</i> -Diiso-propylethylamine
DMA	<i>N,N</i> -Dimethylacetamide
DMAP	<i>N,N</i> -Dimethylpyridin-4-amine
DMF	<i>N,N</i> -Dimethylformamide
DMPK	Drug Metabolism and Pharmacokinetics
DMSO	Dimethyl sulfoxide
DNA	Deoxyribonucleic acid
DPU	Discovery Performance Unit
DTT	Dithiothreitol
E ₀	Standard electrochemical potential
EC	Electrochemical detection
EDG	Electron donating group
EDTA	Ethylenediaminetetraacetic acid
eNOS	Endothelial NOS
EWG	Electron withdrawing group
FaSSIF	Fasted State Simulated Intestinal Fluid
FLINT	Fluorescence intensity
FP	Fluorescence polarisation (Chapter 1)
FP	Furanopyridone (Chapter 2)
GSK	GlaxoSmithKline
GSK215	Fluorescein-labelled ligand used in the FP assay
GST	Glutathione S-transferase
HAC	Heavy Atom Count
HAT	Histone acetyltransferase
HDAC	Histone deacetylase
HEPES	4-(2-Hydroxyethyl)-1-piperazineethanesulfonic acid
hERG	Human Ether-a-go-go gene related gene
HL-60	Human promyelocytic leukemia cells; the cell line was derived from a 36-year-old woman with acute promyelocytic leukemia at the National Cancer Institute
HMBC	Heteronuclear multiple-bond correlation spectroscopy
HPLC	High pressure liquid chromatography
HRMS-FAB	High resolution mass spectrometry – fast atom bombardment
HT-29	Hypertriploid cell line; isolated from a primary colon adenocarcinoma tumour in a 44 year old Caucasian female
HTS	High Throughput Screen
hWB	Human whole blood
ii TAU	Immunoinflammation Therapeutic Area Unit
IL	Interleukin
IL6	Interleukin 6
iNOS	Inducible nitric oxide synthases
<i>iPr</i>	<i>Iso</i> -propyl

IR	Infrared spectroscopy
IVC	<i>In Vitro</i> Clearance in microsomes
<i>J</i>	Coupling value
Jmj	Jumonji
KDM	Lysine demethylase
LBF	Liver Blood Flow
LC	Liquid chromatography
LC-MS	Liquid chromatography mass spectrometry
LC-UV-MS	Liquid chromatography-Ultra violet light-mass spectrometry
LE	Ligand Efficiency
LLE	Lipophilic Ligand Efficiency
L-NMA	L- <i>N</i> ^ω -methylarginine
L-NNA	L- <i>N</i> ^ω -nitroarginine
LogP	Log ₁₀ of the partition coefficient
LPS	Lipopolysaccharide
LSD1	Lysine-specific histone demethylase 1
LSD2	Lysine-specific histone demethylase 2
m	Multiplet
<i>m/z</i>	Mass to charge ratio
MAPK	Mitogen-activated protein kinase
MCF-7	Michigan Cancer Foundation-7 cell line; MCF-7 is a breast cancer cell line isolated in 1970 from a 69-year-old Caucasian woman
MDAP	Mass directed autoperative HPLC
MMFF	Merck Molecular Force Field
MMPs	Matched Molecular Pairs
MOE	Molecular Operating Environment
MOI	Multiplicity of infection
MS	Mass spectrometry
MW	Molecular weight
NADPH	Nicotinamide adenine dinucleotide phosphate
NETs	Neutrophil Extracellular Traps
NMC	Nut Midline Carcinoma
NMR	Nuclear Magnetic Resonance
nNOS	Neuronal NOS
NO	Nitric oxide
NOHLA	<i>N</i> ^ω -hydroxy-L-arginine
NOS	Nitric oxide synthases
NUT	Nuclear-protein in testis
OPT	Phthalaldehyde
PAD	Protein Arginine Deiminase
PAD4	Protein Arginine Deiminase 4
PBMC	Peripheral Blood Mononucleated Cell assay that measures inhibition of LPS-stimulated IL6 release in whole blood
PDB	Protein Data Bank
PFI	Property Forecast Index
Phthal	Phthalimide protecting group
pIC ₅₀	-Log ₁₀ of the inhibition concentration that achieved 50% of the

	maximum response of a dose-response curve
PK	Pharmacokinetics
PMT	Protein methyltransferases
PRDM	PR domain-containing protein
PRMT	Protein arginine methyltransferase
PTM	Post translational modification
Q-ToF	Quadrupole time-of-flight
RA	Rheumatoid arthritis
RNA	Ribonucleic acid
RRP	Relative redox potential
s	Singlet
SAHA	Suberoylanilide hydroxamic acid
SAM	S-adenosylmethionine
SAMTs	S-adenosylmethionine protein N-methyltransferases
SAR	Structure Activity Relationship
SCX-II	A propylsulfonic acid bonded sorbent used for the extraction of basic compounds from solutions using a strong cation exchange retention mechanism
SDS	Sodium dodecyl sulphate
SLE	Systemic lupus erythematosus
SMILES	Simplified Molecular Input Line Entry String
SPE	Solid phase extraction
SPR	Surface Plasmon Resonance
STAB	Sodium triacetoxylborohydride
t	Triplet
TBDMS	<i>tert</i> -Butyldimethylsilyl
TBL	Tight Binding Limit
TFA	Trifluoroacetic acid
THF	Tetrahydrofuran
TMS	Trimethylsilyl
TP	Thienopyridone
TPPTS	3, 3', 3''-Phosphanetriyltris(benzenesulfonic acid) trisodium salt
t_R	Retention time
TR-FRET	Time-Resolved Fluorescence Resonance Energy Transfer
UPLC	Ultra performance liquid chromatography
UV	Ultraviolet
V_{ss}	Volume of distribution at steady state
w/wo Ca^{2+}	With or without calcium
WB	Whole Blood

Chapter 1: The Design, Synthesis and Optimisation of PAD4 Inhibitors

1.1. Abstract

Dysregulation of citrullination has been implicated in a number of immunoinflammatory diseases in humans, which include rheumatoid arthritis (RA)¹ and Systemic Lupus Erythematosus (SLE).² Protein Arginine Deiminase 4 (PAD4) is an enzyme capable of converting specific arginine and methyl-arginine residues, present in the *N*-terminal tails of histone proteins, to citrulline.³ This process is likely to be a key step in the regulation of levels of histone tail arginine methylation and thence the levels of gene transcription at an epigenetic level;⁴ the genes and levels of transcription ultimately define a cell's overall phenotype, which when regulated may be healthy, or when dysregulated may be diseased.

A first generation PAD4 inhibitor,⁵ developed to elucidate the role of PAD4 in disease progression in animal models, was previously found to be cardiotoxic in a dog safety assessment study. A medicinal chemistry program to identify a second generation chemical probe, chemically distinct from the first probe, was therefore initiated to determine whether cardiotoxicity was mechanism-based or related to the chemical template. Compounds were designed and synthesised by myself, or where specified, were synthesised by GSK colleagues or a Contract Research Organisation (CRO) in support of the PAD4 program.⁶⁻⁸ A High Throughput Screen (HTS) identified four novel lead-like PAD4 inhibitors that were validated as potential start points for lead optimisation towards a chemical probe. Lead optimisation of one hit, pyridazine **8** (**Table 10**, page 46), led to the identification of a novel series of PAD4 pyridazine inhibitors, most notably the cell potent PAD4 inhibitor **19c** (**Table 26**, page 102) which was close to the target profile required for a PAD4 chemical probe. Exploration of therapeutic potential of PAD4 inhibitors in RA and SLE is now one step closer.

1.2. Introduction

1.2.1. Epigenetics

Epigenetics is the biological study of stable heritable changes in cellular gene expression that are caused by mechanisms that at the molecular level do not modify an organism's underlying DNA sequence.⁹ Heritable changes can be brought about by covalent modification of deoxyribonucleic acid (DNA), and also by covalent modification of globular proteins called histones.^{10,11}

A histone consists of eight subunits, two each of H2A, H2B, H3 and H4; the eight subunits form reel-like structures around which strands of DNA (of roughly 165 base-pairs per histone),¹² are tightly wound achieving a five- to ten-fold compaction into nucleosomes (**Figure 1**).^{13,14} Lengths of protein that protrude from the histone subunits are called histone tails and modifications of the *N*-termini regions play important parts in the regulation of gene transcription. The nucleosomes together form chromatin, which condenses further into chromosomes.

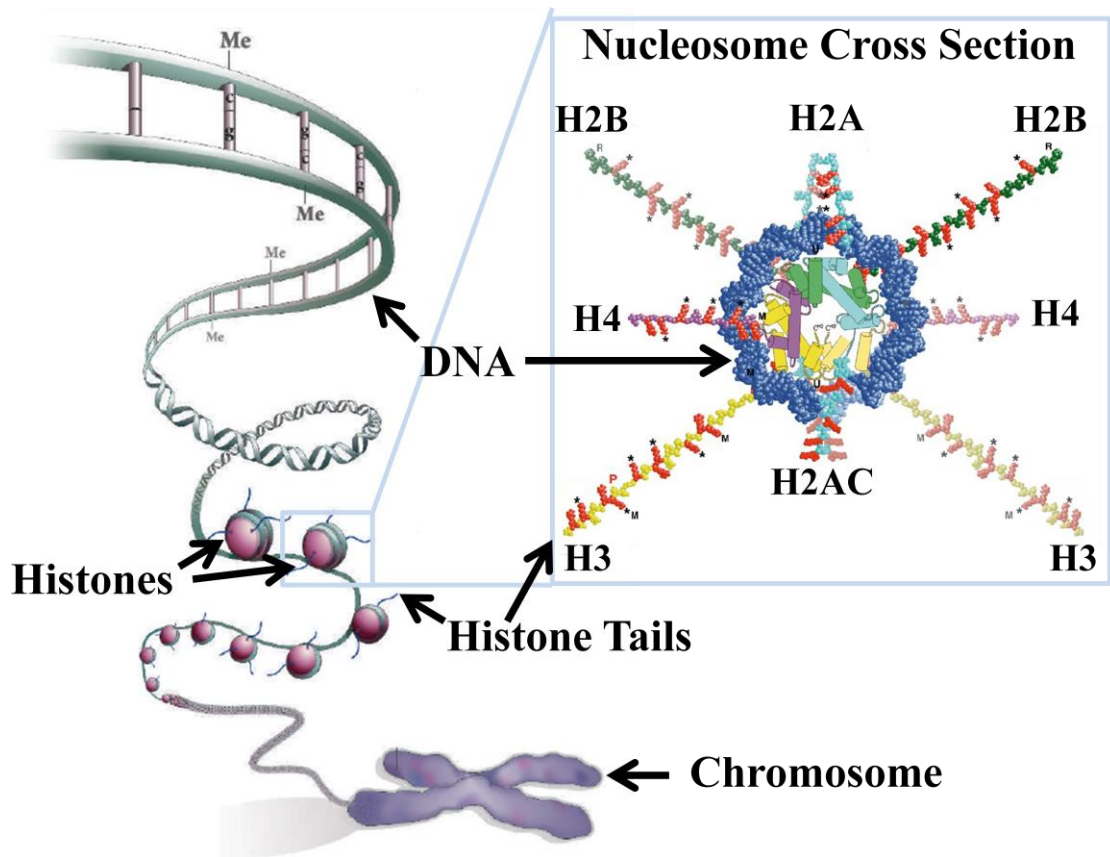


Figure 1. Schematic showing how DNA winds around histones which in turn pack into chromosomes. Reprinted by permission from Macmillan Publishers Ltd: *Nature* 441: 143-145, © 2006.¹⁴ A cross-section of a nucleosome is illustrated (*inset*).¹³

The observable biochemical and physical traits of a cell affected by the change in expression of a gene or a combination of genes is referred to as the cell phenotype. The process of epigenetic-mediated regulation of gene expression is dynamic and reversible and can define both normal healthy cellular phenotypes and those related to human diseases. Progress in linking certain diseases, particularly cancer, with certain cellular phenotypes, has been made in recent decades, as has progress in the identification of the protein families that mediate the epigenetic signalling that affects different cell phenotypes.

The most important epigenetic signalling mediator events are currently thought to be acetylation, methylation, and in the reverse direction, deacetylation and demethylation.¹⁵ These events are affected by histone acetyltransferases, histone deacetylases, protein methyltransferases, lysine demethylases, bromodomain-containing

proteins or proteins that bind to methylated histones. The modulation of these enzymes or protein-protein interaction domains using small molecules to convert diseased cells, or their progeny, into healthier phenotypes is emerging as a realistic and attractive strategy for treatment or management for a wide range of diseases. The potential druggability of these classes of protein has stimulated a number of pharmaceutical companies such as GlaxoSmithKline (GSK) and Pfizer to set up dedicated research departments and collaborations that aim to discover drugs that can treat diseases *via* novel epigenetic-based modes of action.

1.2.1.1. The Role of Epigenetics in Physiological Processes

Epigenetics-mediated gene expression plays an essential role in human physiology by controlling cell differentiation, particularly during *in utero* development, and also throughout childhood. Cell differentiation is the ordered process by which a stem cell, or other precursor cell such as a germ cell, changes into a specialised cell type with a specific function, such as a lung, liver or tissue cell. Every cell within an organism inherits the same genetic material, and it is the heritable differences in the packaging of DNA and chromatin that define the physical characteristics and biological function of cells. These inherited differences determine the distinct programs of cellular gene expression but do not involve changes to the DNA sequence. Indeed the word “epigenetics” literally means “over” or “above genetics”.

The epigenetic state of a cell is malleable and can be influenced at the molecular level by environmental factors such as diet, lifestyle, environmental chemicals, pharmaceuticals and toxins. These factors have been linked to the development and progression of many diseases, including cancer, autoimmune diseases and neuropsychiatric disorders, among many others. Direct modulation of these adverse epigenetic changes at a molecular level could therefore offer potential treatments for the associated diseases. The role of epigenetics in cellular plasticity, cellular reprogramming and response to the environment also gives therapeutic relevance in regenerative medicine.

1.2.1.2. Regulation of Gene Expression by Chromatin Remodelling

Chromatin exists in two main states: euchromatin and heterochromatin (**Figure 2**).¹⁶ Euchromatin is an open, unravelled form that permits access to DNA sequences by DNA transcription machinery, which includes RNA polymerase and associated transcription factors, thus allowing transcription and expression of genes. Conversely, heterochromatin is a closed, tightly ravelled form that blocks transcription of DNA and therefore inhibits transcription of genes. The state of chromatin therefore influences DNA transcription and gene expression which ultimately define the cell phenotype, and any changes in structure are referred to as chromatin remodeling.

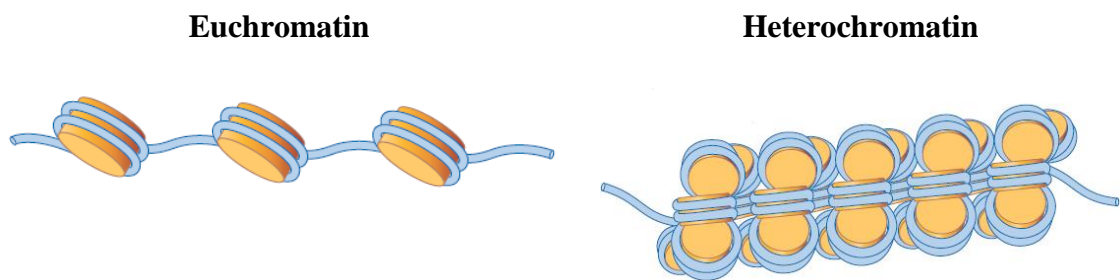


Figure 2. Representation of euchromatin (*left*) which is transcriptionally active and heterochromatin which is transcriptionally inactive (*right*).¹⁶ DNA is coloured blue, and histones are coloured orange.

Chromatin remodeling can be affected by three main events: the addition of methyl groups to DNA,¹⁷ the post translational modification (PTM) of the histone tails that protrude from the reel-like structures, and non-coding RNA-mediated scaffolding and complex formation.¹⁸

DNA methylation occurs mostly at Cytosine-phosphate-Guanine (CpG) rich sites, called CpG islands, at which the cytosine is tagged by a methyl group to form 5-methylcytosine.¹⁷ The CpG islands tend to reside at or near gene promoter regions or first exons of genes, and are unmethylated in normal cells, except those on the inactive X-chromosome in females. CpG islands tend to have a markedly open chromatin structure which is conducive to gene expression, but on methylation can form transcriptionally repressive heterochromatin.

A PTM of a histone tail is a chemical modification that acts as a signal to other proteins that recognise the modification, and is often referred to as a “mark”. The addition or removal of a histone tail mark can alter the histone’s tertiary structure and may in turn either induce or impede DNA from being completely unwound from the histone during replication, thereby altering gene expression. Histone tail modification is thought to occur mainly at the *N*-termini through acetylation and methylation, and to a lesser extent through ubiquitylation, phosphorylation, sumoylation and citrullination, though direct modification of histone subunits has been reported. Acetylated histones are typically less tightly wound and therefore more accessible to the transcriptional machinery, thereby allowing transcription of nearby genes. Methylated histones can be either activating or repressive, depending on the degree and location of methylation. The mapping and quantification of multivalent post translational modified proteins has been made possible with a combination of chromatin immunoprecipitation (ChIP) and mass spectrometry, and most recently using DNA sequencing (ChIP-seq).¹⁹

1.2.1.3. Histone Modification and Recognition

The proteins that affect PTMs of histones fall into three classes according to their function; these are: writers, erasers and readers (**Figure 3**).²⁰ Writers include histone acetyltransferases (also known as acetylases) and histone methyl transferases (also known as methylases), which covalently attach acetyl groups or methyl groups to histone tails respectively. Erasers remove histone marks and include histone deacetylases and lysine demethylases. Readers include bromodomains and methyl-lysine-binding domains which recognise and bind to histone modifications. The combination of histone and DNA post-translational modifications and related interacting proteins that package the genome and define the transcriptional programming of a cell is referred to as the epigenome.

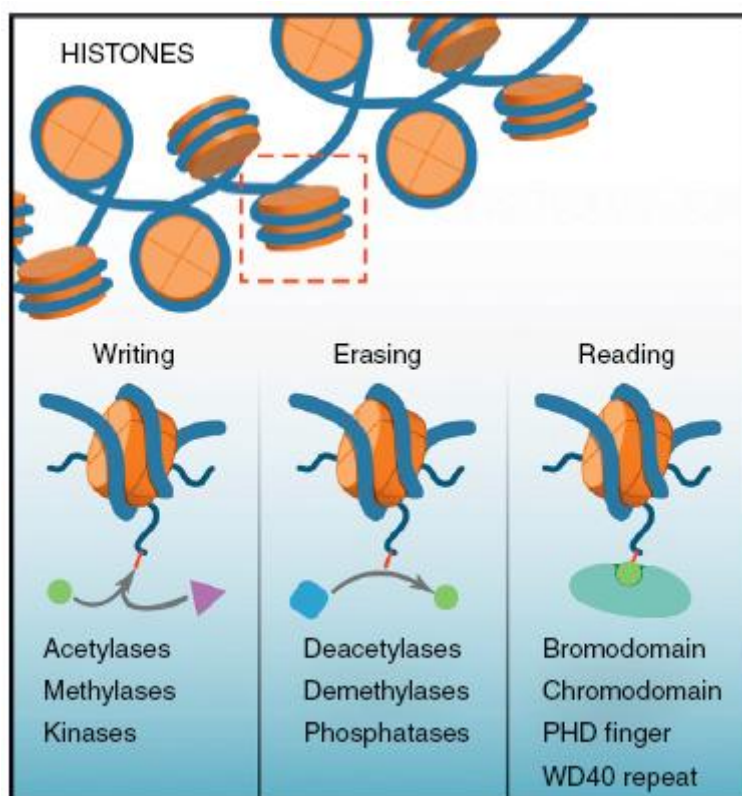


Figure 3. The *N*-termini of histone tails are subject to the activity of the various groups of proteins indicated and are categorised by function as writing, erasing and reading.²⁰

A large component of the human epigenome is comprised of acetylation and methylation networks. Single marks and combinations of marks can be recognised by numerous classes of conserved protein domains usually as part of larger, multi-protein complexes. The majority of writer enzymes that catalyse the formation of methyl and acetyl histone marks are large proteins that possess additional domains, or other regions, that read histone marks or interact with DNA or other proteins in addition to their catalytic domain. The proteins together form larger complexes that affect cellular and environmental signals, define cellular identity and contribute to the formation and/or continuation of disease states. A selection of the key classes and functions of regulatory proteins that write, read and erase the major histone marks are summarised in **Table 1**.¹⁵




Class	Family	Activity	Number of Proteins	Major Class / Function
Writers	Histone acetyltransferases	K→KAc	18	MYST family: DNA damage and oncogenic translocation GNAT: EGF signalling and cell cycle progression EP300: involved in numerous cellular events
	Protein methyltransferases	K→KMe R→RMe	60	SET domain: methylation of histone lysines and non-histone lysines PRMTs: methylate histone arginines and non-histone arginines PRDMs: SET domain-like tissue-specific factors
Erasers	Histone deacetylases	KAc→K	17	Class I, IIb and IV enzymes: gene silencing Class IIa enzymes: scaffolding proteins Sirtuins (class III): deacetylation and ADP-ribosylation
	Lysine demethylases	KMe→K	25	Lysine-specific demethylases: regulation of transcription during development Jmj domain: unknown
Readers	Bromodomain-containing proteins		61	Targeting of chromatin-modifying enzymes to specific sites; often linked to the catalytic domain of histone acetyl transferases
	Methyl-lysine and/or, methyl-arginine-binding-domain containing proteins e.g. Tudor domains		95	Tudor domains: bind di- and tri-methylated lysine and di-methylated arginine MBT domains: bind mono- and di-methylated lysines Chromodomains: bind tri-methylated lysine PWWP domains: bind tri-methylated lysine and DNA
	PHD-containing proteins		104	Large and diverse family that interacts with multiple substrates

Table 1. Major protein families that form the epigenome and write, remove or read methyl- (Me) or acetyl- (Ac) marks on specific lysines (K) or arginine (R) residues. MYST: histone deacetylases, MOZ, Ybf2/Sas3, Sas2 and Tip60; EGF: epidermal growth factor; EP300: E1A-associated protein p300; SET-domain: Su(var), Enhancer of zest, and Trithorax domain; PRMT: protein arginine methyltransferase; PRDM: PR domain-containing protein; Jmj: Jumonji; MBT: malignant brain tumour domain; PWWP: Pro-Trp-Trp-Pro domain.¹⁵ Reprinted (adapted) by permission from Macmillan Publishers Ltd: *Nature* 11: 384-400, © 2012.

1.2.1.4. The Epigenome and the Histone Code

Histone tails and nucleosomes may dynamically and reversibly undergo multiple modifications at any one time and the modifications can change the overall transcriptional behaviour of the cell to give it a specific phenotype. The number of

possible permutations of histone and/or nucleosome modifications is enormous, given the high number of different possible modifications and number of locations at which the modifications can occur, particularly since the location of the modification can cause different events. For example, methylation at one position can cause gene activation, while methylation at another may cause gene repression. The hypothesis that the combination of modifications creates a complex code that relates to the transcriptional state of nearby genes and ultimately defines the cell's phenotype is referred to as the histone code hypothesis. The histone code is increasingly being found to be context-dependent, with the generation of one specific histone mark potentially influencing the placement of the next; the process could therefore be considered to be more of a language than a code.²⁰ The mapping and interpretation of the histone code is currently at a rudimentary stage.

1.2.1.5. Epigenetic Links with Disease

Epigenetic mark readers, writers and erasers are believed to drive the development and progression of a wide range of diseases by altering cellular gene expression patterns either by mutation or alteration of the epigenetic factors themselves, or by upstream signals caused by environmental or tissue-specific events. The potential opportunity to modulate epigenetic events implicated in diseases such as cancer, neuropsychiatric and immunoinflammatory disorders is attractive for drug discovery.

Cancer

Cancer is fundamentally a genetic disease driven by irreversible genomic mutations that cause activation of oncogenes, or inactivate tumour suppressor genes. However epigenetic mechanisms, particularly DNA methylation whereby tumour suppressor genes may be inactivated by hypermethylation of promoter regions, have long been implicated in cancer.²¹ This has led to the development of DNA methyltransferase inhibitors which modulate levels of DNA methylation; some are now in the clinic, such as 5-*aza*-2'-deoxycytidine (decitabine, marketed as Dacogen^(R), **Figure 4**), which is used in the treatment of acute myeloid leukemia (AML) and works by inhibiting DNA methyltransferase.²²

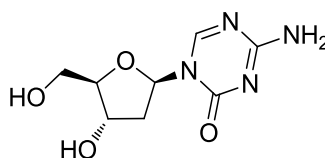


Figure 4. Structure of 5-*aza*-2'-deoxycytidine (decitabine, marketed as Dacogen^(R)) which is a DNA-methyltransferase inhibitor used in the treatment of AML.

Epigenetic regulatory proteins have also been identified as being dysregulated in cancer, leading to both local and global alternation of histone marks within cancer epigenomes and cancer cell phenotypes. Several mechanisms can cause deregulation of epigenetic regulatory proteins and signalling networks, such as deactivating or activating mutations, gene amplification, indirect enzyme up-regulation or inactivation, and translocations that lead to the expression of “gain-of-function” fusion proteins. These contain reader domains and change the gene product so that it gains a new and abnormal function and usually has a dominant phenotype. This information led to the development of histone deacetylase (HDAC) inhibitors, such as suberoylanilide hydroxamic acid (SAHA, also known as vorinostat and marketed as Zolinza^(R), **Figure 5**), which are now being used in the clinic as cancer treatments. This compound is used for the treatment of the haematological malignancy cutaneous T-cell lymphoma (CTCL) when other treatments have not worked.²³ This compound was a proof of concept for the potential of epigenetic disease therapies that work through histone modification. SAHA works by chelating zinc ions present in the active site of HDACs, thereby inhibiting the function of multiple HDACs. The resulting accumulation of acetylated histones and acetylated proteins, which include transcription factors crucial for the expression of genes needed to induce terminal cell differentiation, prevents further cell growth.

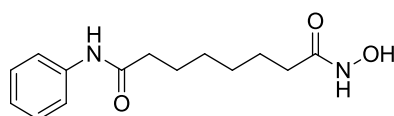


Figure 5. Structure of the HDAC inhibitor, SAHA (vorinostat, which is marketed as Zolinza^(R)).

The main disadvantage of existing epigenetic-based therapies, such as HDAC inhibitors, is that these agents are not selective within their target protein families and therefore have substantial side effects. Side effects may be reduced or removed using target specific HDACs with greater selectivity and this may also be beneficial in the treatment of certain cancers, though this is yet to be demonstrated in the clinic. A number of second generation HDAC inhibitors that are more selective are currently undergoing clinical trials for different types of cancer.

Neuropsychiatric Disorders

Neuropsychiatric disorders that seem to result in intellectual disability have also been linked to abnormal levels of epigenetic proteins.¹⁵ Brachydactyl mental retardation syndrome is characterised by delays in development and behavioural problems, and is caused by reduced HDAC4 function. Rubinstein-Taybi syndrome results in cognitive dysfunction and is caused by reduced levels of the Histone Acetyl Transferase (HAT) Cyclic adenosine monophosphate (cAMP) response element-binding protein (CREB) binding protein, CREBBP. Additionally a polymorphism in Bromodomain 1 (BRD1) has been linked with schizophrenia and bipolar affective disorder.

Immunoinflammatory Disorders

The adaptive immune system operates in a manner which strongly implicates regulation by epigenetic mechanisms of action because it is comprised of cells with multiple roles that undergo differentiation and clonal expansion on exposure to an appropriate stimulus,²⁴ such as an antigen, to become activated lymphocytes; lymphocytes then retain a memory against future exposure to that antigen.

Rheumatoid arthritis (RA) is a chronic, systemic autoinflammatory disorder that can affect many tissues and organs, principally the flexible synovial joints such as those in the knee or elbow; when advanced, it can be a disabling and painful condition. HDAC inhibitors have been found to be anti-rheumatic in collagen-induced arthritis (CIA) models in rodents, potentially through suppression of RA fibroblast-like synoviocyte and macrophage Interleukin-6 (IL-6) production, evidence of which has come from clinical samples of patients with autoimmune disease.²⁵ System Lupus Erythematosus (SLE) is a systemic autoimmune disease in which the immune system attacks cells and

tissues in any part of the body, resulting in inflammation and tissue damage. Abnormal histone modification patterns have been observed in lupus CD4⁺ T-cells.²⁶ There is also evidence for an epigenetic-based role in the aberrant upregulation of autoantigen genes in humans with Anti-Neutrophil Cytoplasmic Autoantibody (ANCA)-associated vasculitis in which the immune system attacks small vessels in different tissues and organs, and can lead to organ failure.²⁷

Evidence for the involvement of epigenetic-based mechanisms in regulating the immune system through modulation of transcription factors and histone modification is continually increasing and there is clinical evidence that suggests these mechanisms can be dysregulated in autoimmune diseases.¹⁵

1.2.1.6. Histone Acetylation

The most studied histone modification is acetylation²⁸ which was first described in 1964. The acetylation of a histone tail is affected by HATs while HDACs remove acetyl groups (**Figure 6**).¹⁵ Together HDACs and HATs complement each other in the regulation of this highly dynamic process. HATs catalyse the transfer of an acetyl group onto the ε-amino group of lysine side chains of the histone tail using acetyl-CoA as a cofactor. The sidechain amino groups of lysine are normally protonated at physiological pH, so lysine is typically positively charged which allows the histone tail to interact strongly with negative phosphate backbone of DNA. Acetylation neutralises positive charge and in turn loosens the nucleosome's interaction with DNA. This allows increased euchromatin character thus allowing the transcriptional machinery to bind and affect gene transcription. HDACs reverse the process by removal of the acetyl group, re-establishing the positive charge on the lysine which allows the nucleosome to form a stable interaction with DNA, increasing heterochromatin character.

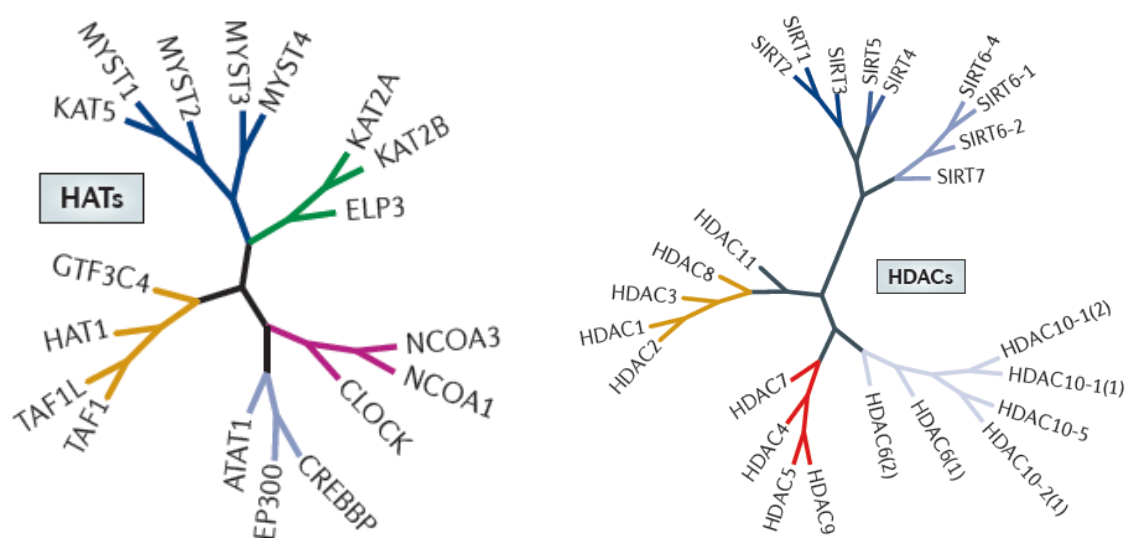


Figure 6. Phylogenetic trees of HAT and HDAC epigenetic protein families.¹⁵ Proteins are clustered on branches on the basis of the similarity of their amino acid sequences. The phylogenetic representation tends to cluster structurally, and sometimes functionally, related proteins. A compound that inhibits a given protein on one branch is more likely to be active against other proteins on the same branch. Reprinted by permission from Macmillan Publishers Ltd: *Nature* 11: 384-400, © 2012.

Various sites of histone lysine acetylation are linked to the formation of transcriptionally active euchromatin from transcriptionally inactive heterochromatin, particularly histone lysine acetylation of lysine 16 of histone 4 (shortened to H4K16).²⁹ There is also evidence for the direct acetylation of histone core at H3K56 which may affect interaction, between DNA and histones.

Histone acetylation also provides binding sites for proteins that are involved in gene activation, particularly the bromodomain-containing family of proteins that recognise or read modified lysines of histone proteins. The activity of an important but diverse set of proteins that affect transcriptional co-activation relies on the ability of bromodomains to recognise and bind to acetylated lysines.

1.2.1.7. Histone Methylation

Protein methyltransferases (PMTs) affect the methylation of histone tails, such as *S*-adenosylmethionine (SAM)-dependent methyltransferases. Conversely lysine

sequence of amino acids. For example, trimethylated H3K4 (H3K4me3) and H3K9 (H3K9me3) are recognised by a distinct set of reader domains.

Methylated histone lysines are associated with transcriptional activation and with repression by induction of euchromatin or heterochromatin respectively. H3K4me3 is associated with transcriptional activation, while H3K9me3 and H3K27me3 are associated with transcriptional repression.¹⁰

Histone arginine methylation, a common but less studied PTM, was recently recognised as playing an important role in transcriptional regulation³⁰ because this PTM can inhibit or agonise the interaction of nuclear factors with nearby histone marks.^{31,32}

1.2.2. What is a Chemical Probe?

A large number of previously unknown and unexplored potential drug targets has emerged over the past decade as a result of advances in genome sequencing efforts, screening technologies and platforms.^{33,34} The development of a small molecule drug is highly complex, time consuming and costly, so some efforts have focussed on the generation of small molecule tools, or chemical probes, to help elucidate the role of biological targets, such as proteins, receptors or enzymes, in healthy and diseased cells and tissues, in a potentially more time- and cost-effective manner.³⁴ Whereas a drug must be safe and effective in the treatment of a disease or condition, a chemical probe must ask a specific biological question; the differing purpose of a drug *versus* a chemical probe leads to different requirements for each (**Table 2**).³³

Drug	Chemical Probe
<ul style="list-style-type: none"> • May have an undefined Mode of Action • Intellectual Property restrictions • High bar for physicochemical and pharmaceutical properties 	<ul style="list-style-type: none"> • Defined Mode of Action • Must have good selectivity • Can be freely available • Drug-like properties not necessarily required • Value is increased by use of structurally related inactive and structurally unrelated active compounds

Table 2. Requirements for chemical probes and drugs.³³

A chemical probe is typically a small molecule that is capable of modulating a target protein's function, usually rapidly and reversibly, to such an extent that mechanistic and

phenotypic questions can be answered in biochemical and cell-based assays or using animal studies.^{33,35} The molecule needs to be potent, selective and adequately characterised so that biological data generated using the probe can be interpreted reliably and usefully in validating or invalidating a biological target which may be therapeutically relevant. The results obtained using chemical probe can be complementary to those using genetic approaches, such as siRNA or shRNA, and are usually more relevant for translational studies than when a drug is used, because they are more likely to mimic the pharmacology *in vivo*.

The common goal shared between the academic and industrial communities for validating biological targets with the potential of translating the research into improved treatments for patients has stimulated a number of collaborations to optimise the validation process. A notable example is the Structural Genomics Consortium (SGC), a public-private partnership that supports the delivery of new medicines through open access research.³⁶ The SGC provides a list of high quality chemical probes, such as those shown in **Table 3**, that will allow the elucidation of the role of a range of biological targets, and should seed the development of new medicines that will benefit patients. GSK has therefore contributed, and is continuing to contribute, a number of chemical probes to the SGC and thence to the wider drug discovery community to support the acceleration of the drug discovery process.

Probe	Target	Target Class	Mode of Action
(+)-JQ1	BET family bromodomains	Bromodomains	Inhibitor
GSK484	PAD4	Arginine deiminases	Inhibitor
UNC0642	G9a/GLP	Histone Methyltransferase	Inhibitor
DDR1-IN-1	Collagen receptor kinase DDR1	Kinase	Inhibitor

Table 3. High quality chemical probes that are offered *via* the SGC.³⁶

Biologically meaningful data can only be generated using high-quality chemical probes and the specific properties required for a high quality probe have been widely debated in the the scientific community.

On-target activity in cells and minimal cell-based toxicity is likely to be required for a high quality chemical probe in order to maximise the probability of observing mechanistic and phenotypic effects in animal models.^{33,35,37} A chemical probe will typically need to have drug-like physicochemical properties to enable penetration into cells and to achieve cell-based potency, such as high permeability and high solubility;^{35,37} these factors often require optimisation and are discussed in later sections.

A widely agreed requirement for a chemical probe is high potency and selectivity for the biological target because the use of a promiscuous chemical probe can at best confound the interpretation of results, and at worst impede the drug discovery process.³³⁻³⁵ The protein kinase inhibitor staurosporine has been used as a chemical probe by many groups to explore specific target pathways, with over 8000 related publications,³⁵ however, over the last decade compound has been found to be promiscuous by virtue of its ability to mimic ATP with a K_D measured against over 20% of all known protein kinases which, in retrospect, would make it difficult to interpret any biological results.³⁸

An SGC chemical probe for epigenetic targets must satisfy the following criteria: 1. *in vitro* IC_{50} or $K_D < 100$ nM ($pIC_{50}/pK_D > 7$); 2. >30-fold selectivity over proteins in the same family; 3. significant on-target cellular activity at 1 μ M.³⁶ Criteria for other biological targets are open to interpretation and are likely to need definition on a case-by-case basis. In an ideal situation a chemical probe would be used in conjunction with both an inactive close analogue of the compound as a negative control, and additionally a second chemical probe with a completely different chemical structure to the first probe to reduce the probability of off-target effects, with its own inactive but structurally related negative control.

In practice biological investigations using the first discovered chemical probe (often referred to as a First Generation probe) in tandem with those using a second structurally unrelated probe (referred to as a Second Generation probe) are usually not realistic, nor necessary; for example, a First Generation probe may be used to confirm that a more potent or more selective Second Generation probe than had been initially thought would be required to validate a biological target.

A chemical probe must have high on-target potency but usually does not need to meet other requirements that a small molecule drug needs to meet, such as good bioavailability, as long as the required level of exposure *in vivo* can be achieved by other means, for example, by intravenous infusion.³³ Many medicines manifest their clinical effects through polypharmacology,³⁹ so many small molecule drugs do not need to be as selective as a chemical probe. Ultimately high quality chemical probes have started to enable an improved understanding of targets and pathways and have created opportunities for proprietary drug discovery efforts to an extent that would not have been possible otherwise.³³ A significant example of success for the chemical probe approach has been the use of small molecule *pan*-BET inhibitors (+)-JQ1 and iBET762 as chemical probes to interrogate BET family bromodomain function; this effort has led to the identification of the potential benefits of inhibiting BET family function in a wide range of therapeutic scenarios, from oncology, inflammation and virology to male contraception.^{33,37}

1.2.3. The Biological Significance of Arginine

L-Arginine (**Figure 8**) is an α -amino acid that is reported to have been first characterised in 1886 by Swiss chemist Ernst Schultze.⁴⁰ The amino acid is a precursor to creatine which is required for metabolism in muscle, nerves and in the testis, and for the synthesis of numerous protein scaffolds; L-arginine is also a precursor to L-ornithine which plays an important part in the urea cycle.⁴¹ L-Arginine has been found to play an important role in a number of important biological functions in mammals, such as soft tissue,⁴² vasculature⁴³ and skeletal wound healing.^{44,45} L-Arginine also plays an essential part in the generation of nitric oxide (NO) which acts as a neurotransmitter, is the primary signal generator involved in regulation of angiogenesis⁴⁶ and cardiac function, and is also involved in insulin generation⁴⁷ and modulation of vasculature and airway tone.⁴¹

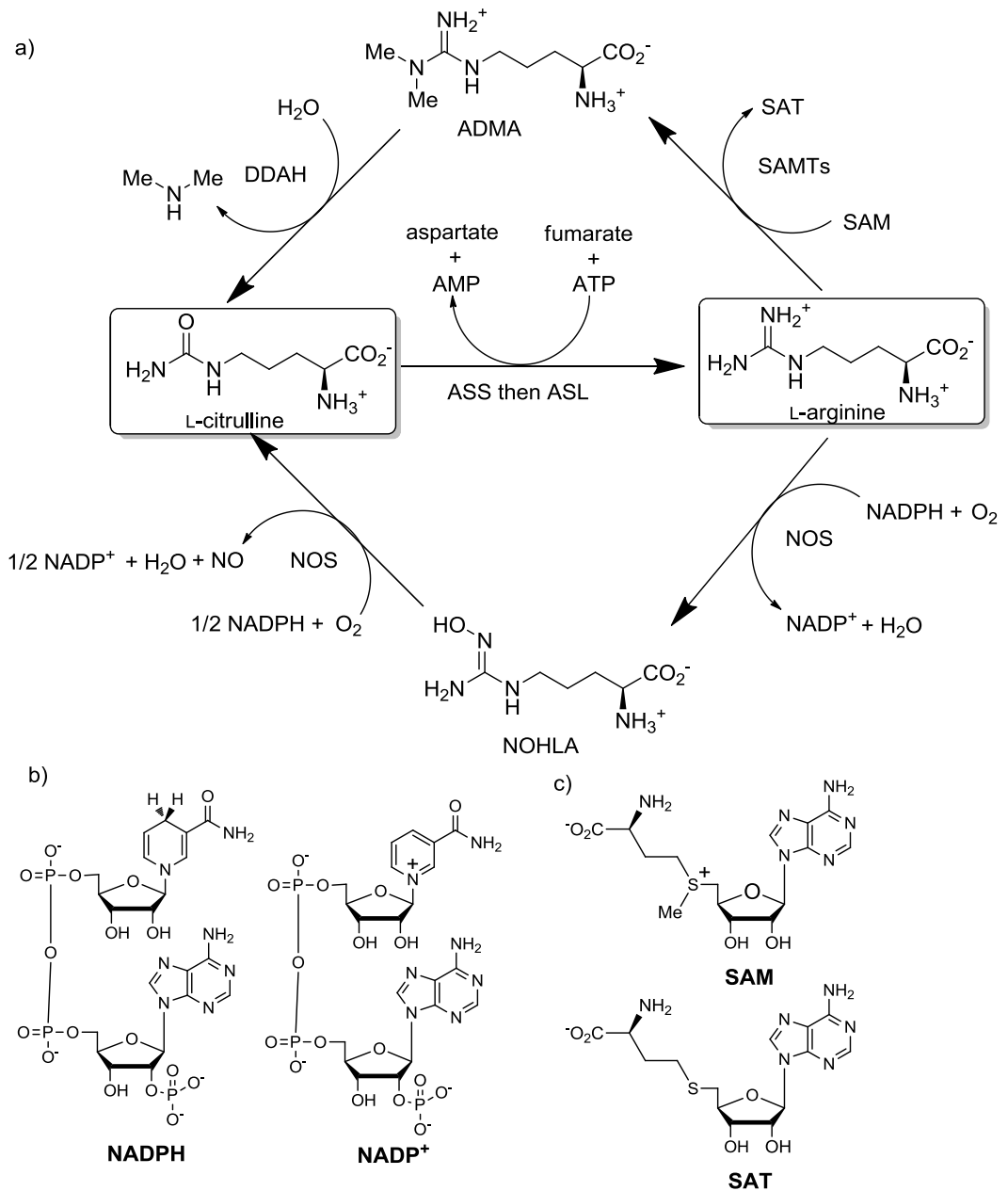


Figure 8. a) Biosynthesis of L-citrulline and L-arginine. ASS = argininosuccinate synthetase, ASL = argininosuccinate lyase, ATP = adenosine triphosphate, AMP = adenosine monophosphate, NADPH = nicotinamide adenine dinucleotide phosphate (reduced form), NADP^+ = nicotinamide adenine dinucleotide phosphate (oxidised form), NOHLA = N^{ω} -hydroxy-L-arginine, SAMTs = S-adenosylmethionine protein N-methyltransferases, SAM = S-adenosylmethionine and SAT = S-adenosyl thionine, DDAH = dimethylarginine dimethylaminohydrolase, ADMA = asymmetric dimethylarginine. b) structure of NADPH and NADP^+ . c) Structure of SAM and SAT.

NO is also critical for vasodilation and reducing arterial pressure and is used as a gas in the clinic to treat patients suffering from pulmonary hypertension.^{48,49} L-Arginine is usually generated in significant amounts by healthy individuals, but can be obtained from a range of animal- and plant-based dietary sources. The guanidine group has a basic pK_a of 12 and is therefore positively charged at physiologically-relevant pHs.⁵⁰

The biosynthesis of arginine from citrulline is effected by two cytosolic enzymes, argininosuccinate synthetase (ASS) and then argininosuccinate lyase (ASL) *via* the intermediate argininosuccinate; the process requires adenosine triphosphate (ATP) to proceed and is therefore energetically costly.⁵¹ The name citrulline is derived from the Latin word for watermelon *citrullus*, from which the compound was first isolated in 1914 by Koga and Odake, and later identified in 1930 by Wada.⁵² Nitric oxide synthases (NOSs) catalyse the conversion of L-arginine to L-citrulline and NO (**Figure 8**) *via* N^ω-hydroxy- L-arginine (NOHLA) in the presence of molecular oxygen using the reduced form of nicotinamide adenine dinucleotide phosphate (NADPH) as a cofactor.⁵³ In addition to the role of NO in cellular signaling, NO is known to be a proximate cause for septic shock⁵⁴ and is also reported to play a role in autoimmune diseases.^{55,56}

Methylated arginines, such as asymmetric dimethylarginine (ADMA, **Figure 8**), circulate in human plasma and have been found to interfere reversibly with the L-arginine mediated generation of NO;⁵⁷ exposure to methylated arginines such as ADMA is thought to cause conditions such as heart disease and arterial stiffness by continued vasoconstriction.⁵⁸ Methylated arginines are formed by a PTM of L-arginine by S-adenosylmethionine protein N-methyltransferases (SAMTs) using S-adenosylmethionine (SAM).⁵⁹ Conversion of ADMA back to L-citrulline is affected by dimethylarginine dimethylaminohydrolase (DDAH).⁵⁸

The calcium-calmodulin controlled isoenzymes, neuronal NOS (nNOS or NOS-1) and endothelial NOS (eNOS or NOS-3) mediate levels of NO in mammals, while the cytokine inducible isoform iNOS (iNOS or NOS-2) is expressed in macrophages and is therefore involved in immune responses.^{53,60} nNOS and iNOS are predominantly found in the cytosol, whereas eNOS is mainly membrane-associated in the endothelial lining of blood vessels. A significant amount of effort has been invested over the last two decades to find specific inhibitors of NOSs, primarily for the management of ischemic

reperfusion injury, hypotensive effects of drugs or hemorrhagic trauma and inflammatory response to cytokines, such as that seen in asthma. Numerous NOS inhibitors have been developed that are analogues of arginine and have high potential for clinical application, such as the amidine GW274150 (**Figure 9**), which was potent and relatively selective for recombinant human iNOS, and had the potential to treat migraine, RA and allergic asthma. GW274150 had a reasonable oral pharmacokinetic profile and was well tolerated by healthy volunteers and patients when administered for the indications mentioned.⁶¹ However, dose-related erosion of the gastrointestinal tract was observed in a rat carcinogenicity study after administration of GW274150 for 13 weeks, which precluded its use in the clinic beyond this time. This molecule was not progressed beyond Phase 2 clinical trials.

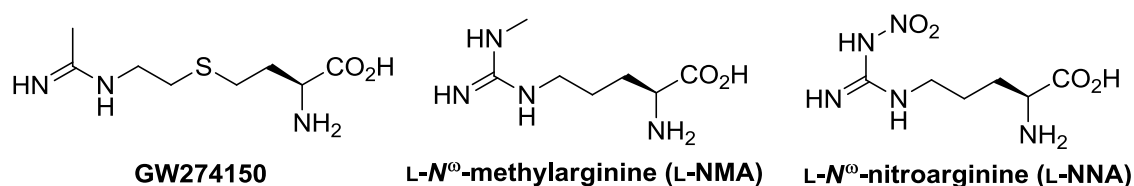


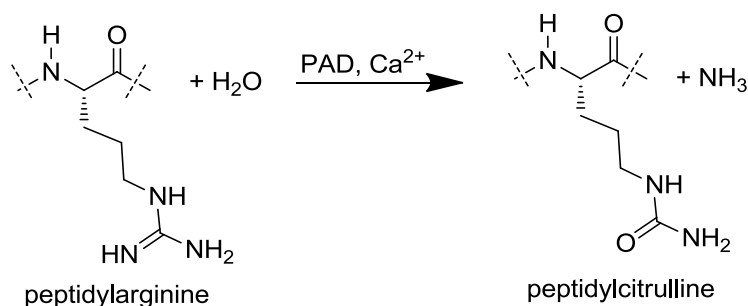
Figure 9. Structure of three noteworthy arginine analogue NOS inhibitors that have progressed to clinical trials: GW274150, L-NMA and L-NNA.

Although a number of arginine-based NOS inhibitors have been found to be potent, of low toxicity and possess reasonable pharmacokinetics, to date the major issue has been the little or low selectivity among isoforms of NOS which can result in pronounced side effects *in vivo*, such as hypertension due to inhibition of eNOS. A small number of arginine-based NOS inhibitors, such as L-N^o-methylarginine (L-NMA, **Figure 9**) and L-N^o-nitroarginine (L-NNA, **Figure 9**), have some subtype selectivity and are being assessed in clinical trials, but to date none have progressed beyond this.

1.2.4. Protein Arginine Deiminase (PAD) Regulation of Histone Methylation

Recently the methylation PTM of arginine residues present on histone tails by PRMTs has been shown to be involved in the regulation of transcription.⁶² The Protein Arginine Deiminase (PAD) enzyme catalyses the conversion of peptidylarginine residues to citrulline (**Scheme 1**)³ and is capable of deiminating specific arginine and methyl-arginine residues present in the *N*-terminal tails of histone proteins. This process is

thought to be key step in the regulation of levels of histone tail arginine methylation, and thence the levels of transcription at an epigenetic level,⁴ that define a cell's phenotype.



Scheme 1. Process of PAD-catalysed deimination of peptidylarginine to citrulline. The guanidine functional group is hydrolysed to give the ureido group and ammonia.

Five related isoforms of PAD enzymes have been identified in mammals; all rely on the presence of Ca²⁺ for activity (**Table 4**).³ The chemical reaction catalysed by PAD enzymes is de-amination, but is also be referred to as citrullination. Although there is a high degree of sequence homology between PAD isotypes, their expression is tissue-specific.

Isotype	Protein	mRNA
PAD1	Epidermis, uterus	Brain, colon, embryonic stem cells, eye (retina), inner ear, kidney, muscle, nerve, placenta, skin, thymus, uterus, vagina
PAD2	Brain, spinal cord (glial cells), uterus, salivary gland, macrophages, pituitary gland, sweat gland, spleen, pancreas, bone marrow, oligodendrocytes, yolk-sac (leucocytes), skin (ambiguous)	Aorta, brain, breast, bone (marrow), cervix, colon, embryo, epididymus, eye (retinal), inner ear, kidney, leukocyte, lung, lymph node, macrophage, muscle, ovary, pancreas, placenta, prostate, salivary gland, skin, spleen thymus, uterus
PAD3	Hair follicles	Muscle, skin, thymus
PAD4	Eosinophils, neutrophils, granulocytes	Brain, bone (marrow), eye, fetal liver/spleen, inner ear, kidney, leukocyte, macrophage, placenta, prostate, skin, thymus
PAD5	Egg, ovary, early embryo	Embryo, ovary (egg), thymus

Table 4. Overview of PAD expression in humans.³

The most widely expressed isotype of PAD is PAD2; its expression is thought to be regulated at both transcriptional and translational level by local concentrations of Ca^{2+} , for example in macrophages, or by hormones such as estrogen in tissues such as the pituitary gland and uterus. The ubiquitous expression of PAD2 makes this isotype an unlikely drug target because of likely widespread and wide-ranging effects of PAD2 modulation.

Conversely, human PAD4 is mainly expressed in white blood cells, specifically granulocytes and monocytes, and is the only type of PAD that resides in the cell nucleus. Human PAD4 was originally named PAD5 because it was believed to be a novel PAD as it shows slightly different reaction kinetics to rat PAD4 towards artificial substrates; however, evidence built from sequence data, expression data, and the genomic organisation of the PAD genes indicate human PAD5 corresponds to the rodent PAD4 so human PAD5 was renamed PAD4.

PAD4 is a transcriptional coregulator that causes repression of gene expression, most likely through the modification of histone arginine residues; this is known to affect or suppress gene transcription by altering local chromatin structure directly or indirectly by the recruitment of additional transcriptional coregulators.⁶³ PAD4 can target multiple sites such as H3 and H4, and those that are methylated, Co-activator-Associated Arginine Methyltransferase 1 (CARM1) at H3R17, and PRMT1 at H4R3. A decrease in levels of histone methylation with concomitant increase in citrullination levels requires PAD4 activity in human HL-60 granulocytes. PAD4 activity has also been linked with transcriptional regulation of estrogen-responsive genes in a human breast adenocarcinoma cell line, MCF-7.

1.2.5. PAD4 as a Drug Target

Increased PAD2 and PAD4 expression and anti-citrullinated protein antibodies have been observed in the inflamed synovium of RA patients, which suggests PAD4 inhibition may halt the progression of RA.⁶⁴ PAD4-mediated citrullination of histones has also been linked to the formation of Neutrophil Extracellular Traps (NETs), which are web-like structures composed of chromatin backbones and granular molecules.² NETs are released by activated neutrophils and have been described as a novel host defence mechanism to trap and kill foreign pathogens. Neutrophils from SLE patients are more susceptible to producing NETs and a subset of SLE patients have impaired ability to clear NETs, which when persistent may directly damage tissues and augment the autoimmune response of the patients. Therefore PAD4 inhibition may reduce levels of NET formation in SLE patients thus reducing tissue damage and autoimmune response augmentation.

Two small molecule PAD4 inhibitors, the F- and Cl-amidine (**Figure 10**) have been reported to display cytotoxic effects towards several cancer cell lines such as HL-60 and MCF-7, and were even shown to induce differentiation of HL-60 and HT-29 cells with no effect on non-cancerous lines.⁶⁵ This suggests a PAD4 inhibitor may also have role in oncology treatments. Furthermore, the Cl-amidine was found to significantly inhibit the formation of CIA in a mouse RA model, whereas the F-amidine was ineffective.⁶⁶

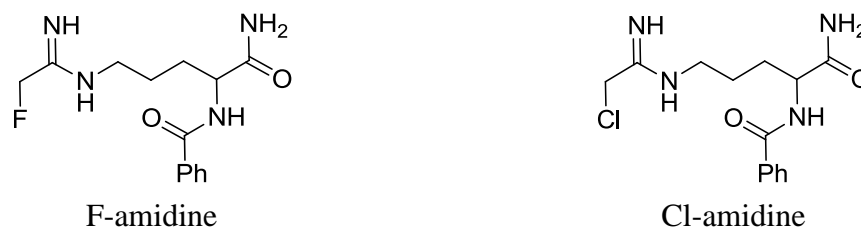


Figure 10. Structures of two small molecule PAD4 inhibitors, the F- and Cl-amidine, that have been previously reported.⁶⁵

Oncology, RA and SLE are in the main poorly managed using existing treatments, so the discovery of a PAD4 inhibitor that modulates citrullination and downstream cellular mechanisms of disease development and progression was therefore attractive from a pharmaceutical perspective. A campaign to identify a small molecule PAD4 inhibitor with good *in vivo* DMPK properties, and which could be used to elucidate the role of PAD4 in RA and SLE, and potentially oncology, was initiated by the Epinova Discovery Performance Unit (DPU).

1.2.6. PAD4 X-ray Crystal Structure

The X-ray crystal structure of full length wild-type human PAD4 was first reported in 2004 by Arita *et al.* who aimed to elucidate the Ca^{2+} -dependent molecular mechanism of peptidyl citrullination by PADs.¹ Crystal structures were determined for Ca^{2+} -free wild-type PAD4 and a Ca^{2+} -bound C645A inactive mutant PAD4, with and without *N*- α -benzoyl-L-arginine amide (**BAA**), which is a close structural analogue to a known substrate, *N*- α -benzoyl-L-arginine ethyl ester (**BAEE**). Marked conformational differences between the Ca^{2+} -free PAD4 and Ca^{2+} -bound PAD4 were evident (**Figure 11**).

The structure of Ca^{2+} -bound PAD4 was found to be similar to that of the substrate-PAD4 complex with an active site cleft created from well-ordered residues in the surrounding region. In contrast, the same residues were highly disordered in Ca^{2+} -free PAD4 which exposed an acidic concave surface to solvent. The active conformation of PAD4 is therefore likely to be the Ca^{2+} -bound form, which is consistent with results observed in biological assays which require the addition of Ca^{2+} to allow the turnover of **BAEE**. Key interactions between **BAA** and PAD4 are highlighted in **Figure 12**.

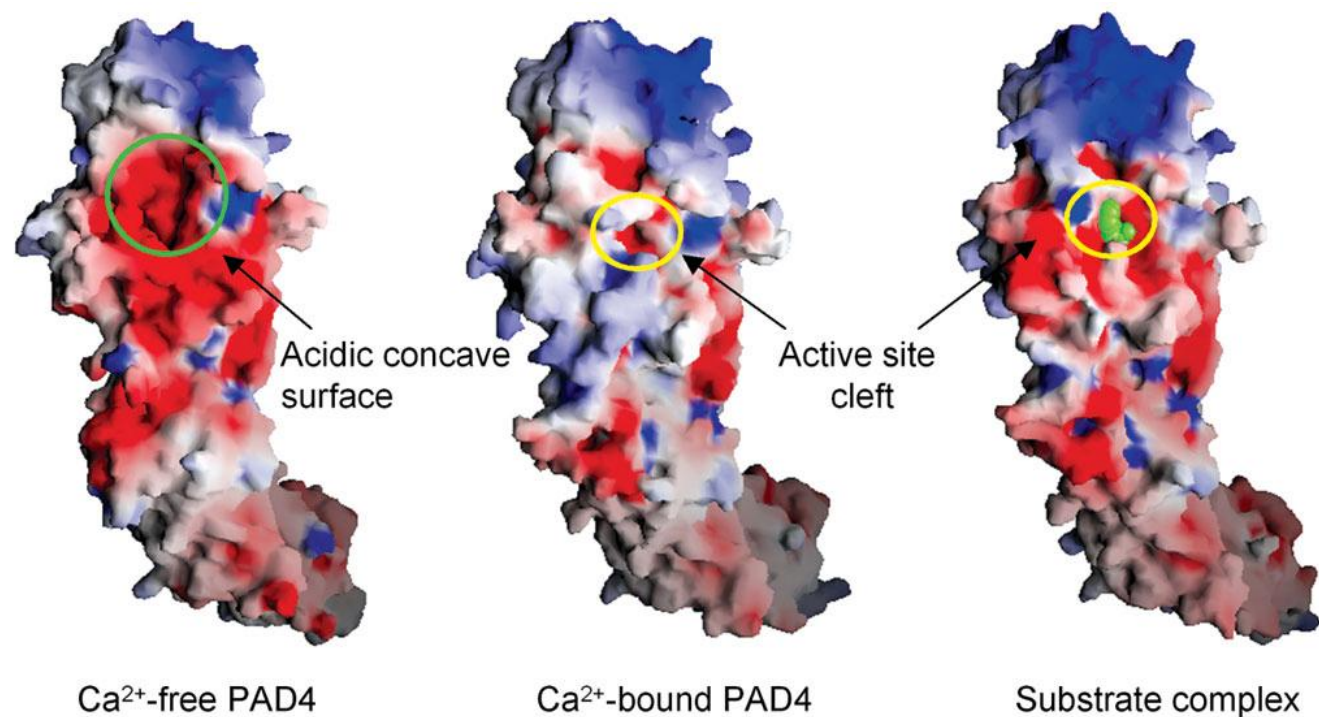


Figure 11. Electrostatic surface potentials of Ca²⁺-free PAD4 (*left*, 2.8 Å resolution, PDB code 1WD8), Ca²⁺-bound PAD4 (*middle*, 2.6 Å, 1WD9) and substrate-PAD4 complex (*right*, 2.3 Å, 1WDA) with highlighted acidic concave surface and active site clefts highlighted by coloured circles (green and yellow respectively).¹ Acidic, basic and hydrophobic surface potentials are coloured red, blue and white respectively. *N*- α -benzoyl-L-arginine amide (**BAA**) is coloured green. Reprinted by permission from Macmillan Publishers Ltd: *Nature* 11: 777-783, © 2004.

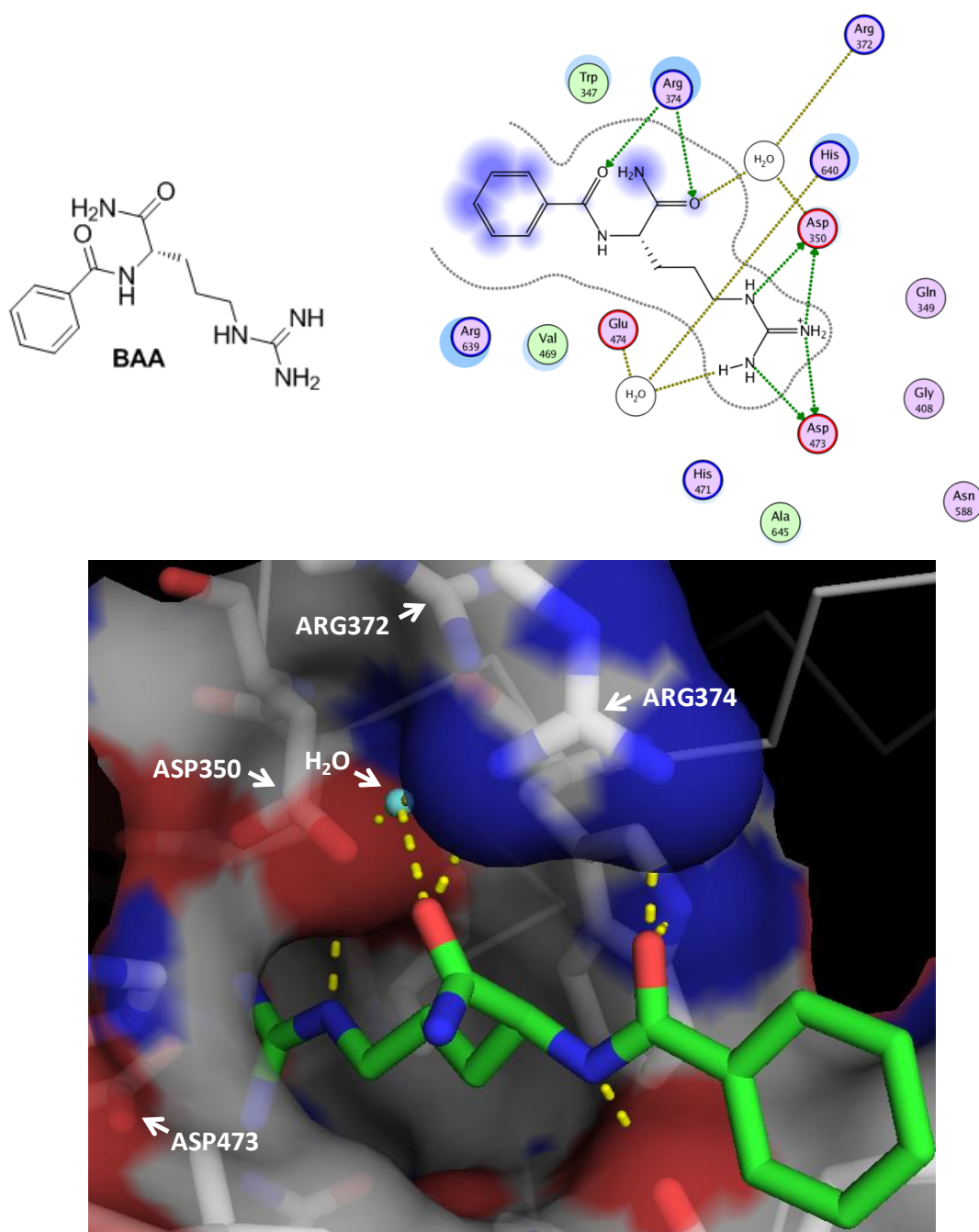
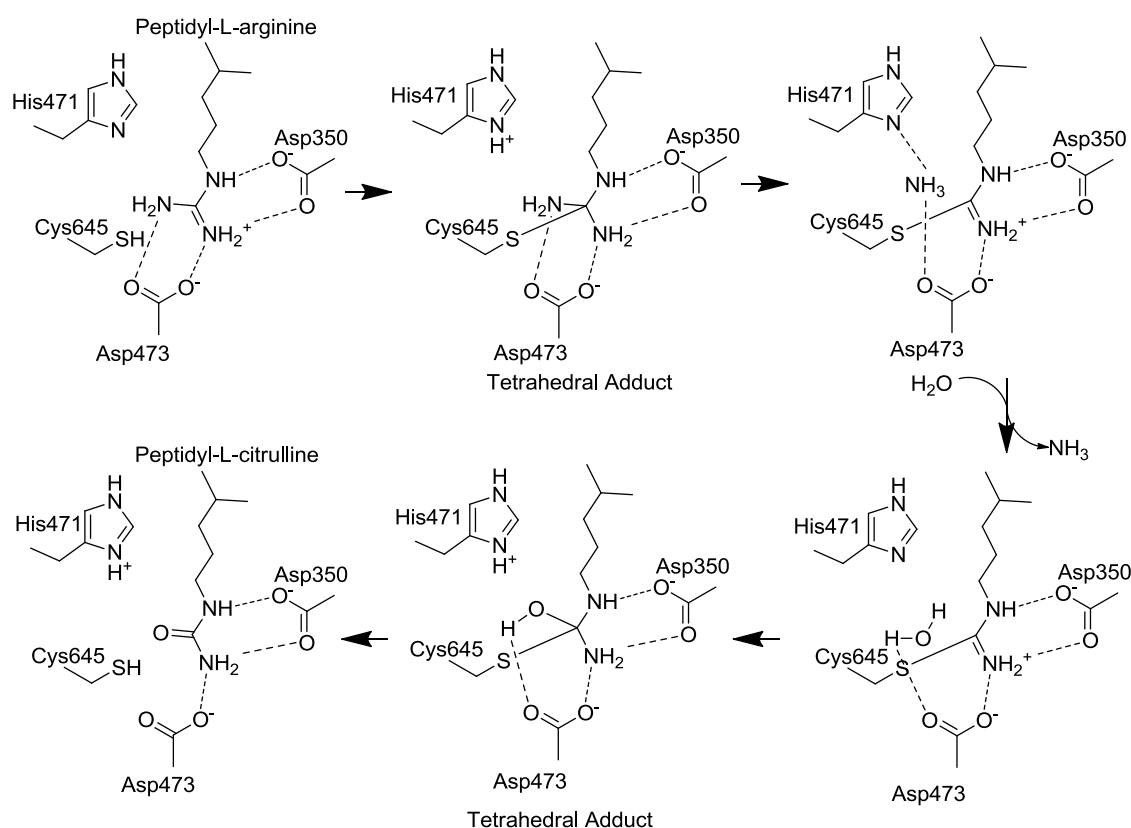


Figure 12. Structure of *N*- α -benzoyl-L-arginine amide (**BAA**, *top left*) and two dimensional representation of key interactions made with the C645A PAD4 mutant in the PAD4 active site (*top right*, 2.3 Å resolution, PDB code 1WDA). A three dimensional representation of **BAA** (*green*) bound in the active site of PAD4 is also shown (*bottom*) with acidic, basic and hydrophobic surface potentials coloured red, blue and white respectively; key residues are labelled in white and hydrogen bonds are represented as yellow dashed lines.

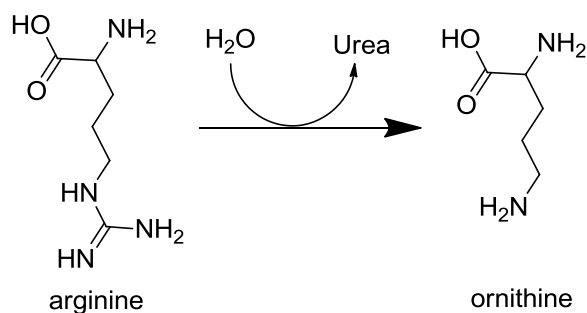
A mechanism of the PAD4-catalysed citrullination reaction was inferred from the crystal structure of the substrate-PAD4 complex to proceed *via* nucleophilic attack by the Cys645 thiol on the substrate's central guanidine carbon (**Scheme 2**). The guanidine carbon is activated by hydrogen bonds with adjacent carboxylate groups of Asp350 and Asp473 residues. The resultant tetrahedral adduct collapses to liberate ammonia. A water molecule subsequently acts as a nucleophile, attacking the thiourea to generate another tetrahedral adduct which then collapses to give the peptidyl-L-citrulline as the final product and regenerates the Cys645 thiol. Throughout the process, His471 is believed to shuttle a proton to and from the substrate, acting as a general acid or general base as required.



Scheme 2. Proposed PAD4-mediated citrullination mechanism.¹ Reprinted by permission from Macmillan Publishers Ltd: *Nature* 11: 777-783, © 2004.

The hydrolysis of arginine using chemical rather than enzymatic methods of hydrolysis typically leads to the formation of ornithine rather than citrulline, and requires forcing conditions, such as strong alkaline or strong acidic solution with long reaction times. (**Scheme 3**).^{67,68} Arginine is unlikely to form citrulline under normal physiological

conditions, so the PAD4 active site must stabilise the transition state required for citrulline formation effectively.



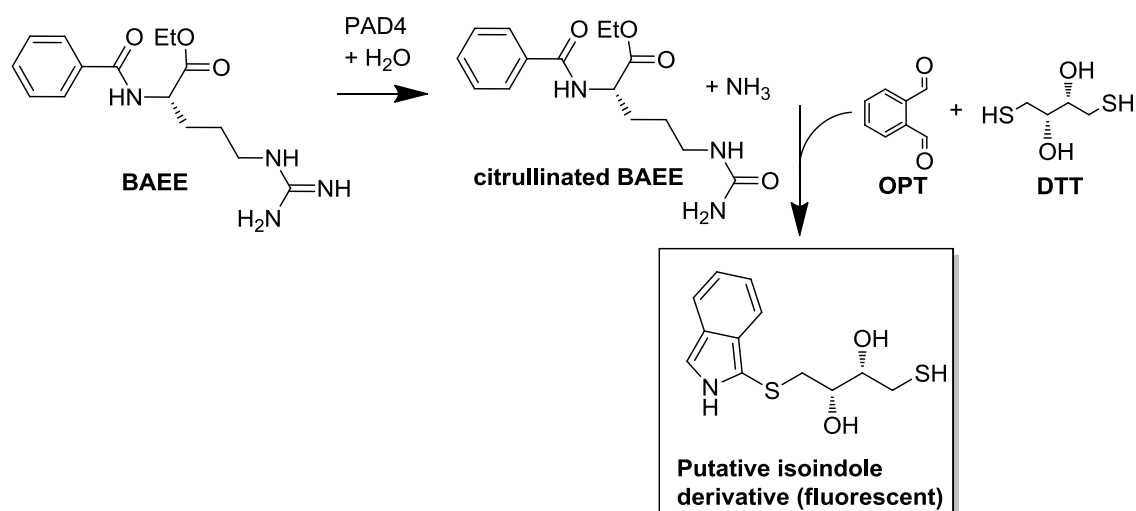
Scheme 3. Hydrolysis of arginine to ornithine.^{67,68}

The inferred catalytic mechanism for the conversion of arginine to citrulline is consistent with the general acid-base catalysis mechanism observed with other common enzyme hydrolase and transferase enzyme classes, such as proteases, esterases and lipases.⁶⁹ These enzymes employ a catalytic triad of nucleophilic, basic and acidic residues which form a proton relay network that effectively catalyses nucleophilic attack on a substrate. Whereas serine proteases, such as chymotrypsin, utilise a Ser-His-Asp triad to catalyse the cleavage of peptide bonds in proteins, PAD4 is likely to use a Cys-His-Asp triad to affect citrullination. Cysteine proteases that employ the same Cys-His-Asp triad include a number of cathepsins which are reported to play a vital role in a wide range of biological processes, such as human immune responses and bone development.⁷⁰

1.2.7. PAD4 Fluorescence Intensity Assay

A PAD4 Fluorescence Intensity (FLINT) assay that had been originally developed by Gribbon *et al.*⁷¹ was identified as a suitable assay for the discovery of novel PAD4 inhibitors a part of an HTS campaign. The assay utilised the known PAD4-mediated conversion of **BAEE** to the citrullinated product and ammonia in the presence of a Ca²⁺ buffer to assess the potencies of test compounds (**Scheme 4**).⁷² Potent PAD4 inhibitors allow little or no ammonia to be produced, while inactive compounds allow maximum conversion to ammonia. On quenching the reaction, phthalaldehyde (**OPT**) and dithiothreitol (**DTT**) are added which react with ammonia to form an isoindole derivative which fluoresces at characteristic wavelengths (460 and 476 nm) when

excited at other known wavelengths (405 and 413 nm).^{73,74,75} The amount of ammonia present in the assay mixture can then be accurately and sensitively quantified relative to a known standard.



Scheme 4. Citrullination of **BAEE** during the PAD4 FLINT assay.

1.3. Aims

This project aimed to identify a novel potent PAD4 inhibitor with the potential to probe the involvement of PAD4 in disease development and progression *in vivo* at an epigenetic level. A chemical probe that had been previously identified by the program team⁵ proved unsuitable for this application because the compound caused cardiotoxicity in the rat and dog, which are the species used for safety assessment studies. An alternative probe differentiated by chemical structure was required to elucidate whether inhibition of PAD4 itself caused cardiotoxicity, or whether the structure of the first chemical probe was cardiotoxic. The identification of novel PAD4 hit molecules by HTS, and the rationale behind the design, synthesis and iterative optimisation steps of the newly discovered chemical templates towards the ideal target profile of a probe molecule (**Table 5**) were the focus of this project.

Parameter	Target Value
Human PAD4 FLINT pIC ₅₀	>7.0
MW / cLogP	<500 / <5.0
LE / LLE	>0.30 / >5.0
PAD4 Human Neutrophil Citrullination Cell pIC ₅₀	>6.0

Table 5. PAD4 probe target profile, defined by lead program biologists and medicinal chemists. FLINT = Fluorescence Intensity; MW = molecular weight; cLogP = calculated LogP; LE= Ligand Efficiency; LLE = Lipophilic Ligand Efficiency.

1.4. Results and Discussion

1.4.1. Discovery of Novel Lead-like PAD4 Hits using an HTS

An HTS campaign was initiated with the aim of finding a high quality starting point (or hit) that had the potential to be optimised into a chemical probe to elucidate the role that PAD4 plays in disease development and progression. The GSK compound collection of roughly two million compounds, the majority of which (>80%) had drug-like *in silico* properties according to Lipinski's rules,⁷⁶ were screened using the PAD4 Fluorescence Intensity (FLINT) assay.

Over 53,000 compounds (or hits) showed statistically significant PAD4 inhibition at a single high concentration of 10 μM ; this was too high a number to allow all compounds to be followed up, so compounds were prioritised according to **Figure 13**.

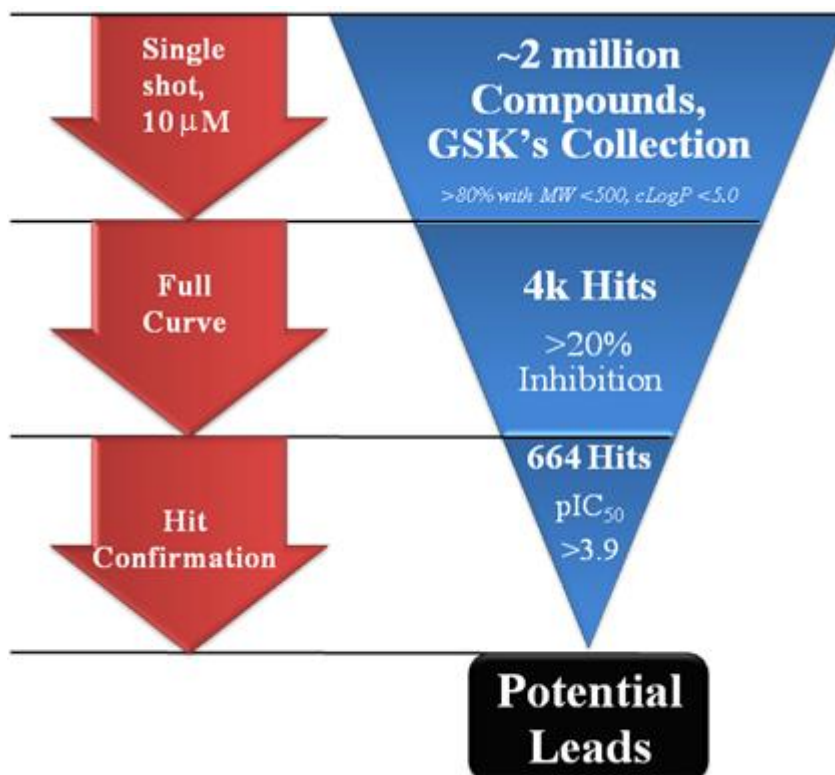


Figure 13. HTS triaging strategy.

Of the 53,000 compounds, 32,000 compounds had greater than 20% inhibition, so these were re-tested at a single high concentration; only 3,947 hits were confirmed active and progressed to full ten-point curves to determine potency. A total of 664 hits were

confirmed to have a PAD4 FLINT pIC_{50} of greater than 3.9. An additional assay, the Fluorescence Polarisation Binding assay (or FP-assay) was employed to further validate these hits as PAD4 inhibitors.

1.4.2. Fluorescence Polarisation Binding Assay

The Fluorescence Polarisation (FP) binding assay employed a fluorescent FP-ligand GSK215 (**Figure 14, left**) to determine the potency of the 664 HTS hits.⁷⁷ The FP-ligand consisted of a previously discovered in-house PAD4-active compound (*black*) attached to a fluorescent tag (*red*) via a polyamide linker (*blue*).

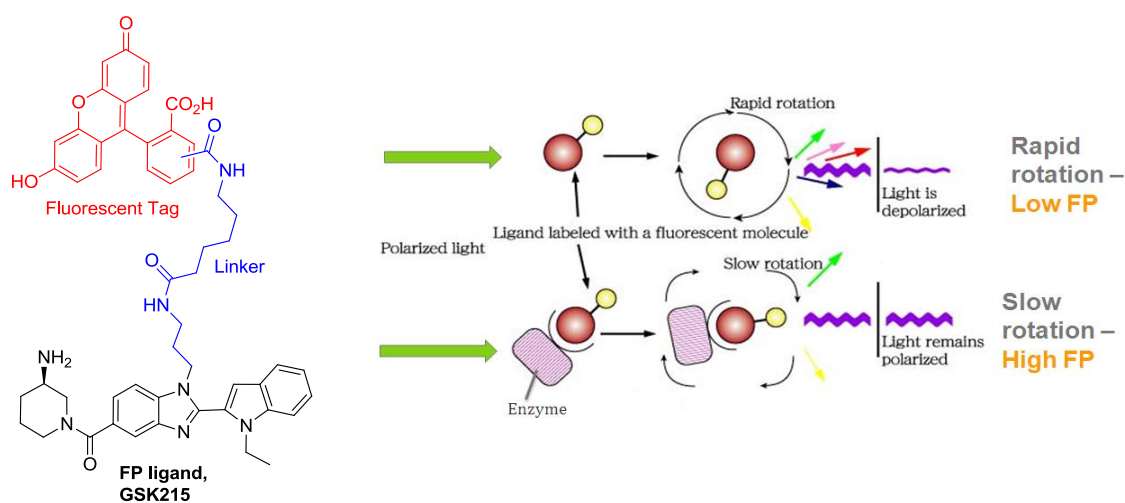


Figure 14. Structure of FP-binding ligand, GSK215 (*left*) and principles of FP signal measurement (*right*). The position of attachment of the amide linker to the fluorescent tag is a mixture of *ortho*- and *meta*- to the carboxylic acid.⁷⁸

To run the FP-binding assay, a mixture of test compound and PAD4 was irradiated with polarized light, before and after the addition of the FP-ligand (**Figure 14, right**). The relative amount of light depolarization was used to determine the relative displacement of FP-ligand by the test compound from PAD4. Free FP-ligand molecules rotate rapidly due to their relatively low MW and this rapid rotation depolarizes light to give a low FP signal; conversely FP-ligand molecules bound to PAD4 rotate slowly due to increased MW, depolarising light to a lesser extent than when unbound to give a high FP signal. Test compounds that bound to PAD4 in preference to the FP-ligand therefore gave a low FP signal in the FP-binding assay and the ratio of polarized to depolarized light at

different known test compound concentrations was used to determine a compound's pIC₅₀.

Unlike the FLINT assay, the FP-binding assay could be run with or without the presence of Ca²⁺ (abbreviated as “w/wo Ca”), in this case in the form of aqueous 2 mM CaCl₂. The compound's binding preference to the active or inactive form of PAD4 can then be determined. The physiological significance of PAD4 binding mode preference is yet to be determined.³

The FP-assay confirmed that all 664 potential hits were PAD4 inhibitors. However, not all the hits could be followed up because resource was limited, so LE and LLE indices were used to prioritise which to progress first. LE and LLE were used to assess subsequent SAR iterations of the hits to ensure modifications were both atom- and lipophilicity-efficient.

1.4.3. Prioritisation of the HTS PAD4 Hits

A high quality PAD4 lead needed to be a potent and selective inhibitor of PAD4, be chemically tractable and stable, exhibit Structure Activity Relationships (SAR), be novel for intellectual property purposes and ideally have good adsorption-distribution-metabolism and excretion (ADME) properties.⁷⁹ MW and lipophilicity are two key parameters used to assess a lead's quality because both typically increase during the development stages towards a probe, and from this to a drug candidate. The overall PAD4 probe target profile is summarised in **Table 5** and relevant parameters, including LE, LLE and MW were used to prioritise HTS initial hits.

Lipophilicity is expressed as LogP, where P is the partition coefficient for the neutral compound between octanol and water,⁸⁰ and is typically calculated using software such as Daylight, ACD⁸¹ or ChemAxon⁸² to give calculated LogP (cLogP). The cLogP values for each HTS hit were calculated using the Daylight package.⁸³

Increasing MW and cLogP can adversely affect a compound's final physicochemical properties by pushing them outside drug-like space; according to Lipinski's findings for oral drugs, an upper MW limit of 500 and a cLogP of 5 are likely to be required to achieve good ADME properties.⁷⁶ In reality limits can depend on the biological target

family⁸⁴ and since limits for PAD enzymes were unknown and a chemical probe was required as a priority rather than an oral drug, the limits defined by Lipinski for LogP and MW were considered, but not adhered to strictly during the identification of PAD4 leads and their SAR iterations. For reference, drug-like space can be used interchangeably with probe-like space, given that the ultimate aim is to deliver a drug candidate from a probe.

A number of efficiency indices have been defined to assess a hit's fitness for optimisation based on a range of variables, which includes physicochemical parameters like MW and more complex parameters related to toxicity and bioavailability.⁸⁵ Two indices that allow easy assessment of a compound's fitness for development with respect to MW and cLogP are LE and LLE respectively.⁸⁶ LE is used to determine how much the individual atoms of a ligand contribute to the overall potency (**Equation 1**), while LLE takes into account both the compound's potency and cLogP (**Equation 2**).

$$LE = -\Delta G/HAC = -RT\ln K_i/HAC \approx 1.37 \times pXC_{50}/HAC$$

Equation 1. Calculation of LE; HAC is the Heavy Atom Count, or non-hydrogen atoms. pXC₅₀ is a measure of a compound's potency as an antagonist (pEC₅₀) or inhibitor (pIC₅₀).

$$LLE = pXC_{50} - cLogP$$

Equation 2. Calculation of LLE.

A typical drug candidate endpoint is taken to be a molecule that has an HAC of 36, which corresponds to Lipinski's maximum MW of 500, with a pXC₅₀ of 8; this equates to an LE value of 0.3 kcal mol⁻¹ per heavy atom. An LE of 0.3 is therefore the lower target value for any given lead for development into a probe or drug candidate. A suitable target value for LLE is defined as 5.0, based on an analysis of properties of oral drugs by Leeson *et al.*⁸⁶

1.4.3.1. PAD4 Hit Validation

The 664 hits were profiled *in silico* using a proprietary web-based tool called A Daylight Enumeration and Profiling Tool (ADEPT).⁸⁷ ADEPT was an in-house process-orientated web-based tool that allowed bench chemists access to simple computational

tools. ADEPT was used to convert each compound's GSK unique registration number into a Simplified Molecular Input Line Entry String (SMILES).⁸⁸ From SMILES, MW, HAC and Daylight cLogP were calculated. LE and LLE could then be determined using the associated PAD4 FLINT pIC₅₀. Prioritisation of the 664 compounds was required because some of the HTS follow-up services offered by internal GSK partners required smaller sample sets. For example, compound solution quality control LC-UV-MS checks offered by Computational and Analytical Scientific Services required fewer than 200 for a two week turnaround. Of the 664 hits, 164 compounds had drug-like LEs of ≥ 0.30 , and of these, only four had drug-like LLEs of ≥ 5.0 .

1.4.3.2. Redox Stability

Compounds capable of redox cycling can generate hydrogen peroxide (H₂O₂) in μ M concentrations in the presence of common buffer components of HTS assays; H₂O₂ can then inhibit the catalytic activity of enzymes by oxidising accessible residues such as cysteine, falsely suggesting that the compounds are inhibitors of the enzyme and generating false hits.⁸⁹ This was of particular concern during the interpretation of the PAD4 HTS output because Cys645 in the PAD4 active site is required for the catalytic cycle, and may be oxidised and inactivated by H₂O₂.

To determine which of the 664 compounds were capable of redox cycling and were therefore potentially false hits, all the hits were routed through a redox assay that used an electrochemical detection (EC) method.⁹⁰ Known voltages were applied to each molecule in a series of electrochemical cells and the current generated by the flow of electrons from the analyte was measured. The voltage at which half the concentration of compound had transformed to its oxidised form was determined to give a relative redox potential (RRP): those with a standard electrochemical potential (E₀) of 1000 mV or greater have a high redox stability and therefore only low risk of redox cycling. Any hits of this type are likely to be real hits. Hits with a relative redox potential of below 650 mV had a low redox stability and were considered to have a high risk of redox cycling, and were likely to be false hits.

Of the set, 144 compounds were classified as low stability (*red*, **Figure 15**), 186 as medium stability (*orange*, **Figure 15**) and 175 as high stability (*green*, **Figure 15**). A

further 159 compounds failed in the assay due to instrument failure, and so were grouped together with the medium and high stability set as high priority for further assessment.

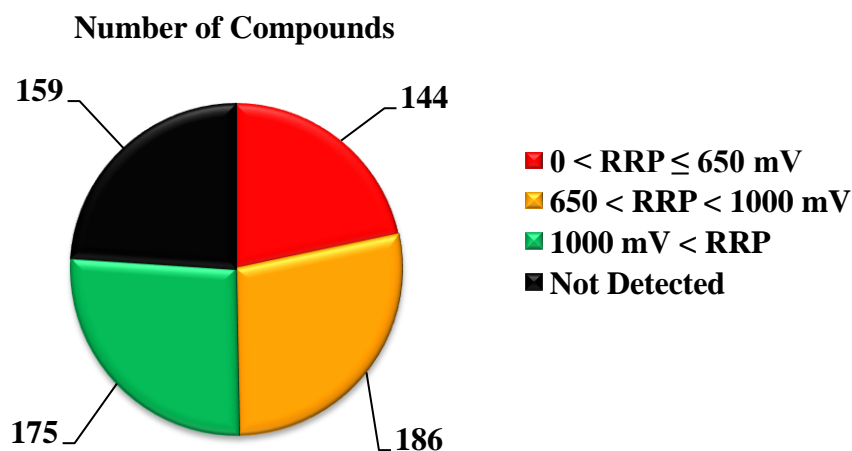


Figure 15. Count of compounds within each binned Relative Redox Potential (RRP, E_0 / mV).

1.4.3.3. Purity Determination

Each compound in GSK's HTS collection had been stored in automated liquid stores as a frozen 10 μ M solution in dimethyl sulfoxide (DMSO). Each sample was therefore likely to have undergone multiple freeze-thaw cycles before reaching the PAD4 HTS, as GSK scientists accessed the compound stores.⁹¹ In addition to a compound's potential chemical instability in solution over time, caused for example by reaction with impurities or the storage container itself, compound decomposition may have been accelerated on exposure to oxidative conditions and moisture by standing in air during the thaw process.⁹² Freeze-thaw cycles can amplify the presence of impurities as the original compound precipitates from solution over time, leaving more soluble, and potentially more potent, impurities in solution.

To help confirm the identity and purity of the 200 highest priority PAD4 actives, solutions were run through an LC-UV-MS screen; the results are summarised in **Figure 16**.

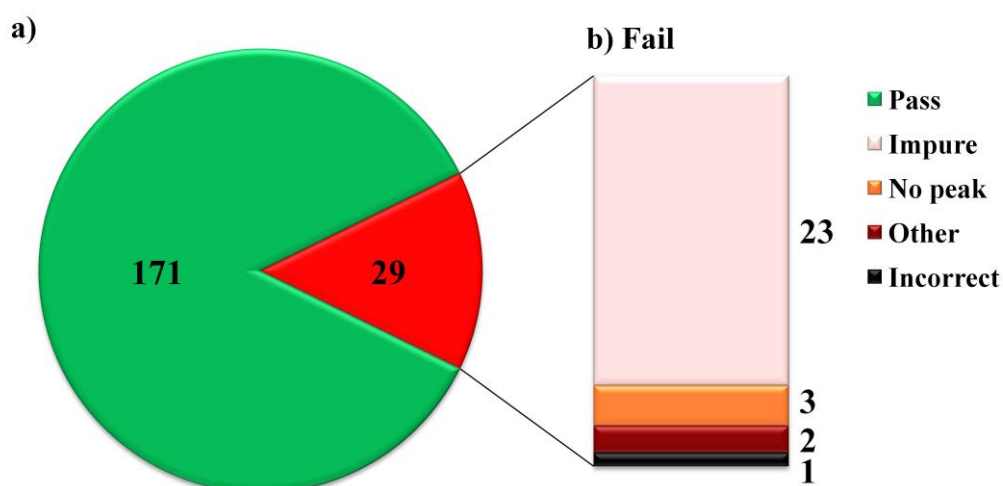


Figure 16. LCMS analysis of 200 highest priority PAD4 actives: a) pie chart shows number of compounds that passed (*green*) and failed (*red*) identity quality control checks; b) bar chart shows breakdown of reasons for failure.

A set of 171 solutions (85.5%) passed with the expected molecular ion and >80% purity by peak area, whereas 29 (14.5%) failed. Of the failures, 79% were low purity and 10% were caused by no peak being detected, presumably because the compound had precipitated out of solution. Only 3% of failures were caused by the presence of a pure compound with the incorrect ionisation. A further 6% of failures were attributed to other factors such as instrument error. The pass rate was comparable to the 89.5% cumulative pass rate found for a sample set of 14,692 compounds analysed at GSK between 2005 and 2010.⁹³

Evidently compounds that failed the quality control check were still potential PAD4 leads and were still worth following up, but at lower priority because it was unclear whether their inhibition arose from the presence of the indicated compound, or from impurities.

1.4.3.4. Cluster Analysis and Analogue Screening

The identification of a number of structurally similar compounds with potential PAD4 inhibition potency would have resulted in increased confidence that any given member of that series was a real PAD4 inhibitor because of apparent SAR. To help identify potential PAD4 active series and obtain any insightful SAR, substructure searches were

performed on the highest priority hits using an application called Instant JChem. Instant JChem is commercial software used for searching and visualising chemical, physicochemical and biological data stored in remote GSK databases⁸² and is useful for creating and refining lists of compounds. Analogues available in-house and commercially were requested for test in the PAD4 FLINT assay. Additionally, a cluster analysis of the 664 hits was performed using ADEPT, having first used compound SMILES to generate Daylight fingerprints. Here ADEPT employed Ward's algorithm to create hierarchical groups of mutually exclusive subsets of compounds (clusters), each of which had members which are maximally similar with respect to structure;⁹⁴ Ward's algorithm is particularly useful in studies of groups with greater than one hundred members. In total, 551 clusters were identified.

3-Amino isoquinolin-1(2*H*)-one Clusters

Clusters 7 and 36 appeared the most interesting to follow up because cluster members had average drug-like LEs of 0.40 and 0.33 respectively (**Table 6**). All nine compounds shared the 3-amino isoquinolin-1(2*H*)-one template, and looked chemically tractable according to literature based syntheses.⁹⁵ Clusters differed only in the nature of the attached amine: cluster 7 consisted of 3-cycloalkylamines, while cluster 36 consisted of 3-phenylamines. Although average LLEs were low at 3.9 and 1.7 for the respective clusters, the structure of both clusters offered potential points of modification to lower the templates' cLogP.

The majority of compounds were of greater than 80% purity by LC-UV-MS; however, three compounds (**1d**, **1e** and **1f**) showed signs of potential degradation because their purities had decreased from a previous LC-UV-MS assay. The redox potentials measured for seven compounds in this cluster suggested that **1c** was highly redox stable, **1e** was of medium stability, and the five other compounds were of low stability (**1a**, **1b**, **1d**, **1f** and **1i**). Overall confidence in the potential of the 3-amino isoquinolin-1(2*H*)-ones as true PAD4 inhibitors was therefore not high.

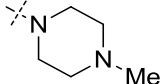
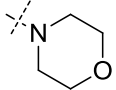
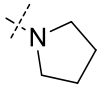
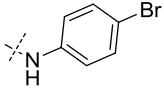
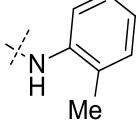
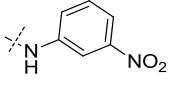
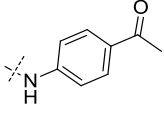
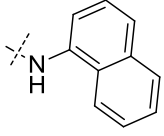
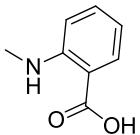
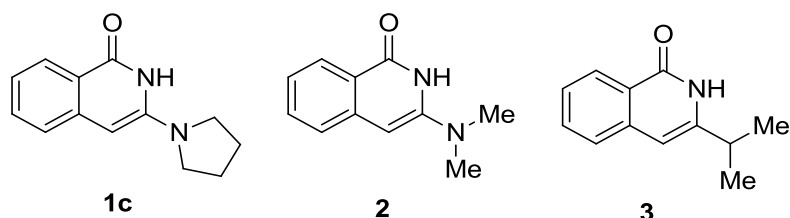
#	R	Cluster #	PAD4 pIC ₅₀	Day cLogP			LE	LLE	Redox, First Potential, E ₀ /mV	LC-UV-MS Purity, %	LCMS Comments
				MW	HAC	HAC					
1a		7	5.1	261	18	1.2	0.39	3.9	462	85	
1b		7	5.0	230	17	0.6	0.40	4.4	461	N/a	
1c		7	4.7	214	16	1.4	0.40	3.3	2000	87	
1d		36	5.2	315	19	3.8	0.37	1.4	434	64	Possible decomposition
1e		36	5.1	250	19	3.3	0.37	1.8	679	73	Possible decomposition
1f		36	5.1	281	21	2.9	0.33	2.2	420	83	Possible decomposition
1g		36	4.8	278	21	2.5	0.31	2.3	Assay failed	90	
1h		36	4.6	286	22	4.0	0.29	0.6	Assay failed	N/a	
1i		36	4.4	315	19	2.5	0.32	1.9	545	86	

Table 6. Profiles of 3-amino isoquinolin-1(2H)-one clusters 7 and 36.

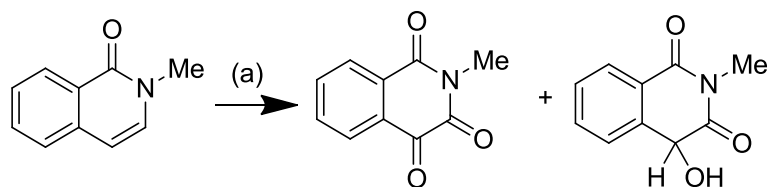
A set of 18 available analogues with the 3-amino isoquinolin-1(2*H*)-one substructure was tested in the PAD4 FLINT assay. Only **1c** retested with measurable potency (**Table 7**), but a 3-dimethylamino analogue **2** with PAD4 potency an apparently high LE and LLE was identified from the analogue screen. However, the 3-*iso*-propyl analogue **3**, which should be less susceptible to redox cycling than **2**, was inactive.



Compound	PAD4 FLINT pIC ₅₀	LE	LLE
1c	4.7	0.40	3.3
2	≤4.5	≤0.42	≤3.0
3	<4.1	-	-

Table 7. Active compounds identified from a screen of 3-amino isoquinolin-1(2*H*)-one analogues.

The 3-amino isoquinolin-1(2*H*)-one template may have been liable to oxidation and hydrolysis in the 3- or 4-positions, creating a decomposition product that is potent against PAD4. Air oxidation of 2-methylisoquinolin-1(2*H*)-one, which is chemically similar to **2**, has been reported (**Scheme 5**).^{96,97}



Scheme 5. Air-mediated oxidation of 2-methylisoquinolin-1(2*H*)-one, which is similar in structure to **1c**.^{96,97} Reagents and conditions: (a) refluxing benzene in air.

3-Amino isoquinolin-1(2*H*)-ones such as **1c** are likely to be more susceptible to oxidation than 2-methylisoquinolin-1(2*H*)-one: the 3-amino nitrogen of **1c** can push electron density into the 4-position, which would activate this position to oxidation.

Identification of the potent component of **1c** became of paramount importance given the high LE and LLE.

Compound **2** was of >99% purity by LCMS analysis on submission for test, but at the time the PAD4 FLINT assay was run, this figure had decreased to 93%. However, the solid sample had retained its high purity. Similarly the purity of compound **1c** was found to have decreased from 97% at submission to 86% at the time of test, whereas the solid sample had retained its purity. Both compounds must therefore have decomposed after being dissolved in DMSO to make the 10 μ M solution required for test.

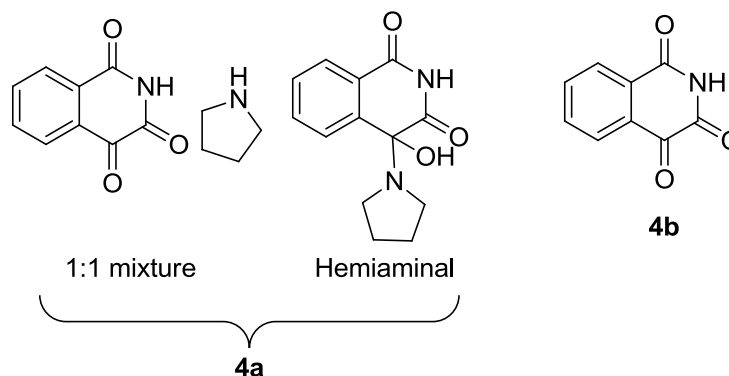
1.4.4. Identification of Isoquinoline Hit, **4b**

Pyrrolidine, a potential decomposition product of **1c** after oxidation and hydrolysis, proved inactive against PAD4, so a larger batch of **1c** was synthesised and a portion was left to stir in DMSO solution in the presence of air. After two weeks, enough decomposition product for isolation had been formed. LCMS and NMR studies (not shown) tentatively confirmed that the decomposition product was a 1:1 mixture of pyrrolidine and isoquinoline-1,3,4(2*H*)-trione (**4a**, **Table 8**). Compound **4a** proved to be a potent PAD4 inhibitor with excellent LE (0.46) and LLE (6.5).

The isoquinoline-1,3,4(2*H*)-trione (calculated pK_a , cpK_a , 5.6) is acidic enough to protonate the basic pyrrolidine (calculated pK_b 11.4) and form a 1:1 salt mixture, but it is unlikely the salt could remain intact during purification by mass directed autopreparative LCMS (MDAP). This purification used an ammonium formate modifier; formic acid (cpK_a 4.3) should have displaced the less acidic isoquinoline-1,3,4(2*H*)-trione from the salt. Alternatively **4a** may exist as a hemiaminal (**Table 8**); however, no HMBC correlation between the pyrrolidine protons and isoquinoline-1,3,4(2*H*)-trione carbons (^{13}C) were evident, so the structure of **4a** remained unconfirmed.

Given that the pyrrolidine alone was inactive at PAD4, a solid sample of isoquinoline-1,3,4(2*H*)-trione (**4b**, **Table 8**) was obtained from in-house stores, analysed by LCMS and NMR then sent for test at PAD4. Compound **4b** had high PAD4 FLINT potency and had excellent LE and LLE. A PAD4 FP binding assay confirmed the PAD4 potency of **4b**, which had higher potency against the inactive form of PAD4 than against the

active form, given that the pIC_{50} of **4b** was higher in the absence of calcium than in the presence of calcium. It was likely that enough oxidised product **4b** was present in DMSO solutions of all 3-amino isoquinolin-1(2*H*)-ones (**1a** to **1i** and **2**), to confer PAD4 potency to the solutions.

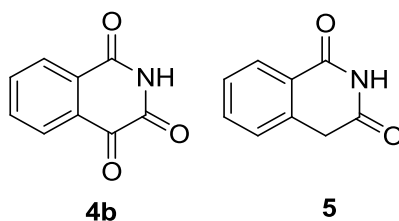


Compound	PAD4 FLINT pIC_{50}	LE	LLE	PAD4 FP pIC_{50} w/wo Ca^{2+}
4a	6.0	0.46	6.5	N/a
4b	5.7	0.60	6.2	<4.0 / 5.4

Table 8. Profile of the putative decomposition product **4a** which may form from **1c**, and the corresponding data for the possible single component **4b**. Pyrrolidine was inactive. Data is from solid retest.

1.4.4.1. Isoquinoline Template SAR

Isoquinoline-1,3,4(2*H*)-trione hit **4b** was resynthesised then retested against PAD4 which confirmed **4b** as a PAD4 inhibitor (**Table 9**). However, analogue **5** which had lower HAC showed no improvement in PAD4 potency. In the absence of an X-ray crystal structure the progression of **5** to lead optimisation was suspended: it was unclear where to begin optimisation, given that the compound was so small and had multiple vectors from which to grow.

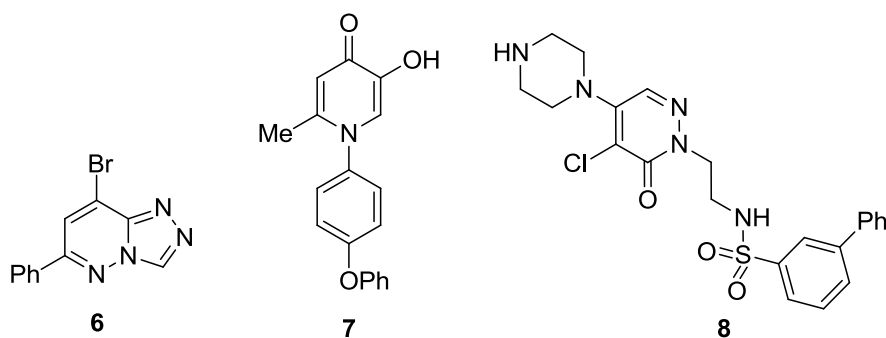


Compound	HAC	PAD4 FLINT pIC ₅₀	LE	LLE
4b , original batch	13	5.7	0.60	6.2
4b , new batch	13	5.6	0.59	6.1
5	12	5.3	0.61	4.3

Table 9. Isoquinoline template hit **4b**, with the newly synthesised batch for comparison with previous batch, and the structural analogue **5**.⁹⁸

1.4.5. Identification of Further PAD4 Hits

Three additional HTS hits retested with PAD4 FLINT potency (**6**, **7** and **8**, **Table 10**). Compounds **7** and **8** had confirmed potency in the PAD4 FP assay, and data was consistent for further test occasions in both FLINT and FP assays when retested from resynthesised solid. Compound **6** also had confirmed potency in the FLINT assay on retest, though on some occasions **6** tested inactive in the FP assay.

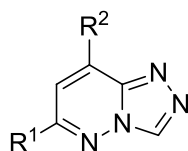


Compound	HAC	PAD4 FLINT pIC ₅₀	LE	LLE	PAD4 FP pIC ₅₀ w/wo Ca ²⁺	Redox E ₀ /mV
6	16	4.4	0.38	2.0	<4.0/≤4.2	2000
7	22	5.3	0.33	2.2	5.4/<4.0	Not measured: assay failed.
8	32	6.0	0.26	3.8	5.2/5.9	808

Table 10. Profiles of three further hits discovered using the HTS, **6**, **7** and **8**. Data is from retest from solid.

1.4.6. Lead Optimisation of Triazolopyridazine Hit, **6**

Triazolopyridazine **6** was the least potent HTS hit but had excellent LE because of a low HAC. Compound **6** was a weak inhibitor of the inactive form of PAD4, but not the active form in the FP assay, and had high redox stability. Both LE and LLE required improvement. A small set of compounds (**9a-9c**) was synthesised by a colleague to obtain SAR around the R² substituent, as well as the truncate **9d** and the original hit **6** (Table 11).⁶



Compound	R ¹	R ²	HAC	PAD4 FLINT pIC ₅₀	LE	LLE	PAD4 FP pIC ₅₀ w/wo Ca ²⁺
6	Ph	Br	16	4.4	0.38	2.0	<4.0/≤4.2
9a	Ph	Cl	16	4.3	0.37	2.1	<4.0/<4.0
9b	Ph	Me	16	<4.1	-	-	-
9c	Ph	H	15	<4.1	-	-	-
9d	Me	Br	11	<4.1	-	-	-

Table 11. SAR for triazolopyridazine analogues varied at R¹- and R²-positions. Original hit **6** is included for reference.

Only **9a** had measurable PAD4 FLINT potency, but this compound offered no significant advantage over the original hit **6** because neither LE nor LLE had improved, and **9a** was inactive in the FP assay. Replacement of the R¹-phenyl with a methyl group (**9b**) or a proton (**9c**) lowered HAC but was not tolerated; a set of 30 available analogues was inactive. Work on this template was suspended to focus resource on the remaining hits, **7** and **8**, which had more developable overall profiles.

1.4.7. Lead Optimisation of Hydroxypyridinone Hit, **7**

1.4.7.1. X-ray Crystal Structure of Hydroxypyridinone Hit, **7**

The redox assay failed for the hydroxypyridinone hit **7**, but an X-ray crystal structure was solved with **7** bound in the PAD4 active site at a resolution of 2.83 Å; the structure confirmed that compound **7** could bind in the PAD4 active site (**Figure 17, left**) and was therefore likely to be a true PAD4 inhibitor.⁹⁹

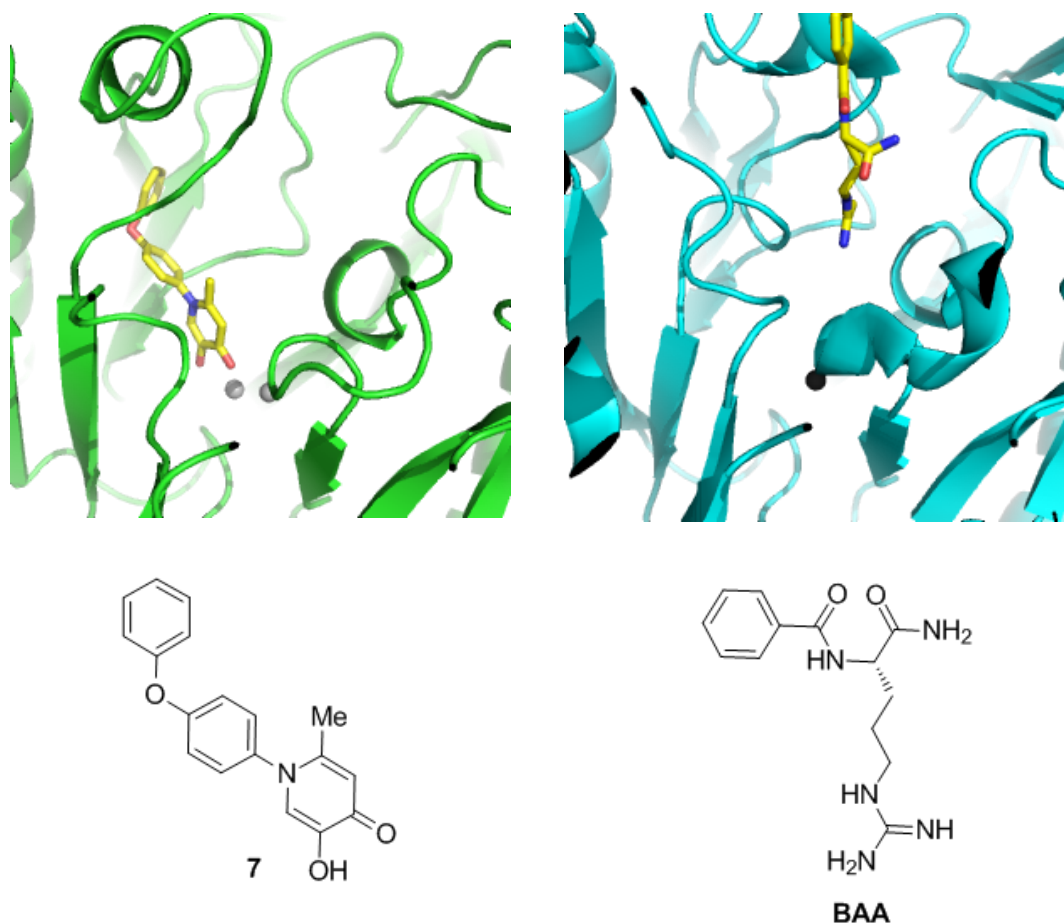


Figure 17. Comparison of PAD4 Cys645Ala X-ray crystal structures with **7** (*left*, 2.8 Å resolution, PDB code 80TLN)⁹⁹ and **BAA** (*right*, 2.3 Å, 1WDA)¹ bound in the PAD4 active site separately. Ligands are coloured yellow; in-house and Arita *et al.*'s enzyme structures are coloured light green (*left*) and cyan (*right*) respectively. Calcium ions are represented by grey spheres.

Comparison of the GSK X-ray crystal structure of compound **7** bound in the PAD4 Cys645Ala mutant (**Figure 17, left**)⁹⁹ with that previously determined by Arita *et al.* with *N*-α-benzoyl-L-arginine amide (**BAA, Figure 17, right**) bound¹ indicated that a previously unknown pocket had opened up for **7** to bind in. The new binding pocket appeared to have a channel adjacent to the 2-methyl substituent which was relatively polar in nature (**Figure 18a**) because it consisted of polar residues Asp350 and Glu351.

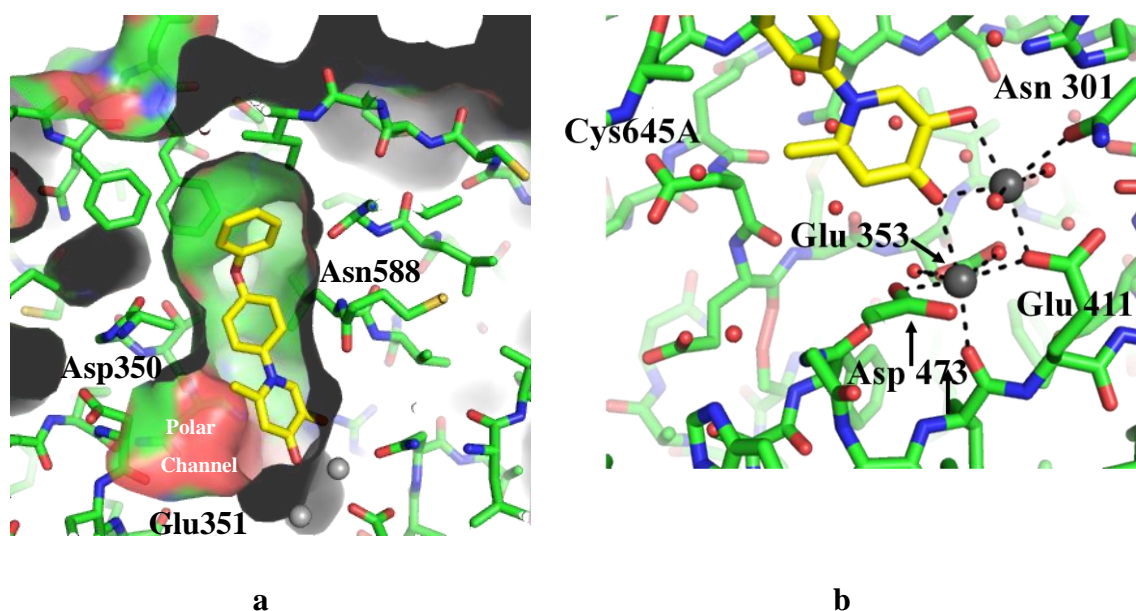


Figure 18. X-ray crystal structure of **7** (yellow) bound in the active site of the PAD4 Cys645Ala mutant, with site residues coloured green (2.8 Å resolution, 80TLN). The electrostatic surface has been added (**Figure 18a**) to indicate relative size of the active site with hydrophobic, polar donor and polar acceptor areas coloured green, red and blue respectively. Key residues are labelled (**Figure 18b**) with hydrogen bond interactions represented by dashed lines. Water molecules and Ca^{2+} ions are represented by red and grey spheres respectively.

A complex network of interactions between the pyridinone carbonyl oxygen and hydroxyl group with two Ca^{2+} ions, and Asp473, Glu353, Glu411 and Asn301 residues was evident (**Figure 18b**); these were likely to be key interactions for achieving PAD4 potency.

The electron density around the middle phenyl ring (**Figure 19**) was mostly missing, so it was likely that this ring could adopt a number of conformations when bound to the active site. The middle ring was likely to be twisted out of plane to relieve a steric clash with the 2-methyl group; the representation drawn is one possible conformation that positions the ring along the small amount of electron density that was visible.

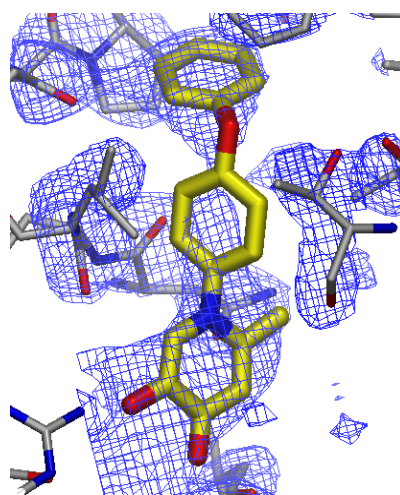


Figure 19. Structure of **7** bound (yellow) in the PAD4 active site with the electron density map (blue mesh) superimposed on top (2.8 Å resolution, 80TLN).

Hydroxypyridinone **7** was a more potent inhibitor of the active form of PAD4 in the FP binding assay, and was the only hit compound to show this profile (**Table 10**). Optimised analogues could therefore have proven useful for probing the physiological significance of inhibiting both the inactive and active forms of PAD4. A set of 18 available analogues based on the 5-hydroxy-pyridin-4(1*H*)-one substructure was submitted for test (data not shown) but none offered any improvement in LE nor LLE, so lead optimisation was initiated on **7**. The template had a high LE but low HAC and LLE for a lead, so initial efforts focussed on improving the latter two parameters.¹⁰⁰

1.4.7.2. Variation of the Hydroxypyridinone Headgroup

Compound **7** has four main structural features; these are: the hydroxypyridinone head group, the middle ring, the linker and the distal ring (**Figure 20**). Hydroxypyridinone is a catechol bioisostere,¹⁰¹ and compounds containing this moiety are known to inhibit CNS targets such as the catechol oxygen methyl transferase (COMT) enzyme;¹⁰² the catechol structural feature is also associated with a number of other toxicities.¹⁰³ Compound **7** has a COMT pIC₅₀ of 6.9 so potential unwanted effects on the CNS were a concern, given that they could limit the template's usefulness as a PAD4 probe *in vivo*.

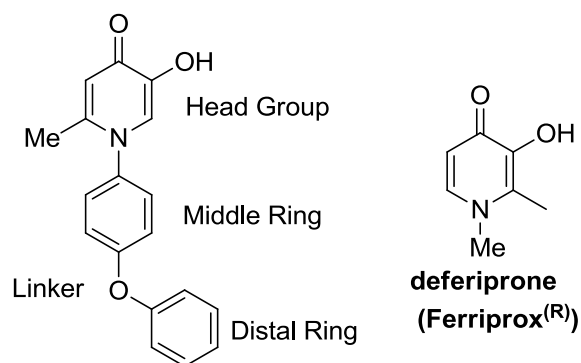


Figure 20. Structural features of the hydroxypyridinone hit **7** and structure of deferiprone, which is marketed as Ferriprox^(R).¹⁰¹

Some confidence in the biological safety of hydroxypyridinones came from a structurally similar analogue known as deferiprone which has been marketed since 1999 as Ferriprox^(R) (**Figure 20**), an iron chelator for the treatment of thalassemia patients who have blood overloaded with iron, which sometimes occurs after a blood transfusion.¹⁰⁴

The X-ray crystal structure of **7** bound with PAD4 (**Figure 18a**) showed a polar channel in close proximity to the 2-methyl substituent of the head group. The channel consisted of polar residues including Asp350 and Glu351; an additional polar residue Asn588 was situated adjacent to the middle ring. This suggested that the introduction of a hydroxyl group substituent onto the methyl group at C-2 to give compound **10** (**Figure 21**) should have been tolerated and would reduce LogP leading to improved LLE. At best, the introduction of an additional hydrogen bond interaction with these adjacent polar residues might have improved potency. Typically a single full hydrogen bond can increase binding energy by 1.1 kcal mol⁻¹, which can translate to a six-fold improvement in potency.¹⁰⁵

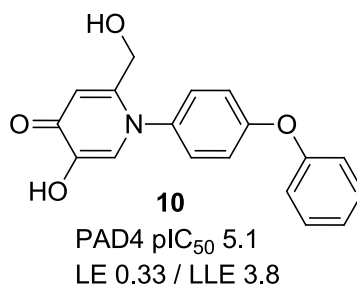
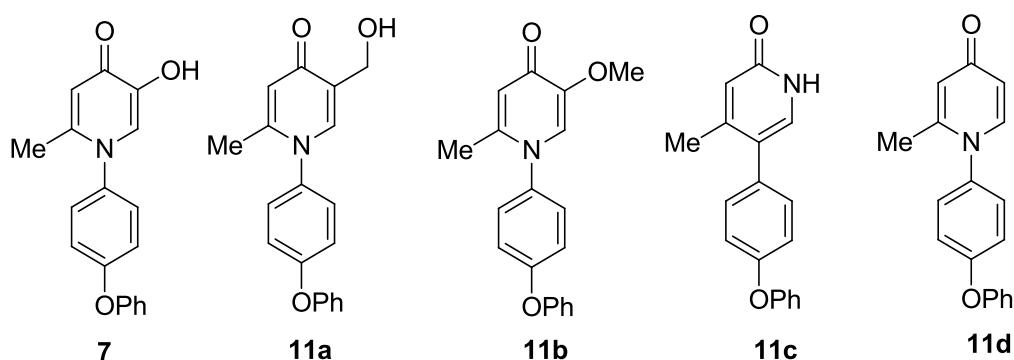


Figure 21. Compound **10** was designed to improve LLE and introduce extra hydrogen bonds between the hydroxypyridone molecule and the polar residues, such as Asp350 and Glu351, present in the polar channel in the PAD4 active site.

Compound **10** had a similar PAD4 potency to **7** which suggested an extra hydrogen bond with the PAD4 active site had not been achieved. It is possible that the linker to the hydroxyl group adopted a position more than 3 Å away from the targeted residues, which is the typical distance reported for an hydrogen bond, or that the hydroxyl group adopted a poor vector for the hydrogen bond to form, which is important given the directionality of hydrogen bonds.¹⁰⁶ The introduction of an hydroxyl group did however lead to a significant increase of +1.6 in LLE relative to **7**.

A set of four analogues (**11a-11d**, **Table 12**) which all lacked the catechol-like feature, was synthesised in an attempt to remove the potential safety risk of COMT inhibition. Compounds **11c** and **11d** were synthesised by a GSK colleague, Preston.⁸ Each compound was theoretically capable of making the same interactions as **7** with the Ca²⁺ ions in the PAD4 active site. However, confidence in binding mode could not be gleaned from Schrödinger's® Grid-based Ligand Docking with Energetics (Glide)-based computational docking studies: the ability to model interactions between the hydrogen bond acceptors and donor with multiple Ca²⁺ ions was beyond the capabilities of the Glide software (data not shown).^{107,108} All compounds were less potent than the original hit and were not pursued.

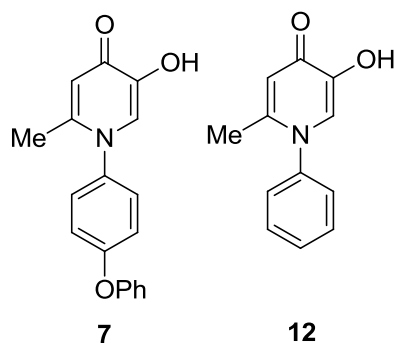


Compound	HAC	PAD4 FLINT pIC ₅₀
7	22	5.3
11a	23	<4.1
11b	23	<4.1
11c	21	<3.4
11d	21	<4.1

Table 12. Profiles of hydroxypyridinone head group replacement analogues **11a-11d**. Compounds **11c** and **11d** were synthesised by Preston, a GSK colleague.⁸

1.4.7.3. Variation of the Hydroxypyridone Template Distal Ring

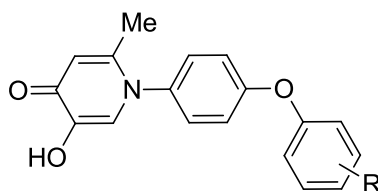
Compound **12** (**Table 13**) was synthesised to determine if the distal phenoxy moiety was required for potency, and to reduce HAC relative to **7**, but it was inactive. The distal phenyl ring of **7** may interact through dispersion forces with three surrounding hydrophobic residues Phe319, Ile630 and Pro599, that are evident in the PAD4 X-ray. Dispersion forces offer an energetically weak contribution of around 0.71 kcal mol⁻¹ per Å² of interaction,¹⁰⁵ but the possible hydrophobic interaction associated with the displacement of water molecules on binding of a ligand such as **7**, to a protein such as PAD4, can contribute a significant increase in overall entropy for the PAD4-**7** complex relative to the PAD4-**12** complex. This entropic contribution may increase potency,¹⁰⁹ and may explain why **7** is more potent than **12**.



Compound	HAC	PAD4 FLINT pIC ₅₀
7	22	5.3
12	15	<3.4

Table 13. Profile of analogue **12**⁸ with reduced HAC.

The movement of a single methyl group around the distal phenyl ring to optimise fit and probe the flexibility of the PAD4 active site (**Table 14**) led to a three-to six-fold reduction in potency when positioned in the 2- and 3-positions (**13a** and **13b** respectively), whereas substitution of a methyl group in the 4-position (**13c**) was not tolerated.



R Position	H		Me		OMe		OH	
	2-	7	5.3	13a	4.8	13d	4.3	13f
3-	13b			4.5	13e	≤4.2	13g	4.8
4-	13c			<4.1	-	-	13h	4.3

Table 14. PAD4 FLINT assay profiles of the distal ring analogues, **13a-13h**, that probed the flexibility of the PAD4 active site (R = Me) or the potential to make extra hydrogen bond interactions (R = OMe or OH).

The X-ray crystal structure of **7** bound in the PAD4 active site showed a number of backbone residues, such as Gly597 and Leu590, which are in close proximity to the distal ring (~3 Å in distance); these residues could be potential loci for the introduction of extra hydrogen-bond interactions between **7** and the PAD4 active site. Substitution was not tolerated at the 4-position with R = Me, so OMe and OH substituents that were capable of making hydrogen bond interactions were introduced into the 2- and 3-positions. The OH group was also placed in the 4-position with the aim of making a specific hydrogen bond with the Asp632 residue that was in close proximity to this position.

Positioning the hydrogen bond acceptor OMe in 2-(**13d**) and 3-(**13e**) positions led to at least a ten-fold reduction in potency. Movement of the hydrogen bond donor and acceptor OH to the 2-position (**13f**) was tolerated but a three-fold reduction in potency was observed in the 3-position (**13g**) and a ten-fold reduction in potency was observed from substitution in the 4-position (**13h**). The lack of improvement in potency suggested that extra hydrogen bonds were not being made with these substituents, probably because the correct geometries required for hydrogen bonding to the adjacent residues had not been achieved.¹⁰⁶

Of all the hydroxypyridone analogues made, only 2-hydroxy compound **10** offered any improvement in profile relative to the original hydroxypyridone hit **7** by increasing LLE. However, the PAD4 potency still required a substantial increase of at least fifty-fold to meet the target profile required for a probe molecule (**Table 5**). The lack of improvement in potency, together with the potential developability issues introduced by the hydroxypyridone headgroup that may cause unwanted COMT inhibition, caused work on the hydroxypyridone template to be suspended to allow resource to focus on the pyridazine template.

1.4.8. Lead Optimisation of the Pyridazine Hit **8**

Pyridazine **8** was a more potent inhibitor of the inactive form of PAD4 than of the active form in the FP binding assay and a medium redox potential gave no cause to suspect the compound to be a false hit. The potential lability of the 5-Cl substituent in the presence of nucleophiles, such as Cys645 in the PAD4 active site, was a concern,

because an irreversible inhibitor was not sought by the program team. The potential liability was discharged, at least partially, on incubation of compound **8** with *N*-acetyl cysteine over a number of days at close to physiological temperature (37 °C); no displacement of the chloride was evident by LCMS. In retrospect, a base should have been added to emulate conditions in the PAD4 active site more closely.

Compound **8** had five main structural features; these were: the piperazine headgroup, the pyridazine core, a linker region and the middle- and distal-rings (**Figure 22**). The template had a high HAC of 32 and low LE and LLE for a lead,¹⁰⁰ so initial targets aimed to reduce HAC, while at least retaining PAD4 potency, to increase LE and LLE. A smaller, less lipophilic and more potent lead would have been closer to drug-like space, and therefore more likely to have a DMPK profile closer to that required for a probe to be administered to a test animal *via* an intravenous or oral route.¹¹⁰ In-house efforts to obtain an X-ray crystal structure of **8** bound in the PAD4 active site were unsuccessful and computational docking studies did not present sensible representations of how **8** might bind to the active site; structure-guided design was therefore not possible and iterative point changes to the structure were undertaken instead. To complement the lead optimisation effort, more than 400 available analogues of compound **8** were sent for biological evaluation,¹¹¹ but none offered any improvement in LE or LLE over **8**.

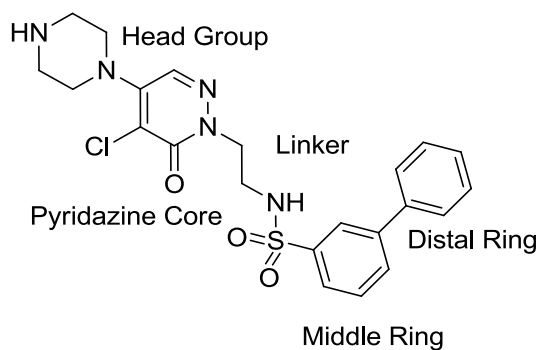
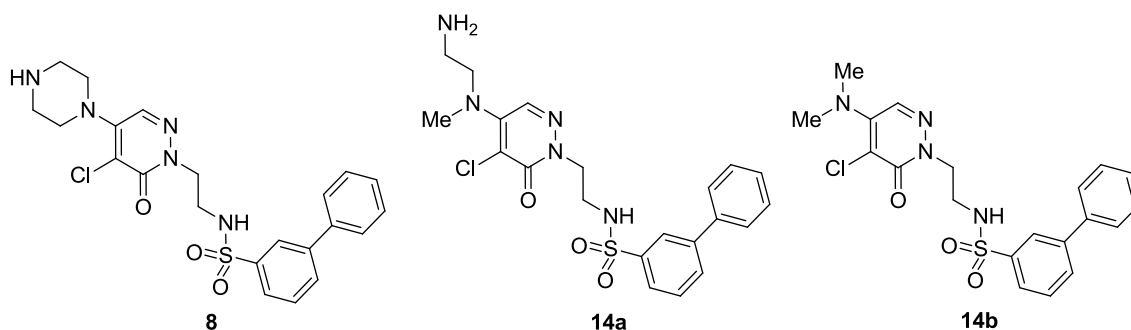


Figure 22. Structural features of the pyridazine hit **8**.

1.4.8.1. Reducing HAC of the Pyridazine Template Headgroup

The basic piperazine nitrogen in **8** was likely to be protonated at physiological pH (7.4) because the calculated pK_a (cpK_a) is 10.1.¹¹² The resulting piperidinium ion would be

capable of making a salt-bridge interaction with a side-chain of an acidic amino acid such as an Asp residue present in the PAD4 active site, which would be energetically strong at ~ 2.0 kcal mol⁻¹ under ideal conditions.¹⁰⁵ There are many examples of this type of interaction in the literature; for example, the active ingredient of the asthma treatment salmeterol interacts with an Asp residue of the β_2 -receptor through a protonated amine.¹¹³ Compound **14a** was also synthesised to explore whether the positioning of the headgroup basic centre was important: the steric clash between the amino functional group of **14a** and the *N*-methyl moiety would force the amino group to adopt a different position (as drawn in **Table 15**) to that adopted by **8**. Compound **14b** was synthesised to confirm if the basic centre and piperazino group were really required for potency.



Compound	HAC	PAD4 FLINT pIC ₅₀	LE	LLE	Terminal Amine cpK _a
8	32	6.0	0.26	3.8	9.6
14a	31	≤4.3	≤0.19	≤2.0	9.5
14b	29	<4.1	-	-	-

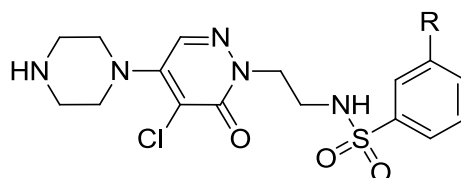
Table 15. Profile of pyridazine template headgroup analogues with lower HAC, **14a** and **14b**.

Compound **14a** was at least 50-fold less potent than **8** and had lower LE and LLE. The cpK_as of the terminal amines of **8** and **14a** were 9.6 and 9.5 respectively which indicated that they were of similar basicity, so the positioning of the piperazine basic centre was critical in achieving PAD4 potency. Replacement of the piperazine headgroup with a dimethylamino group to give **14b** substantially reduced potency which indicated a

cyclic amino group was required at this position. The piperazine headgroup was therefore retained for future analogues.

1.4.8.2. Removal of the Pyridazine Template Distal Ring

Replacement of the distal phenyl ring with an *iso*-propyl group, methyl group or proton in **15a**, **15b** and **15c** respectively, led to substantially decreased PAD4 potency, LE and LLE relative to **8** (Table 16). The only truncated species with any measurable potency was **15a** which was >79-fold less active than **8**. The distal phenyl ring must therefore be required for PAD4 potency. It may be able to make favourable π -interactions with an aromatic residue, such as a Phe or Tyr, in the PAD4 active site; such an interaction would strengthen the binding enthalpically.^{114,115}



Compound	R	HAC	PAD4 FLINT pIC ₅₀	LE	LLE
8	Ph	32	6.0	0.26	3.8
15a	<i>i</i> Pr	29	<4.1	<0.18	<2.0
15b	Me	27	<4.1	-	-
15c	H	26	<4.1	-	-

Table 16. Profiles of pyridazine headgroup analogues with reduced HAC in the distal ring, **15a-15c**.

π -Interactions are non-covalent interactions that, alongside hydrogen bonds, salt-bridge, and hydrophobic interactions, play a major role in protein stability and the biological recognition of ligands.¹¹⁵⁻¹¹⁷ Three main classes of π -interactions have been observed in protein structures; these are π -stacking, ion- π and XH- π interactions (**Figure 23**).¹¹⁸

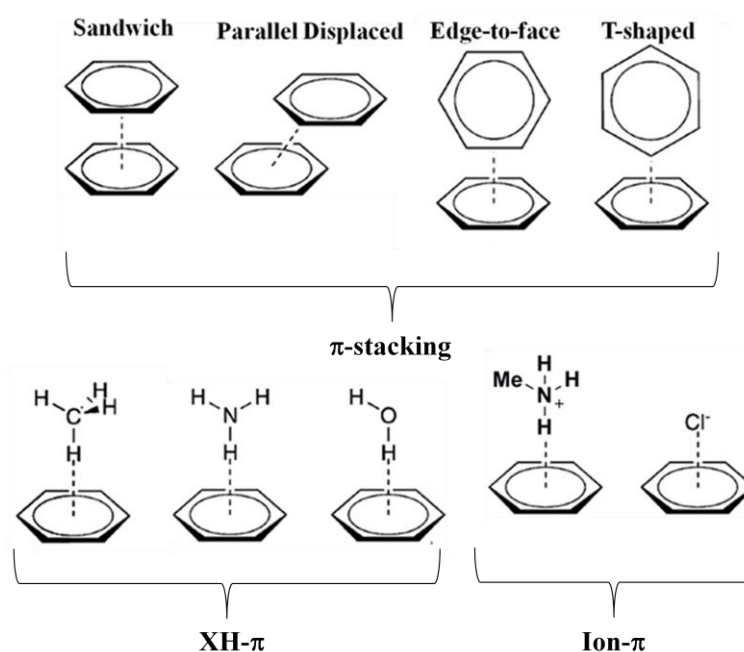


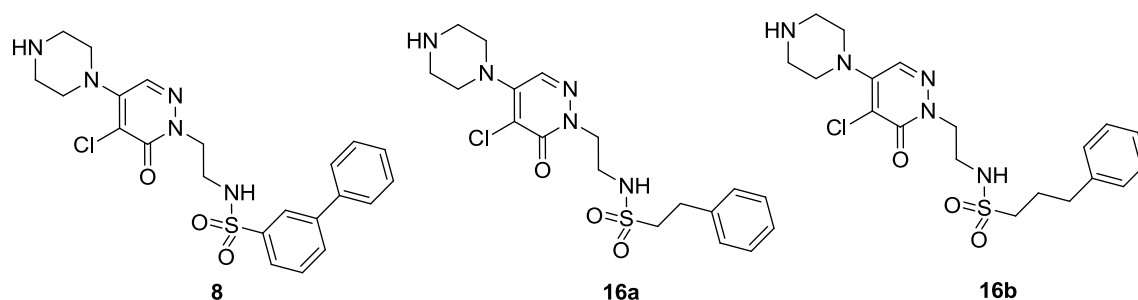
Figure 23. Representations of non-covalent interactions involving aromatic rings.¹¹⁸

Estimated values for the strengths of these interactions in terms of contribution to binding energy in kcal mol^{-1} vary according to the test systems used. Anion- π interactions have been reported to be $<1 \text{ kcal mol}^{-1}$ using experimental host-guest models.¹¹⁹ Computational studies of cation- π interactions between benzene and protonated methylamine in water indicate a contribution of $\sim 5.5 \text{ kcal mol}^{-1}$ to binding energy;¹²⁰ this was higher than the $\sim 2.2 \text{ kcal mol}^{-1}$ predicted for a salt bridge between protonated methylamine and acetate in the same study. Protonated methylamine was chosen to emulate protonated amino acid residues such as phenylalanine, tryptophan and tyrosine which are known to form cation- π interactions with ligands in biological systems.¹²¹ Cation- π interactions occur with the cation directly above the aryl ring but may also adopt off-axis or even a perpendicular orientation to the aryl ring.¹²² π -Stacking interactions are predicted to vary between 1.6 and $2.4 \text{ kcal mol}^{-1}$ using computational studies; benzene dimers adopt sandwich, parallel displaced, edge-to-face or T-shaped configurations. These configurations are all thought to exist in dynamic equilibrium due to the low difference in energies between configurations.^{123,124} XH- π interactions such as the one present in the water-benzene complex have been determined to be worth up to $3.0 \text{ kcal mol}^{-1}$ using infrared (IR) -spectroscopy.

In summary there is general agreement that whereas anion- π interactions are typically very weak, XH- π interactions, π - π stacking interactions may be of similar magnitude or stronger than hydrogen bonds, while cation- π interactions can be stronger than a hydrogen bond. π - π Stacking, cation- π and XH- π interactions may therefore make significant contributions to ligand inhibition potency. The distal ring of **8** is essential for PAD4 potency which suggests the ring may be able to make at least one π - π interaction with the PAD4 active site.

1.4.8.3. Removal of the Pyridazine Template Middle Ring

Replacement of the middle phenyl ring with ethyl- and propyl- chains to give **16a** and **16b** (Table 17) respectively led to a reduction in PAD4 potency, LE and LLE relative to **8**.



Compound	HAC	PAD4 FLINT pIC ₅₀	LE	LLE
8	32	6.0	0.26	3.8
16a	28	<4.1	-	-
16b	29	≤4.2	≤0.20	≤3.2

Table 17. Profiles of pyridazine middle ring replacement analogues with reduced HAC in the middle-ring, **16a** and **16b**.

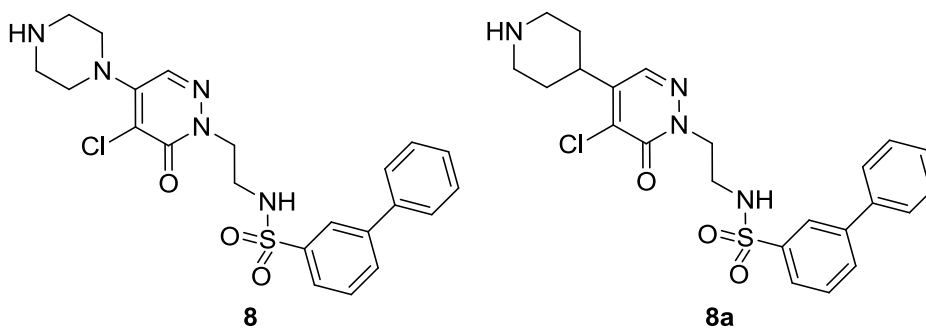
The terminal phenyl ring of **16b** was initially thought to be able to access the same area of the PAD4 active site as that occupied by the phenyl ring of **8** to make a favourable π - π interaction with an aromatic residue in the active site. However, the introduction of a propyl linker introduced two extra degrees of freedom relative to **8** which increased the

entropic penalty paid by PAD4-**16b** ligand system relative to that for the PAD4-**8** ligand system and may account for the lowered PAD4 potency of **16b** relative to **8**;¹⁰⁶ a penalty of ~ 0.7 kcal mol⁻¹ of binding energy has been estimated per degree of freedom.¹¹⁷ Alternatively **8** may fit better in the PAD4 active site than **16b** because the extra phenyl ring of **8** provides an increased hydrophobic area for favourable dispersive interactions to form between the ligand and the active site, for example through a π - π interaction; this extra interaction cannot be achieved with the ethyl chain of **16b**. The ethyl chain of compound **16a** may have been too short to allow the terminal phenyl ring to access the area that the slightly longer **8** could access, to make, for example, a favourable π - π interaction with the PAD4 active site. An energy minimisation study using a variant of the Merck Molecular Force Field (MMFF), MMFF94s,¹²⁵ which was embedded in the Molecular Operating Environment (MOE) interface¹²⁶ suggested the lowest energy conformers of **16a** and **16b** would not place the distal phenyl ring in a similar region to those accessed by the distal ring of energy minimised conformers of **8**. A more detailed investigation into the most likely conformations to be adopted by the middle and distal phenyl rings of **8** is discussed later (see section 1.4.8.5).

All analogues with reduced HAC in the piperazine headgroup, middle- and distal- ring regions had significantly reduced PAD4 potency, LE and LLE relative to hit **8**. Since all these structural features seemed to be required for PAD4 potency and the template's potency needed to be increased by at least tenfold to meet the probe target profile (**Table 5**), optimisation efforts focussed on changing regions of the molecule that were the most synthetically tractable, which were the the piperazine headgroup, and the distal aromatic ring.

1.4.8.4. Replacement of the Pyridazine Template Headgroup

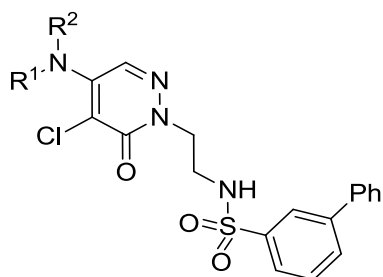
Replacement of the piperazine headgroup of **8** with a piperidine to generate **8a**⁷ removed PAD4 potency (**Table 18**), which suggested that the flatter conformation of the piperazine was favoured over the more three-dimensional piperidine for achieving PAD4 potency.



Compound	PAD4 FLINT pIC ₅₀	LE	LLE
8	6.0	0.26	3.8
8a	<4.1	-	-

Table 18. Structure and profile of first headgroup replacement **8a**.⁷

A set of *N*-linked headgroup variations was designed to explore the result of constraining or removing the basic centre of the headgroup (**17a-17e**, **Table 19**).



Compound	R ¹ R ² N	HAC	PAD4 FLINT pIC ₅₀	LE	LLE
8		32	6.0	0.26	3.4
17a		33	<4.1	-	-
17b		33	4.2	0.17	1.4
17c		32	<4.1	-	-
17d		32	<4.1	-	-
17e		32	<4.1	-	-

Table 19. Headgroup variations, **17a-17e**, that explored the result of constraining or removing the basic centre present in the headgroup.

Replacement of the basic centre of **8** with O and CH₂ (**17c** and **17d**) respectively reduced PAD4 pIC₅₀ to <4.1; replacement with a neutral amide-NH that was able to make a hydrogen bond interaction (**17e**) had the same negative effect on potency. These data together confirmed that a basic centre was required in the headgroup for PAD4 potency, and suggested that **8** may interact with the PAD4 active site potentially through a salt bridge interaction between the piperidinium ion and a negatively charged residue such as Asp. Methylation of the piperidine nitrogen (**17b**) reduced potency by

63-fold which suggested that the methyl group may clash sterically with this key residue in the PAD4 active site, given that the the pK_a of the methyl-piperazine headgroup (9.6)¹¹² was of similar magnitude to that of the piperazine headgroup. Constraining the headgroup in racemic **17a** reduced PAD4 pIC_{50} to <4.1, either because this introduced a steric clash between the bridgehead carbon and the protein, or because the positioning of the basic centre in the rigid 2,5-diazabicyclo[2.2.1]heptane moiety of **17a** was suboptimal relative to the more flexible piperazine of **8**.

A second set of headgroup variations investigated the effect of varying the pK_a and directionality of the basic centre (**18a-18i**, **Table 20**). All analogues apart from **18b** were less potent than the hit compound **8**; **18b** was equipotent with **8** and differs only in the addition of a methyl group in the 2-position of the piperazine. Compound **18b** was assumed to be a racemic mixture of enantiomers because the Boc-2-methylpiperazine starting material used to make **18b** was labelled as racemic. Intriguingly, the addition of a second methyl group in the 6-position (**18a**) substantially reduced PAD4 potency. Compound **18a** was assumed to be a 1:1 mixture of diastereomers because the commercially available Boc-protected dimethylpiperazine starting material used to make **18a** was labelled as racemic. Although the HAC of **18b** was higher than that of **8**, one of the separated enantiomers may have offered improved potency relative to the racemate; however, the LLE was unlikely to have been improved so isolation of the each unique diastereoisomer was not pursued.

Compound	R ¹ R ² N	cpK _a ¹¹²	HAC	PAD4 FLINT pIC ₅₀	LE	LLE
8		10.1	32	6.0	0.26	3.4
18a		10.1	34	<4.1	-	-
18b		10.1	33	6.1	0.25	3.3
18c		9.8	32	4.9	0.21	2.4
18d		10.2	33	<4.1	-	-
18e		9.8	33	≤4.2	≤0.17	≤2.5
18f		10.2	33	<4.1	-	-
18g		10.3	33	5.1	0.21	2.8
18h		9.9	33	<4.1	-	-
18i		10.1	31	4.5	0.20	2.5

Table 20. Headgroup analogues, **18a-18i**, that explored the result of varying the pK_a and directionality of the basic centre present in the headgroup.

1.4.8.5. Substitution on the Pyridazine Template Distal Ring

The Topliss operational scheme for aromatic substitutions (or Topliss tree, **Figure 24**)¹²⁷ was employed to design a set of compounds (**Table 22**) aimed at improving the PAD4 potency of the pyridazine hit **8** with the minimum number of compounds. The Topliss analysis makes a fundamental assumption of the Hansch method¹²⁸ that a particular substituent on an aromatic ring may modify potency relative to the hit by virtue of changes in hydrophobicity (π), electronic effects (σ) and steric effects (E_s) (**Table 21**),¹²⁷ and is used to improve the chance of increasing potency of a hit compound with the minimum number of compounds.

The hit **8** contained an unsubstituted phenyl ring ($\pi = 0.00$, $\sigma = 0.00$, $E_s = 1.28$) so according to a Topliss analysis, the next compound to be made should incorporate a hydrophobic and electronegative 4-Cl substituent ($\pi = 0.70$, $\sigma = 0.23$, $E_s = 0.27$). Should the 4-Cl compound be less potent than the unsubstituted **8**, then a hydrophilic and electron donating 4-MeO substituent ($\pi = -0.04$, $\sigma = -0.27$, $E_s = 0.69$) should be made, and the left-hand branch of the decision tree should be followed to conclusion. Should the 4-Cl compound be equipotent to **8**, then a neutral and slightly less hydrophobic 4-Me group ($\pi = 0.60$, $\sigma = -0.17$, $E_s = -0.14$) should be made, and the middle branch of the decision tree should be followed to conclusion. If the 4-Cl compound is more potent than **8**, then the highly hydrophobic and electron deficient 3,4-Cl compound should be made and the right-hand side of the decision tree followed to conclusion.

To investigate the effect of the Hansch parameters π , σ and E_s on PAD4 potency in the minimum amount of time, four analogues of **8** were synthesised with distal ring substituents that are proposed by the top two tiers of the Topliss tree, namely 4-Cl (**19a**), 4-Me (**19b**), 4-OMe (**19d**) and 3,4-Cl (**19c**, **Table 22**).

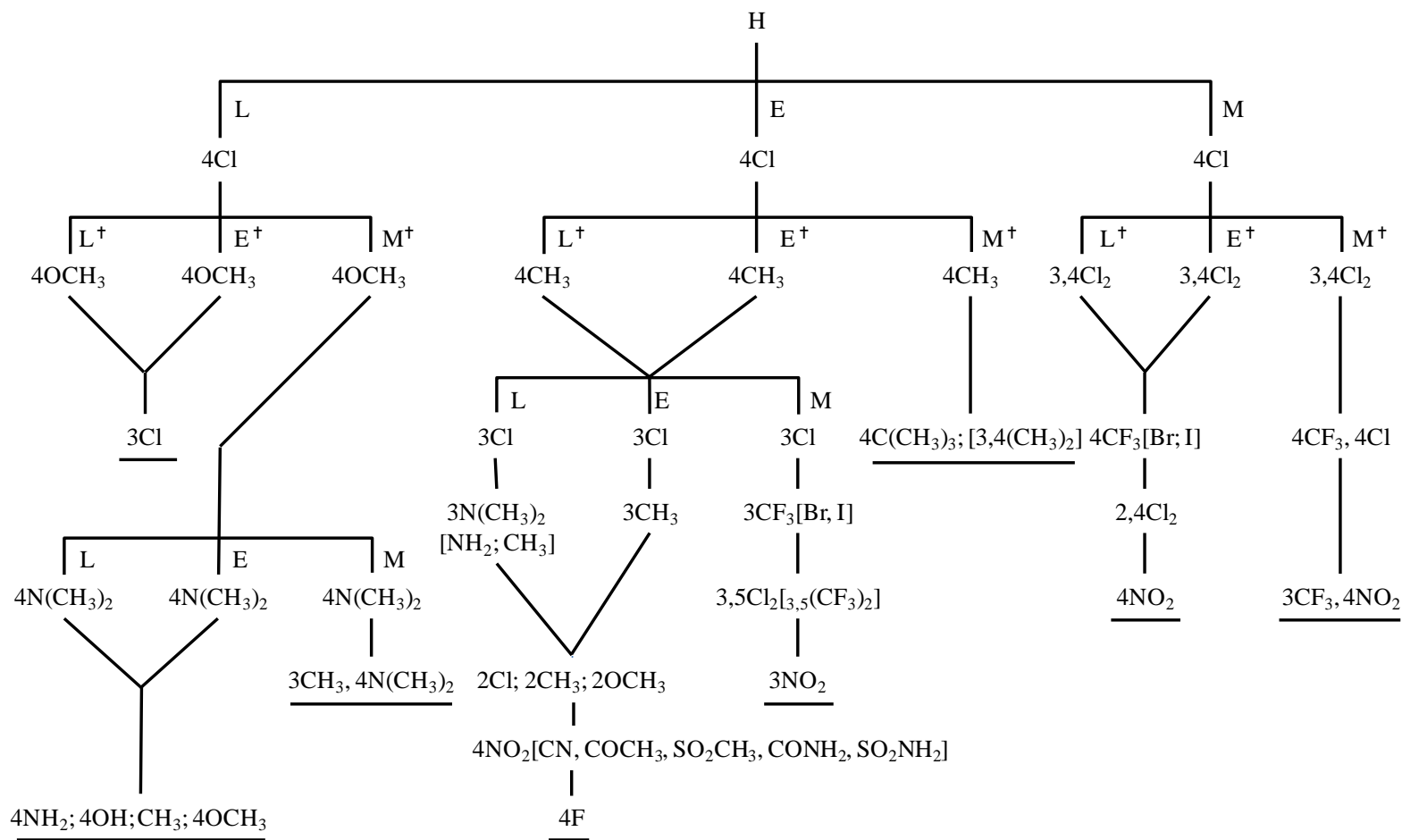
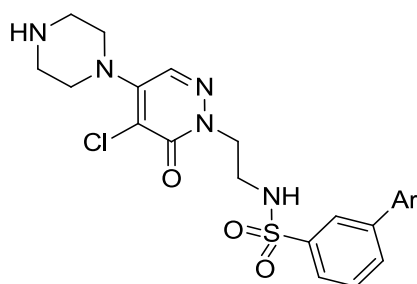


Figure 24. Topliss operational scheme for aromatic substitutions, or Topliss tree.¹²⁷ M = More active, E = equiactive, L = less active. Descending lines indicate sequence. Square brackets indicate alternates. †Compared to 4H compound.

Substituent	Aromatic		E_s
	π	σ	
H	0.00	0.00	1.28
4-Cl	0.70	0.23	0.27
3-Cl	0.76	0.37	0.27
3-ClF ₃	1.21	0.43	-0.98
4-NO ₂	0.24	0.78	-1.28
4-CF ₃	1.07	0.54	-0.98
4-Br	1.19	0.23	0.08
4-I	1.43	0.28	-0.16
2-Cl	0.76	0.23	0.27
4-CH ₃	0.60	-0.17	-0.14
4-C(CH ₃) ₃	1.68	-0.20	-1.65
3-CH ₃	0.54	-0.07	-0.14
3-Br	0.94	0.39	0.08
3-I	1.15	0.35	-0.16
3-NO ₂	0.11	0.71	-1.28
2-CH ₃	0.68	-0.17	-0.14
2-OCH ₃	-0.33	-0.27	0.69
4-CN	-0.32	0.66	
4-COCH ₃	-0.37	0.38	
4-SO ₂ CH ₃	-1.26	0.72	
4-CONH ₂	-1.49	0.40	
4-SO ₂ NH ₂	-1.82	0.57	
4-F	0.15	0.06	0.78
3-N(CH ₃) ₂	0.18	-0.21	
3-NH ₂	-1.23	-0.16	0.63
4-OCH ₃	-0.04	-0.27	0.69
4-NH ₂	-1.23	s0.66	0.63
4-OH	-0.61	-0.37	0.69

Table 21. Substituent Constant Values.¹²⁷



Compound	Ar	HAC	PAD4 FLINT pIC ₅₀	LE	LLE
8		32	6.0	0.26	3.4
19a		33	6.7	0.28	3.7
19b		33	5.8	0.24	3.1
19c		34	7.2	0.29	3.6
19d		35	4.9	0.20	2.7

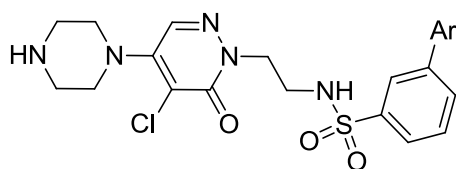
Table 22. Distal ring analogues, **19a-19d**, that explored the effect of varying electronics and lipophilicity on potency with the minimum number of compounds according to the Topliss tree.

The addition of a methoxy group into the 4-position of the distal aryl ring (**19d**) led to a thirteen-fold decrease in potency relative to **8**, while a neutral methyl group in the 4-position (**19b**) was tolerated. Conversely the addition of a chlorine atom on to the 4-position of the distal aryl ring (**19a**) increased potency by five-fold relative to the initial hit **8**. Additional chlorine atoms in both the 3- and 4-positions (**19c**) improved potency by sixteen-fold relative to **8** thereby surpassing the target PAD4 pIC₅₀ 7.0 required for a

PAD4 probe. Improvements in both LE and LLE were also achieved with **19a** and **19c**. These data were consistent with those predicted by the Topliss analysis and confirmed that potency could be maximised by the incorporation of hydrophobic and electronegative substituents on the distal ring.

In the absence of a PAD4-**8** X-ray crystal structure and suitable computational molecular models, the distal phenyl ring of **8** was previously postulated to make a π - π interaction with the PAD4 active site because removal of the aryl ring (**15a-15c**) rendered the template impotent. Substituents are known to affect π - π interactions according to whether they are electron withdrawing groups (EWGs) or electron donating groups (EDGs).¹¹⁸ Generally EWGs deplete the aryl π -electron density which is thought to decrease the unfavourable electrostatic interaction with the π -cloud of the other aryl system and ultimately enhance π -stacking interactions. Conversely, EDGs are reported to hinder stacking interactions through the opposite mechanism, but are likely to improve cation- π interactions. The Topliss investigation confirmed hydrophobic EWGs were favourable for PAD4 potency which is consistent with the distal ring of pyridazinone compounds **8** and **19a-19c** making favourable π - π stacking interactions with aromatic residues in the PAD4 active site, such as Tyr and Phe.

An additional set of distal ring analogues which probed the space and flexibility of the PAD4 active site around the distal ring with neutral methyl substituents in the 2-(**20a**) and 3-(**20b**) positions, and also with the smaller thiophene analogue (**20c**), was synthesised (**Table 23**).



Compound	Ar	HAC	PAD4 FLINT pIC ₅₀	LE	LLE
8		32	6.0	0.26	3.4
20a		33	6.6	0.27	4.2
20b		33	6.5	0.27	3.8
20c		31	5.1	0.23	2.9

Table 23. Distal ring analogues, **20a-20c**, that probed the space and flexibility of the PAD4 active site around the distal ring.

An MMFF dihedral coordinate scan (**Table 24a**)¹²⁹ for the biphenyl ring system present in **8** indicated global energy minima at 50°, 130°, 230° and 310°, with a maximum energy barrier of 1 kcal mol⁻¹ to rotate from 50° to 130° (and the equivalent 230° to 310°), and a maximum energy barrier of 3 kcal mol⁻¹ to rotate from 310° to 50° (and the equivalent 130° to 230°). The biphenyl ring system of **8** was therefore predicted to favour a non-coplanar configuration, probably to avoid a steric clash between adjacent protons on the two rings.

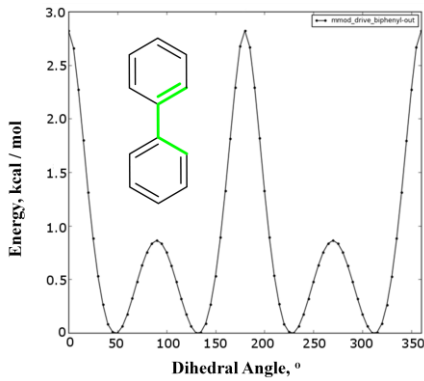
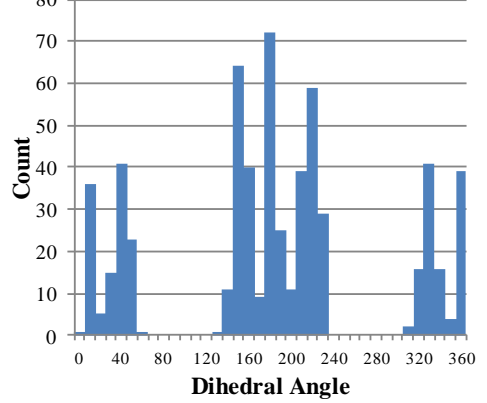
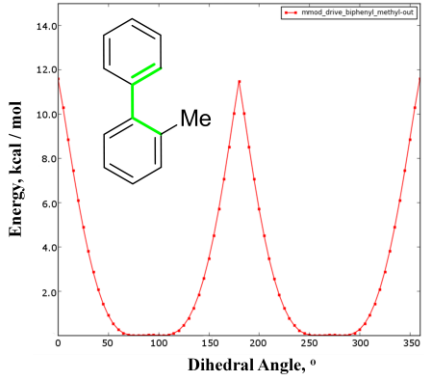
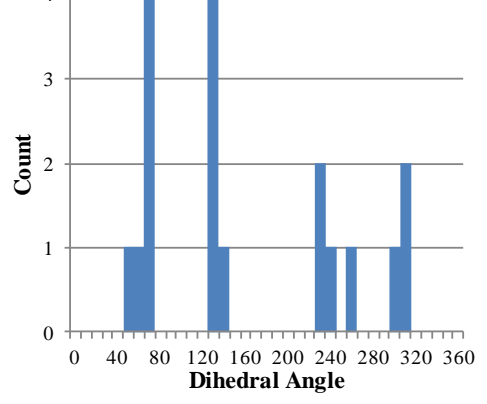
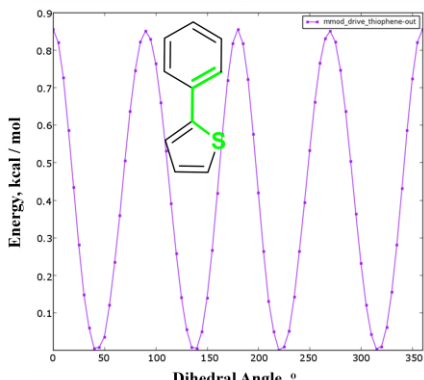
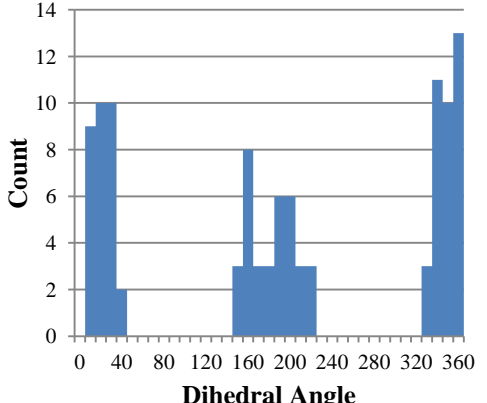
Compound	a) MMFF Dihedral Coordinate Scan	b) Frequency of Dihedral Angles According to the CSD
8		
20a		
20c		

Table 24. a) Plot of MMFF-calculated relative energy (kcal mol^{-1}) for dihedral angles of 0 to 360° between the middle and distal rings of compounds **8**, **20a** and **20c** in 5° increments. The dihedral angle is highlighted in green on inset structures. b) Count of the number of entries found in the Cambridge Structural Database (CSD) for each

dihedral angle from 0 to 360°, binned in 10° increments; 600 entries were found with a phenyl-phenyl ring system similar to **8**, 18 entries were found with a phenyl-2-Me-phenyl ring system similar to **20a**, and 103 entries were found with a phenyl-thiophene ring system similar to **20c**.

The observed frequency distribution of the set of 600 available entries in the Cambridge Structural Database (CSD, **Table 24b**)¹³⁰ roughly mirrored what was predicted using the MMFF forcefield scan given the maximum distribution of experimentally determined dihedral angles at 40 to 50°, 140 to 150°, 220 to 230° and 320 to 330°. However, the CSD showed a much larger than expected number of compounds with coplanar biphenyl rings. This phenomenon has been attributed to improved intermolecular or intramolecular interactions in crystal structures of around 1.2 to 2.4 kcal mol⁻¹ above the global minimum when a crystallographic inversion centre coincides with a centre of symmetry of a C₁-symmetric molecule such as a biphenyl moiety; such an effect has been referred to as a “crystal packing effect” which is known to be relevant in defining the limits of accuracy of molecular and protein modelling.^{131,132}

The crystal packing effect is thought to arise when compounds pack close together in the solid phase, allowing higher energy conformations to be adopted, such as the coplanar biphenyl conformation. In the crystal environment, the coplanar biphenyl moiety may pack more efficiently than a twisted, non-planar biphenyl moiety, for example in a “herringbone” formation.¹³³ Discrepancies between the MMFF results and the CSD results probably arose because while the CSD results were experimentally observed using small molecule X-ray crystal structures, the MMFF predictions used mathematical algorithms that assumed solvation in water. In reality the biphenyl moiety of **8** was likely to be able to adopt any dihedral angle when bound to the PAD4 active site, with a possible small preference towards non-coplanarity given the relative lower energy of this conformation.

For 2-Me phenyl analogues such as **20a**, no coplanar exemplars existed in the set of 18 entries found in the CSD (**Table 24b**), which was consistent with the high energy barrier to coplanarity of 12 kcal mol⁻¹ predicted using the MMFF forcefield (**Table 24a**). A steric clash between the 2-Me group and a proton on the adjacent phenyl ring

makes this conformation energetically unfavourable. The majority of exemplars in CSD adopted dihedral angles of 70 to 80°, 120 to 130°, 220 to 230° and 310 to 320° which was again broadly consistent with the MMFF scan but there was a surprisingly small number of compounds with dihedral angles between 80 and 120° (equivalent to 270 and 300°) which were at the MMFFs-predicted global minima. Perhaps the sample set was small to be statistically significant at 18 members, but together the MMFF and CSD results suggested the biaryl motif of **20a** was very unlikely to be coplanar.

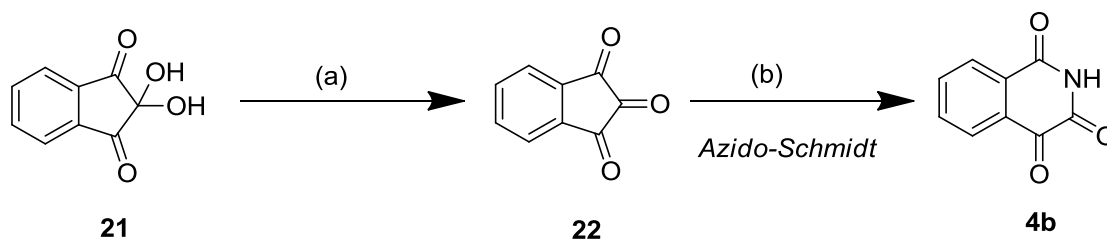
The MMFF dihedral coordinate scan for the thiophene-phenyl ring system present in **20c** indicated energy minima at 40°, 130°, 230° and 310° with a barrier to rotation of less than 1 kcal mol⁻¹ (**Table 24a**); this that suggested any dihedral angle may be adopted. However, these data were inconsistent with the frequency distribution pattern of dihedral angles of the 103 exemplars in the CSD (**Table 24b**). Analysis indicated that the majority of compounds with thiophene-phenyl ring systems adopted dihedral angles of 150 to 220° and 330 to 40°. Very few compounds were able to adopt dihedral angles between these values. This suggested the MMFF model was not accurate for this ring system; the CSD was likely to be more accurate because the dihedral angles were observed experimentally.

The thiophene analogue **20c** was eight-fold less potent than **8** while the incorporation of 2-Me and 3-Me substituents onto the phenyl group (**20a** and **20b** respectively) improved potency three- to four-fold relative to **8** (**Table 23**). Given that the 4-Me analogue **19b** (**Table 22**) was 1.6-fold less potent than **8**, the preferred substitution points on the distal ring for PAD4 potency seemed to be the 2- or 3- position, or potentially both. Additionally, the improvement in PAD4 potency for the 2-Me analogue **20a** suggested that the middle ring and the distal ring should not be coplanar to optimise PAD4 potency. The SAR altogether suggested the potency of the 3,4-Cl₂ analogue **19c** may be further improved, for example, by removing the 4-Cl substituent, because this position may not be an optimal point for substitution. Options for further optimisation are discussed later (see 1.7 Future Work).

1.5. Chemistry

1.5.1. Resynthesis of Isoquinoline Hit 4b

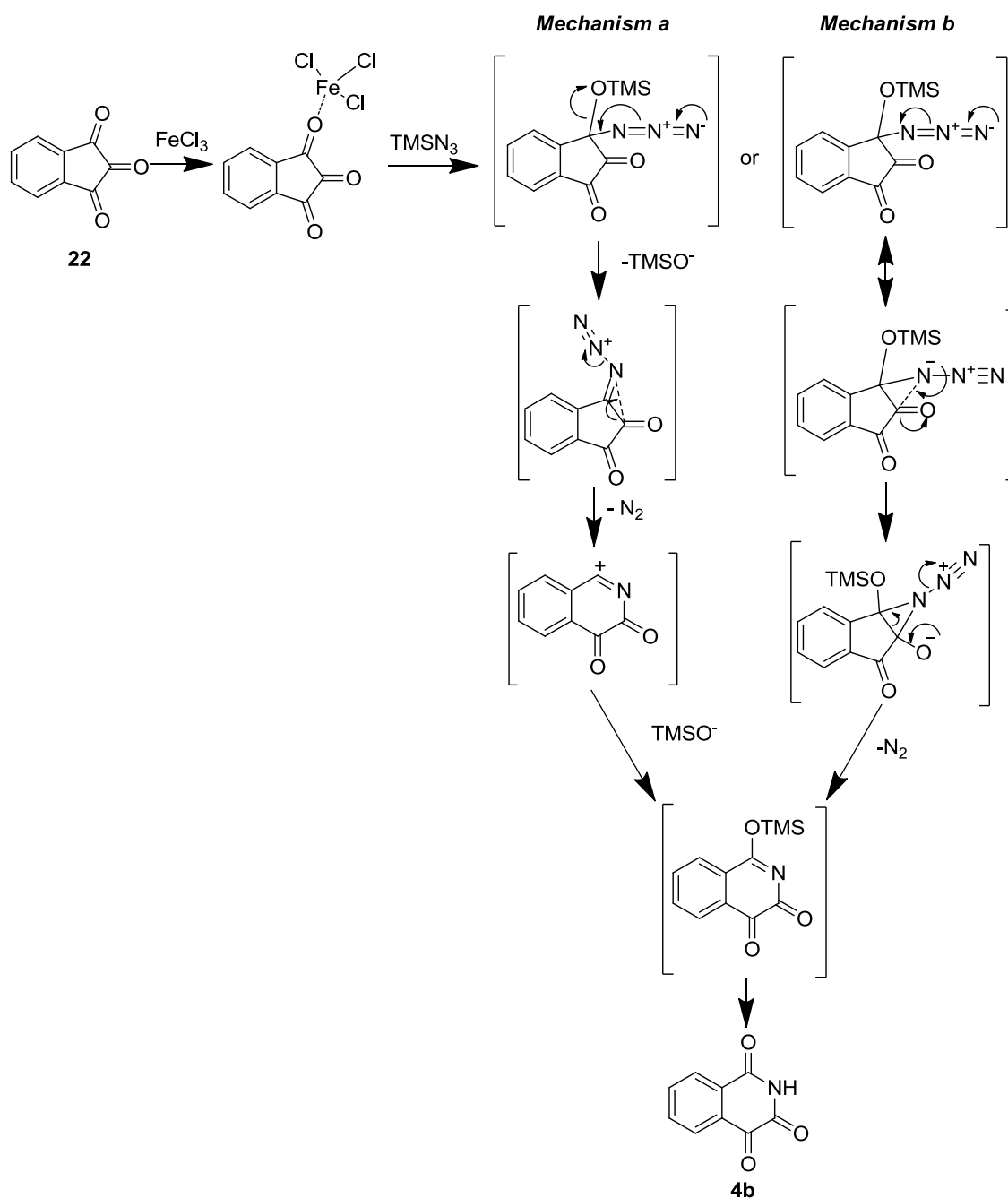
Isoquinoline lead **4b** was prepared *via* a two step reaction in which commercially available **21** underwent dehydration to ninhydrin **22**, followed by an azido-Schmidt reaction by which **23** underwent rearrangement and ring expansion using TMSN_3 in the presence of FeCl_3 to give compound **4b** (**Scheme 6**).¹³⁴



Scheme 6. Preparation of isoquinoline hit **4b** from commercially available starting material **21**. Reagents and conditions: (a) chlorobenzene, reflux, >99%. (b) TMSN_3 , FeCl_3 , DCE, 40 min, 7%.

In contrast to the classical Schmidt reaction which uses strongly acidic media to activate the ketone carbonyl to azide attack, FeCl_3 was used as a Lewis acid catalyst, (**Scheme 7**). Following TMS-azide addition to **22**, the formation of **4b** may occur *via* **Mechanism a** (**Scheme 7**), which is reported without mechanistic studies,¹³⁴ or *via* **Mechanism b** (**Scheme 7**) which is suggested to circumvent the unlikely formation of the immonium ion present in **Mechanism a**. The iminodiazonium ion in **Mechanism a** decomposes to release nitrogen gas while the carbonyl group *anti* to the electron deficient nitrogen migrates to this nitrogen; subsequent attack by TMSO^- on the resultant immonium group gives **4b** after *in situ* TMS removal. **Mechanism b** circumvents the unlikely formation of the immonium ion *via* formation of an azirine on ring expansion then emission of nitrogen to form **4b**.

A low yield of 7% was obtained in the final step, possibly because a time longer than forty minutes may be required. Enough material was secured for analytical and biological evaluation, so no further optimisation steps were undertaken.

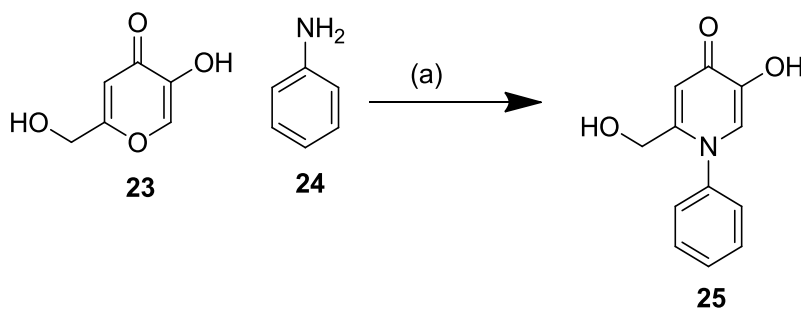


Scheme 7. Proposed mechanisms for the formation of **5** via an azido-Schmidt reaction from ninhydrin **22**.

1.5.2. Hydroxypyridinone Chemistry

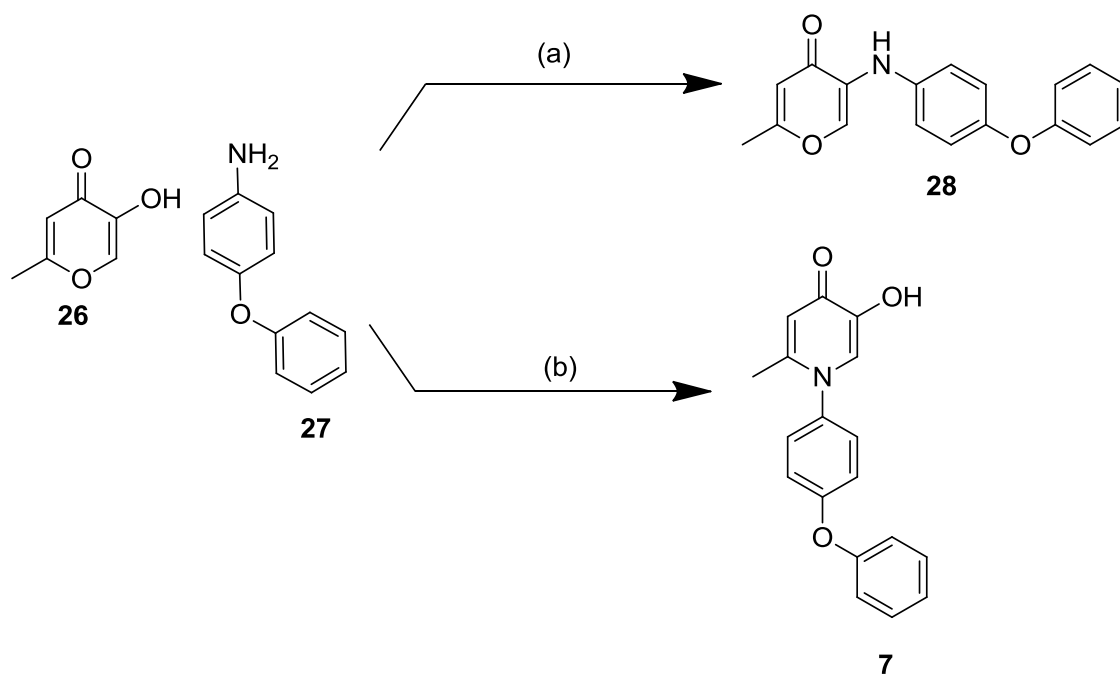
1.5.2.1. Synthesis of Hydroxypyridinone, **7**

The synthesis of **7** was undertaken using the route originally developed by Imafuku *et al.* to make 1-aryl-5-hydroxy-2-hydroxymethyl-4-pyridones such as **25** (**Scheme 8**). Heating kojic acid **23**, with aniline **24**, using hydrochloric acid and water as solvents in a sealed glass tube afforded **25**.¹³⁵ The reaction temperature was not stated.



Scheme 8. Synthesis of **25** reported by Imafuku *et al.*¹³⁵ Reagents and conditions: (a) 12M HCl, water, heat, 18% reported yield.

In a similar manner, **26** was heated with 4-phenoxyaniline **27** in a sealed glass tube in the presence of hydrochloric acid using microwave irradiation (**Scheme 9, Route a**). Instead of the desired pyridinone product **7**, the major product was identified as pyranone **28**. When the reaction was repeated by thermally heating in a sealed glass tube (Reacti-VialTM) at a higher temperature, the major product was **7** (**Scheme 9, Route b**), though a small amount of **28** was evident in the crude LCMS, according to relative LC retention times. The structure of **28** was confirmed using a combination of ¹³C/¹H HMBC (**Figure 25**) and ¹⁵N/¹H COSY (**Figure 26**) NMR experiments.¹³⁶



Scheme 9. Preparation of **7** and **28**. Reagents and conditions: (a) 7% $\text{HCl}_{(\text{aq})}$, H_2O , 100 °C, 4 h, microwave, then 110 °C, 2 h, microwave, 9%, (b) 6% $\text{HCl}_{(\text{aq})}$, 150 °C, 16 h, sealed glass tube, 8%.

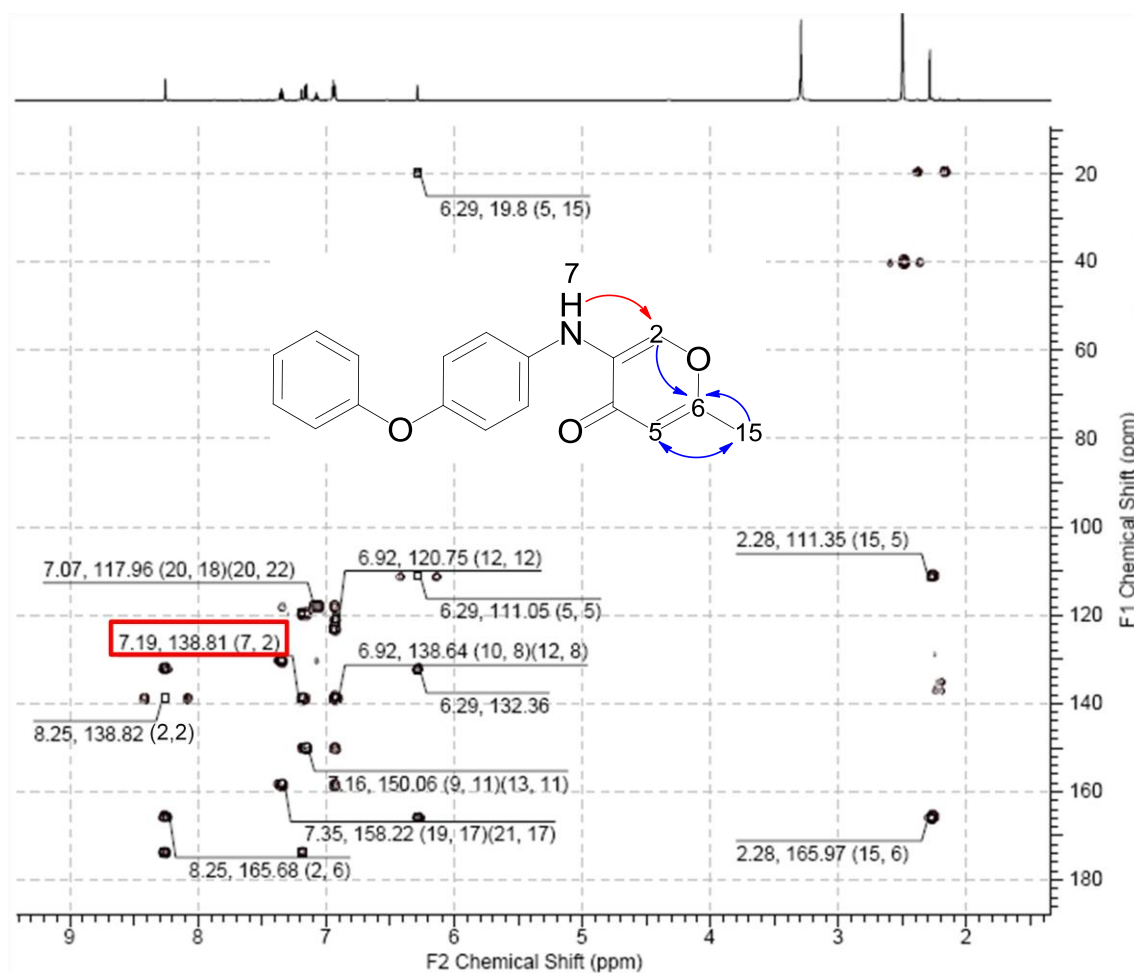


Figure 25. $^{13}\text{C}/^1\text{H}$ HMBC NMR spectrum of **28**.¹³⁶ Key correlations between ^1H and ^{13}C nuclei are represented by red and blue arrows. The key crosspeak that indicated a correlation between the anilinic N7-proton (singlet, 7.19 ppm) and the C2-carbon (138.8 ppm) is highlighted in red and suggested the aniline was likely to be attached to C3-carbon as drawn. Further evidence for this structure was provided by the $^{15}\text{N}/^1\text{H}$ COSY NMR spectrum (**Figure 26**).

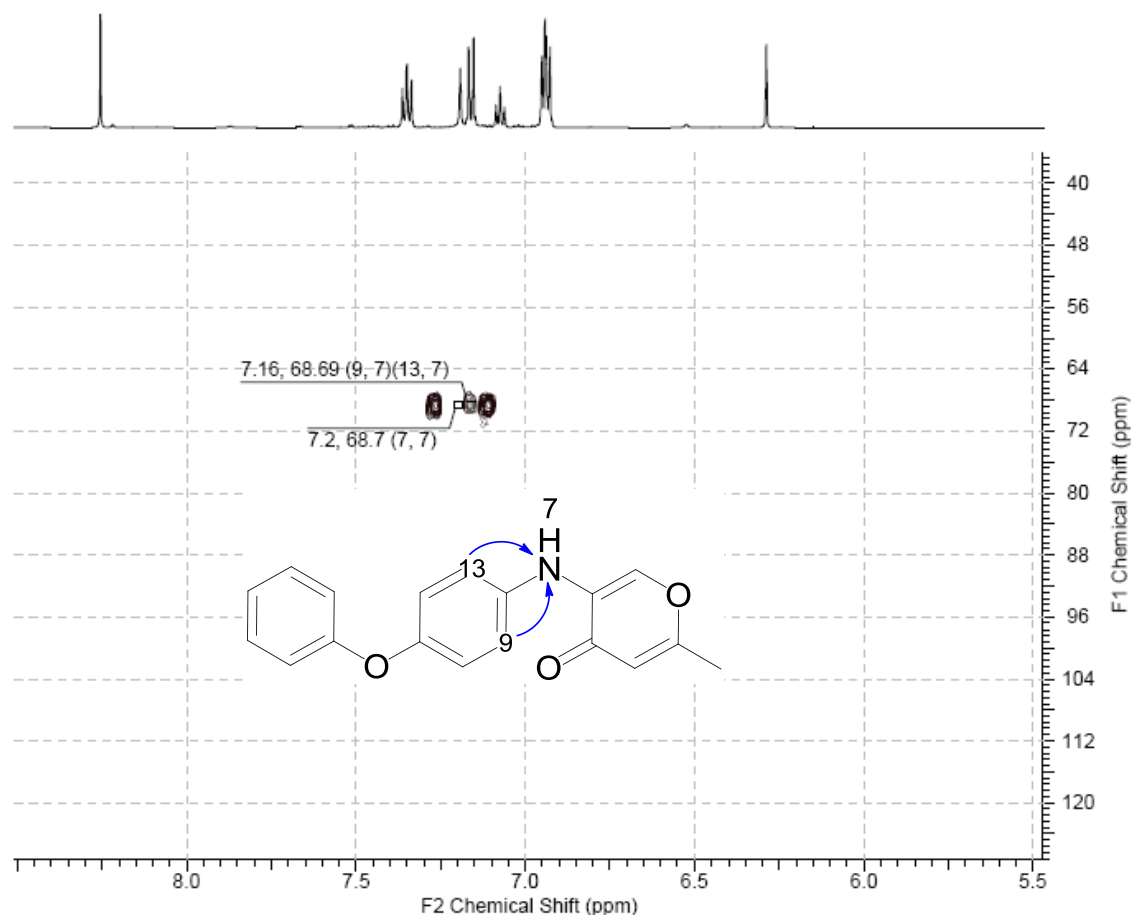
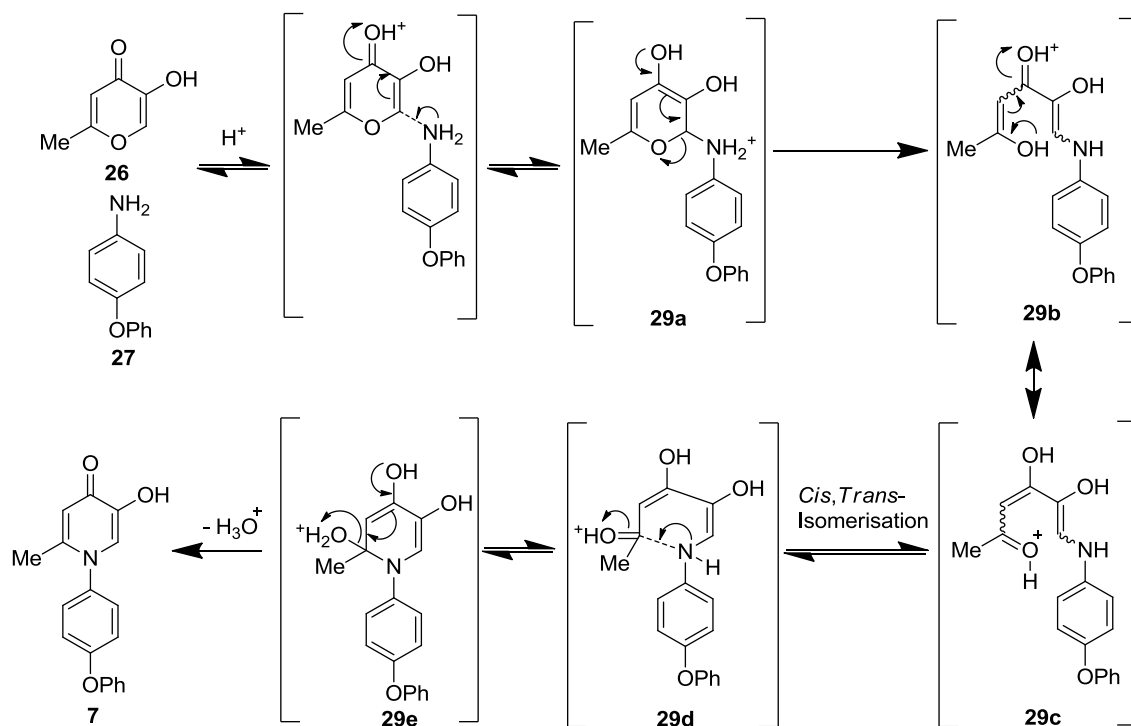


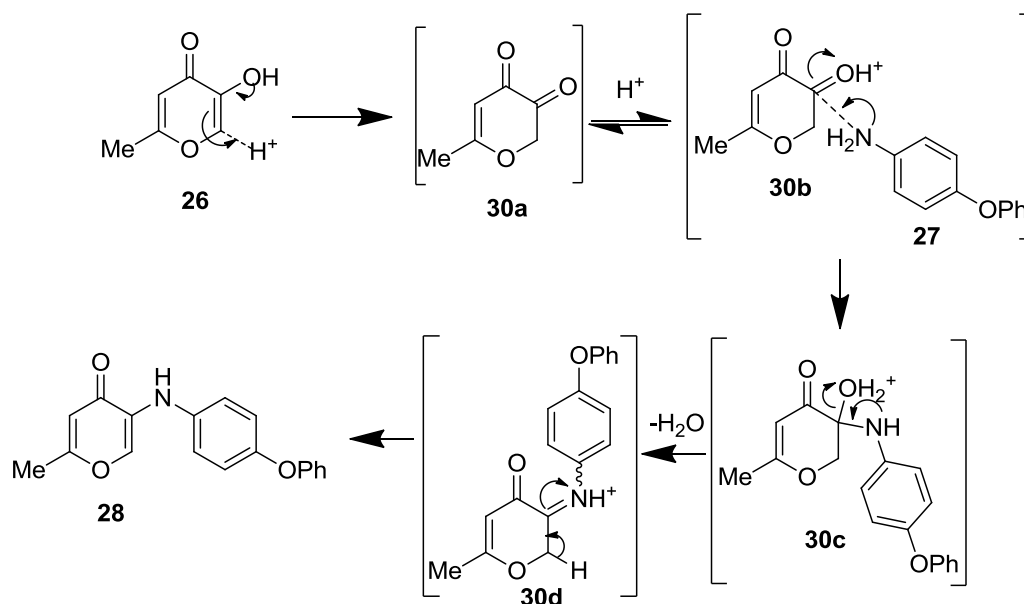
Figure 26. $^{15}\text{N}/^1\text{H}$ COSY NMR spectrum of **28**.¹³⁶ The key correlations between the C9- and C13-protons (doublet, 7.16 ppm) and N7-nitrogen (68.8 ppm), are represented by blue arrows.

The mechanisms for the formation of **7** and **28** are not discussed in the literature. One possible mechanism for the formation of **7** is shown in **Scheme 10**, where the protonated unsaturated α,β -keto ester **26** can undergo nucleophilic attack by aniline **27** to form reactive intermediate **29a**. Ring opening to **29b** and isomerisation to **29c**, followed by *cis,trans*-isomerisation aided by the polar-protic ethanol and water solvent gives **29d**, then intramolecular nucleophilic attack by the anilinic nitrogen on the newly formed protonated ketone can give intermediate **29e**. This can then collapse, eliminating water to form desired product **7**.



Scheme 10. Proposed mechanism for formation of **7**.

The proposed mechanism for the formation of **28** is much more tentative (**Scheme 11**). Protonation of **26** gives diketone **30a** which on protonation to give **30b** can then undergo nucleophilic attack by aniline **27** on the less conjugated carbonyl group to give tetrahedral intermediate **30c**. Elimination of water gives imine **30d** which can then tautomerise to form **28**.

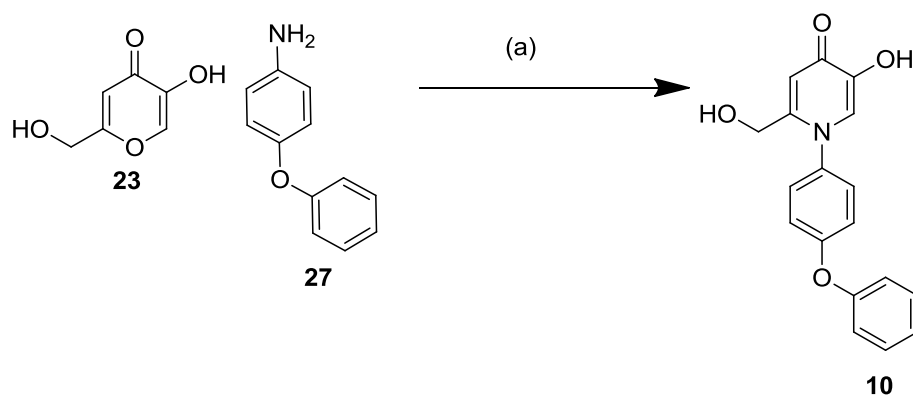


Scheme 11. Proposed mechanism for formation of **28**.

Preference for the formation of **7** over **28** using **Route b** instead of **Route a** may have occurred due to a number of variables such as the higher temperature, the use of thermal heating instead of microwave heating, the much longer heating time, the higher concentration of hydrochloric acid, or indeed a combination of all four variables. Some **28** was evident in the LCMS of the crude reaction mixture during **Route b** which suggested **28** might have been a stable intermediate on the way to **7**, and that **28** may have been the most thermodynamically stable product.

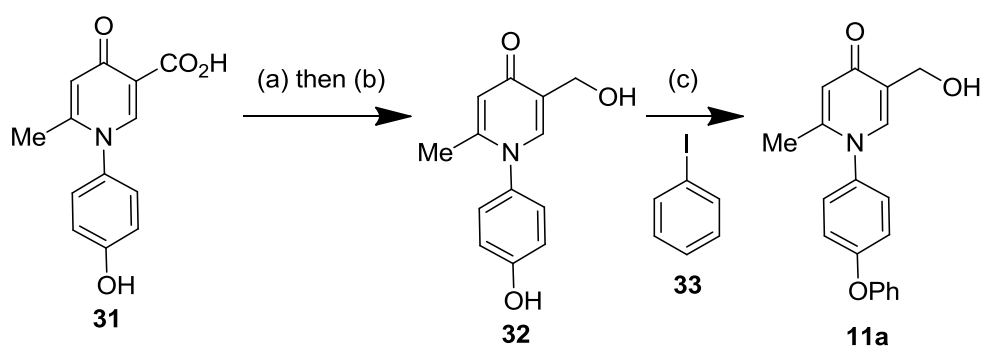
1.5.2.2. Synthesis of Hydroxypyridinone Analogues with Varied Headgroups

The 2-hydroxymethyl analogue **10** was synthesised (**Scheme 12**) using a method similar to that described by Imafuku *et al.*¹³⁵ and used to make 1-aryl-5-hydroxy-2-hydroxymethyl-4-pyridones such as **25** (**Scheme 8**). Kojic acid **23** was heated with 4-phenoxyaniline **27** in the presence of hydrochloric acid in a sealed glass tube.¹³⁵ No overpressures were evident during the synthesis of **10** using this method, though a blast shield was used as a precaution. No putative regioisomers were evident in the LCMS.



Scheme 12. Preparation of **10** from kojic acid **23** and **27**. Reagents and conditions: (a) 4% HCl_(aq.), 150 °C, 16 h, sealed glass tube, 12%.

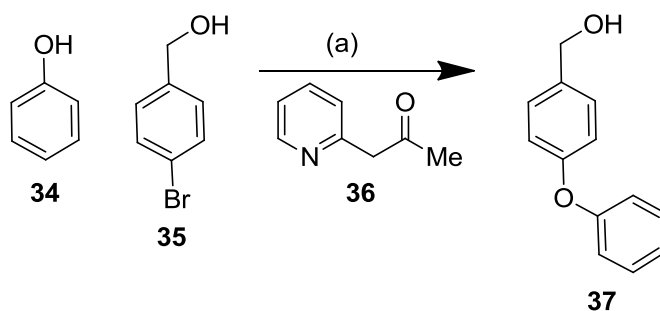
The hydroxypyridinone headgroup analogue **11a** (**Scheme 13**) was synthesised *via* a reduction followed by an Ullman reaction. Reduction of the 4-oxo-1,4-dihydropyridine-3-carboxylic acid moiety of **31**⁸ to alcohol **32** was achieved by treatment with ethyl chloroformate, followed by sodium borohydride; this is a general method used for the reduction of benzoic acids to the corresponding benzylic alcohols but was previously unreported on this type of heterocyclic core.¹³⁷



Scheme 13. Preparation of hydroxypyridinone headgroup analogue **11a**. Reagents and conditions: (a) ethyl chloroformate, triethylamine, THF, (b) sodium borohydride, EtOH, >99%, (c) (2-pyridyl)acetone **36**, CuBr, Cs₂CO₃, DMSO, 120 °C, 24 h, 12%.

The conditions that were used to access **11a** from phenol **32** and iodobenzene **33** were identified from conditions that had been reported previously by Zhang *et al.* (**Scheme 14**) to synthesise biaryl ether **37** from phenol **34** and benzylic alcohol **35**.¹³⁸ Zhang's conditions were chosen because they reported good functional group compatibility and

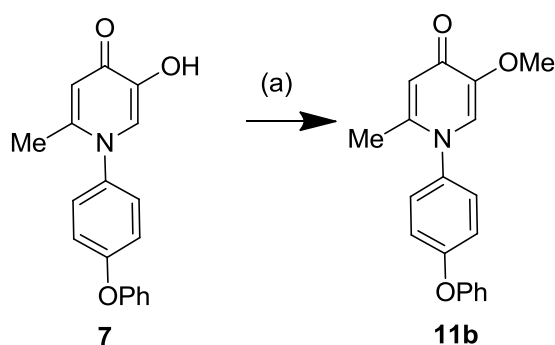
excellent reaction selectivity at moderate temperatures using ligand (2-pyridyl)acetone (**36**).



Scheme 14. Ullman reaction that Zhang *et al.* used to access biaryl ether **37** using (2-pyridyl)acetone **36**.¹³⁸ Reagents and conditions: CuBr, Cs₂CO₃, 120 °C, 80%.

A much lower yield was achieved than Zhang *et al.*'s reported yield of 80%, possibly because the hydroxymethylpyridinone moiety of **32** is capable of forming a complex with the copper catalyst. The yield may be improved by increasing the loading of CuBr and the (2-pyridyl)acetone ligand **36**, or by using a protecting group on the alcohol. For example, a TBDMS group could be used to protect the alcohol which can then be removed after the Ullman coupling.

Compound **11b** (**Scheme 15**) was secured *via* methylation of the hydroxyl group of **7** using methyl iodide. No starting material was evident in the reaction mixture, and **11b** was the major product according to LCMS (99%) so the low yield could perhaps be attributed to a preparation step used to remove the caesium carbonate before MDAP purification: the sample was dissolved in DMSO then filtered, and not all the material might entered solution before purification.

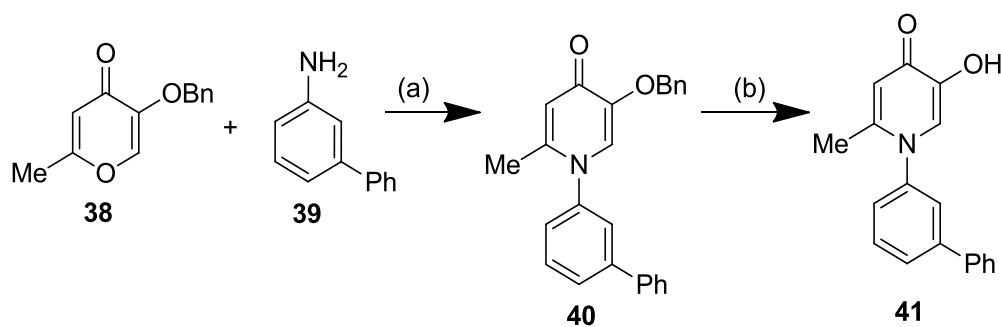


Scheme 15. Synthesis of **11b** from **7**. Reagents and conditions: (a) MeI, Cs₂CO₃, 2 h, DMF, 46%.

1.5.2.3. Synthesis of Hydroxypyridone Distal Ring Analogues

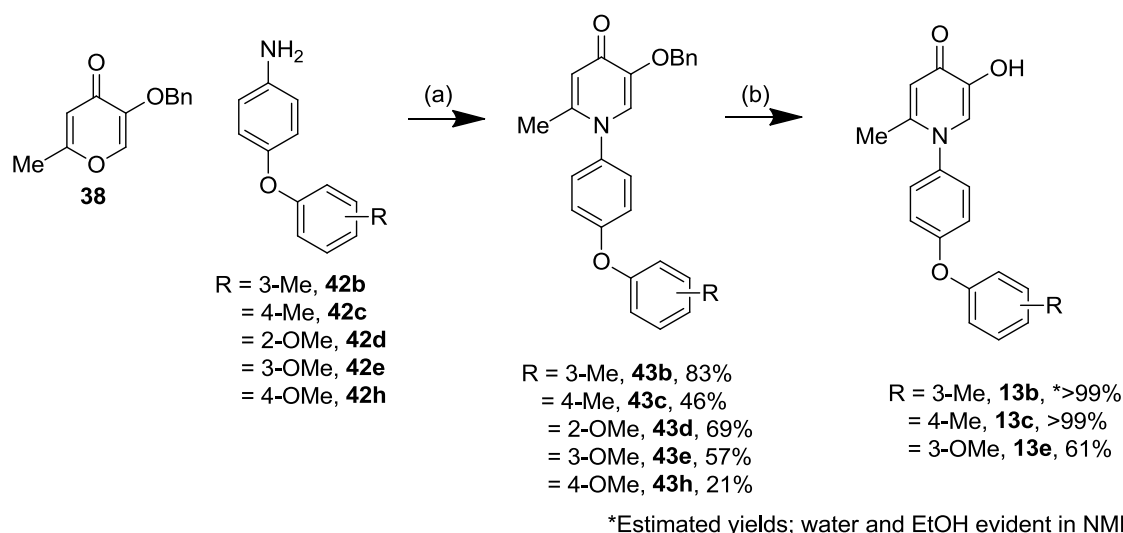
The successful route used to access **7**, **Route b** (**Scheme 9**) produced a number of by-products which may explain the poor yield. The conditions also proved hazardous because high overpressures were generated, and a number of initial attempts to synthesise analogues with alternative distal rings caused the sealed glass tubes to fail.

The poor yields and hazardous nature of this method prompted investigations into alternative methods, one of which accessed scaffolds similar to **7** *via* benzyl-protected starting material **38**.⁸ This material was reported in a patent application that described the synthesis of COMT inhibitors such as **41** from benzyl protected kojic acid analogue **38** (**Scheme 16**).¹³⁹



Scheme 16. Alternative route to hydroxypyridinone analogues that was reported in a patent *via* benzyl-protected acid analogue **38**.¹³⁹ The closest reported structural analogue to **7** is illustrated, **41**. Reagents and conditions: (a) 30% AcOH/water, 160 °C, 18 h, yield unreported, (b) 4 M HCl_(aq.), 160 °C, 18 h, yield unreported.

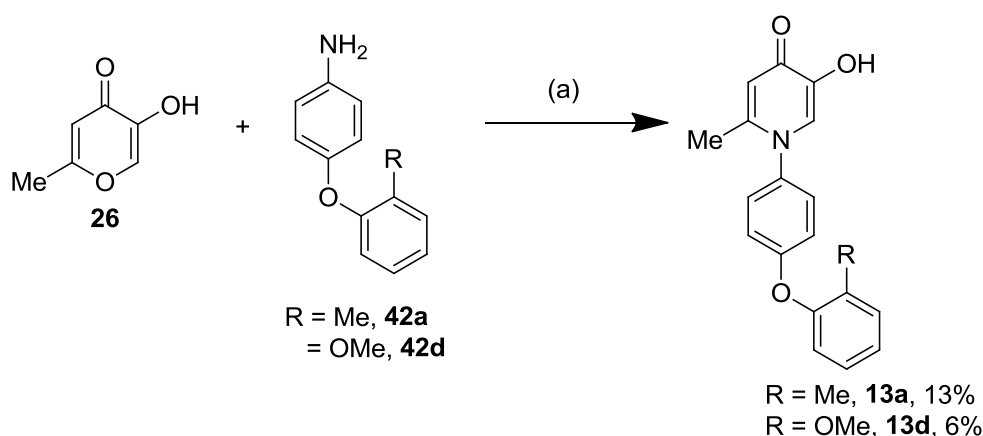
Similar conditions allowed syntheses of substituted phenyl analogues **13b**, **13c** and **13e** in high yield over two steps from intermediate **38** that had been synthesised by Preston,⁸ though hydrogenolysis was used to remove the benzyl protecting group, rather than the previously reported acid-mediated hydrolysis (**Scheme 17**). Nucleophilic attack of the appropriate aniline, **42b-42d**, **42e** or **42h**, on benzyl-protected kojic acid analogue **38**, followed by cyclisation to benzyl-protected intermediates **43b-43d**, **43e** or **43h**, was effected using microwave irradiation. Subsequent hydrogenolysis of **43b**, **43c** and **43e** to **13b**, **13c** and **13e** respectively was achieved using a 10% Pd/C catalyst in the presence of hydrogen with an H-cubeTM hydrogenator; further purification of the hydrogenolysed products was not required. This alternative two step route proved safer and higher yielding than the sealed glass tube route. The mechanism for the acid-mediated cyclisation mechanism is anticipated to be similar to that discussed previously for the formation of **7** (**Scheme 10**).



Scheme 17. Route used to access distal ring analogues **13b**, **13c** and **13e**. Reagents and conditions: (a) 40% AcOH in water, 170 °C, microwave irradiation, 2 h, (b) hydrogen, 10% Pd/C CatCart^{30 TM}, EtOH, H-CubeTM.

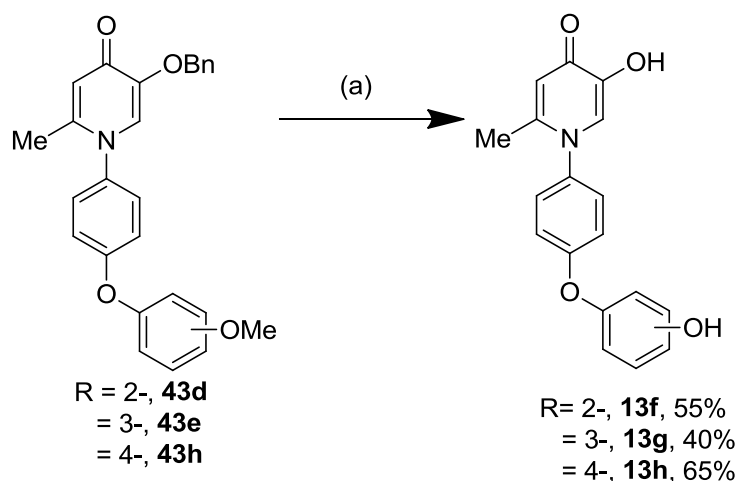
Given the success of the single-step HCl/water-mediated route to **10**, the route was revisited for the synthesis of **13a** and **13d** from kojic acid analogue **26**; this time the reactions were heated at the higher temperature of 170 °C using a microwave reactor (**Scheme 18**). This proved successful, if low yielding, but gave the desired product as

the major product, as opposed to the regioisomer **28** previously detected during the synthesis of **7**. However, the putative regioisomer (unisolated) and a number of unidentified byproducts were visible in the LCMS, which may explain the low yields. The evidence suggested that the higher temperature was required for formation of the desired regioisomer, which may be the more thermodynamically favoured product; the alternative regioisomer may be the more kinetically favoured product. However, the two-step synthetic route *via* benzyl protected kojic acid analogue **38** remained superior to the single-step route because of its improved safety, reproducibility and higher yields.



Scheme 18. Route used to access distal ring analogues **13a** and **13d**. Reagents and conditions: (a) 6% HCl in water, EtOH, microwave irradiation, 170 °C, 4 h.

An alternative strategy was used to access the 2-, 3- and 4- substituted distal ring phenols **13f-13h** (**Scheme 19**). The appropriate methyl ether intermediates **43d**, **43e** and **43h** were treated with excess boron tribromide which led to debenzoylation and demethylation to afford the target compounds **13f-13h** in one pot. Unlike the hydrogenolysis products, these compounds required further purification by MDAP.

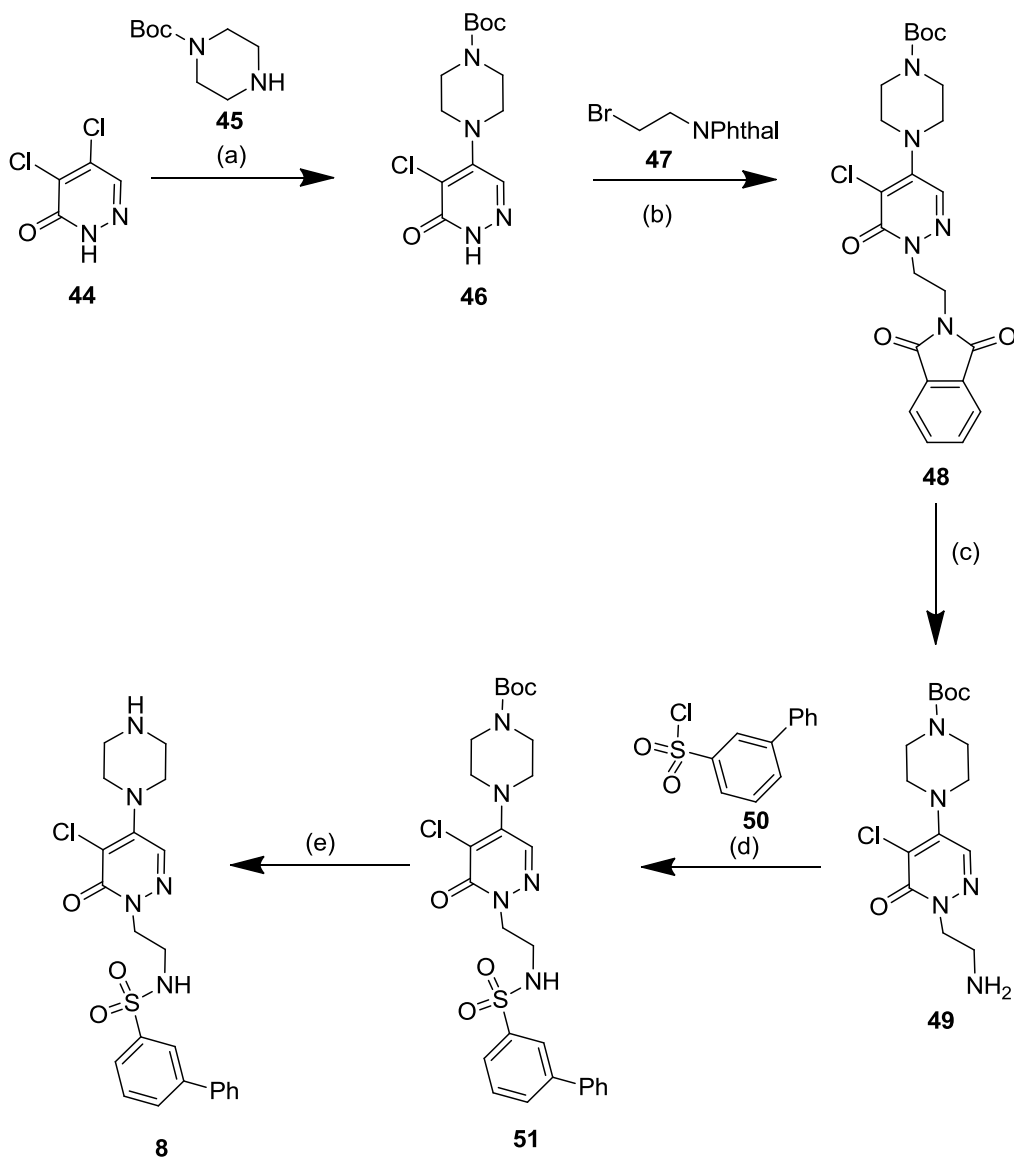


Scheme 19. Route used to access distal ring phenol analogues. Reagents and conditions: (a) 1 M solution of BBr_3 in DCM, 0 °C to room temperature, DCM.

1.5.3. Pyridazine Chemistry

1.5.3.1. Resynthesis of Pyridazine Hit, **8**

A fresh sample of the pyridazine lead **8** was obtained after a facile five-step synthesis from commercially available starting material **44** (**Scheme 20**). The first step involved nucleophilic displacement of the 4-chloro substituent of **44** by Boc-piperazine **45** to give **46** in analogy to a synthesis reported by Varga *et al.*¹⁴⁰ Compound **46** has been reported by Ting *et al.*,¹⁴¹ but the exact conditions for preparation were not described. However, conditions that were used to make close analogues and that were described were the same as those used here, except triethylamine was used instead of DIPEA. Compound **44** is a cyclic vinylogous acid chloride with *trans*-configuration so the 4-position is more susceptible to nucleophilic substitution than the 5-position.¹⁴² No regioisomer was evident by LCMS. Alkylation of the pyridazine N1-position with **47** to give **48** was effected using a method that was well precedented for the synthesis of pyridazinone-aryl piperazine α 1- and α 2-adrenoreceptor antagonists (not shown).¹⁴³ Removal of the phthalimide protecting group from the *bis*-protected primary amine using methylamine¹⁴⁴ gave the key amine intermediate **49**. Sulfonylation using the sulfonyl chloride **50** and pyridine as base¹⁴⁵ yielded **51**. Subsequent TFA-mediated Boc-deprotection¹⁴⁶ secured the pyridazine lead compound **8**.

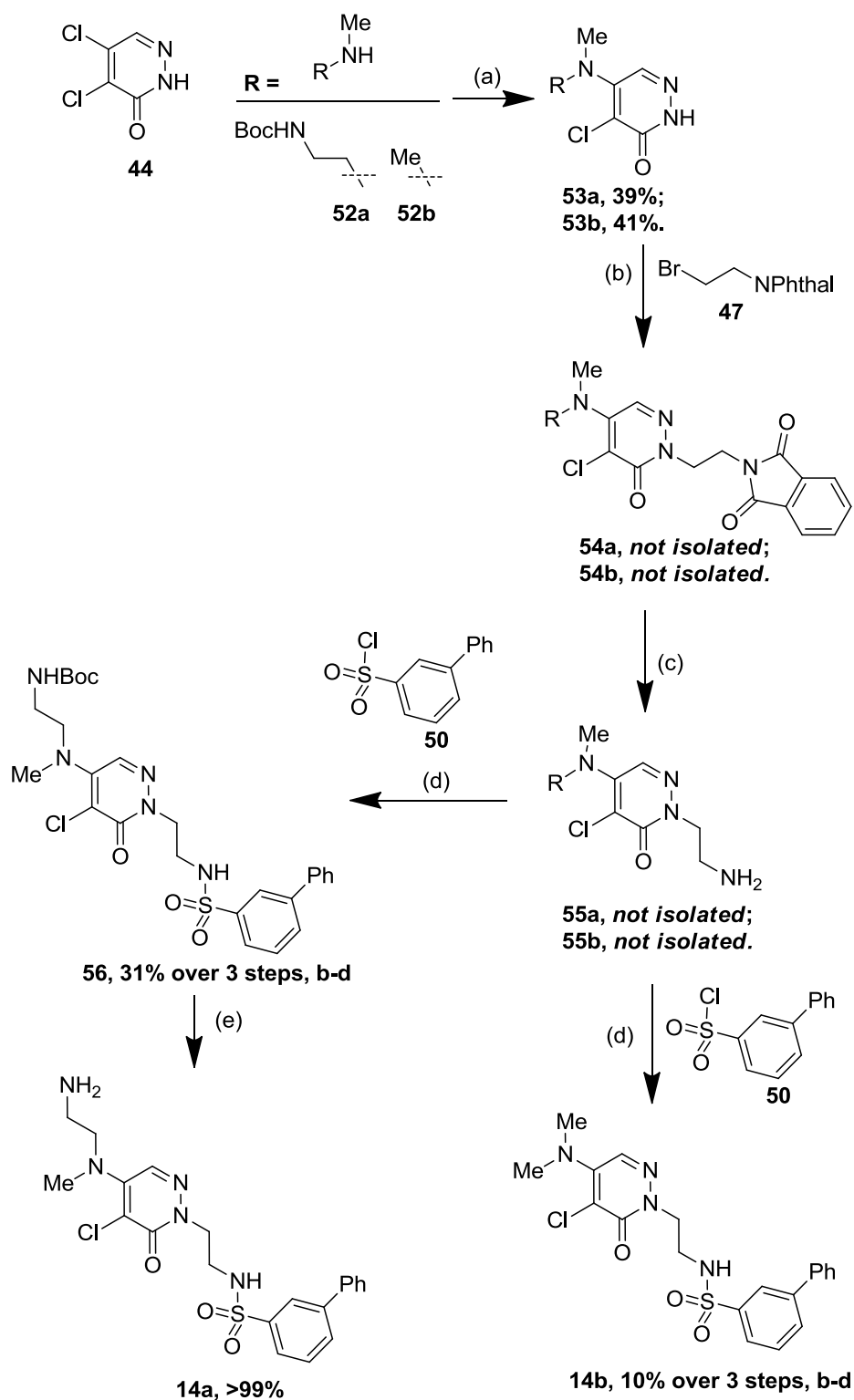


Scheme 20. Preparation of pyridazine hit **8** from commercially available starting materials **44** and **45**. Reagents and conditions: (a) DIPEA, EtOH, reflux, 20 h, >99%, (b) K_2CO_3 , DMF, 72 h, 74%, (c) methylamine (33% by weight in EtOH), 92% at 85% purity, (d) pyridine, DCM, 50%, (e) TFA, DCM, 81%.

1.5.3.2. Synthesis of Pyridazine Template Headgroup Analogues

Pyridazine template headgroup analogues **14a** and **14b** (**Scheme 21**) were accessed using a route similar to that used to secure **8** using the appropriate amine, **52a** or **52b**, as the nucleophile in the first step instead of Boc-piperazine **45**; no regioisomer was

evident by LCMS. An acid-mediated deprotection final step was required for **14a**, where RMeNH was Boc-ethylamine.



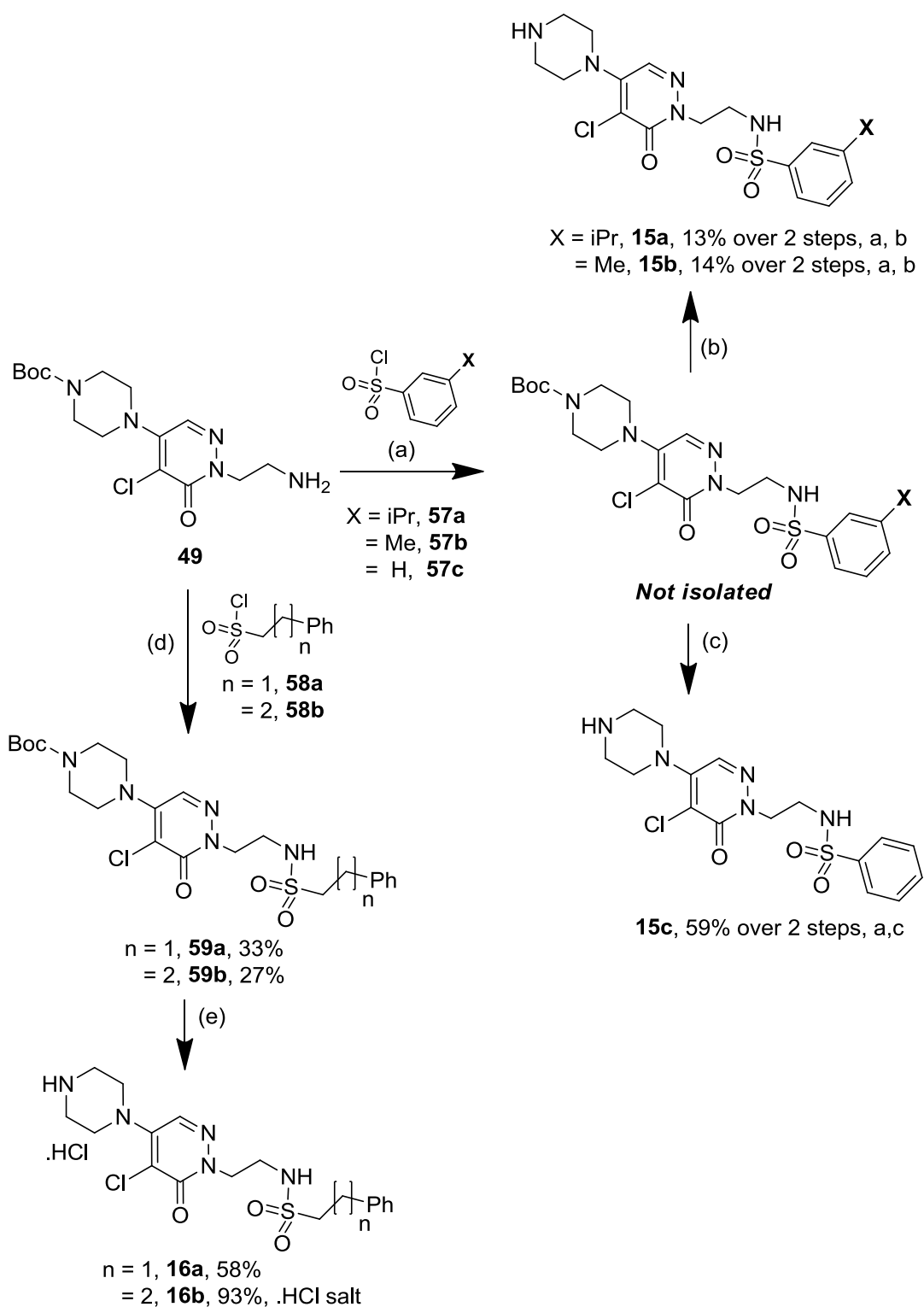
Scheme 21. Preparation of pyridazine template headgroup truncates **14a** and **14b** from commercially available starting material. Reagents and conditions: (a) DIPEA, EtOH, Reflux, (b) K_2CO_3 , DMF, (c) methanamine (33% solution by weight in EtOH), (d) pyridine, DMF, (e) TFA, DCM.

1.5.3.3. Synthesis of Pyridazine Template Middle- and Distal- ring Analogues

Middle- and distal ring analogues **15a-15c** and **16a** and **16b** (Scheme 22) were obtained in two steps: sulfonylation of amine intermediate **49**, followed by acid-mediated Boc-deprotection.

DMAP was used in sub-stoichiometric quantities to effect sulfonylations that were low yielding on the first attempt of synthesis of **16a** and **16b**, probably because the alkyl sulfonyl chlorides are less activated to nucleophilic attack by pyridine than the aryl sulfonyl chlorides used to make **15a-15c**. DMAP is known to be more effective than pyridine at activating electrophilic species such as acid chlorides and sulfonyl chlorides to nucleophilic attack by amines, and in sequestering the HCl acid that is generated as a by-product.¹⁴⁷ The electron donating effect of the 4-dimethylamino group makes DMAP more nucleophilic and a stronger base than pyridine: the pK_a of DMAP is 9.2 while the pK_a of pyridine is 5.1.¹⁴⁸

A range of Boc-deprotection methods were utilised based on the availability of fresh, newly bought-in materials to minimise the requirements for a final purification step, rather than based on synthetic rationale.

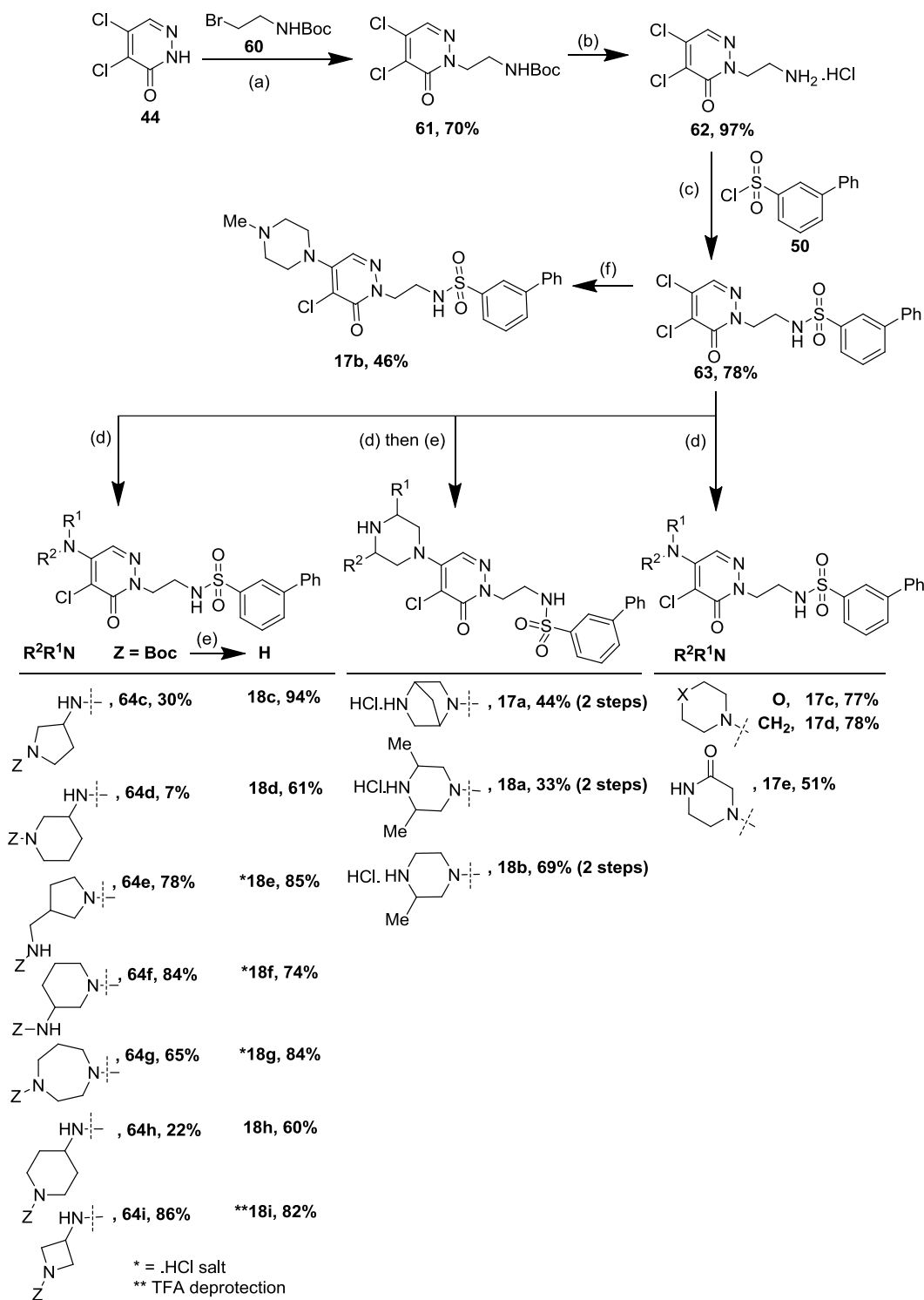


Scheme 22. Preparation of pyridazine middle- and distal-ring analogues **15a-15c** and **16a** and **16b** from common intermediate **49**. Reagents and conditions: (a) pyridine, DCM, (b) HCl in DCM, (c) TFA, DCM, (d) DMAP, DCM, (e) HCl_(g) in EtOAc.

1.5.3.4. Pyridazine Template Headgroup Variation

Pyridazine template headgroup analogues **17a-17e** and **18a-18i** were obtained after facile four- to five- step syntheses from starting material **44** (**Scheme 23**). Alkylation of the pyridazine N1-position with **60** gave **61** then removal of the Boc-protecting group using gaseous hydrochloric acid in ethyl acetate gave the key amine intermediate **62** in high yield. Subsequent sulfonylation with **50** using pyridine as base¹⁴⁵ yielded late stage intermediate **63** which was then used to access final compounds **17b-17e** or Boc-protected intermediates of **17a** and **18a-18i** *via* nucleophilic displacement of the 4-chloro substituent by the appropriate amine, R¹R²NH. Amine monomers used to make **17a** and **18a-18i** contained two nucleophilic amino groups so to avoid potential nucleophilic attack of the second amino group, appropriate monomers were chosen with the second amino group protected with a Boc-group.

On some occasions during the reactions of the amines with **63**, a second minor peak (<5%) which had a similar mass ion to the desired product was evident in the LCMS; this component was assumed to be the regioisomer formed as a byproduct from displacement of the 5-chloro substituent. The putative regioisomer could be easily separated from the desired product by HPLC, though efforts to isolate this component failed because too small an amount formed to be isolated. Subsequent deprotection was effected using HCl to give final compounds **17a** and **18a-18h**, or using TFA to give final compound **18i**.

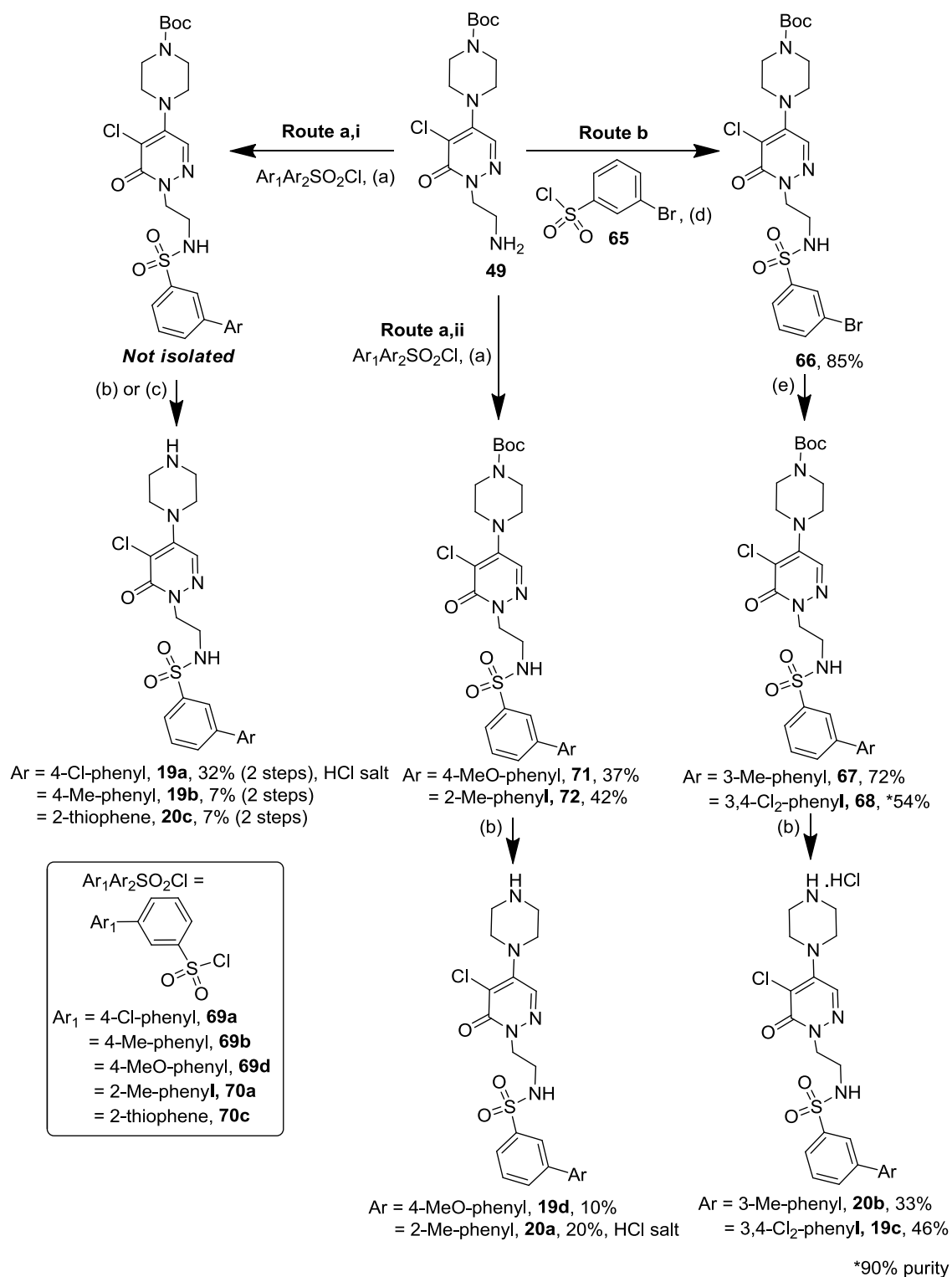


Scheme 23. Preparation of pyridazine template headgroup analogues **17a-17e** and **18a-18i** from commercially available starting material. Reagents and conditions: (a) K_2CO_3 , DMF, 70%, (b) gaseous HCl, DCM, 97%, (c) pyridine, 78%, (d) R^2R^1NH , DIPEA, EtOH or *n*-BuOH, Reflux, (e) gaseous HCl in EtOAc, or TFA (f) methylpiperazine, potassium carbonate, DMF.

1.5.3.5. Distal Ring Variation

Pyridazine template distal ring analogues **19a-19d** and **20a-20c** were obtained using facile syntheses *via* either **Route a** from common intermediate **49** when the appropriate sulfonyl chloride was available (**Scheme 24**), or *via* **Route b** from common intermediate **66**. In this case, when the sulfonyl chloride was unavailable, the distal ring was introduced using a Suzuki coupling. **Route a** involved sulfonylation of amine intermediate **49** using the appropriate biaryl sulfonyl chloride and pyridine, followed by acid-mediated Boc-deprotection¹⁴⁶ to give target compounds **19a**, **19b**, **19d**, and **20a** and **20c**. The Boc-protected intermediates were isolated and characterised where possible (**Route a,ii**), but on occasions time pressures were high or only a small amount of Boc-protected intermediate was obtained, so material was converted directly to the desired product without isolation of the intermediate (**Route a,i**).

Route b involved a Suzuki reaction between aryl bromide intermediate **66** and the appropriate aryl boronic acid, followed by hydrochloric acid-mediated Boc-deprotection to give target compounds **19c** and **20b**. Again a range of Boc-deprotection methods were utilised based on the availability of fresh, newly bought in materials to minimise the requirements for a final purification step, rather than based on any synthetic rationale.



Scheme 24. Preparation of pyridazine template distal ring analogues **19a-19d** and **20a-20c** from commercially available starting materials. Reagents and conditions: (a) pyridine, DCM, (b) HCl in EtOAc or DCM, (c) TFA in DCM, (d) pyridine, (e) aryl boronic acid, *tetrakis*(triphenylphosphino)palladium(0), Na₂CO₃, DMF, water, 100 °C.

1.6. Conclusions

The compounds in **Table 25** are discussed in the conclusions for Chapter 1 that follow.

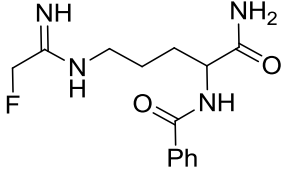
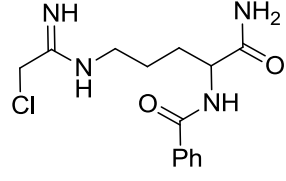
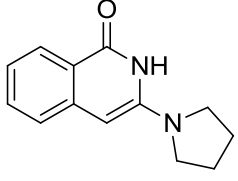
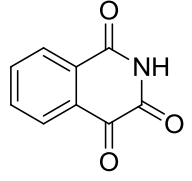
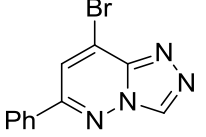
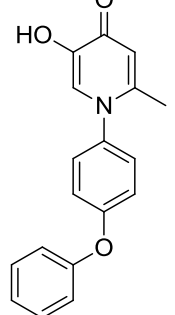
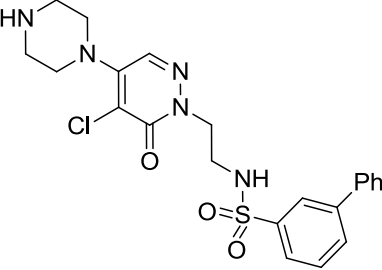
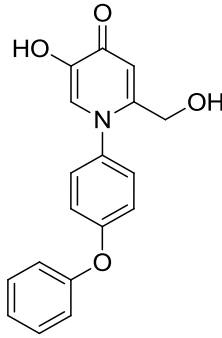
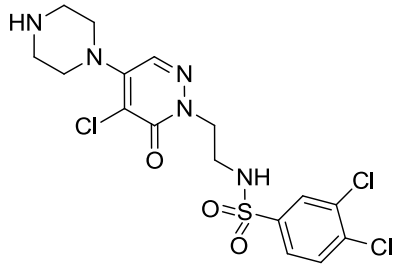
		
F-amidine	Cl-amidine	1c
		
*4b	6	*7
		
*8	*10	*19c

Table 25. Compounds discussed in the conclusions for Chapter 1. *Compounds prepared, or reprepared, as part of the investigations reported herein.

Autoimmune diseases such as RA and SLE are attractive therapeutic targets for the pharmaceutical industry because they are currently poorly managed in patients: existing therapies generally treat the symptoms rather than the disease. Disease development has a significant and progressively negative impact on the quality of a patient's life, and can eventually cause death; for example advanced SLE can lead to multiple organ failure.⁵

The biological mechanisms that underpin the development of RA and SLE are currently poorly understood.^{1,149,150} The emerging links between the dysregulation of PAD4-mediated citrullination in RA and the dysregulation of NET formation in SLE prompted the GSK Epinova DPU to identify a novel PAD4 inhibitor that could be used to elucidate the role of PAD4 in biological processes at a cellular level and in the first instance *in vivo* in an animal species; a suitable compound would be referred to as a chemical probe.

Small molecule PAD4 inhibitors previously reported in the literature include the F- and Cl-amidine (**Figure 10**) which inhibited the formation of CIA in a mouse RA model.^{65,66} Both compounds are covalent irreversible binders which is particularly undesirable for a chemical probe: alkylation of other macromolecules can take place *in vivo* which could lead to deleterious effects, and the reactive species may be scavenged by ubiquitous low MW nucleophiles such as glutathione.¹⁵¹ The Epinova DPU initially identified a suitable novel drug-like chemical probe⁵ that was a reversible PAD4 inhibitor but cardiotoxicity in rat and dog safety assessment studies halted further progression of this molecule into the clinic. This triggered a second campaign to find another novel PAD4 inhibitor chemically distinct from the previous chemical probe, to elucidate if PAD4 inhibition or the chemical structure itself caused cardiotoxicity; this work is described herein. The new campaign began with an HTS to identify a suitable starting point, or hit.

The HTS campaign utilised a FLINT assay which identified around four thousand PAD4 hits at a high single compound concentration of 10 μ M, a relatively high hit rate of 2%. The number of hits dropped to 664 when the compound set was retested at ten dilution concentrations up to 10 mM, which was a more practical hit rate to follow up of 0.03%. The reason for the high number of false positives at 10 μ M is unclear, but at high concentration there was a higher chance of interference occurring between the compound and reagents in the assay, such as **BAEE**, **OPT**, **DTT** or even ammonia itself, which might have inhibited the detection of ammonia. Full dose response curves are therefore essential for the confirmation of true hit potency. The HTS FP assay was useful for gaining confidence that the hits in the FLINT assay were true PAD4 inhibitors and for the identification of compounds that selectively inhibited the inactive

or active forms of PAD4 and may therefore exhibit different pharmacology *in vivo*. However, the pharmacological consequence of such selectivity is to date still unknown.

A cluster of nine hits (**1a-1i**, **Table 6**) with the 3-amino isoquinolin-1(2*H*)-one substructure was identified. The existence of SAR across the series gave confidence that these compounds were true PAD4 inhibitors, but only one compound, **1c**, appeared stable to redox cycling with an RRP >2000 mV. The isoquinoline hit, **4b** (**Table 9**), was subsequently identified as the PAD4-active decomposition product of this template which is at odds with the high RRP of **1c**. This suggests a requirement to consider the RRP of a whole cluster in conjunction with the SAR when dealing with an enzyme that contains active site residues that are prone to oxidation, such as PAD4.

The isoquinoline hit **4b** had moderate PAD4 potency (FLINT pIC₅₀ 5.7), high LE (0.60) and LLE (6.2), and may have been an excellent starting point for lead optimisation to find a chemical probe that selectively bound to the inactive form of PAD4 (FP pIC₅₀ w/wo Ca²⁺ <4.0/5.4). However, in the absence of an X-ray crystal structure of **4b** bound in the PAD4 active site, the vectors to build out from and improve the template's ADME properties were not obvious, and a purely iterative approach would have been required which would have potentially taken a long time. A similar situation existed with the lower potency triazolopyridazine hit **6** (FLINT pIC₅₀ 4.4, FP pIC₅₀ Ca²⁺_{w/wo} <4.0/≤4.2, **Table 11**); SAR suggested substitution at positions R¹ and R² was viable, though no improvement in PAD4 potency was achieved with a brief investigation around these points. Therefore resource was refocused on the remaining confirmed hits, the hydroxypyridinone **7** and the pyridazine **8**.

The hydroxypyridinone hit **7** had moderate PAD4 potency (FLINT pIC₅₀ 5.3) and LE (0.33), but low LLE (2.2) for a chemical probe. In contrast to the other hits, hydroxypyridinone **7** selectively bound to the active form of PAD4 (FP pIC₅₀ w/wo Ca²⁺ 5.4/<4.0) which may have exhibited *in vivo* pharmacology different to the other hits.

An in-house X-ray crystal structure of the hydroxypyridinone **7** bound in the PAD4 active site was solved; it showed that the compound adopted a new and previously unseen binding mode compared with a previously reported X-ray crystal structure of **BAA** bound in the PAD4 active site.¹ The X-ray crystal structure indicated the existence

of polar channel adjacent to the 2-methyl substituent so a polar hydroxyl substituent was introduced into this position to give compound **10** to improve LLE and potentially introduce extra hydrogen bond interactions between the headgroup and residues present in the polar channel such as Asp350 and Glu351. A substantial improvement in LLE was observed, from 2.2 to 3.8, but potency was not improved which suggested extra hydrogen bonds had not been introduced.

The hydroxypyridone headgroup of **7** was likely to be responsible for the high COMT potency (COMT pIC₅₀ of 6.9) which indicated the headgroup had high potential to cause unwanted CNS effects *in vivo*. Some confidence in the biological safety of hydroxypyridinones came from the structurally similar analogue Ferriprox^(R) which has been used since 1999 to treat thalassemia patients. However, any PAD4 inhibitor-based therapy for RA or SLE patients is likely to require administration over a long period of time, so the potential to cause CNS effects, or indeed any other side-effects, would need to be negligible. Four compounds were synthesised with alternative headgroups (**11a-11d**) to remove the potential CNS liability, but all were inactive against PAD4 so work on this template was suspended and resource refocused on the pyridazine lead **8**. The X-ray crystal structure of compound **7** also showed a network of interactions between the pyridinone carbonyl oxygen and the hydroxyl group with two Ca²⁺ ions and Asp473, Glu353, Glu411 and Asn301 residues of the PAD4 active site. The high number of interactions suggested they were likely to be key interactions for achieving PAD4 potency and therefore difficult to replace.

The pyridazine lead **8** had moderate PAD4 potency (FLINT pIC₅₀ 6.0) and LE (0.26), but low LLE (3.8) for a chemical probe. The FP assay showed compound **8** bound to both the inactive and active forms of PAD4 (FP pIC₅₀ w/wo Ca²⁺ w/wo 5.2/5.9). In the absence of an X-ray crystal structure of compound **8** bound in the PAD4 active site and in the absence of a rational binding mode from computational docking studies, iterative point changes to the structure were undertaken.

The two most chemically tractable positions to vary on the pyridazine template were identified to be the headgroup and the distal aryl ring. The SAR of an array of 16 different cyclic and acyclic headgroups (compounds **14a-14b**, **17a-17e** and **18a-18i**) with a range of calculated pK_a values suggested that the the piperazine headgroup was

close to optimal for PAD4 potency. A Topliss approach was applied to vary the distal aryl ring to explore electronic effects (π), hydrophobicity (σ) and steric effects (E_s) on PAD4 potency. With four compounds (**19a-d**), it was possible to show that electronegative and hydrophobic substituents on the distal ring were optimal for PAD4 potency: a significant increase in PAD4 potency of 16-fold relative to the original pyridazine hit **8** was achieved with compound **19c** (FLINT pIC₅₀ 7.2) with 3,4-Cl disubstitution on the distal ring. Both the LE (0.29) and LLE (3.6) were improved for **19c** relative to **8**.

The overall profile of compound **19c** was better than the original HTS hit **8** and approached the overall target profile required for a PAD4 chemical probe (**Table 26**). The first evidence for cell potency, obtained from a neutrophil citrullination assay that used human neutrophil cells, was highly encouraging for this series's potential for PAD4 inhibition *in vivo*. In conclusion this work has successfully identified a series of novel, cell potent PAD4 inhibitors, that has the potential to be developed into a chemical probe to elucidate the role of PAD4 in RA and SLE.

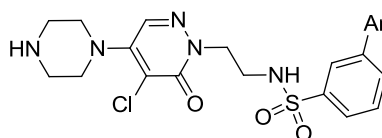
Ar =

Assay	Target	8	19c
Human PAD4 FLINT pIC ₅₀	>7.0	6.0	7.2
MW / cLogP	<500 / <5.0	474 / 2.6	542 / 3.6
LE / LLE	>0.30 / >5.0	0.26 / 3.4	0.29 / 3.6
PAD4 FP pIC ₅₀ w/w/o Ca ²⁺	Unknown	5.2 / 5.9	6.2 / 6.8
PAD4 Human Neutrophil Citrullination pIC ₅₀	>6.0	Inactive	Moderate potency

Table 26. Comparison of the PAD4 probe target profile with the profiles of compound **19c**, and the HTS hit **8**.

1.7. Future Work

Further improvements in cell potency of the pyridazine series are likely to be required before a probe can be identified from the series, and the SAR gained from this work suggests certain combinations of template modifications would make this eminently possible. The SAR from compounds **19a-d** and **20a-b** suggests that potency, LE and LLE may be increased using a combination of electronegative and hydrophobic substituents on the distal aryl ring. For example, compound **19a** showed that the introduction of an electronegative and hydrophobic Cl atom in the 4-position of the distal aryl ring improved PAD4 potency five-fold relative to compound **8**, whereas compound **19b** showed that the introduction of a 4-Me substituent lowered potency by nearly two-fold. Substitution in the 4-position may therefore be unfavourable for PAD4 potency, perhaps because the 4-substituent introduces a steric clash with the PAD4 protein, so the 3-Cl analogue **21a** should be made (**Table 27**).



Compound	Ar	MW
19c		543
21a		508
21b		508
21c		492
21d		492

Table 27. Profile of selected proposed target molecules **21a-d** which aim to match or exceed the target profile for a PAD4 chemical probe.

Furthermore, the introduction of 2-Me or 3-Me substituents (compounds **20a** and **20b** respectively) led to a three- to four-fold improvement in PAD4 potency; this suggests a 2-Cl analogue **21b** should be made. The MWs of **21a** and **21b** are still higher than the target MW, so the introduction of electronegative substituents with a lower MW, such as a 2-F or 3-F substituent (**21c** and **21d** respectively, **Table 27**), could improve cell permeability and therefore improve cell potency.

Pyridazine compounds such as **8** and **19c** exhibited >10-fold selectivity for PAD4 *versus* targets in the extended cross-assay panel (eXP panel, data not shown) that are associated with *in vivo* toxic events; this suggested the series was unlikely to be toxic, at least due to activity at these targets. The selectivity of **8** for PAD4 *versus* PAD2 was found to be >10-fold (data not shown), but the selectivity of **19c** and associated pyridazines for PAD4 *versus* PAD2 and other PAD isotypes, such as PAD1, 3 and 5, is unknown due to technical issues developing a reproducible assay to assess inhibition of these isotypes. Poor selectivity across the PAD isotypes could complicate investigations into the role of PAD4 in autoimmune diseases: the risks of toxic events occurring, such as cardiotoxicity, are increased because off-target effects are more likely with an inhibitor that has low selectivity, and it would be difficult to determine if any observed desired effects were directly a result of PAD4 inhibition itself. However, the understanding of the effects of PAD4 inhibition on therapeutically-relevant biological events in *in vivo* animal models is still at such an early stage that a cell potent PAD4 inhibitor would still be invaluable for probing the potential for a PAD4 inhibitor to treat these autoimmune diseases. Such a PAD4 inhibitor would still be anticipated to favourably modulate levels of NET formation in animal models, which could halt or reverse the SLE phenotype; a PAD4 inhibitor would also still be anticipated to reduce levels of citrullination in synovial fluid of mice in the collagen induced arthritis model which should reduce joint inflammation in RA.

1.8. General Methods

All animal studies performed as part of this research were ethically reviewed and carried out in accordance with Animals (Scientific Procedures) Act 1986 and the GSK Policy on the Care, Welfare and Treatment of Animals. Human biological samples were sourced ethically and their research use was in accord with the terms of the informed consents.

1.8.1. Analytical Methods

1.8.1.1. Nuclear Magnetic Resonance Methods

^1H , ^{13}C and ^{15}N Nuclear Magnetic Resonance (NMR) spectra were recorded using Bruker AVI or AVII NMR machines. ^1H NMR spectra were recorded at 300 MHz, 400 MHz or 600 MHz, referenced to tetramethylsilane and internally referenced to the residual solvent peak. ^{13}C NMR spectra were recorded at 101 MHz, 126 MHz or 151 MHz, referenced to the residual solvent peak. ^{15}N NMR spectra were recorded at 60 MHz referenced to the ^{15}N chemical shift of liquid ammonia.

1.8.1.2. Infra-red Spectrometry Methods

Infrared (IR) spectra were generated using a Perkin Elmer Spectrum One FT-IR spectrometer with an Attenuated Total Reflectance (ATR) accessory.

1.8.1.3. Melting Point Methods

Melting points were generated using Stuart SMP10 Bibby Scientific Ltd. melting point apparatus.

1.8.1.4. Liquid Chromatography Mass Spectrometry Methods

Method A

Liquid Chromatography Mass Spectrometry (LCMS) was conducted on an Acquity ultra performance liquid chromatography (UPLC) ethylene bridged hybrid (BEH) C18 column (50 mm x 2.1 mm in dimensions, 1.7 μm packing diameter) at 40 °C, eluting with 0.1% v/v solution of formic acid in water (Solvent A) and 0.1% volume to volume (v/v) solution of formic acid in acetonitrile (Solvent B) using the following elution

gradient 0 to 1.5 min 3 to 100% B, 1.5 to 1.9 min 100% B, 1.9 to 2.1 min 3% B at a flow rate of 1 ml/min. The ultraviolet (UV) detection was a summed signal from wavelength of 210 nm to 350 nm. The mass spectra were recorded on a Waters ZQ Mass Spectrometer using Alternate-scan Positive and Negative Electrospray.

Method B

LCMS was conducted on an Halo C18 column (150 mm x 50 mm in dimensions, 5 µm packing diameter) at ambient temperature, then elution with 0.1% v/v solution of formic acid in water (Solvent A) and 0.1% v/v solution of formic acid in acetonitrile (Solvent B) using an elution gradient of between 5 and 95% Solvent B over over 2.5 min using a flow rate of 1.8 mL/min. The UV detection was an averaged signal from wavelength of 210 nm to 350 nm. The mass spectra were recorded on an Agilent 1200-6110 Mass Spectrometer.

1.8.1.5. Mass Directed Autopreparative Chromatography Methods

Method A

Mass directed autopreparative chromatography (MDAP) involved purification by HPLC using a Sunfire C18 column (150 mm x 30 mm in dimensions, 5 µm packing diameter) at ambient temperature, then elution with 0.1% formic acid in water (Solvent A) and 0.1% formic acid in acetonitrile (Solvent B) using an elution gradient of between 0 and 100% Solvent B over 15 or 25 minutes. The UV detection was an averaged signal from wavelength of 210 nm to 350 nm. The mass spectra were recorded on a Waters ZQ Mass Spectrometer using Alternate-scan Positive and Negative Electrospray.

Method B

An Agilent 1100 Liquid Chromatograph equipped with a model G1367A autosampler, a model G1312A binary pump and an HP1100 model G1315B diode array detector was used. All separations were achieved using a Phenomenex Luna C18(2) reversed phase column (100 x 2.1 mm, 3 µm particle size). Gradient elution was carried out with the mobile phases as (Solvent A) water containing 0.1% (v/v) formic acid and (Solvent B) acetonitrile containing 0.1% (v/v) formic acid. The conditions for the gradient elution were initially 5% B, increasing linearly to 100% B over 6 minutes, remaining at 100%

B for 2.5 minutes then decreasing linearly to 5% B over 1 minute followed by an equilibration period of 2.5 minutes prior to the next injection. The flow rate was 0.5 mL/min, temperature controlled at 35 °C with an injection volume of between 2 to 5 µL. All samples were diluted with DMSO (99.9%) prior to LC/MS analysis.

1.8.1.6. Preparative HPLC Method

Preparative HPLC involved purification by HPLC using a Gilson Gemini column (150 mm x 21 mm in dimensions, 5 µm packing diameter) at a flow rate of 20 mL per minute at ambient temperature, then elution with 0.1% formic acid in water (Solvent A) and 0.1% formic acid in acetonitrile (Solvent B) with an elution gradient of between 0 and 100% Solvent B over up to 20 minutes. The UV detection wavelength was 214 nm.

1.8.1.7. High Resolution Mass Spectrometry

Positive ion mass spectra were acquired as accurate mass centroided data using a Micromass Q-ToF Ultima hybrid quadrupole time-of-flight mass spectrometer, equipped with a Z-spray (ESI) interface, over a mass range of 100 to 1100 Da, with a scan time of 0.9 s and an interscan delay of 0.1 s. Reserpine was used as the external mass calibrant ($[M+H]^+ = 609.2812$ Da). The Q-ToF Ultima mass spectrometer was operated in W reflectron mode to give a resolution (FWHM) of 16,000 to 20,000. Ionisation was achieved with a spray voltage of 3.2 kV, a cone voltage of 100 V, with cone and desolvation gas flows of 10 to 20 and 600 L/h respectively. The source block and desolvation temperatures were maintained at 120 °C and 250 °C respectively. The elemental composition was calculated using MassLynx v4.1 for the $[M+H]^+$ and the mass error quoted as ppm.

1.8.2. Assay Methods

1.8.2.1. PAD4 Biochemical Assay¹⁵²

Recombinant human PAD4 (residues 1-663) was expressed in *Escherichia coli* as an N-terminal Glutathione S-transferase (GST)-tagged fusion protein. During purification of the protein, the GST tag was removed by cleavage with PreScission Protease (GE Healthcare). Activity of the final product was determined using a Fluorescence Intensity (FLINT) NH₃ release assay.

An aliquot of 8 μ L of PAD4 enzyme was diluted to an assay concentration of 30 nM or 75 nM in assay buffer ((a): 100 mM 4-(2-hydroxyethyl)-1-piperazineethanesulfonic acid (HEPES), 50 mM NaCl, 2 mM (dithiothreitol) DTT and 0.6 mg/ml bovine serum albumin (BSA) at pH 8), or in assay buffer (b): 100 mM HEPES, 50 mM NaCl, 2 mM DTT, 7.5% glycerol and 1.5 mM 3-[(3-cholamidopropyl)dimethylammonio]-1-propanesulfonate (CHAPS) at pH 8)), and added to wells containing 0.1 μ L of various concentrations of compound or dimethyl sulfoxide (DMSO) vehicle (0.8% final) in a Greiner high volume 384-well black plate. Following 30 min pre-incubation at room temperature, the reaction was initiated by the addition of 4 μ L of substrate buffer containing 3 mM *N*- α -benzoyl-L-arginine ethyl ester (**BAEE**), 100 mM HEPES, 50 mM NaCl, 600 μ M CaCl₂ (2H₂O) and 2 mM DTT, at pH 8.0. The reaction was stopped after between 60 and 100 min with the addition of 38 μ L stop/detection buffer containing 50 mM ethylenediaminetetraacetic acid (EDTA), 2.6 mM phthalaldehyde (OPT) and 2.6 mM DTT. The assay was incubated at room temperature for 90 min before measuring fluorescence signal (λ_{ex} 405/ λ_{em} 460 or λ_{ex} 413/ λ_{em} 476) on an Envision plate reader (Perkin Elmer Life Sciences, Waltham, MA, USA).

1.8.2.2. PAD4 Fluorescence Polarisation Assay, with and without Calcium¹⁵²

For the assay in the absence of calcium, 8 μ L of PAD4 enzyme diluted to an assay concentration of 81.3 nM in assay buffer (100 mM HEPES, 50 mM NaCl, 1 mM DTT, 5% glycerol and 1 mM CHAPS at pH 8), and added to wells containing 0.1 μ L of various concentrations of compound or DMSO vehicle (0.8% final) in a Greiner low volume 384-well black plate. The reaction was initiated by the addition of 2 μ L of FP ligand buffer containing 50 nM **GSK215** (fluorescein labelled), 100 mM HEPES, 50 mM NaCl, 1 mM DTT, 5% glycerol and 1 mM CHAPS at pH 8.0. The assay was incubated at room temperature for 50 min before measuring fluorescence signal (λ_{ex} 485/ λ_{em} 530) on an Envision plate reader (Perkin Elmer Life Sciences, Waltham, MA, USA).

For the assay in the presence of calcium, 8 μ L of PAD4 enzyme diluted to an assay concentration of 337 nM in assay buffer (100 mM HEPES, 50 mM NaCl, 1 mM DTT, 5% glycerol, 1 mM CHAPS and 2.5 mM calcium chloride at pH 8), and added to wells containing 0.1 μ L of various concentrations of compound or DMSO vehicle (0.8%

final) in a Greiner low volume 384 well black plate. Following 15 min pre-incubation at room temperature, the reaction was initiated by the addition of 2 μ L of FP ligand buffer containing 50 nM **GSK215** (Fluorescein labelled), 100 mM HEPES, 50 mM NaCl, 1 mM DTT, 5% glycerol and 1 mM CHAPS at pH 8.0. The assay was incubated at room temperature for 50 min before measuring fluorescent signal (λ_{ex} 485/ λ_{em} 530) on an Envision plate reader (Perkin Elmer Life Sciences, Waltham, MA, USA).

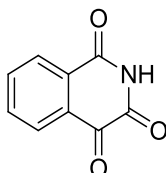
1.8.2.3. Neutrophil Citrullination Blots¹⁵³

Neutrophils were isolated from human peripheral blood using 3% dextran density gradient, followed by centrifugation in ficoll and red blood cell lysis in 0.2% w/v saline. Neutrophils were at least 90-95% pure. Cells were diluted to a density of 2×10^5 /mL and pre-treated with compounds for 30 min. Cells were then stimulated with either calcium ionophore at 1 μ M final concentration for 45 min or *Staphylococcus aureus* (ATCC 13709) at 10x MOI (multiplicity of infection) for 90 min or left unstimulated as controls. During treatment, the cells were placed in an incubator at 37 °C, 5% CO₂. At the end of stimulation cells were spun and the pellets lysed on ice with 250 μ L lysis buffer (62.5 mM Tris-HCl pH 6.8, 1% sodium dodecyl sulfate (SDS), 5% 2-mercaptoethanol) and frozen overnight. The next day, the lysates were thawed on ice, sonicated for 6 x 30 sec bursts at 4 °C in a Bioruptor (Diagenode) connected to a refrigerated bath circulator (Thermo scientific NESLAB RTE7). Lysates were separated by SDS-PAGE. Western immunoblotting was performed to detect citrullination using the polyclonal H3Cit antibody (Abcam, 5103), with Mitogen-Activated Protein Kinase (MAPK) being used as a loading control (Cell Signalling #9102). Pan-citrullination was detected using the AMC kit (Millipore 17-347). All blots were probed with an horseradish peroxidase secondary antibody and exposed on a Carestream 4000 MM PRO Image station generating digital images of the blots.

1.9. Experimental

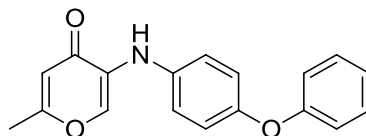
Compound purity is assumed to be $\geq 95\%$ purity by LC-MS and ^1H NMR, unless otherwise stated.

Isoquinoline-1,3,4(2H)-trione, **4b**

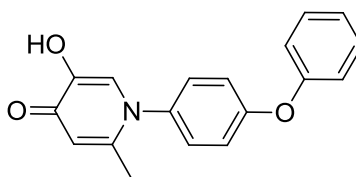


A mixture of **21** (178 mg, 1.0 mmol) in chlorobenzene (8 mL) was gently refluxed under reduced light for 30 min. The reaction mixture was concentrated under reduced pressure then cooled using iced-water to afford red crystals of **22**. The crystals were filtered then washed with dry hexane to give **22** as a red solid (160 mg, >99%). ^1H NMR (400 MHz, DMSO- d_6 , δ): 8.00 (s); LC-MS (Method B) m/z : $[\text{M} + \text{H}]^+$ 161.0, t_R 1.07 mins.

A solution of **22** (160 mg, 1.0 mmol) in DCE (5 mL) under nitrogen was treated with azidotrimethylsilane (0.199 mL, 1.5 mmol) followed by iron(III) chloride (162 mg, 1.0 mmol). The reaction mixture was stirred at room temperature for 40 min then concentrated under reduced pressure. The crude material was partitioned between water and EtOAc (10 mL each) and the organic layer separated. The aqueous layer was extracted once more with EtOAc (10 mL) and the combined organic extracts were dried (sodium sulphate) then concentrated under reduced pressure. The crude product was purified by preparative TLC (1:1 EtOAc/petroleum ether) followed by column chromatography (EtOAc/petroleum ether (0 to 100%)) to afford **4b** as a yellow solid (12 mg, 7%). ^1H NMR (400 MHz, CDCl_3 , δ): 8.57 (br. s, 1H), 8.35 (dd, $J = 8$, 1 Hz, 1H), 8.28 (dd, $J = 8$, 1 Hz, 1H), 7.95 (td, $J = 8$, 1 Hz, 1H), 7.92-7.87 (m, 1H), consistent with literature; ^{13}C NMR (151 MHz, DMSO- d_6 , δ): 175.5, 163.2, 157.4, 135.0, 134.0, 132.3, 129.8, 128.2, 126.7, consistent with literature values. ^{13}C LC-MS (Method B) m/z : $[\text{M} + \text{H}]^+$ 176.1, t_R 1.15 mins.

2-Methyl-5-((4-phenoxyphenyl)amino)-4H-pyran-4-one, 28

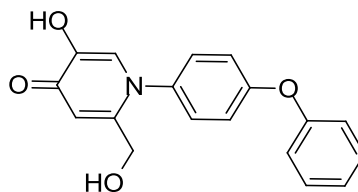
A mixture of **27** (147 mg, 0.79 mmol) and **26** (100 mg, 0.79 mmol) in hydrochloric acid (0.60 mL of a 7% v/v aqueous solution) was heated at 100 °C for 4 h by microwave irradiation, then at 110 °C for a further 2 h, then concentrated under reduced pressure. The crude product was purified by MDAP (Method A) to afford **28** as a yellow solid (22 mg, 9%). IR (cm⁻¹): 3318, 1639, 1610, 1582, 1504, 1487; ¹H NMR (400 MHz, DMSO-d₆, δ): 8.26 (s, 1H), 7.38-7.31 (m, 2H), 7.25-7.12 (m, 3H), 7.07 (t, *J* = 7 Hz, 1H), 6.98-6.91 (m, 4H), 6.29 (s, 1H), 2.29 (s, 3H); ¹³C NMR (101 MHz, DMSO-d₆, δ): 173.1, 165.2, 157.8, 149.5, 138.3 (2C), 131.6, 129.8, 122.6, 120.2, 119.2, 117.4, 110.7, 19.3; HRMS–FAB (*m/z*): [M + H]⁺ calcd for C₁₈H₁₅NO₃, 294.1125; found, 294.1127; LC-MS (Method A) *m/z*: [M + H]⁺ 294.0, *t*_R 1.13 mins; mp 127 – 129 °C.

5-Hydroxy-2-methyl-1-(4-phenoxyphenyl)pyridin-4(1H)-one, 7

A mixture of **26** (500 mg, 4.0 mmol) and **27** (734 mg, 4.0 mmol) in a Reacti-VialTM was treated with water (2 mL) followed hydrochloric acid (2.0 mL of a 6% v/v aqueous solution). The Reacti-VialTM was capped and heated at 150 °C for 16 h then allowed to stand for 48 h. The reaction mixture was concentrated under reduced pressure, then the crude material was purified by MDAP (Method A) to afford **7** as an orange-brown solid (92 mg, 8%). IR (cm⁻¹): 3300-2800 (br. s), 1639, 1576, 1503, 1486; ¹H NMR (400 MHz, DMSO-d₆, δ): 7.48-7.42 (m, 4H), 7.29 (s, 1H), 7.22 (t, *J* = 7 Hz, 1H), 7.13-7.10 (m, 2H), 7.11-7.08 (m, 2H), 6.21 (s, 1H), 1.98 (s, 3H), *the hydroxyl proton underwent exchange and was not observed*; ¹³C NMR (151 MHz, DMSO-d₆, δ): 171.2, 157.2, 155.7, 146.1, 144.8, 136.7, 130.2, 128.7, 124.3, 123.1, 119.4, 118.6, 113.2, 19.7;

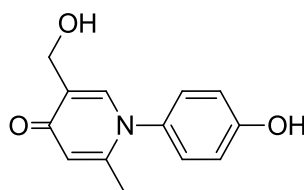
HRMS–FAB (m/z): $[M + H]^+$ calcd for $C_{18}H_{15}NO_3$, 294.1125; found, 294.1127; LC-MS (Method A) m/z : $[M + H]^+$ 294.0, t_R 0.87 mins.

5-Hydroxy-2-(hydroxymethyl)-1-(4-phenoxyphenyl)pyridin-4(1H)-one, 10



A mixture of **23** (250 mg, 1.76 mmol) and **27** (326 mg, 1.76 mmol) in a ReactiVial™ was treated with 4% aq. HCl (2.5 mL) then heated behind a blast shield at 150 °C for 16 h. The reaction mixture was concentrated then purified by MDAP (Method A) to afford **10** as an off-white solid (63 mg, 12%). 1H NMR (400 MHz, DMSO- d_6 , δ) 7.50-7.41 (m, 4H), 7.29 (s, 1H), 7.22 (t, $J = 7$ Hz, 1H), 7.15-7.03 (m, 4H), 6.39 (s, 1H), 5.41 (br. s., 1H), 4.04 (s, 2H), *the phenolic proton underwent exchange in wet deuterated solvent and was not observed*; LC-MS (Method A) m/z $[M + H]^+$ 310.3, t_R 0.81 mins.

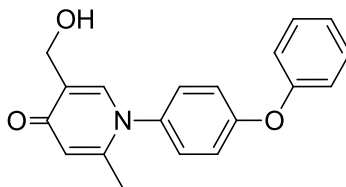
5-(Hydroxymethyl)-1-(4-hydroxyphenyl)-2-methylpyridin-4(1H)-one, 32



A heterogeneous mixture of **31** (292 mg, 1.19 mmol)¹⁵⁴ and triethylamine (458 mg, 630 μ L, 4.52 mmol) in THF (5 mL) was treated with ethyl chloroformate (431 μ L, 4.52 mmol). The reaction mixture was stirred at room temperature for 1 h then sodium tetrahydridoborate (541 mg, 14.29 mmol) in EtOH (5 mL) was added and the reaction mixture stirred at room temperature for 2 h. Aqueous HCl (1 M, 10 mL of an aqueous solution) was added and the mixture was stirred vigorously for 1 h then concentrated under reduced pressure. The mixture was partitioned between water and EtOAc (20 mL each) and the aqueous layer was then isolated. The aqueous layer was loaded onto a 20 g C18 SPE column and the column washed with water (210 mL) then crude product eluted using a solution of MeCN in water (1:9, 500 mL) to give **32** as a yellow solid (350 mg, >99%). 1H NMR (400 MHz, DMSO- d_6 , δ): 7.41 (s, 1H), 7.22 (d, $J = 9$ Hz,

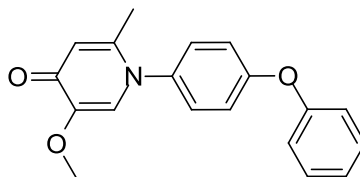
2H), 6.90 (d, $J = 9$ Hz, 2H), 6.11 (s, 1H), 4.96 (br. s., 1H), 4.29 (s, 2H), 1.96 (s, 3H), *the phenolic proton underwent exchange in wet deuterated solvent and was not observed*; LC-MS (Method A) m/z $[M + H]^+$ 232.1, t_R 0.40 mins.

5-(Hydroxymethyl)-2-methyl-1-(4-phenoxyphenyl)pyridin-4(1H)-one, 11a



A solution of **32** (100 mg, 0.43 mmol) in anhydrous DMSO (1 mL) was treated with copper (I) bromide (13 mg, 0.09 mmol), iodobenzene **33** (88 mg, 0.43 mmol), **36** (24 mg, 0.18 mmol) and caesium carbonate (282 mg, 0.87 mmol). Further DMSO (2.5 mL) was added and the reaction vessel was flushed with nitrogen then heated at 120 °C for 24 h. The crude product was purified by MDAP (Method A) to give **11a** as a brown solid (16 mg, 12%). IR (cm^{-1}) 3400-3000 (br. s), 1646, 1558, 1501, 1487, 1242, 1225; ^1H NMR (400 MHz, DMSO- d_6 , δ): 7.51-7.41 (m, 5H), 7.22 (dd, $J = 7$ Hz, 1H), 7.16-7.09 (m, 4H), 6.13 (s, 1H), 4.99 (br. s, 1H), 4.30 (s, 2H), 2.00 (s, 3H); ^{13}C NMR (126 MHz, DMSO- d_6 , δ): 176.7, 157.2, 155.8, 147.5, 137.8, 136.6, 130.2, 128.8, 128.4, 124.3, 119.4, 118.8, 115.8, 57.0, 19.8; HRMS-FAB (m/z): $[M + H]^+$ calcd for $\text{C}_{19}\text{H}_{17}\text{NO}_3$, 308.1281; found, 308.1282; LC-MS (Method A) m/z $[M + H]^+$ 308.2, t_R 0.82 mins; mp 173 – 175 °C.

5-Methoxy-2-methyl-1-(4-phenoxyphenyl)pyridin-4(1H)-one, 11b

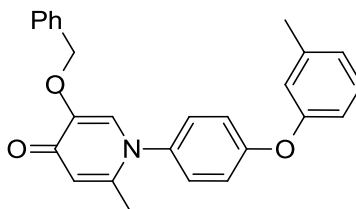


A solution of **7** (49 mg, 0.167 mmol) in DMF (5 mL) was treated with caesium carbonate (109 mg, 0.334 mmol) followed by iodomethane (10 μL , 0.167 mmol). The reaction mixture was stirred at room temperature under nitrogen for 2 h then concentrated under reduced pressure. The crude product was purified by MDAP (Method A) to afford **11b** as a brown gum (23 mg, 46%). ^1H NMR (400 MHz, CD_3OD ,

δ): 7.52 (s, 1H), 7.48-7.38 (m, 4H), 7.23 (dd, $J = 8$ Hz, 1H), 7.18-7.07 (m, 4H), 6.46 (s, 1H), 3.76 (s, 3H), 2.12 (s, 3H); LC-MS (Method A) m/z $[M + H]^+$ 308.3, t_R 0.88 mins.

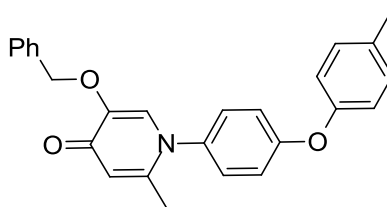
General Cyclisation Procedure 1

5-(Benzyloxy)-2-methyl-1-(4-(*m*-tolylloxy)phenyl)pyridin-4(1*H*)-one, 43b



A mixture of **42b** (230 mg, 1.16 mmol) and **38** (250 mg, 1.16 mmol) in a solution of AcOH (2.4 mL) and water (3.6 mL) was heated at 170 °C for 2 h using microwave irradiation. The reaction mixture was concentrated under reduced pressure then purified by silica chromatography (EtOAc/cyclohexane solvent system (0 to 100%) then MeOH/DCM (1:4)) to afford **43b** as a pale brown gum (383 mg, 83%). IR (cm^{-1}) 1629, 1580, 1500, 1250, 1215, 1161, 731, 696; ^1H NMR (400 MHz, DMSO- d_6 , δ): 7.49-7.26 (m, 9H), 7.14-7.01 (m, 3H), 6.95 (s, 1H), 6.89 (d, $J = 8$ Hz, 1H), 6.21 (s, 1H), 4.96 (s, 2H), 2.33 (s, 3H), 1.98 (s, 3H); ^{13}C NMR (101 MHz, DMSO- d_6 , δ): 171.8, 157.4, 155.6, 146.8, 145.6, 140.1, 137.0, 136.5, 129.9, 128.8, 128.2, 127.9, 127.8, 127.0, 125.1, 120.0, 118.5, 116.5, 116.1, 70.5, 20.9, 19.6; HRMS-FAB (m/z): $[M + H]^+$ calcd for $\text{C}_{26}\text{H}_{23}\text{NO}_3$, 398.1751; found, 398.1743; LC-MS (Method A) m/z $[M + H]^+$: 398.4, t_R 1.14 mins; mp 130 – 132 °C.

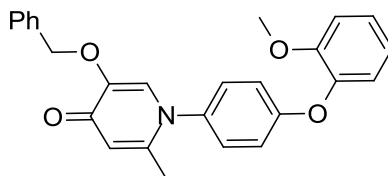
5-(Benzyloxy)-2-methyl-1-(4-(*p*-tolylloxy)phenyl)pyridin-4(1*H*)-one, 43c



Prepared from **42c** (25 mg, 0.125 mmol) and **38** (25 mg, 0.116 mmol) using general cyclisation procedure 1 to afford **43c** as a white solid (21 mg, 46%); ^1H NMR (400 MHz, DMSO- d_6 , δ): 7.49-7.30 (m, 8H), 7.27 (d, $J = 8$ Hz, 2H), 7.07 (d, $J = 9$ Hz, 2H),

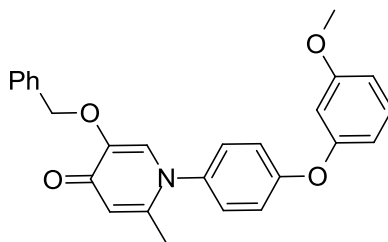
7.02 (d, $J = 9$ Hz, 2H), 6.21 (s, 1H), 4.96 (s, 2H), 2.32 (s, 3H), 1.98 (s, 3H); LC-MS (Method A) $[M + H]^+$ 398.4, t_R 1.15 mins.

5-(Benzyloxy)-1-(4-(2-methoxyphenoxy)phenyl)-2-methylpyridin-4(1H)-one, 43d

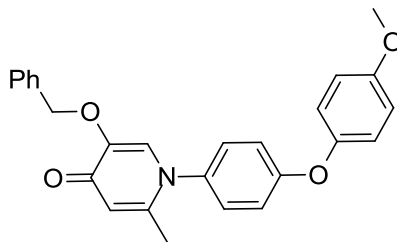


Prepared from **42d** (249 mg, 1.16 mmol) and **38** (250 mg, 1.16 mmol) using general cyclisation procedure 1 to afford **43d** as a brown gum (330 mg, 69%); 1H NMR (400 MHz, CD_3OD , δ): 7.47 (s, 1H), 7.46-7.41 (m, 2H), 7.38-7.20 (m, 6H), 7.16 (dd, $J = 8, 2$ Hz, 1H), 7.10 (dd, $J = 8, 2$ Hz, 1H), 7.01 (td, $J = 7, 2$ Hz, 1H), 6.98-6.92 (m, 2H), 6.46 (s, 1H), 5.04 (s, 2H), 3.78 (s, 3H), 2.08 (s, 3H); LC-MS m/z (Method A) $[M + H]^+$ 414.4, t_R 1.03 mins.

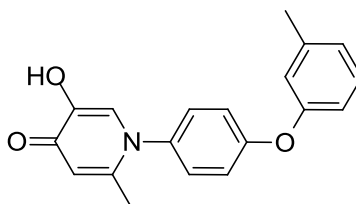
5-(Benzyloxy)-1-(4-(3-methoxyphenoxy)phenyl)-2-methylpyridin-4(1H)-one, 43e



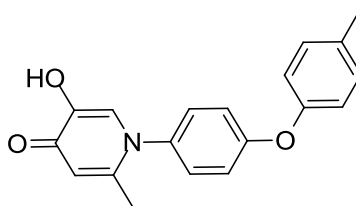
Prepared from **42e** (249 mg, 1.16 mmol) and **38** (250 mg, 1.16 mmol) using general cyclisation procedure 1 to afford **43e** as a pale brown gum (270 mg, 57%). 1H NMR (400 MHz, CD_3OD , δ): 7.51 (s, 1H), 7.49-7.43 (m, 2H), 7.40-7.29 (m, 6H), 7.17-7.11 (m, 2H), 6.83-6.77 (m, 1H), 6.69-6.62 (m, 2H), 6.49 (s, 1H), 5.08 (s, 2H), 3.81 (s, 3H), 2.12 (s, 3H); LC-MS (Method A) m/z $[M + H]^+$ 414.4, t_R 1.08 mins.

5-(Benzyloxy)-1-(4-(4-methoxyphenoxy)phenyl)-2-methylpyridin-4(1H)-one, 43h

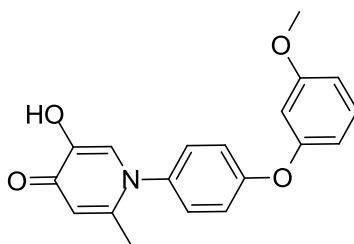
Prepared from **42h** (249 mg, 1.16 mmol) and **38** (250 mg, 1.16 mmol) using general cyclisation procedure 1 to afford **43h** as a pale brown gum (100 mg, 21%). ¹H NMR (400 MHz, DMSO-d₆, δ): 7.48-7.29 (m, 8H), 7.13-7.06 (m, 2H), 7.06-6.97 (m, 4H), 6.20 (s, 1H), 4.96 (s, 2H), 3.77 (s, 3H), 1.96 (s, 3H); LC-MS (Method A) *m/z* [M + H]⁺ 414.4, *t_R* 1.06 mins.

General Hydrogenolysis Procedure**5-Hydroxy-2-methyl-1-(4-(*m*-tolylloxy)phenyl)pyridin-4(1H)-one, 13b**

A solution of **43b** (120 mg, 0.30 mmol) in EtOH (5 mL) was passed through a catalyst cartridge (10% palladium on carbon CatCart³⁰™) using an H-cube™ hydrogenator. The resulting solution was concentrated under reduced pressure to afford **13b** as a pink solid (100 mg, >99%, *estimated yield: ~2% ethanol by wt is evident, and additional water*). IR (cm⁻¹) 3313 – 2638 (br. s), 1638, 1573, 1501; ¹H NMR (400 MHz, DMSO-d₆, δ): 7.48-7.39 (m, 2H), 7.36-7.26 (m, 2H), 7.12-7.01 (m, 3H), 6.95 (s, 1H), 6.90 (d, *J* = 8 Hz, 1H), 6.22 (s, 1H), 2.32 (s, 3H), 1.98 (s, 3H), *the hydroxyl proton underwent exchange in wet deuterated solvent and was not observed*; ¹³C NMR (101 MHz, DMSO-d₆, δ): 171.2, 157.3, 155.6, 146.1, 144.8, 140.1, 136.6, 129.9, 128.7, 125.1, 123.2, 120.0, 118.5, 116.5, 113.3, 20.9, 19.7. HRMS–FAB (*m/z*): [M + H]⁺ calcd for C₁₉H₁₇NO₃, 308.1281; found, 308.1280; LC-MS *m/z* (Method A) [M + H]⁺ 308.3, *t_R* 0.99 mins.

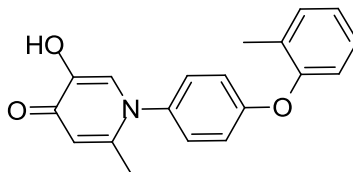
5-Hydroxy-2-methyl-1-(4-(*p*-tolylloxy)phenyl)pyridin-4(1*H*)-one, 13c

Prepared from **43c** (21 mg, 0.053 mmol) using general hydrogenolysis procedure to afford **13c** as a white solid (19 mg, >99%). IR (cm⁻¹) 3300 - 2750 (br. s), 1575, 1496, 1230, 1206, 1162, 858, 843, 823; ¹H NMR (400 MHz, DMSO-d₆, δ): 7.46-7.39 (m, 2H), 7.31-7.23 (m, 3H), 7.09-6.98 (m, 4H), 6.21 (s, 1H), 2.32 (s, 3H), 1.97 (s, 3H), *the hydroxyl proton underwent exchange in wet deuterated solvent and was not observed*; ¹³C NMR (126 MHz, DMSO-d₆, δ): 171.2, 157.7, 153.2, 146.1, 144.9, 136.4, 133.6, 130.6, 128.6, 123.2, 119.7, 118.0, 113.2, 20.3, 19.7; HRMS–FAB (*m/z*): [M + H]⁺ calcd for C₁₉H₁₇NO₃, 308.1281; found 308.1277; LC-MS (Method A) *m/z* [M + H]⁺ 308.3, *t_R* 0.97 mins; mp 230 – 232 °C.

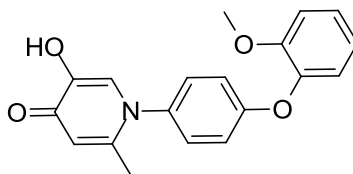
5-Hydroxy-1-(4-(3-methoxyphenoxy)phenyl)-2-methylpyridin-4(1*H*)-one, 13e

Prepared from **43e** (21 mg, 0.051 mmol) using the general hydrogenolysis procedure to afford **13e** as a white solid (10 mg, 61%). ¹H NMR (400 MHz, DMSO-d₆, δ): 7.48-7.42 (m, 2H), 7.35 (t, *J* = 8 Hz, 1H), 7.30 (s, 1H), 7.15-7.08 (m, 2H), 6.80 (d, *J* = 8 Hz, 1H), 6.72-6.61 (m, 2H), 6.21 (s, 1H), 3.76 (s, 3H), 1.98 (s, 3H), *the hydroxyl proton underwent exchange in wet deuterated solvent and was not observed*; LC-MS (Method A) *m/z* [M + H]⁺ 324.3, *t_R* 0.89 mins.

General Cyclisation Procedure 2

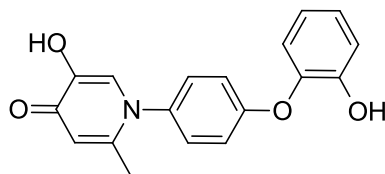
5-Hydroxy-2-methyl-1-(4-(*o*-tolylloxy)phenyl)pyridin-4(1*H*)-one, **13a**

A mixture of **42a** (79 mg, 0.40 mmol) and **26** (50 mg, 0.40 mmol) in HCl (6% solution v/v in water, 2 mL) and EtOH (1.5 mL) was heated at 170 °C by microwave irradiation for 4 h (*care: 20 bar pressure recorded*). The reaction mixture was filtered, then purified by MDAP (Method A) to afford **13a** as a purple solid (16 mg, 13%). ¹H NMR (400 MHz, CD₃OD, δ): 7.44 (s, 1H), 7.40-7.31 (m, 3H), 7.27 (t, *J* = 8 Hz, 1H), 7.18 (t, *J* = 8 Hz, 1H), 7.07-6.98 (m, 3H), 6.46 (s, 1H), 2.23 (s, 3H), 2.11 (s, 3H), *the hydroxyl proton underwent exchange and was not observed*; LC-MS (Method A) *m/z* [M + H]⁺ 308.3, *t_R* 0.96 mins.

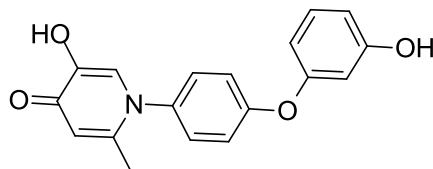
5-Hydroxy-1-(4-(2-methoxyphenoxy)phenyl)-2-methylpyridin-4(1*H*)-one, **13d**

Prepared from **42d** (171 mg, 0.79 mmol) and **26** (100 mg, 0.79 mmol) using the general cyclisation procedure 2 to afford **13d** as a white solid (16 mg, 6%). ¹H NMR (400 MHz, CD₃OD, δ): 7.41 (s, 1H), 7.33-7.21 (m, 3H), 7.19-7.08 (m, 2H), 7.05-6.92 (m, 3H), 6.44 (s, 1H), 3.78 (s, 3H), 2.08 (s, 3H), *the hydroxyl proton underwent exchange and was not observed*; LC-MS (Method A) *m/z* [M + H]⁺ 324.3, *t_R* 0.84 mins.

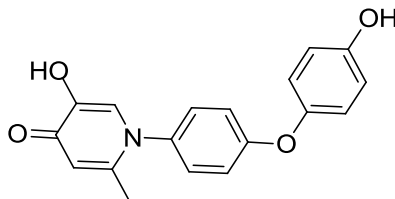
General One Pot Debenzylation and Demethylation Procedure

5-Hydroxy-1-(4-(2-hydroxyphenoxy)phenyl)-2-methylpyridin-4(1H)-one, **13f**

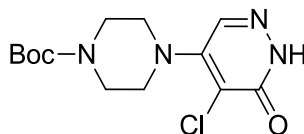
A rapidly stirred solution of **43d** (80 mg, 0.193 mmol) in anhydrous DCM (5 mL) under nitrogen was cooled over 15 min using an ice/water bath. The solution was treated dropwise with BBr_3 (3 mL, 1 M solution in DCM, 3.00 mmol) and the mixture stirred for 15 min then allowed to warm to room temperature over 2 h. The reaction mixture was treated with MeOH (3 mL) then concentrated three times, then crude product purified by MDAP (Method A) to afford **13f** as a white solid (33 mg, 55%). ^1H NMR (400 MHz, DMSO-d_6 , δ): 9.64 (br. s, 1H), 7.40-7.33 (m, 2H), 7.26 (s, 1H), 7.15-7.04 (m, 2H), 7.01 (dd, $J = 8$, 2 Hz, 1H), 6.97-6.89 (m, 2H), 6.87 (dd, $J = 8$, 2 Hz, 1H), 6.20 (s, 1H), 1.96 (s, 3H), *a phenol proton underwent exchange in wet deuterated solvent and was not observed*; LC-MS (Method A) m/z $[\text{M} + \text{H}]^+$ 310.2, t_R 0.75 mins.

5-Hydroxy-1-(4-(3-hydroxyphenoxy)phenyl)-2-methylpyridin-4(1H)-one, **13g**

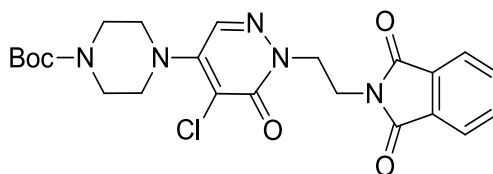
Prepared from **43e** (100 mg, 0.24 mmol) using the general one pot debenzylation and demethylation procedure to give **13g** as a white solid (30 mg, 40%). ^1H NMR (400 MHz, DMSO-d_6 , δ) 9.68 (br. s, 1H), 7.48-7.40 (m, 2H), 7.29 (s, 1H), 7.21 (t, $J = 8$ Hz, 1H), 7.14-7.06 (m, 2H), 6.61 (dd, $J = 8$, 2 Hz, 1H), 6.51 (dd, $J = 8$, 2 Hz, 1H), 6.48-6.44 (m, 1H), 6.21 (s, 1H), 1.98 (s, 3H), *a phenol proton underwent exchange and was not observed in wet deuterated solvent*; LC-MS (Method A) m/z $[\text{M} + \text{H}]^+$ 310.2, t_R 0.76 mins.

5-Hydroxy-1-(4-(4-hydroxyphenoxy)phenyl)-2-methylpyridin-4(1H)-one, 13h

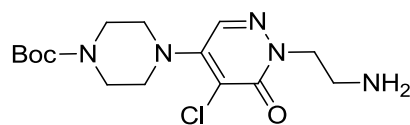
Prepared from **43h** (90 mg, 0.22 mmol) using the general one pot debenzoylation and demethylation procedure to give **13h** as a white solid (44 mg, 65%). ¹H NMR (400 MHz, DMSO-d₆, δ): 9.45 (br. s, 1H), 7.43-7.34 (m, 2H), 7.26 (s, 1H), 7.03-6.93 (m, 4H), 6.87-6.78 (m, 2H), 6.20 (s, 1H), 1.96 (s, 3H), *a phenol proton underwent exchange in wet deuterated solvent and was not observed*; LC-MS (Method A) *m/z* [M + H]⁺ 310.2, *t_R* 0.70 mins.

General Nucleophilic Substitution Procedure 1***tert*-Butyl 4-(5-chloro-6-oxo-1,6-dihydropyridazin-4-yl)piperazine-1-carboxylate, 46**

A solution of **44** (10.0 g, 60.6 mmol) and **45** (11.3 g, 60.6 mmol) in EtOH (80 mL) was treated with DIPEA (10.6 mL, 60.6 mmol) and the reaction mixture refluxed for 20 h then left to cool to room temperature for 36 h. The resultant solid was filtered under reduced pressure and washed with EtOH then dried under reduced pressure to give **46** as a pale yellow solid (19.3 g, >99%). IR (cm⁻¹) 3108, 2973, 2925, 2849, 1685, 1627, 1592; ¹H NMR (400 MHz, DMSO-d₆, δ): 12.95 (br. s, 1H), 7.86 (s, 1H), 3.50-3.40 (m, 4H), 3.39-3.33 (m, 4H), 1.42 (s, 9H); ¹³C NMR (101 MHz, DMSO-d₆, δ): 158.5, 153.7, 148.2, 132.2, 115.2, 79.2, 48.3, 42.9, 28.0; HRMS-FAB (*m/z*): [M + H]⁺ calcd for C₁₃H₁₉ClN₄O₃, 315.1216; found, 315.1218; LC-MS (Method A) *m/z* [M + H]⁺ 315.2, *t_R* 0.81 mins; mp 216 – 219 °C; *compound 46 has been reported in the literature, but without preparation details or characterising data.*¹⁴⁰

***tert*-Butyl 4-(5-chloro-1-(2-(1,3-dioxoisindolin-2-yl)ethyl)-6-oxo-1,6-dihydropyridazin-4-yl)piperazine-1-carboxylate, 48**

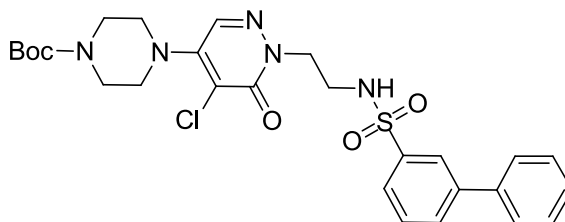
A solution of **46** (5.0 g, 15.9 mmol) in DMF (50 mL) was treated with potassium carbonate (2.20 g, 15.9 mmol) followed by **47** (4.44 g, 17.5 mmol) and the reaction mixture stirred under nitrogen at room temperature for 16 h. The reaction mixture was concentrated under reduced pressure then partitioned between water and EtOAc (200 mL each). The organic layer was isolated and the aqueous layer re-extracted with EtOAc (2 x 200 mL). The combined organic extracts were dried over magnesium sulphate then concentrated under reduced pressure to give crude **48**. The crude product was purified using a silica column (0 to 70% cyclohexane/EtOAc) to give **48** as a white solid (5.76 g, 74%). IR (cm⁻¹) 3100, 2975, 1773, 1714, 1674, 1634, 1590, 1501; ¹H NMR (400 MHz, DMSO-d₆, δ): 7.88-7.81 (m, 4H), 7.80 (s, 1H), 4.28 (t, *J* = 6 Hz, 2H), 3.94 (t, *J* = 6 Hz, 2H), 3.50-3.36 (m, 4H), 3.38-3.31 (m, 4H), 1.41 (s, 9H); ¹³C NMR (101 MHz, DMSO-d₆, δ): 168.3, 158.1, 154.4, 148.1, 135.1, 132.4, 132.1, 123.7, 115.5, 79.8, 50.5, 48.9, 43.5, 36.7, 28.6; HRMS–FAB (*m/z*): [M + H]⁺ calcd for C₂₃H₂₆ClN₅O₅, 488.1695; found, 488.1680; LC-MS (Method A) *m/z* [M + H]⁺ 488.3, *t_R* 1.05 mins; mp 179 – 181 °C.

***tert*-Butyl 4-(1-(2-aminoethyl)-5-chloro-6-oxo-1,6-dihydropyridazin-4-yl)piperazine-1-carboxylate, 49**

A solution of **48** (820 mg, 1.68 mmol) in EtOH (20 mL) and 1,4-dioxane (10 mL) was treated with methanamine (10 mL of a 33% solution by weight in EtOH, 80.0 mmol). The reaction mixture was stirred at room temperature for 16 h then concentrated under reduced pressure. The crude material was partitioned between EtOAc and water (100 mL each) and the organic layer isolated. The aqueous layer was re-extracted with

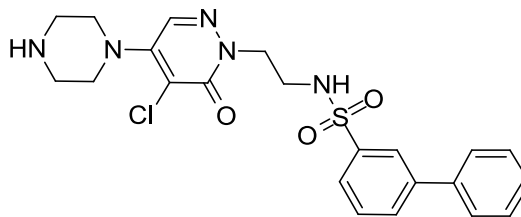
EtOAc (2 x 100 mL) and the combined organic extracts passed through a hydrophobic frit then concentrated under reduced pressure to afford **49** as a colourless gum 511.15 (650 mg, 92% at 85% purity by LCMS and NMR). IR (cm⁻¹) 3399, 3102, 3069, 2977, 2917, 2859, 1682, 1624; ¹H NMR (400 MHz, DMSO-d₆ δ) 7.90 (s, 1H), 4.02 (t, *J* = 7 Hz, 2H), 3.54-3.39 (m, 4H), 3.39-3.26 (m, 4H), 2.83 (t, *J* = 7 Hz, 2H), 1.51 (br. s, 2H), 1.42 (s, 9H); ¹³C NMR (101 MHz, DMSO-d₆, δ): 157.4, 153.7, 147.5, 131.4, 115.5, 79.2, 54.4, 48.3, 43.3, 40.2, 28.0; HRMS–FAB (*m/z*): [M + H]⁺ calcd for C₁₅H₂₄ClN₅O₃, 358.1640; found, 358.1640; LC-MS (Method A) *m/z* [M + H]⁺ 358.1, *t_R* 0.64 mins; mp 148 - 149 °C.

***tert*-Butyl 4-(1-(2-([1,1'-biphenyl]-3-ylsulfonamido)ethyl)-5-chloro-6-oxo-1,6-dihydropyridazin-4-yl)piperazine-1-carboxylate, 51**

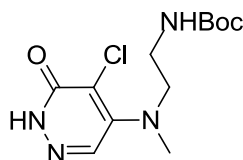


A solution of **49** (150 mg, 0.42 mmol) in DCM (2 mL) was treated with pyridine (0.068 mL) and **50** (127 mg, 0.50 mmol). The reaction mixture was stirred at room temperature for 16 h then concentrated under reduced pressure. The crude material was purified by MDAP (Method A), to give **51** as a white solid (120 mg, 50%). IR (cm⁻¹) 3189, 1691, 1622, 1593, 1412; ¹H NMR (400 MHz, DMSO-d₆, δ): 8.00 (s, 1H), 7.93 (t, *J* = 8 Hz, 1H), 7.90-7.81 (m, 2H), 7.77-7.62 (m, 4H), 7.57-7.49 (m, 2H), 7.45 (d, *J* = 8 Hz, 1H), 4.08 (t, *J* = 6 Hz, 2H), 3.48-3.37 (m, 4H), 3.31-3.26 (m, 4H), 3.23-3.12 (m, 2H), 1.42 (s, 9H); ¹³C NMR (101 MHz, DMSO-d₆, δ): 157.3, 153.7, 147.4, 141.1, 141.0, 138.5, 131.6, 130.6, 129.9, 129.1, 128.2, 126.9, 125.3, 124.3, 115.0, 79.2, 51.1, 48.2, 43.2, 40.4, 28.0; HRMS–FAB (*m/z*): [M + H]⁺ calcd for C₂₇H₃₂ClN₅O₅S, 574.1886; found, 574.1861; LC-MS (Method A) *m/z* [M + H]⁺ 574.1, *t_R* 1.18 mins; mp 101 – 104 °C.

General Boc Deprotection Procedure 1

N*-(2-(5-Chloro-6-oxo-4-(piperazin-1-yl)pyridazin-1(6*H*)-yl)ethyl)-[1,1'-biphenyl]-3-sulfonamide, **8*

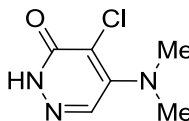
A solution of **51** (120 mg, 0.21 mmol) in DCM (2 mL) was treated with TFA (2 mL) and stirred at room temperature for 2 h. The mixture was concentrated under reduced pressure and dissolved in MeOH then loaded onto a 1 g SCX-2 SPE column. The column was washed with MeOH (~9 mL) then product eluted using a solution of ammonia in MeOH (2 M, ~9 mL) to give **8** as a white solid (67 mg, 81%). IR (cm⁻¹) 3027, 2953, 2813, 2470, 1642, 1593; ¹H NMR (600 MHz, DMSO-d₆, δ): 8.00 (t, *J* = 2 Hz, 1H), 7.93 (d, *J* = 8 Hz, 1H), 7.84 (br. s, 1H), 7.80 (s, 1H), 7.74 (d, *J* = 8 Hz, 1H), 7.73-7.70 (m, 2H), 7.68-7.64 (m, 1H), 7.52 (t, *J* = 8 Hz, 2H), 7.46-7.42 (m, 1H), 4.06 (t, *J* = 6 Hz, 2H), 3.27-3.23 (m, 4H), 3.16 (t, *J* = 6 Hz, 2H), 2.79-2.73 (m, 4H), *the basic piperazine proton underwent exchange in wet deuterated solvent and was not observed*; ¹³C NMR (151 MHz, DMSO-d₆, δ): 157.4, 147.6, 141.1, 141.0, 138.5, 131.5, 130.5, 129.9, 129.1, 128.2, 126.8, 125.2, 124.3, 113.8, 51.0, 49.8, 45.6, 40.5; HRMS–FAB (*m/z*): [M + H]⁺ calcd for C₂₂H₂₄N₅O₃SCl, 474.1367; found, 474.1363; LC-MS (Method A) *m/z* [M + H]⁺ 474.0, *t_R* 0.72 mins; mp 95 – 97 °C.

tert*-Butyl-(2-((5-chloro-6-oxo-1,6-dihydropyridazin-4-yl)(methyl)amino)ethyl)carbamate, **53a*

Prepared from **52a** (2.1 g, 12.1 mmol) and **44** (2.0 g, 12.1 mmol) using the general nucleophilic substitution procedure 1 to afford **53a** as a yellow solid (1.4 g, 39%). ¹H NMR (400 MHz, DMSO-d₆, δ) 12.66 (br. s, 1H), 7.77 (s, 1H), 6.89 (br. s, 1H), 3.50 (t, *J*

= 6 Hz, 2H), 3.21-3.10 (m, 2H), 3.06 (s, 3H), 1.33 (s, 9H). LC-MS (Method A) m/z [$M + H$]⁺ 303.1, t_R 0.67 mins.

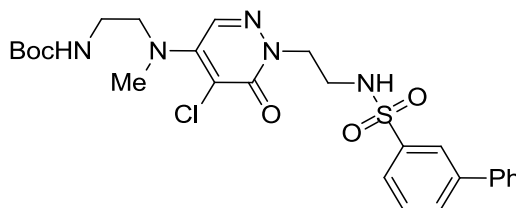
4-Chloro-5-(dimethylamino)pyridazin-3(2H)-one, **53b**



Prepared from **52b** (3.0 mL of a 2 M solution in THF, 6.0 mmol) and **44** (1.0 g, 6.1 mmol) using the general nucleophilic substitution procedure 1 to afford **53b** as a clear colourless gum (430 mg, 41%). ¹H NMR (400 MHz, DMSO-*d*₆, δ): 12.69 (br. s, 1H), 7.81 (s, 1H), 3.06 (s, 6H). LC-MS (Method A) m/z [$M + H$]⁺ 174.0, t_R 0.45 mins.

General Alkylation, Phthalimido-group Removal and Sulfonylation Procedure

tert-Butyl (2-((1-(2-([1,1'-biphenyl]-3-ylsulfonamido)ethyl)-5-chloro-6-oxo-1,6-dihydropyridazin-4-yl)(methyl)amino)ethyl)carbamate, **56**



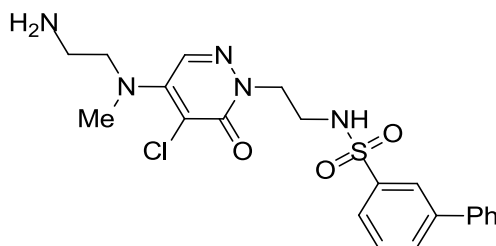
A solution of **47** (420 mg, 1.65 mmol) in DMF (5 mL) and **53a** (500 mg, 1.65 mmol) was treated with potassium carbonate (228 mg, 1.65 mmol). The reaction mixture was stirred at room temperature for 16 h and concentrated under reduced pressure then partitioned between water and EtOAc (100 ml). The organic layer was isolated then the aqueous layer re-extracted with EtOAc (2 x 100 ml). The combined organic extracts were passed through a hydrophobic frit then concentrated under reduced pressure to give crude **54a** as a pale yellow gum (910 mg at 42% purity by LCMS). LC-MS (Method A) m/z [$M+H$]⁺ 476.1, t_R 0.95 mins.

Crude **54a** (910 mg) was treated with methanamine (40 mL of a 33% solution by weight in EtOH) and the reaction mixture stirred at room temperature for 72 h then concentrated under reduced pressure to give crude **55a** as a pale yellow gum. The gum was dissolved in MeOH (~5 mL) and loaded onto a 20 g SCX-II SPE column. The

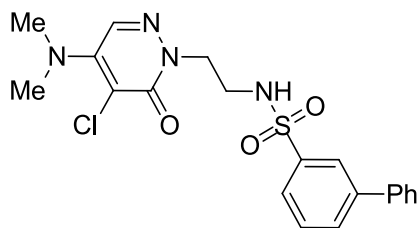
column was washed with MeOH (100 mL) then product eluted with ammonia in MeOH (2 M, 100 mL). Crude **55a** was isolated as a pale yellow gum (720 mg, 81% purity by LCMS). LC-MS (Method A) m/z $[M + H]^+$ 346.1, t_R 0.54 mins.

A solution of **55a** (310 mg) in DMF (2 mL) was treated with **50** (272 mg, 1.08 mmol) and pyridine (0.145 mL, 1.79 mmol). The reaction mixture was stirred at room temperature for 16 h and concentrated under reduced pressure then purified by MDAP (Method A) to give **56** (122 mg, 31% yield over three steps) as a white solid. 1H NMR (400 MHz, DMSO- d_6 , δ): 8.02 (s, 1H), 7.94 (d, $J = 7$ Hz, 1H), 7.86 (br. s, 1H), 7.78-7.64 (m, 5H), 7.57-7.49 (m, 2H), 7.43 (t, $J = 7$ Hz, 1H), 6.84 (br. s, 1H), 4.03 (t, $J = 7$ Hz, 2H), 3.46 (t, $J = 6$ Hz, 2H), 3.19-3.08 (m, 4H), 3.03 (s, 3H), 1.28 (s, 9H); LC-MS (Method A) m/z $[M + H]^+$ 562.1, t_R 1.10 mins.

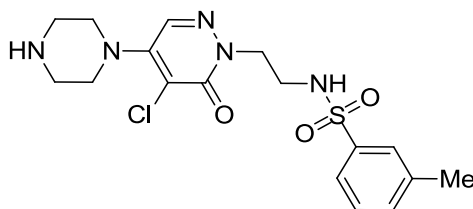
N*-(2-(4-((2-Aminoethyl)(methyl)amino)-5-chloro-6-oxopyridazin-1(6*H*)-yl)ethyl)-[1,1'-biphenyl]-3-sulfonamide, **14a*



Prepared from **56** (122 mg, 0.22 mmol) using the general Boc deprotection procedure 1, followed by an additional azeotrope step with cyclohexane to afford **14a** as a cream coloured solid (105 mg, >99%, *estimated 3% cyclohexane present by wt, plus additional water*). 1H NMR (400 MHz, DMSO- d_6 , δ): 8.01 (s, 1H), 7.93 (d, $J = 8$ Hz, 1H), 7.82 (s, 1H), 7.78-7.62 (m, 4H), 7.52 (t, $J = 8$ Hz, 2H), 7.45 (t, $J = 8$ Hz, 1H), 4.04 (t, $J = 6$ Hz, 2H), 3.62 (t, $J = 6$ Hz, 1H), 3.37 (t, $J = 7$ Hz, 2H), 3.15 (t, $J = 6$ Hz, 2H), 3.06 (s, 3H), 2.75 (t, $J = 7$ Hz, 2H), *the sulfonamide proton and an ethylamine proton underwent exchange in wet deuterated solvent and were not visible*. LC-MS (Method A) m/z $[M + H]^+$ 462.0, t_R 0.71 mins.

***N*-(2-(5-Chloro-4-(dimethylamino)-6-oxopyridazin-1(6*H*)-yl)ethyl)-[1,1'-biphenyl]-3-sulfonamide, 14b**

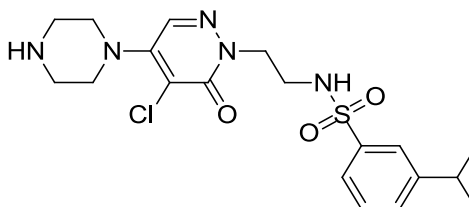
Prepared from **53b** (430 mg, 2.48 mmol) using the general alkylation, phthalimido-group removal and sulfonylation procedure to afford **14b** as a white solid (105 mg, 10% over three steps). ¹H NMR (400 MHz, DMSO-d₆, δ): 8.00 (s, 1H), 7.93 (d, *J* = 8 Hz, 1H), 7.83 (t, *J* = 6 Hz, 1H), 7.79-7.62 (m, 5H), 7.56-7.49 (m, 2H), 7.44 (t, *J* = 7 Hz, 1H), 4.05 (t, *J* = 6 Hz, 2H), 3.21-3.11 (m, 2H), 2.50 (s, 6H); LC-MS (Method A) *m/z* [M + H]⁺ 433.0, *t_R* 1.00 mins.

General Sulfonylation and Deprotection Procedure***N*-(2-(5-Chloro-6-oxo-4-(piperazin-1-yl)pyridazin-1(6*H*)-yl)ethyl)-3-methylbenzenesulfonamide, 15b**

A solution of **49** (418 mg, 1.17 mmol) in DCM (20 mL) was treated with pyridine (0.2 mL, 2.34 mmol) then **57b** (267 mg, 1.40 mmol) was added. The mixture was stirred at 25 °C for 58 h then partitioned between DCM (50 mL) and brine (50 mL). The organic layer was isolated then dried (sodium sulphate) then concentrated under reduced pressure to afford the crude intermediate as a yellow oil. The yellow oil was purified by column chromatography (1:1 hexane/EtOAc) to afford *tert*-butyl 4-(5-chloro-1-(2-(3-methylphenylsulfonamido)ethyl)-6-oxo-1,6-dihydropyridazin-4-yl)piperazine-1-carboxylate (265 mg, 44%). LC-MS (Method B) *m/z* [M+H]⁺ 512.1, *t_R* 1.56 min.

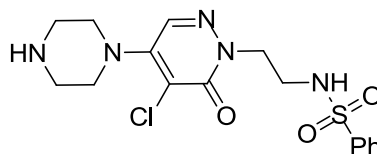
tert-Butyl 4-(5-chloro-1-(2-(3-methylphenylsulfonamido)ethyl)-6-oxo-1,6-dihydropyridazin-4-yl)piperazine-1-carboxylate (265 mg, 0.52 mmol) was treated with hydrochloric acid (15 ml of a 4 M solution in DCM). The reaction mixture was stirred at 25 °C under nitrogen overnight then concentrated under reduced pressure. The solid was washed with DCM (15 ml) followed by MeCN (1 ml) and ether (0.5 ml) then purified by MDAP (Method B) to afford **15b** (80 mg, 39%, 14% over 2 steps). ¹H NMR (400 MHz, CD₃OD, δ) 7.89 (s, 1H), 7.63–7.58 (m, 2H), 7.43–7.42 (m, 2H), 4.22 (t, *J* = 6 Hz, 2H), 3.79–3.64 (m, 4H), 3.45–3.30 (m, 6H), 2.43 (s, 3H), *the piperazine proton and sulfonamide proton underwent exchange and were not observed*. LC-MS (Method B) *m/z* [M + H]⁺ 412.1, *t_R* 1.10 mins.

***N*-(2-(5-Chloro-6-oxo-4-(piperazin-1-yl)pyridazin-1(6*H*)-yl)ethyl)-3-*iso*-propylbenzenesulfonamide, 15a**



Prepared from **49** (253 mg, 0.71 mmol) and **57a** (186 mg, 0.85 mmol) using the general sulfonylation and deprotection procedure to afford **15a** (40 mg, 13% over two steps). IR (cm⁻¹) 3500-2300 (m), 1601, 1422, 1319, 1141, 864, 771, 749, 692; ¹H NMR (400 MHz, CD₃OD, δ): 7.92 (s, 1H), 7.70 (s, 1H), 7.62 (d, *J* = 8 Hz, 1H), 7.56-7.43 (m, 2H), 4.24 (t, *J* = 6 Hz, 2H), 3.76-3.65 (m, 4H), 3.45-3.38 (m, 4H), 3.30 (t, *J* = 6 Hz, 2H), 3.00 (septet, *J* = 7 Hz, 1H), 1.30 (d, *J* = 7 Hz, 6H), *the piperazine and sulfonamide protons underwent exchange and were not observed*; ¹³C NMR (126 MHz, DMSO-d₆, δ): 157.2, 149.6, 146.9, 140.3, 131.7, 130.5, 129.2, 124.0, 123.9, 115.8, 51.1, 45.5, 42.7, 40.4, 33.2, 23.6; LC-MS (Method B) *m/z* [M + H]⁺ 440.0, *t_R* 1.24 mins; mp 195 – 197 °C.

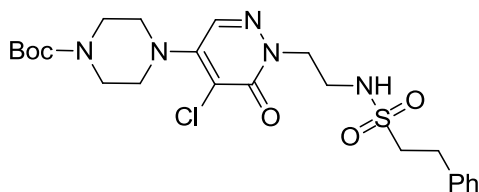
N*-2-(5-Chloro-6-oxo-4-(piperazin-1-yl)pyridazin-1(6*H*)-yl)ethylbenzenesulfonamide, **15c*



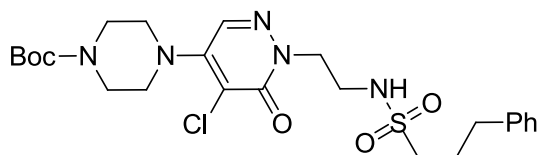
A solution of **49** (150 mg, 0.42 mmol) and **57c** (0.065 mL, 0.50 mmol) in DCM (2 mL) was treated with pyridine (0.068 mL, 0.84 mmol). The reaction mixture was stirred under nitrogen for 16 h then concentrated under reduced pressure and purified by MDAP (Method A) to give *tert*-butyl 4-(5-chloro-6-oxo-1-(2-(phenylsulfonamido)ethyl)-1,6-dihydropyridazin-4-yl)piperazine-1-carboxylate as a white solid (160 mg, 77%). LC-MS (Method A) m/z $[M + H]^+$ 498.2, t_R 1.02 mins.

tert-Butyl 4-(5-chloro-6-oxo-1-(2-(phenylsulfonamido)ethyl)-1,6-dihydropyridazin-4-yl)piperazine-1-carboxylate (160 mg, 0.3 mmol) was dissolved in DCM (2 mL) and treated with TFA (2 mL) and stirred at room temperature for 2 h then concentrated under reduced pressure. The mixture was concentrated under reduced pressure and loaded in MeOH (~2 mL) onto a 1 g SCX-II SPE column. The column was washed with MeOH (~9 mL) then product eluted with ammonia in MeOH (2 M, ~9 mL). Ammonia/MeOH fractions were concentrated under reduced pressure to give **15c** as a white solid (99 mg, 59% over two steps). 1H NMR (400 MHz, DMSO- d_6 , δ): 7.83 (s, 1H), 7.78-7.70 (m, 3H), 7.67-7.50 (m, 3H), 4.04 (t, $J = 6$ Hz, 2H), 3.29-3.28 (m, 4H, obscured by residual solvent peak), 3.14-3.08 (m, 2H), 2.82-2.77 (m, 4H), the sulfonamide proton underwent exchange in wet deuterated solvent and was not observed; LC-MS (Method A) m/z $[M + H]^+$ 398.1, t_R 0.46 mins.

General Sulfonylation Procedure 1

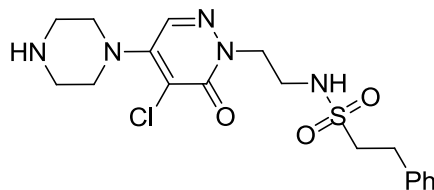
***tert*-Butyl 4-(5-chloro-6-oxo-1-(2-(2-phenylethylsulfonamido)ethyl)-1,6-dihydropyridazin-4-yl)piperazine-1-carboxylate, 59a**

A solution of **49** (670 mg, 1.87 mmol) in DCM (30 mL) was treated with DMAP (46 mg, 0.37 mmol) followed by **58a** (460 mg, 2.25 mmol). The reaction mixture was stirred at 25 °C under nitrogen for 24 h, then water, DCM and brine were added (50 mL each). The organic layer was isolated and washed with brine (50 mL) then dried (sodium sulphate) and concentrated under reduced pressure. The crude product was purified by silica chromatography using a hexane/EtOAc (1:1) to afford **59a** (320 mg, 33%). ¹H NMR (300 MHz, CDCl₃, δ): 7.59 (s, 1H), 7.40-7.10 (m, 5H), 4.28 (t, *J* = 4 Hz, 2H), 3.64-3.49 (m, 6H), 3.40–3.26 (m, 6H), 3.13–3.03 (m, 2H), 1.49 (s, 9H), *the sulfonamide proton underwent exchange in the wet deuterated solvent and was not observed*. LC-MS (Method B) *m/z* [M + H]⁺ 526.1, *t_R* 1.57 mins.

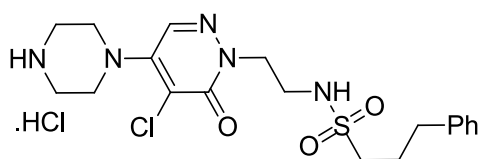
***tert*-Butyl 4-(5-chloro-6-oxo-1-(2-(3-phenylpropylsulfonamido)ethyl)-1,6-dihydropyridazin-4-yl)piperazine-1-carboxylate, 59b**

Prepared from **58b** (233 mg, 1.1 mmol) and **49** (318 mg, 0.89 mmol) using the general sulfonylation procedure 1 to afford **59b** (130 mg, 27%). ¹H NMR (400 MHz, CDCl₃, δ): 7.61 (s, 1H), 7.33–7.18 (m, 6H), 4.33 (t, *J* = 6 Hz, 2H), 3.65–3.50 (m, 6H), 3.43–3.33 (m, 4H), 3.00 (t, *J* = 6.0 Hz, 2H), 2.75 (t, *J* = 6 Hz, 2H), 2.18–2.06 (m, 2H), 1.50 (s, 9H). LC-MS (Method B) *m/z* [M + H]⁺ 540.0, *t_R* 1.61 mins.

General Boc Deprotection Procedure 2

***N*-(2-(5-Chloro-6-oxo-4-(piperazin-1-yl)pyridazin-1(6*H*)-yl)ethyl)-2-phenylethanesulfonamide, 16a**

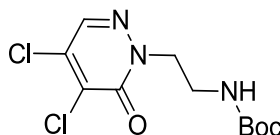
A solution of **59a** (320 mg, 0.61 mmol) in EtOAc (15 mL) that had been saturated with HCl gas was stirred at 25 °C under nitrogen overnight. The mixture was filtered and the solid washed with EtOAc (5 x 1 mL) then purified by MDAP (Method B) to afford **16a** (150 mg, 58%). IR (cm⁻¹) 3348-2400 (m), 1600, 1419, 1313, 1140, 1005, 747, 721, 696; ¹H NMR (400 MHz, CD₃OD, δ): 8.31 (br. s, 1H), 7.93 (s, 1H), 7.36-7.29 (m, 2H), 7.29-7.20 (m, 3H), 4.30 (t, *J* = 6 Hz, 2H), 3.69-3.60 (m, 4H), 3.52 (t, *J* = 6 Hz, 2H), 3.40-3.34 (m, 4H), 3.30-3.22 (m, 2H), 3.07-2.96 (m, 2H), *the sulfonamide proton underwent exchange and was not observed*; ¹³C NMR (126 MHz, DMSO-d₆, δ): 157.4, 147.1, 138.5, 131.7, 128.5, 128.4, 126.4, 115.6, 52.3, 51.8, 46.3, 43.3, 40.3, 29.2; HRMS–FAB (*m/z*): [M + H]⁺ calcd for C₁₈H₂₄ClN₅O₃S, 426.1361; found, 426.1354; LC-MS (Method B) *m/z* [M + H]⁺ 426.0, *t*_R 1.13 mins; mp 136 – 138 °C.

***N*-(2-(5-Chloro-6-oxo-4-(piperazin-1-yl)pyridazin-1(6*H*)-yl)ethyl)-3-phenylpropane-1-sulfonamide, hydrochloride salt, 16b**

Prepared from **59b** (130 mg, 0.24 mmol) using the general Boc deprotection procedure 2 to afford **16b** (110 mg, 93%) with the MDAP purification step omitted. IR (cm⁻¹) 3400-2400 (m), 1614, 1419, 1313, 1270, 1138, 928, 747, 699; ¹H NMR (400 MHz, DMSO-d₆, δ): 9.07 (br. s., 2H), 8.00 (s, 1H), 7.36-7.16 (m, 6H), 4.12 (t, *J* = 6 Hz, 2H), 3.66-3.52 (m, 4H), 3.31-3.14 (m, 6H), 2.98 (t, *J* = 8 Hz, 2H), 2.68 (t, *J* = 8 Hz, 2H), 1.98-1.83 (m, 2H); ¹³C NMR (126 MHz, DMSO-d₆, δ): 157.3, 146.9, 140.8, 131.6,

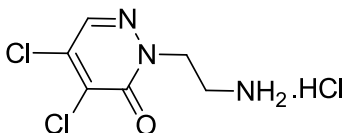
128.4, 128.3, 126.0, 116.0, 51.7, 50.7, 45.5, 42.8, 40.2, 33.3, 25.1; HRMS–FAB (m/z): $[M + H]^+$ calcd for $C_{19}H_{26}ClN_5O_3S$, 440.1518; found, 440.1503; LC-MS (Method B) m/z $[M + H]^+$ 440.0, t_R 1.18 mins; 116 – 118 °C.

tert*-Butyl (2-(4,5-dichloro-6-oxopyridazin-1(6*H*)-yl)ethyl)carbamate, **61*



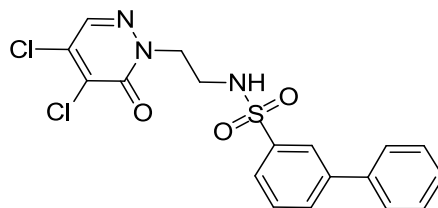
A solution of **44** (10 g, 60.6 mmol) and **60** (14.9 g, 66.7 mmol) in DMF (100 mL) was treated with K_2CO_3 (9.2 g, 66.7 mmol). The reaction mixture was stirred at room temperature overnight then partitioned between EtOAc and water (50 mL each). The organic layer was separated, washed with water (50 mL) and brine (50 mL), then dried (sodium sulphate) and concentrated. The crude material was purified using silica column chromatography to afford **61** as a white solid (13.0 g, 70%). 1H NMR (400 MHz, $CDCl_3$, δ): 7.82 (s, 1H), 4.90 (br. s, 1H), 4.33 (t, $J = 6$ Hz, 2H), 3.59–3.58 (m, 2H), 1.42 (s, 9H); LC-MS (Method B) m/z $[M - tBu]^+$ 251.9, t_R 1.52 mins.

2-(2-Aminoethyl)-4,5-dichloropyridazin-3(2*H*)-one, hydrochloride salt, **62**



A solution of **61** (13.0 g, 42.2 mmol) in DCM (500 mL) was cooled to 0 °C then treated with gaseous HCl for 2 h and stirred at room temperature overnight. The mixture was concentrated to afford **62** as a white solid (10.0 g, 97%). 1H NMR (400 MHz, $DMSO-d_6$, δ): 8.27 (s, 1H), 8.18 (br. s, 3H), 4.36 (t, $J = 6$ Hz, 2H), 3.21–3.17 (m, 2H), *previously reported in literature but no spectral data reported*.¹⁵⁵ LC-MS (Method B) m/z $[M + H]^+$ 208.0, t_R 0.52 mins.

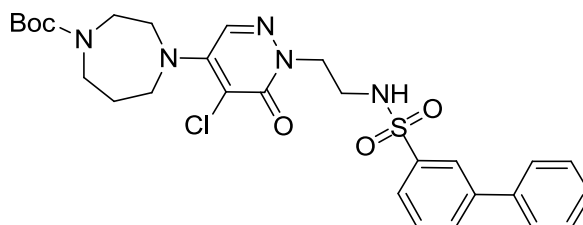
N*-(2-(4,5-Dichloro-6-oxopyridazin-1(6*H*)-yl)ethyl)-[1,1'-biphenyl]-3-sulfonamide, **63*



A solution of **62** (10.0 g, 40.9 mmol) in pyridine (10 mL) was treated with **50** (10.3 mL, 49.1 mmol) then stirred under nitrogen at room temperature for 16 h. The reaction mixture was concentrated and partitioned between EtOAc (50 mL) and water (50 mL). The organic layer was separated and washed with water (50 mL), saturated sodium carbonate (50 mL) and brine (50 mL) then dried (sodium sulphate) and concentrated. Purification of the crude material by silica column chromatography afforded **63** as a yellow solid (13.5 g, 78%). IR (cm⁻¹) 3294, 1650, 1322; ¹H NMR (400 MHz, DMSO-d₆, δ): 8.11 (s, 1H), 7.98 (br. s, 1H), 7.96-7.85 (m, 2H), 7.77-7.61 (m, 4H), 7.58-7.49 (m, 2H), 7.49-7.40 (m, 1H), 4.15 (t, *J* = 6 Hz, 2H), 3.29–3.21 (m, 2H); ¹³C NMR (101 MHz, DMSO-d₆, δ): 156.5, 141.6 (2C), 139.0, 136.3 (2C), 133.3, 131.1, 130.5, 130.0, 128.8, 127.4, 125.7, 124.8, 52.6, 41.2; HRMS–FAB (*m/z*): [M + H]⁺ calcd for C₁₈H₁₅Cl₂N₃O₃S, 424.0284; found, 424.0273; LC-MS (Method B) *m/z* [M + H]⁺ 423.9/424.9, *t*_R 1.59 mins; mp 140 – 142 °C.

General Nucleophilic Substitution Procedure 2

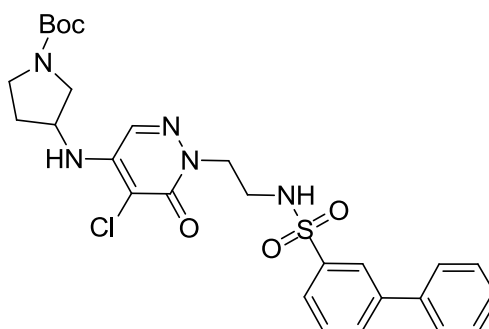
tert*-Butyl 4-(1-(2-([1,1'-biphenyl]-3-ylsulfonamido)ethyl)-5-chloro-6-oxo-1,6-dihydropyridazin-4-yl)-1,4-diazepane-1-carboxylate, **64g*



A solution of **63** (200 mg, 0.47 mmol) and *tert*-butyl 1,4-diazepane-1-carboxylate (142 mg, 0.71 mmol) in EtOH (10 mL) was treated with DIPEA (0.30 mL, 1.72 mmol). The reaction mixture was refluxed overnight, concentrated then purified by silica

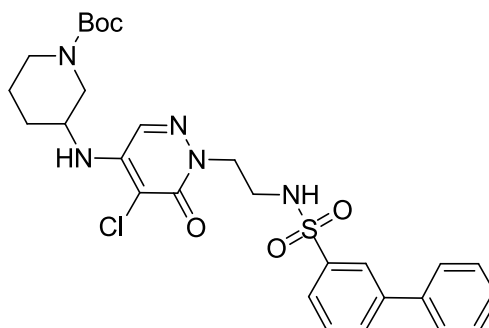
chromatography to afford **64g** as a white solid (180 mg, 65%). ^1H NMR (400 MHz, CDCl_3 , δ): 8.07 (s, 1H), 7.64-7.62 (m, 2H), 7.57-7.43 (m, 7H), 5.59 (br. s, 1H), 4.23 (t, $J = 6$ Hz, 2H), 3.71-3.43 (m, 10H), 2.00-1.90 (m, 2H), 1.45 (s, 9H). LC-MS (Method B) m/z $[\text{M} + \text{H}]^+$ 588.1, t_R 1.63 mins.

tert*-Butyl 3-((1-(2-([1,1'-biphenyl]-3-ylsulfonamido)ethyl)-5-chloro-6-oxo-1,6-dihydropyridazin-4-yl)amino)pyrrolidine-1-carboxylate, **64c*



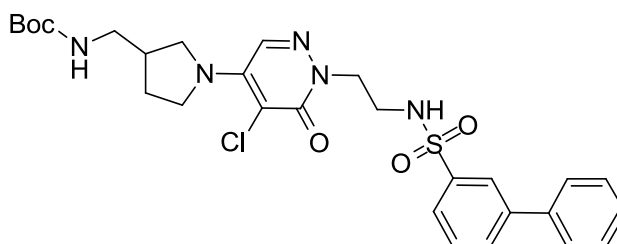
Prepared from **63** (200 mg, 0.47 mmol) and racemic *tert*-butyl 3-aminopyrrolidine-1-carboxylate (122 mg, 0.71 mmol), using the general nucleophilic substitution procedure 2, but using BuOH in the place of EtOH, to afford **64c** (80 mg, 30%). ^1H NMR (400 MHz, CDCl_3 , δ): 8.04 (s, 1H), 7.77-7.67 (m, 2H), 7.62-7.28 (m, 7H), 5.76 (br. s, 1H), 4.66-4.63 (m, 1H), 4.24 (t, $J = 5$ Hz, 2H), 4.10-3.99 (m, 1H), 3.68-3.66 (m, 1H), 3.49 (t, $J = 5$ Hz, 2H), 3.48-3.45 (m, 1H), 2.21-2.17 (m, 1H), 1.91-1.77 (m, 1H), 1.47 (s, 9H), 1.45-1.42 (m, 1H), the *sulfonamide proton underwent exchange in wet deuterated solvent and was not visible*. LC-MS m/z $[\text{M} - t\text{Bu}]^+$ 517.9, t_R (Method B) 1.60 mins.

tert*-Butyl 3-((1-(2-([1,1'-biphenyl]-3-ylsulfonamido)ethyl)-5-chloro-6-oxo-1,6-dihydropyridazin-4-yl)amino)piperidine-1-carboxylate, **64d*



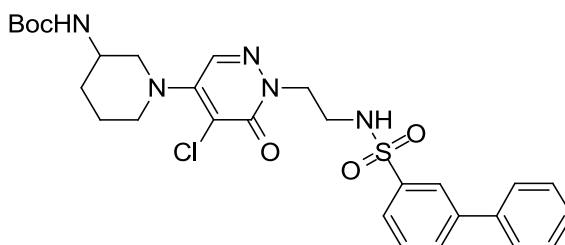
Prepared from **63** (200 mg, 0.47 mmol) and racemic *tert*-butyl 3-aminopiperidine-1-carboxylate (142 mg, 0.71 mmol) using the general nucleophilic substitution procedure 2, but using BuOH instead of EtOH, to afford **64d** (20 mg, 7%). ¹H NMR (400 MHz, CDCl₃, δ): 8.06 (s, 1H), 7.78-7.73 (m, 2H), 7.64-7.28 (m, 7H), 5.76 (br. s, 1H), 4.80-4.70 (m, 1H), 4.28-4.21 (m, 2H), 3.78-3.72 (m, 1H), 3.51-3.12 (m, 6H), 1.93-1.92 (m, 1H), 1.77-1.50 (m, 3H), 1.48 (s, 9H). LC-MS *m/z* [M - *t*Bu]⁺ 531.9, *t*_R (Method B) 1.63 mins.

***tert*-Butyl ((1-(1-(2-([1,1'-biphenyl]-3-ylsulfonamido)ethyl)-5-chloro-6-oxo-1,6-dihydropyridazin-4-yl)pyrrolidin-3-yl)methyl)carbamate, 64e**



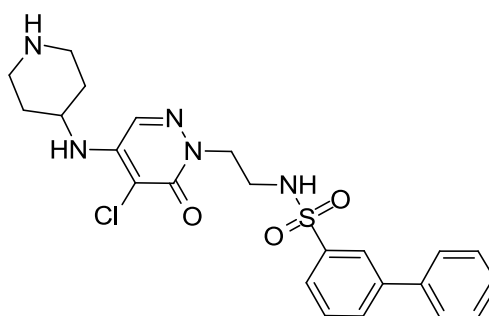
Prepared from **63** (212 mg, 0.50 mmol) and *tert*-butyl (pyrrolidin-3-ylmethyl)carbamate (140 mg, 0.70 mmol) using the general nucleophilic substitution procedure 2 to afford **64e** (230 mg, 78%). ¹H NMR (400 MHz, CDCl₃, δ): 8.03 (s, 1H), 7.80-7.69 (m, 2H), 7.63-7.40 (m, 6H), 7.29 (s, 1H), 4.70 (br. s, 1H), 4.13 (t, *J* = 6 Hz, 2H), 3.75-3.60 (m, 3H), 3.50-3.32 (m, 3H), 3.30-3.12 (m, 2H), 2.37-2.35 (m, 1H), 2.02-1.98 (m, 1H), 1.65-1.63 (m, 1H), 1.46 (s, 9H), *sulfonamide proton underwent exchange in the wet deuterated solvent and was not visible*. LC-MS *m/z* [M+H]⁺ 588.2, *t*_R (Method B) 1.60 mins.

***tert*-Butyl (1-(1-(2-([1,1'-biphenyl]-3-ylsulfonamido)ethyl)-5-chloro-6-oxo-1,6-dihydropyridazin-4-yl)piperidin-3-yl)carbamate, 64f**



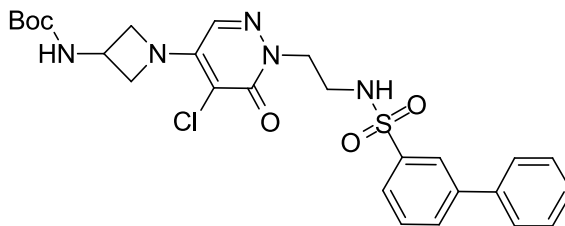
Prepared from **63** (212 mg, 0.50 mmol) and *tert*-butyl (piperidin-3-ylmethyl)carbamate (140 mg, 0.70 mmol) using the general nucleophilic substitution procedure 2 to afford **62f** (247 mg, 84%). ¹H NMR (400 MHz, CDCl₃, δ): 8.05 (s, 1H), 7.80-7.74, (m, 2H), 7.62-7.47 (m, 7H), 5.59 (br. s, 1H), 4.26-4.23 (m, 2H), 3.27-3.23 (m, 1H), 3.60-3.35 (m, 4H), 3.20-2.98 (m, 2H), 2.00-1.50 (m, 4H), 1.46 (s, 9H), *sulfonamide proton underwent exchange in wet deuterated solvent and was not visible*. LC-MS [M - *t*Bu]⁺ 532.1, *t*_R (Method B) 1.65 mins.

***N*-(2-(5-Chloro-6-oxo-4-(piperidin-4-ylamino)pyridazin-1(6*H*)-yl)ethyl)-[1,1'-biphenyl]-3-sulfonamide, 18h**

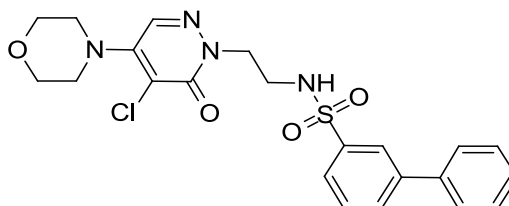


A solution of **63** (200 mg, 0.47 mmol) in DMA (2 mL) was treated with *tert*-butyl 4-aminopiperidine-1-carboxylate (0.1 mL, 0.47 mmol) and K₂CO₃ (130 mg, 0.94 mmol) then the reaction mixture was heated at 100 °C for 24 h. The reaction mixture was allowed to cool to room temperature then partitioned between EtOAc (25 mL) and water (25 mL). The organic extract was isolated then washed with water (25 mL) then brine (25 mL) and dried (sodium sulphate) to afford **64h** as a yellow oil (60 mg, 22%). LC-MS *m/z* [M + H]⁺ 588.8, *t*_R (Method B) 1.51 mins.

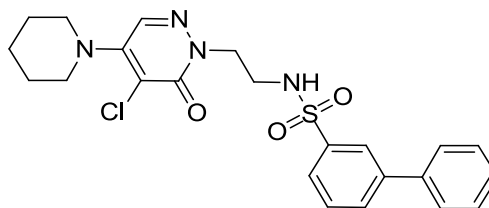
A solution of **64h** (60 mg, 0.10 mmol) in EtOAc (15 mL) was treated with gaseous HCl overnight then concentrated under reduced pressure. Crude product was purified by MDAP (Method B) to afford **18h** (30 mg, 60%). ¹H NMR (400 MHz, CD₃OD, δ): 8.54 (br. s, 1H), 8.08 (s, 1H), 7.99-7.87 (m, 2H), 7.83-7.46 (m, 7H), 4.28 (t, *J* = 6 Hz, 2H), 3.94-3.76 (m, 1H), 3.67-3.44 (m, 4H), 3.11 (t, *J* = 6 Hz, 2H), 2.25-2.00 (m, 2H), 2.01-1.78 (m, 2H), *amino piperidine proton and sulfonamide proton underwent exchange and were not visible*; LC-MS *m/z* [M + H]⁺ 487.9, *t*_R (Method B) 1.21 mins.

tert*-Butyl (1-(1-(2-([1,1'-biphenyl]-3-ylsulfonamido)ethyl)-5-chloro-6-oxo-1,6-dihydropyridazin-4-yl)azetidin-3-yl)carbamate, **64i*

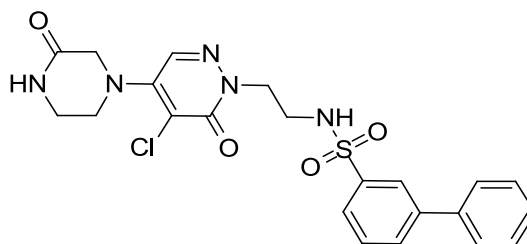
Prepared from **63** (200 mg, 0.47 mmol) and *tert*-butyl azetidin-3-ylcarbamate, hydrochloride salt (118 mg, 0.57 mmol) using the general nucleophilic substitution procedure 2 to afford **64i** (227 mg, 86%). ¹H NMR (400 MHz, CDCl₃, δ): 8.04 (s, 1H), 7.85-7.75 (m, 2H), 7.68-7.65 (m, 2H), 7.60-7.40 (m, 4H), 6.96 (s, 1H), 4.86 (br. s, 1H), 4.61-4.39 (m, 3H), 4.20 (t, *J* = 6 Hz, 2H), 4.11-4.00 (m, 2H), 3.50 (t, *J* = 6 Hz, 2H), 1.49 (s, 9H), *sulfonamide proton underwent exchange in wet solvent and was not visible*; LC-MS *m/z* [M + H]⁺ 559.9, *t_R* (Method B) 1.57 mins.

N*-(2-(5-Chloro-4-morpholino-6-oxopyridazin-1(6*H*)-yl)ethyl)-[1,1'-biphenyl]-3-sulfonamide, **17c*

Prepared from **63** (150 mg, 0.354 mmol) and morpholine (62 mg, 0.707 mmol) using the general nucleophilic substitution procedure 2 to afford **17c** (130 mg, 77%). ¹H NMR (400 MHz, DMSO-*d*₆, δ): 7.98-7.92 (m, 2H), 7.80-7.65 (m, 5H), 7.54-7.44 (m, 3H), 4.07 (t, *J* = 6 Hz, 2H), 3.70-3.67 (m, 4H), 3.35-3.25 (m, 4H), 3.21 (t, *J* = 6 Hz, 2H), *sulfonamide proton underwent exchange and was not visible*. LC-MS *m/z* [M + H]⁺ 474.9, *t_R* (Method B) 1.49 mins.

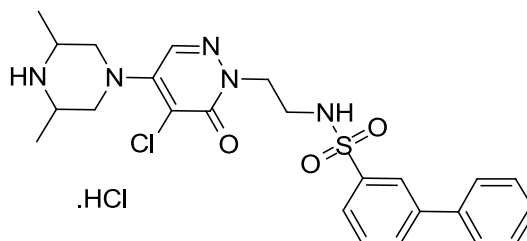
***N*-(2-(5-Chloro-6-oxo-4-(piperidin-1-yl)pyridazin-1(6*H*)-yl)ethyl)-[1,1'-biphenyl]-3-sulfonamide, 17d**

Prepared from **63** (150 mg, 0.354 mmol) and piperidine (60 mg, 0.707 mmol) using the general nucleophilic substitution procedure 2 to afford **17d** (130 mg, 78%). IR (cm⁻¹) 3200 - 3000 (br. s), 2939, 2853, 1623, 1591, 1329, 1306, 1152, 1088, 854, 753, 692; ¹H NMR (400 MHz, CDCl₃ δ) 8.07 (s, 1H), 7.82 (d, *J* = 8 Hz, 1H), 7.76 (d, *J* = 8 Hz, 1H), 7.66-7.60 (m, 2H), 7.56 (t, *J* = 8 Hz, 1H), 7.53-7.46 (m, 3H), 7.43 (t, *J* = 7 Hz, 1H), 5.65 (br. s, 1H), 4.25 (t, *J* = 6 Hz, 2H), 3.50 (t, *J* = 6 Hz, 2H), 3.38-3.25 (m, 4H), 1.75-1.61 (m, 6H); ¹³C NMR (126 MHz, DMSO-*d*₆, δ): 157.4, 147.9, 141.1, 141.0, 138.5, 131.7, 130.6, 129.9, 129.1, 128.2, 126.9, 125.3, 124.3, 113.6, 51.0, 49.6, 40.5, 25.6, 23.4; HRMS-FAB (*m/z*): [M + H]⁺ calcd for C₂₃H₂₅ClN₄O₃S, 473.1409; found, 473.1397; LC-MS *m/z* [M + H]⁺ 473.0, *t*_R (Method B) 1.65 mins; mp 123 – 125 °C.

***N*-(2-(5-Chloro-6-oxo-4-(3-oxopiperazin-1-yl)pyridazin-1(6*H*)-yl)ethyl)-[1,1'-biphenyl]-3-sulfonamide from piperazin-2-one, 17e**

Prepared from **63** (212 mg, 0.50 mmol) and piperazin-2-one (70 mg, 0.70 mmol) using the general nucleophilic substitution procedure 2 to afford **17e** (125 mg, 51%). ¹H NMR (400 MHz, CDCl₃, δ): 8.06 (s, 1H), 7.86-7.74 (m, 2H), 7.67-7.60 (m, 2H), 7.57 (t, *J* = 8 Hz, 1H), 7.54-7.46 (m, 3H), 7.44 (t, *J* = 7 Hz, 1H), 6.44 (br. s, 1H), 5.71 (br. s, 1H), 4.29 (t, *J* = 5 Hz, 2H), 4.01 (s, 2H), 3.65 (t, *J* = 5 Hz, 2H), 3.57-3.46 (m, 4H). LC-MS *m/z* [M + H]⁺ 487.9, *t*_R (Method B) 1.36 mins.

General Nucleophilic Substitution then Deprotection Procedure

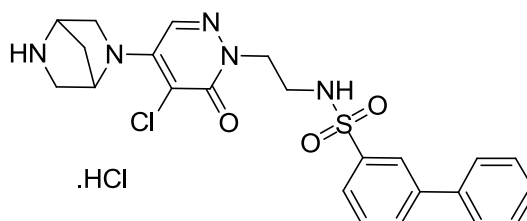
N*-2-(5-Chloro-4-(3,5-dimethylpiperazin-1-yl)-6-oxopyridazin-1(6*H*)-yl)ethyl)-[1,1'-biphenyl]-3-sulfonamide, hydrochloride salt, **18a*

A solution of **63** (106 mg, 0.25 mmol) in EtOH (5 mL) was treated with racemic *tert*-butyl 2,6-dimethylpiperazine-1-carboxylate (75 mg, 0.35 mmol) followed by DIPEA (0.087 mL, 0.50 mmol) then the reaction mixture stirred at 80 °C for 94 h. The mixture was concentrated under reduced pressure then crude product purified by prep-TLC (1:1 EtOAc/petroleum ether) to afford *tert*-butyl 4-(1-(2-([1,1'-biphenyl]-3-ylsulfonamido)ethyl)-5-chloro-6-oxo-1,6-dihydropyridazin-4-yl)-2,6-dimethylpiperazine-1-carboxylate as an off-white solid (74 mg, 49%). LC-MS m/z $[M + H]^+$ 601.9, t_R (Method B) 1.75 mins.

tert-butyl 4-(1-(2-([1,1'-biphenyl]-3-ylsulfonamido)ethyl)-5-chloro-6-oxo-1,6-dihydropyridazin-4-yl)-2,6-dimethylpiperazine-1-carboxylate (74 mg, 0.12 mmol) was treated with a saturated solution of hydrochloric acid in EtOAc (15 mL) then the reaction mixture was stirred at 25 °C overnight. Solid product was filtered under reduced pressure then washed with EtOAc (5 x 1 mL) to afford **18a** (45 mg, 84%, 33% over two steps), assumed to be a mono-HCl salt. IR (cm^{-1}) 3600-2500 (m), 1616, 1595, 1326, 1153, 760, 697; ^1H NMR (400 MHz, CD_3OD , δ): 8.03 (s, 1H), 7.93-7.83 (m, 2H), 7.78 (d, $J = 8$ Hz, 1H), 7.72-7.60 (m, 3H), 7.58-7.49 (m, 2H), 7.44 (t, $J = 7$ Hz, 1H), 4.25 (t, $J = 6$ Hz, 2H), 3.97-3.87 (m, 2H), 3.55-3.44 (m, 2H), 3.41 (t, $J = 6$ Hz, 2H), 3.05-2.93 (m, 2H), 1.36 (d, $J = 7$ Hz, 6 H), *sulfonamide, piperazine and hydrochloride protons underwent exchange and were not visible*; ^{13}C NMR (126 MHz, DMSO-d_6 , δ): 157.3, 146.3, 141.1, 140.9, 138.5, 132.0, 130.6, 129.9, 129.2, 128.3, 126.9, 125.3, 124.3, 115.2, 51.1 (2C), 50.8, 40.4, 15.3; HRMS-FAB (m/z): $[M + H]^+$ calcd for

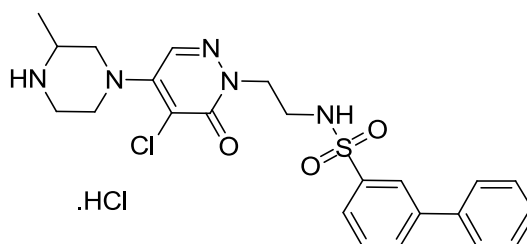
$C_{24}H_{28}ClN_5O_3S$, 502.1674; found, 502.1662; LC-MS m/z $[M+H]^+$ 501.9, t_R (Method B) 1.24 mins; mp 151 – 153 °C.

***N*-(2-(4-((2,5-Diazabicyclo[2.2.1]heptan-2-yl)-5-chloro-6-oxopyridazin-1(6*H*)-yl)ethyl)-[1,1'-biphenyl]-3-sulfonamide, hydrochloride salt, 17a**



Prepared from **63** (212 mg, 0.50 mmol) and racemic *tert*-butyl 2,5-diazabicyclo[2.2.1]heptane-2-carboxylate (139 mg, 0.70 mmol) using the general nucleophilic substitution then deprotection procedure to afford **17a** (115 mg, 44% over 2 steps), *assumed to be mono-HCl salt*. 1H NMR (400 MHz, DMSO- d_6 , δ): 9.56 (br. s, 1H), 8.94 (br. s, 1H), 8.01 (s, 1H), 7.96 (d, $J = 8$ Hz, 1H), 7.90 (t, $J = 6$ Hz, 1H), 7.81 (s, 1H), 7.78-7.65 (m, 4H), 7.58-7.50 (m, 2H), 7.46 (t, $J = 7$ Hz, 1H), 4.15-3.93 (m, 3H), 3.80 (d, $J = 11$ Hz, 1H), 3.40-3.20 (m, 4H), 3.14 (q, $J = 6$ Hz, 2H), 2.13-1.89 (m, 2H), *piperazine and hydrochloride protons underwent exchange and were not visible in wet deuterated solvent*; LC-MS m/z $[M + H]^+$ 486.0, t_R (Method B) 1.31 mins.

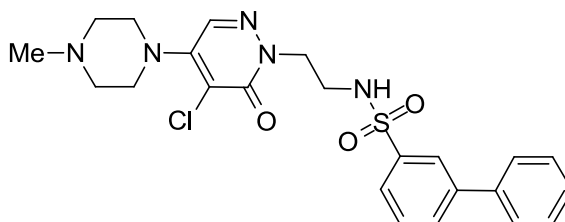
***N*-(2-(5-Chloro-4-(3-methylpiperazin-1-yl)-6-oxopyridazin-1(6*H*)-yl)ethyl)-[1,1'-biphenyl]-3-sulfonamide, hydrochloride salt, 18b**



Prepared from **63** (212 mg, 0.50 mmol) and racemic *tert*-butyl 2-methylpiperazine-1-carboxylate (140 mg, 0.70 mmol) using the general nucleophilic substitution then deprotection procedure to afford **18b** (180 mg, 69% over 2 steps), *assumed to be a mono-HCl salt*. 1H NMR (400 MHz, CD $_3$ OD, δ): 8.02 (s, 1H), 7.93-7.83 (m, 2H), 7.79 (d, $J = 8$ Hz, 1H), 7.73-7.60 (m, 3H), 7.57-7.50 (m, 2H), 7.44 (t, $J = 7$ Hz, 1H), 4.23 (t,

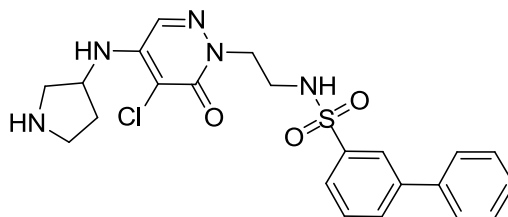
$J = 6$ Hz, 2H), 3.96-3.80 (m, 2H), 3.55-3.44 (m, 2H), 3.40 (t, $J = 6$ Hz, 2H), 3.32-3.26 (m, 2H), 3.17-3.03 (m, 1H), 1.37 (d, $J = 7$ Hz, 3H), *piperazine, sulfonamide and hydrochloride protons underwent exchange and were not visible*; LC-MS m/z $[M + H]^+$ 487.9, t_R (Method B) 1.22 mins.

N*-(2-(5-Chloro-4-(4-methylpiperazin-1-yl)-6-oxopyridazin-1(6*H*)-yl)ethyl)-[1,1'-biphenyl]-3-sulfonamide, **17b*

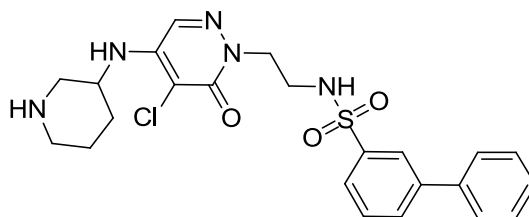


A solution of **63** (150 mg, 0.35 mmol) in DMF (2 mL) was treated with potassium carbonate (98 mg, 0.71 mmol) and 1-methyl piperazine (0.10 mL, 0.35 mmol), then stirred at room temperature overnight. The reaction mixture was filtered then concentrated under reduced pressure and the crude product washed with EtOH then diethyl ether to afford **17b** as a white solid (80 mg, 46%). IR (cm^{-1}) 3200 - 3100, 2842, 2795, 1625, 1589, 1331, 1154, 1087, 1005, 856, 801, 757, 692; ^1H NMR (400 MHz, DMSO- d_6 δ) 8.00 (s, 1H), 7.94 (d, $J = 8$ Hz, 1H), 7.91-7.85 (br. s, 1H), 7.83 (s, 1H), 7.78-7.63 (m, 4H), 7.57-7.49 (m, 2H), 7.45 (t, $J = 7$ Hz, 1H), 4.07 (t, $J = 6$ Hz, 2H), 3.41-3.27 (m, 4H), 3.22-3.12 (m, 2H), 2.44-2.34 (m, 4H), 2.20 (s, 3H); ^{13}C NMR (126 MHz, DMSO- d_6 , δ): 157.3, 147.4, 141.1, 140.9, 139.0, 131.6, 130.6, 129.9, 129.1, 128.3, 126.9, 125.3, 124.3, 114.1, 54.5, 51.1, 48.3, 45.6, 40.5; HRMS-FAB (m/z): $[M + H]^+$ calcd for $\text{C}_{23}\text{H}_{26}\text{ClN}_5\text{O}_3\text{S}$, 488.1518; found, 488.1496; LC-MS m/z $[M + H]^+$ 488.0, t_R (Method B) 1.27 mins; mp 169 – 171 $^\circ\text{C}$.

General Boc Deprotection Procedure 3

***N*-(2-(5-Chloro-6-oxo-4-(pyrrolidin-3-ylamino)pyridazin-1(6*H*)-yl)ethyl)-[1,1'-biphenyl]-3-sulfonamide, 18c**

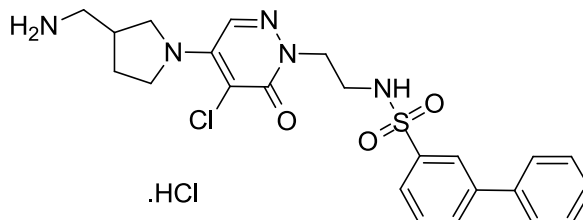
A solution of **64c** (80 mg, 0.139 mmol) in was treated with a saturated solution of HCl in EtOAc (15 mL). The reaction mixture was allowed to stir overnight then concentrated under reduced pressure. Crude material was purified using the preparative HPLC method to afford **18c** as a yellow oil (62 mg, 94%, *estimated yield because a large amount water is evident by NMR*). ¹H NMR (400 MHz, CD₃OD, δ): 8.46 (br. s, 1H), 8.02 (s, 1H), 7.87 (d, *J* = 8 Hz, 1H), 7.82 (s, 1H), 7.77 (d, *J* = 8 Hz, 1H), 7.72-7.65 (m, 2H), 7.61 (t, *J* = 8 Hz, 1H), 7.55-7.47 (m, 2H), 7.44 (t, *J* = 8 Hz, 1H), 4.52-4.42 (m, 1H), 4.21 (t, *J* = 6 Hz, 2H), 3.60-3.45 (m, 2H), 3.40 (t, *J* = 6 Hz, 2H), 3.38-3.35 (m, 1H), 3.30 (d, *J* = 5 Hz, 1H), 2.44-2.29 (m, 1H), 2.14-2.00 (m, 1H), *sulfonamide proton and amino pyrrolidine proton underwent exchange and were not visible*; LC-MS *m/z* [M + H]⁺ 474.0, *t_R* (Method B) 1.33 mins.

***N*-(2-(5-Chloro-6-oxo-4-(piperidin-3-ylamino)pyridazin-1(6*H*)-yl)ethyl)-[1,1'-biphenyl]-3-sulfonamide, 18d**

Prepared from **64d** (20 mg, 0.036 mmol) using the general Boc deprotection procedure 3 to afford **18d** (10 mg, 61%). ¹H NMR (400 MHz, CD₃OD, δ): 8.01 (s, 1H), 7.87 (d, *J* = 8 Hz, 1H), 7.83-7.73 (m, 2H), 7.72-7.66 (m, 2H), 7.61 (t, *J* = 8 Hz, 1H), 7.56-7.48 (m, 2H), 7.43 (t, *J* = 7 Hz, 1H), 4.30-4.07 (m, 2H), 3.84-3.69 (m, 1H), 3.41 (t, *J* = 6 Hz, 2H), 3.31-3.18 (m, 2H, *obscured by residual solvent peak*), 2.88-2.73 (m, 2H), 2.05-

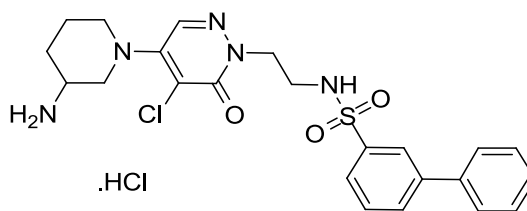
1.87 (m, 2H), 1.80-1.58 (m, 2H), *the sulfonamide proton and both amino piperidine protons, underwent exchange and were not visible*; LC-MS m/z $[M + H]^+$ 487.9, t_R (Method B) 1.22 mins.

N*-(2-(4-(3-(Aminomethyl)pyrrolidin-1-yl)-5-chloro-6-oxopyridazin-1(6*H*)-yl)ethyl)-[1,1'-biphenyl]-3-sulfonamide, hydrochloride salt, **18e*



Prepared from **64e** (230 mg, 0.39 mmol) using the general Boc deprotection procedure 3, but with the preparative HPLC step omitted, to afford **18e** (180 mg, 85%). 1H NMR (400 MHz, CD_3OD , δ): 8.02 (s, 1H), 7.89 (d, $J = 8$ Hz, 1H), 7.78 (d, $J = 8$ Hz, 1H), 7.74-7.68 (m, 2H), 7.64 (t, $J = 8$ Hz, 1H), 7.59 (s, 1H), 7.56-7.49 (m, 2H), 7.44 (t, $J = 7$ Hz, 1H), 4.18 (t, $J = 6$ Hz, 2H), 3.95-3.86 (m, 1H), 3.82-3.65 (m, 2H), 3.54-3.46 (m, 1H), 3.42 (t, $J = 6$ Hz, 2H), 3.10-2.97 (m, 2H), 2.55-2.44 (m, 1H), 2.25-2.12 (m, 1H), 1.77-1.63 (m, 1H), *hydrochloride proton, sulfonamide proton and both primary amine protons underwent exchange and were not visible*; LC-MS m/z $[M + H]^+$ 487.9, t_R (Method B) 1.21 mins.

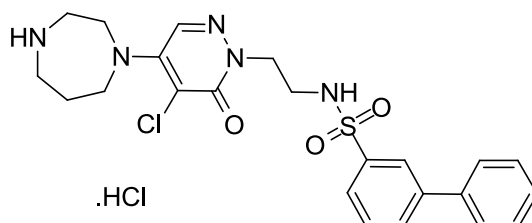
N*-(2-(4-(3-Aminopiperidin-1-yl)-5-chloro-6-oxopyridazin-1(6*H*)-yl)ethyl)-[1,1'-biphenyl]-3-sulfonamide, hydrochloride salt, **18f*



Prepared from **64f** (247 mg, 0.42 mmol) using the general Boc deprotection procedure 3, but with the preparative HPLC step omitted, to afford **18f** (163 mg, 74%). 1H NMR (400 MHz, $DMSO-d_6$, δ): 8.13 (br. s, 3H), 8.01 (s, 1H), 7.99-7.83 (m, 3H), 7.80-7.64 (m, 4H), 7.59-7.49 (m, 2H), 7.46 (t, $J = 7$ Hz, 1H), 4.08 (t, $J = 6$ Hz, 2H), 3.85-3.66 (m,

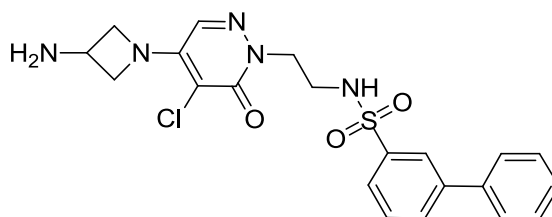
2H), 3.32- 3.09 (m, 3H), 3.09-2.94 (m, 2H), 2.08-1.92 (m, 2H), 1.72-1.49 (m, 2H); LC-MS m/z $[M + H]^+$ 488.0, t_R (Method B) 1.34 mins.

***N*-(2-(5-Chloro-4-(1,4-diazepan-1-yl)-6-oxopyridazin-1(6H)-yl)ethyl)-[1,1'-biphenyl]-3-sulfonamide, hydrochloride salt, 18g**



Prepared from **64g** (200 mg, 0.34 mmol) using the general Boc deprotection procedure 3, but with the preparative HPLC step omitted, to afford **18g** (150 mg, 84%). IR (cm^{-1}) 3600 - 2600 (m), 1593, 1327, 1153, 760, 698; ^1H NMR (400 MHz, DMSO-d_6 , δ): 7.99 (s, 1H), 7.93 (d, $J = 8$ Hz, 1H), 7.81 (s, 1H), 7.76-7.64 (m, 4H), 7.57-7.49 (m, 2H), 7.44 (t, $J = 7$ Hz, 1H), 4.05 (t, $J = 6$ Hz, 2H), 3.83-3.74 (m, 2H), 3.58 (t, $J = 6$ Hz, 2H), 3.34-3.09 (m, 6H), 2.13-2.01 (m, 2H), *secondary amino, hydrochloride and sulfonamide protons underwent exchange in wet deuterated solvent and were not visible*; ^{13}C NMR (126 MHz, DMSO-d_6 , δ): 157.4, 146.7, 141.1, 140.9, 138.5, 130.6 (2C), 129.9, 129.1, 128.3, 126.9, 125.3, 124.3, 110.3, 50.9, 49.6, 47.1, 46.1, 44.3, 40.5, 25.0; HRMS-FAB (m/z): $[M + H]^+$ calcd for $\text{C}_{23}\text{H}_{26}\text{ClN}_5\text{O}_3\text{S}$, 488.1518; found, 488.1507; LC-MS m/z $[M + H]^+$ 488.1, t_R (Method B) 1.23 mins; mp 160 – 163 °C.

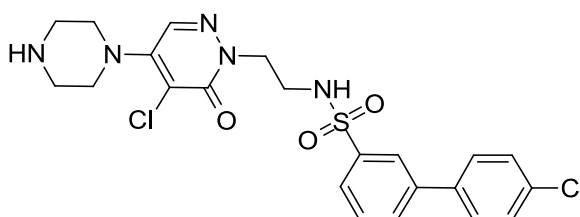
***N*-(2-(4-(3-Aminoazetididin-1-yl)-5-chloro-6-oxopyridazin-1(6H)-yl)ethyl)-[1,1'-biphenyl]-3-sulfonamide, 18i**



Compound **64i** (207 mg, 0.37 mmol) was treated with TFA (10 mL) and the reaction mixture was stirred at 25 °C for 3 h. The reaction mixture was concentrated under reduced pressure then partitioned between DCM (100 mL) and saturated sodium bicarbonate solution (50 mL). The organic layer was isolated, washed with brine, dried

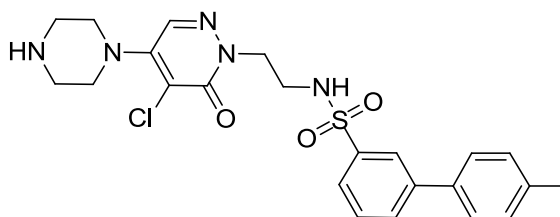
over sodium sulphate then concentrated under reduced pressure. The crude product was triturated with ether (3 x 5 mL) to afford **18i** as an off-white solid (140 mg, 82%). ¹H NMR (400 MHz, CD₃OD, δ): 8.01 (s, 1H), 7.93 (d, *J* = 8 Hz, 1H), 7.79-7.70 (m, 3H), 7.64 (t, *J* = 8 Hz, 1H), 7.58-7.49 (m, 2H), 7.45 (t, *J* = 7 Hz, 1H), 7.23 (s, 1H), 4.55-4.44 (m, 2H), 4.14 (t, *J* = 6 Hz, 2H), 4.04-3.94 (m, 2H), 3.87-3.76 (m, 1H), 3.40 (t, *J* = 6 Hz, 2H), *primary amino and sulfonamide protons underwent exchange and were not visible*; LC-MS *m/z* [M + H]⁺ 460.9, *t_R* (Method B) 1.20 mins.

4'-Chloro-N-(2-(5-chloro-6-oxo-4-(piperazin-1-yl)pyridazin-1(6H)-yl)ethyl)-[1,1'-biphenyl]-3-sulfonamide, hydrochloride salt, 19a



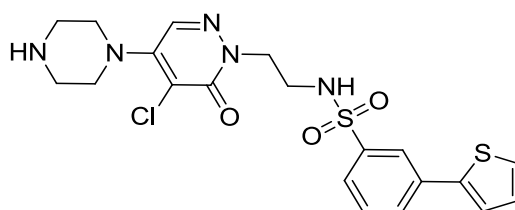
Prepared from **49** (188 mg, 0.53 mmol) and **69a** (181 mg, 0.63 mmol) using the general sulfonylation and deprotection procedure to afford **19a** (90 mg, 32% over two steps). IR (cm⁻¹) 3700 - 2400 (m), 1595, 1311, 1153, 1092, 795, 691; ¹H NMR (400 MHz, CD₃OD, δ): 8.03 (s, 1H), 7.92-7.85 (m, 2H), 7.80 (d, *J* = 8 Hz, 1H), 7.73-7.61 (m, 3H), 7.56-7.49 (m, 2H), 4.25 (t, *J* = 6 Hz, 2H), 3.68-3.61 (m, 4H), 3.43-3.36 (m, 6H), *the piperazine and sulfonamide protons underwent exchange and were not observed*; ¹³C NMR (126 MHz, DMSO-d₆, δ): 157.3, 146.9, 141.0, 139.8, 137.4, 133.2, 131.7, 130.6, 130.0, 129.1, 128.7, 125.6, 124.3, 115.8, 51.1, 45.5, 42.8, 40.4; HRMS-FAB (*m/z*): [M + H]⁺ calcd for C₂₂H₂₃Cl₂N₅O₃S, 508.0971; found, 508.0962; LC-MS (Method B) *m/z* [M + H]⁺ 507.9, *t_R* 1.32 mins; mp 158 – 160 °C.

N-(2-(5-Chloro-6-oxo-4-(piperazin-1-yl)pyridazin-1(6H)-yl)ethyl)-4'-methyl-[1,1'-biphenyl]-3-sulfonamide, 19b



Prepared from **49** (204 mg, 0.57 mmol) and **69b** (182 mg, 0.68 mmol) using the general sulfonylation and deprotection procedure to afford **19b** (20 mg, 7% over two steps). ^1H NMR (400 MHz, CD_3OD , δ): 8.43 (br. s, 1H), 8.02 (s, 1H), 7.90-7.79 (m, 2H), 7.74 (d, $J = 8$ Hz, 1H), 7.66-7.50 (m, 3H), 7.39-7.33 (d, $J = 8$ Hz, 2H), 4.22 (t, $J = 6$ Hz, 2H), 3.63-3.53 (m, 4H), 3.40 (t, $J = 6$ Hz, 2H), 3.31-3.24 (m, 4H), 2.42 (s, 3H), *the sulfonamide proton underwent exchange and was not observed*; LC-MS (Method B) m/z $[\text{M} + \text{H}]^+$ 488.0, t_{R} 1.30 mins.

N*-(2-(5-Chloro-6-oxo-4-(piperazin-1-yl)pyridazin-1(6*H*)-yl)ethyl)-3-(thiophen-2-yl)benzenesulfonamide, **20c*



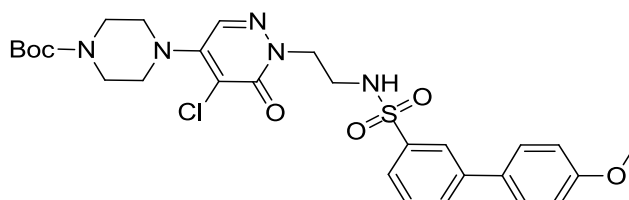
A solution of **49** (100 mg, 0.28 mmol) in DMF (5 mL) was treated with pyridine (45 μL , 0.56 mmol) and **70c** (87 mg, 0.34 mmol). The reaction mixture was stirred at room temperature for 16 h then concentrated under a stream of nitrogen. Crude product was purified by MDAP (Method A) to give *tert*-butyl 4-(5-chloro-6-oxo-1-(2-(3-(thiophen-2-yl)phenylsulfonamido)ethyl)-1,6-dihydropyridazin-4-yl)piperazine-1-carboxylate as a white solid (20 mg, 12%). LC-MS (Method A) m/z $[\text{M} + \text{H}]^+$ 580.3, t_{R} 1.16 mins.

A solution of *tert*-butyl 4-(5-chloro-6-oxo-1-(2-(3-(thiophen-2-yl)phenylsulfonamido)ethyl)-1,6-dihydropyridazin-4-yl)piperazine-1-carboxylate (20 mg, 0.034 mmol) in DCM (5 mL) was treated with TFA (5 mL) and the reaction mixture was stirred at room temperature for 3 h then concentrated under reduced pressure. The crude product was dissolved in MeOH (~2 mL) then loaded onto a 1g SCX-II SPE column which was eluted with MeOH (~9 mL) followed by ammonia (9 mL of a 2M solution in MeOH) to afford **20c** as a colourless gum (9 mg, 63%, 7% over 2 steps). ^1H NMR (400 MHz, $\text{DMSO}-d_6$, δ): 7.99-7.88 (m, 3H), 7.83 (s, 1H), 7.70-7.57 (m, 4H), 7.20 (dd, $J = 5, 4$ Hz, 1H), 4.07 (t, $J = 6$ Hz, 2H), 3.39-3.23 (m, 4H, *obscured by residual solvent peak*), 3.16 (t, $J = 6$ Hz, 2H), 2.93-2.83 (m, 4H), *piperazine proton*

underwent exchange in the wet deuterated solvent and was not observed; LC-MS (Method A) m/z $[M + H]^+$ 480.2, t_R 0.66 mins.

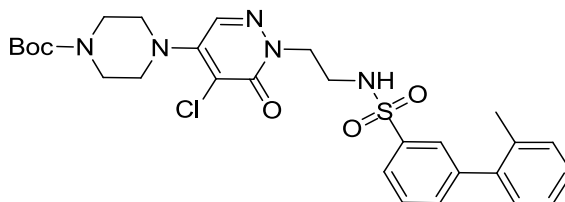
General Sulfonylation Procedure 2

***tert*-Butyl 4-(5-chloro-1-(2-(4'-methoxy-[1,1'-biphenyl]-3-yl)sulfonamido)ethyl)-6-oxo-1,6-dihydropyridazin-4-yl)piperazine-1-carboxylate, 71**



A solution of **49** (224 mg, 0.63 mmol) in DCM (11 mL) was treated with pyridine (0.10 mL, 1.30 mmol) and **69d** (212 mg, 0.75 mmol). The mixture was stirred at 25 °C for 58 h then diluted with further DCM (11 mL) and partitioned with brine (25 mL). The organic extract was isolated then dried (sodium sulphate) and concentrated under reduced pressure to give crude product as a yellow oil. The yellow oil was purified by silica column chromatography (1:1 hexane/EtOAc) to afford **71** (141 mg, 37%). 1H NMR (400 MHz, $CDCl_3$, δ): 8.02 (s, 1H), 7.77-7.71 (m, 2H), 7.58-7.51 (m, 3H), 7.48 (s, 1H), 7.03 (d, $J = 8$ Hz, 2H), 4.27 (t, $J = 5$ Hz, 2H), 3.89 (s, 3H), 3.56-3.55 (m, 4H), 3.51 (t, $J = 5$ Hz, 2H), 3.30-3.28 (m, 4H), 1.51 (s, 9H), *the sulfonamide proton underwent exchange in wet deuterated solvent and was not observed*. LC-MS (Method B) m/z $[M + H]^+$ 603.9, t_R 1.63 mins.

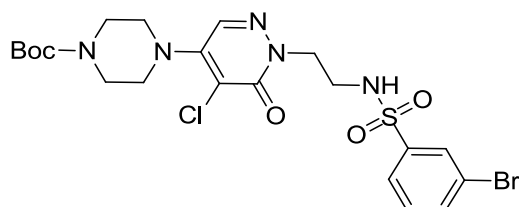
***tert*-Butyl 4-(5-chloro-1-(2-(2'-methyl-[1,1'-biphenyl]-3-yl)sulfonamido)ethyl)-6-oxo-1,6-dihydropyridazin-4-yl)piperazine-1-carboxylate, 72**



Prepared from **49** (204 mg, 0.57 mmol) and **70a** (182 mg, 0.69 mmol) using general sulfonylation procedure 2 to afford **72** (139 mg, 42%). 1H NMR (300 MHz, $CDCl_3$ δ) 7.87–7.84 (m, 2H), 7.58-7.55 (m, 3H), 7.33-7.24 (m, 4H, *obscured by residual solvent*)

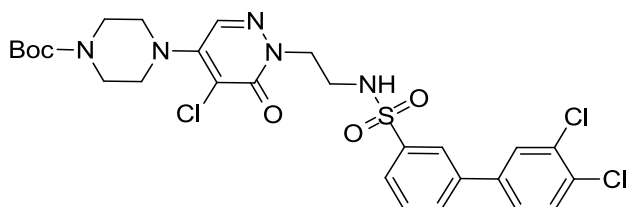
peak), 4.31 (t, $J = 5$ Hz, 2H), 3.62-3.60 (m, 4H), 3.51 (t, $J = 5$ Hz, 2H), 3.39-3.36 (m, 4H), 2.30 (s, 3H), 1.53 (s, 9H), *sulfonamide proton underwent exchange in the wet deuterated solvent and was not visible*. LC-MS (Method B) m/z $[M + H]^+$ 587.9, t_R 1.69 mins.

***tert*-Butyl 4-(1-(2-(3-bromophenylsulfonamido)ethyl)-5-chloro-6-oxo-1,6-dihydropyridazin-4-yl)piperazine-1-carboxylate, 66**



A solution of **49** (2.0 g, 5.6 mmol) in pyridine (30 mL) was treated with **65** (1.6 g, 6.2 mmol). The reaction mixture was stirred at room temperature for 10 min, then concentrated and the crude material was purified by silica chromatography to afford **66** (2.9 g, 85% yield at 95% purity). IR (cm^{-1}) 3120, 1698, 1616, 1597, 1406, 1329; ^1H NMR (400 MHz, DMSO-d_6 , δ): 7.96 (br. s, 1H), 7.90-7.82 (m, 3H), 7.74 (d, $J = 8$ Hz, 1H), 7.54 (d, $J = 8$ Hz, 1H), 4.06 (t, $J = 6$ Hz, 2H), 3.52–3.39 (m, 4H), 3.40-3.32 (m, 4H), 3.25-3.07 (m, 2H), 1.42 (s, 9H); ^{13}C NMR (101 MHz, DMSO-d_6 , δ): 158.6, 155.0, 148.7, 143.7, 136.5, 132.9, 132.7, 130.0, 126.7, 123.4, 116.2, 80.5, 61.0, 52.4, 49.5, 41.6, 29.3; HRMS–FAB (m/z): $[M + H]^+$ calcd for $\text{C}_{21}\text{H}_{27}\text{BrClN}_5\text{O}_5\text{S}$, 576.0678; found, 576.0664; LC-MS (Method B) m/z $[M + H]^+$ 576.1/578.0, t_R 1.60 mins; mp 145 – 147 °C.

***tert*-Butyl 4-(5-chloro-1-(2-(3',4'-dichloro-[1,1'-biphenyl]-3-yl)sulfonamido)ethyl)-6-oxo-1,6-dihydropyridazin-4-yl)piperazine-1-carboxylate, 68**

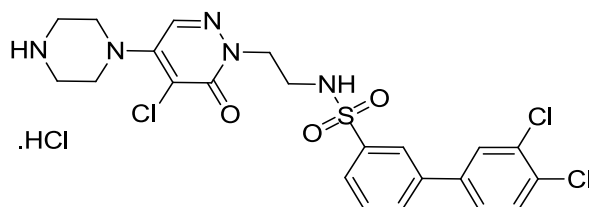


Tetrakis(triphenylphosphino)palladium(0) (60 mg, 0.052 mmol, 10 mol%) was added to a mixture of **66** (300 mg, 0.52 mmol), (3,4-dichlorophenyl)boronic acid (109 mg, 0.57

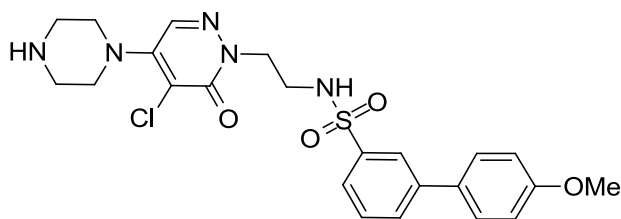
mmol) and sodium carbonate (165 mg, 1.56 mmol) in DMF (15 mL) and water (2 mL) under nitrogen. The mixture was heated overnight at 100 °C then concentrated. The crude material was purified by silica chromatography to afford **68** as a yellow oil (200 mg, 54% at 90% purity). ¹H NMR (400 MHz, CDCl₃, δ): 8.03 (s, 1H), 7.88 (d, *J* = 9 Hz, 1H), 7.75-7.72 (m, 2H), 7.61-7.55 (m, 3H), 7.47 (d, *J* = 9 Hz, 1H), 5.65 (br. s, 1H), 4.27 (t, *J* = 8 Hz, 2H), 3.60–3.57 (m, 4H), 3.55–3.48 (m, 2H), 3.34–3.32 (m, 4H), 1.51 (s, 9H); LC-MS (Method B) *m/z* [M + H]⁺ 642.2, *t_R* 1.76 mins.

General Boc Deprotection Procedure 4

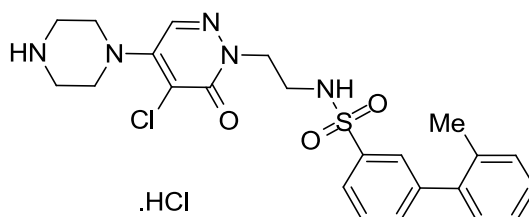
3',4'-Dichloro-*N*-(2-(5-chloro-6-oxo-4-(piperazin-1-yl)pyridazin-1(6*H*)-yl)ethyl)-[1,1'-biphenyl]-3-sulfonamide, hydrochloride salt, **19c**



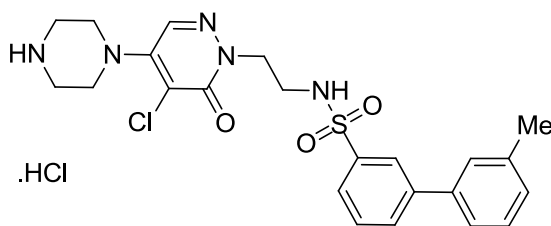
A stirred solution of **68** (200 mg, 0.31 mmol) in EtOAc (20 mL) was treated with a solution of concentrated HCl (9.5 μL, 0.31 mmol) in EtOAc (20 mL). The reaction mixture was stirred at room temperature overnight then filtered. The solid was washed with EtOAc (20 mL) then purified by MDAP (Method B) and acidified with HCl to afford **19c** as a white solid (80 mg, 46%). IR (cm⁻¹) 3700 - 2400 (m), 1594, 1310, 1153, 1092, 796, 692, 678; ¹H NMR (600 MHz, DMSO-d₆, δ): 9.18 (br. s, 2H), 8.05 (s, 1H), 8.02 (d, *J* = 2 Hz, 1H), 7.99 (d, *J* = 8 Hz, 1H), 7.93 (s, 1H), 7.90 (t, *J* = 6 Hz, 1H), 7.82-7.76 (m, 2H), 7.76-7.72 (m, 1H), 7.71-7.66 (m, 1H), 4.08 (t, *J* = 6 Hz, 2H), 3.61-3.51 (m, 4H), 3.23 - 3.18 (m, 4H), 3.17 - 3.12 (m, 2H); ¹³C NMR (126 MHz, DMSO-d₆, δ): 157.2, 146.8, 141.1, 139.1, 138.5, 131.9, 131.6, 131.1, 131.0, 130.7, 130.0, 128.7, 127.1, 126.0, 124.5, 115.8, 51.1, 45.4, 42.7, 40.4; HRMS-FAB (*m/z*): [M + H]⁺ calcd for C₂₂H₂₂Cl₃N₅O₃S, 542.0582; found, 542.0583; LC-MS *m/z* [M + H]⁺ 542.1, *t_R* (Method B) 1.30 mins; mp 152 – 153 °C.

N*-(2-(5-Chloro-6-oxo-4-(piperazin-1-yl)pyridazin-1(6*H*)-yl)ethyl)-4'-methoxy-[1,1'-biphenyl]-3-sulfonamide, **19d*

Prepared from **71** (141 mg, 0.23 mmol) using the general Boc deprotection procedure 4 to afford **19d** (12 mg, 10%) without the HCl-mediated acidification step. ¹H NMR (400 MHz, CD₃OD, δ): 7.99 (s, 1H), 7.88-7.80 (m, 2H), 7.72 (d, *J* = 8 Hz, 1H), 7.66-7.56 (d, *J* = 8 Hz, 3H), 7.13-7.00 (m, 2H), 4.24 (t, *J* = 6 Hz, 2H), 3.87 (s, 3H), 3.67-3.57 (m, 4H), 3.43-3.32 (m, 6H, *obscured by residual solvent peak*), *sulfonamide proton and piperazine proton underwent exchange and were not visible*; LC-MS [M + H]⁺ 504.0, *t_R* (Method B) 1.27 mins.

N*-(2-(5-Chloro-6-oxo-4-(piperazin-1-yl)pyridazin-1(6*H*)-yl)ethyl)-2'-methyl-[1,1'-biphenyl]-3-sulfonamide, hydrochloride salt, **20a*

Prepared from **72** (139 mg, 0.24 mmol) using the general Boc deprotection procedure 4, with DCM in the place of EtOAc. The reaction mixture was acidified with HCl to afford **20a** (25 mg, 20%). ¹H NMR (600 MHz, DMSO-*d*₆, δ): 9.29 (br. s, 2H), 7.93 (s, 1H), 7.86 (t, *J* = 5 Hz, 1H), 7.76 (d, *J* = 7 Hz, 1H), 7.69 (br. s, 1H), 7.68-7.60 (m, 2H), 7.37-7.28 (m, 3H), 7.25 (d, *J* = 7 Hz, 1H), 4.09 (t, *J* = 6 Hz, 2H), 3.67 - 3.54 (m, 4H), 3.24-3.13 (m, 6H), 2.23 (s, 3H); ¹³C NMR (151 MHz, DMSO-*d*₆, δ) 157.2, 146.9, 142.0, 140.2, 139.6, 134.7, 132.9, 131.7, 130.5, 129.5, 129.2, 128.0, 126.6, 126.1, 124.9, 115.8, 51.1, 45.5, 42.7, 40.4, 19.9; LC-MS *m/z* [M + H]⁺ 488.0, *t_R* (Method B) 1.31 mins.

N*-(2-(5-Chloro-6-oxo-4-(piperazin-1-yl)pyridazin-1(6*H*)-yl)ethyl)-3'-methyl-[1,1'-biphenyl]-3-sulfonamide, hydrochloride salt, **20b*

Tetrakis(triphenylphosphino)palladium(0) (40 mg, 0.035 mmol, 10 mol%) was added to a mixture of **66** (200 mg, 0.35 mmol), *m*-tolylboronic acid (52 mg, 0.38 mmol) and sodium carbonate (110 mg, 1.04 mmol) in DMF (15 mL) and water (2 mL) under nitrogen. The mixture was heated overnight at 100 °C then concentrated. The crude material was purified by silica chromatography (EtOAc) to afford **67** as a yellow oil (150 mg, 63% at 85% purity). LC-MS (Method B) *m/z* [M + H]⁺ 588.0, *t_R* 1.71 mins.

Compound **67** (150 mg, 0.26 mmol at 85% purity) was dissolved in EtOAc (20 mL). The mixture was treated with hydrochloric acid (8 μL solution in 10 mL EtOAc) then stirred at room temperature overnight. The mixture was concentrated then purified by MDAP (Method B). Isolated material was acidified with HCl to give **20b** as a white solid (60 mg, 33%). IR (cm⁻¹) 3700 - 2400 (m), 1594, 1319, 1151, 1093, 782, 693; ¹H NMR (600 MHz, DMSO-*d*₆, δ): 9.28 (br. s, 2H), 8.00 (s, 1H), 7.94-7.90 (m, 2H), 7.87 (t, *J* = 6 Hz, 1H), 7.74 (d, *J* = 8 Hz, 1H), 7.69-7.63 (m, 1H), 7.53 (s, 1H), 7.50 (d, *J* = 8 Hz, 1H), 7.40 (dd, *J* = 8, 8 Hz, 1H), 7.25 (d, *J* = 7 Hz, 1H), 4.09 (t, *J* = 6 Hz, 2H), 3.67-3.49 (m, 4H), 3.25-3.11 (m, 6H), 2.41 (s, 3H); ¹³C NMR (151 MHz, DMSO-*d*₆, δ): 157.2, 146.8, 141.2, 140.9, 138.5, 138.3, 131.6, 130.5, 129.8, 129.0, 128.8, 127.4, 125.2, 124.3, 123.9, 115.8, 51.1, 45.4, 42.7, 40.4, 21.0; HRMS-FAB (*m/z*): [M + H]⁺ calcd for C₂₃H₂₆ClN₅O₃S, 488.1518; found, 488.1496; LC-MS (Method B) *m/z* [M + H]⁺ 488.0, *t_R* 1.31 mins; mp 148 – 149 °C.

1.10. References

- (1) Arita, K.; Hashimoto, H.; Shimizu, T.; Nakashima, K.; Yamada, M.; Sato, M. *Nat. Struct. Mol. Biol.* **2004**, *11*, 777-783.
- (2) Yu, Y., Su, K. *J. Clin. Cell Immunol.* **2013**, *4*, 139-145.
- (3) Vossenaar, E. R.; Zendman, A. J. W.; van Venrooij, W. J.; Pruijn, G. J. M. *BioEssays* **2003**, *25*, 1106-1118. **Table 3** is reprinted with permission, © 2003 Wiley Periodicals, Inc.
- (4) Wang, Y.; Wysocka, J.; Sayegh, J.; Lee, Y.-H.; Perlin, J. R.; Leonelli, L.; Sonbuchner, L. S.; McDonald, C. H.; Cook, R. G.; Dou, Y.; Roeder, R. G.; Clarke, S.; Stallcup, M. R.; Allis, C. D.; Coonrod, S. A. *Science* **2004**, *306*, 279-283.
- (5) Atkinson, S. J.; Barker, M. D.; Campbell, M.; Diallo, H.; Douault, C.; Garton, N. S.; Liddle, J.; Sheppard, R. J.; Walker, A. L.; Wellaway, C.; Wilson, D. M.; WO2014/015905A1: 2014.
- (6) Atkinson, S. *GSK colleague responsible for synthesis, unpublished results.*
- (7) Atkinson, S. *GSK colleague responsible for synthesis, via Contract Research Organisation, unpublished results.*
- (8) Preston, A. *GSK colleague responsible for synthesis, unpublished results.*
- (9) *Epigenetic Mechanisms of Gene Regulation*; Russo, V. E. A., Martienssen, R. A., Riggs, A. D. , Ed.; Cold Spring Harbor Laboratory Press,; Woodbury, 1996.
- (10) Kouzarides, T. *Cell* **2007**, *128*, 693-705.
- (11) Tarakhovsky, A. *Nat. Immunol.* **2010**, *11*, 565-568.
- (12) Felsenfeld, G.; Groudine, M. *Nature* **2003**, *421*, 448-453.
- (13) Wolffe, A. P.; Hayes, J. J. *Nucleic Acids Res.* **1999**, *27*, 711-720. **Figure 1** (inset) is reproduced by permission of Oxford University Press.
- (14) Qiu, J. *Nature* **2006**, *441*, 143-145.
- (15) Arrowsmith, C. H.; Bountra, C.; Fish, P. V.; Lee, K.; Schapira, M. *Nat. Rev. Drug Discov.* **2012**, *11*, 384-400.
- (16) Bottomley, M. J. *EMBO Rep.* **2004**, *5*, 464-469. **Figure 2** is reprinted with permission, © 2004, European Molecular Biology Organization.
- (17) Robertson, K. D.; Wolffe, A. P. *Nat. Rev. Genet.* **2000**, *1*, 11-19.
- (18) Lee, J. T. *Science* **2012**, *338*, 1435-1439.

- (19) Sidoli, S.; Cheng, L.; Jensen, O. N. *J. Proteomics* **2012**, *75*, 3419-3433.
- (20) Prinjha, R. K.; Witherington, J.; Lee, K. *Trends Pharmacol. Sci.* **2012**, *33*, 146-153. **Figure 3** is reprinted from this publication entitled Place your BETs: the therapeutic potential of bromodomains, © 2012 with permission from Elsevier.
- (21) Sugimura, T.; Ushijima, T. *Mutat. Res.* **1999**, *462*, 235-246.
- (22) Marks, P. W. *Expert Rev. Anticancer Ther.* **2012**, *12*, 299–305.
- (23) Marks, P. A.; Breslow, R. *Nat. Biotechnol.* **2007**, *25*, 84-90.
- (24) Cedar, H.; Bergman, Y. *Nat. Rev. Immunol.* **2011**, *11*, 478-488.
- (25) Lin, H. S.; Hu, H.-S.; Chan, H.-Y.; Liew, Y.-Y.; Huang, H.-P.; Lepescheux, L.; Bastianelli, E.; Baron, R.; Rawadi, G.; Clément-Lacroix, P. *Br. J. Pharmacol.* **2007**, *150*, 862-872.
- (26) Hu, N.; Qiu, X.; Luo, Y.; Yuan, J.; Li, Y.; Lei, W.; Zhang, G.; Zhou, Y.; Su, Y.; Lu, Q. *J. Rheumatol.* **2008**, *35*, 804-810.
- (27) Ciavatta, D. J.; Yang, J.-J.; Preston, G. A.; Badhwar, A. K.; Xiao, H.; Hewins, P.; Nester, C. M.; Pendergraft, W. F.; Magnuson, T. R.; Jennette, J. C.; Falk, R. *J. Clin. Invest.* **2010**, *120*, 3209-3219.
- (28) Muller, S.; Filippakopoulos, P.; Knapp, S. *Expert Rev. Mol. Med.* **2011**, *13*, 1-21.
- (29) Shogren-Knaak, M.; Ishii, H.; Sun, J.-M.; Pazin, M. J.; Davie, J. R.; Peterson, C. L. *Science* **2006**, *311*, 844-847.
- (30) Lorenzo, A. D.; Bedford, M. T. *FEBS Lett.* **2011**, *585*, 2024-2031.
- (31) Guccione, E.; Bassi, C.; Casadio, F.; Martinato, F.; Cesaroni, M.; Schuchlantz, H.; Luescher, B.; Amati, B. *Nature* **2007**, *449*, 933-938.
- (32) Kirmizis, A.; Santos-Rosa, H.; Penkett, C. J.; Singer, M. A.; Vermeulen, M.; Mann, M.; Bähler, J.; Green, R. D.; Kouzarides, T. *Nature* **2007**, *449*, 928-932.
- (33) Arrowsmith, C. H.; Audia, J. E.; Austin, C.; Baell, J.; Bennett, J.; Blagg, J.; Bountra, C.; Brennan, P. E.; Brown, P. J.; Bunnage, M. E.; Buser-Doepner, C.; Campbell, R. M.; Carter, A. J.; Cohen, P.; Copeland, R. A.; Cravatt, B.; Dahlin, J. L.; Dhanak, D.; Edwards, A. M.; Frye, S. V.; Gray, N.; Grimshaw, C. E.; Hepworth, D.; Howe, T.; Huber, K. V. M.; Jin, J.; Knapp, S.; Kotz, J. D.; Kruger, R. G.; Lowe, D.; Mader, M. M.; Marsden, B.; Mueller-Fahrnow, A.; Muller, S.; O'Hagan, R. C.; Overington, J. P.; Owen, D. R.; Rosenberg, S. H.; Roth, B.; Ross, R.; Schapira, M.; Schreiber, S. L.; Shoichet, B.; Sundstrom, M.;

- Superti-Furga, G.; Taunton, J.; Toledo-Sherman, L.; Walpole, C.; Walters, M. A.; Willson, T. M.; Workman, P.; Young, R. N.; Zuercher, W. J. *Nat. Chem. Biol.* **2015**, *11*, 536-541.
- (34) Sweis, R. F. *ACS Med. Chem. Lett.* **2015**, *6*, 618-621.
- (35) Frye, S. V. *Nat. Chem. Biol.* **2010**, *6*, 159-161.
- (36) Structural Genomics Consortium (SGC), <http://www.thesgc.org/>, accessed 28th May 2016.
- (37) Bunnage, M. E.; Chekler, E. L. P.; Jones, L. H. *Nat. Chem. Biol.* **2013**, *9*, 195-199.
- (38) Tanramluk, D.; Schreyer, A.; Pitt, W. R.; Blundell, T. L. *Chem. Biol. Drug Des.* **2009**, *74*, 16-24.
- (39) Reddy, A. S.; Zhang, S. *Expert Rev. Clin. Pharmacol.* **2013**, *6*, 41-47.
- (40) Tenenbaum, A.; Fisman, E. Z.; Motro, M. *Cardiology* **1998**, *90*, 153-159.
- (41) Tapiero, H.; Mathé, G.; Couvreur, P.; Tew, K. D. *Biomed. Pharmacother.* **2002**, *56*, 439-445.
- (42) Arana, V.; Paz, Y.; González, A.; Méndez, V.; Méndez, J. D. *Biomed. Pharmacother.* **2004**, *58*, 588–597.
- (43) Napoli, C.; Maione, C.; Schiano, C.; Fiorito, C.; Ignarro, L. J. *Trends Mol. Med.* **2007**, *13*, 278-286.
- (44) Dort, J.; Sirois, A.; Leblanc, N.; Cote, C. H.; Jacques, H. *App. Physiol. Nutr. Metab.* **2012**, *37*, 489-498.
- (45) Witte, M. B.; Barbul, A. *Wound Repair Regen.* **2003**, *11*, 419-423.
- (46) Pipili-Synetos, E.; Sakkoula, E.; Haralabopoulos, G.; Andriopoulou, P.; Peristeris, P.; Maragoudakis, M. E. *Br. J. Pharmacol.* **1994**, *111*, 894-902.
- (47) Eckersten, D.; Henningsson, R. *Regul. Pept.* **2012**, *174*, 32-37.
- (48) Cannon III, R. O. *Clin. Chem.* **1998**, *44*, 1809-1819.
- (49) Hayward, C. S.; Kelly, R. P.; Macdonald, P. S. *Cardiovasc. Res.* **1999**, *43*, 628–638.
- (50) Andre, I.; Linse, S.; Mulder, F. A. A. *J. Am. Chem. Soc.* **2007**, *129*, 15805-15813.
- (51) Haines, R. J.; Pendleton, L. C.; Eichler, D. C. *Int. J. Biochem. Mol. Biol.* **2011**, *2*, 8-23.

- (52) Wada, M. *Biochemische Z.* **1930**, 224, 420-429.
- (53) Knowles, R. G.; Moncada, S. *Biochem. J.* **1994**, 298, 249-258.
- (54) Thiemermann, C. *Gen. Pharmacol.* **1997**, 29, 159-166.
- (55) Bogdan, C. *Nat. Immunol.* **2001**, 2, 907-916.
- (56) Singh, V. K.; Mehrotra, S.; Narayan, P.; Pandey, C. M.; Agarwal, S. S. *Immunol. Res.* **2000**, 22, 1-19.
- (57) Vallance, P., Leone, A., Calver, A., Collier, J., Moncada, S. *J. Cardiovasc. Pharm.* **1992**, 20, S60-S62.
- (58) Bedford, M. T.; Clarke, S. G. *Mol. Cell* **2009**, 33, 1-13.
- (59) Bedford, M. T. *J. Cell Sci.* **2007**, 120, 4243-4246.
- (60) Vítěček, J.; Lojek, A.; Valacchi, G.; Kubala, L. *Mediators Inflamm.* **2012**, 2012, 1-22.
- (61) National Center for Advancing Translational Sciences (NCATS) website, <http://www.ncats.nih.gov/files/GW274150.pdf>, accessed 28th May 2016.
- (62) Molina-Serrano, D.; Schiza, V.; Kirmizis, A. *Biochem. Soc. Trans.* **2013**, 41, 751-759.
- (63) Thompson, P. R.; Fast, W. *Chem. Biol.* **2006**, 1, 433-441.
- (64) Foulquier, C.; Sebbag, M.; Clavel, C.; Chapuy-Regaud, S.; Al Badine, R.; Méchin, M.-C.; Vincent, C.; Nachat, R.; Yamada, M.; Takahara, H.; Simon, M.; Guerrin, M.; Serre, G. *Arthritis Rheum.* **2007**, 56, 3541–3553.
- (65) Slack, J. L.; Causey, C. P.; Thompson, P. R. *Cel. Mol. Life Sci.* **2011**, 68, 709-720.
- (66) Willis, V. C.; Gizinski, A. M.; Banda, N. K.; Causey, C. P.; Knuckley, B.; Cordova, K. N.; Luo, Y.; Levitt, B.; Glogowska, M.; Chandra, P.; Kulik, L.; Robinson, W. H.; Arend, W. P.; Thompson, P. R.; Holers, V. M. *J. Immunol.* **2011**, 186, 4396-4404.
- (67) Murray, K.; Rasmussen, P. S.; Neustaedter, J.; Luck, J. M. *J. Biol. Chem.* **1965**, 240, 705-709.
- (68) Warner, R. C. *J. Biol. Chem.* **1942**, 142, 705.
- (69) Dodson, G.; Wlodawer, A. *Trends Biochem. Sci.* **1998**, 23, 347.
- (70) Chapman, H. A.; Riese, R. J.; Shi, G.-P. *Annu. Rev. Biophys. Biomol. Struct.* **1999**, 28.

- (71) Gribbon, P.; Sewing, A. *Drug Discov. Today* **2003**, *8*, 1035-1043.
- (72) Luo, Y.; Arita, K.; Bhatia, M.; Knuckley, B.; Lee, Y.-H.; Stallcup, M. R.; Sato, M.; Thompson, P. R. *Biochem.* **2006**, *45*, 11727-11736.
- (73) Banerjee, A.; Sharma, R.; Banerjee, U. C. *Biotech. Appl. Biochem.* **2003**, *37*, 289-293.
- (74) Suguwara, K.; Oyama, F. *Biochem. J.* **1981**, *89*, 771-774.
- (75) Huang, G.; Hou, J.; Zhou, X. A. *Environ. Sci. Technol.* **2009**, *43*, 5851-5856.
- (76) Lipinski, C. A.; Lombardo, F.; Dominy, B. W.; Feeney, P. J. *Adv. Drug Deliv. Rev.* **1997**, *23*, 3-25.
- (77) Moerka, N. *Curr. Protoc. Chem. Biol.* **2009**, *1*, 1-15.
- (78) Locke, K.; Craggs, P.; Traynor, H., GSK internal presentation: "Biochemical assays: how to see molecules".
- (79) Oprea, T. I.; Davis, A. M.; Teague, S. J.; Leeson, P. D. *J. Chem. Inf. Comput. Sci.* **2001**, *41*, 1308-1315.
- (80) Leo, A. H., C.; Elkins, D. *Chem. Rev.* **1971**, *71*, 525-616.
- (81) Mannhold, R. *Molecular Drug Properties: Measurement and Prediction.*; Wiley-VCH publishing: Weinheim, 2008.
- (82) Instant JChem, ChemAxon Kft, and Informatics Matters Ltd.
- (83) cLOGP Reference Manual, Daylight Chemical Information Systems, Inc. <http://www.daylight.com/dayhtml/doc/clogp/index.html>, accessed 28th May 2016.
- (84) Morphy, R. *J. Med. Chem.* **2006**, *49*, 2969-2978.
- (85) Abad-Zapatero, C. *Expert Opin. Drug Discov.* **2007**, *2*, 469-488.
- (86) Leeson, P. D.; Springthorpe, B. *Nat. Rev. Drug Discov.* **2007**, *6*, 881-890.
- (87) ADEPT, GSK Internal Online Tool: <http://adept.gsk.com/adept/adept>, accessed 8th October 2014. The website is no longer supported.
- (88) Weininger, D. *J. Chem. Inf. Model.* **1988**, *28*, 31-36.
- (89) Johnston, P. A. *Curr. Opin. Chem. Biol.* **2011**, *15*, 174-182.
- (90) Lochansky, M. *GSK colleague, unpublished results.*
- (91) Blaxill, Z.; Holland-Crimmin, S.; Lively, R. *J. Biomol. Screen.* **2009**, *14*, 547-556.

- (92) Cheng, X.; Hochlowski, J.; Tang, H.; Hepp, D.; Beckner, C.; Kantor, S.; Schmitt, R. *J. Biomol. Screen.* **2003**, *8*, 292-304.
- (93) Areri, I. *GSK Internal Communication.*
- (94) Ward, J. H. *J. Amer. Statist. Assoc.* **1963**, *58*, 236-244.
- (95) Kucherenko, T.; Kysil, V.; Kovtunencko, V. *Synth. Commun.* **2003**, *33*, 1163-1166.
- (96) Mruk, N. J.; Tieckelmann, H. *Tetrahedron Lett.* **1970**, *14*, 1209-1212.
- (97) Henry, R. A.; Heller, C. A.; Moore, D. W. *J. Org. Chem.* **1975**, *40*, 1760-1766.
- (98) *Synthesis completed independently by contract research organisation (CRO), unpublished results.*
- (99) Bax, B. *GSK colleague responsible for X-ray crystallography, unpublished results.*
- (100) Mortenson, P. N.; Murray, C. W. *J. Comput.-Aided Mol. Des.* **2011**, *25*, 663–667.
- (101) Tsuji, K.; Tsubouchi, H.; Yasumura, K.; Matsumoto, M.; Ishikawa, H. *Bioorg. Med. Chem.* **1996**, *4*, 2135-2149.
- (102) Waldmeier, P. C.; Buchle, A.-M.; Steulet, A. F. *Biochem. Pharmacol.* **1993**, *45*, 2417-2424.
- (103) Meanwell, N. A. *J. Med. Chem.* **2011**, *54*, 2529-2591.
- (104) Hanspeter, N. *Curr. Opinion Chem. Biol.* **2007**, *11*, 419-423.
- (105) Böhm, H.-J. *J. Comput.-Aided Mol. Des.* **1994**, *8*, 243-256.
- (106) Bissantz, C.; Kuhn, B.; Stahl, M. *J. Med. Chem.* **2010**, *53*, 5061-5084.
- (107) Friesner, R. A.; Banks, J. L.; Murphy, R. B.; Halgren, T. A.; Klicic, J. J.; Mainz, D. T.; Repasky, M. P.; Knoll, E. H.; Shelley, M.; Perry, J. K.; Shaw, D. E.; Francis, P.; Shenkin, P. S. *J. Med. Chem.* **2004**, *47*, 1739-1749.
- (108) Schrödinger Desmond Molecular Dynamics System in Maestro-Desmond Interoperability Tools 34 edn New York D E Shaw Research.
- (109) Cozzini, P.; Fornabaio, M.; Marabotti, A.; Abraham, D. J.; Kellogg, G. E.; Mozzarelli, A. *Curr. Med. Chem.* **2004**, *11*, 1345-1359.
- (110) Johnson, T. W.; Dress, K. R.; Edwards, M. *Bioorg. Med. Chem.* **2009**, *19*, 5560-5564.
- (111) Barker, M. *GSK Internal Communication.*

- (112) ChemAxon software, ChemAxon Kft., Záhony u. 7, Building HX 1031, Budapest, Hungary.
- (113) Isogaya, M.; Yamagiwa, Y.; Fujita, S.; Sugimoto, Y.; Nagao, T.; Kurose, H. *Mol. Pharmacol.* **1998**, *54*, 616-622.
- (114) Waters, M. L. *Curr. Opinion Chem. Biol.* **2002**, *6*, 736–741.
- (115) Meyer, E. A.; Castellano, R. K.; Diederich, F. *Angew. Chem. Int. Ed.* **2003**, *42*, 1210-1250.
- (116) Ma, J. C.; Dougherty, D. A. *Chem. Rev.* **1997**, *97*, 1303-1324.
- (117) Andrews, P. R.; Craik, D. J.; Martin, J. L. *J. Med. Chem.* **1984**, *27*, 1648-1657.
- (118) Raju, R. K.; Bloom, J. W. G.; An, Y.; Wheeler, S. E. *ChemPhysChem* **2011**, *12*, 3116 -3130. **Figure 23** is reprinted with permission, © 2011 Wiley-VCH Verlag GmbH & Co. KGaA, Weinheim.
- (119) Ballester, P. *Acc. Chem. Res.* **2013**, *46*, 874-884.
- (120) Gallivan, J. G.; Dougherty, D. A. *J. Am. Chem. Soc.* **2000**, *122*, 870-874.
- (121) Burley, S. K.; Petsko, G. A. *FEBS Lett.* **1986**, *203*, 139-143.
- (122) Marshall, M. S.; Steele, R. P.; Thanthiriwatte, K. S.; Sherrill, C. D. *J. Phys. Chem. A* **2009**, *113*, 13628-13632.
- (123) Burley, S. K.; Petsko, G. A. *Science* **1985**, *229*, 23-28
- (124) McGaughey, G. B.; Gagné, M.; Rappé, A. K. *J. Biol. Chem.* **1998**, *273*, 15458-15463.
- (125) Halgren, T. A. *J. Comput. Chem.* **1999**, *20*, 720-729.
- (126) Molecular Operating Environment (MOE), Chemical Computing Group Inc., 1010 Sherbooke St. West, Suite #910, Montreal, QC, Canada, H3A 2R7, 2012.
- (127) Topliss, J. G. *J. Med. Chem.* **1972**, *15*, 1006-1011. The Topliss operational scheme (**Figure 24**) and table of substituent Constant Values (**Table 21**) are reprinted (adapted) from this reference with permission, © 1972 American Chemical Society.
- (128) Hansch, C.; Fujita, T. *J. Am. Chem. Soc.* **1964**, *86*, 1616-1626.
- (129) Percy, J. M. *University of Strathclyde Glasgow, unpublished results.*
- (130) Thomas, P. *GSK colleague, unpublished results.*
- (131) Cruz-Cabeza, A. J.; Liebeschuetz, J. W.; Allen, F. H. *CrystEngComm* **2012**, *14*, 6797-6811.

- (132) Eyal, E.; Gerzon, S.; Potapov, V.; Edelman, M.; Sobolev, V. *J. Mol. Biol.* **2005**, *351*, 431–442.
- (133) Brock, C. P. *J. Res. Natl. Inst. Stan.* **1996**, *101*, 321-.
- (134) Yadav, J. S.; Reddy, B. V. S.; Reddy, U. V. S.; Praneeth, K. *Tetrahedron Lett.* **2008**, *49*, 4742–4745.
- (135) Imafuku, K.; Takahashi, K.; Matsumura, H. *Bull. Chem. Soc. Jpn.* **1983**, *56*, 1879-1880.
- (136) Upton, R. *GSK colleague, unpublished results.*
- (137) Minami, N.; Kijima, S. *Chem. Pharm. Bull.* **1979**, *27*, 816-820.
- (138) Zhang, Q.; Wang, D.; Wang, X.; Ding, K. *J. Org. Chem.* **2009**, *74*, 7187-7190.
- (139) Wolkenberg, S.; Barrow, J. C.; Poslusney, M. S.; Harrison, S. T.; Trotter, B. W.; Mulhearn, J.; Nanda, K. K.; Manley, P. J.; Zhao, Z.; Schubert, J. W.; Kett, N.; Zartman, A.; WO2011/109254A1: 2011.
- (140) Ting, P. C.; Herr, R. J.; Kim, D. W. S.; Yang, J.; Zhou, G.; Kuang, R.; Zorn, N.; Zych, A. J.; Aslanian, R. G.; Cao, J.; Wu, H.; WO2008/08115381A1:2008.
- (141) Varga, I.; Jerkovich, G.; Mátyus, P. *J. Heterocyclic Chem.* **1991**, *28*, 493-496.
- (142) Dury, K. *Angew. Chem. Int. Ed.* **1965**, *4*, 292-300.
- (143) Betti, L.; Zanelli, M.; Giannaccini, G.; Manetti, F.; Schenoned, S.; Strappaghetti, G. *Bioorg. Med. Chem.* **2006**, *14*, 2828–2836.
- (144) Motawia, M. S.; Wengel, J.; Abdel-Megid, A. E. S.; Pedersen, E. B. *Synthesis* **1989**, 384-387.
- (145) Ming Lei, X.-L. T.; Wang, Y.-G. *Helv. Chim. Acta.* **2006**, *89*, 532-536.
- (146) Ripka, A. S.; Bohacek, R. S.; Rich, D. H. *Bioorg. Med. Chem.* **1998**, *8*, 357-360.
- (147) Höfle, G.; Steglich, W.; Vorbrüggen, H. *Angew. Chem. Int. Ed.* **1978**, *17*, 569-583.
- (148) Brown, H. C.; McDaniel, D. H.; Hafliger, O., Eds. *Determination of Organic Structures by Physical Methods*; Academic Press: New York, 1955.
- (149) Tan, W.; Hung, W.; Tsao, B. P. *Adapt. Med.* **2011**, *3*, 73-84.
- (150) Dwivedi, N.; Upadhyay, J.; Neeli, I.; Khan, S.; Pattanaik, D.; Myers, L.; Kirou, K. A.; Hellmich, B.; Knuckley, B.; Thompson, P. R.; Crow, M. K.; Mikuls, T. R.; Csernok, E.; Radic, M. *Arthritis Rheum.* **2012**, *64*, 982-992.

- (151) Johnson, D. S.; Weerapana, E.; Cravatt, B. F. *Future Med. Chem.* **2010**, *2*, 949–964.
- (152) Locke, K. *GSK colleague, unpublished results.*
- (153) Davis, R. *GSK colleague, unpublished results.*
- (154) Bassini, C. *GSK colleague responsible for synthesis, unpublished results.*
- (155) Hensel, H. R.; Baumann, H.; DE1420969A 1971.

Chapter 2: The Design, Synthesis and Optimisation of BET BD1 Inhibitors

2.1. Abstract

The Bromodomain Extra-terminal (BET)-containing bromodomain (BRD) family of proteins consists of four main BRDs which are involved in the regulation of gene transcription; these are BRD2, BRD3, BRD4 and BRDT.^{1,2} The *pan*-BET BRD inhibitor **iBET762** (**Figure 27**) developed by GSK was found to have anti-proliferative and anti-inflammatory effects;³⁻⁵ this suggested a *pan*-BET BRD inhibitor could be used to treat cancers, or to treat autoimmune diseases,⁶ such as rheumatoid arthritis (RA) and systemic lupus erythematosus (SLE). However, the toxic effects observed in preclinical safety species (rat and dog), including testicular changes and cardiovascular effects,⁷ have to date limited the clinical progress of *pan*-BET inhibitors to oncology indications where the benefit to risk ratio is higher than for the treatment of chronic autoimmune diseases. Clinical trials are underway using **iBET762** as an experimental treatment of nuclear-protein in testis (NUT) midline carcinoma patients,³ and more recently in patients with other tumours.^{8,9}

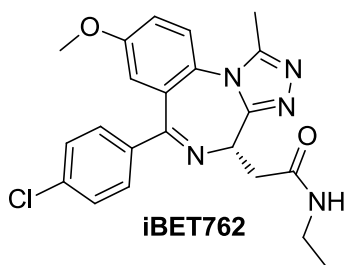


Figure 27. Antagonist **iBET762**, that is efficacious *in vivo* and a selective inhibitor of BRD2, BRD3, BRD4 and BRDT.

It was postulated that a selective inhibitor of one of the two binding domains (BDs) of the BET BRDs could have the potential to retain the beneficial anti-proliferative or anti-inflammatory effects of BET BRD inhibition observed using *pan*-BET BRD inhibitors, while also mitigating the toxic effects; an inhibitor with this profile could be used as a chronic treatment for autoimmune diseases.

A campaign to identify a novel BET BRD BD1 selective inhibitor that could be used to investigate preclinical toxicity was initiated by the Epinova Discovery Performance Unit (DPU). Compounds were designed and synthesised by myself, and where specified, were synthesised or purified by GSK colleagues, with access to array or large scale

synthesis or chiral HPLC equipment, in support of the BET BRD BD1 program.¹⁰⁻²⁰ As a result of this research, the novel furanopyridone (FP) **89** (Figure 28) was discovered, which is a potent and highly selective inhibitor of BET BRD BD1, and met anti-inflammatory endpoints *in vivo*. Compound **89** had a sufficiently good PK profile to be progressed to the dog safety study that aimed to determine whether selective BET BRD BD1 inhibition could be beneficial for the chronic treatment of autoimmune diseases without the toxic effects seen with *pan*-BET inhibitors.

An 11 g amount of **89** of greater than 97% purity, was delivered to meet the requirements of the dog safety study; the delivery of this amount of material was made possible as a result of the development of a chiral synthesis of oxetanyl moiety of **89**. During this development work, a number of steps in the synthesis were optimised, particularly the boronylation step, which led to an improvement in overall yield of **89** (12%) by three-fold relative to the route used to make the material the first time (4%).

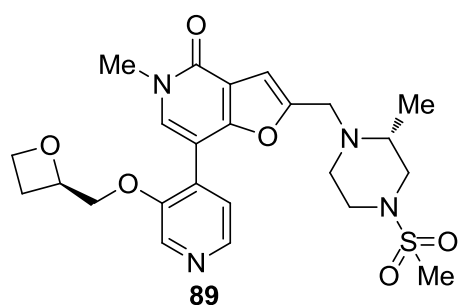


Figure 28. Novel furanopyridone antagonist **89**, a potent and highly selective inhibitor of BET BRD BD1, that met anti-inflammatory endpoints *in vivo*, and was progressed to a dog safety study.

The dog safety study showed that sufficient exposure to the selective BET BD1 inhibitor **89** had been achieved by intravenous infusion. Although no cardiovascular issues were conclusively observed, testicular changes in a number of dogs were evident. The testicular changes were milder in severity than those seen with *pan*-BET inhibitors, which suggested a greater benefit to risk ratio might be achieved with another generation of BET BRD BD1 inhibitor with an improved profile, for example, with even higher selectivity for BD1 *versus* BD2.^{7,21,22} The Epinova DPU has used learnings from this work to inform the BET inhibitor franchise and has since refocussed efforts on

the development of highly selective BET BRD BD2 inhibitors with the aim of identifying treatments for immunoinflammatory diseases.

2.2. Introduction

2.2.1. Bromodomains

The first BRD was first described in 1992 and consists of around 110 amino acids; the bromodomain is conserved in a number of transcriptionally important genes in species from yeasts to humans.²³ The human genome is known to encode 42 bromodomain-containing proteins, each of which can contain between one and six binding domains;²⁴ binding domain 1 is referred to as BD1, binding domain 2 as BD2, *et cetera*. A total of 57 unique human bromodomains are known and they have been clustered into nine subgroups according to sequence identity and structural similarity (**Figure 29**); a number have had their structures determined experimentally.²⁵ BRDs play a role in the regulation of gene transcription by acting as readers of epigenetic modifications, specifically *N*-acetylation marks on histone tails which can be created by HATs.²

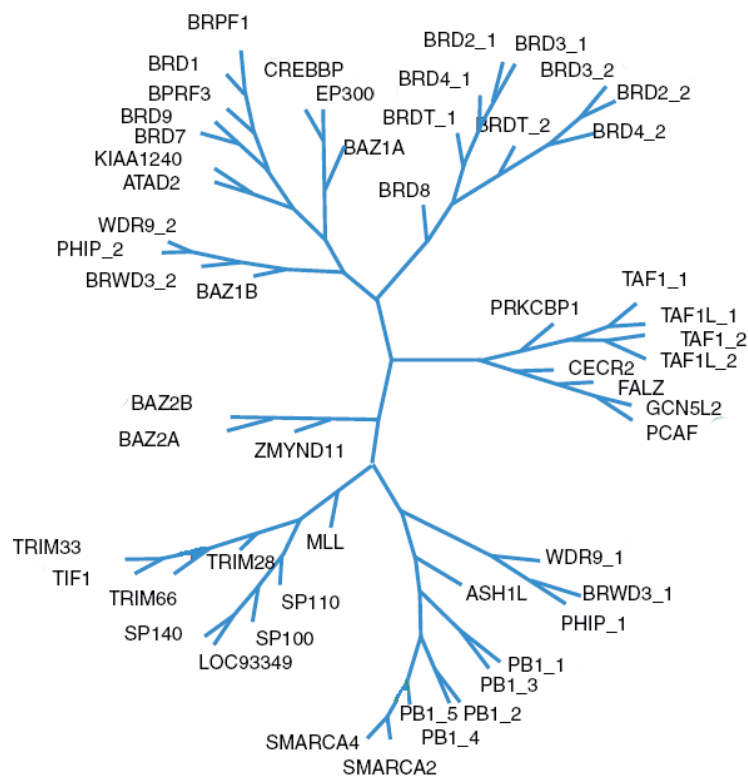


Figure 29. Phylogenetic tree of the bromodomain family of histone modification reader proteins which is also referred to as the bromonome.²⁵

Bromodomains are found in a number of proteins that also contain an enzymatic domain, such as HATs, or other reader domains, such as plant homeodomains (PHDs); the specific reader/writer/eraser abilities of each protein allow the creation of a unique combination of histone marks.

2.2.1.1. The BET Family of Bromodomains and Known Inhibitors

The BET-containing BRD family of proteins consists of four main BRDs which are structurally similar; these are BRD2, BRD3, BRD4 and BRDT^{2,4} (**Figure 30**).²⁶ Each BET BRD contains two BDs, BD1 and BD2. BET BRDs are involved in the regulation of gene transcription.

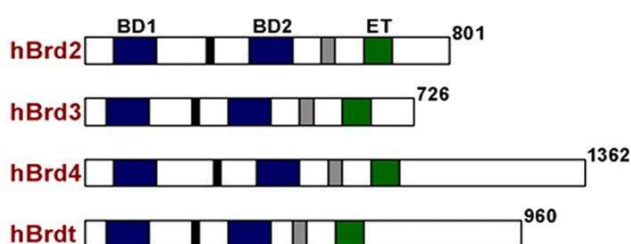


Figure 30. Representation of the BET family of BRDs.²⁶

The first selective small molecule inhibitors with low nanomolar affinity for BET BRDs, (+)-**JQ1** and **iBET762**, were independently reported to be BET BRD inhibitors in 2010 by Filippakopoulos *et al.*²⁷ and Nicodeme *et al.*⁴ respectively (**Figure 31**). These compounds are cell permeable and selectively inhibit the structurally similar BET BRD family of activity of BD1 and BD2 across the BET family, BRD2, 3, 4 and T.

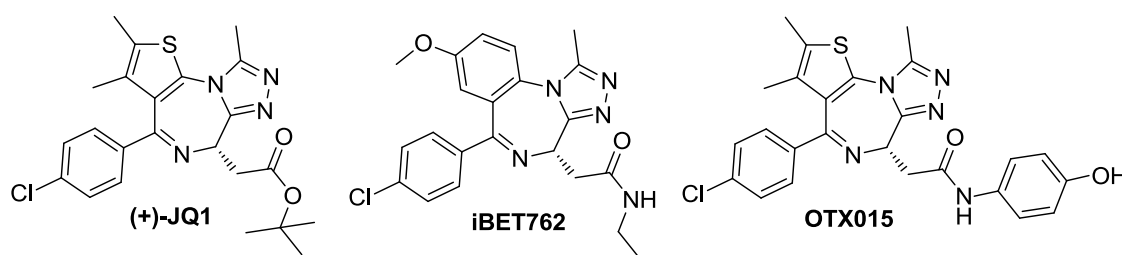


Figure 31. Bromodomain antagonists, (+)-**JQ1**, **iBET762**, and **OTX015** that are efficacious *in vivo* and are selective inhibitors of BRD2, BRD3, BRD4 and BRDT.^{4,27,28-}

Although both compounds possess a benz-[1,2,4]triazolo[4,3-*a*][1,4]diazepin backbone, they represented a novel chemical template that differed from previously reported templates by the absence of an acetyl moiety which is typically required for bromodomain recognition.

Compound **iBET762** had been originally identified by GSK France as **GSK525768A** during efforts to identify oral inducers of apolipoprotein A1 for the treatment of dyslipidaemias in heart disease to prevent heart attacks and strokes, but the class of compound was terminated because found to have poor oral human oral exposure.^{32,33} However, the GSK Epinova DPU found **iBET762** had anti-proliferative effects which led to its progression to clinical trials in patients as an experimental treatment of nuclear-protein in testis (NUT) midline carcinoma, solid tumours,^{3,5} and more recently for the treatment of other cancers such as haematologic malignancies.³⁴ NUT midline carcinoma (NMC) is a rare incurable aggressive epithelial cancer that can affect any tissue type or organ but is most likely to affect the head, neck and mediastinum.³⁵ The median age of patients at diagnosis is 25 years old;³⁶ there is a mean survival of 6.7 months.³⁵ NMC is driven by chromosomal translocation that leads to the expression of a “gain-of-function” fusion protein containing BRD4 and a testis-specific transcription factor, NUT. The BRD4 fusion oncoprotein was found to be displaced from chromatin by *pan*-BET inhibitors, leading to anti-proliferative effects in patient-derived xenograft models. Hence *pan*-BET inhibitors are being investigated as anti-cancer agents for this indication and clinical dose escalation studies are currently underway with **iBET762**.^{3,5,34} The *pan*-BET inhibitor OTX015, which is structurally related to (+)-JQ1, has been recently progressed by OncoEthix (now Merck) to clinical trials for evaluation as an anti-cancer agent (**Figure 31**).²⁸⁻³¹

The *pan*-BET inhibitor **iBET762** was also found by the Epinova DPU to have anti-inflammatory effects: **iBET762** inhibited IL-6 production with sub-micromolar potency after a lipopolysaccharide LPS challenge in a cell assay, the PBMC assay;⁵ **iBET762** was subsequently found to confer protection against both LPS-induced endotoxic shock and bacteria-induced sepsis in mice by disrupting chromatin complexes responsible for key inflammatory genes in activated macrophages.⁴ However, the use of **iBET762** to treat chronic auto-inflammatory diseases, such as SLE and RA, is challenging due to the

testicular and cardiovascular toxicities observed in the dog and rat. The outcome of the oncology clinical trials will ultimately help to determine if the pre-clinical toxicity events are observed in humans or not, at therapeutic doses. In the meantime, the Epinova DPU initiated efforts to discover more selective BET inhibitors that might retain the favourable anti-inflammatory effects while removing the toxic effects that were observed in preclinical safety species with a *pan*-BET inhibitor such as **iBET762**. The research described herein focuses on the development of a selective inhibitor of BD1 of the BET family of BRDs (**Figure 32**).

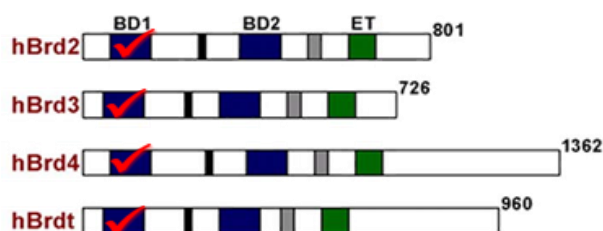


Figure 32. Diagrammatic representation of the main aim of the research described herein: the discovery of a selective inhibitor of BET BRD family BD1.²⁶

2.2.1.2. Structural features of BRDs and Early BRD Inhibitors

Bromodomains share a conserved fold of a left-handed, four-helix bundle made of four amphipathic helices; these are: αZ , αA , αB , and αC , and they are linked together by two different loop regions, ZA and BC, that contribute to ligand specificity.^{4,25} These key features can be seen clearly in the X-ray crystal structure of BRD4 BD1 bound to **iBET762** (**Figure 33a**, *orange*) overlaid with that of the H4Ac peptide (**Figure 33a**, *green*); in this case the H4Ac peptide is being used as a mimetic of an acetylated lysine (AcK) histone tail, and the H4Ac moiety is positioned in the acetyl-lysine pocket. The αZ and αA helices run alongside each other to create a hydrophobic channel, called the ZA channel, that is involved in recognition of the acetylated ligand, such as the H4Ac peptide.²⁵ Another feature that facilitates ligand binding is the lipophilic WPF shelf, so called because it consists of W81 (Trp 81), P82 (Pro 82) and F83 (Phe 83) residues. The Gatekeeper residue varies in size across the BRD family and controls access to the lipophilic WPF shelf, which is adjacent to the ZA channel (**Figure 33b**).

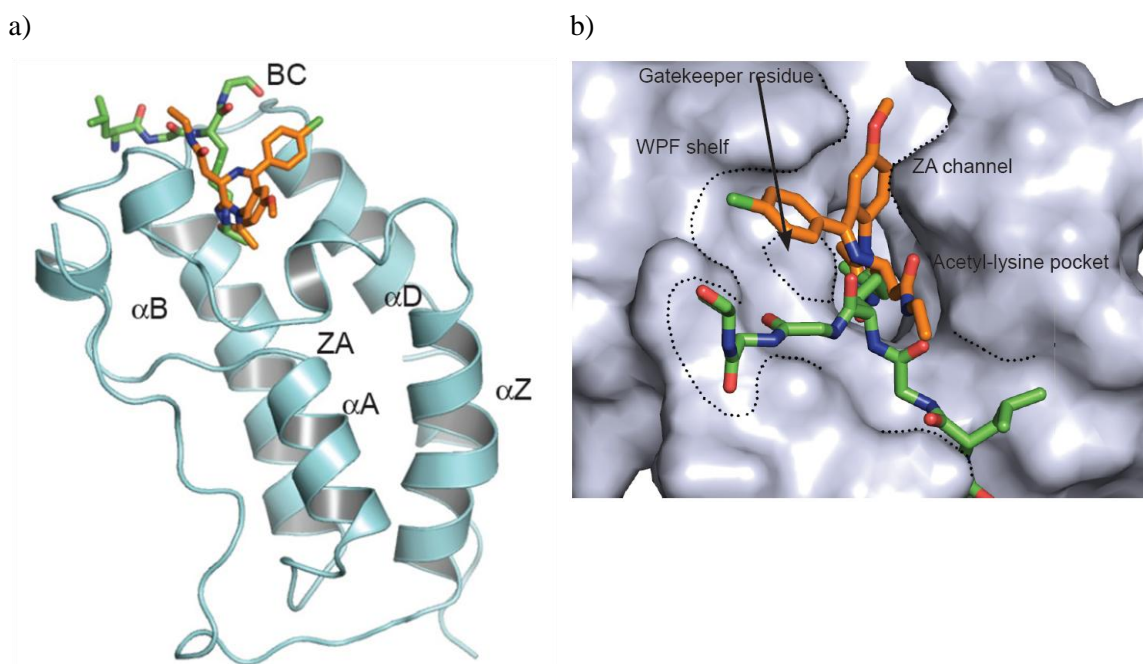


Figure 33. a) Ribbon representation of BRD4 BD1 bound to **iBET762** (orange) overlaid with acetylated histone H4 peptide, H4(1-15)K12Ac (H4Ac, green), at 1.6 Å resolution (PDB code 3P5O).⁴ Structural features of BRD4 BD1 are labelled. b) Structure of **iBET762** (orange) bound to the acetyl-binding pocket of BRD4 BD1 overlaid with (H4Ac, green).⁴ The WPF shelf (W81, P82 and F83, which corresponds to Trp 81, Pro 82 and Phe 83 respectively), the ZA channel and acetyl-lysine (AcK) pocket are indicated. Reprinted by permission from Macmillan Publishers Ltd: *Nature* 468: 1119-1123, © 2010.

The methyl and methylene groups of the acetylated ligand, the acetylated histone H4 peptide, make significant contacts with the side chains of Val 752, Ala 757, Tyr 760, Tyr 802, Asn 803 and Tyr 809, residues which are highly conserved across the BRD family.²⁵ The Acetyl-lysine pocket recognises the AcK portion of the ligand through a hydrogen bond with Asn 140 (**Figure 34**).

The crystal structure of **iBET762** bound in BRD4 BD1 showed that the 1,2,4-triazole moiety of iBET was able to occupy the acetyl-lysine (AcK)-binding pocket (**Figure 33b**) by making an essential hydrogen bond to Asp 140, and through water, to Tyr 97 (**Figure 34**).⁴ The compound **iBET762** was found to be highly selective for BRD2, BRD3, BRD4 and BRDT, and did not interact with other bromodomain-containing

proteins from other arms of the phylogeny tree (**Figure 29**), nor with 38 unrelated proteins. Selectivity is thought to be determined by the relative size of the hydrophobic ZA channel and the WPF-shelf adjacent to the AcK binding pocket, where spatial constraints on the size of molecules that can gain access to the WPF shelf are imposed by a conserved isoleucine or valine. The WPF shelf is lipophilic in character and is likely to make favourable interactions with the lipophilic chlorophenyl substituent of **iBET762** through dispersion forces. Favourable lipophilic contacts have been estimated to contribute 0.71 kcal per mol Å² to binding energy,³⁷ so the chlorophenyl substituent is likely to contribute to the potency of **iBET762**.

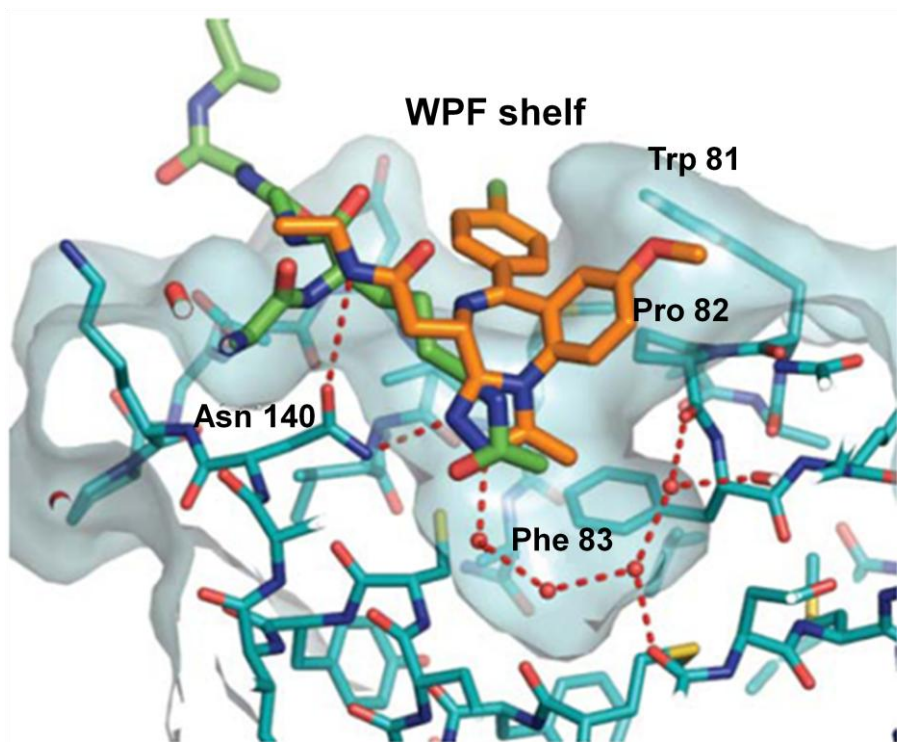


Figure 34. Structure of **iBET762** (orange) bound to the acetyl-binding pocket of BRD4-BD1 overlaid with H4Ac (green) at 1.6 Å resolution (PDB code 3P5O), reprinted by permission from Macmillan Publishers Ltd: *Nature* 468: 1119-1123, © 2010.^{4,125} The WPF shelf (W81, P82 and F83, which corresponds to Trp 81, Pro 82 and Phe 83 respectively), as well as the network of essential hydrogen bonds (red dashed lines) made between the triazole of **iBET762** and Asn 140 and the adjacent network of waters (red spheres) are shown.

A number of additional small molecule BET family inhibitors with alternative chemotypes to the benz-[1,2,4]triazolo[4,3-*a*][1,4]diazepin template have been reported, including the 3,5-dimethylisoxazole **iBET151** (**Figure 35**) for the treatment of MLL-fusion leukaemia,³⁸ a set of 1-acyltetrahydroquinolines (THQ) that are dual BET/HDAC inhibitors, represented by **iBET295** (**Figure 35**)³⁹ and the benzimidazole **BIC1** (**Figure 35**).⁴⁰

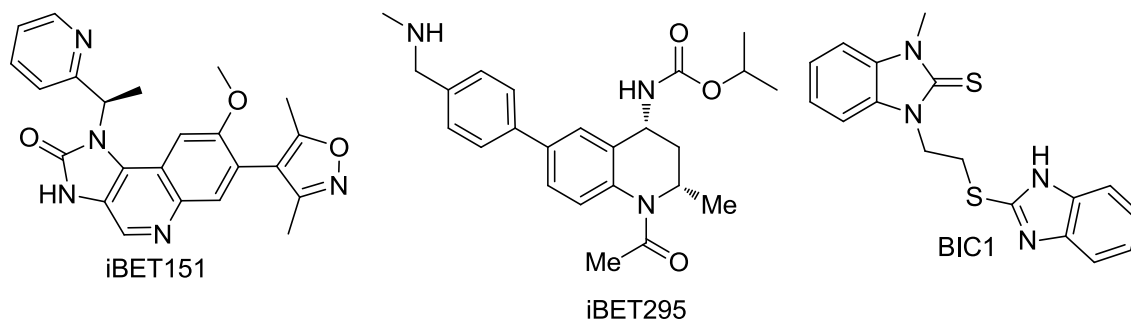


Figure 35. Structures of recently reported BET BRD-selective ligands.

The triazole units of **iBET762** and (+)-**JQ1** each act as an AcK mimic (**Figure 36a**), with one of the nitrogen atoms forming a hydrogen bond with a highly conserved Asn residue, Asn 140 in BRD4 BD1.⁴ A second triazolyl nitrogen atom forms a hydrogen bond with a conserved water molecule that is also hydrogen bonded to the conserved Tyr residue, Tyr 97 in BRD4 BD1. Similarly the 3,5-dimethylisoxazolyl oxygen atom of **iBET151** forms a hydrogen bond directly with the Asn residue while the nitrogen atom forms a hydrogen bond through water to the Tyr residue (**Figure 36b**).³⁸ The carbonyl oxygen atom of the 1-acetyl substituent of **iBET295**, and related compounds, forms a hydrogen bond with the Asn residue (**Figure 36c**).⁴⁰ These hydrogen bond interactions closely mimic those of the natural KAc ligand located on the *N*-termini of histone tails. An overlay of the BRD4 BD1 X-ray crystal structures of **iBET762**, (+)-**JQ1**, **iBET151** and **iBET295** shows the major hydrogen bond interactions made between the AcK mimetics and the BRD4 BD1 active site (**Figure 37**).

The KAc binding pocket is highly conserved between bromodomain subtypes and the interactions between ligand and the bromodomain Asn and Tyr residues are clearly important for the recognition and orientation of the ligand.⁴¹ Consequently it was highly

unlikely that selectivity between subtypes might be achieved with alternative AcK bioisosteres.

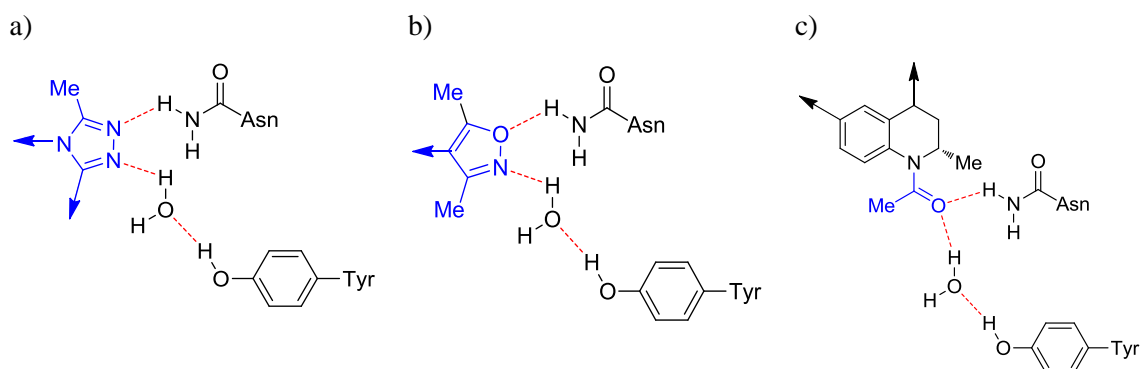


Figure 36. Schematic representations of the BRD-binding interactions of a) the benz-[1,2,4]triazolo[4,3-*a*][1,4]diazepines, **iBET762** and **(+)-JQ1**,^{4,27} b) the 3,5-dimethylisoxazole, **iBET151**,³⁸ c) the 1-acyltetrahydroquinoline **iBET295**.⁴⁰ For simplicity only partial structures are shown. Portions of each structure that act as AcK mimics are coloured blue and hydrogen bonds are represented by red dotted lines.

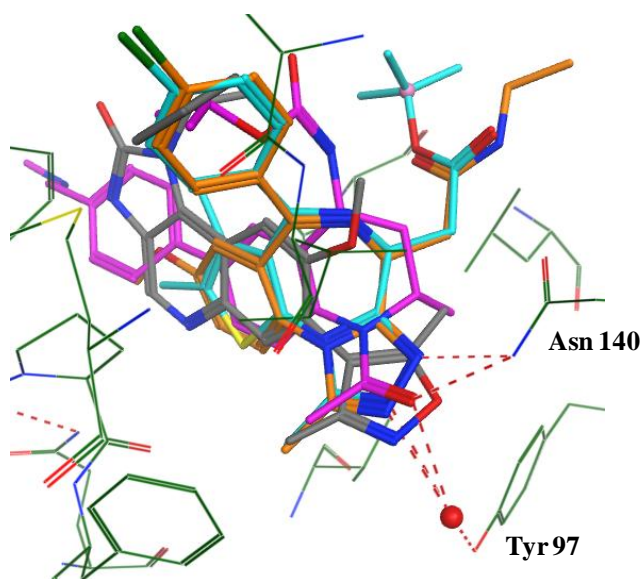
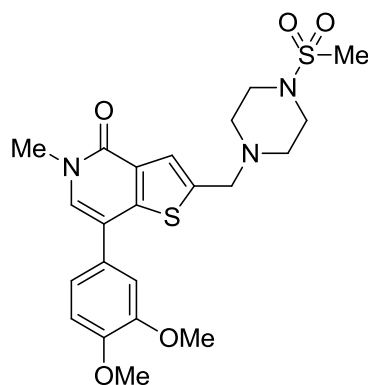


Figure 37. Overlay of BRD4 BD1 X-ray crystal structures of **iBET762** (orange, 1.6 Å resolution, PDB code 1HGKI), **(+)-JQ1** (cyan, 3MXF, 1.6 Å), **iBET151** (grey, 1.5 Å, 3ZYU), and **iBET295** (magenta, 1.6 Å, 3PMEN). Hydrogen bonds are represented by red dotted lines.

2.2.2. Discovery of a BET BD1 Selective Lead Series and First Generation *in vivo* Probe

The thienopyridone (TP) **1** (Table 28) was identified by the BET BRD program team⁴² following a knowledge-based screen of around 1400 *N*-acetyl lysine mimetics using a BET BRD4 Fluorescence Polarisation (FP) assay, and was confirmed using Time Resolved-Fluorescence Resonance Energy Transfer (TR-FRET) assays.⁴³



Compound	1
BRD2/3/4/T BD1 pIC ₅₀	6.5/6.4/6.7/6.1
Selectivity for BD1 vs. BD2	>40x

Table 28. BRD2, 3, 4 and T BD1 and BD2 potency of the initial TP hit **1**, identified from a knowledge-based screen.

TR-FRET assays combine Time Resolved Fluorescence (TRF), and Fluorescence Resonance Energy Transfer (FRET) principles to assess the level of competitive inhibition of any given compound (**Figure 38**).

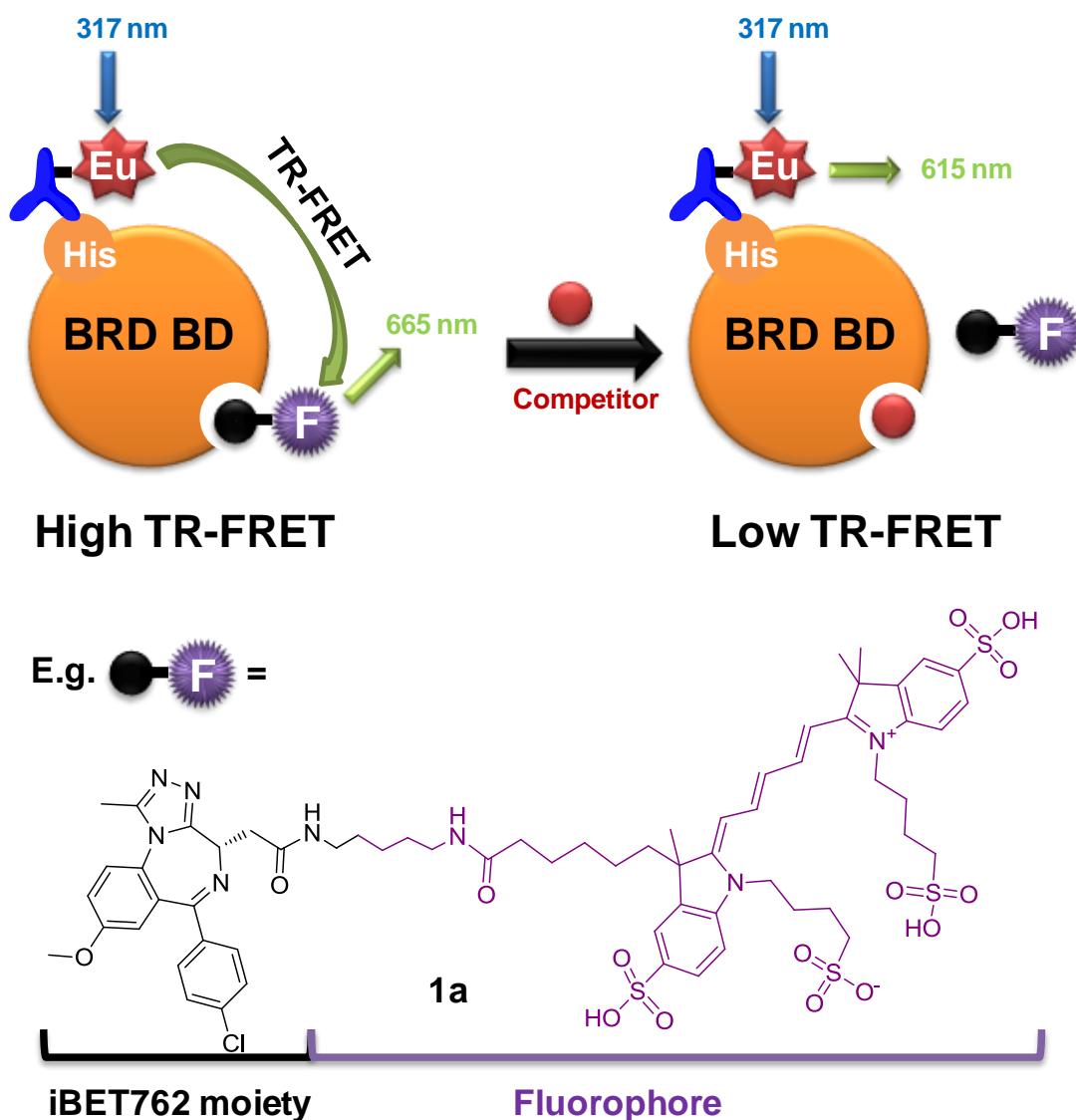


Figure 38. Diagrammatic representation of the BET BRD TR-FRET assay that used **1a** to measure the inhibition potency of BET BRD BD1 inhibitors *versus* BRD2, 3, 4 and T BD1 and BD2.

TRF allows the negation of natural fluorescence from proteins and compounds in solution by the use of long-lived donor fluorophores when combined with time-resolved detection; this incorporates a time delay between excitation and emission reads. The long lived donor fluorophore that is used in the BET BRD TR-FRET assays is the lanthanide europium. Europium, when complexed with a chelate, acts as light harvesting device: on stimulation with light of a defined wavelength (such as 317 nm used in the BET BRD2/3/4/T assays), a portion of the light energy is captured by the

chelate while a portion is transferred to an acceptor fluorophore attached to a molecule that is able to bind to the BET BRD BD active site (such as **iBET762**, **Figure 38**) and is in close proximity to the donor fluorophore; the acceptor fluorophore then emits light at a defined wavelength, such as 665 nm in the BET BRD2/3/4/T assays. A competitive inhibitor can displace the molecule **1a** that is labelled with the acceptor fluorophore, halting emission of light at 665 nm. Meanwhile the lanthanide donor fluorophore emits light at a specific wavelength and is used as an internal standard, 615 nm. The acceptor emission is the measure of the FRET: with high inhibition, no FRET count is detected; with low inhibition, high FRET counts are detected.

Compound **1** was only a moderately potent inhibitor of BD1 of the BET family of BRDs, BRD2, 3, 4 and T, and selectivity for BD1 *versus* BD2 was lower than the 50-fold target that was initially pursued by the BET BRD program team. Subsequent optimisation efforts focussed on improving BRD BD1 potency and selectivity. The potency for inhibition of BD1 across the BET BRD2, 3, 4 and T was of a similar magnitude for **1** (pIC₅₀ range of 6.1 to 6.7), as were the potencies of all compounds synthesised from this point; BRD4 BD1 pIC₅₀ is quoted from this point onwards to give an indication of a compound's potency against the BET family of BRDs.

2.2.2.1. X-ray Crystal Structure of **1**

The X-ray crystal structure of **1** complexed to BRD4 BD1 was obtained at high resolution (1.2 Å, **Figure 39**).⁴⁴ The methylpyridinone oxygen acted as a hydrogen bond acceptor with the Asn 140 residue (**Figure 39a**, orange) and through water with Tyr 97 in a similar manner to the acetyl oxygen of acetylated histone H4 peptide (**Figure 39a**, pale green, thick bonds), while the *N*-methyl group overlaid directly with the acetyl methyl group of acetylated histone H4 peptide; the methylpyridinone was therefore an effective AcK mimetic. A sulfonamide oxygen acted as a hydrogen bond acceptor with a hydrogen bond to the backbone NH of Ile 146 (**Figure 39a** and **b**). The lipophilic WPF shelf that the potent **iBET762** was able to interact with through the chlorophenyl moiety²⁵ was unoccupied with **1** (**Figure 39c**), so the introduction of a lipophilic substituent onto the dimethoxyphenyl ring that had the potential to interact with the WPF shelf was likely to increase potency.

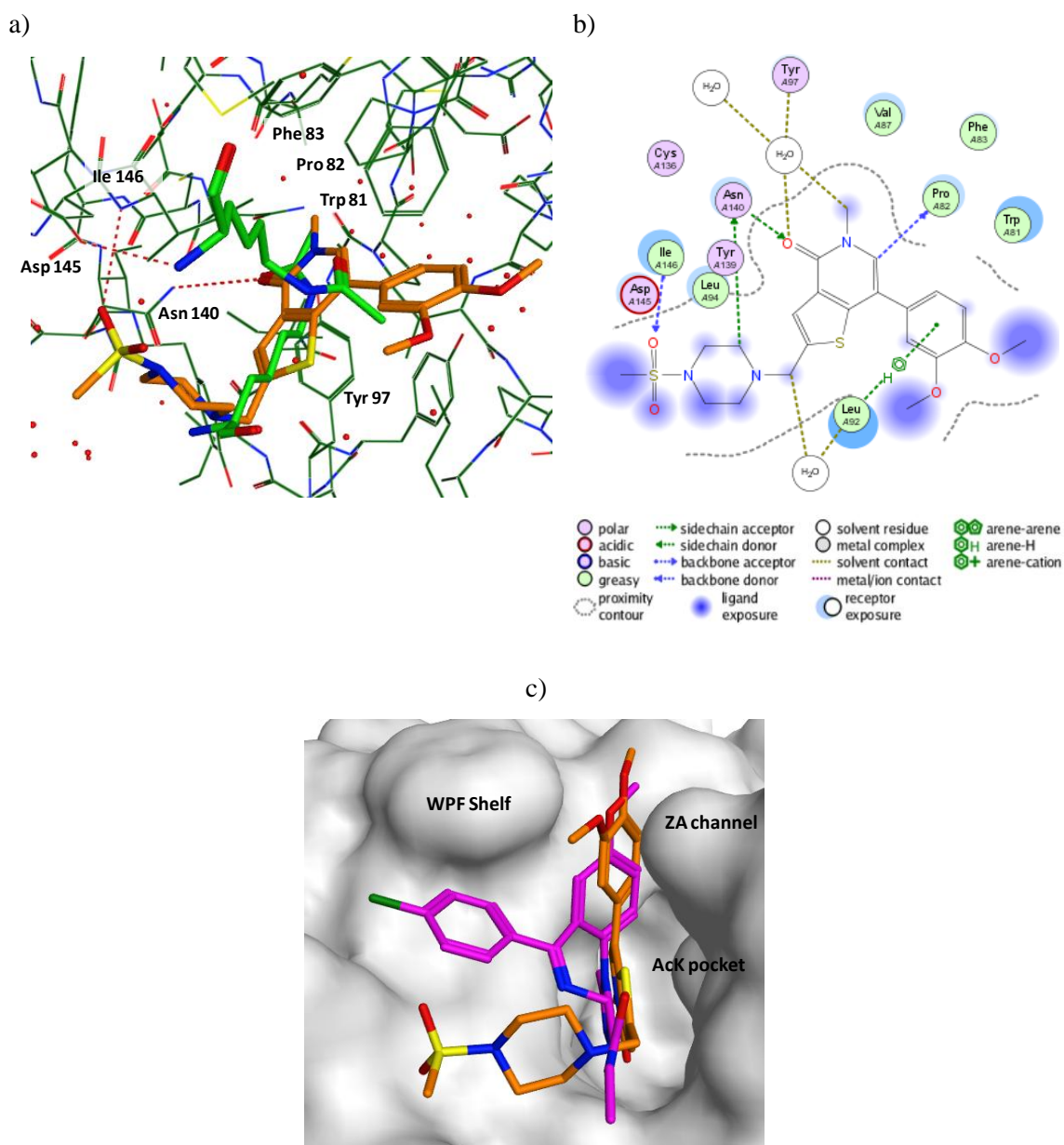


Figure 39.⁴⁴ a) A three dimensional representation of **1** (orange) and acetylated histone H4 peptide (pale green, thick bonds) bound in the active site of BRD4 BD1 (dark green, thin bonds) at 1.2 Å resolution (PDB code 2INSC). Key residues are labelled in black and hydrogen bonds represented as red dashed lines. Water molecules are represented by red spheres. b) Two dimensional representation of key interactions made between **1** and the BRD4 BD1 active site. c) Space-filling representation that shows the bioactive conformation of **1** (orange, 2INSC) overlaid with **iBET762** (magenta, 1.6 Å, 1HGKI); the dimethoxyphenyl moiety of **1** sits in close proximity to the lipophilic WPF shelf

which suggests substitution of this ring would allow access to the WPF shelf in analogy to the chlorophenyl substituent of **iBET762**.

2.2.2.2. Selectivity of **1** for BET BD1 versus BD2

Compound **1** was >40-fold more selective for the inhibition of BET BRD BD1 over BD2. Comparison of the space-filling representation of the X-ray crystal structure of **1** complexed with BRD4 BD1, with an X-ray crystal structure of BRD4 BD2 without a ligand present⁴⁴ (**Figure 40**), shows this could be a result of the headgroup piperazine methylsulfonamide moiety of **1** having a steric clash with the bulky His 437 residue in BD2, which would lead to a reduction of potency against BD2. The residue in the same position in BD1, Asp 144, is less bulky and therefore more accommodating of the headgroup piperazine methylsulfonamide.

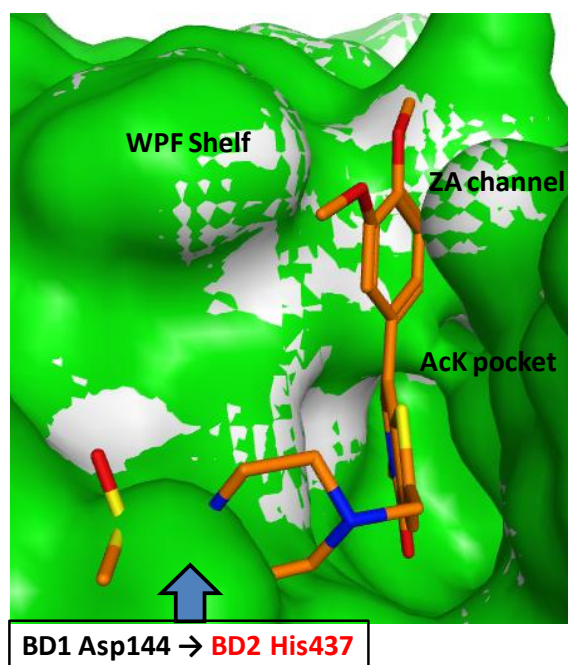
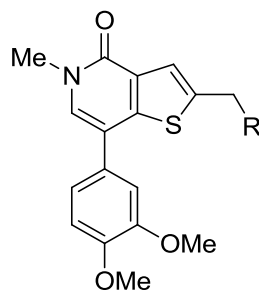


Figure 40. Overlay of the space-filling representation of the X-ray crystal structure of BRD4 BD1 (*grey*, 1.2 Å resolution, PDB code 2INSC) with that of BRD4 BD2 (*green*, 2.0 Å, 2FFTZ,). The piperazine methylsulfonamide moiety of **1** (*orange*, 2INSC) is likely to clash sterically with the bulky His 437 moiety of BD2 where indicated.

2.2.2.3. Optimisation of the TP Headgroup

A limited expansion of SAR of the TP headgroup R, was completed (**Table 29**).



R =		Me					
Compound	1 ⁴²	2 ¹⁷	3 ⁴²	4 ⁴²	5 ⁴²	6 ⁴²	7 ⁴²
BRD4 BD1 pIC ₅₀	6.7	6.3	6.3	5.7	7.1	6.3	6.7
BRD4 BD2 pIC ₅₀	≤4.9	5.9	5.9	4.6	4.6	4.9	4.9
Minimum Fold Selectivity for BET BD1 <i>vs.</i> BD2	40x	2.5x	2.5x	5x	100x	5x	32x

Table 29. Variation of the TP headgroup.

Replacement of the piperazinomethylsulfonamide headgroup of **1** with a methyl group gave **2** which led to a nearly 2.5-fold drop in BRD4 BD1 potency relative to **1**. Compound **2** was also less selective for BRD4 BD1 *versus* BD2 (2.5-fold) relative to **1**. Compound **2** has lower potency than **1** because it lacks the methylsulfonamide oxygen which makes a hydrogen bond with Ile 146 in BRD4 BD1. An ideal hydrogen bond in terms of location and direction can increase potency by up to 10-fold, so the 2.5-fold the reduction in potency of **2** relative to **1** indicates the hydrogen bond with Ile 146 is less than ideal. The reduced steric bulk of **2** in the headgroup region was likely to cause the reduced selectivity for inhibition of BD1 *versus* BD2 as previously described. Compound **3** also lacks the methylsulfonamide portion of **1**, and like **1** was unable to make a hydrogen bond with Ile 146 in the active site of BRD4 BD1. Compounds **2** and

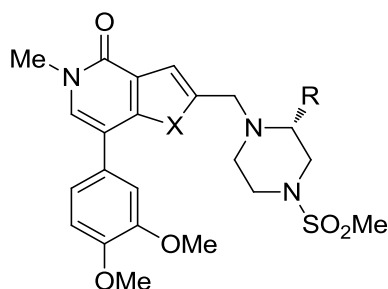
3 had the same potency, which confirmed that the extra hydrogen bond that the piperazinomethylsulfonamide oxygen of **1** can make with Ile 146 improves BRD4 BD1 potency by 2.5-fold.

Introduction of the methyl substituent at the 2-position of the piperazine ring to give compound **4**, the *S*-stereoisomer, led to a 10-fold drop in potency relative to **1**; however, the *R*-isomer, **5** had 2.5-fold higher potency than **1**. An improvement in selectivity for BET BD1 *versus* BD2 was also evident for **5** (100-fold *versus* 40-fold for **1**). The extra methyl-group in **5** may allow the piperazine ring to adopt a lower energy conformation to deliver the methylsulfonamide oxygen to the Ile 146 residue at a more favourable vector that can make the hydrogen bond interactions which would lead to improved potency. An X-ray crystal structure of compound **5** would have confirmed this, but one was not obtained by the program team. The improved selectivity of compound **5** for BET BD1 *versus* BD2 relative to **1** is caused by improved potency *versus* BD1 because the two compounds have similar potencies *versus* BRD4 BD2.

Two further headgroup analogues compounds **6** and **7** were synthesised to optimise the hydrogen-bond interaction with Ile 146 using a S=O moiety. Both were less potent and less selective than **5** which suggested that the vector adopted by the oxygen in both compounds was less than optimal. A more thorough attempt to optimise the headgroup is described later (see section 2.4.2).

2.2.3. Discovery of the FP Template

Replacement of the TP sulfur with oxygen to give the furanopyridone (FP) template was found to be favourable in terms of BRD4 BD1 potency and physicochemical properties. The lipophilicity of the FP template relative to the TP template was lower, as is indicated by lower measured ChromLogD_{7.4} and Property Forecast Index (PFI), which is related to ChromLogD_{7.4}, and is discussed later in this section (**Table 30**).⁴⁵



Compound	R	X	Series	ChromLogD _{7.4}	PFI	BRD4 BD1 pIC ₅₀	BRD4 BD2 pIC ₅₀	Minimum Fold Selectivity for BET BD1 vs. BD2
1 ⁴²	H	S	TP	3.3	6.3	6.7	≤4.9	40x
5 ⁴²	Me	S	TP	3.8	6.8	7.1	4.6	100x
8 ⁴⁶	H	O	FP	2.5	5.5	7.7	5.5	80x
9 ⁴⁶	Me	O	FP	3.0	6.0	7.8	5.6	158x

Table 30. Comparison of potency and selectivity for BET BD1 *versus* BD2 of the TP and FP series. PFI = Property Forecast Index = ChromLogD_{7.4} + Number of aryl rings.⁴⁵

The *des*-methyl FP analogue, compound **8**, was 10-fold more potent for BRD4 BD1 than the equivalent TP analogue **1**, and selectivity for BET BD1 *versus* BD2 was slightly higher (80-fold). The 2-methylpiperazine FP analogue, compound **9**, was five-fold more potent for BD1 than the equivalent TP analogue, compound **5**, and was similar in selectivity for BD1 *versus* BD2 (158-fold *versus* 100-fold); however, the selectivity was still within an acceptable region for a target compound for the dog safety assessment study.

Unlike in the TP series, the introduction of a 2-methyl group into the piperazine to give compound **9** led to no real improvement in BRD4 BD1 potency over compound **8**; however, an improvement in selectivity *versus* BRD4 BD2 was observed which cannot be rationalised using X-ray crystal structures. The addition of a 2-methyl substituent was later found to also improve solubility due to reduced planarity which thereby reduces crystal packing energy,⁴⁷ and this modification is discussed later (see section 2.4.2).

Importantly the FP series was inherently lower in lipophilicity than the TP series which brought analogues closer to drug-like physicochemical space; compounds with lower

lipophilicities are more likely to have favourable absorption, distribution, metabolism, excretion and toxicity (ADMET) profiles.⁴⁵ The PFI was developed at GSK to allow an approximate quantification of the drug-likeness of a compound according to lipophilicity measured using an HPLC method, chromatographic LogD at pH_{7.4} (ChromLogD_{7.4}), together with the number of aromatic rings (**Equation 3**).

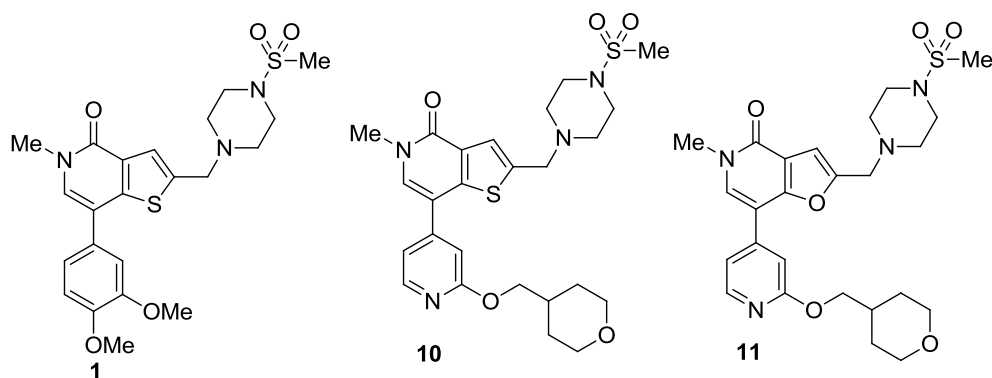
$$\text{Property Forecast Index (PFI)} = \text{ChromLogD}_{7.4} + \text{Number of aryl rings}$$

Equation 3. Equation used to calculate Property Forecast Index (PFI).⁴⁵

The PFI of FP analogues are 5.5 and 6.0 for compounds **8** and **9** respectively, which are closer to drug-like upper-limit of 6.0 than the equivalent analogues of the TP template which have higher PFIs of 6.3 and 6.8 for compounds **1** and **5** respectively.

2.2.4. Identification of the First Generation Probe, 10

Optimisation of the TP and FP template explored the possibility to improve BRD BD1 potency by introducing groups that may be able to interact favourably with the WPF shelf onto the aryl tail group. This led to the identification of **10** which had similar potency to **1**, but which exceeded the initial potency, selectivity and PK target values defined at the time by the BRD program team (**Table 31**).



	1	10 ⁴²	11
Series	TP	TP	FP
BRD4 BD1 pIC ₅₀	6.7	6.7	7.3
BRD4 BD2 pIC ₅₀	≤4.9	4.5	5.2
BRD9 pIC ₅₀	6.6	6.6	6.3
Minimum Fold Selectivity for BET BD1 vs. BD2	40x	50x	63x
Minimum Fold Selectivity for BET BD1 vs. BRD9	<1x	0.3x	6.3x
PBMC pIC ₅₀	5.8	6.2	6.8
FaSSIF Solubility, μg/mL	Not tested	10	Not tested
ChromLogD _{7.4}	3.3	3.9	2.9
PFI	6.3	6.9	5.9
Rat Cl _b , ml/min/kg	Not tested	36	88
Dog Cl _b , ml/min/kg	Not tested	15	Not tested
Rat F%	Not tested	8	15

Table 31. Profiles of the knowledge-based hit **1**, the first-generation probe **10** and its FP analogue, **11**. PFI = Property Forecast Index.⁴⁵ Cl_b = Clearance from blood after 1 mg per Kg intravenous dose; Rat F% = rat oral bioavailability after 3 mg per Kg dose.⁷

The equivalent FP analogue **11** was four times more potent, was similar in magnitude for selectivity and had a slightly higher oral bioavailability, but had an overall inferior PK profile to **10** because of higher clearance, Cl_b, in the rat. The higher Cl_b of the FP compound **11** was surprising since its ChromLogD_{7.4} is lower, and it is therefore less likely to be a substrate for metabolising enzymes such as cytochrome p450 enzymes (CYP450s)⁴⁸ which are thought to be responsible for metabolism of 70-80% of all drugs.⁴⁹

The dog PK profile of **10** was deemed suitable for progression to 14 day dog safety studies *via* intravenous administration which aimed to differentiate the safety profile of a BET BRD BD1-selective compound from the safety profile of *pan*-BET inhibitors such as **iBET762** which had been shown to be toxic in the rat and dog.^{7,21} Interestingly **10** had *pan*-BET like toxicities *in vivo*. As shown in **Table 31**, **10** was equipotent *versus* BRD4 BD1 and BRD9. The biological consequence of inhibiting the non-BET BRD, BRD9, was unknown but it was proposed that dual BRD BD1/BRD9 inhibition could be deleterious as additional transcriptional / remodelling roles which may lead to toxic events. Lead optimisation efforts were then refocused on finding a more selective compound for another dog *in vivo* safety study, with >100-fold selectivity for BET BD1 *versus* BD2 and BRD9.

2.2.4.1. X-ray Crystal Structures of the First Generation Probe and Related Analogues

The BRD4 BD1 X-ray crystal structures of the TP **10**⁴⁴ and the corresponding FP analogue **11**⁴⁴ showed that the two compounds bound to the active site in a similar manner to the original lead **1** (**Figure 41**). The methyltetrahydropyranyl substituent of **10** pointed along a vector away from the piperazine methylsulfonamide headgroup that did not allow any interaction with the WPF shelf (**Figure 41**). However, that of **11** pointed along an alternative vector, towards the piperazine methylsulfonamide headgroup, which allowed it to make at least a partial interaction with the WPF shelf; this extra interaction may explain the increased BRD BD1 potency of **11** relative to **10**. This result also suggested SAR around the aryl-tail group in the TP series should be different for the FP series because the substituents pointed towards differing parts of the protein.

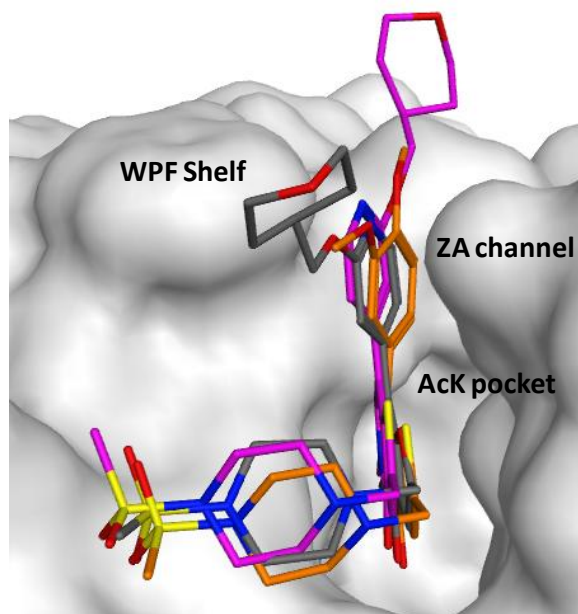
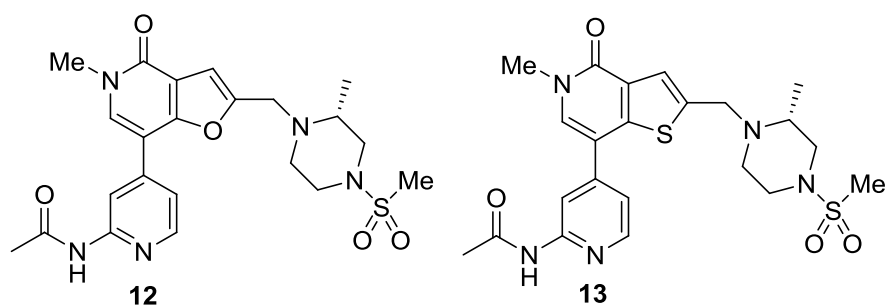


Figure 41. BRD4 BD1 X-ray crystal structure of **10** (*magenta*, 1.3 Å resolution, PDB code 9NZGW) overlaid with that of **11** (*dark grey*, 1.6 Å, 3VXUJ), and with the original lead **1** (*orange*, 1.2 Å, 2INSC).⁴⁴

Subsequent optimisation efforts were still undertaken in both the TP and FP series because the TP series had a superior PK profile to the FP series, whereas the FP series had superior potency and physicochemical properties to the TP series.

2.2.4.2. Identification of the Pyridylacetamide **12**

Further optimisation of the aryl tail group led to the identification of the pyridylacetamides **12** and **13**.⁵⁰ Although compound **12** exceeded the target potency and solubility required for the dog safety assessment study (**Table 32**), the clearance in dog and selectivity were not optimal.



	12	13 ⁴²
Series	FP	TP
BRD4 BD1 pIC ₅₀	7.6	6.7
Minimum Fold Selectivity for BET BD1 <i>vs.</i> BD2	126x	40x
Minimum Fold Selectivity for BET BD1 <i>vs.</i> BRD9	79x	1x
PBMC pIC ₅₀	6.7	6.5
FaSSIF Solubility, μg/mL	982	18
ChromLogD _{7.4}	1.7	2.3
PFI	4.7	5.3
Dog Cl _b , ml/min/kg	24	24

Table 32. Profile of the lead TP and FP pyridylacetamides, **12** and **13** respectively.

The corresponding TP analogue **13**, was even less selective for BET BD1 *versus* BRD9. The methyl group that had been introduced into the piperidine head group consistently led to improved FaSSIF solubility for the FP series relative to the unsubstituted piperidine due to reduced planarity and reduced crystal packing energy;⁴⁷ the *R*-stereoisomer was consistently around two-fold more potent *versus* BRD BD1 than the *S*-stereoisomer (data not shown).

2.2.4.3. X-ray Crystal Structures **12** and **13**

The BRD4 BD1 X-ray crystal structure of the FP **12**⁴⁴ showed that it bound to the BD1 active site in a similar manner to the corresponding previous FP lead **11**, with the substituent on the aryl tail group pointed towards the piperazine methylsulfonamide headgroup (**Figure 42a**, orange and **Figure 42b**). Similarly the BRD4 BD1 X-ray crystal structure of the TP **13**⁴⁴ showed it bound to the BD1 active site in a similar manner to the corresponding previous TP lead **10**, with the substituent on the aryl tail group pointed away from the piperazine methylsulfonamide headgroup (**Figure 42a**, magenta and **Figure 42c**).

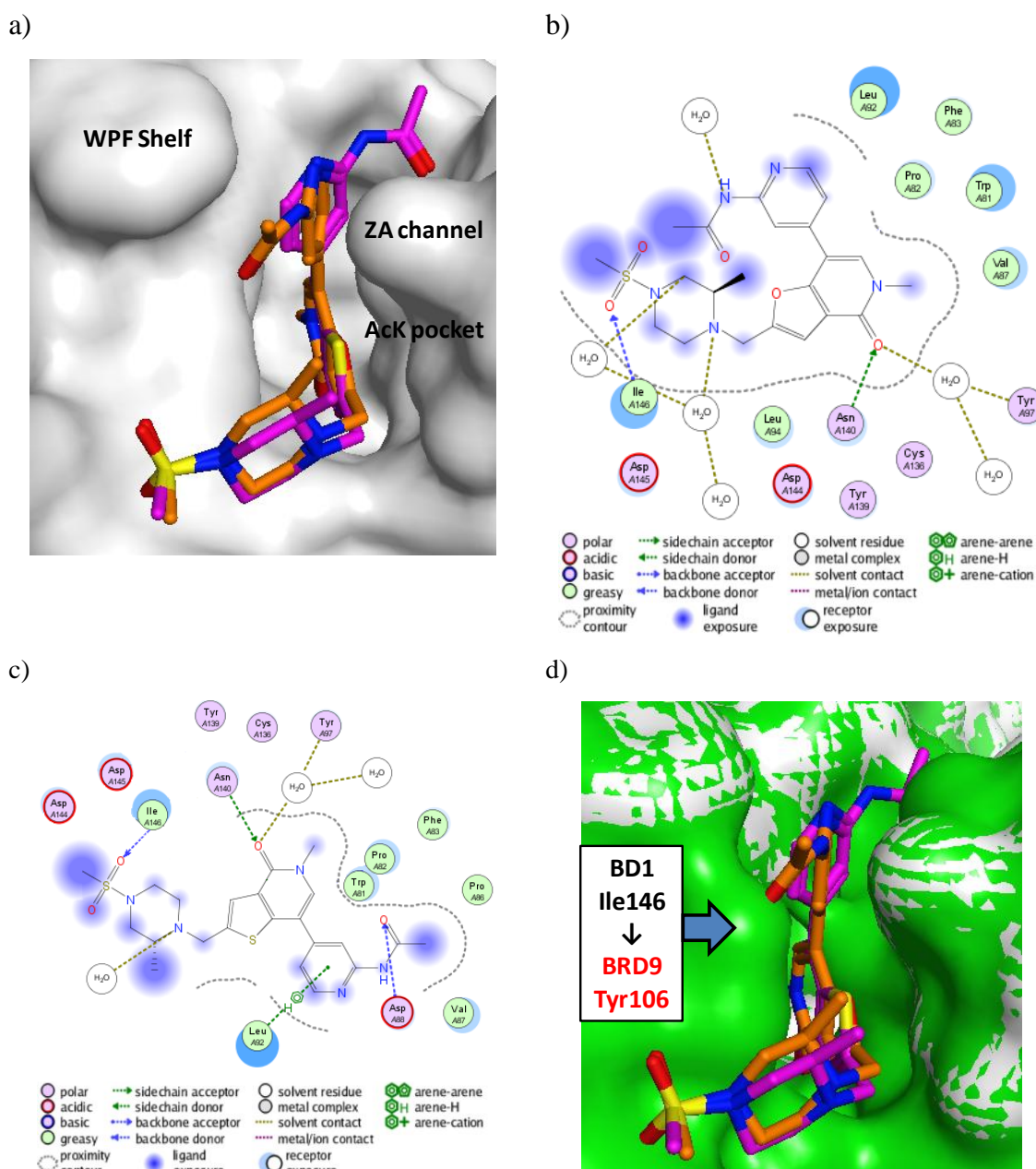


Figure 42. a) Space-filling representation of the BRD4 BD1 X-ray crystal structure of **12** (orange, 1.3 Å resolution, PDB code 2PSMP) overlaid with that of **13** (magenta, 1.3 Å, 7OGRV).⁴⁴ The pyridyl nitrogen is exposed to solvent and is not close to any residues. b) Two dimensional representation of key interactions made between **12** and BRD4 BD1. c) Two dimensional representation of key interactions made between **13** and BRD4 BD1. d) Space-filling representation of the BRD4 BD1 X-ray crystal structure (grey, 1.3 Å, 2PSMP), with **12** (orange, 2PSMP) and **13** (magenta, 7OGRV) bound, overlaid with a ligandless X-ray crystal structure of BRD9 (green, 1.7 Å, 8XLGJ).⁴⁴

An hypothesis for the difference in selectivity for BRD BD1 *versus* BRD9 of the FP **12** and the TP **13** is based on the consideration of the overlays of the X-ray crystal structures of these compounds with BRD4 BD1 and the *apo* X-ray crystal structure of BRD9 (**Figure 42d**).⁴⁴ The 79-fold selectivity of **12** for BET BRD BD1 *versus* BRD9 could be a result of the acetamide substituent of the pyridyl tail group that points towards the piperazine methylsulfonamide headgroup, having a steric clash with Tyr 106 of BRD9 but not with Ile 146; the equivalent residue in BRD BD1 is Ile 146 which makes a hydrogen bond with the S=O of the piperazine methylsulfonamide headgroup. This clash might not be possible for **13** which points the acetamide along a different vector, away from the piperazine methylsulfonamide headgroup; the acetamide substituent may be preferentially accommodated by BRD9, thereby lowering selectivity for BRD BD1 *versus* BRD9. Confirmation of this hypothesis could have been possible by obtaining X-ray crystal structures of **12** and **13** in BRD9, or by docking studies, but these activities were not undertaken. The putative extra hydrogen bond made between the acetamide oxygen of **13** and Asp 88 (that **12** cannot make) does not seem to improve BRD4 BD1 potency which suggests that this hydrogen bond is not optimal.

Lead optimisation efforts continued to focus on improving clearance, Cl_b, and selectivity of both the FP and TP series starting with point changes to the two lead compounds, **10** and **12**.

2.3. Aims

This project aimed to identify a novel potent and selective small molecule BET BRD BD1 inhibitor with the potential to determine *via* rat and dog preclinical safety species if BD1 inhibition could retain the anti-inflammatory/anti-proliferative effects that were observed with *pan*-BET inhibitors such as **iBET762**,³⁻⁵ but with a greater margin over the associated toxic effects. A compound with a suitable profile (**Table 33**) could help pave the way towards new treatments of chronic auto-inflammatory diseases⁶ such as RA and SLE, or towards new treatments of cancers with minimal or no side effects.

The identification of novel BET BRD BD1 inhibitors and the rationale behind the design, synthesis and iterative optimisation steps of these compounds towards the ideal target profile were the initial focus of this project, followed by the delivery of multi-gram quantities of a chosen inhibitor to take forwards into a dog safety study.

Parameter	Target
BET BD1 TR-FRET pIC ₅₀	>7.0
Selectivity for BRD2, 3, 4, T BD1 <i>vs.</i> BD2	>100-fold
Selectivity for BRD2, 3, 4, T BD1 <i>vs.</i> BRD9	>100-fold
Inhibition of LPS-Stimulated PBMC IL6 dog/human WB pIC ₅₀	≥6.5
MW / cLogP	<500 / <5.0
LE / LLE	>0.30 / >5.0
FaSSIF solubility, µg/mL	>100
hERG pIC ₅₀	<4.5
Dog Cl _b , mL/min/Kg (% Liver Blood Flow)	<22 (<40%)
Dog V _{ss} , L/Kg	0.6 to 5.0
Dog t _{1/2} , h	1 to 6

Table 33. BET BRD BD1 probe target profile, defined by lead program biologists and medicinal chemists. TR-FRET = Time-Resolved Fluorescence Resonance Energy Transfer; LPS = Lipopolysaccharide; PBMC = peripheral blood mononucleated cell assay; IL6 = Interleukin 6; WB = Whole Blood; MW = molecular weight; cLogP = calculated LogP; LE= Ligand Efficiency; LLE = Lipophilic Ligand Efficiency; FaSSIF = Fasted State Simulated Intestinal Fluid; Cl_b = Clearance from the blood; V_{ss} = Volume of distribution at steady state.

2.4. Results and Discussion

2.4.1. Reducing Clearance in the FP and TP Series

Drug metabolism is the process used by living organisms to biochemically modify pharmaceutical substances that are potentially toxic, usually using specialised enzymatic systems, so that the substances may be excreted.^{51,52} Typically, lipophilic chemical compounds are converted by these enzymes into more readily excreted hydrophilic products, a process referred to as metabolic clearance. The liver is the most important site of drug metabolism in the body and approximately 70-80% of marketed drugs are cleared by metabolism within the liver, catalysed by the CYP450 enzyme.⁴⁹ There are six main isozymes of CYP450: 1A2, 2B6, 2C19, 2C9, 2D6 and 3A4. CYP450 3A4 is the most clinically relevant isozyme, thought to be accountable for the metabolism of more than 50% of all drugs.⁴⁸

The process of metabolism and excretion of potentially toxic compounds is essential to maintain a healthy *status quo*; however higher levels of clearance are likely to limit the *in vivo* exposure of test species to a test compound which means that too little material may reach the site of action that is being investigated. GSK is actively reducing the numbers of animals involved in research through a process called replacement, reduction and refinement in practice.⁵³ This means that before a compound can be tested *in vivo*, test compounds must be pre-screened using *in vitro* clearance (IVC) methods, typically using liver microsomes, to give an indication of the level of clearance *in vivo*.^{45,51} All microsomal IVC assays were outsourced to a contract research organisation called Cyprotex.⁵⁴

Liver microsomes are subcellular fractions that contain membrane-bound metabolising enzymes such as CYP450 and are used to determine *in vitro* intrinsic clearance of a compound;⁵⁵ this is the potential ability of the liver to metabolise the compound in the absence of other factors, such as blood flow and protein binding. Species-specific microsomes are used to improve understanding of interspecies differences in drug metabolism,⁵⁶ and are easy to prepare, use and store, which makes their use cost-effective over whole cell models, such as those using hepatocytes. The IVC may then be scaled-up to predict potential clearance in the relevant *in vivo* species.^{55,57} It is important

to regard IVCs as only a guide to likely *in vivo* clearances because predictability can vary from chemical template to chemical template, due to confounding factors such as Phase II metabolism which is absent in microsomal IVC assays. This is in contrast to the hepatocyte IVC assay which is capable of undertaking Phase II metabolism,⁵⁷ but the price of this assay is prohibitive relative to the microsomal assay for routine screening.

Microsomal and hepatocyte IVC values for a compound are typically quoted in units of mL/min/g of liver tissue. The IVC value can be scaled based on liver weight as a proportion of bodyweight to determine intrinsic clearance ($Cl_{int.}$) in units of mL/min/Kg, according to **Equation 4**. Liver weight proportion varies between species and values have been standardised across GSK (**Table 34**).⁵⁸

$$Cl_{int.} = IVC \times \text{Liver weight proportion}$$

Equation 4. Calculation used to determine intrinsic clearance ($Cl_{int.}$) from IVC.

	Human (70 Kg)	Rat (0.25 Kg)	Dog (10 Kg)
Liver weight proportion, g/Kg bodyweight	24.5	36.0	32.5

Table 34. Standardised liver weight values for human, rat and dog in g/Kg bodyweight.⁵⁸

The non-restrictive well-stirred clearance model can then be used to estimate the likely *in vivo* rate of clearance (Cl) in mL/min/Kg from intrinsic clearance ($Cl_{int.}$) and liver blood flow ($Q_{Hep.}$) using **Equation 5**.⁵⁹ This approach assumes the majority compound is cleared from the blood by just the liver, so liver blood flow is the maximum rate that a compound may be cleared from the blood.

$$Cl_b = \frac{Q_{Hep.} \times Cl_{int.}}{Q_{Hep.} + Cl_{int.}}$$

Equation 5. Calculation of predicted *in vivo* clearance (Cl) based on IVC. $Q_{Hep.}$ = liver blood flow; $Cl_{int.}$ = intrinsic clearance.⁵⁹

Compounds can then be classed as having low, moderate or high predicted clearance relative to the maximum liver blood flow, and only compounds with low to moderate

IVC are progressed to *in vivo* PK experiments to measure clearance. Compounds with a predicted clearance of up to a third of liver blood flow are classed as having low clearance, those with a predicted liver blood flow between a third to two thirds of liver blood flow have moderate clearance, while those with above two thirds liver blood flow have high clearance. Different species have different liver blood flows, so low, moderate or high IVC values have different cut-off points across the species; these are shown in **Table 35**.⁵⁸

	Species		
	Human (adult male)	Rat	Dog
Q_{Hep}	18	78	56
Low IVC, mL/min/g	≤ 0.35	≤ 1.0	≤ 0.8
Moderate IVC, mL/min/g	>0.35 to 1.45	>1.0 to 4.1	>0.8 to 3.2
High IVC, mL/min/g	>1.45	>4.1	>3.2

Table 35. IVC values that correspond to low, moderate and high predicted clearance for human, rat and dog.⁵⁸

Meteor®⁶⁰ and Metasite®⁶¹ software tools were used⁶² to predict sites that were likely to be metabolised *in vivo* by metabolising enzymes such as CYP3A4 on the first generation probe **10**, and the subsequent lead **12** (**Figure 43a** and **b** respectively), to determine which parts of the molecule could be altered to block or reduce metabolism.

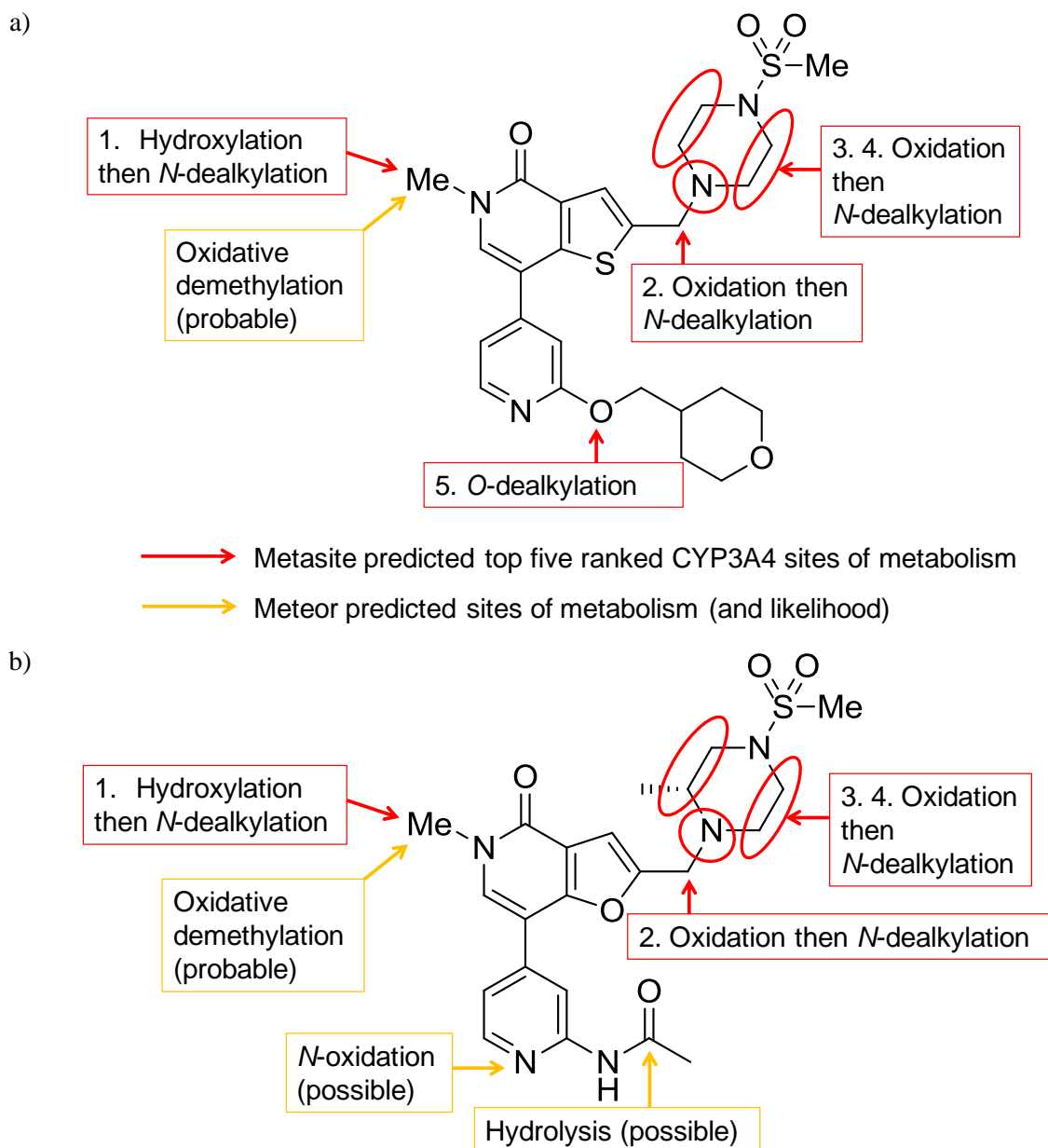


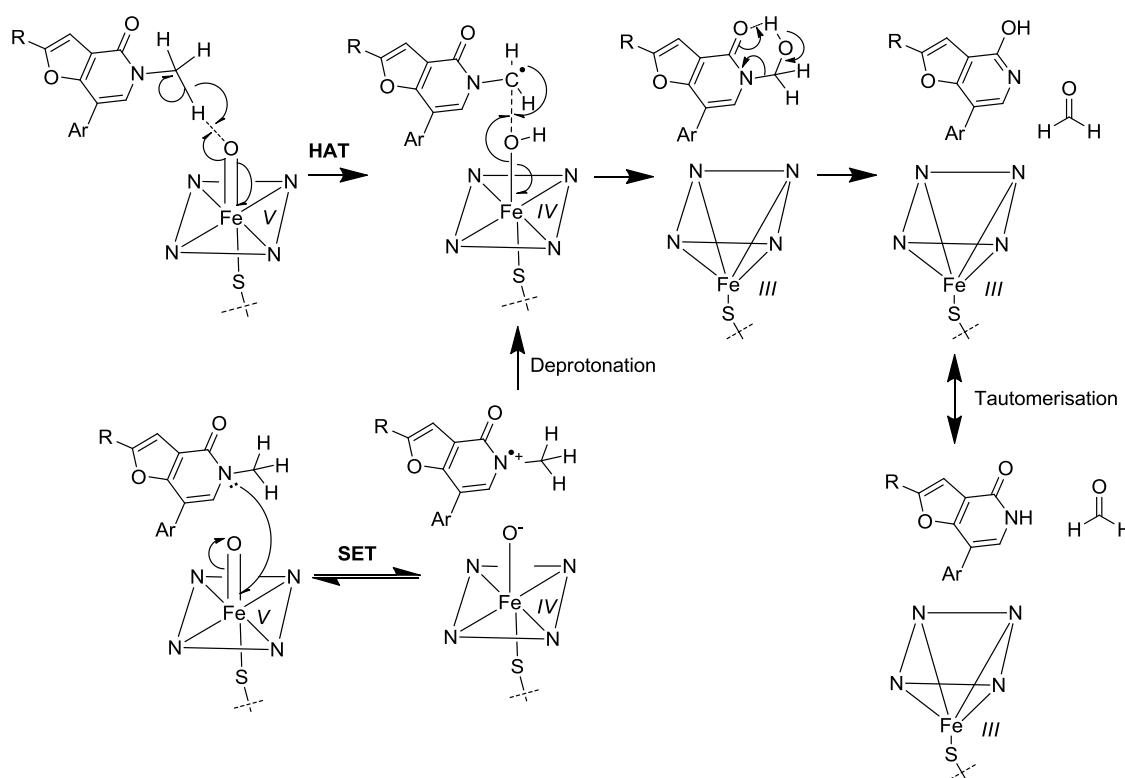
Figure 43. Sites of metabolism on a) the first generation TP probe **10**, and b) the FP lead **12**, predicted using Meteor®⁶⁰ and Metasite®⁶¹ software.⁶²

Meteor® is a rule-based tool that employs an algorithm that asks three main questions in succession to assess the likelihood of routes of metabolism for the molecule being queried: firstly, does the molecule contain any substructures that are labile to biotransformations present in its knowledgebase? Secondly, what is the likelihood of each biotransformation taking place (for example, according to logP)? And thirdly, based on a set of defined preferences, what is the relative ranking of biotransformations that can occur concomitantly on the same compound?⁶³ Conversely, Metasite® is

designed to predict CYP450-mediated phase I metabolism *via* an automated docking model. The software uses Grid descriptors for CYP450 enzymes and the molecule in query to evaluate metabolism at all possible sites; a likelihood for metabolism is then assigned to each atom.

Metabolism of **10** and **12** was predicted to proceed *via* *N*-dealkylation at four main sites in the following order of probability (highest first): 1, the *N*-methyl position; 2, the benzylic carbon and 3, and 4, the piperazine carbons. CYP450-mediated oxidations that lead to *N*-dealkylations are reported to occur *via* two main free radical based routes; Direct Hydrogen Atom Transfer (HAT) and Single Electron Transfer (SET).⁶⁴

Scheme 25 illustrates potential routes of CYP450-mediated *N*-demethylation of the FP template.⁶⁵

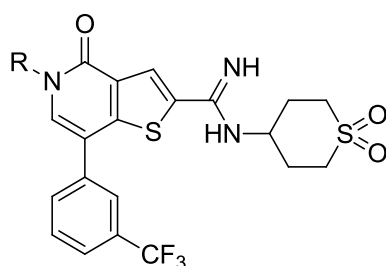


Scheme 25. Proposed routes of CYP450-mediated *N*-dealkylation of the FP methylpyridinone: Hydrogen Atom Transfer (HAT) and Single Electron Transfer (SET).⁶⁴ Adapted from Timbrell (1991).⁶⁵

The two main approaches that were considered to reduce metabolism at the four likely sites were removal or replacement of the metabolically liable group with a group that is likely to be less metabolically labile, or steric blocking of those positions with a group that is less likely to be metabolically labile.

2.4.1.1. Replacement of the *N*-Me Group

The methyl pyridone acts as an AcK mimetic, so the methyl group was likely to be required to achieve BRD potency. This was evident from SAR of a similar series that was being investigated by another colleague in house that aimed to identify a BRD9 inhibitor (compounds **14** to **17**, Table 36).⁶⁶



Compound #	14	15	16	17
R =	H	Me	Et	<i>i</i>Pr
BRD4 BD1 pIC ₅₀	<4.3	5.6	5.3	<4.3
Minimum Fold Selectivity for BET BD1 vs. BD2	-	2.5x	1.6x	-
BRD9 pIC ₅₀	5.2	7.8	7.3	5.5

Table 36. Potencies of an analogous TP series under investigation by a colleague for the BRD9 program.⁶⁶

The BRD9 TP series was found using X-ray crystallography to bind to BRD4 BD1 in the same mode as the BRD BD1 FP and TP series in that the methylpyridone group acts as an AcK mimetic (data not shown).⁶⁶ The observed SAR, in which the N-H of compound **14** is alkylated with a methyl (**15**), an ethyl (**16**) or isopropyl group (**17**) confirmed optimal BRD4 BD1 potency for **15** with the methyl group. Compounds **14** and **17**, which lacked an alkyl group or contained an isopropyl group respectively had no detectable BRD BD1 potency. This SAR was highly likely to be transferable to the BRD BD1 FP and TP series due to the similarity in binding mode.

An *N*-CD₃ was investigated as a viable replacement of the *N*-methyl group because it is an isosteric replacement for a methyl group that is theoretically more stable to metabolism: the rate of cleavage of a C-D bond is slower than that of a C-H bond.¹⁸

The effect on the rate of bond cleavage by the introduction of a deuterium in the place of a hydrogen is called a kinetic isotope effect (KIE);⁶⁷ when the isotope effect can be attributed to a bond breaking event at the X-H/X-D bond, it is referred to as a primary isotope effect, or in this case a primary deuterium isotope effect. The primary deuterium effect arises from the heavier mass of a deuterium atom relative to a hydrogen atom: a deuterium atom is twice as heavy as a hydrogen atom because the nucleus consists of a proton and a neutron, whereas the nucleus of a hydrogen atom consists of a proton alone. A C-D bond therefore has a lower zero point energy than C-H bond so a higher activation energy is required to cleave that bond.⁶⁸ The C-D bond is therefore more resistant to enzymatic or chemical cleavage than the C-H bond. If cleavage of a C-H bond is implicated as the rate determining step in metabolism, as was predicted for the *N*-Me group using the Meteor® and Metasite® software, then substitution of the hydrogen with a deuterium should slow down metabolism at this position and therefore should reduce the IVC of **12**. Because deuterium is twice the mass of hydrogen, its KIE is far greater than observed for isotopes of other elements whose mass differs from the most abundant isotope by a much smaller percentage.

The ratio of the rate constant for cleavage of a C-H bond, k_H , to the rate constant for cleavage of a C-D bond, k_D , is usually between two and ten if hydrogen abstraction is the rate determining step in a transformation.^{69,70} For a CYP450-mediated hydrogen abstraction, a k_H/k_D range of 5.2 to 7.4 has been determined experimentally using microsomes. However, an investigation into the *N*-demethylation of a series of *para*-substituted (H, Cl, CN, NO₂) dimethylanilines catalyzed by CYP1A2, CYP2B1, CYP4B1, and CYP101 showed that the magnitude of k_H/k_D varied between substrates of values between 2.4 and 4.1.⁷¹ The magnitude was virtually identical across all the enzymes; these data suggested that any given CYP450-catalyzed reaction is likely to proceed by the same mechanism with the same value for the intrinsic isotope effect, irrespective of the isoform catalysing the reaction.

The electron clouds of the component atoms of a molecule define the shape of a molecule, so deuterated compounds have shapes and sizes that are essentially indistinguishable from the all hydrogen analogue.⁷² No deuterated compound has been approved as a medicine to date, but the early clinical evaluation of several candidate compounds has been encouraging. One important example is **SD-254**, which is a deuterated version of the blockbuster anti-depression drug venlafaxine (**Figure 44**) made by Auspex.^{73,74}

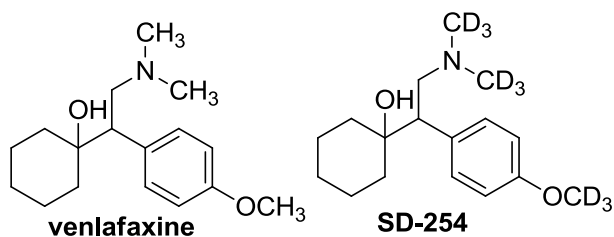
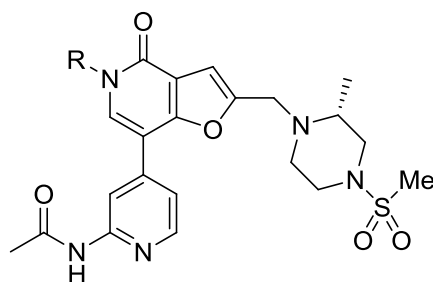


Figure 44. Structure of venlafaxine and **SD-254**.^{73,74}

Venlafaxine is a selective serotonin-norepinephrine reuptake inhibitor and was originally marketed by Wyeth as Effexor® from 1993.⁷³ Venlafaxine contains a methoxy group that is rapidly converted to a hydroxyl group in the liver, and also has a dimethylamino group that is metabolised to the primary amine. Compound **SD-254** was found to be metabolised half as quickly as venlafaxine in Phase I clinical trials using sixteen healthy volunteers; the slower metabolism allows **SD-254** to persist at therapeutic doses in the body for far longer than venlafaxine.

The *N*-CD₃ analogue of **12** was made by Garton, compound **18**,¹⁸ to reduce IVC (**Table 37**).

**12** **18**¹⁸

	R =	Me	CD₃
BRD4 BD1 pIC ₅₀		7.6	7.6
Minimum Fold Selectivity for BRD4 BD1 vs. BD2		126x	398x
Minimum Fold Selectivity for BET BD1 vs. BRD9		79x	251x
PBMC (LPS) Il6 pIC ₅₀		6.7	6.5
IVC _{mics. rat}		3.1	3.4

Table 37. Profiles of the *N*-Me FP **12** and the *N*-CD₃ FP **18**.¹⁸

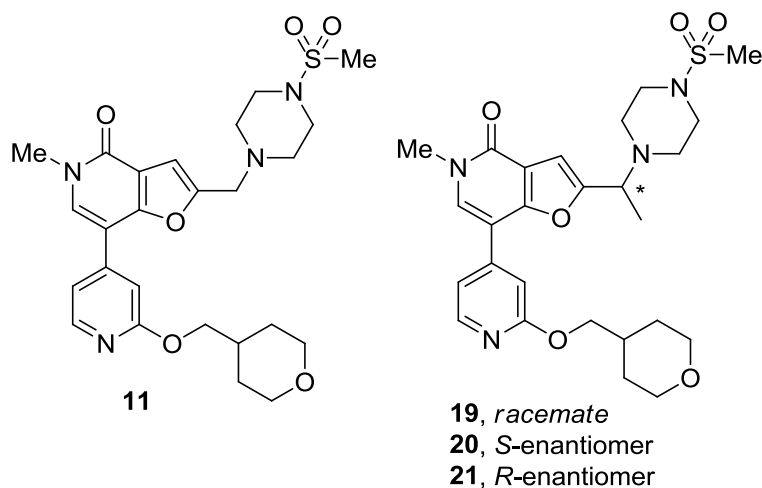
Replacing the *N*-Me of **12** with CD₃ to give **18** unsurprisingly led to the same BRD4 BD1 and PBMC potency. Microsomal IVC_{rat} was comparable for the two compounds which suggested *in vivo* clearance would also be comparable. The reduction in IVC may not have been achieved with **18** because of a phenomenon called “metabolic switching”, which is also known as “metabolic shunting” whereby the suppression of one metabolic pathway promotes metabolism at another site.⁷⁵ Inhibition of metabolic demethylation of **18** is likely to have caused metabolism of an alternative site of the FP template, most likely one of the remaining three sites of metabolism. Compound **18** offered no real advantage over **12**, so this compound was not progressed to PK studies.

The benzylic position of the FP and TP templates was the next most likely place to be metabolically oxidised then dealkylated *in vivo*. It was anticipated that the vulnerability of this position to metabolism could be lowered by the introduction of deuterium due to the KIE effect,⁶⁷ or by the introduction of a methyl group to clash sterically with the active sites of metabolising enzymes, or by the introduction of two methyl groups to remove the hydrogens vulnerable to metabolism.^{76,77} Only the introduction of methyl groups was investigated at this point, but deuterated analogues could be investigated in future studies. However, the deuterated analogue was not guaranteed to be lower clearance than the hydrogenated analogue due to metabolic switching, as was previously seen with **18** (Table 37). As proof of concept, introduction of lipophilic methyl groups

was initiated in the FP series as opposed to the TP series because the FP series offered a less lipophilic starting point than the TP series.

2.4.1.2. Blocking the Benzylic Position of 11

Compound **19** was synthesised as a racemate then separated into the two constituent enantiomers by chiral HPLC¹⁰ to give the mono-methyl substituted analogues of **11**, compounds **20** and **21** (Table 38).



#	e.e. by chiral HPLC ¹⁰	BRD4 BD1 pIC ₅₀	PBMC pIC ₅₀	Minimum Fold Selectivity for BET BD1 vs. BD2 / BRD9	IVC			Chrom LogD _{7.4}	PFI
					Human	Dog	Rat		
11	-	7.3	6.8	63x / 6x	1.0	-	2.1	2.9	5.9
20	98	7.4	7.0	79x / 200x	2.7	1.4	5.1	3.4	6.4
21	>99	7.6	7.6	50x / 20x	4.9	3.2	4.1	3.4	6.4

Table 38. Profiles of the mono-methyl substituted analogues of **11**, compounds **20** and **21**.

Too little of each compound was isolated to perform complete characterisation, but enough of **21** was secured to obtain an X-ray crystal structure of the compound bound to BRD4 BD1, which showed the compound to be unambiguously the *R*-enantiomer (Figure 45).⁴⁴ By inference **20** is then the *S*-enantiomer.

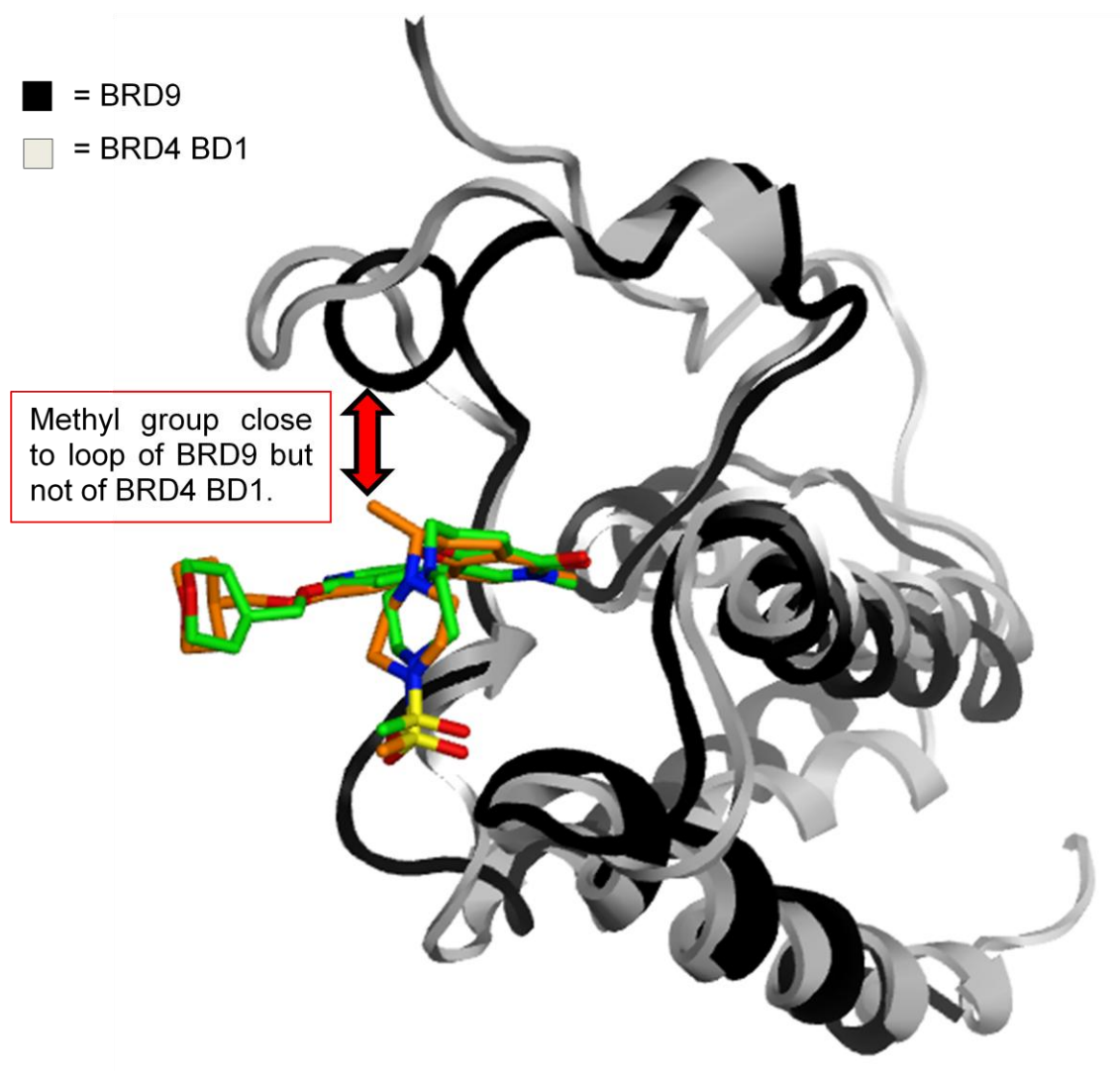


Figure 45. X-ray crystal structure of BRD4 BD1 (grey, 1.6 Å resolution, PDB code 3VXUJ) bound to **11** (green, 3VXUJ) and **21** (orange, 1.7 Å, 4PERF) overlaid with the ligandless X-ray crystal structure of BRD9 (black, 1.7 Å, 9OZAS).⁴⁴

The *R*-stereoisomer, compound **21**, is slightly more potent at BRD4 BD1 than the *des*-methyl **11**, but is of similar selectivity *versus* BD2, probably because the piperazine methylsulfonamide headgroup of **21** binds in the same manner to that of **11**. Compound **21** is slightly more selective *versus* BRD9 than **11**.

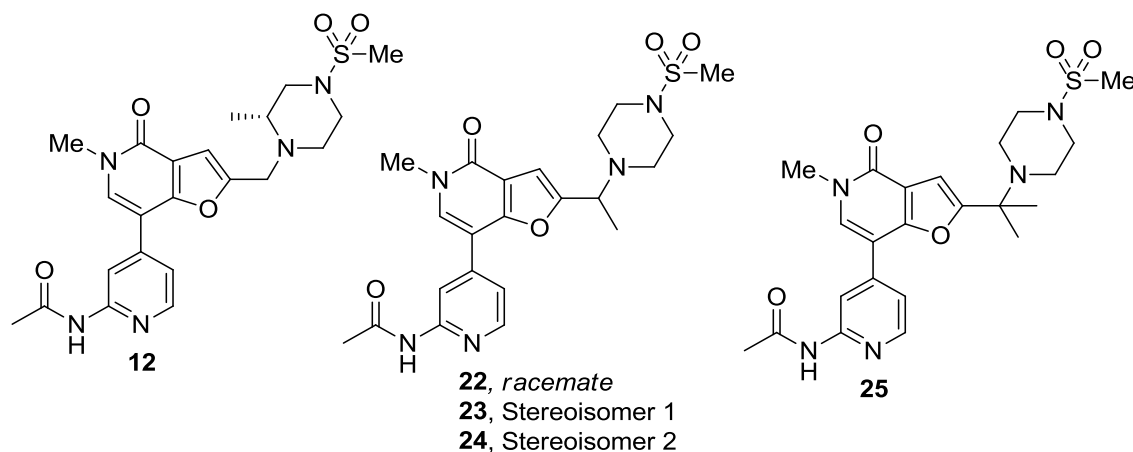
The *S*-stereoisomer, compound **20** was equipotent to **11** and their selectivities *versus* BD2 were similar. However, compound **20** was highly selective *versus* BRD9 which suggested that the methyl group of **20** may clash even more extensively with BRD9 than that of **21**. One hypothesis for improved BRD9 selectivity may be inferred from an

overlay of the BRD4 BD1 X-ray crystal structure of **20** with an X-ray crystal structure of BRD9 (**Figure 45**): the extra methyl group is positioned relatively close to a backbone loop of BRD9 (<2 Å to the closest residue), whereas the equivalent backbone loop of BRD4 BD1 is further away (~4 Å). The extra methyl is likely to clash sterically with BRD9 but not BRD4 BD1, making BRD9 binding less favoured for **21** than for **11**, and even less favoured for **20** than for **11**.

Unfortunately the IVCs of both compounds **20** and **21** were higher than those of the *des*-methyl analogue **11**. Although the benzylic position would be protected to some extent against metabolic oxidation, the lipophilicity of **20** and **21** has increased relative to **11**; the increased lipophilicity seems to have been enough to increase clearance. Further lead optimisation based on **11** was therefore not pursued. Meanwhile the introduction of mono- and di-methyl substituents into the alternative lead **12** was initiated because **12** had a relatively low starting lipophilicity.

2.4.1.3. Blocking the Benzylic Position of **12**

The mono-methyl substituted analogue of **12**, compound **22**, was synthesised as a racemate then separated into the two constituent enantiomers, compounds **23** and **24**, by chiral HPLC,¹¹ (**Table 39**). The absolute configuration of these compounds remains undefined because not enough material was obtained to resolve BRD4 BD1 X-ray crystal structures. The di-methyl analogue of **12**, compound **25**, was also synthesised, but it was not possible to obtain an X-ray crystal structure with this compound bound to the protein.



#	% e.e. by chiral HPLC ¹¹	BRD4 BD1 pIC ₅₀	PBMC pIC ₅₀	Minimum Fold Selectivity for BET BD1 vs. BD2 / BRD9	IVC, mL/min/g			Chrom LogD _{7.4}	PFI
					Human	Dog	Rat		
12	-	7.6	6.7	126x / 79x	<0.5	0.6	3.1	1.7	4.7
23	99.6	7.6	7.2	79x / 251x	<0.5	<0.5	3.4	1.9	4.9
24	99.2	7.1	*6.3	40x / 200x	<0.5	<0.5	2.8	1.9	4.9
25	-	7.6	6.8	100x / 1000x	0.9	<0.5	9.1	2.2	5.2

Table 39. Profiles of the mono- and dimethyl-substituted analogues of **12**, compounds **23-25**. *One test occasion (n = 1).

Compound **23**, the mono-methyl substituted analogue of **12**, had similar potency *versus* BRD4 BD1 to **12** and had similar selectivity over BD2. However, **23** was more potent in the PBMC assay; the reason for this anomaly is unknown because the compounds' physicochemical properties are similar (data not shown). The other mono-methyl substituted analogue **24** was less potent and slightly less selective *versus* BD2 than **12** and **23**, whereas the dimethyl-substituted analogue **25** was similar in potency to **12** but had similar selectivity *versus* BD2.

Selectivity of **23** *versus* BRD9 was higher than **12** which is consistent with the SAR for other mono- and the di-methyl substituted compounds, **24** and **25** respectively. The increased selectivity *versus* BRD9 is also consistent with that seen with the methyl analogues of **11**, compounds **20** and **21**. In the absence of X-ray crystal structures of **23-25**, it was possible that the introduction of a methyl group at the benzylic position may

introduce a steric clash with BRD9, making binding with BRD9 disfavoured as was proposed with compounds **20** and **21** (**Figure 45**). The introduction of two methyl groups to give **25** further increased the steric clash relative to the single methyl compounds **23** and **24**, which would explain the 1000-fold selectivity for BRD BD1 *versus* BRD9; this was the highest ever selectivity achieved in this series of investigations.

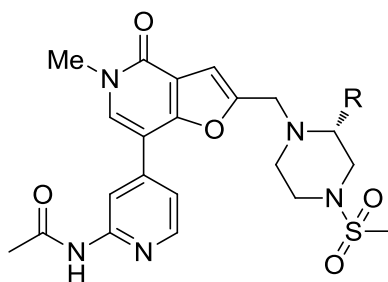
The introduction of a single methyl group at the benzylic position of **12** to give **23** and **24** kept IVC_{human} and IVC_{dog} below the lowest level of detection. The measured IVC_{dog} of **12** was too close to the lower limit of detection to conclude that the IVC_{dog} values of **23** and **24** were lower. However, IVC_{rat} values seemed unaffected and remained high. Similarly, the introduction of two methyl groups at the benzylic position of **12** to give **25** led to a modest improvement in IVC_{dog} , but led to increased IVC_{human} and IVC_{rat} .

The introduction of one or two extra methyl groups at the benzylic position of **12** may well have lowered the vulnerability of this position to metabolic oxidation by sterically blocking access by CYP450 enzymes, or by removing the hydrogen susceptible to metabolism respectively. However, the consequent increase in lipophilicity may have increased the susceptibility of other regions of the molecule to CYP450-mediated metabolism. The low-to-moderate values of IVC_{dog} suggested that the lipophilicities of these compounds may be on the cusp of achieving low IVC. This suggested the lipophilicity of future compounds needed to be even lower than the $\text{ChromLogD}_{7.4\text{s}}$ of **23** to **25** (< 2.2) in order to further lower IVC_{dog} and to increase the potential to achieve low Cl_b in the dog. This implied an upper PFI limit of 5.2 was required to achieve low IVC_{dog} with this series.

Compounds **23** to **25** did not meet the target profile required for progression into the dog safety assessment study, so attention was turned to optimising the piperazine methylsulfonamide headgroup of **12** which was predicted to be the next most likely position to be prone to metabolic oxidation and dealkylation, and could be a handle to reduce lipophilicity.

2.4.2. Optimisation of the Piperazine Methylsulfonamide Headgroup

Adding a methyl group to the 2-position of the TP piperazine methylsulfonamide headgroup to give the *R*-stereoisomer **5** was previously found to improve BRD4 BD1 potency and selectivity *versus* BD2 relative to the unsubstituted analogue **1** (**Table 29**); the *S*-stereoisomer **4** was substantially less potent and less selective. However, the introduction of a methyl group at the 2-position of the FP template headgroup piperazine to give **9** did not seem to affect potency or selectivity for BET BD1 *versus* BD2 relative to the unsubstituted analogue, **8** (**Table 30**, section 2.2.3). Indeed the additional substituent only seemed to increase ChromLogD_{7.4} by 0.5 log units which was likely to be detrimental to IVC. Similarly the introduction of a methyl group at the 2-position of the methylpiperazine sulfonamide headgroup of **26** to give **12**, increased ChromLogD_{7.4} by 0.3 log units and did not improve BRD BD1 potency (**Table 40**). The modification did however marginally improve selectivity *versus* BD2 and BRD9, and led to a substantial improvement in solubility, and to a possible marginal improvement in permeability.



Compound #	12	26
R =	Me, <i>R</i> -stereoisomer	H
BRD4 BD1 pIC ₅₀	7.6	7.4
Minimum Fold Selectivity for BET BRD BD1 vs. BD2	126x	63x
Minimum Fold Selectivity for BET BD1 vs. BRD9	79x	32x
PBMC (LPS) II6 pIC ₅₀	6.7	6.8
ChromLogD _{7.4} / PFI	1.7 / 4.7	1.4 / 4.4
CLND solubility, μg / mL	≥171	18
AMP at pH 7.4, nm/s	≤24	<3

Table 40. Profiles of the 2-methyl piperazine methylsulfonamide headgroup analogue **12** and the *des*-methyl analogue **26**. CLND = chemiluminescent nitrogen detection of solubility; AMP = artificial membrane permeability.

The introduction of an extra methyl group into the piperazine methylsulfonamide headgroup of **26** to give the *R*-stereoisomer **12** is likely to have increased solubility by disrupting planarity and reducing crystal packing energy.⁴⁷ The 2-methyl *S*-enantiomer was not made due to time constraints, but perhaps could have been made for completeness to confirm if headgroup SAR of the TP template was divergent from that of the FP template. A comparison between the BRD4 BD1 X-ray crystal structure of 2-methyl analogue **12**, and that of *des*-methyl analogue **8**,⁴⁴ showed that the piperazine methylsulfonamide headgroups overlaid closely, which may explain why potency and selectivity were of similar magnitude for the 2-methyl analogues and *des*-methyl analogues **12** and **26** respectively (**Figure 46**). The X-ray crystal structure also suggested the 2-methyl group of the hypothetical *S*-enantiomer of **12** might clash sterically with the acetamide of the pyridyl tail group; the *S*-methyl group might force the tail group substituent to adopt an unfavourable conformation which is likely to be disadvantageous for potency and selectivity.

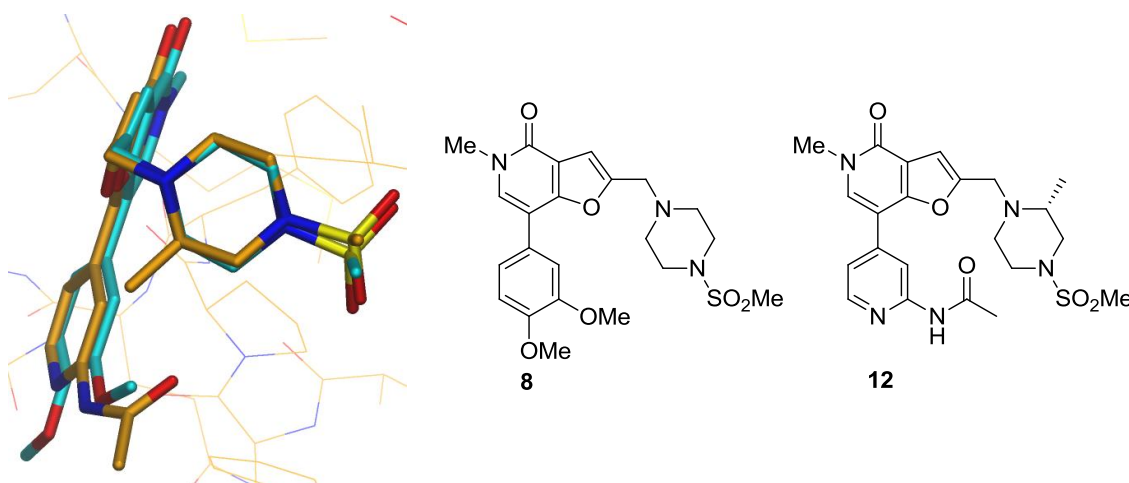
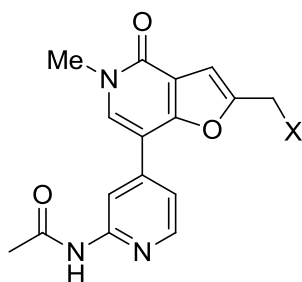


Figure 46. Overlay of the X-ray crystal structure of **12** (*orange*, 1.3 Å resolution, PDB code 2PSMP) bound with BRD4 BD1 with that of **8** (*cyan*, 1.2 Å, 2INSC) with BRD4 BD1.⁴⁴ The headgroups overlay closely, and the 2-methyl substituent of **12** was found to be in close proximity to the tail group acetamido substituent.

An array of analogues of **12** with alternative headgroups was synthesised by Barnett and Watson in order to optimise potency for BD1 and selectivity *versus* BD2 and BRD9, and to potentially reduce the propensity for metabolic oxidation and dealkylation of the headgroup (compounds **27** to **48**, **Table 41**, page 206).^{16,19} Compounds were designed to be drug-like (MW <500, calculated PFI (cPFI) <6)⁷⁸ and to explore the requirement for the incorporation of a hydrogen bond acceptor with the potential to hydrogen-bond to the backbone Ile 146 in a similar manner to the S=O of the piperazine methylsulfonamide of **12**. Compounds with stereogenic centres were synthesised with known absolute configuration where starting materials were available in house or commercially (**34** and **48**); where material was not available, compounds were made as racemates (compounds **30**, **33**, **36**, **38**, **39**, and **41**).



Compound Number	X	TR-FRET BRD4 BD1 pIC ₅₀	Minimum Fold Selectivity for BET BD1 vs. BD2	Minimum Fold Selectivity for BET BD1 vs. BRD9	PFI
12		7.6	126x	79x	4.7
27 ¹⁶		5.7	13x	Not tested	3.2
28 ¹⁶		5.8	16x	Not tested	3.5
29 ¹⁶		5.7	8x	Not tested	3.6
30 ¹⁶		5.6	20x	Not tested	4.0
31 ¹⁶		6.2	32x	Not tested	3.4
32 ¹⁶		6.4	50x	Not tested	3.5
33 ¹⁶		7.3	50x	16x	5.2
34 ¹⁹		7.3	50x	25x	4.8
35 ¹⁶		6.1	13x	Not tested	4.3
36 ¹⁶		6.2	13x	Not tested	4.7

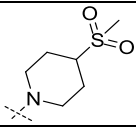
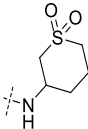
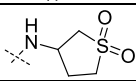
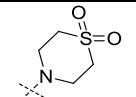
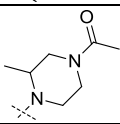
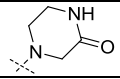
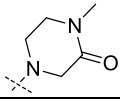
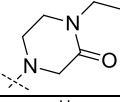
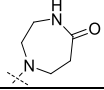
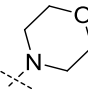
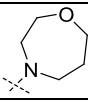
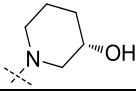
Compound Number	X	TR-FRET BRD4 BD1 pIC ₅₀	Minimum Fold Selectivity for BET BD1 vs. BD2	Minimum Fold Selectivity for BET BD1 vs. BRD9	PFI
37 ¹⁶		5.9	16x	Not tested	4.1
38 ¹⁶		6.0	13x	Not tested	4.1
39 ¹⁶		6.2	13x	Not tested	4.0
40 ¹⁶		7.0	32x	Not tested	4.1
41 ¹⁹		6.9	50x	13x	4.0
42 ¹⁶		6.1	16x	Not tested	3.6
43 ¹⁹		5.8	10x	Not tested	3.7
44 ¹⁶		5.9	10x	Not tested	4.3
45 ¹⁶		7.1	32x	8x	3.7
46 ¹⁶		5.8	10x	Not tested	4.1
47 ¹⁶		6.0	20x	Not tested	4.5
48 ¹⁶		5.7	10x	Not tested	4.0

Table 41. Profile of the array of analogues with alternative headgroups to the piperazine methylsulfonamide present in **12**. Compounds were synthesised by Barnett and Watson.^{16,19}

The piperazine **27** and *N*-alkyl analogues **28-30** were considerably less potent *versus* BD1 than **12**, and also less selective *versus* BD2 and BRD9, as was the 1,4-diazepane **31**, and the corresponding *N*-Me analogue **32**; this suggested that a hydrogen acceptor,

such as a sulfone oxygen, were required for potency, as has been discussed previously, or that basic nitrogens were not tolerated in this position. The dimethyl analogue **33** was similar in potency to **12**, but had lower selectivity for BD1 *versus* BD2 and BRD9, and was more lipophilic, offering no advantage over **12**. Regioisomer **34** was also of similar potency to **12** but was less selective *versus* BD2 and BRD9. Piperidine methylsulfonamide analogues **35** and **36** were less potent and selective than **12**, as were the sulfone analogues **37** to **40**. The *N*-acetamido analogue **41**, amides **42** to **45**, morpholine **46**, oxazepane **47** and hydroxy piperidine **48** were all less potent and selective than **12**. These data suggest the constituent oxygens of compounds **35** to **48** could not pick up an hydrogen bond interaction with Ile 146 as efficiently as the S=O of **12**. Although lower in potency and selectivity than **12**, the sulfone **40** and the diazepamone **45** met the BD1 TR-FRET potency criterion of ≥ 7.0 for a probe and the *N*-acetamide **41** came close to the target value; additionally all three compounds were considerably lower in lipophilicity than **12** which was postulated to be likely to improve IVC. However, the PBMC IL6 pIC₅₀s and selectivities of **40** (6.0), **41** (5.4) and **45** (6.2) were too low to progress the compounds; a follow-up array based on these compounds was therefore designed to improve these parameters, while retaining low lipophilicity. An X-ray crystal structure of **41** bound in the BRD4 BD1 active site was resolved in order to gain some insights into how this might be achieved (**Figure 47**). Attempts to obtain X-ray crystal structures of **40** and **45** were unsuccessful.

The BRD4 BD1 X-ray crystal structure of **41** obtained by Chung⁴⁴ showed that the piperazine acetamide oxygen was positioned in a similar region to the piperazine methylsulfonamide of **12** as predicted (**Figure 47**); the acetamide oxygen of **41** acted as a hydrogen bond acceptor to the NH of Ile 146 in the same manner as the methylsulfonamide oxygen of **12**.

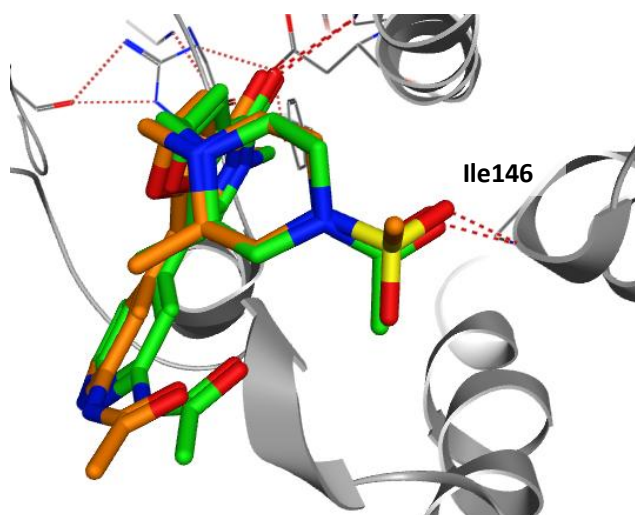
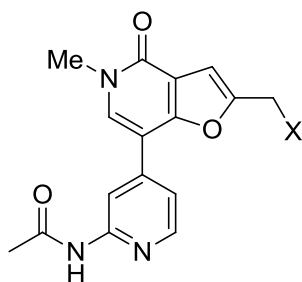


Figure 47. X-ray crystal structure of **12** (*orange*, 1.3 Å resolution, PDB code 2PSMP) overlaid with that of **41** (*green*, 1.3 Å, 3XCXR) in BRD4 BD1 (*grey*, 2PSMP). Hydrogen bonds are depicted by red dashed lines.⁴⁴

However, the lower BRD4 BD1 potency of **41** relative to **12** was difficult to rationalise from the X-ray crystal structure because all key interactions with BRD4 BD1 seemed to be made with **41** as well as with **12**. The main difference between the bioactive conformation of **12** and **41** was in the tail group pyridine acetamide, which seemed to be positioned away from the headgroup in **12**, potentially due to a steric clash with the methyl substituent on the headgroup of **12**; conversely, the tail group pyridine acetamide was positioned closer to headgroup of **41**. The conformation of the acetamido moiety in **12** may be preferred to that adopted in **41** because it may make more favourable interactions with the WPF shelf. From the X-ray crystal structure, it was not obvious how to improve the potency and selectivity of **41**, so the follow-up headgroup array was instead based on the structures of the two headgroup hits, **40** (compounds **49** to **51**) and **45** (compounds **52** to **55**, **Table 42**). Compounds **52** to **55** were prepared by Barnett.¹⁶



Compound Number	X	BRD4 BD1 pIC ₅₀	Minimum Fold Selectivity for BET BD1 vs. BD2	Minimum Fold Selectivity for BET BD1 vs. BRD9	PFI
12		7.6	126x	79x	4.5
40 ¹⁶		7.0	32x	Not tested	4.1
49 ¹⁶		7.0	251x	Not tested	4.4
50 ¹⁶		6.9	126x	Not tested	4.5
51 ¹⁶		6.9	100x	Not tested	4.4
45 ¹⁶		7.1	32x	8x	3.7
52 ¹⁶		5.7	6x	Not tested	3.7
53 ¹⁶		7.0	158x	Not tested	3.9
54 ¹⁶		5.9	20x	Not tested	3.8

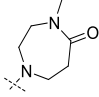
Compound Number	X	BRD4 BD1 pIC ₅₀	Minimum Fold Selectivity for BET BD1 vs. BD2	Minimum Fold Selectivity for BET BD1 vs. BRD9	PFI
55 ¹⁶		6.7	100x	40x	3.8

Table 42. Profiles of the second headgroup array that aimed to optimise analogues **40** and **45** that were made in the first headgroup array, shown in **Table 41**. Compounds were prepared by Barnett.¹⁶

The methyl analogues of sulfone **40**, compounds **49** and **50**, and thiazepane dioxide **51** had similar BD1 potencies to **40**; compound **49** offered slightly improved selectivity *versus* BD2 over **40**, whereas **50** and **51** were similar in selectivity. The regioisomer of **45**, compound **52**, was significantly less potent and selective, as was the methyl analogue of **45**, compound **54**. The alternative methyl analogue **53** was similar in potency to **45** but had higher selectivity *versus* BD2, whereas the *N*-methyl analogue **55** was slightly lower in potency.

Although all were lower in lipophilicity, none of the compounds with alternative headgroups (**27-55**) offered neither sufficiently improved potency, nor selectivity over compounds with the 2-methyl piperazine methylsulfonamide headgroup in **12**. The 2-methyl piperazine methylsulfonamide headgroup was therefore retained in all subsequent optimisation efforts.

2.4.3. Investigating the Optimum Position of the Pyridine Nitrogen

The tail group pyridine nitrogen of **12** did not seem to be involved in binding to the BRD4 BD1 active site: the X-ray crystal structure of **12** within the active site showed the nitrogen was exposed to solvent and did not seem to interact with any residue (**Figure 48**).

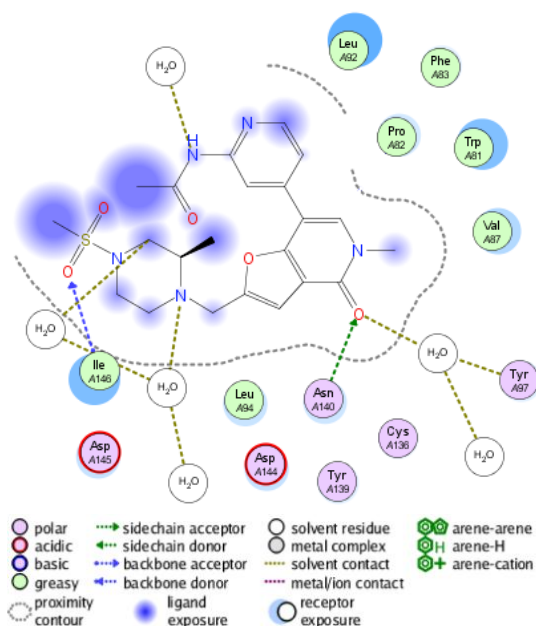
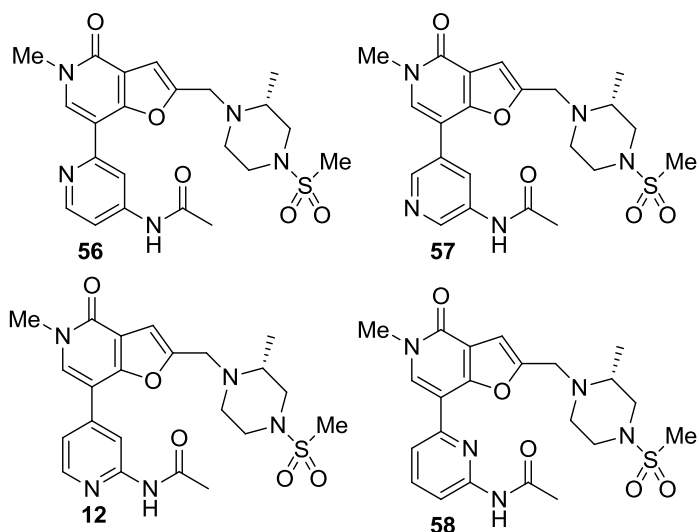


Figure 48. Two dimensional representation of key interactions made between **12** and BRD4 BD1 (PDB code 2PSMP).⁴⁴ The pyridine nitrogen was exposed to solvent and did not seem to interact with any residue.

The tail group 4-position nitrogen was originally introduced to reduce the overall template lipophilicity which was thought to be likely to be favourable for reducing clearance. However, the 4-position nitrogen and the position directly adjacent to this nitrogen were prone to metabolic oxidation and therefore likely to predispose the template to increased clearance.⁷⁹ Placement of the nitrogen in the 2-, 3- and 6-positions (compounds **56**, **57** and **58** respectively) was investigated because different steric characteristics of each of these systems can influence the IVC characteristics of the template (**Table 43**).



#	TR-FRET BRD4 BD1 pIC ₅₀	Minimum Fold Selectivity for BET BD1 versus:		PBMC pIC ₅₀	Calculated Chrom LogD _{7,4} ⁷⁸	Measured Chrom LogD _{7,4}	AMP, nm/s	CLND Sol. mg/mL	IVC _{mic} , mL/min/g		
		BD2	BRD9						Rat	Dog	Human
56	-	-	-	-	1.6	-	-	-	-	-	-
57	7.7	200x	79x	6.0	1.2	1.2	<3	216	-	-	-
12	7.6	126x	79x	6.7	1.8	1.7	≤24	≥171	3.1	0.6	<0.5
58	7.0	126x	32x	6.5	2.9	2.3	57	≥213	0.7	<0.5	1.1

Table 43. Profiles of the pyridine regioisomers of **12**, compounds **56** to **58**.

Compound **56** was unlikely to offer much of an advantage for reducing IVC relative to **12** because, like **12**, a position adjacent to the nitrogen remained vulnerable to microsomal oxidative metabolism in addition to the nitrogen itself, and the two compounds were calculated to be of similar lipophilicity.⁷⁸ A number of unsuccessful attempts were made to synthesise **56**, but a decision was made not to pursue this compound further due to synthetic difficulties and the probability that the IVC was unlikely to be any better than for **12**.

Similarly, compound **57** was thought to be more vulnerable to metabolism than **12** because **57** had an additional site adjacent to the nitrogen that could potentially be oxidised by metabolising enzymes. However, it not known at the time whether this could have been offset by the reduction in lipophilicity quantified by the reduction in ChromLogD_{7,4}. BRD4 BD1 potency and selectivity of **57** were maintained relative to **12** in the TR-FRET assay; however, a significant reduction in PBMC cell potency to below

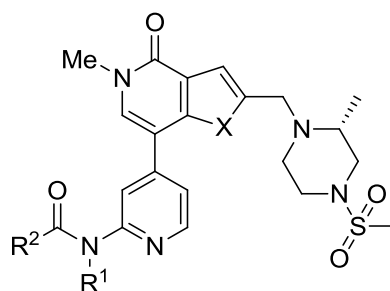
the target pIC_{50} of 6.5 was observed, possibly because **57** was less cell permeable. Compound **57** was therefore not progressed to the IVC assays.

The pyridyl ring of compound **58** was likely to be less vulnerable to metabolic oxidation than **12** because it is sterically less accessible to metabolising enzymes and both sites adjacent to the pyridyl nitrogen were blocked to oxidation by metabolising enzymes whereas only one adjacent position is blocked in **12**. However, **58** is more lipophilic than **12**, which could have made the compound more susceptible to metabolism elsewhere on the molecule. A clear reduction in IVC_{rat} was observed for **58** relative to **12**, as was a tentative reduction in IVC_{dog} ; blocking positions to either side of the nitrogen was therefore likely to be more important in achieving a reduction in IVC_{rat} than reducing lipophilicity of the template (at least by 0.6 log units). However, IVC_{human} was higher and illustrates that the interspecies differences in metabolism can be unpredictable.

Compound **58** was four-fold less potent than **12** in the TR-FRET assay, but had similar, if not slightly lower potency in the PBMC cell assay, possibly because **58** was more permeable and soluble than **12**; this meant that a higher concentration of **58** was achievable in cells. Given that compound **12** had a lower IVC_{human} and lower $ChromLogD_{7.4}$ than **58**, compound **12** remained the lead compound on which optimisation was focussed.

2.4.4. Optimisation of the Pyridyl Amide Substituent

Another possible route of metabolism of **12** involved hydrolysis of the aryl tailgroup acetamide by amidases that are present in microsomes.⁸⁰ In order to investigate the possibility of making the amide less susceptible to hydrolysis while retaining or improving potency and selectivity, a set of amide analogues, compounds **59** to **64**, in both the TP and FP series was made with varying steric bulk at this position (**Table 44**).



Compound	X	R ¹	R ²	BRD4 BD1 pIC ₅₀	Minimum Fold Selectivity for BET BD1 <i>vs.</i> :		PBMC pIC ₅₀	TR- FRET/ PBMC difference	CLND sol., µg/mL	AMP, nm/s
					BD2	BRD9				
12	O	H	Me	7.6	126x	79x	6.7	-0.9	≥171	≤24
59		Me	Me	7.6	79x	25x	6.4	-1.2	≥200	36
60		H	Et	7.4	158x	13x	6.9	-0.5	150	<3
61		H	cPr	7.7	126x	25x	7.0	-0.7	≥203	66
13	S	H	Me	6.7	40x	1x	6.5	-0.2	202	35
62		Me	Me	7.0	126x	1x	6.2	-0.8	100	130
63		H	Et	6.5	158x	2x	5.5	-1.0	≥179	39
64		H	cPr	6.9	158x	2x	6.4	-0.5	26	200

Table 44. Amide analogues made in the TP series (X = S) and FP series (X = O).

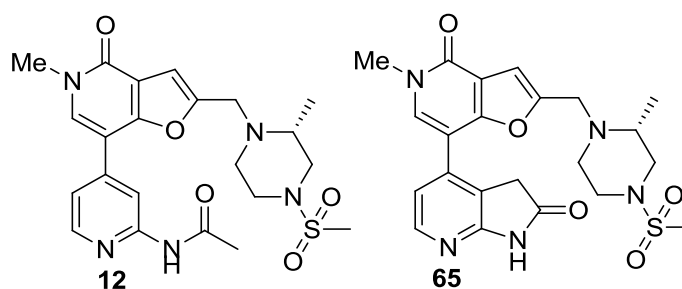
Each of the FP analogues (**59** to **61**) was more potent than the corresponding TP analogues (**62** to **64**) in the BRD4 BD1 TR-FRET assay which was in agreement with previous findings. Selectivity for BD1 *versus* BD2 was variable between matched pairs of TP and FP analogues; for example, the TP **13** was less selective than the corresponding FP **12**, whereas the TP **64** was slightly more selective than the FP **61**. However, the FP series was more selective overall for BD1 *versus* BRD9. Although the FP analogues were all more potent in the TR-FRET assay, there seemed to be little difference in potency in the PBMC cell assay between some of the matched pairs, for example the TP **13** and the FP **12**, and the TP **62** and the FP **59**, whereas there was a more substantial difference between other matched pairs, such as the TP **63** which was much less potent than the FP **60**, and the TP **64** which was also less potent than the FP **61**.

An approximate one log unit difference between TR-FRET and PBMC cell potency was expected because the TR-FRET assay is a biochemical assay which mixes the

compound in solution with the BRD4 BD1 protein, whereas the PBMC cell assay requires compounds to first permeate then cross the cell membrane and enter the cell cytosol before it can reach the BRD4 BD1 protein. Two factors that can affect cell potency are solubility and permeability which are represented here by CLND solubility and AMP respectively. All compounds but **64** were highly soluble, but a range of permeabilities were evident: the FPs were low to moderate in permeability while the TPs are low or high in permeability. There did not seem to be a trend between PBMC potency and solubility or permeability, possibly because the CLND and AMP assays are artificial and do not always give representative values of what happens in a cell in this case.

Increasing the size of the amide substituent R² from methyl (**12** and **13**) to ethyl (**60** and **63**) to cyclopropyl (**61** and **64**) did not seem to have a significant impact on either BRD4 BD1 TR-FRET potency or PBMC potency in either series; similarly the dimethyl amides in the FP series (**59**) and TP series (**62**) were of similar potency to the monosubstituted analogues, **12** and **13** respectively. The most potent FPs, **59** to **61**, had lower selectivity for BET BD1 *versus* BRD9 relative to **12**, so these changes offered no advantage over **12** and these compounds were not progressed to the IVC assays.

In one further attempt to stabilise the amide substituent on the tail group against metabolism, the acetamide was fused to the adjacent position of the pyridyl ring (**65**, **Table 45**), creating a lactam.



Compound	12	65
BRD4 BD1 pIC ₅₀	7.6	6.4
Minimum Fold Selectivity for BET BD1 <i>vs.</i> BD2	126x	50x
Minimum Fold Selectivity for BET BD1 <i>vs.</i> BRD9	79x	10x
PBMC pIC ₅₀	6.7	5.4
ChromLogD _{7.4}	1.7	1.6
IVC _{human/dog} , mL/min/g	<0.5 / 0.6	<0.5 / 0.5

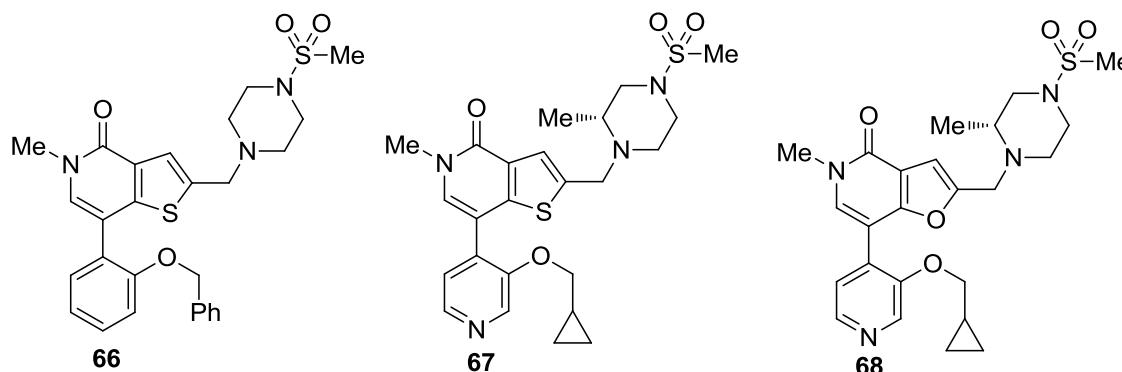
Table 45. Comparison of the profile of **12** with the cyclised amide analogue **65**.

A substantial drop in potency and selectivity *versus* BD2 and BRD9 was observed for **65** relative to **12**, whereas the IVC_{human} and IVC_{dog} were comparable for **12** and **65**. The profile of **12** had not been improved by all the lead optimisation attempts to date, but was close to the target profile required for a probe for *in vivo* dog safety studies. However, the moderate dog clearance remained a risk in terms of progression into these studies, so subsequent lead optimisation efforts focussed on incorporating substituents at different positions of the aryl tail group, initially by substitution in the *ortho*-position.

2.4.5. Improving Selectivity for BRD4 BD1 *versus* BRD9: *ortho*-substitution on the Aryl Tail Group

The *ortho*-substituted benzyloxy TP **66**¹⁵ was identified as the first ever TP to be ≥ 100 -fold more selective for inhibition of BRD4 BD1 *versus* BRD9 (**Table 46**).⁵⁰ However the PBMC potency and the selectivity *versus* BD2 were lower than required and lipophilicity was high which meant the compound was likely to have high IVC and had a high risk of non-mechanistic toxicity *in vivo*. In order to reduce lipophilicity and improve potency and selectivity of the template, two analogues were made; these were the TP **67**, and the FP **68** (**Table 46**), by which a nitrogen was introduced into the 4-position of the pyridyl ring, which was known from **12** to be tolerated, and the aryl group was replaced with a cyclopropyl group, respectively. Cyclopropane ring bonds exhibit some π -character, reacting with electrophiles like bromine, and undergoing

hydrogenolysis.⁸¹⁻⁸³ The replacement of a phenyl ring with a cyclopropane group therefore retains an element of π -character with a significant reduction in size and lipophilicity.



Compound	66 ¹⁵	67	68
BRD4 BD1 pIC ₅₀	7.0	*7.9	*8.1
Minimum Fold Selectivity for BET BD1 vs. BD2	25x	*251x	*32x
Minimum Fold Selectivity for BRD4 BD1 vs. BRD9	126x	*316x	*631x
PBMC pIC ₅₀	5.8	7.0	≥8.2
ChromLogD _{7.4}	5.5	3.7	2.7
IVC _{dog} , mL/min/g	Not tested	23	7.5

Table 46. Profiles of the the first TP and FP compounds that were ≥ 100 -fold more selective for BD1 *versus* BRD9. *BRD4 BD1 pIC₅₀s close to TR-FRET assay tight binding limit (TBL), therefore pIC₅₀s and selectivity values are likely to be underestimated.

The potencies of **67** and **68** were close to the tight binding limit (TBL) of the BRD4 BD1 TR-FRET assay and both compounds met or exceeded the required levels of PBMC potency and selectivity for BD1 *versus* BRD9. The selectivities of **67** and **68** *versus* BD2 were likely to be underestimated because the potency was at the TBL of the TR-FRET assays. Surface Plasmon Resonance (SPR) experiments indicated the BRD4 BD1 pIC₅₀s to be closer to 9 with greater than 100-fold selectivity for BRD2, 3, 4, T BD1 *versus* BD2 (data not shown).⁸⁴

Both the TP **67** and the FP **68** were moderately lipophilic but IVC_{dog} values were too high to progress to *in vivo* dog PK studies; the IVC of **67** was substantially higher than

that of **68**, probably because **67** was more lipophilic than **68**. This suggested a reduction in lipophilicity to $\text{ChromLogD}_{7.4} < 2.7$ might be required to reduce IVC_{dog} to acceptable levels of $< 0.53 \text{ ml/min/g}$. Given that the TP **67** was also substantially less potent in the PBMC assay than the FP **68**, further lead optimisation focussed on improving IVC of FP analogues of **68**. An X-ray crystal structure of **68** bound to the BRD4 BD1 active site was obtained to aid structure-based design of the next iterations of compounds.

2.4.5.1. X-ray Crystal Structure of **68**

Compound **68** was found to bind to the BRD4 BD1 active site in a manner similar to **12**, according to the X-ray crystal structure (**Figure 49a and b**).⁴⁴ Similarly to **12**, the methyl group on the piperazine methylsulfonamide headgroup does not make any clear interactions with the active site.

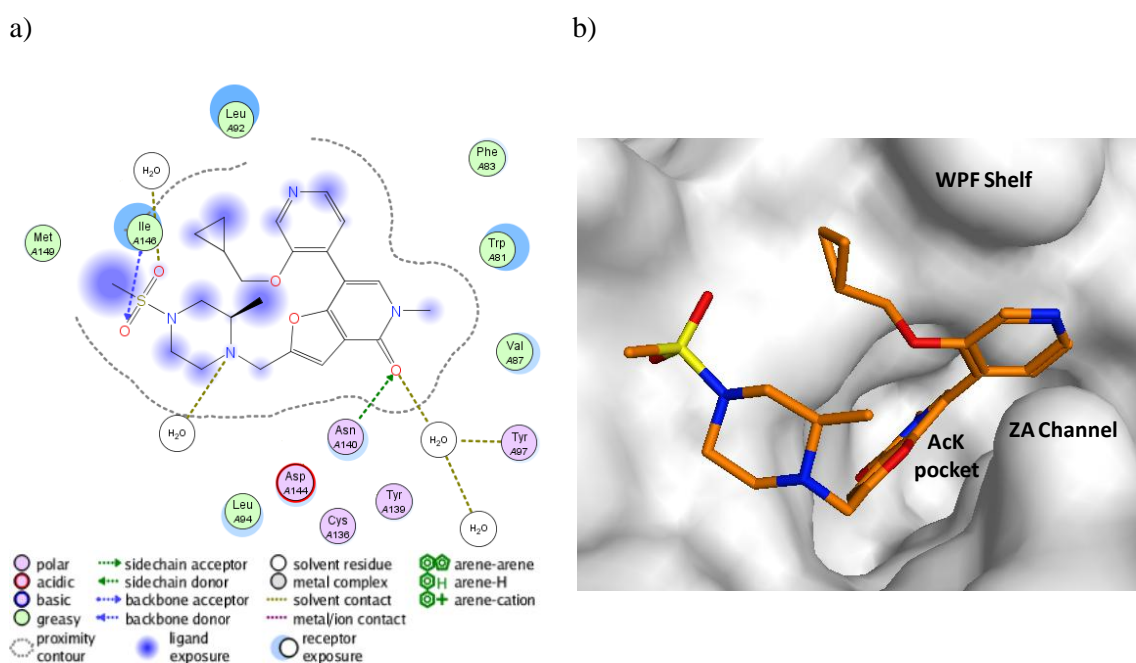


Figure 49. X-ray crystal structure of **68** in the BRD4 BD1 active site (1.5 Å resolution, PDB code 2ZSNN).⁴⁴ a) Two dimensional representation to show the major interactions made with the BRD4 BD1 active site. b) Space filling representation to show the conformation adopted by **68** in the BRD4 BD1 active site and the positioning of the cyclopropyl methyl moiety against the hydrophobic WPF shelf.

A hypothesis for the reason that **68** is so selective for BD1 *versus* BRD9 was developed by comparing the BRD4 BD1 active site with that of BRD9;⁴⁴ an overlay of a space-

filling representation of the X-ray crystal structure of **68** bound in the active site of BRD4 BD1 with an *apo* structure of BRD9 is shown in **Figure 50**. The *ortho*-cyclopropylmethyl ether substituent was likely to clash sterically with the bulky Tyr 106 residue in BRD9 but not with the equivalent residue in BRD4 BD1, Ile 146, which occupies a smaller volume of space than Tyr 106 and also makes a hydrogen bond with the S=O in the headgroup. This would make binding in the BRD9 active site disfavoured, but would increase BRD4 BD1 potency, thus increasing selectivity for BET BD1 *versus* BRD9. The lipophilic *ortho*-cyclopropylmethyl ether substituent is also likely to interact favourably with the WPF shelf of BD1, which does not exist in BRD9, and would therefore further improve BRD4 BD1 potency and selectivity for BRD4 BD1 over BRD9.

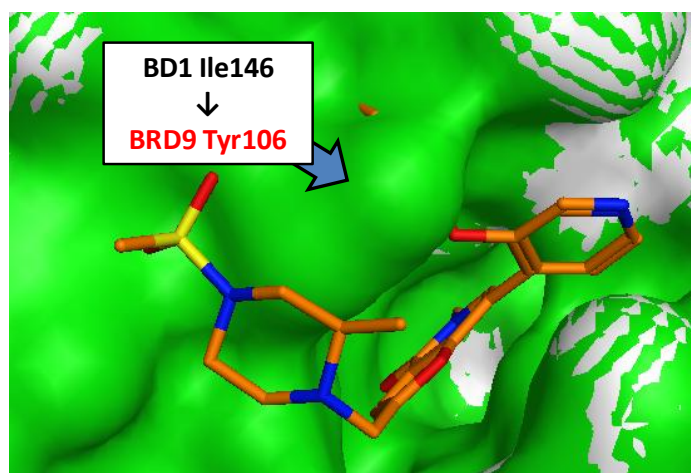


Figure 50. Overlay of the space-filling representation of the X-ray crystal structure of **68** (*orange*, 1.5 Å resolution, PDB code 2ZSNN) in the BRD4 BD1 active site (*grey*, 2ZSNN) with a ligandless X-ray crystal structure of BRD9 (*green*, 1.7 Å, 8XLGJ).⁴⁴

Subsequent lead optimisation steps looked at three potential methods of reducing the IVC of the FP template by replacing or moving structural features on the aryl tailgroup that were likely to be liable to metabolism.⁷⁷ These were:

1. variation of the position of the nitrogen in the pyridyl tail group;⁵¹
2. replacement of the linker oxygen atom in the *ortho*-position of the tail group with an alternative linker group;

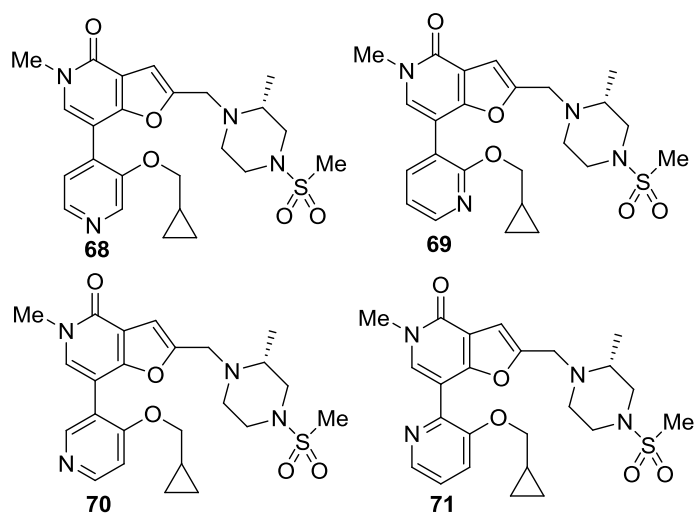
3. replacement of the *ortho*-cyclopropylmethyl substituent of the tail group with an alternative substituent with lower lipophilicity.^{45,85}

In the interests of efficiency, investigations were limited to the FP series.

2.4.6. Improving *In Vitro* Clearance of the FP Series

2.4.6.1. Investigating the Optimum Position of the Pyridine Nitrogen

The nitrogen in the 4-position of the pyridyl tail group of **68** was thought to be more exposed to metabolism relative to alternative positions in the tail group such as position 3 or position 6 which would lead to increased IVC.⁵¹ The effect of varying the position of the nitrogen in the tail group was investigated with compounds **69-71** (Table 47).

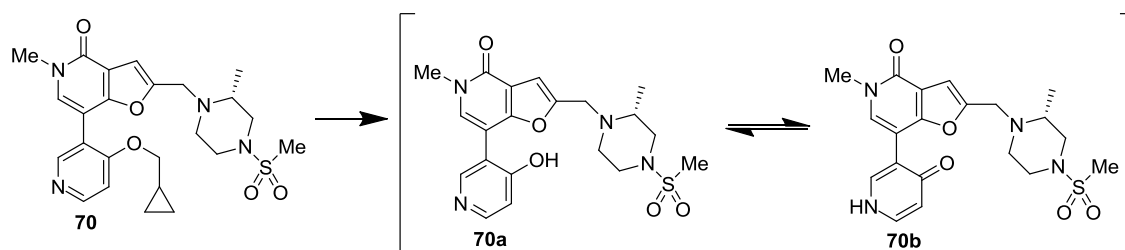


Compound number	68	69	70	71
Nitrogen position	4	3	5	6
BRD4 BD1 pIC ₅₀	*8.1	-	-	*7.9
Minimum Fold Selectivity for BET BD1 vs. BD2	*31x	-	-	*316x
Minimum Fold Selectivity for BRD4 BD1 vs. BRD9	*631x	-	-	*794x
PBMC pIC ₅₀	≥8.2	-	-	7.4
Calculated ChromLogD _{7.4} ⁷⁸	3.0	3.6	2.7	3.3
ChromLogD _{7.4}	2.7	-	-	3.3
IVC _{dog} , mL/min/g	7.5	-	-	9.8

Table 47. Profiles of the 6-*aza* analogue of **68**. *BRD4 BD1 pIC₅₀s at the TR-FRET assay TBL, therefore pIC₅₀s and selectivity values are likely to be underestimated.

Synthesis of the 3-*aza* analogue **69** was not attempted because its higher predicted lipophilicity was likely to increase IVC relative to **68**.

The 5-*aza* analogue **70** was also not made because it was likely to be metabolically unstable, particularly to dealkylation to give **70a** and **70b** (Scheme 26).

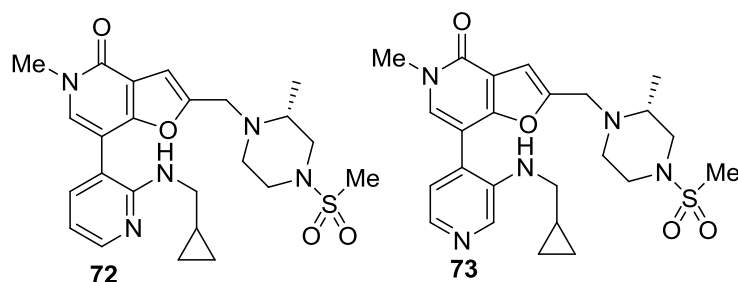


Scheme 26. Likely metabolites of **70**.

The 6-*aza* analogue **71** was less potent in the PBMC assay than 4-*aza* analogue **68**, but still exceeded the target level of potency and selectivity for BD1 *versus* BRD9, and also for BD1 *versus* BD2, even though the BD1 potency was at the TBL of the TR-FRET assay. However, the IVC_{dog} of **71** was of a similar magnitude to **68** which was too high to progress to *in vivo* studies.

2.4.6.2. Replacement of the Oxygen Linker Atom with Less Electronegative Linker

Based on the high IVC_{dog} values of **68** and **71** (Table 47), the cyclopropylmethyl substituent was likely to be susceptible to metabolic oxidation then dealkylation *in vivo*. Replacement of the oxygen linker atom with a nitrogen linker atom was undertaken to investigate the effect this would have on potency, selectivity and IVC. Two *N*-linked analogues of **68**, the 3-*aza* analogue **72** and the 4-*aza* analogue **73** were made (Table 48). For both compounds, the BRD4 BD1 and PBMC potencies, and selectivities for BD1 *versus* BRD9 were higher than target values. The selectivity of **72** for BD1 *versus* BD2 exceeded the required level, and this was likely to be the case for **73** because the BD1 potency was at the TBL of the TR-FRET assays. However, the IVC_{dog} values of these compounds remained too high to progress to dog PK studies. The remaining 6-*aza* and 5-*aza* analogues were not pursued because parallel investigations into replacement of the *ortho*-cyclopropylmethyl group were more promising for reducing IVC.



Compound number	72	73
Nitrogen position	3	4
BRD4 BD1 pIC ₅₀	*7.8	*7.9
Minimum Fold Selectivity for BET BD1 vs. BD2	*200x	*79x
Selectivity for BRD4 BD1 vs. BRD9	*1259x	*794x
PBMC pIC ₅₀	7.5	7.4
Calculated ChromLogD _{7,4} ⁷⁸	3.1	2.9
Measured ChromLogD _{7,4}	3.5	2.6
IVC _{dog} , mL/min/g	16.3	14.3

Table 48. Profiles of *N*-linked analogues of **68**. *BRD4 BD1 pIC₅₀s close to TR-FRET assay TBL, therefore pIC₅₀s and selectivity values may be underestimated.

2.4.6.3. Variation of the 2-position of the Pyridyl Ring Tail group

The *ortho*-cyclopropylmethyl ether substituent of the pyridyl ring of **68** conveyed excellent potency and selectivity for BRD2,3,4 and T BD1 *versus* BRD9 but the compound was too metabolically unstable *in vitro* for progression to *in vivo* dog PK studies. Variation of substituents at this position was explored with the aim of reducing IVC while at the same time retaining or improving potency and selectivity. In the first instance, BioDig, an in-house software tool was employed to facilitate the choice of substituents that were likely to reduce IVC.⁸⁶

BioDig is an add-on to the TIBCO™ SpotFire® data visualisation package⁸⁷ that allows access to IVC data that has been generated at GSK and uses Matched Molecular Pair (MMP) approach⁸⁸ to identify potential substructure replacements for given substructures. BioDig is set up to query data for approximately 47,000 compounds, eight million MMPs and six million transformations.⁸⁶ BioDig allows a substructure to be inputted, which in this case is the cyclopropylmethyl ether group, and then mines the GSK databases containing human and rat IVC data. Substructure replacements that have been tried and shown to increase, reduce or have no effect on IVC for given sets of MMPs are then identified by the tool. Data is displayed in the form of a histogram,

whereby the number of occasions an MMP has been tested is plotted *versus* binned change in IVC.

At this time the BioDig software did not offer an option to mine the IVC_{dog} dataset, probably because the dataset was too small. A large dataset was found for IVC_{human} so this was used as a surrogate. The BioDig software was used to identify 85 MMPs for the cyclopropylmethyl ether substituent present in GSK databases that had IVC_{human} data (Figure 51).

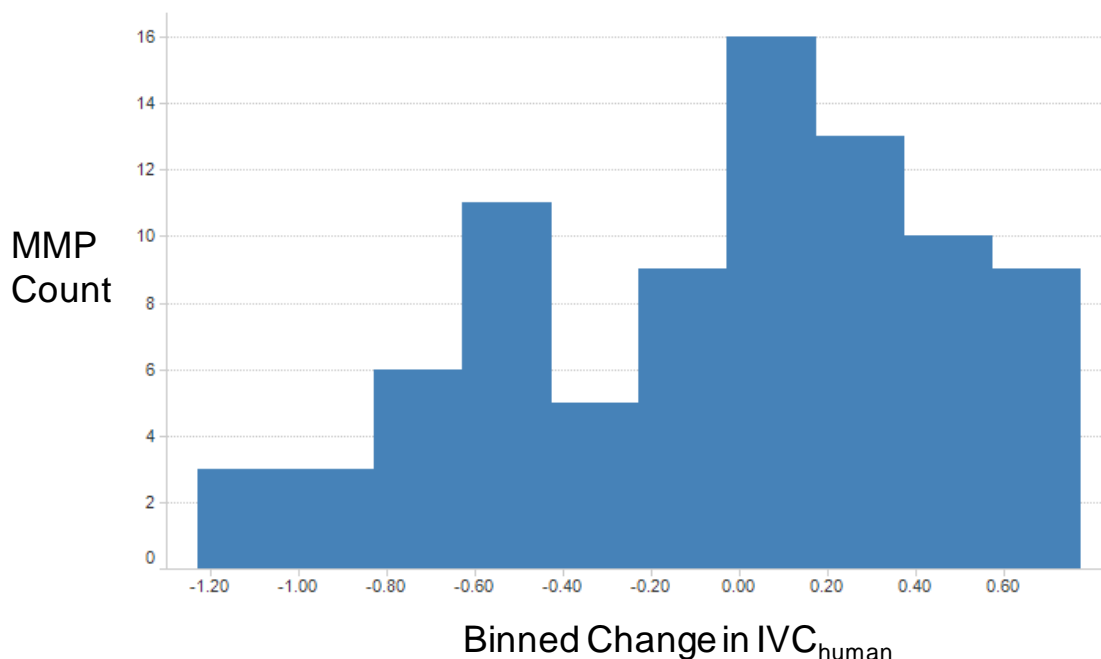
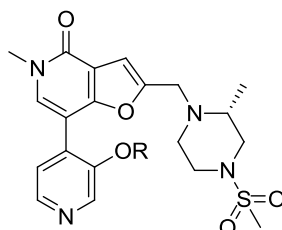


Figure 51. Histogram generated using BioDig software that showed numbers of MMPs found for the cyclopropylmethyl substructure activity versus change in human IVC.

Of the 85 MMPs identified, 37 showed a reduction in IVC_{human} whereby the cyclopropylmethyl group had been replaced with an alternative substituent; note this does not mean 37 alternative substituents were identified because a number of the MMPs had the same alternative substituent. For example three MMPs had reduced IVC_{human} when a cyclopropylmethyl ether group was replaced with a hydroxyl group. Intriguingly two MMPs had reduced IVC_{human} when a cyclopropylmethyl ether group was replaced with a cyclopropylmethyl amino group; these data contradicted previous findings whereby the cyclopropylmethyl ether group of **68** was replaced with a

cyclopropylmethyl amino group to give **73** which actually had a higher IVC_{dog} than **68**. The reasons for the latter finding are unknown.

In addition to the hydroxyl group, a number of other substituents that were likely to reduce IVC_{human} were identified using BioDig; the appropriate analogues were synthesised and tested (compounds **74** to **77**, **Table 49**).



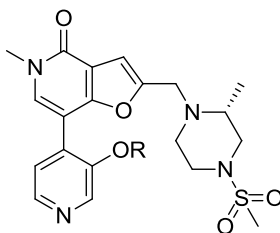
#	R	BRD4 BD1 pIC ₅₀	PBMC pIC ₅₀	Minimum Fold Selectivity for BET BD1 vs. BD2	Minimum Fold Selectivity for BET BD1 vs. BRD9	Chrom LogD _{7.4}	IVC _{dog} , mL/min/g
68		*8.1	≥8.2	*32x	*631x	2.7	7.5
74 ²⁰		7.5	6.9	63x	50x	2.4	1.3
75		7.6	7.0	79x	63x	2.0	3.2
76		6.8	6.0	79x	16x	1.4	0.7
77 ²⁰		7.3	5.2	126x	50x	1.1	-

Table 49. Profiles of *ortho*-substituted analogues of **68** where R-groups were chosen using the BioDig tool.⁸⁶ Compounds are ordered according to decreasing lipophilicity. *Potency at assay TBL, so selectivity is likely to be underestimated. Compounds **74** and **77** were prepared by Westaway.²⁰

Replacement of the cyclopropylmethyl ether substituent of **68** with the three R-groups in compounds **74-76**, and removal of the substituent to give **77**, led to a decrease in IVC_{dog}, though only **74** and **76** had IVC_{dog} values that approached target levels; however, their selectivities were too low. Apparent selectivity for BD1 *versus* BD2 improved for **74-77** relative to **68**, but this was not the case for selectivity over BRD9 which was lower and suggested that the R-groups present in **74-77** were unlikely to have enough steric bulk to clash significantly with the Tyr 106 residue in BRD9; the reduced levels of BRD4 BD1 potency also suggested these R-groups may not interact

with the lipophilic WPF shelf of BD1 as favourably as the cyclopropylmethyl substituent in **68**.

A further set of R-groups that might have enough lipophilic character to interact favourably with the lipophilic WPF shelf of BD1 but at the same time would incorporate enough hydrophilic character to further lower the ChromLogD_{7.4} of **68** and achieve lower IVC was chosen (**78-88**, **Table 50**). Calculated ChromLogD_{7.4}⁷⁸ was initially used to design these compounds to ensure they were less lipophilic than **68** (data not shown). Only compounds with close to or >100-fold selectivity for BD1 *versus* BRD9 were progressed to IVC studies.



Compound	R	BRD4 BD1 pIC ₅₀	PBMC pIC ₅₀	Minimum Fold Selectivity for BET BD1 vs. BD2	Minimum Fold Selectivity for BET BD1 vs. BRD9	Chrom LogD _{7.4}	IVC _{dog} , mL/min/g
68		*8.1	≥8.2	*32x	*631x	2.7	7.5
78		*7.9	8.0	*50x	*63x	2.6	10.0
79		6.4	-	16x	25x	2.5	-
80		7.0	6.2	50x	79x	2.5	-
81		7.4	7.0	100x	1000x	2.3	2.8
82		*7.9	8.0	*40x	*100x	2.3	8.3
83		7.4	6.7	126x	501x	2.1	3.0
84		7.3	7.1	100x	316x	2.1	2.0
85		7.4	6.4	79x	398x	1.9	0.8
86		7.0	-	63x	32x	1.9	-
87		7.3	6.8	126x	501x	1.8	0.7
88		7.7	-	126x	8x	1.6	-

Table 50. Profiles of compounds **78-88** which had varied R-groups to lower lipophilicity of the FP template relative to **68**. Compounds are listed in order of

decreasing lipophilicity. *At TBL of the BRD4 BD1 TR-FRET assay, so selectivity is likely to be underestimated.

A general trend in which IVC_{dog} was found to decrease with decreasing lipophilicity, as measured by $ChromLogD_{7.4}$, was observed for compounds **78-88**. Only **87** had a good enough overall profile to be considered for the dog *in vivo* PK. Given that **87** was a racemate, the material was separated into constituent diastereoisomers, **89** and **90** (**Figure 52**) using chiral HPLC⁸⁹ so that the individual compounds could be fully profiled separately. The oxetane chirality of **89** and **90** was assigned using X-ray crystallography (**Figure 53**, overleaf),⁴⁴ **89** was confirmed to be the *R,R*-stereoisomer and **90** the *R,S*-stereoisomer, and both compounds had acceptable BRD4 BD1 potency.

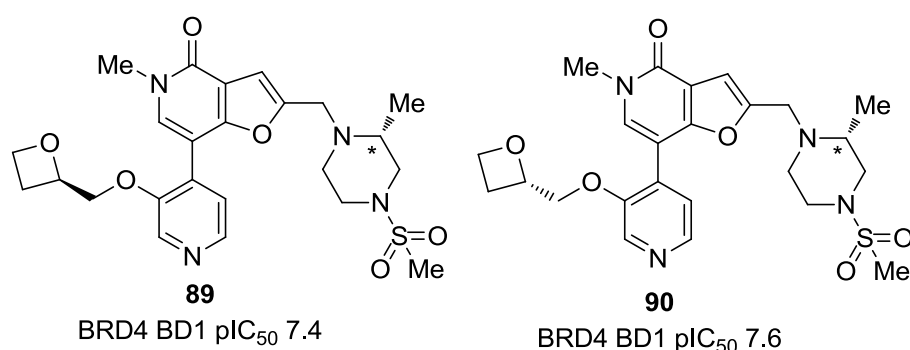


Figure 52. Structures of the epimers, **89** and **90** that were isolated from racemate **87** using chiral HPLC.¹² X-ray crystallography was used to confirm that **89** was the *R,R*-stereoisomer and **90** was the *R,S*-stereoisomer.⁴⁴

2.4.6.4. X-ray Crystal Structures of **89** and **90**

The BRD4 BD1 X-ray crystal structures of **89** and **90** (**Figure 53a** and **b** respectively)⁴⁴ showed that the two compounds bound to the active site in the same manner as previous FP compounds, such as **68** (**Figure 49**). The main difference between the oxetane *R*-stereoisomer **89** and the *S*-stereoisomer **90** was that the oxetane oxygen was either exposed to solvent, in **90**, or not, in **89**, which did not have an impact on the relative BRD4 BD1 potency (**Table 51**). The *ortho*-oxetanemethyl substituent of **89** and **90** was lipophilic enough and in close enough proximity to the lipophilic WPF shelf of BD1 to retain the required BD1 potency (**Figure 52**), though both compounds were lower in potency than **68**, probably because the *ortho*-oxetanemethyl substituent is not as

lipophilic as the *ortho*-cyclopropylmethyl substituent present in **68**. Both compounds were fully profiled in order to determine which would be the most appropriate compound to progress to the dog safety study.

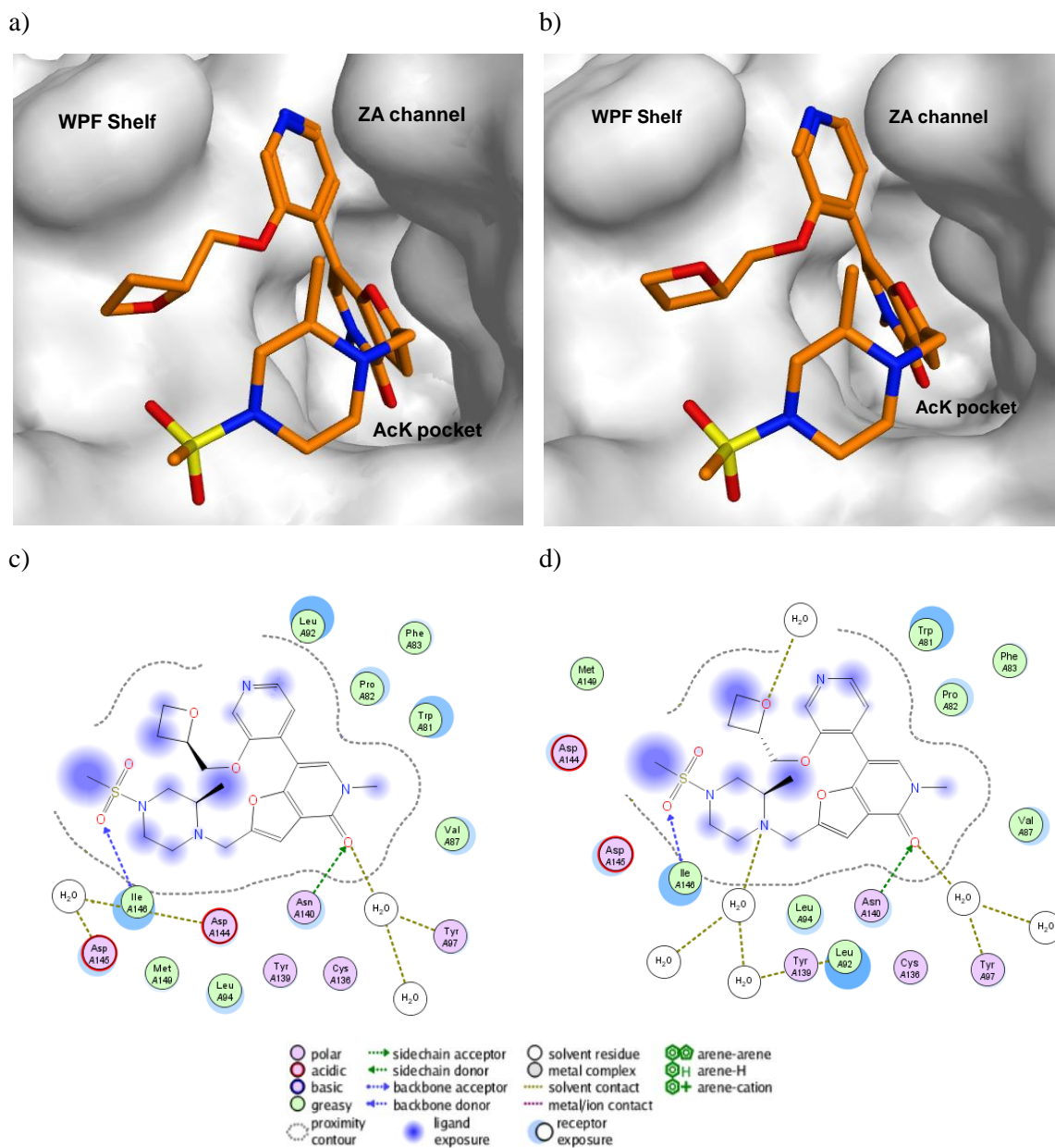
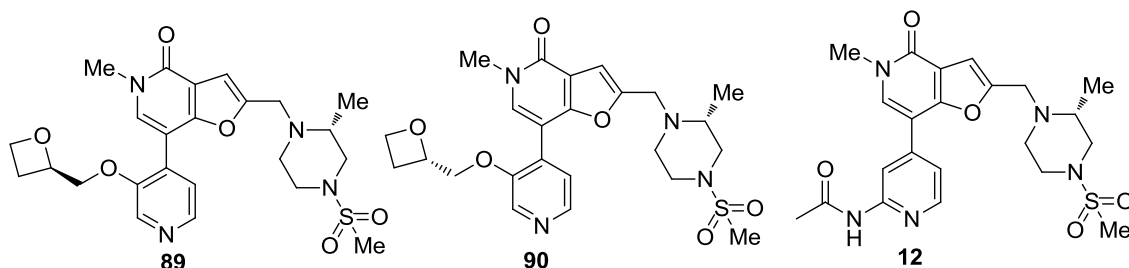


Figure 53. BRD4 BD1 X-ray crystal structures of a) the *R*-oxetane **89** (1.3 Å resolution, PDB code 9MMFY), and b) the *S*-oxetane **90** (1.4 Å, 3CFBS), and the key interactions made with the active site by c) **89** and d) **90**.⁴⁴

2.4.7. Selection of the BRD4 BD1 Selective *in vivo* Probe

The two epimers **89** and **90** had very similar potency and selectivity, and had similar IVC profiles that exceeded the target values (**Table 51**). Both compounds were progressed into dog PK studies to determine which compound might have a suitable PK profile to then progress into the dog safety study.^{7,21}



Parameter	Target Value	Compound Number		
		89	90	12
BET BRD4 BD1 pIC ₅₀	>7.0	7.4	7.6	7.6
Minimum Fold Selectivity for BET BD1 vs. BD2	>100x	>158x	>126x	>126x
Minimum Fold Selectivity for BET BD1 vs. BRD9	>100x	>501x	>631x	>79x
PBMC dog / human pIC ₅₀	≥6.5	6.6 / 6.5	6.9 / 6.5	6.8 / 6.7
MW / cLogP / ChromLogD _{7.4}	<500 / <5.0 / <6.0	503 / 1.0 / 1.7	503 / 1.0 / 1.7	474 / 1.3 / 1.7
LE / LLE	>0.30 / >5.0	0.29 / 6.4	0.30 / 6.6	0.32 / 6.3
FaSSiF solubility, μg/mL	>100	>725	>940	982
hERG pIC ₅₀	<4.5	<4.2	<4.2	<4.2
IVC _{dog} , mL/min/g	<1.9	0.5	0.8	0.6
Dog Cl _b , mL/min/Kg	<22	*21	*52	**24
Dog V _{d,ss} , L/Kg	0.6 to 5.0	*1.9	*2.7	**6.0
Dog t _{1/2} , h	1 to 6	*1.2	*0.6	**6.1

Table 51. Profiles of epimers **89** and **90**, and the previous lead **12**. Compounds **89** and **90** exceeded target values for potency and selectivity. Compound **89** had a much lower dog Cl_b than **90**. *3 mg/Kg dosed intravenously.⁷ **1 mg/Kg dosed intravenously.

Dog PK studies confirmed that **89** had much lower clearance than **90**, and had a comparable PK profile to **12**, and was therefore suitable for progression to the dog safety study. The difference in clearance for different stereoisomers such as **89** and **90** is

a well known phenomenon for each of the ADME processes and has been used by pharmaceutical companies to their advantage. For example, the racemate omeprazole, a proton pump inhibitor, was developed by AstraZeneca for the treatment of gastroesophageal reflux and was marketed initially as Losec® and then Prilosec® and became a blockbuster drug (**Figure 54**).⁹⁰

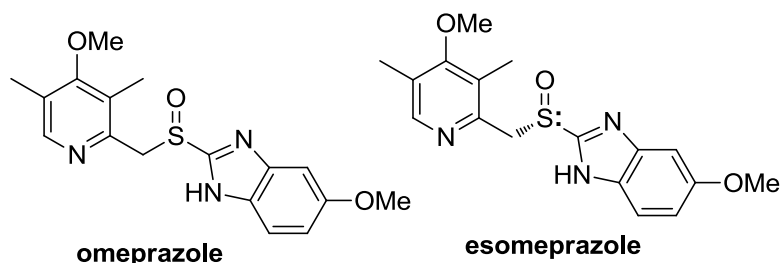


Figure 54. Structures of proton pump inhibitors omeprazole and esomeprazole developed by AstraZeneca for the treatment of gastroesophageal reflux.⁹⁰

Subsequently, AstraZeneca discovered that (*S*)-omeprazole (also known as esomeprazole) was superior to its racemic formulation due to higher bioavailability of (*S*)-omeprazole than the (*R*)-omeprazole in clinical trials. When Prilosec's U.S. patent expired in April 2001, AstraZeneca introduced esomeprazole onto the market as Nexium®.

Compound **12** was less selective than **89** for BET BD1 *versus* BRD9, and both compounds were profiled against 17 additional non-BET family BRDs using the BROMOScan® assay service run by DiscoverRx (**Figure 55** and **Figure 56**).⁹¹

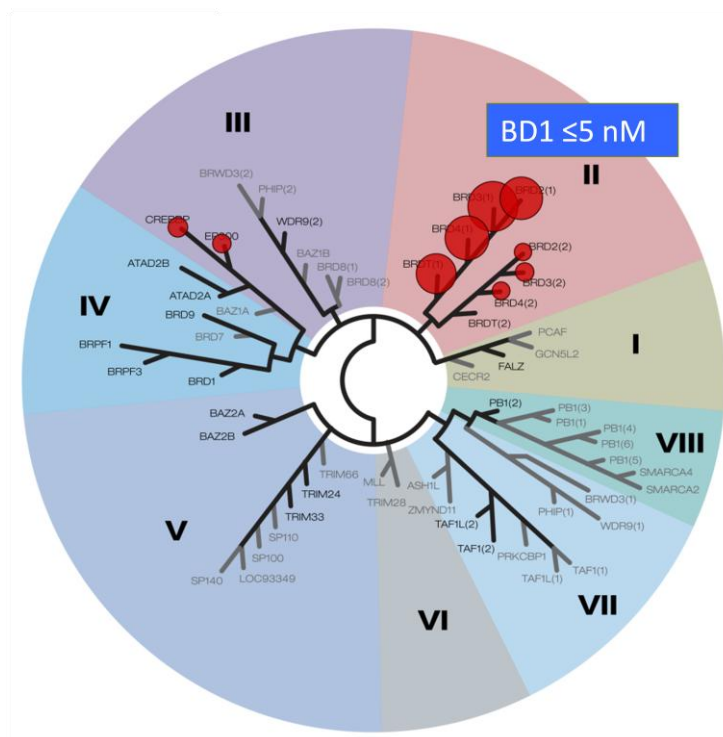
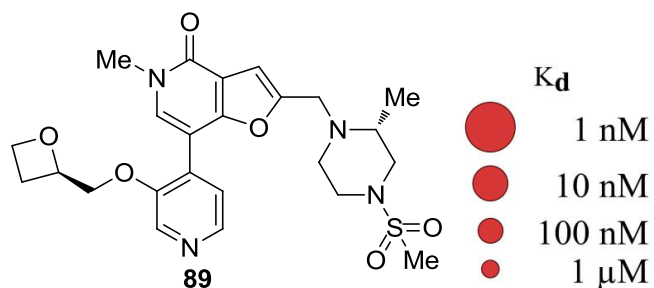


Figure 55. BROMOScan^{®91} selectivity profile of compound **89** which was >100-fold selective for BD1 *versus* BD2 for BRD2, 3, 4 and T, and >140-fold more selective for BD1 *versus* 17 non-BET family BRDs.

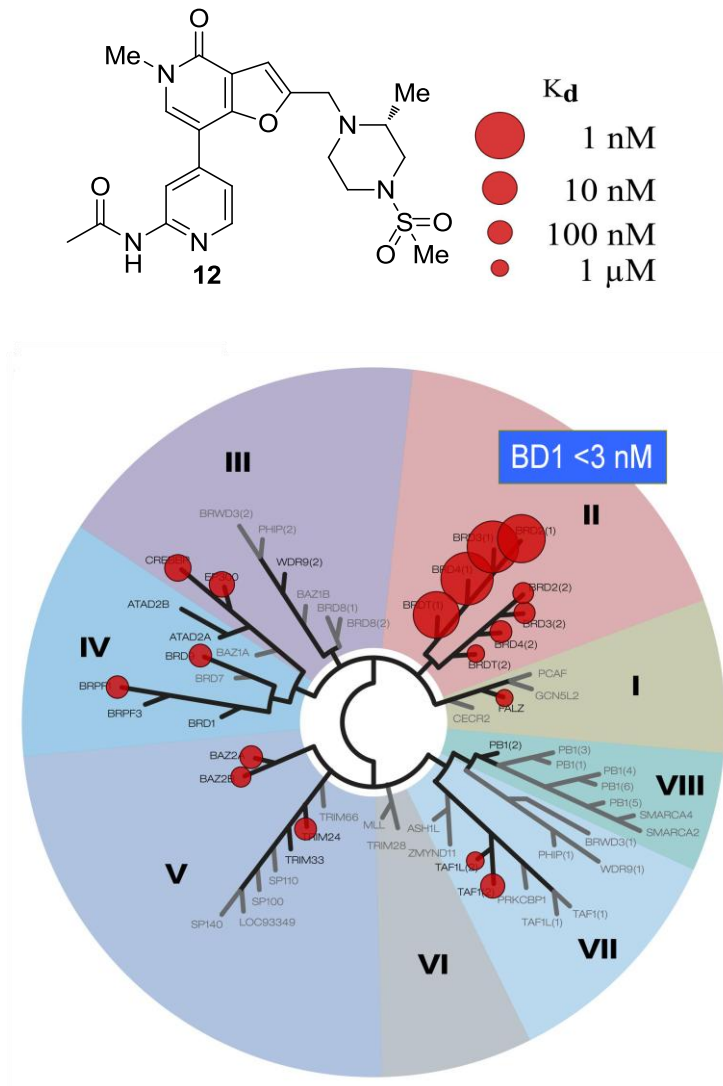


Figure 56. BROMOScan^{®91} selectivity profile of **12** which was >100-fold more selective for BD1 *versus* BD2 for BRD2, 3, 4 and T, and >40-fold more selective for BRD BD1 *versus* 17 non-BET family BRDs.

The BROMOScan^{®91} assays confirmed that compound **89** (**Figure 55**) had comparable potency to **12** (**Figure 56**) for BRD2, 3, 4 and T, and that both compounds were at least 100-fold more selective inhibitors of BD1 *versus* BD2 for BRD2, 3, 4 and T. However, the overall selectivity profile of **89** was superior to that for **12**: **89** was at least 140-fold selective for BD1 *versus* 17 non-BET family BRDs, whereas **12** was at least 40-fold selective. The selectivity of **89** for BD1 *versus* BRD9 was higher than **12**, so **89** had the highest potential to address the hypothesis that BET BRD BD1 inhibition may retain the beneficial anti-proliferative or anti-inflammatory effects of BET BRD inhibition observed using *pan*-BET BRD inhibitors, while also mitigating the toxic effects seen with *pan*-BET inhibitors. Compound **89** was chosen to progress to dog safety studies which required 10 g of material at greater than 95% purity. An 11 g amount of **89** was delivered after method development on a small scale, followed by scale-up synthesis by colleagues, Watson and Mitchell (see section 2.5.13).^{14,16} Results from the dog safety study are discussed in the next section (see section 2.4.8).

2.4.8. Dog Toxicity Study Using the BET BRD BD1 Selective Inhibitor, **89**

A 14 day exploratory toxicity study was undertaken in Marshall Beagle® dogs to evaluate the safety profile of **89**.^{21,22} The dogs were sexually mature, which was important to ensure testicular effects could be investigated, and were housed two dogs to a pens with 450 g food provided, and water provided *ad libitum*. The compound was administered intravenously to maximise systemic exposure because **89** was not orally bioavailable. Doses given were 1, 3 and 12 mg/Kg/day over 1 h, with three dogs in each dosing group. The doses were chosen based on dog PK and dog WB potency from previous *pan*-BET inhibitors, such as **iBET762**, and the First Generation BET BD1 probe **10**, whereby one or more toxicities associated with *pan*-BET inhibition were seen, including testicular lesions, and abnormal electrocardiogram profiles, which are indicative of cardiotoxicity. The Marshall Beagle® was chosen as the species for toxicity studies because there is considerable knowledge of this strain's general pathology and of its response to a wide variety of drugs, and an additional non-rodent species is required for most test guidelines. Dogs have also been found to be more sensitive to the *pan*-BET related testicular changes than other species, such as rat. Only male dogs were included in this study to assess the formation of testicular lesions that had been seen previously with *pan*-BET inhibitors and the First Generation BET BD1 probe **10** and **iBET762**.

A normal electrocardiogram has a P-wave, a QRS complex and a T wave (**Figure 57**).⁹² Each wave represents an electrical activity in a region of the heart.⁹³ The QT interval represents the time interval required for depolarization and repolarization of the ventricles in the heart. The time interval is measured in milliseconds, from the beginning of the Q wave to the end of the T wave, and the QTc interval is QT corrected for heart rate, since QT interval is inversely related to heart rate and different species have different heart rates.⁹⁴

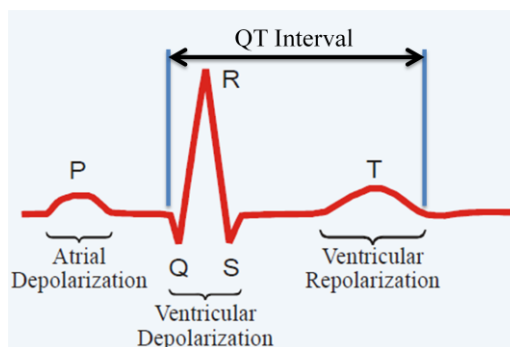


Figure 57. Representation of a normal electrocardiogram, which has a P-wave, QRS complex and T wave. Each wave represents electrical activity in a region of the heart.⁹³

Clinically relevant parameters, such as body weight, food consumption and haematology, were assessed during the study in addition to electrocardiogram monitoring. There were no **89**-related clinical changes observed at any dose, but some variability in the QTc intervals was seen for two dogs, one dog that had been given a 3 mg/Kg/day dose and another that had been given a 12 mg/Kg/day dose. It was inconclusive whether the effect on QTc was treatment-related or due to the low resting heart rate that these dogs had at the start of the study, which was almost half the usual heart rate of Beagle dog of 90 beats per minute.⁹⁵ No effects in QTc were observed, and no changes in other cardiovascular parameters, such as heart rate, was seen in any other animal. Mild to moderate testicular changes were seen in the dogs for which the QTc was prolonged, and also in another dog that had been given the highest 12 mg/Kg/day dose of **89**.

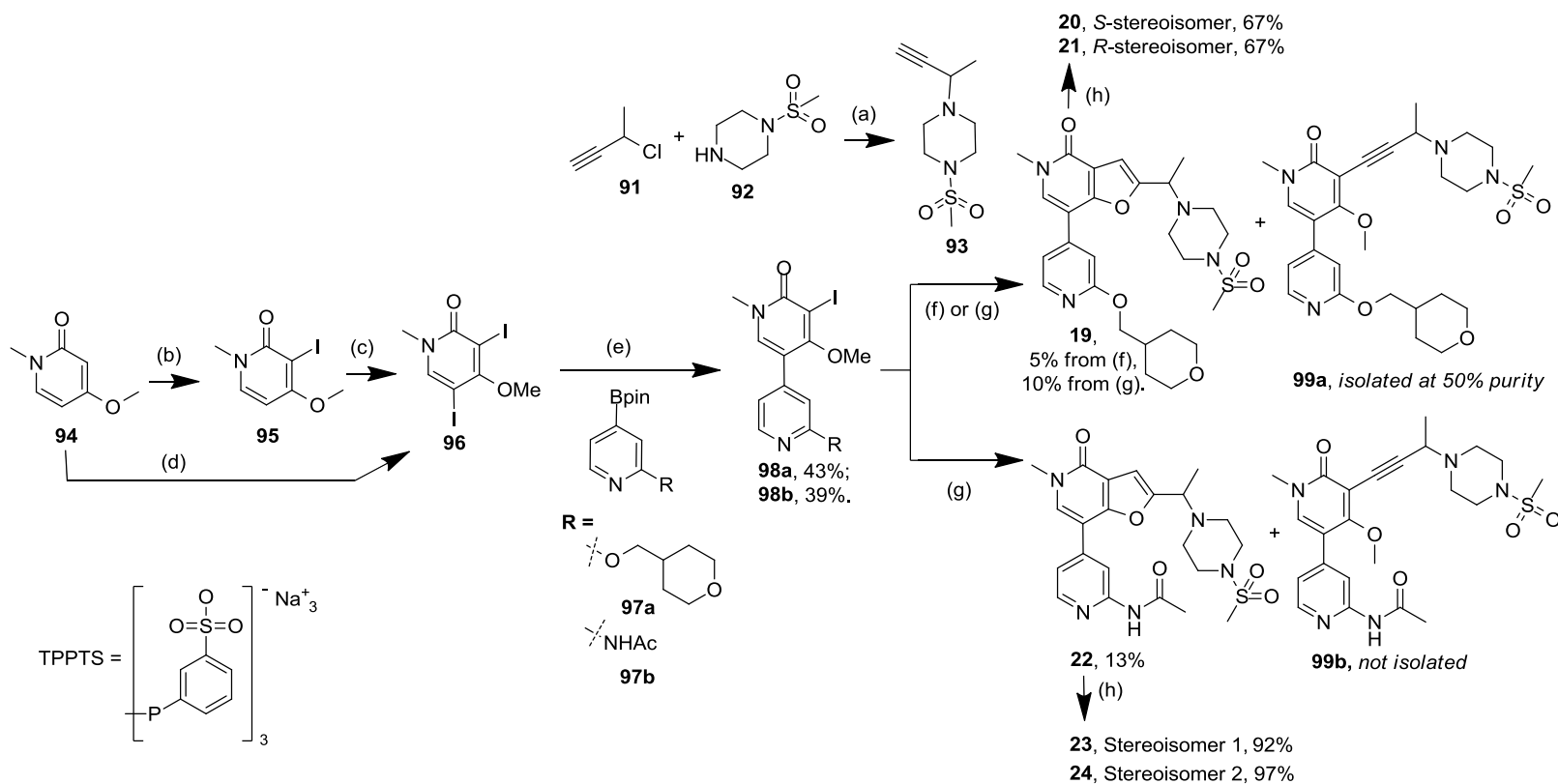
Although none of the dogs on the intermediate dose showed testicular changes, the incidence of testicular changes seems to have been only tentatively dose-related because two of the three dogs on the highest dose showed testicular pathology, as did one of the three dogs on the lowest dose. A possible **89**-related effect therefore could not be excluded. Given **89** was a highly selective BET BRD BD1 inhibitor and sufficient exposure had been achieved, the observed testicular changes could be attributed to BET BRD BD1 inhibition. However, the testicular changes were less severe than those seen with *pan*-BET inhibitors, which suggested a greater benefit to risk ratio could be potentially achieved with a next generation BET BRD BD1 inhibitor with an improved profile, for example, with even higher selectivity for BD1 *versus* BD2. The Epinova

DPU has used learnings from this work to inform the BET inhibitor franchise and has since focussed efforts on the development of highly selective inhibitors of BET BRD BD2, with the aim of identifying treatments for immunoinflammatory diseases.

2.5. Chemistry

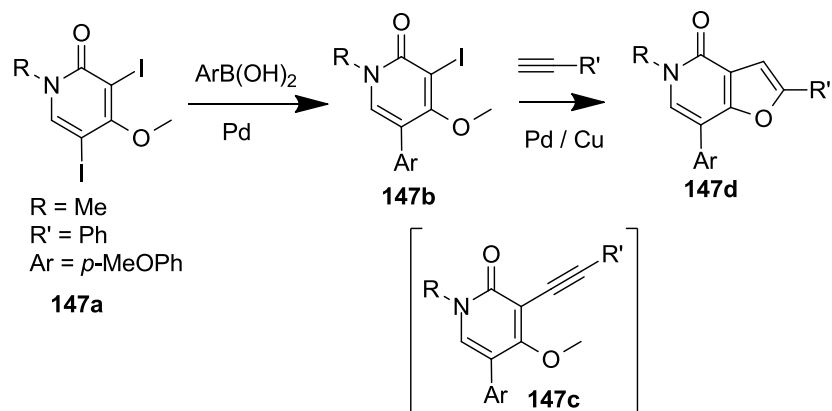
2.5.1. Synthesis of Mono-methyl Substituted Analogues 20, 21, 23 and 24

Compounds **19** and **22** were prepared as racemates using common intermediates **93** and **96**, following a Suzuki coupling between **96** and the appropriate iodo pyridininone **98a** or **98b** and a one-step Sonogashira/cyclisation (**Scheme 27**). Compound **93** was prepared from **91** and **92** in one step, and **96** was prepared from **94** in one to two steps. Chiral HPLC of **19** secured *S*- and *R*-stereoisomers **20** and **21** respectively,¹⁰ and chiral HPLC of **22** secured the two stereoisomers **23** and **24**.¹¹



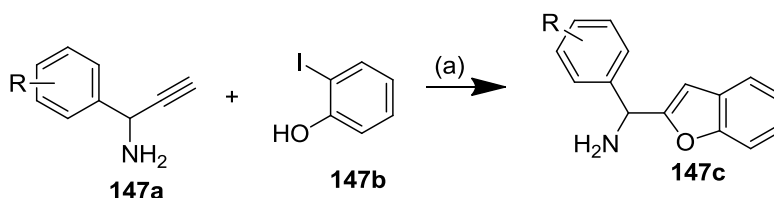
Scheme 27. Preparation of **19-21** and **22-24**. Reagents and conditions: (a) 2 mol% Cu, 2 mol% CuCl, diethylether/H₂O (3:1 v/v mixture), 16 h, 66%; (b) NIS (1 equiv.), MeCN, 16 h, >99%; (c) NIS (1.3 equiv.), TFA, MeCN, 16 h, 86%; (d) NIS (2.5 equiv.), TFA, MeCN, 18 h, >99%; (e) 6 mol% Pd(OAc)₂, 8 mol% TPPTS, DIPEA, MeCN/H₂O (3:1 v/v mixture), 60 °C, 16-20 h; (f) 11 mol% CuI, 5 mol% PdCl₂(PPh₃)₂, NEt₃, MeCN, 80 °C, 96 h; (g) 24% CuI, 4 to 6 mol% PdCl₂(PPh₃)₂, NEt₃, DMF, 120 °C, microwave, 6 h; (h) chiral HPLC;^{10,11} yields assumed **19** and **22** were 1:1 mixtures of enantiomers.

The synthetic strategy used to access **19** and **22** was defined in analogy to that developed by Conreaux *et al.* for the synthesis of 2-substituted furan-fused heterocycles such as **147d** by means of *in situ* sequential Sonogashira-acetylide coupling, dealkylation and regioselective furan annulation reactions (**Scheme 28**).⁹⁶



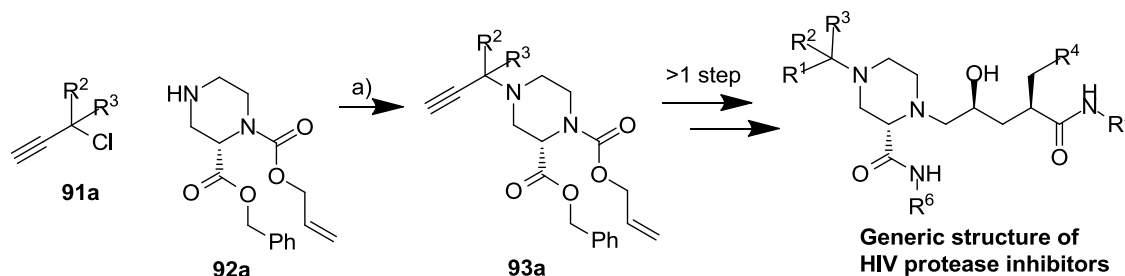
Scheme 28. Access to furo[3,2-*c*]pyridin-4-ones *via* site-selective functionalisation of 3,5-diiodopyridin-2-ones, reported by Conreaux *et al.*⁹⁶

The conditions were originally serendipitously discovered by the authors during attempts to isolate **147c**, but the formation of **147d** as a side-product was observed when the reaction time was prolonged beyond that required for the Sonogashira reaction. The authors propose a mechanism which is discussed later (**Scheme 34**). Numerous analogous transformations of iodophenols into 2-benzofuranmethanamines have been reported; for example, Messina *et al.* reported the synthesis of α -aryl-2-benzofuranmethanamines through palladium-catalyzed heteroannulation of 2-iodophenol with enantiomerically pure or enriched α -arylpropargylamines (**Scheme 29**).⁹⁷



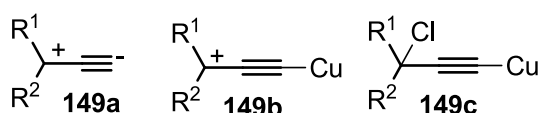
Scheme 29. Transformation of iodophenol into 2-benzofuranmethanamines reported by Messina *et al.*⁹⁷ Reagents and conditions: (a) PdCl₂(PPh₃)₂, tetramethylguanidine, CuI, DMF, 40 °C for 16 to 20 h. Yields ranged from 69% to 82%, depending on R.

Alkyne intermediate **93** was formed *via* a copper-mediated alkylation of **92** with **91** (Scheme 27) in analogy to a method reported by Tata *et al.* used for the preparation of γ -hydroxy-2-fluoroalkylaminocarbonyl-1-piperazinepentanamides as HIV protease inhibitors from chloromethyl alkynes **91a** and piperazines such as **92a** (Scheme 30).⁹⁸



Scheme 30. Method reported by Tata *et al.* for the preparation of γ -hydroxy-2-fluoroalkylaminocarbonyl-1-piperazinepentanamides as HIV protease inhibitors from chloromethyl alkynes **91a** and piperazines such as **92a**.⁹⁸ Reagents and conditions: a) Cu powder, CuCl, NEt₃, 0 °C to room temperature, overnight, yield not given.

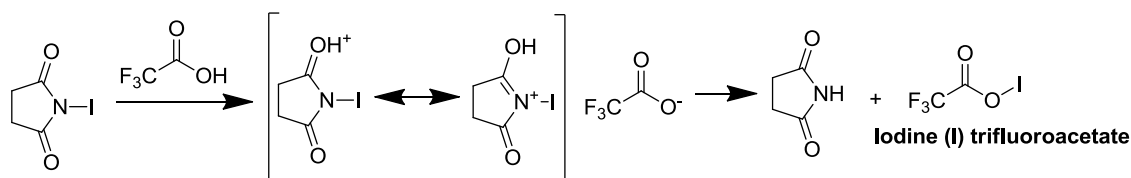
Hennion *et al.* originally reported the mild copper-mediated conditions for the alkylation of weakly basic amines, such as piperazines, with *t*-acetylenic chlorides that are sterically hindered.⁹⁹ The mechanistic role of cuprous salts is not known but Hennion *et al.* proposed the dipolar ion intermediate **149a** is made more reactive in the form of acetylide **149b**; alternatively the *t*-acetylenic chloride might form its acetylide **149c** in the alkaline reaction mixture which could produce reactive species **149a** and/or **149b** (Scheme 31).



Scheme 31. Reactive species proposed by Hennion *et al.* that may be formed from *t*-acetylenic chloride in the presence of Cu and CuCl.⁹⁹

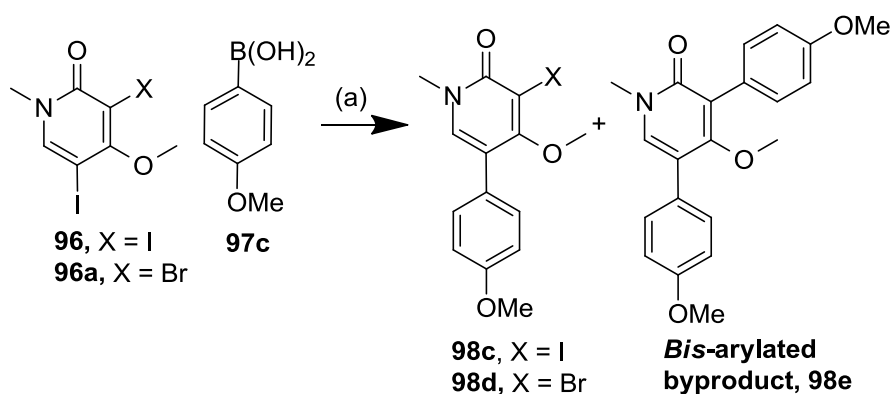
Iodination in the 3-position of **94** using NIS-based conditions reported by Devadas *et al.* gave **95** in >99% yield (Scheme 27).¹⁰⁰ Further iodination in the 5-position to give **96** was achieved in 86% yield using a combination of NIS and TFA which was reported for this substrate by Conreux *et al.*¹⁰¹ The combination of NIS and TFA for iodination of

deactivated aromatics was first reported by Castanet *et al.* who proposed that the active species was iodine(I) trifluoroacetate that is generated *in situ* (**Scheme 32**);¹⁰² however, these types of reagent are not widely reported, so the reactive species capable of bringing about iodination is debatable. Iodination in both the 3- and 5-positions of **94** to give **96** in >99% yield was achieved using the NIS/TFA combination, in accordance with Conreaux *et al.*'s findings.¹⁰¹



Scheme 32. Active species for the 5-position iodination, iodine (I) trifluoroacetate.¹⁰²

A Suzuki coupling between **96** and the relevant aryl boronate ester **97a** and **97b** afforded **98a** and **98b**. Conditions that had been developed by Conreaux *et al.* were used; they reported 3,5-diiodo-4-methoxy-*N*-methylpyridin-2(1*H*)-ones could undergo palladium-catalysed coupling reactions selectively in the 5-position, leaving the C-I bond at the 3-position free for further functionalisation to access differentially 3,5-disubstituted 2-pyridones. The approach was used previously by Conreaux *et al.* to synthesise differentially substituted 3,5-disubstituted 4-oxypyridin-2(1*H*)-ones (**Scheme 33**).¹⁰¹



Scheme 33. Synthesis of differentially substituted 3,5-disubstituted 4-oxypyridin-2(1*H*)-ones which started with site-selective Suzuki coupling of **96** and **96a**.¹⁰¹ Reagents and conditions: 1.4 equivs boronic acid, 5 mol% Pd(OAc)₂, 15 mol% TPPTS, *i*Pr₂NH, MeCN/water, 60 °C, 36 h.

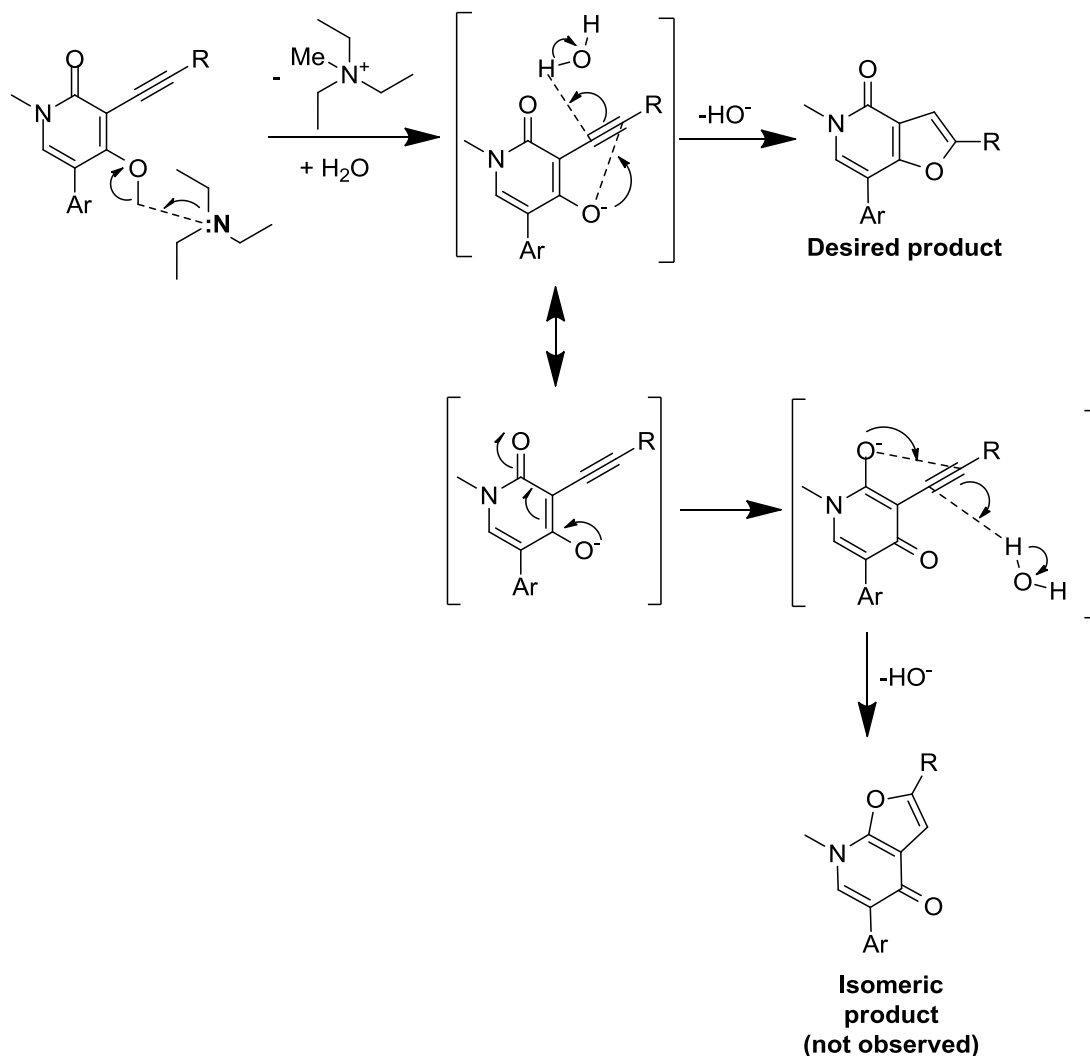
The authors reported the formation of the mono-5-arylated product **98c** in 72% yield from diiodide **96** and boronic acid **97c**, with only 15% of the *bis*-arylated product **98e** being formed (**Scheme 33**). Selectivity for Pd-catalysed cross-coupling in the 5-position in preference to the 3-position was attributed to steric factors, with a higher relative rate of cross-coupling occurring at the less-hindered 5-position. A slight improvement in isolated yield to 88% was reported using the iodo/bromo starting material **96a**, but it was not reported how much of the *bis*-arylated product had been formed.

However, such selectivity was not achieved for the Suzuki coupling, step (e) (**Scheme 27**), towards **98a** and **98b**. LCMS analysis of the reaction mixtures of step (e), towards **98a** and **98b** at 16 h indicated approximate ratios of mono-arylated product to *bis*-arylated material of 3:2; starting material had been consumed fully and the isolated yields of **98a** and **98b** were 43% and 39% respectively.

Conreux *et al.*'s conditions were used to introduce **93** into **98a** via a Sonogashira reaction to give **99a**, which could then undergo a 5-*endo-dig* reaction *in situ* to form the FP core ring system **19** (**Scheme 27**).⁹⁶ The reaction was monitored by LCMS and was found to proceed very slowly, with very gradual consumption of starting materials leading to the formation of the Sonogashira intermediate **99a** and desired product **19**; a number of byproducts were also evident but were not isolated or characterised. After 96 h at 80 °C, the reaction was halted and **19** was isolated from the reaction mixture in poor yield (5%). Modified Sonogashira conditions, which were used to introduce **93** into **98b** employed microwave heating at 120 °C for 6 h to secure **22** in poor yield (13%) due to the formation of a number of byproducts and the lack of ring closure from Sonogashira intermediate **99b**. In this case, MeCN solvent was replaced with DMF to ensure better solvation of reagents and to allow a high temperature to be achieved. Yields were comparable for both the thermal heating and microwave heating protocols, assessed from the similar reaction profiles (by LCMS analysis), but microwave heating allowed material to be secured in a much faster time. Step (g) (**Scheme 27**), was therefore repeated using **98a** and **93** to secure more **19** for chiral separation, and a slightly improved yield of 10% was achieved. The increased yield of **19** using microwave irradiation compared with heating could be a result of using an increased amount of CuI in the microwave reaction (24 mol% *versus* 11 mol%) which occurred due to a

miscalculation. A direct comparison of yields between microwave irradiation and heating cannot be made in the synthesis of **20**.

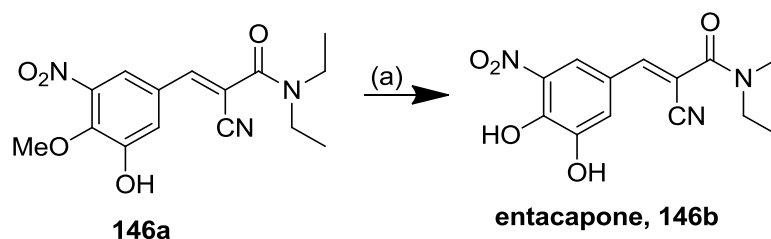
The mechanism of ring closure is likely to be similar to the mechanism suggested by Conreux *et al.* (Scheme 34).⁹⁶



Scheme 34. Proposed mechanism for the Et_3N -induced dealkylation-cyclisation of 3-alkynyl-4-alkoxypyridin-2-ones.⁹⁶

Triethylamine was proposed by the authors to attack the methyl group of the Sonogashira product *via* $\text{S}_{\text{N}}2$ displacement.⁹⁶ The reaction has been reported by a small number of other groups, such as Harisha *et al.*, who reported triethylamine-mediated demethylation of a range of anisoles such as **146a**, which was transformed into entacapone **146b**, a catechol-*O*-methyl transferase (COMT) inhibitor used in the

treatment of Parkinson's disease (**Scheme 35**).¹⁰³ The phenolate of **146a** is stabilised by the adjacent nitro group.



Scheme 35. Triethylamine-mediated dealkylation used by Harisha *et al.* for the synthesis of entacapone **146b**.¹⁰³ Reagents and conditions: (a) NEt₃, EtOH, 70-75 °C, 12 h, 45%.

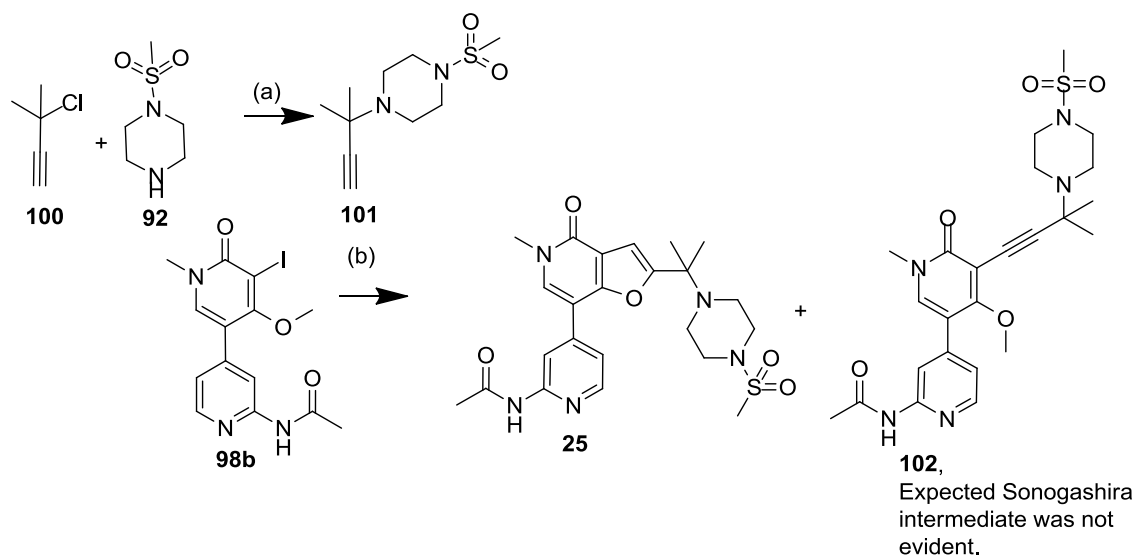
The delocalised enolate undergoes a regioselective anionic *5-endo-dig* cyclisation then proton capture from water to deliver the desired furo[3,2-*c*]pyridin-4-one. The isomeric furo[3,2-*c*]pyridin-2-one was not observed.

Chiral HPLC separation of the racemate **19** secured the *S*-enantiomer **20** in 67% yield, and the *R*-enantiomer **21**, also in 67% yield, assuming **19** was a 1:1 mixture of enantiomers.¹⁰ Too little of each compound was isolated to perform complete characterisation because of the poor overall yields, but enough **21** was secured to obtain a BRD4 BD1 X-ray crystal structure which showed the compound to be the *R*-enantiomer (**Figure 45**).⁴⁴ By inference **20** was likely to be the *S*-enantiomer.

Similarly chiral HPLC separation of the racemate **22** gave the enantiomer 1 **23** in 92% yield, and enantiomer 2 **24** in 97% yield, assuming **19** was a 1:1 mixture of enantiomers.¹¹ Too little of each compound was isolated to perform complete characterisation or to obtain an X-ray crystal structure because of the poor overall yields, so the chirality of each compound remains unknown.

2.5.2. Synthesis of Dimethyl Analogue, **25**

Compound **25**, was synthesised in an analogous fashion to compounds **19** and **22** from **98b** and **101** (**Scheme 36**).

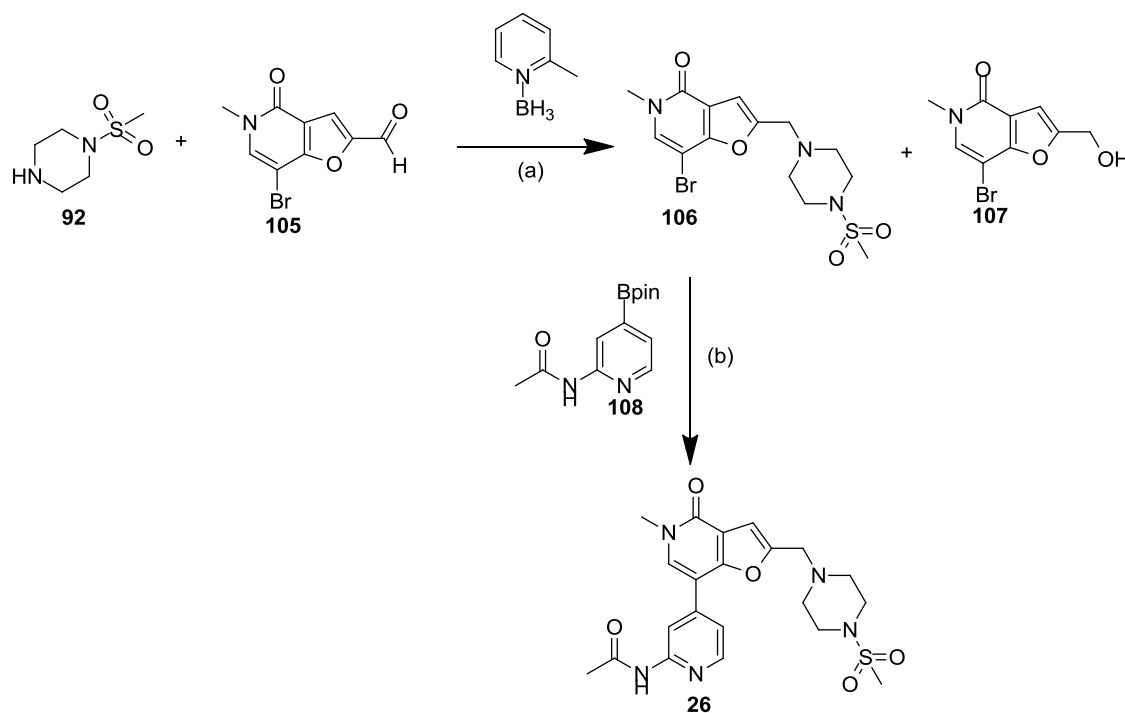


Scheme 36. Synthetic route used to access dimethyl substituted analogue of **12**, compound **25**. Reagents and conditions: (a) 2 mol% Cu, 2 mol% CuCl, ether/H₂O (3:1 v/v mixture), 16 h, 78%; (b) **101**, 24 mol% CuI, 6 mol% PdCl₂(PPh₃)₂, NEt₃, 120 °C, DMF, microwave, 6 h, 8%.

Alkyne intermediate **101** was formed *via* a copper-mediated alkylation of **92** with **100** using conditions previously reported by Tata *et al.* for the preparation of γ -hydroxy-2-fluoroalkylaminocarbonyl-1-piperazinepentanamides as HIV protease inhibitors (**Scheme 30**).⁹⁸ Microwave-mediated Sonogashira conditions were used to couple **101** and **98b**, then a 5-*endo-dig*¹⁰⁴ ring closing reaction afforded the FP **25** in 8% yield. Low yields were due to the formation of a large number of byproducts which was evident by LCMS. However, the expected Sonogashira intermediate **102** was not detected, so the low yield was unlikely to be caused by incomplete ring closure.

2.5.3. Synthesis of Des-methyl Headgroup Analogue 26

Compound **26** was prepared from intermediates **92** and **105** in two steps (**Scheme 37**).



Scheme 37. Reagents and conditions: (a) 2-picoline borane, AcOH, MeOH, 1.5 h, 78%; (b) 5 mol% Pd(PPh₃)₄, K₂CO₃, DME, 120 °C, microwave, 2 h, 40%.

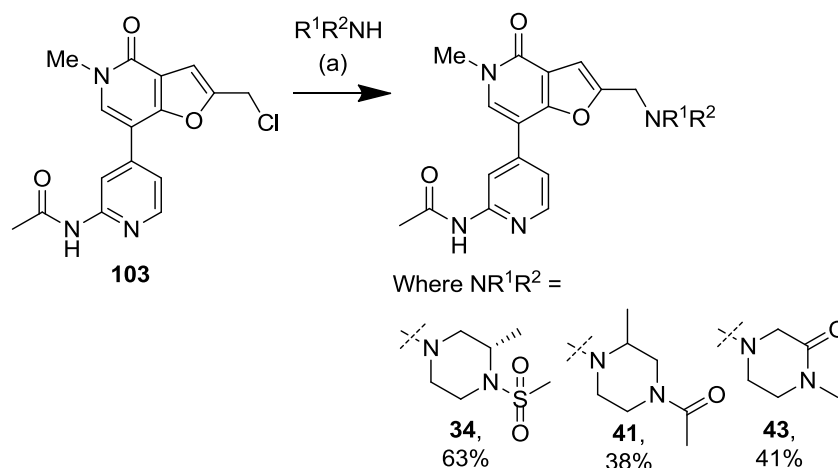
Intermediate **106** was prepared from **92** and **105** by reductive amination using 2-picoline borane. 2-Picoline borane was chosen because it is a mild reducing agent and was reported to be effective “one-pot” reductive aminations because it selectively reduces the iminium intermediate before the aldehyde or ketone starting materials.¹⁰⁵ The formation of the alcohol byproduct **107** was therefore expected to be limited, which was indeed observed, as indicated by the high yield of **106** (78%).

Generic Suzuki coupling conditions originally reported by Miyaura *et al.* were then used to couple boronate ester **108** with the aryl bromide **106** to afford **26** in low yield.¹⁰⁶ LCMS analysis of the crude reaction mixture indicated that approximately 75% of the mixture was desired product, and that all starting material had been consumed. After workup, product was also present in the aqueous layer; this was not isolated, which may explain the recovery of material, which was lower than expected.

2.5.4. Synthesis of Array of Headgroup Analogues 27-55

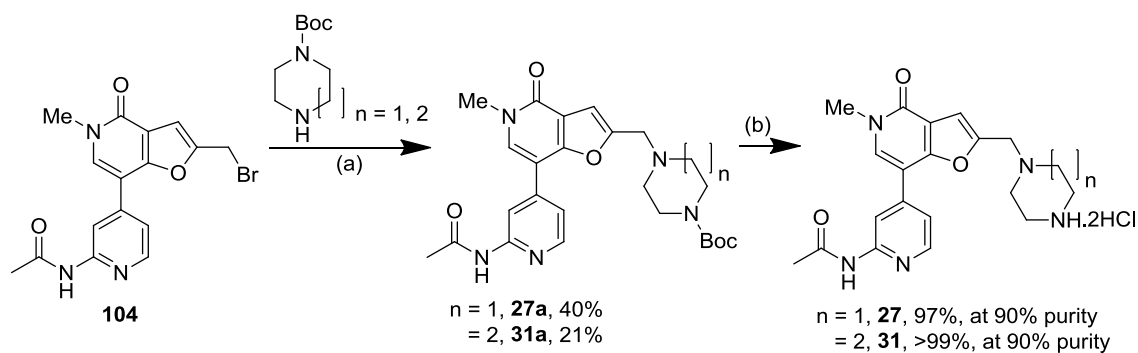
Compounds **34**, **41**, and **43** were made from chloride **103** that had been previously prepared by a colleague supporting the program chemistry, Watson,¹⁹ and the

appropriate amines, R^1R^2NH , using K_2CO_3 to sequester the HCl byproduct, in **38** to 63% yield (**Scheme 38**). Compounds were synthesised by Barnett, a colleague in the Chemical Arrays Team,¹⁶ and Watson.¹⁹



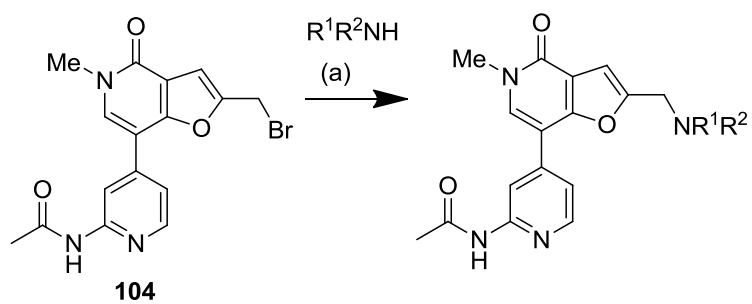
Scheme 38. Synthetic route used to access **34**, **41** and **43**. Reagents and conditions: (a) K_2CO_3 , DMF, 3 h, room temperature.

Compounds **27** and **31** were made from the bromide **104** that had been previously prepared by Watson,¹⁹ and Boc-protected amine which gave **27a** and **31a**, and then acid-mediated deprotection (**Scheme 39**).



Scheme 39. Synthetic route used to access compounds **27** and **31**. Reagents and conditions: (a) DIPEA, DMF, 110 °C, microwave, 30 min; (b) DCM, 4 M HCl in dioxane, 2 h to 18 h.

Compounds **28-30**, **32**, **33**, **35-40**, **42** and **44-55** were made by Barnett using an array approach from bromide **104** and the appropriate amines, R^1R^2NH (**Scheme 40**).¹⁹ Yields of between 9% and 46% were achieved, and are shown in **Table 52**.



Scheme 40. Synthetic route used to access compounds **28-30, 32, 33, 35-40, 42** and **44-55**. Reagents and conditions: (a) DIPEA, DMF, 110 °C, microwave, 30 min. Yields are shown in **Table 52**; all compounds were 90% purity by LCMS and ¹H NMR.

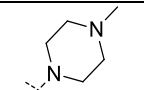
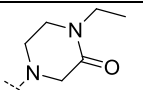
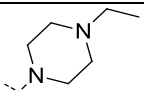
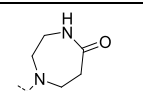
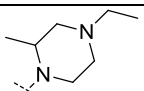
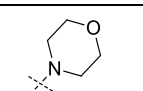
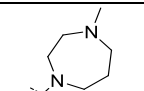
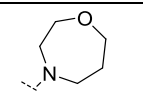
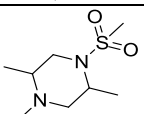
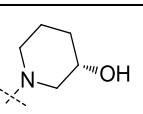
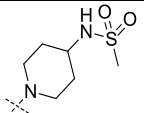
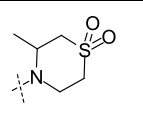
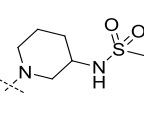
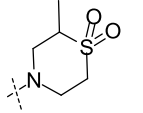
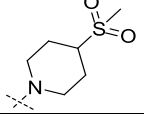
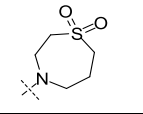
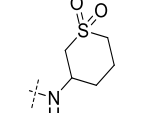
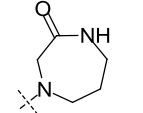
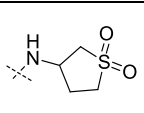
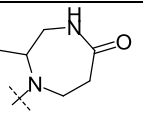
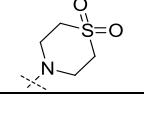
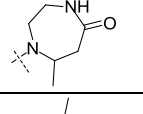
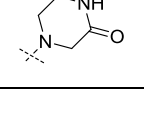
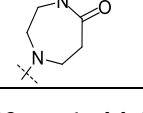
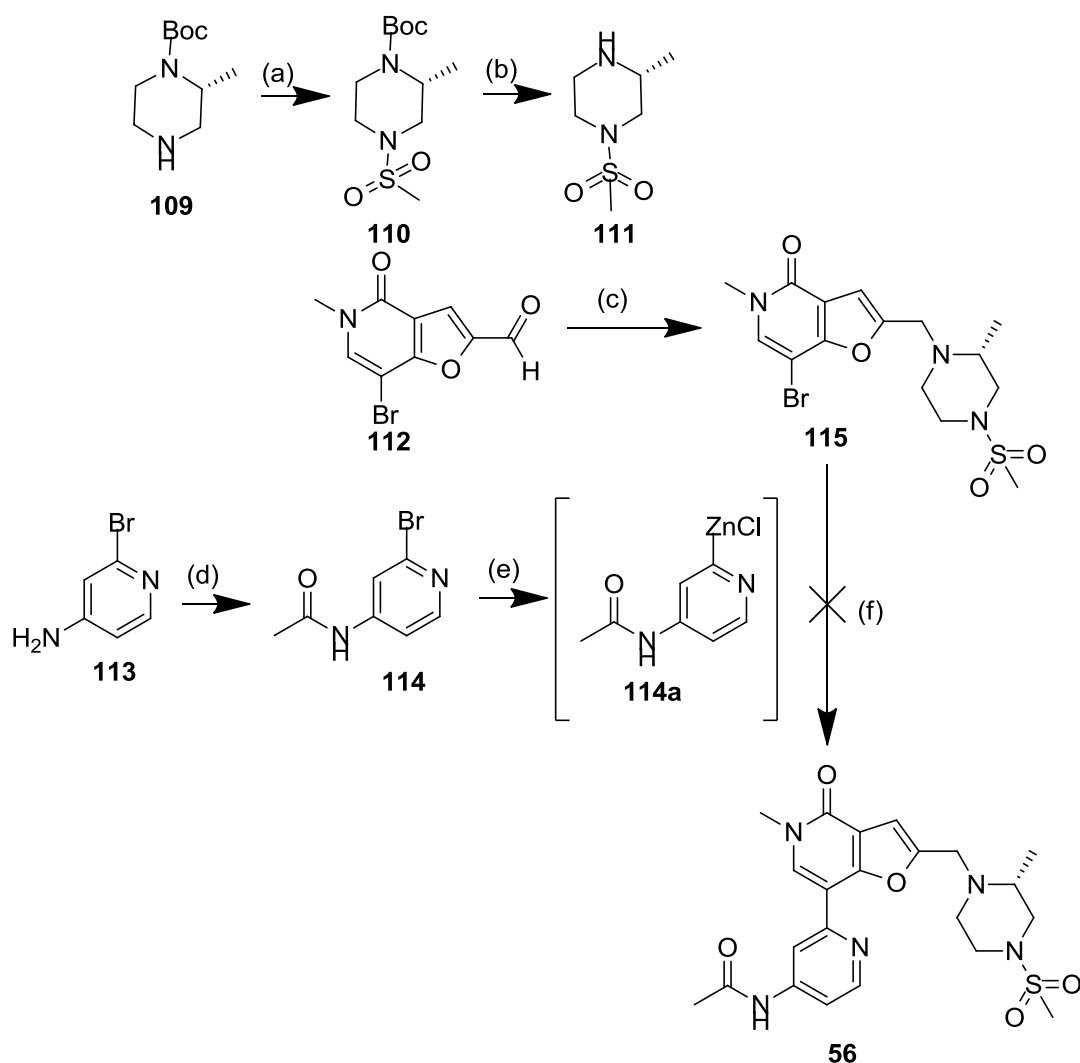
Compound Number	NR ¹ R ²	*% Yield	Compound Number	NR ¹ R ²	*% Yield
28		30	44		35
29		40	45		23
30		27	46		46
32		14	47		39
33		42	48		39
35		31	49		28
36		37	50		35
37		32	51		29
38		23	52		18
39		26	53		25
40		30	54		14
42		9	55		25

Table 52. Yields for compounds **28-30, 32, 33, 35-40, 42** and **44-55**, which were synthesised according to **Scheme 40**. *Compounds were isolated at 90% purity and were prepared by Barnett.¹⁶

2.5.5. Synthesis of Pyridine Regioisomers 56 to 58

2.5.5.1. 2-position Isomer, Compound 56

Compound **56** (**Scheme 41**) contained a 2-pyridyl moiety which is typically a challenging structural motif to introduce into functionalised organic molecules.¹⁰⁷ Intermediate **111** was synthesised in two steps from commercially available **109**, and was used to make bromopyridinone intermediate **115** in one step from **112**, which had been synthesised using a contract research organisation. An attempt to generate the organozinc intermediate **114a** from **113**, and couple with **115** using Negishi-coupling conditions failed to give **56**.



Scheme 41. Reagents and conditions: (a) MsCl, 2 M NaOH_(aq), THF, 0 °C to room temperature, 2 h, 79%; (b) 4 M HCl in dioxane, dioxane, 16 h, aminopropyl SPE, 98%; (c) 2-picoline borane, AcOH, MeOH, 40 °C, 16 h, 58%; (d) acetyl chloride, pyridine, DCM, 3 h, 93%; (e) 2M *i*PrMgCl in THF, 3 h, then 1M ZnCl₂ in ether, THF, 0 °C (material was taken forward without isolation, so no yield is given); (f) 17 mol% Pd(PPh₃)₄, THF/ether, reflux, 16 h, 0%.

The scope for cross-coupling involving 2-pyridyl nucleophiles is limited because 2-pyridyl nucleophiles are often of low stability, or need to be generated at low temperatures, or need to be synthesised according to technically demanding reaction protocols. A Suzuki-Miyaura coupling between the aryl bromide 115 and a 2-pyridyl boronate was likely to be difficult because 2-pyridyl boronates are not usually very stable. The employment of 2-pyridyl MIDA and a pinacol boronate was one option to

circumvent the stability problem,¹⁰⁸ but was likely to require bespoke synthesis of the 2-pyridyl MIDA boronate which can require significant method development and time investment.¹⁰⁷ Trifluoroborate salts, such as pyridine-2- trifluoroborate salts, have been reported to possess outstanding air-stability, but would also have required bespoke synthesis.^{109,110} An alternative option was the use of 2-pyridyl zinc reagents which are reported to be excellent nucleophiles in cross-coupling reactions that often proceed at room temperature.¹⁰⁸ The synthetic strategy to access **56** relied on the generation of the organozinc reagent **114a** and a Negishi coupling between **114a** and the aryl bromide **115** (Scheme 41).

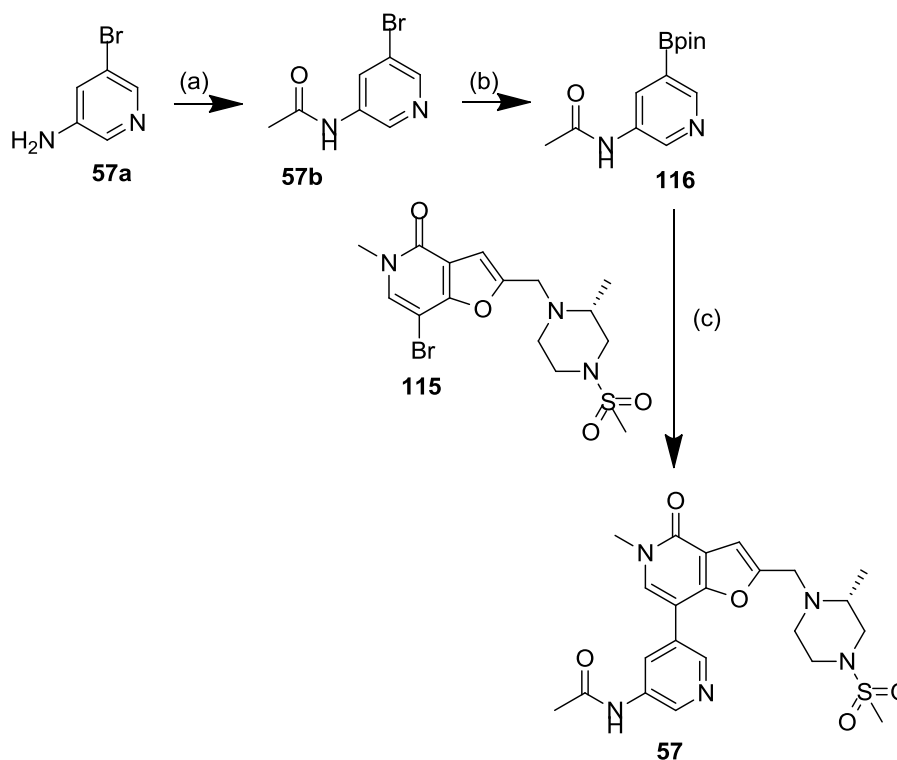
The piperidine **111** was prepared from **109** by mesylation to form **110**, followed by HCl-mediated Boc-deprotection, and free-based using aminopropyl SPE. A reductive amination reaction between aldehyde **112** and **111** afforded **115**. Meanwhile, acetamide **114** was prepared from **113** using acetyl chloride, and then used to make the organozinc reagent **114a** using Jensen *et al.*'s¹¹¹ method that had been modified by Luzung *et al.* to tolerate ambient temperatures.¹¹² The pK_a of *i*PrMgCl is approximately 31 in THF,¹¹³ while the pK_a of secondary amide of **114a** is calculated to be much lower at approximately 13, according to the Chemaxon pK_a prediction tool which uses partial charge, polarisability, structure-specific, and ionisation elements to predict pK_a.¹¹⁴ The amide was likely to be deprotonated by the Grignard reagent, so an excess of *i*PrMgCl (four equivalents) was used to form the organozinc in step (e), Scheme 41. The organozinc reagent was used directly in the Negishi coupling step between **114a** and **115** using established conditions; however, no trace of desired product **56** was obtained.^{107,115}

In retrospect it was unknown whether the organozinc intermediate **114a** had formed. This could have been confirmed with a simple test Negishi coupling reaction, for example, by adding a sample of **114a** to a simple surrogate for **115**, such as bromobenzene, or by deuteration. Alternative strategies to access **56**, such as the employment of 2-pyridyl MIDA and a pinacol boronate, were not undertaken because the target was unlikely to solve the high IVC of **12**.

The same Negishi protocol was however successful in preparing **71** which also contained a 2-pyridyl moiety, but not the amide functional group (**Scheme 53**, section 2.5.9.2).

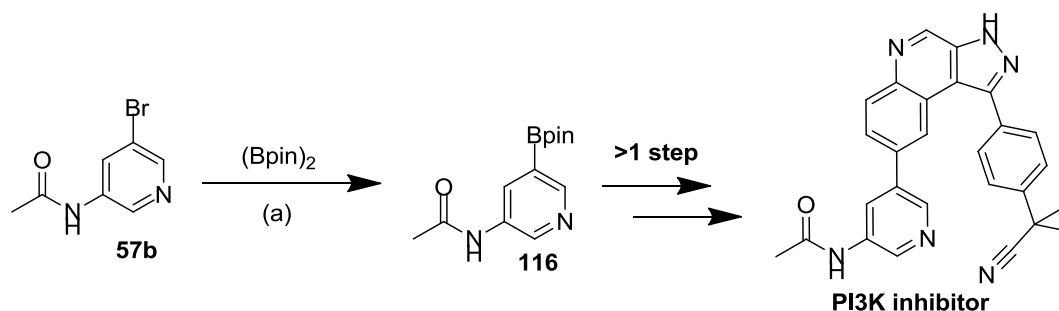
2.5.5.2. 3-position Isomer, Compound **57**

A two-step synthesis from **57a** afforded **116**, which was coupled with **115** to deliver **57** (**Scheme 42**).



Scheme 42. Reagents and conditions: (a) acetyl chloride, DCM, 3 h, 91%; (b) $(\text{Bpin})_2$, 10 mol% $\text{Pd}(\text{dppf})\text{Cl}_2$, KOAc , dioxane, 100 °C, 1 h, microwave (material was taken forward without purification, so no yield is given); (c) 5 mol% $\text{Pd}(\text{PPh}_3)_4$, K_2CO_3 , DME, 120 °C, microwave, 2 h, 5% over two steps (step (b) and step (c), assuming **115** was the limiting reagent).

The pyridyl boronate ester **116** was prepared from **57a** via acetylation then boronylation using pinacol borane. The borylation conditions that were used were developed by Ishiyama *et al.*;¹¹⁷ they were employed by Qian *et al.* to prepare **116** and subsequently phosphatidylinositol 3 kinase (PI3K) inhibitors for therapeutic applications (**Scheme 43**).¹¹⁶



Scheme 43. Miyaura borylation conditions employed by Quian *et al.* to prepare **116** as an intermediate for the preparation of PI3K inhibitors such as that shown. Reagents and conditions: (a) (Bpin)₂, 5 mol% Pd(dppf)Cl₂, KOAc, dioxane, 85 °C, 8 h.

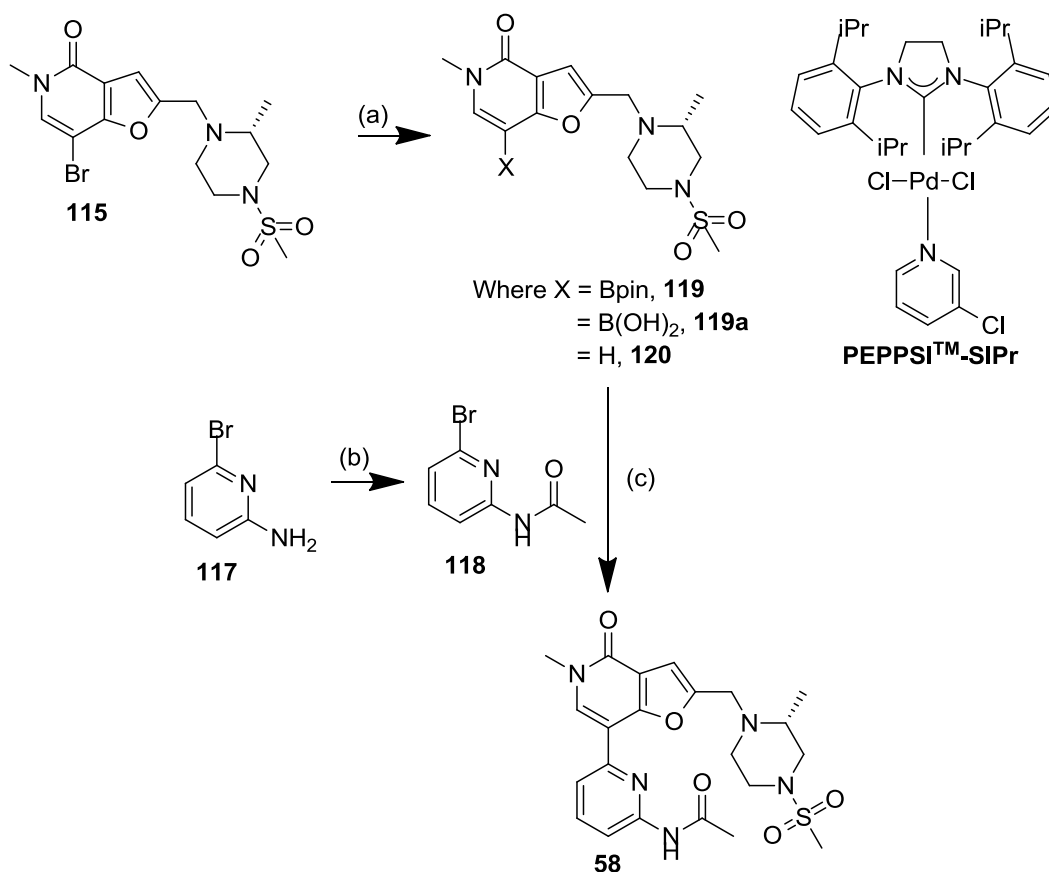
The mass ion of the boronate ester **116** could not be identified by LCMS, but ¹H NMR of the crude material indicated the presence of of desired material, as well as a number of pinacol-related impurities that were difficult to identify.

Compound **116** proved difficult to purify due to poor separation by TLC, and purification by reverse phase methods failed, so crude material was taken forward to the Suzuki coupling step, and the 5% yield quoted for **57** assumed excess **116** was present in the crude mixture. A low yield was obtained for this step, presumably because the boronate ester was low in purity.

Poor chromatography was found to be a major issue for purifying pyridyl boronate esters, so crude material was generally taken forward for Suzuki coupling.

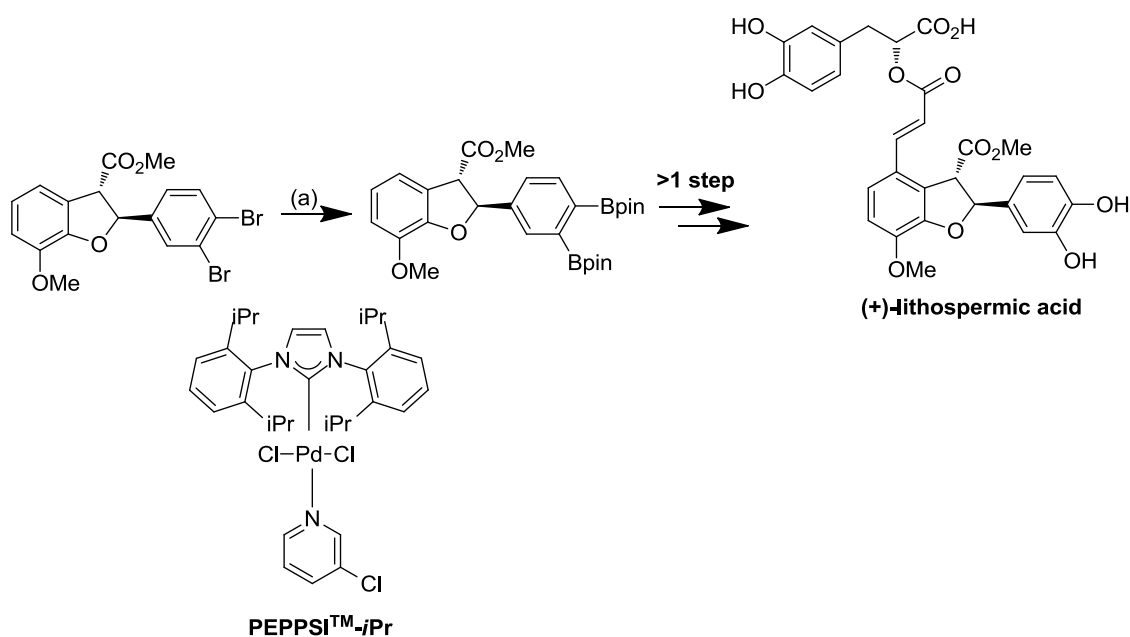
2.5.5.3. 6-position Isomer, **58**

Compound **58** was prepared from **118** and **119** / **119a** using a three step synthesis (**Scheme 44**).



Scheme 44. Reagents and conditions: (a) HBpin, NEt₃, 10 mol% PEPPSI™-SiPr^(R), dioxane, 100 °C, 3 h; material was taken forward without purification, so no yield is given; (b) acetyl chloride, pyridine, DCM, 3 h, 96%; (c) 5 mol% Pd(PPh₃)₄, 2 M Na₂CO_{3(aq)}, DME, 120 °C, microwave, 30 min, 23%, *over two steps* (step (a) and step (c)).

A mixture of the boronate ester **119**, boronic acid **119a** and proto-deborylated product **120** was synthesised from aryl bromide **115** using the Miyaura borylation conditions similar to those that Ghosh *et al.* developed as part of the synthesis of (+)-lithospermic acid (**Scheme 45**).¹¹⁸ Ghosh *et al.* reported that the PEPPSI™-iPr^(R) precatalyst enabled the *bis*-Bpin intermediate to be secured in 57% yield where previous catalyst systems had proven ineffective and therefore demonstrated the effectiveness of this precatalyst in borylation reactions.



Scheme 45. Miyaura borylation conditions that Ghosh *et al.* developed for the synthesis of (+)-lithospermic acid.¹¹⁸ Reagents and conditions: (a) 10 mol% PEPPSI™-iPr^(R), HBpin, Et₃N, 110 °C, 12 h, 57%.

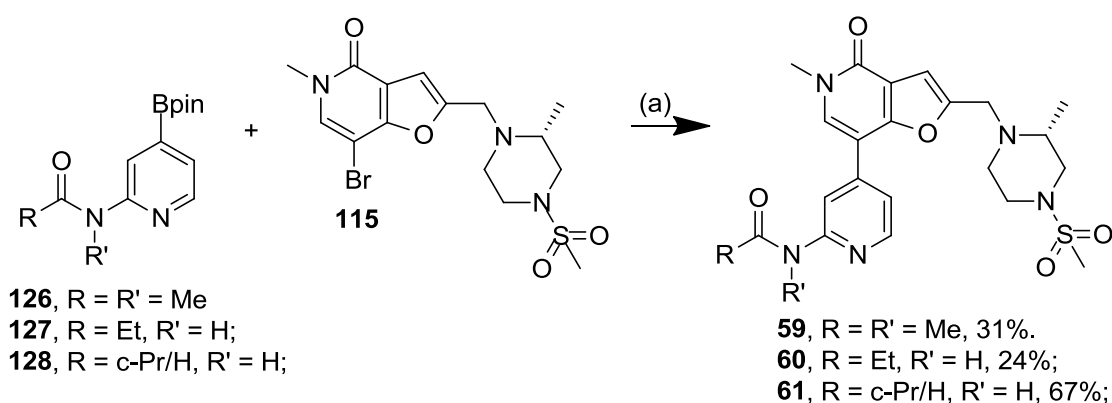
PEPPSI™-iPr^(R) and PEPPSI™-SiPr^(R) belong to a family of *N*-heterocyclic carbenes (NHCs) that has found widespread use as precatalysts for a range of transformations, including Negishi couplings,¹¹⁹ Suzuki couplings,¹²⁰ Buchwald-Hartwig aminations¹²¹ and Kumada-Tamao-Corriu¹²² reactions. The strong σ -electron-donating ability of NHCs is reported to enable oxidative addition in challenging substrates, while steric bulk assists fast reductive elimination.¹²⁰ The active species of NHC-based precatalysts are robust because Pd-NHC bonds are strong, even at low ligand/Pd ratios and high temperatures. PEPPSI™ is an acronym for pyridine-enhanced precatalyst preparation, stabilization and initiation, while *iPr* describes the *diisopropylphenylimidazolium* portion of the molecule; a set of closely related alternative precatalysts exists, including PEPPSI™-SiPr^(R) which is the saturated version of PEPPSI™-iPr^(R).

The PEPPSI™-SiPr^(R) precatalyst was chosen for borylation of **115** instead of PEPPSI™-iPr^(R) because PEPPSI™-SiPr^(R) has been reported to be instrumental in promoting some reactions at lower temperatures than PEPPSI™-iPr^(R).^{122,123} LCMS analysis of the borylation step (step (a), **Scheme 44**), indicated an approximate total of 69% of borylated products **119** (12% by peak area) and **119a** (57% by peak area) were

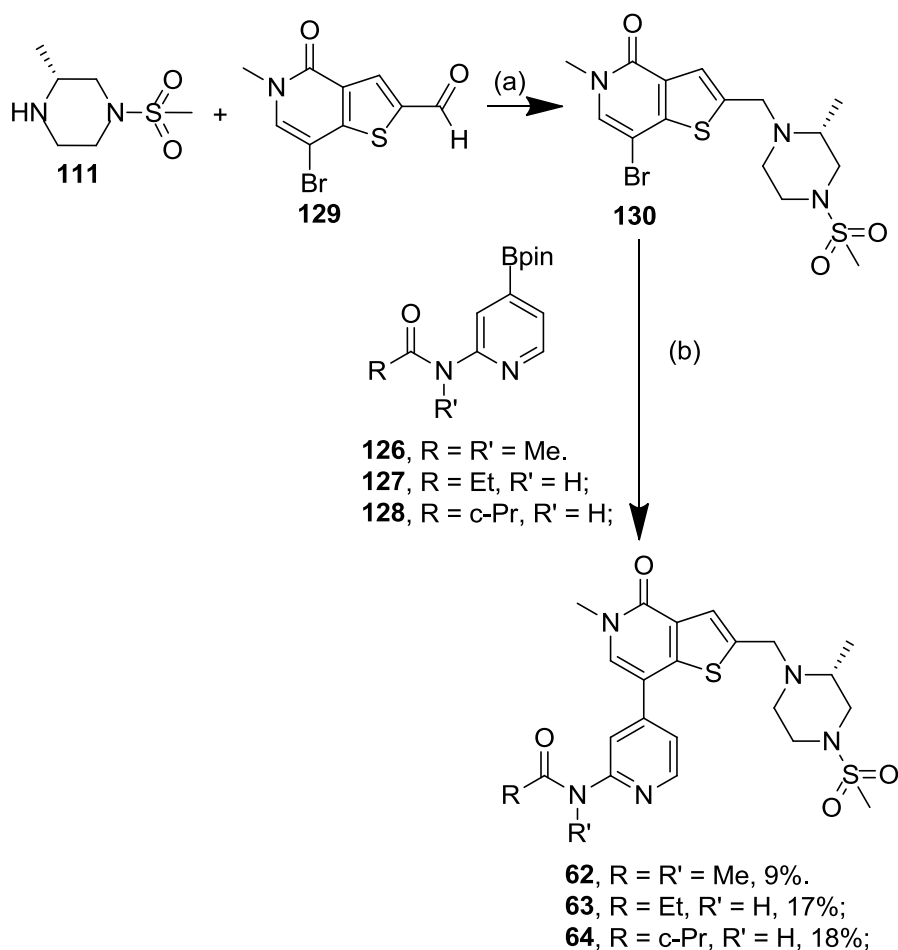
present which were capable of undergoing Suzuki coupling in step (c), with approximately 27% (by peak area) of the proto-deborylated byproduct **120**. It was assumed the boronate ester **119** could undergo hydrolysis to the boronic acid **119a** under LCMS conditions, but this was not confirmed by NMR. Purification of the boronic acid/boronate ester mixture of **119** and **119a** proved difficult due to poor separation by TLC, and reverse phase methods failed. The crude mixture of **119**, **119a** and **120** was therefore taken forward to the Suzuki coupling step with acetamide **118** using Pd(PPh₃)₄-based Suzuki cross-coupling conditions.¹⁰⁶ A low yield of 23% was achieved for **58** probably because the boronic acid/boronate ester coupling partner was low in purity. The yield is quoted over two steps, step (a) and step (c).

2.5.6. Synthesis of Pyridyl Amide Analogues 59-64

Compounds **59** to **64** were synthesised using Suzuki coupling conditions from the pyridyl boronate ester **126-128**, and either the FP intermediate **115** (Scheme 46), or the TP intermediate **130** (Scheme 47). Pyridyl boronate esters **126-128** were made in two to three steps from common intermediate **121** (Scheme 48). The TP intermediate **130** was made from amine **111** and aldehyde **129** *via* a reductive amination reaction using 2-picoline borane. A much lower yield of the TP intermediate **130** was achieved than the analogous reaction using the FP intermediate **112** (step (c), Scheme 41), because the TP intermediate **129** was not as soluble as **112**, at least visually.¹⁰⁵

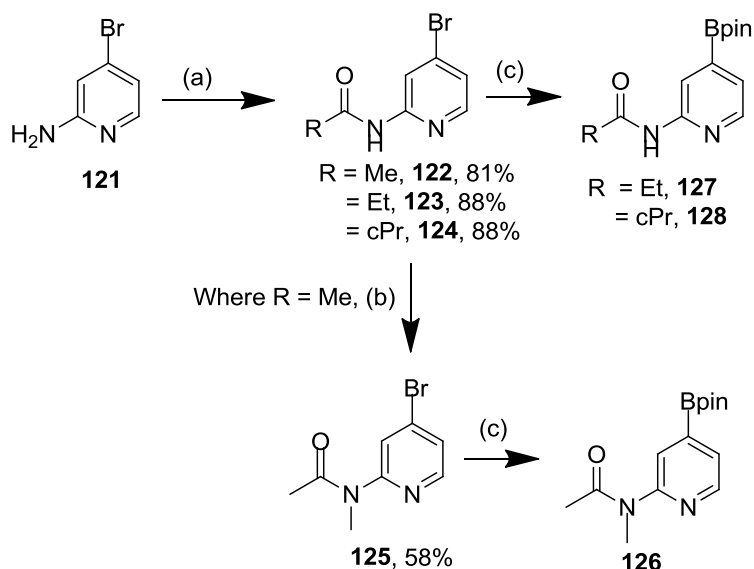


Scheme 46. Suzuki cross-coupling reaction between boronate esters **126-128** and the FP intermediate **115**. Reagents and conditions: (a) 5 mol% Pd(PPh₃)₄, 2 M Na₂CO_{3(aq)}, DME, 120 °C, microwave, 2 h.



Scheme 47. Synthetic route used to access TP amides **62-64**. Reagents and conditions: (a) 2-picoline borane, AcOH, MeOH, 50 °C, 16 h, 29%; (b) 5 mol% Pd(PPh₃)₄, 2 M Na₂CO_{3(aq)}, DME, 120 °C, microwave, 2 h.

Boronate ester intermediates **126-128** (**Scheme 48**) were synthesised from bromo pyridines **122-125** using boronylation conditions developed by Qian *et al.* and had previously been used to make pyridine boronate ester **116** (**Scheme 42**) and have been previously discussed.¹¹⁶



Scheme 48. Synthesis of boronate ester intermediates **126-128** used to make pyridyl amide analogues **59-64**. Reagents and conditions: (a) acid chloride, pyridine, DCM, room temperature, 16 h, amino propyl SPE; (b) MeI, NaH (60% w/w dispersion in mineral oils), DMF, 0 °C to room temperature, 2 h; (c) (Bpin)₂, 10 mol% Pd(dppf)Cl₂, KOAc, dioxane, 100 °C, microwave, 30 min, material was taken forward without purification, so no yield is given.

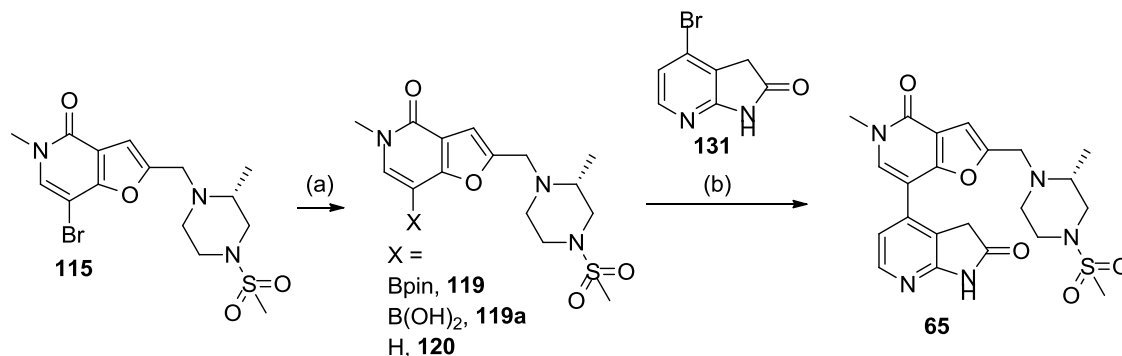
Compounds **126-128** were made using similar boronylation conditions to those used previously. As with previous boronate esters, **126-128** were difficult to purify due to poor separation by TLC, and reverse phase methods failed, so in each case crude material was taken forward to the Suzuki step. By LCMS, only the mass ion for the corresponding boronic acids of the boronate esters **126-128** were observed, and it was assumed the boronate esters hydrolysed under LCMS conditions in each case, as had happened with **116**. NMR would have confirmed this, but not taken.

The yields quoted for the Suzuki step relate to the amount of the aryl bromide used, **115** or **130**, because the amount of boronate ester **126-128** was assumed to be in excess. The low purities of **126-128** may explain the low yields of Suzuki step used to access **59-64**.

Compounds **122-125** were made from the common intermediate **121** *via* acylation and compound **126** was made *via* methylation of **125**.

2.5.7. Synthesis of Cyclic Amide, 65

A Suzuki cross-coupling reaction between **131** and a crude mixture of the boronate ester **119**, boronic acid **119a** and proto-deborylated product **120** that had been generated from **115**, delivered **65** (Scheme 49).

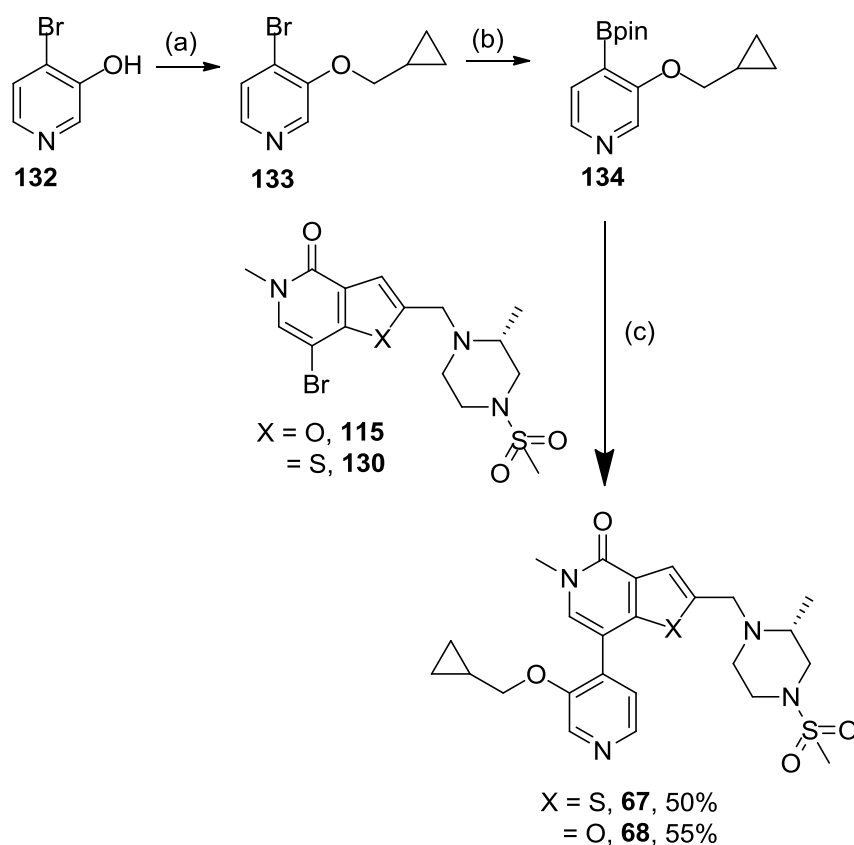


Scheme 49. Suzuki cross-coupling reaction used to secure **65**. Reagents and conditions: (a) HBpin, NEt₃, 10 mol% PEPPSITM-SiPr^(R), dioxane, 100 °C, 3 h, material was taken forward without purification, so no yield is given; (b) 10 mol% Pd(PPh₃)₄, 2 M Na₂CO_{3(aq)}, DME, 120 °C, microwave, 30 min, 4% over the two steps.

The same boronylation conditions were used to boronylate **115** that had been used towards the synthesis of **58**, but this time no mass ion for the boronic ester **119** was evident by LCMS. Only mass ions for the boronic acid **119a** (approximately 45% by LCMS peak area) and the proto-deborylated product **120** (approximately 55% by peak area) were evident. This profile did not compare favourably with the previous boronylation reaction, which achieved (by peak area) 12% of **119**, 57% of **119a**, and only 27% of **120**. The apparent lower yield of boronic acid/boronic ester could not be explained, and the amounts of these species required for Suzuki coupling varied substantially from batch to batch in subsequent reactions, for example to make **77** (Scheme 56). The yield for **65**, and yields from boronylation-Suzuki reactions from hereon are therefore quoted for the two steps from **115**. An improved process for generating on a larger scale is described later (Scheme 72).

2.5.8. Synthesis of *ortho*-substituted Tail-group Compounds **67** and **68**

The TP **67** and FP **68** with *ortho*-substituted tail-groups were synthesised from aryl bromide intermediates **130** and **115** respectively *via* a Suzuki cross-coupling reaction with *ortho*-substituted pyridyl boronate ester **134** (Scheme 50). The boronate ester **134** was synthesised *via* a boronylation reaction from *ortho*-substituted bromopyridine **133**, which was made from hydroxyl pyridine **132** *via* an alkylation reaction.



Scheme 50. Route used to secure *ortho*-substituted tail-group analogues **67** and **68**.

Reagents and conditions: (a) (bromomethyl)cyclopropane, NaH (60% w/w dispersion in mineral oils), DMF, 0 °C to room temperature, overnight, 45%; (b) (Bpin)₂, 10 mol% Pd(dppf)Cl₂, KOAc, dioxane, 100 °C, microwave, 30 min. Compound **134** was taken on without purification, so no yield is given; (c) 5 mol% Pd(PPh₃)₄, 2M Na₂CO_{3(aq)}, DME, 120 °C, microwave, 2 h.

Compound **134** was made using similar boronylation conditions to those used previously. As with previous boronate esters, **134** was difficult to purify due to poor separation by TLC, and reverse phase methods failed, so the crude material was taken

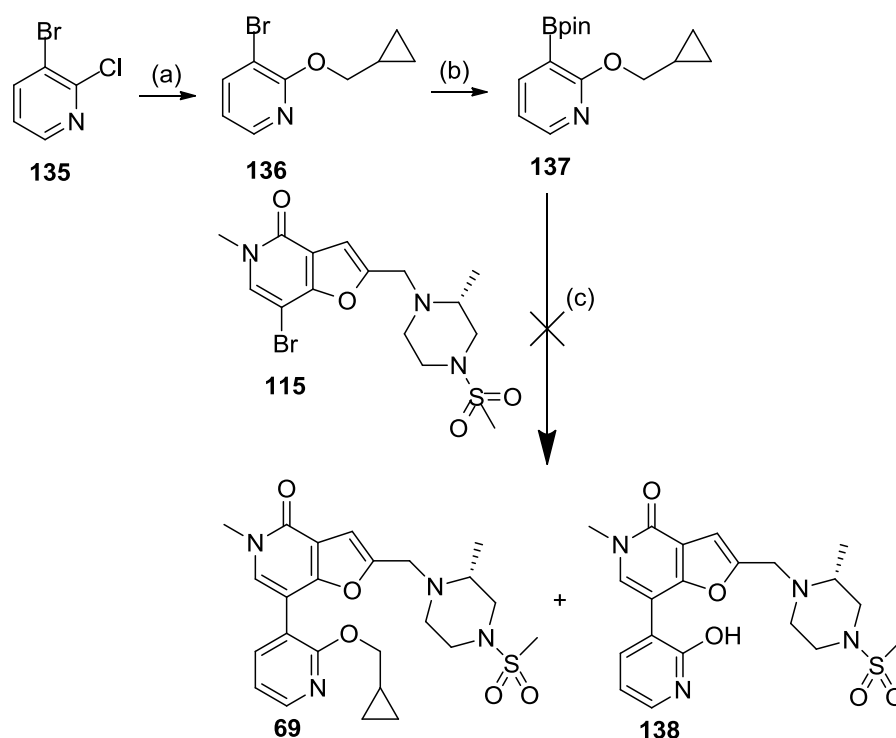
forward to the Suzuki step. By LCMS, only the mass ion for the corresponding boronic acid of the boronate ester was observed, and it was assumed the boronate esters hydrolysed under LCMS conditions, as had happened with **116**. An NMR was not taken to confirm this.

The yields quoted for the Suzuki step relate to the amounts of the FP or TP aryl bromide used, **115** or **130**, because the amount of boronate ester **134** was assumed to be in excess.

2.5.9. Chemistry Towards *ortho*-substituted Pyridine Regioisomers **69** and **71**

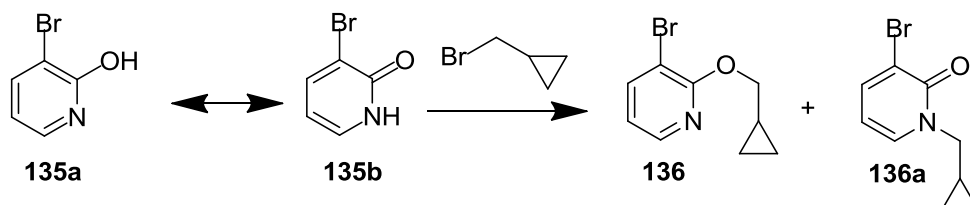
2.5.9.1. 3-position Regioisomer, **69**

The synthesis of **69** was attempted according to **Scheme 51** via three steps.



Scheme 51. Synthetic route undertaken to access **69**. Reagents and conditions: (a) cyclopropylmethanol, NaH (60% w/w dispersion in mineral oils), DMF, 0 °C to room temperature, overnight, 36% at 80% purity by LCMS and ¹H NMR; (b) (Bpin)₂, 10 mol% Pd(dppf)Cl₂, KOAc, dioxane, 100 °C, microwave, 30 min, then 120 °C, microwave 1 h, material was taken forward without purification, so no yield is given; (c) 5 mol% Pd(PPh₃)₄, 2 M Na₂CO_{3(aq)}, DME, 120 °C, microwave, 2 h, 0% (isolated).

The *ortho*-substituted bromo pyridine **136** was accessed *via* a nucleophilic displacement of the 2-chlorine of **135**. The 2-cyclopropylmethyl substituent of **136** was installed *via* an S_NAr reaction rather than an alkylation reaction, which had been used to access **133**, because S_NAr at the 2-position of a 2-chloropyridyl species is facile and avoids the *N*-alkylated by-product that could also be formed if the alkylation of the ambident 3-bromopyridin-2-ol **135a** was attempted (Scheme 52).



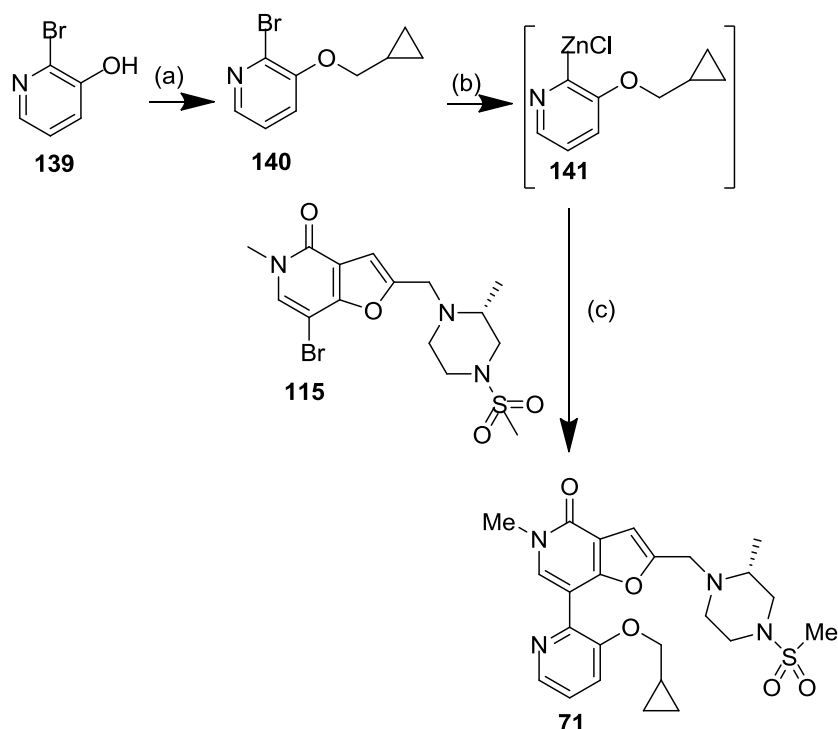
Scheme 52. Alkylation of **135a** using (bromomethyl)cyclopropane was anticipated to be possible on the oxygen or nitrogen, because two major tautomers were possible, **135a** and **135b**, and *O*-alkylation and *N*-alkylation is known.

Compound **136** was converted to the boronate ester **137** using conditions previously described, and as with previous pyridyl boronate esters, **137** was difficult to purify due to poor separation by TLC, and reverse phase methods failed, so the crude material was taken forward to the Suzuki step. By LCMS, only the mass ion for the corresponding boronic acid of the boronate ester was observed, but ¹H NMR spectrum was consistent with the presence of the boronate ester. It was assumed therefore that the boronate ester hydrolysed under LCMS conditions.

The Suzuki cross-coupling reaction between the aryl bromide **115** and the boronate ester **137** was successful according to LCMS analysis, but a portion of the material degraded on purification by MDAP to a byproduct with a molecular weight of 432.5 (by LCMS, with approximately 14% by peak area). The degradation product was not isolated and characterised, but a putative structure that corresponded to this molecular weight was **138** (Scheme 51). This step was undertaken twice, but with a similar result each time.

2.5.9.2. 6-position Regioisomer, 71

A Negishi coupling between the aryl bromide **115** and organozinc intermediate **141** allowed access to **71** (Scheme 53).



Scheme 53. Route used to secure 6-position regioisomer **71**. Reagents and conditions:

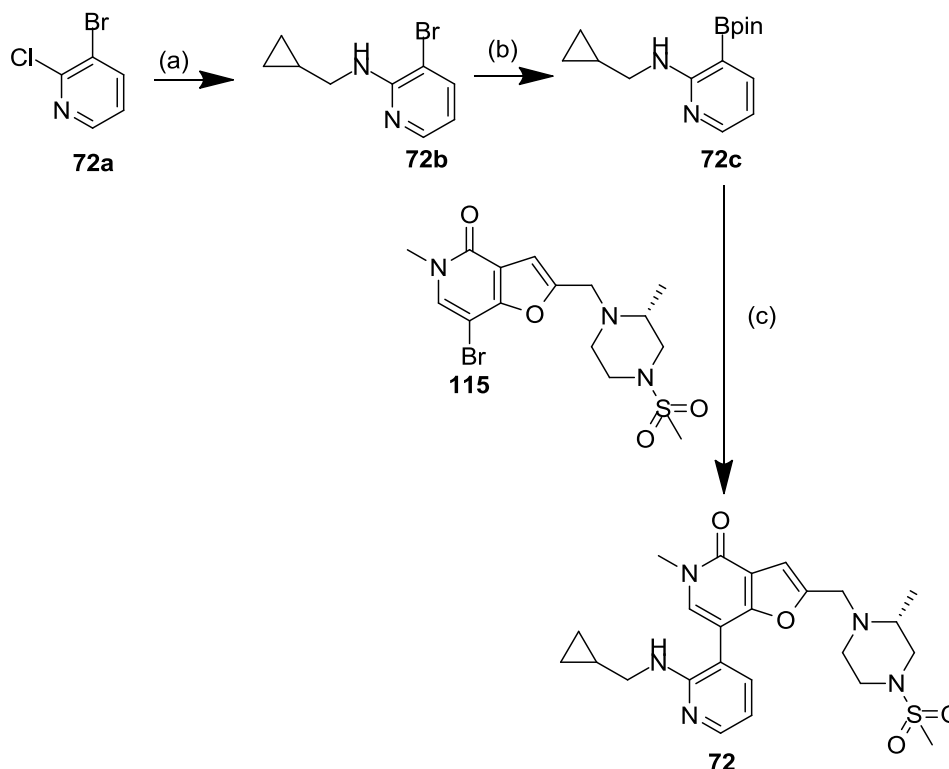
(a) (bromomethyl)cyclopropane, NaH (60% w/w dispersion in mineral oils), DMF, 0 °C to room temperature, 16 h, 87%; (b) 2 M *i*PrMgCl in THF, 4 h, then 1 M ZnCl₂ in ether, 0 °C to room temperature, 4 h (material was taken forward without isolation, so no yield is given); (c) 17 mol% Pd(PPh₃)₄, THF/ether, 80 °C, 16 h, 25%, over steps (b) and (c).

The *ortho*-substituted bromopyridine **140** was accessed *via* an alkylation reaction between (bromomethyl)cyclopropane and pyridinol **139** using NaH (60% w/w dispersion in mineral oils) as a base. The organozinc intermediate **141** was formed using the method reported by Luzung *et al.*,¹¹² and then coupled with **115** using established conditions to give **71**.^{107,115}

2.5.10. Synthesis of *ortho*-Cyclopropylmethyl *N*-linked Pyridyl Ring FP Analogues, 72 and 73

2.5.10.1. 3-position Regioisomer, 72

A three step synthesis was used to prepare **72** from intermediates **72a** and **115** (Scheme 54).

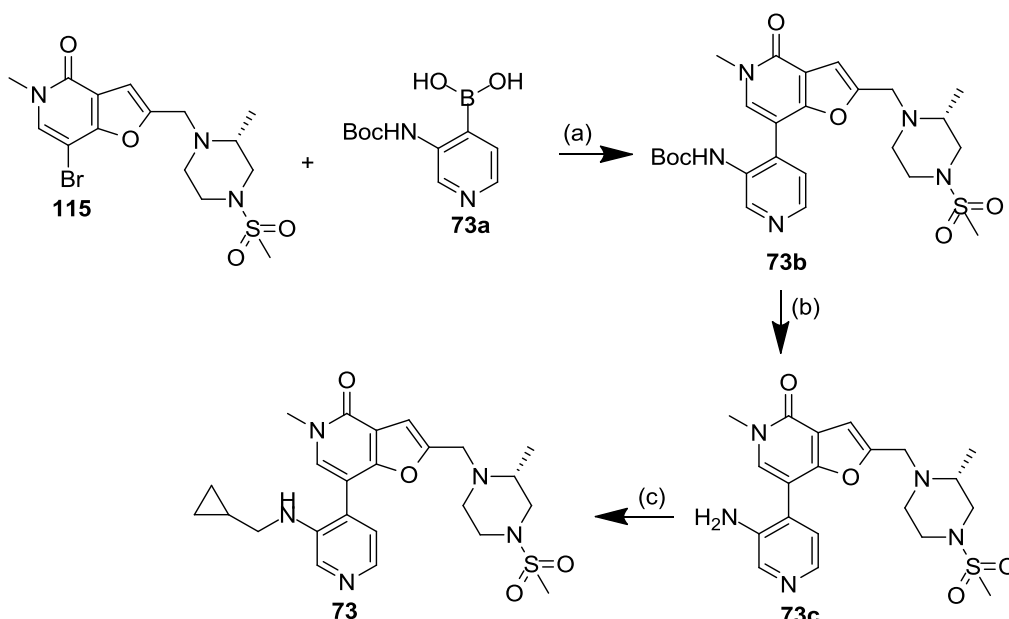


Scheme 54. Synthesis of *N*-linked 3-position regioisomer **72**. Reagents and conditions: (a) cyclopropylmethanamine, DIPEA, IPA, 120 °C, microwave, 1 h, then 180 °C, 4 h, microwave, 79%; (b) (Bpin)₂, 10 mol% Pd(dppf)Cl₂, KOAc, dioxane, 120 °C, microwave, 1 h, material was taken on without purification, so a yield is not given; (c) 4 mol% Pd(PPh₃)₄, 2 M Na₂CO_{3(aq)}, DME, 120 °C, microwave, 2 h, 34% over steps (b) and (c).

The bromopyridine **72b** was prepared from **72a** and cyclopropylmethanamine by S_NAr; Miyaura borylation delivered boronate ester **72c** which was taken forward without purification to the Suzuki coupling reaction with **115** to secure **72**.

2.5.10.2. 4-position Regioisomer, 73

A three step synthesis was used to prepare **73** from **115** and commercially available intermediate **73a** (Scheme 55).

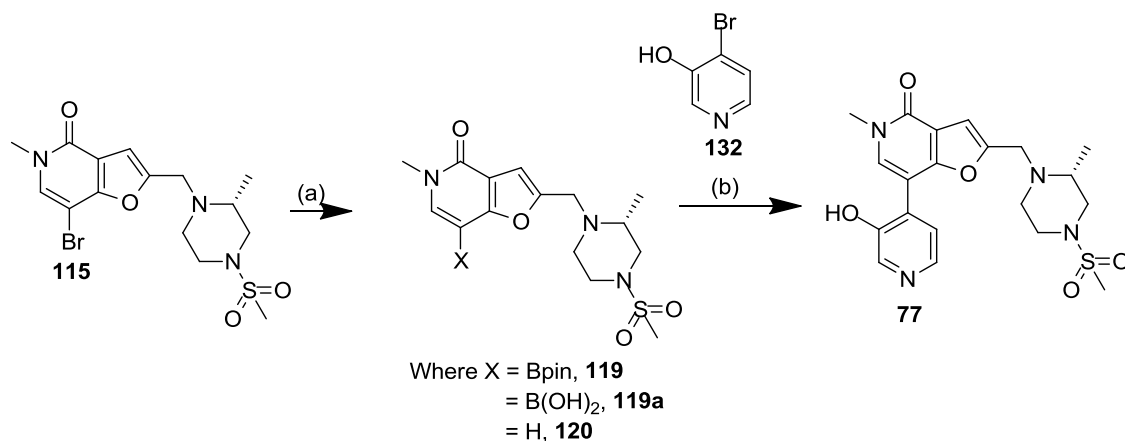


Scheme 55. Synthesis of *N*-linked target **73**. Reagents and conditions: (a) 4 mol% Pd(PPh₃)₄, 2 M Na₂CO_{3(aq)}, DME, 120 °C, microwave, 2 h, 39%; (b) TFA, DCM, 30 min, amino propyl SPE, 97% at 85% purity by LCMS and NMR; (c) cyclopropanecarbaldehyde, 2-picoline borane, MeOH/AcOH (9:1, v/v), 16 h, 28%.

A Suzuki coupling between boronic acid **73a** and the aryl bromide **115** delivered **73b**, then TFA-mediated deprotection to **73c** and subsequent reductive amination with cyclopropanecarbaldehyde afforded **73**.

2.5.11. Synthesis of *ortho*-Hydroxy Pyridyl Ring FP Analogue, 77

Compound **77** was made by boronylation of **115** using Ghosh *et al.*'s conditions to give a mixture of the boronate ester **119**, the boronic acid **119a** and the proto-deborylated product **120**;¹¹⁸ the excess HBpin in the crude mixture was then quenched with IPA, and the reaction mixture filtered, concentrated under reduced pressure and then used in the PEPPITM-SiPr^(R)-based Suzuki coupling with **132** (Scheme 56).

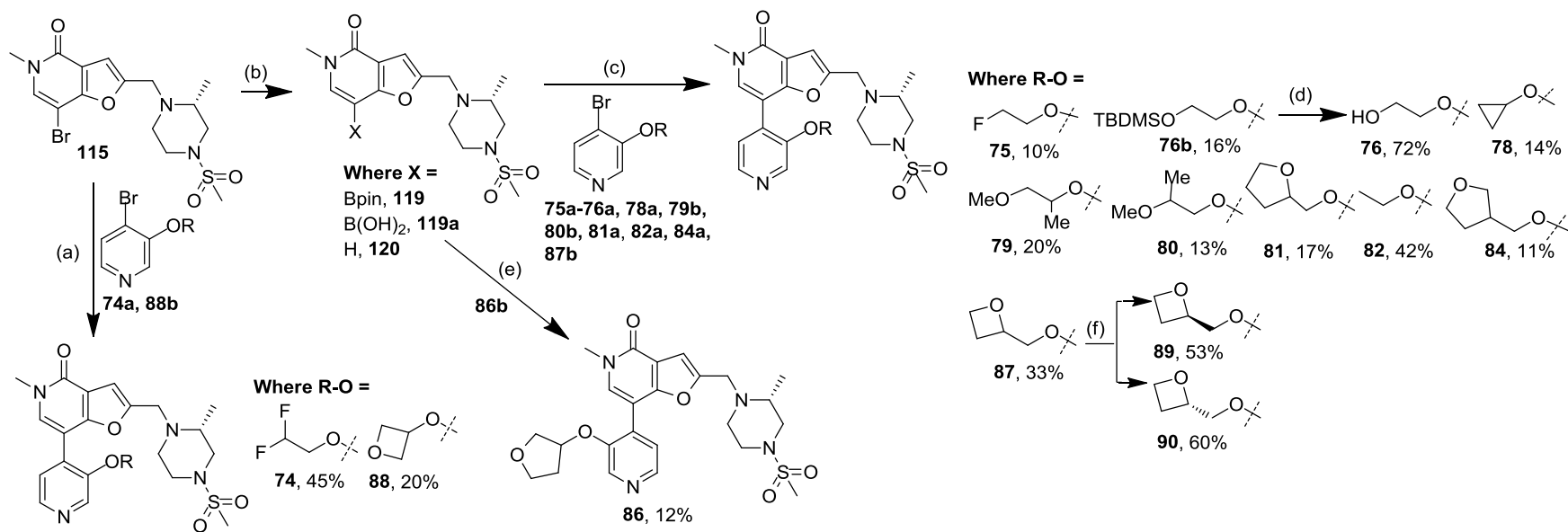


Scheme 56. Synthesis of **77**. Reagents and conditions: (a) HBpin, NEt₃, 10 mol% PEPPSITM-SiPr^(R), dioxane, 100 °C, 2.5 h, material was taken forward without purification, so no yield is given; (b) 8 mol% PEPPSITM-SiPr^(R), K₂CO_{3(aq)}, IPA:water (5:1 v/v), reflux, 1.3 h, 19%, over the two steps.

The use of PEPPSITM-SiPr^(R) for the Suzuki coupling of pyridin-one boronate esters or acids, such as **119** and **119a** respectively, with bromopyridines, such as **132**, has not been widely reported, but PEPPSITM-SiPr^(R) was chosen in an attempt to perform the borylation then Suzuki coupling with the same catalyst, which could have simplified the procedure. A moderate yield of **77** (38%) was achieved, but the yield was lower on a larger scale (results not reported).

2.5.12. Synthesis of *ortho*-Pyridyl Substituted FP Analogues, **74-75**, **76**, **78-82**, **84**, **86-88**, **89** and **90**

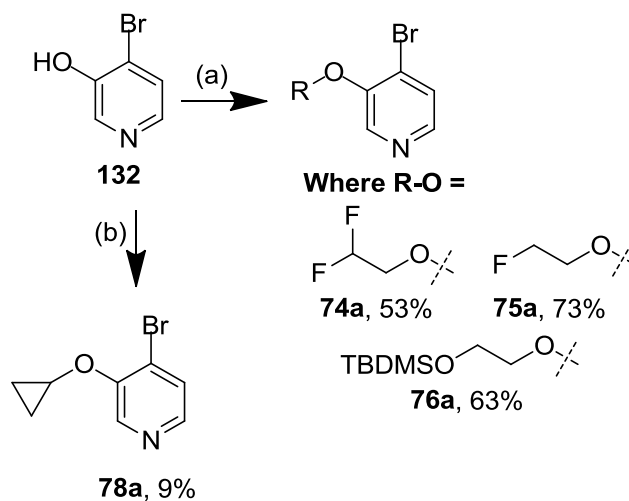
Compounds **74**,²⁰ **75**, **76b**, **78-82**, **84**, and **86-88** were made by borylation of **115** to give a mixture of the boronate ester **119**, boronic acid **119a** and proto-deborylated product **120** (Scheme 57), then the crude mixture was then coupled with the appropriate crude bromopyridine **74a-76a**, **78a**, **79b**, **80b**, **81a**, **82a**, **84a**, and **86b-88b**, using Suzuki coupling conditions. As before, the relative levels of boronate ester **119**, boronic acid **119a**, and proto-deborylated product **120**, varied substantially between preparations (as determined by LCMS), which together with the use of crude bromopyridines in the Suzuki step, may explain the range of yields of final compound (10 to 45%). Compound **76** was obtained by TBAF-mediated deprotection of **76b**; compounds **89** and **90** were secured from **87** following chiral HPLC purification.¹²



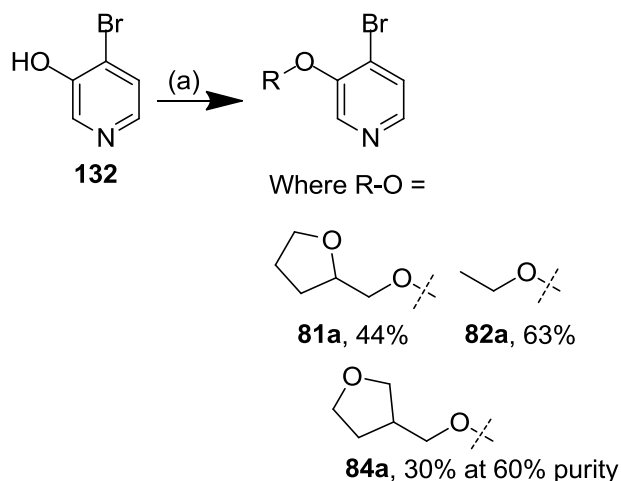
Scheme 57. Route to *ortho*-substituted tail-group analogues **74**²⁰-**82**, **84** and **86-88** to **90**. Reagents and conditions: (a) HBpin, NEt₃, 6 mol% PEPPSITM-SiPr^(R), dioxane, 60 °C for 2h then 100 °C for 3.5 h, then **74a**, 10 mol% PEPPSITM-SiPr^(R), K₂CO₃, IPA:H₂O (5:1 v/v), reflux, 7 h, or HBpin, NEt₃, 10 mol% PEPPSITM-SiPr^(R), dioxane, 100 °C for 3 h, then **88b**, 5 mol% PEPPSITM-SiPr^(R), K₂CO₃, IPA:H₂O (5:1 v/v), reflux, 1 h; (b) HBpin, NEt₃, 10 mol% PEPPSITM-SiPr^(R), dioxane, 100 °C, microwave, 3 h, material was taken forward without purification, so no yield is given; (c) 5 mol% Pd(PPh₃)₄, 2 M Na₂CO_{3(aq)}, DME, 120 °C, microwave, 30 min; (d) TBAF (1 M solution in THF), THF, 2 h; (e) 12 mol% PEPPSITM-SiPr^(R), K₂CO₃, DME:H₂O (3:1 v/v), 120 °C, microwave, 30 min, then 140 °C, 1h, then 6 mol% PEPPSITM-SiPr^(R), IPA:H₂O (5:1 v/v), reflux, 1.5 h; (f) chiral HPLC.¹² Quoted yields for **74**, **88**, **75**, **76b**, **78-82**, **84** and **87** are combined for the boronylation and Suzuki steps. Quoted yields for **89** and **90** assumed the 121 mg of **87** that was used for chiral separation was a 1:1 mixture of enantiomers, with a theoretical maximum of approximately 61 mg of each isomer.

Compounds **74** and **88** were made in 45% and 20% yield respectively, using a protocol whereby **115** was borylated using previously described boronylation conditions, the reaction mixture was quenched with IPA, filtered through Celite^(R), then the crude solution of the boronic ester **119**, the boronic acid **119a**, and the proto-deborylated product **120** was treated with the appropriate bromopyridine, more PEPPSITM-SiPr^(R), K₂CO₃, and a solution of IPA in water to affect Suzuki coupling with **74a** and **88b** respectively. This approach did not seem to offer much advantage over an alternative protocol that was used to make compounds **75**, **76b**, **78-82**, **84**, **86** and **87**, in 10 to 42% yield. The alternative protocol involved borylation of **115** give a mixture of **119**, **119a**, and **120**, the excess HBpin in the crude reaction mixtures was quenched using IPA. The reaction mixtures were then filtered and, in contrast to the previous protocol, concentrated under reduced pressure, then used crude in the Suzuki coupling step with the appropriate bromopyridine, 2 M Na₂CO_{3(aq.)}, DME, and Pd(PPh₃)₄ to give the final compounds.

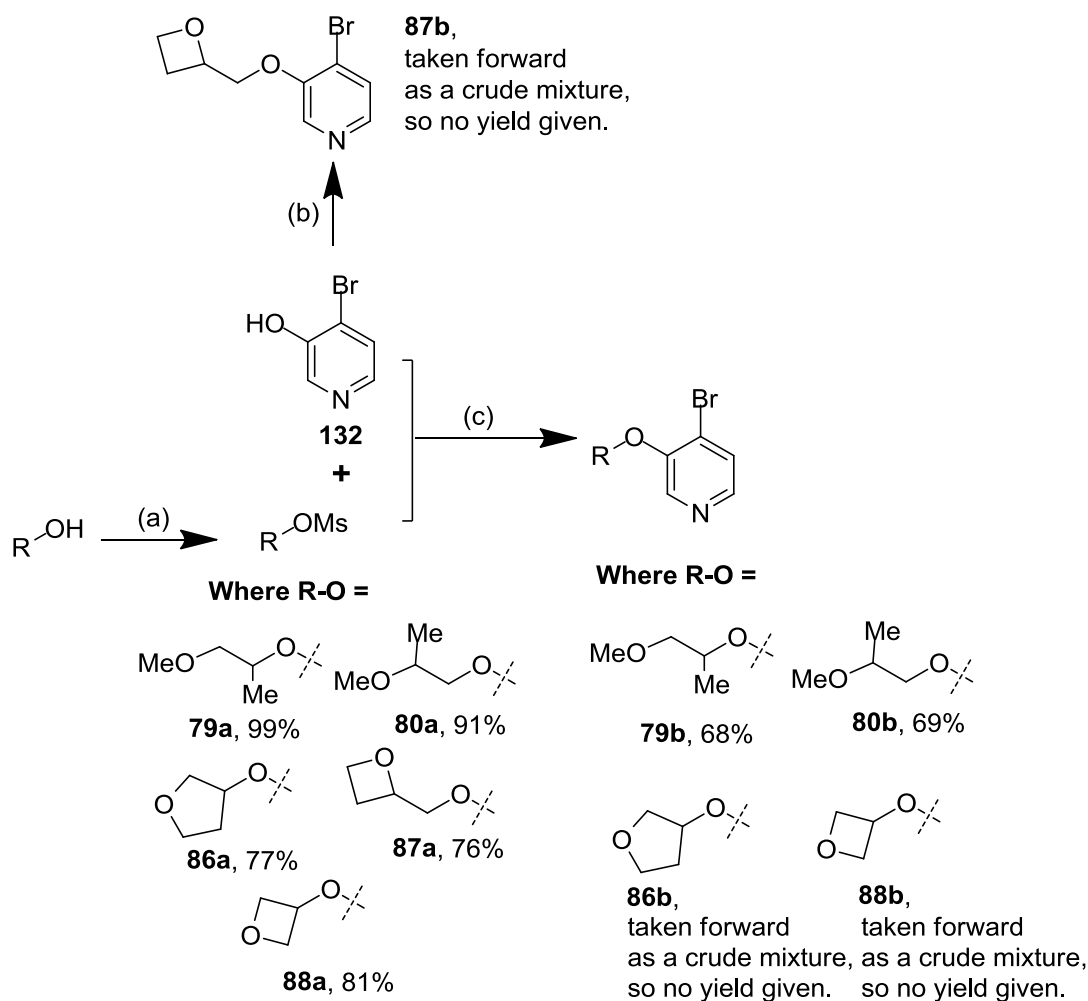
The *ortho-O*-substituted bromopyridine intermediates **74a-76a**, **78a**, **79b**, **80b**, **81a**, **82a**, **84a**, and **86b-88b** were synthesised by alkylation of **132** with alkyl bromide using either Cs₂CO₃ (**Scheme 58**) or NaH (**Scheme 59**) as base to first deprotonate **132**. Where the alkyl bromide was unavailable, the mesylate was used in the alkylation step instead, and was made from the alcohol (**Scheme 60**). The TBDMS-protected intermediate **76a** was made rather than the corresponding free hydroxyethyl intermediate to avoid the formation of by-products that could form by alkylation of hydroxyl group in the presence of alkyl bromide.



Scheme 58. Route used to secure *ortho*-substituted tail-group analogues **74a-76a** and **78a**. Reagents and conditions: (a) RBr, Cs₂CO₃, DMF, 16-48 h, room temperature; (b) bromocyclopropane, Cs₂CO₃, NaI, DMF, 150 °C, 108 h.

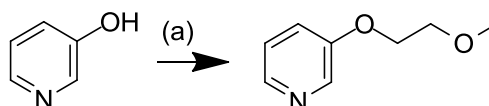


Scheme 59. Route used to secure *ortho*-substituted tail-group analogues **81a**, **82a**, and **84a**. Reagents and conditions: (a) RBr, NaH (60% w/w dispersion in mineral oils), DMF, 60 °C, 24 h.

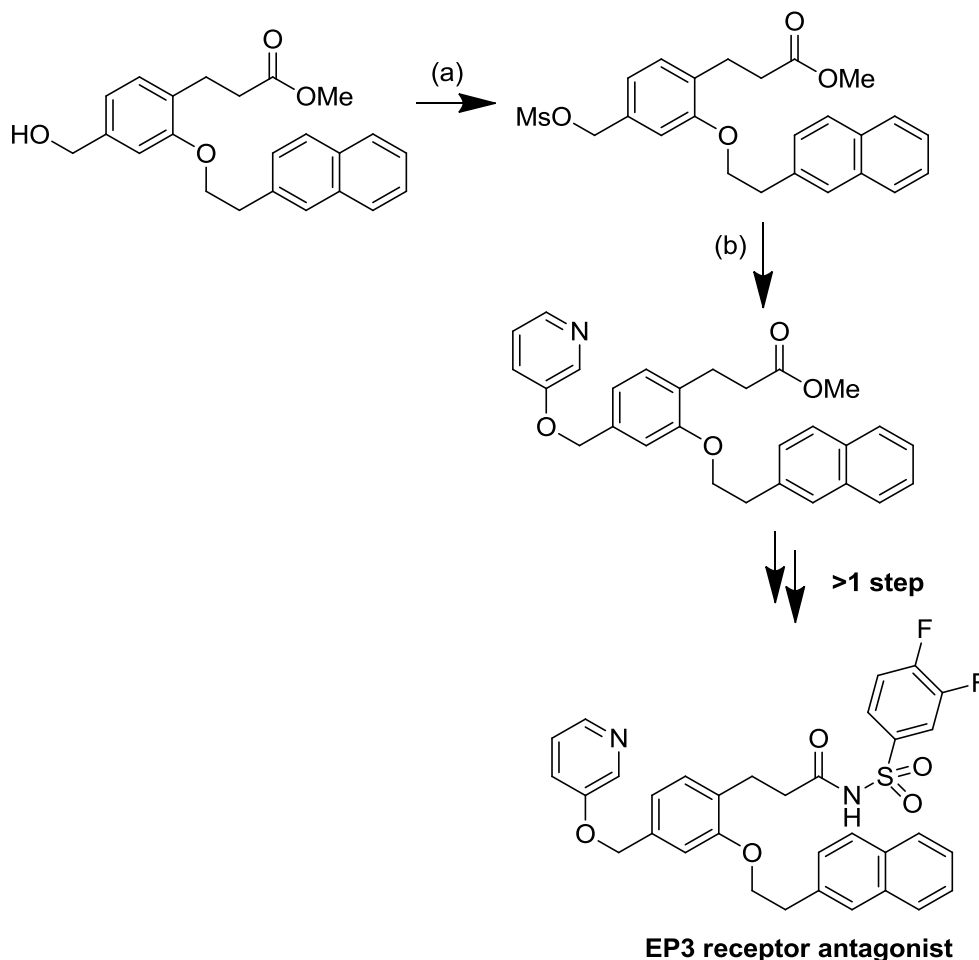


Scheme 60. Route to *ortho*-substituted tail-group analogues **79b**, **80b**, **86b**, **87b** and **88b**. Reagents and conditions: (a) MsCl, NEt₃, DCM, 0 °C, 1 h; (b) NaH (60% w/w dispersion in mineral oils), DMF, 60 °C, 16 h; c) Cs₂CO₃, DMF, 50-120 °C, 40-64 h.

The use of NaH for the alkylation of 3-hydroxypyridines with bromoalkanes or alkylmethanesulfonates is well preceded in the literature. For example, Wada *et al.* treated the hydroxypyridines first with NaH, then with bromoalkanes to synthesise (2-methoxy)ethoxy-arenes (**Scheme 61**).¹²⁴ Asada *et al.* used alkylmethanesulfonates and NaH to synthesise EP3 antagonists (**Scheme 62**).¹²⁵



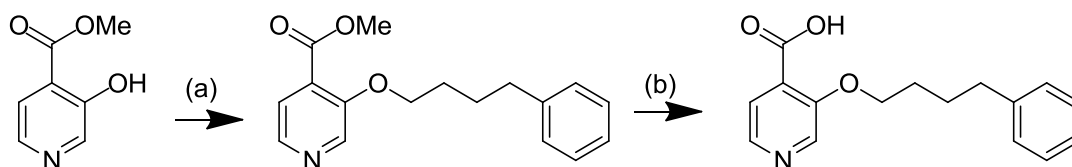
Scheme 61. Route used by Wada *et al.* to synthesise (2-methoxy)ethoxy- arenes from bromoalkanes. Reagents and conditions: (a) NaH (suspension in ether), DMF, then Br(CH₂)₂OMe, 16 h, 38%.¹²⁴



Scheme 62. Route used by Asada *et al.* to synthesise EP3 antagonists from alkylmethanesulfonates and NaH. Reagents and conditions: (a) MsCl, NEt₃, THF, no yield given; (b) 3-hydroxypyridine, NaH, DMF, no yield given.¹²⁵

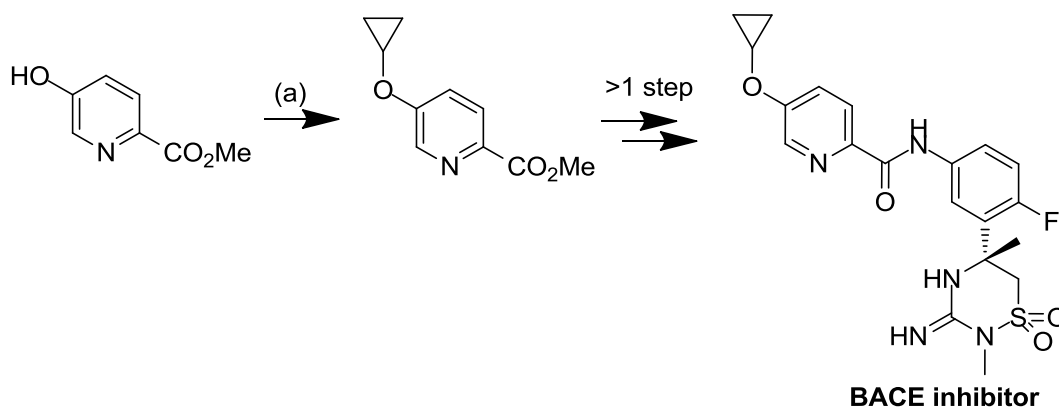
Similar conditions were employed in the first attempts at alkylating **132** (**Scheme 59** and **Scheme 60**), except the suspension of NaH in ether was replaced by NaH as a 60% by weight dispersion in mineral oil because this form is less prone to combustion in the presence of oxygen, and because it is easier to dispense an accurate amount of NaH into

the reaction mixture. The pK_a for the conjugate acid of NaH is 35,¹²⁶ so the conjugate base should have completely deprotonated 3-hydroxypyridine (calculated pK_a 7.3),¹¹⁴ to form the more reactive sodium salt that can then undergo alkylation. High yields using these conditions were not always achieved, probably because the old batches of NaH in mineral oils that were used may have actually mainly contained NaOH,¹²⁶ having reacted over time with water moisture in the air. The NaOH can react with the bromoalkane or alkylmethanesulfonate to form the corresponding alcohol and lower the alkylation yield. Consequently alternative alkylation conditions that used Cs_2CO_3 were chosen in order to make the remaining compounds, using conditions that had been used successfully inhouse to synthesise demethylase inhibitors from 3-hydroxypyridines (**Scheme 63**).¹²⁷ The main role of the much weaker base (CO_3^{2-} pK_a 10.3)¹²⁶ in the alkylation reactions was neutralisation of the alkylation byproducts, HBr or methanesulfonic acid.



Scheme 63. Synthesis of 3-hydroxypyridine-based demethylase inhibitors. Reagents and conditions: (a) $Ph(CH_2)_4Br$, Cs_2CO_3 , DMF, 16h, 66%; (b) LiOH monohydrate, THF/ H_2O (3:1 v/v), 16 h, 12%.¹²⁷

The majority of conditions reported in the literature for alkylating 3-hydroxypyridines with bromocyclopropane employed Cs_2CO_3 as a base, but also included NaI to generate the more reactive iodide *in situ*, and elevated temperatures, such as those used by Scott *et al.* to synthesise BACE inhibitors (**Scheme 64**).¹²⁸ These conditions were successfully applied to the synthesis of **78a** from **132**, albeit in low yield (**Scheme 58**).



Scheme 64. Conditions used by Scott *et al.* to synthesise BACE inhibitors. Reagents and conditions: (a) Cs_2CO_3 , NaI, DMF, $150\text{ }^\circ\text{C}$, 7 h, yield not reported.¹²⁸

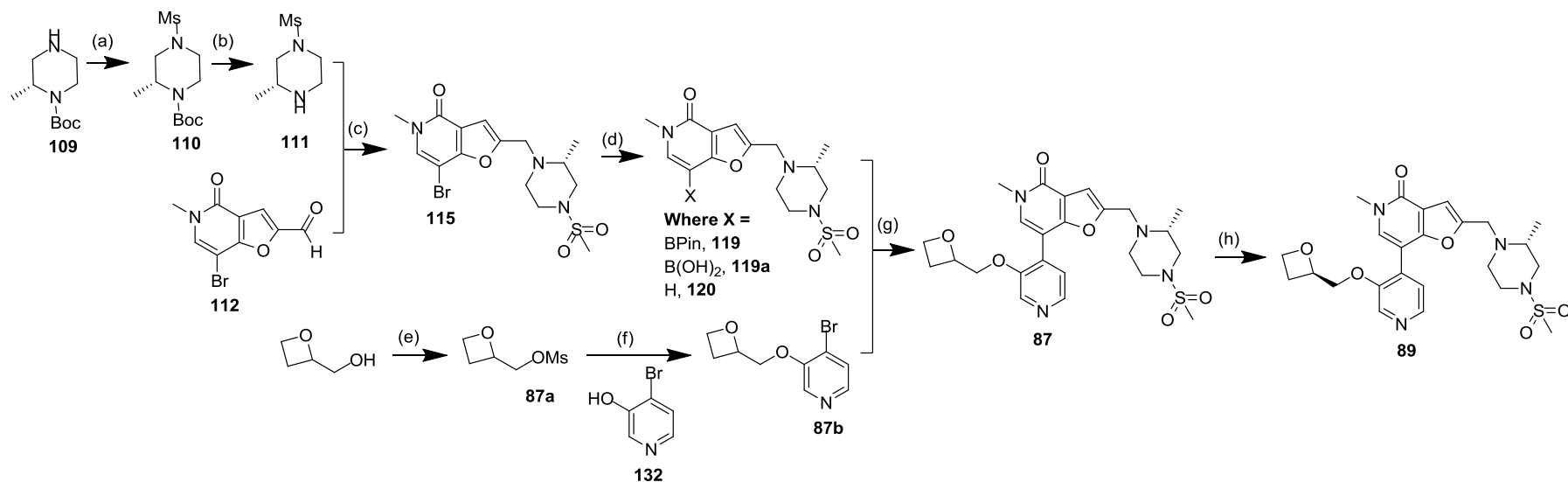
The alkylation using bromocyclopropane was difficult and required a high temperature ($150\text{ }^\circ\text{C}$) for a substantial amount of time (108 h). The $\text{S}_{\text{N}}2$ transition state requires the carbon/carbon/hydrogen substituents to adopt a trigonal planar formation, with 120° bond angles between substituents, which are substantially higher than the existing 60° bond angles in bromocyclopropane.^{129,130} The elevated temperature and long heating time were therefore required to overcome the angle strain to achieve alkylation using bromocyclopropane.

2.5.12.1. Synthesis of *ortho*-Pyridyl Substituted FP Analogues, **83** and **85**

Compounds **83** and **85** were synthesised in three steps from **132**, starting with an alkylation using bromoalkane and NaH, borylation to form the crude boronate esters **83b** and **85b**, then Suzuki coupling with **115** using conditions that have been previously discussed (**Scheme 65**).

2.5.13.Scaled-up Synthesis of **89**

A 10 g quantity of **89** at greater than 95% purity, chemically and enantiomerically, was required for the dog safety study. Compound **89** had been previously secured on a small scale after chiral HPLC of **87** in 53% yield, which assumed the 121 mg of **87** that was used for chiral separation was a 1:1 mixture of enantiomers, with a theoretical maximum of 61 mg of each isomer. However, this also meant for every 100 mg of **87** produced, only 26 mg of **89** was likely to be isolated after chiral HPLC. Compound **87** had been synthesised in 15% yield in five steps with respect to starting material **109**, which gave a projected overall yield of **89** of 4% from **109** (Scheme 66).



Scheme 66. Synthetic route used to deliver **89** on a small scale. Reagents and conditions: (a) MsCl , 2 M $\text{NaOH}_{(\text{aq})}$, THF, 0 °C to room temperature, 2 h, 79%; (b) 4 M HCl in dioxane, DCM, 16 h, aminopropyl SPE, 98%; (c) 2-picoline borane, AcOH, MeOH, 1 h at room temperature, then 40 °C, 16 h, 58%; (d) HBpin, NEt_3 , 10 mol% PEPPSITM-SiPr^(R), dioxane, 100 °C, microwave 3 h, material was taken forward without purification, so no yield is given; (e) MsCl , NEt_3 , DCM, 0 °C, 1 h, 76%; (f) NaH (60% w/w dispersion in mineral oils), DMF, 60 °C, 16 h, material was taken forward without purification, so no yield is given; (g) 6 mol% $\text{Pd}(\text{PPh}_3)_4$, 2 M $\text{Na}_2\text{CO}_3_{(\text{aq})}$, DME, 120 °C, microwave, 30 min, 33% (over steps (d) and (g)); (h) chiral HPLC, 53%, assuming **87** was a 1:1 mixture of enantiomers.

According to equivalents required and yields achieved on a small scale using this route, large amounts of starting materials and intermediates were required to prepare 10 g of **89** were estimated. These are shown in **Table 53**.

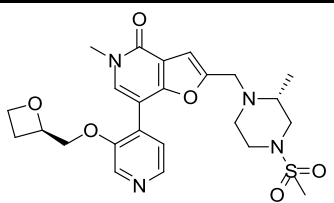
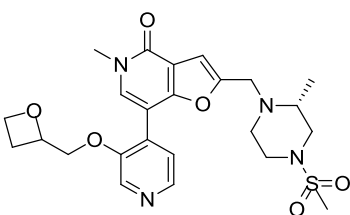
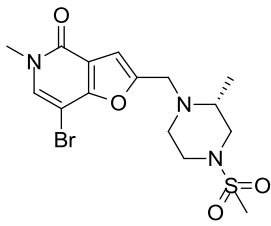
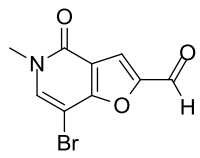
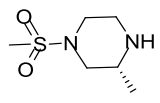
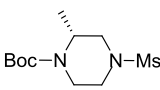
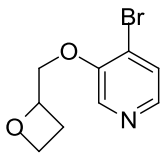
#	Structure	MW	Amount /g	Amount /mmol
89		502.6	10.0	19.9
87		502.6	37.7	75.1
115		418.3	135.8	324.6
112		256.1	143.4	560.0
111		178.3	142.0	796.4
110		278.4	226.3	812.7
87b	 (racemate)	244.1	53.9	220.8

Table 53. Estimated amounts of key intermediates required to make 10 g of **89**. The calculations were based on the assumptions that the yields obtained on the larger scales would be no lower than those for the small scale reactions.

Key intermediates that were commercially available included oxetan-2-ylmethanol, **109** and **132**, whereas **112** required a custom synthesis by an external company at high cost, and the remaining intermediates in **Table 53** required bespoke synthesis on large enough scale. Two major synthetic issues were identified that needed to be addressed before a scaled-up synthesis could be undertaken: intermediate **87b** was found to be unstable by proton NMR and was found to degrade within a few hours at room temperature, and boronylation of **115** yielded variable amounts of boronate ester **119**, boronic acid **119a**, and proto-deborylated product **120** from batch to batch.

Ideally a chiral route to **89** could remove the requirement for chiral HPLC purification at the last stage of the synthesis, or would reduce the amounts of intermediates required for each step of the synthesis. However, the chiral alcohol or alkyl halide starting material **87c** that would allow direct access to the chiral intermediate **87d** was not commercially available (**Figure 58**). An alternative synthetic strategy towards **87d** had to be devised.

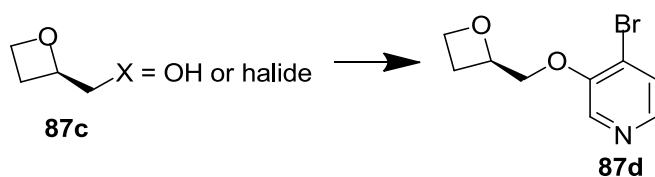
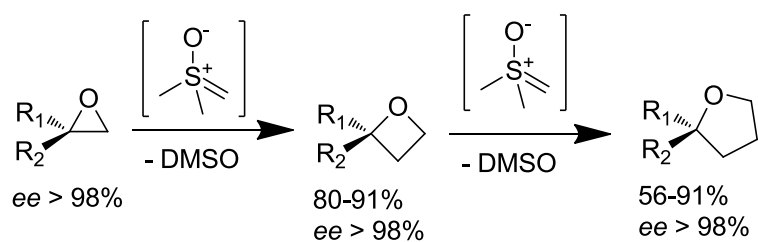


Figure 58. Chiral starting material that would have allowed direct access to chiral intermediate **87d** but was not commercially available.

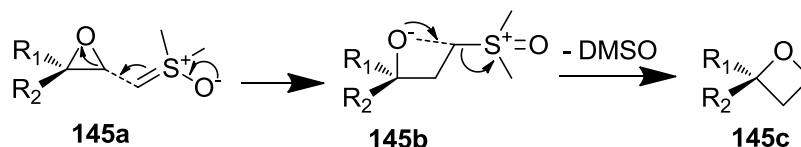
2.5.13.1. Scaled-up Synthesis of **87d**

Butova *et al.* studied the ring-expansion reactions of oxiranes with dimethylsulfoxonium methylide; epoxide to oxetane ring expansion occurred at elevated temperatures *via* a Corey-Chaykovsky mechanism, and further ring expansion to oxolanes could occur with heating at higher temperatures (**Scheme 67**).¹³¹



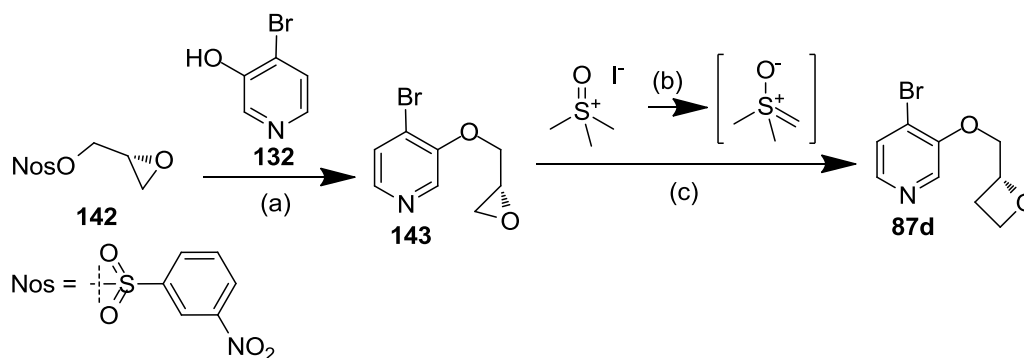
Scheme 67. Ring-expansion reactions of oxiranes with dimethylsulfoxonium methylide *via* a Corey-Chaykovsky mechanism reported by Butova *et al.*;¹³¹ enantiomeric purities of 2-mono- and 2,2-disubstituted epoxides and oxetanes were reported to have been conserved.

Conservation of enantiomeric purities of 2-mono- and 2,2-disubstituted epoxides **145a** was reported by Butova *et al.*, and the mechanism for transformation to oxetane **145c** was proposed to proceed *via* betaine **145b** (**Scheme 68**).



Scheme 68. Proposed mechanism for oxacycle ring expansion with dimethylsulfoxonium methylide.

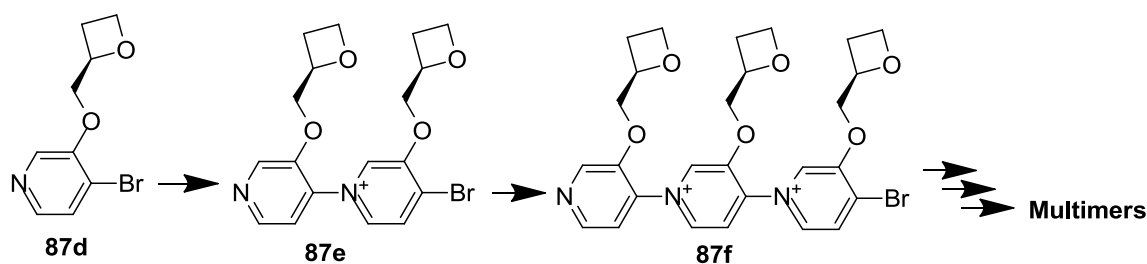
The conditions used by Butova *et al.* to access chirally pure oxetanes were used by Mitchell to access **87d** starting with chiral epoxide **142** which was readily available from a commercial source (**Scheme 69**).¹⁴



Scheme 69. Corey-Chaykovsky reaction used to access chiral intermediate **87d**. Reagents and conditions: (a) Cs_2CO_3 , DMF, 16 h, 80% at 90% purity; (b) $\text{KO}t\text{Bu}$, $t\text{BuOH}$, 80 °C, 10 min; (c) $t\text{BuOH}$, 60 °C, 6 h, 42% at 85% purity by LCMS and NMR, material was taken forward without purification due to instability.

The chiral epoxide **143** was prepared by alkylation of **132** with nosylate **142**, and was treated with dimethylsulfoxonium methylide to give oxetane **87d** in moderate yield. The chiral purity of **87d** could not be determined because, like **87b**, the material was found to degrade in a matter of hours at room temperature.

The ready self-condensation of 4-bromopyridine has been reported to occur by Feast *et al.* who were interested in the synthesis of water soluble polymers; they reported that the reaction occurred at temperatures as low as 10 °C.¹³² The instability of **87b** and **87d** was therefore unsurprising because by analogy the 4-bromopyridine moiety common to **87b** and **87d** was also likely to self-condense; the self condensation of **87d** is shown in **Scheme 70**.



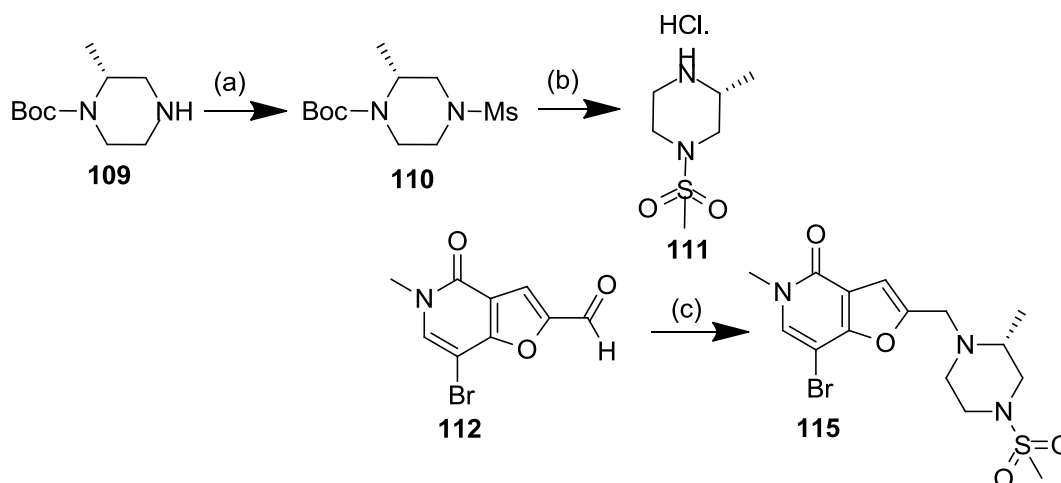
Scheme 70. The expected self-condensation of **87d** to form dimer **87e** and trimer **87f**.

The bromine in the 4-position of the pyridine is susceptible to displacement by nucleophiles such as the pyridine nitrogen, allowing formation of the dimer **87e**, a stable

quaternary salt. The pyridinium species is isoelectronic with benzene. The pyridinium ring of the dimer would be even more susceptible to nucleophilic attack, leading to formation of the trimer **87e**, and so on. To avoid degradation, any batches of **87d** that were prepared were stored at $-20\text{ }^{\circ}\text{C}$, and material was prepared in batches of up to 19 g at a time.¹⁴

2.5.13.2. Scaled-up Synthesis of **115**

Multi-gram quantities of intermediate **115** were prepared in three steps in 65% overall yield with the support of Watson and Mitchell (**Scheme 71**).^{14,19} This was an improvement on the small scale synthesis that achieved an overall yield of 45% for these three steps.

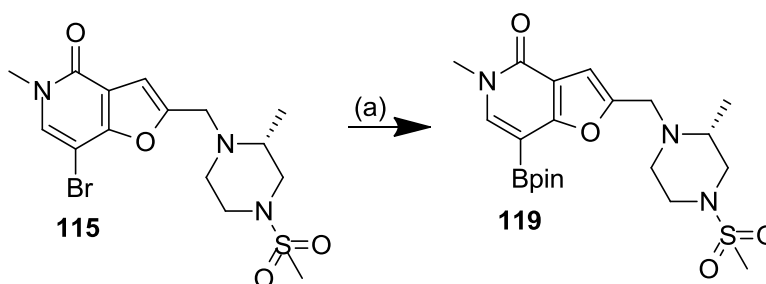


Scheme 71. Route used to prepare multi-gram quantities of **115**. Reagents and conditions: (a) MsCl, 2 M NaOH_(aq), THF, 0 °C to room temperature, 20 h, 87%; (b) 4 M HCl in dioxane, DCM, 0 °C to room temperature, 48 h, >99%; (c) **111**, Et₃N, 10 min, 2Me-THF, then NaBH(OAc)₃, 2 h, 75%.

The route that was used to access **115** on a small scale was similar to that used on a larger scale, except on a larger scale sodium triacetoxyborohydride (STAB) was used during the reductive amination step, step (c), because STAB-based conditions were found by Mitchell to generally deliver higher yields (75%) than 2-picoline borane-based conditions (58%).¹⁴ The reason for the higher yields using STAB for this step is unknown. Batches of up to 64 g of **115** were delivered using this route.

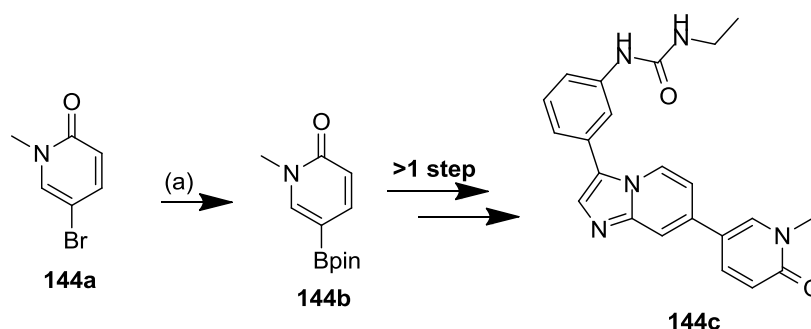
2.5.13.3. Scaled-up Synthesis of **119**

The boronylation of **115** to **119** using PEPPSITM-SiPr^(R) had been previously found to deliver unpredictable yields of **119** with variable amounts of boronic acid **119a** and proto-deboronated byproduct **120**, from batch to batch. Swapping the PEPPSITM-SiPr^(R) catalyst for Pd(PPh₃)₄, keeping the number of equivalents of NEt₃ and HBpin to six relative to **115**, and heating at 100 °C for 18 h instead of using microwave irradiation was found to deliver **119** with reproducible yields of greater than 96%, with levels of **120** that were too low to be detected by LCMS (Scheme 72).



Scheme 72. Optimised route using **115** to access **119**. Reagents and conditions: (a) 6 equiv. HBpin, 10 mol% Pd(PPh₃)₄, 6 equiv. NEt₃, dioxane, 100 °C, 18 h, 96%.

An initial attempt to synthesise **119** applied boronylation conditions employed by Berdini *et al.* to synthesise intermediate **144b** from **144a** (which had a similar substructures to **119** and **115** respectively) towards FGFR inhibitors such as **144c** using *bis*(pinacolato)diboron (**Scheme 73**).¹³³ However, these conditions only led to proto-deborylated product **120**, with no desired intermediate **119**.



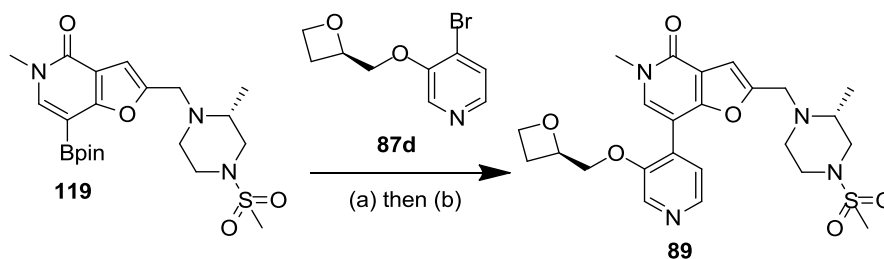
Scheme 73. Conditions employed by Berdini *et al.* to synthesise intermediate **144b** towards FGFR inhibitors such as **144c**.¹³³ Reagents and conditions: (a) (Bpin)₂, AcOK, Pd(dppf)Cl₂, dioxane, 80 °C, overnight, 29%.

Optimisation of conditions for the boronylation of **115** to **119** with minimal formation of **120** was therefore focussed on the use of pinacol borane instead of *bis*(pinacolato)diboron because pinacol borane had previously been successfully used to deliver **115**, even with unoptimised conditions. Murata *et al.* pioneered the palladium-catalysed borylation of aryl halides using pinacol borane to produce aryl boronates, and found that 1,1'-bis(diphenylphosphino)ferrocene with PdCl₂ was the best pre-catalyst/ligand combination.^{134,135} When used with excess NEt₃, this combination delivered the highest yield of aryl boronate with minimal proto-deboronylated product. Matos *et al.* later reported that using a larger excess of triethylamine (nine equivalents as opposed to three) gave more reproducible results.¹³⁶

The boronylation of **115** was initially attempted on a 50 mg scale using one to six equivalents of NEt₃, one to six equivalents of pinacol borane, 1 to 10 mol% of Pd(PPh₃)₄ or Pd(dppf)Cl₂, heating in dioxane at 100 °C for 2 to 18 h, using either microwave irradiation or a stirrer hotplate (experimentals not shown). Optimal conditions were found to deliver **119** in yields of greater than 86% using six equivalents of NEt₃ and pinacol borane and 10 mol% of Pd(PPh₃)₄. The time for heating did not seem to have an impact on yields, but heating using a stirrer hotplate instead of using microwave irradiation enabled larger batches of **119** to be produced. High yields were reproducible on a multigram scale and 5 to 10 g batches of **119** were initially produced, ready for coupling with **87d**.¹⁹ Although LCMS analysis indicated the presence of the boronic acid **119a**, ¹H NMR confirmed material was mainly boronate ester **119** (greater than 90%). Batches of **119** of up to 32 g were successfully produced using the optimised conditions on a standard stirrer hotplate.

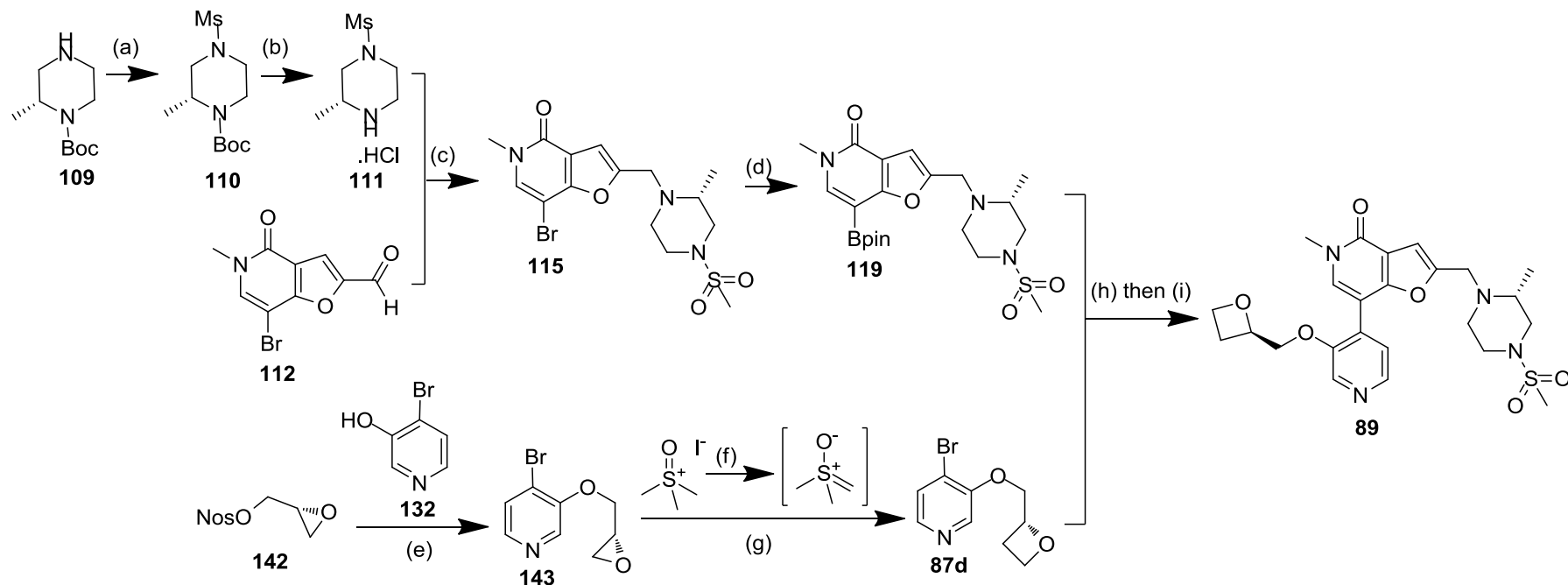
2.5.13.4. Scaled-up Suzuki Coupling to give **89**

Suzuki coupling conditions were used to couple boronate ester **119** with chiral bromo pyridine **87d**,¹⁹ then chiral HPLC was used to secure 11 g of **89** of greater than 97% purity (Scheme 74).¹³



Scheme 74. Suzuki coupling reaction between **119** and **87d** used to deliver **89**. Reagents and conditions: (a) 10 mol% Pd(PPh₃)₄, Cs₂CO₃, toluene/methanol, 100 °C, 38%;¹⁹ (b) chiral HPLC, 49%.¹³

Suzuki coupling conditions developed by Watson delivered 11 g of **89** in 38% yield.¹⁹ However, material was estimated to be at around 95% in purity and an unidentified impurity was found to be difficult to remove using normal phase chromatographic techniques. Another 11 g batch of **89** was produced of similar purity,¹⁹ and the combined batches purified by chiral HPLC with the help of colleagues¹³ to deliver an 11 g batch of **89** of greater than 97% purity which was ready for the dog safety assessment study. The enantiomeric purity of **89** was determined by chiral HPLC to be >99% ee, and the overall yield of this optimised route was 12% (**Scheme 75**), which is three times higher than the original yield of 4% (**Scheme 66**) that was achieved on a smaller scale.

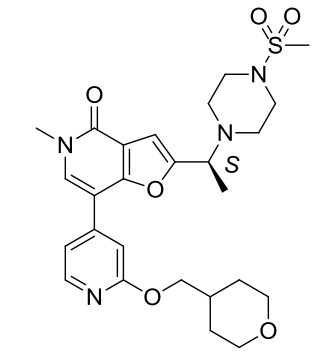
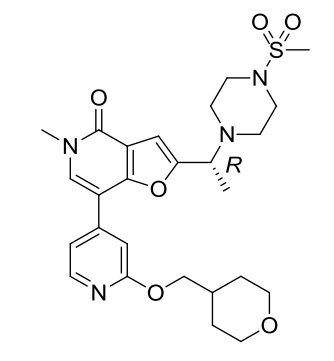
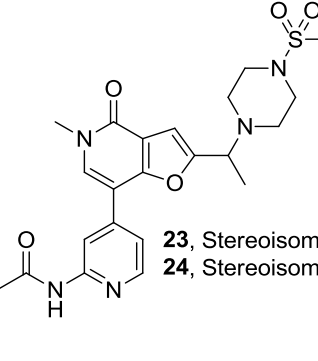
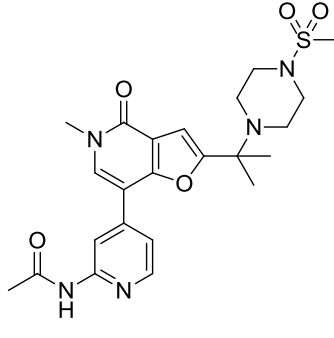
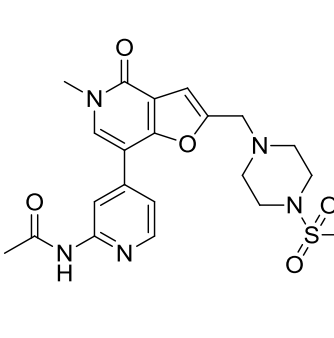
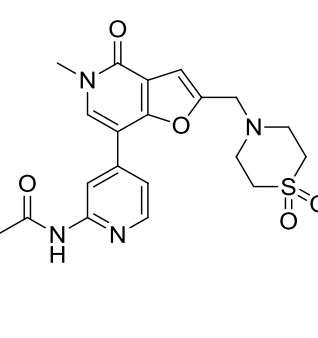
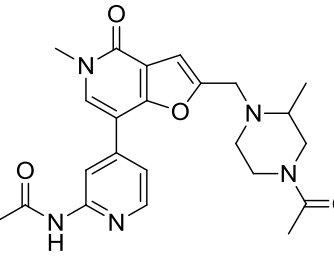
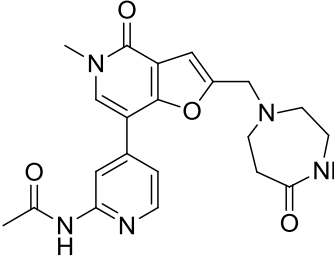
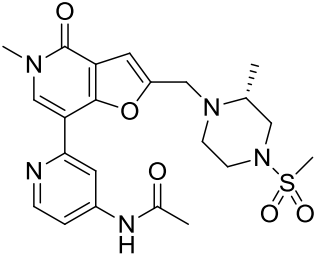
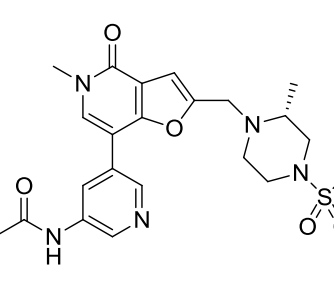
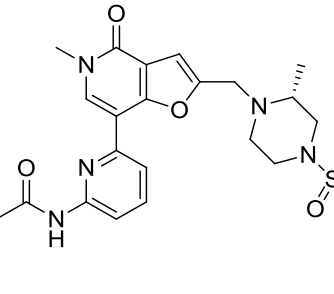
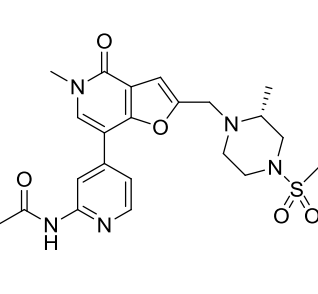


Scheme 75. Optimised scaled-up route that allowed delivery of 11 g batch of **89** of >97% purity ready for the dog safety assessment study in 12% overall yield. Reagents and conditions: (a) MsCl, 2 M NaOH_(aq), THF, 0 °C to room temperature, 20 h, 87%; (b) 4 M HCl in dioxane, DCM, 48 h, >99%; (c) NEt₃, 10 min, 2Me-THF, then NaBH(OAc)₃, 2 h, 75%; (d) 6 equiv. HBpin, 10 mol% Pd(PPh₃)₄, 6 equiv. NEt₃, dioxane, 100 °C, 18 h, 96%; (e) Cs₂CO₃, DMF, 16 h, 80%; (f) *t*BuOK, *t*BuOH, 60 °C, 10 min; (g) *t*BuOH, 80 °C, 4 h, 42% at 85% purity; (h) 10 mol% Pd(PPh₃)₄, Cs₂CO₃, toluene/methanol, 100 °C, 38%; (i) chiral HPLC purification, 49%.

2.6. Conclusions

The compounds in **Table 54** are discussed in the conclusions for Chapter 2 that follow.

iBET762	1	4
5	8	9
10	11	12
	 R = H, 14 Me, 15 Et, 16 iPr, 17	
13	14 to 17	18

		 <p>23, Stereoisomer 24, Stereoisomer</p>
20	21	23, 24
		
25	26	40
		
41	45	56
		
57	58	60

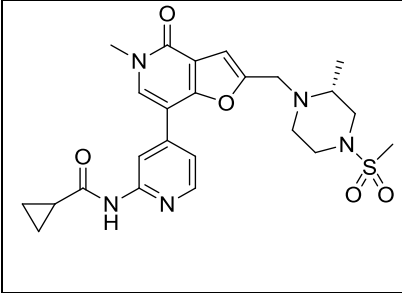
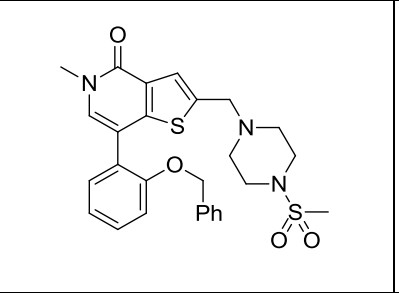
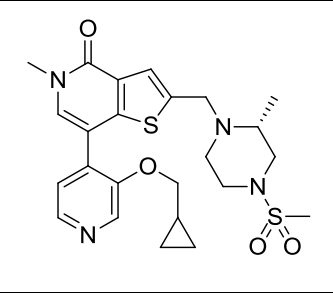
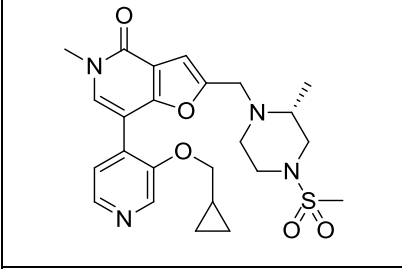
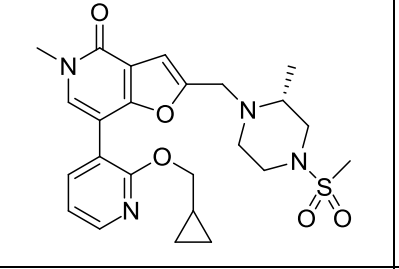
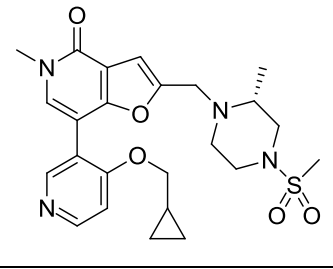
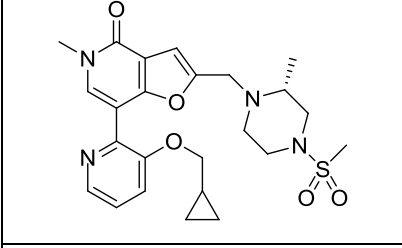
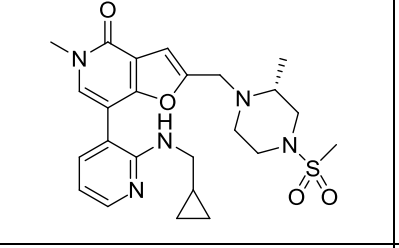
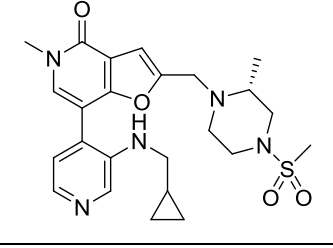
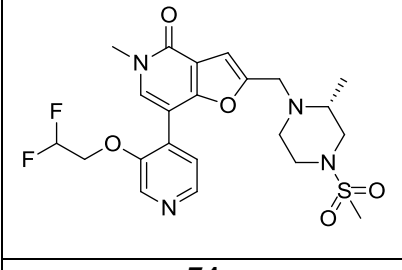
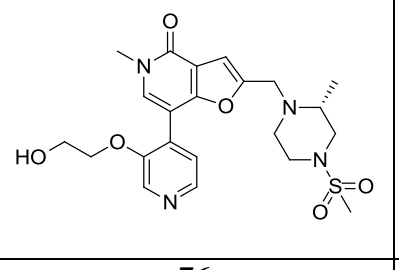
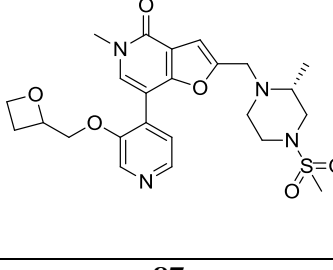
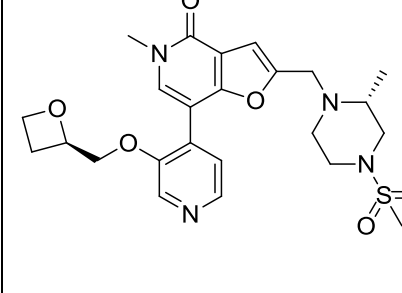
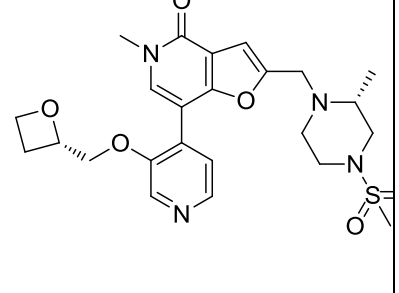
		
61	66	67
		
68	69	70
		
71	72	73
		
74	76	87
		
89	90	

Table 54. Compounds discussed in the conclusions for Chapter 2. Compounds **18** onwards were synthesised as part of the investigations described herein.

The *pan*-BET BRD inhibitor **iBET762** (**Figure 27**) was found by GSK to inhibit BD1 and BD2 of the BET family of BRDs that are involved in the regulation of gene transcription;^{1,2} inhibition of BET BRDs caused anti-proliferative and anti-inflammatory effects^{4,5} which could be useful for the treatment of cancers or autoimmune diseases, such as RA and SLE. The toxic effects observed in preclinical safety species (rat and dog) limited investigations into the use of *pan*-BET inhibitors to oncology indications, where the benefit to risk ratio is likely to be higher than for the treatment of chronic autoimmune diseases. Clinical trials are underway using **iBET762** as an experimental treatment of NUT midline carcinoma patients,³ and more recently in patients with other tumours.^{8,9}

It was thought that a selective inhibitor of one of the two BDs of the BET BRDs would have the potential to retain the beneficial anti-proliferative or anti-inflammatory effects of BET BRD inhibition observed using *pan*-BET BRD inhibitors, while also mitigating the toxic effects. An inhibitor with this profile could be used as a treatment for chronic autoimmune diseases, so a campaign to identify a novel BET BRD BD1 selective inhibitor that could be used to investigate potential toxicity in a dog safety study was initiated by the Epinova DPU.

A knowledge-based screen of around 1400 compounds using a BET BRD4 FP assay identified inhibitor **1** that had a novel TP substructure, and BET BRD2, BRD3, BRD4 and BRDT TR-FRET assays confirmed **1** had sub-micromolar potency *versus* BET BRD BD1s (**Table 28**).⁴² Importantly, **1** was also found to be >40-fold selective for BD1 over BD2 across the BET family of BRDs, which showed that selectivity for BD1 over BD2 could be achieved, and could be potentially improved using the extensive existing structural-based knowledge. Comparison of the BRD4 BD1 X-ray crystal structure of **1** with the *pan*-BET inhibitor **iBET762**,⁴⁴ suggested that BET BD1 potency could be improved by the addition of a lipophilic group at the aryl tail group which was in close proximity to the lipophilic WPF shelf because the chlorophenyl of **iBET762** seemed to be capable of making this interaction (**Figure 39**).

The methylpyridinone portion of the TP **1** was confirmed by X-ray crystallography⁴⁴ to act as an AcK mimetic by making key hydrogen-bond interactions in the BRD4 BD1 active site; similar interactions with Asp 140, and through water with Tyr 97, are also

made by *N*-acetylated histone tails (**Figure 39**). This is an essential event in the BRD-mediated process of reading the histone code at an epigenetic level, so inhibition was likely to have an effect on gene transcription, and subsequently on cell proliferation and inflammation.⁶ All subsequent X-ray crystal structures of TP compounds, and of the related FP series confirmed that the methylpyridinone portion was acting as an AcK mimetic.

An explanation for the selective inhibition of **1** for BET BD1 *versus* BD2 came from the the X-ray crystal structure of the BRD4 BD1 enzyme complex with **1**, when compared with the X-ray crystal structure of BRD4 BD2 (**Figure 40**): the headgroup piperazine methylsulfonamide moiety of **1** is likely to clash sterically with the bulky His 437 residue in BD2 which would lower BD2 potency; the equivalent residue in BD1 is Asp 144, which is less bulky than His 437 and therefore less likely to clash sterically. The incorporation of a methyl group at the 2-position of the piperazine headgroup was subsequently found to improve potency and selectivity in the TP series in the *R*-configured **5**. The *S*-stereoisomer **4** was less potent and less selective than the unsubstituted piperazine (**Table 29**). However, the introduction of a methyl group at the 2-position of the headgroup piperazine had an unpredictable effect on the FP series. The *des*-methyl FP analogue **8** was of similar potency and selectivity to the 2-Me *R*-stereoisomer **9**; however, the 2-Me *R*-stereoisomer **12** had marginally improved selectivity for BET BD1 *versus* BD2 and BRD9, and had substantially improved solubility relative to the *des*-methyl analogue **26** (**Table 40**), probably because the methyl group disrupted planarity and reduced the crystal packing energy.⁴⁷ The corresponding *S*-stereoisomer was not made in the FP series to determine if the headgroup SAR of the FP series was divergent from the TP series, and perhaps could be made in future investigations to complete the explanation.

The PFI of compounds made in the TP series was generally greater than six (e.g. **Table 30**), at the upper limit for drug-like compounds suggested by GSK guidelines.⁴⁵ By definition, a high PFI indicates a high lipophilicity which gives an indication of the potential developability issues that are more likely to be encountered for any given compound, such as toxicity or high *in vivo* clearance, both of which are usually a result of increased vulnerability to metabolising enzymes such as CYP450.⁴⁸ Replacement of

the thiophene substructure with the less lipophilic furan substructure to lower PFI led to the identification of the FP series.⁴⁶ FP compounds were found to be more potent and slightly more selective for BET BD1 *versus* BD2 compared with the corresponding TP analogues. The improved BET BD1 potency of the FP series *versus* the TP series may occur because substituents on the aryl tailgroup seem to interact favourably with the WPF shelf in the FP series, whereas the same substituents seem to instead point through the ZA channel in the TP series; this phenomenon can be seen clearly by comparing the X-ray crystal structures⁴⁴ of the TP **10** with the FP **11** (**Figure 41**) and the TP **13** with the FP **12** (**Figure 42**).

The first compound identified with a profile that exceeded the program team's original target profile for a BET BD1-selective probe (PBMC pIC₅₀ ≥ 6, selectivity of ≥ 50-fold for BET BD1 *versus* BD2, moderate clearance in the dog) was the TP **10** (**Table 31**). The corresponding FP analogue **11** was more potent and selective but had high clearance in the dog which was unexpected, considering that the PFI of **11** was much lower than TP **10**; the electron donor ability of the FP oxygen was likely to activate the adjacent benzylic position towards metabolic oxidation compared with the TP sulfur, thereby increasing clearance. Unfortunately **10** produced *pan*-BET like toxicities in a 14 day dog safety study.⁷ One hypothesis advanced to explain the observed toxicity was that the compound was an equipotent inhibitor of BRD9, so subsequent lead optimisation efforts focussed on finding a more selective compound with low to moderate clearance for another dog safety study. The new target profile (**Table 33**) was substantially more stringent than the original target profile. Investigations into both the TP and FP series were undertaken initially because the TP series seemed to have superior PK profiles to the FP, whereas the FP series seemed to have a superior potency and physicochemical profile to the TP series. After a number of optimisation steps, the FP **12** (**Table 32**) was identified; FP **12** met or exceeded target values for all parameters, except for selectivity for BET BD1 *versus* BRD9. The dog *in vivo* clearance was also moderate-to-high, and **12** became an additional lead for optimisation.

CYP450-mediated metabolism is responsible for the clearance of around 70 to 80% of marketed drugs and was therefore the most likely route of clearance of the FP and TP compounds.⁴⁹ GSK is actively reducing the numbers of animals involved in research⁵³

so all compounds were pre-screened using liver microsome IVC assays.⁵⁴ Liver microsomes contain membrane-bound metabolising enzymes such as CYP450;⁵⁵ only compounds with low IVC clearance were progressed to *in vivo* studies. Meteor®⁶⁰ and Metasite®⁶¹ software was used to identify⁶² four main sites of the TP and FP templates, represented by **10** and **12** respectively (**Figure 43**), that were most likely to undergo *N*-dealkylation by CYP450-mediated metabolism through HAT or SET mechanisms.⁶⁴ The following order of probability was established (highest probability first): 1, the *N*-methyl position of the *N*-methyl pyridinone; 2, the benzylic carbon; 3, and 4, the piperazine carbons of the headgroup. Two main approaches were employed in order to reduce metabolism at these sites; these were removal/replacement of metabolically liable group with a less labile group, or steric blocking of those positions with a metabolically less liable group.

Removal of the *N*-Me group of the *N*-Me pyridinone AcK mimetic to give **14** (**Table 36**), or replacement with other groups, Et (**16**) and *i*Pr (**17**), was undertaken by a colleague who aimed to identify a BRD9 inhibitor in an analogous TP series that bound to the BRD4 BD1 active site in the same way as BET BD1 TP compounds;⁶⁶ the SAR confirmed that the methyl group (**15**) was the optimal substituent. Replacement with CD₃ (**18**),¹⁸ which was likely to be more resistant to metabolism due to the KIE,⁶⁷ allowed retention of BET BD1 potency, PBMC potency, and selectivity for BET BD1 *versus* BD2 and BRD9 (the latter slightly improved) (**Table 37**). However, IVC_{rat} was not reduced, possibly due to metabolic switching in which the suppression of metabolism at the *N*-Me position leads to promoted metabolism at another site.⁷⁵

The benzylic position of the FP and TP templates was the next most metabolically liable position. The vulnerability of this site to metabolism was anticipated to be lowered by the introduction of deuterium due to the KIE,⁶⁷ or by the introduction of one methyl group or two methyl groups due to additional steric clashes with the active sites of metabolising enzymes, or due to the complete removal of the vulnerable benzylic hydrogens.^{76,77} The introduction of methyl groups was investigated, but deuteration was not undertaken and could potentially be investigated in future studies; however, the deuterated analogue was not guaranteed lower clearance because metabolic switching may occur. The introduction of one or two lipophilic methyl groups was only

investigated in the FP series, as opposed to the TP series, because the FP series offered a less lipophilic starting point than the TP series.

The introduction of a single methyl group at the benzylic position of **11** to give the *S*-stereoisomer **20** and the *R*-stereoisomer **21**, retained BET BD1 potency but intriguingly improved selectivity for BD1 *versus* BRD9, particularly for **21** which was >200-fold more selective (**Table 38**). Similarly, the introduction of a single methyl group at the benzylic position of **12** to give the two unresolved stereoisomers **23** and **24**, raised the selectivity for BD1 *versus* BRD9 to >200-fold (**Table 39**); the introduction of two methyl groups to give **25** further improved selectivity to >1000-fold. A hypothesis for the improved BET BD1 selectivity *versus* BRD9 came from the X-ray crystal structure of **21** bound in the active site of BRD4 BD1 overlaid with a BRD9 X-ray crystal structure (**Figure 45**).⁴⁴ This showed the methyl group of **21** to be in close proximity to a protein loop of BRD9 which may clash sterically, thus reducing binding affinity of **21** to BRD9 relative to **11**. X-ray crystal structures of **20** and **23-25** were not available due to lack of material, but by inference, the methyl groups of **20** and **23-25** were likely to be positioned in closer proximity to the BRD9 loop, thereby introducing increased steric clashes with BRD9 relative to **11** and **12**, and further reducing affinity for BRD9. Unfortunately the IVCs of the mono- and di-methylated analogues of **11** or **12** were higher, probably because the extra methyl groups increased ChromLogD_{7.4}; the increased lipophilicity was likely to increase affinity to metabolising enzymes such as CYP450.^{45,48,85}

In order to optimise BET BD1 potency and selectivity *versus* BD2 and BRD9 and reduce the propensity for metabolism at the piperazine headgroup, an array of analogues of **12** with alternative headgroups was synthesised (**27-48**, **Table 41**). Each was designed to have drug-like physico-chemical properties (MW <500, cPFI <6);⁷⁸ headgroups that either lacked or contained the potential to make a hydrogen bond with Ile 146 in BET BD1 in a similar manner to the S=O of the piperazine methylsulfonamide of **12** were included. Only three compounds with PFIs lower than **12** and headgroups capable of making this hydrogen bond achieved a BRD4 BD1 pIC₅₀ in the TR-FRET assay of around 7.0; these were the sulfone **40**, the piperazine acetamide **41** and the diazepanone **45**. The X-ray crystal structure of **41**⁴⁴ bound in the BRD4 BD1

active site (**Figure 47**) clearly showed that the acetamide oxygen acted as hydrogen bond acceptor to the NH of Ile 146 in the same manner as the S=O of the methylsulfonamide. However, **41** may be less potent than **12** because the tailgroup acetamide may be positioned less favourably to interact with the WPF shelf. The three compounds, **40**, **41** and **45**, were too low in PBMC potency, particularly **41**, which had a pIC₅₀ of 5.4. One further attempt to optimise the headgroup was undertaken in which a small array of compounds that contained alternative headgroups with structures based on the most potent compounds from the first headgroup array, **40** and **45**, and that had reduced PFI relative to **12**, was made. These were **49-51** and **52-55** (**Table 42**). Although lower in lipophilicity, none of these compounds with alternative headgroups offered either sufficiently improved potency or selectivity relative to the original 2-Me piperazine methylsulfonamide headgroup present in **12**.

The aryl tailgroup of **12** had a nitrogen in the 4-position, as shown in **Table 43**, which according to the X-ray crystal structure (**Figure 42**)⁴⁴ was exposed to solvent and not involved in binding to the active site of BRD4 BD1. Placement of the nitrogen in alternative positions of the aryl tailgroup was undertaken to investigate the effect on IVC (compounds **56-58**, **Table 43**) in order to lower *in vivo* clearance.⁷⁹ The 2-position analogue **56** was not made due to a number of synthetic issues but was unlikely to offer much of an advantage over **12** because the compounds were of similar lipophilicity, and like **12**, a position adjacent to the nitrogen remained available for oxidative metabolism. Although placement of nitrogen in the 3-position to give **57** would leave two adjacent sites open to oxidation, it was unknown if the reduction in lipophilicity would lower the compound's propensity to metabolism; however this compound was of too low potency in the PBMC assay, probably because the permeability was low. It was anticipated that placement of the nitrogen in the 6-position had the potential to reduce clearance by blocking access of metabolising enzymes to both positions adjacent to the nitrogen. The 6-position regioisomer **58** offered a reduction in IVC_{rat} and a tentative reduction in IVC_{dog}, but increased IVC_{human} and was lower in potency and selectivity for BET BD1 *versus* BRD9. The increased lipophilicity of **58** relative to **12** was thought to be likely to counteract the effect of blocking metabolism at this point by making the compound more susceptible to metabolism elsewhere on the molecule. Compound **12** therefore remained the lead compound on which optimisation was focussed.

A potential route of metabolism of **12** is hydrolysis of the aryl tailgroup acetamide by amidases that are present in microsomes.⁸⁰ A set of amides in both the FP series (**59-61**, and **65**, **Table 44** and **Table 45**) and the TP series (**62-64**, **Table 44**) were made to attempt to lower susceptibility to metabolism by varying steric bulk at this position. Whereas the PBMC potencies of the TPs **62-64** were too low, the ethylacetamide FP **60** and the cyclopropylamide FP **61** offered similar or improved PBMC potency to **12**; however, both compounds had substantially reduced selectivity for BET BD1 *versus* BRD9 and so were not progressed to IVC assays.

A second insight into the potential to achieve selectivity for BET BD1 *versus* BRD9 came from the *ortho*-substituted benzyloxy compound **66** which was the first TP found to be ≥ 100 -fold more selective for inhibition of BRD4 BD1 *versus* BRD9 (**Table 46**). However, considerable improvement in PBMC potency and selectivity *versus* BD2 was required to meet target values required for a compound to be progressed to the dog safety study (**Table 33**). A substantial reduction in lipophilicity was also likely to be required, and was achieved with the introduction of a nitrogen at the 4-position of the aryl tailgroup, which was known from SAR to be tolerated, and replacement of the benzyloxy substituent with a less lipophilic, but semi-aromatic cyclopropyloxy substituent to give **67**.⁸¹ The equivalent FP analogue **68** was also made; both **67** and **68** were highly potent with BET BD1 potencies at the TBLs of the TR-FRET assays, and both were very selective for BET BD1 *versus* BRD9 (>316 -fold). Selectivity for BET BD1 *versus* BD2 and BRD9 based on the TR-FRET assays⁴³ was underestimated because compounds were at TBL, and SPR⁸⁴ confirmed that the compounds had BRD4 BD1 pIC₅₀s closer to 9 with >100 -fold selectivity *versus* BET BD2. Unfortunately both compounds had high IVC_{dog}, so efforts focussed on reducing lipophilicity of the template to reduce affinity to metabolising enzymes.⁴⁸

An X-ray crystal structure of **68** bound to the BRD4 BD1 active site (**Figure 49**) showed that the lipophilic *ortho*-(cyclopropyl)methyl ether substituent interacted favourably with the lipophilic WPF shelf; favourable lipophilic contacts such as this have been estimated to contribute 0.71 kcal per mol Å² to binding energy³⁷ and could explain the high BET BD1 potency. The increased selectivity of **68** for BET BD1 *versus* BRD9 was evident from an overlay of the X-ray crystal structure of **68** bound in BRD4

BD1⁴⁴ with a ligandless structure of BRD9 (**Figure 50**): the *ortho*-(cyclopropyl)methyl ether substituent was likely to clash with the bulky Tyr 106 residue in BRD9, but not with the equivalent and less bulky Ile 146 substituent in BD1 which would disfavour binding in the BRD9 active site. The Ile 146 also made a hydrogen bond with the S=O in the headgroup in BRD4 BD1, which would increase BRD4 BD1 potency, thus increasing selectivity for BET BD1 *versus* BRD9. The lipophilic *ortho*-(cyclopropyl)methyl ether substituent was also likely to interact favourably with the WPF shelf of BD1 which does not exist in BRD9, and would further improve BRD4 BD1 potency and selectivity for BRD4 BD1 over BRD9.

Lead optimisation steps therefore focussed on exploring three potential methods of reducing IVC of **68** by replacing or moving metabolically liable structural features on the pyridyl tailgroup;⁷⁷ these were 1, variation of the position of the nitrogen in the pyridyl ring;⁵¹ 2, replacement of the *ortho*-linker oxygen atom with a less electronegative atom than oxygen, or 3, replacement of the (cyclopropyl)methyl substituent with an alternative to lower lipophilicity.^{45,85} Investigations were limited to the FP series which offered a starting point that was lower in lipophilicity, and tended to be more potent and selective than the TP series.

Synthesis of the analogue **69** with the tailgroup pyridyl nitrogen in the 3-position, as defined in **Table 47**, proved problematic and was abandoned because the predicted lipophilicity of **69** was higher than the 4-position analogue **68**, and so was likely to have increased IVC. Compound **70**, with the nitrogen in the 5-position, was chemically unstable and therefore was not suitable for progression. Compound **71**, with the pyridyl nitrogen in the 6-position, exceeded target values for PBMC and selectivity for BET BD1 over BD2 and BRD9 but had increased IVC_{dog} relative to **68**. Replacement of the electron-rich oxygen linker with a nitrogen linker gave the 3-*aza* and 4-*aza* analogues **72** and **73** (**Table 48**) which also exceeded target values for PBMC and selectivity for BET BD1 *versus* BD2 and BRD9, but also had higher IVC_{dog} relative to **68**.

The final attempt to improve the IVC of **68** involved the replacement of the *ortho*-(cyclopropyl)methyl ether tailgroup substituent with an alternative lower lipophilicity substituent. In house BioDig software⁸⁶ was used to mine the substantial amount of IVC data present in the GSK databases and was then used to determine what potential

replacement substituents to cyclopropylmethyl ether groups had been shown to reduce IVC using a MMP approach.⁸⁸ The BioDig software did not offer an option to mine the IVC_{dog} dataset, so IVC_{human} was used as a surrogate data set. Four alternative *ortho*-substituents were suggested using BioDig which were incorporated into the FP template to make compounds **74-77** (Table 49); all four compounds had lower IVC_{dog} than **68** which justified the use of IVC_{human} as a surrogate for IVC_{dog} and confirmed the MMP approach to be appropriate in this case. Only **74** and **76** had an IVC_{dog} that approached the target value, but these compounds were not selective enough to progress to a dog PK study.

A further set of 11 compounds was made with alternative substituents to cyclopropylmethyl ether substituents (**78-88**, Table 50) which lowered lipophilicity but still had the potential to interact with the lipophilic WPF shelf. A general trend was observed in which IVC_{dog} decreased with decreasing lipophilicity, which reinforced the reported hypothesis that metabolising enzymes that are found in microsomes, such as CYP450s, have higher affinity for compounds which are more lipophilic.^{45,48,85}

The 2-methyl oxetane **87** met all the new target values for potency, selectivity and IVC_{dog} (Table 33); the racemate **87** was therefore separated using chiral HPLC⁸⁹ into constituent stereoisomers, **89** and **90**, which were fully profiled individually (Table 51) and later determined by BRD4 BD1 X-ray crystallography (Figure 53)⁴⁴ to be the *R,R*- and *R,S*-stereoisomers respectively. The *R*-2-methyloxetane **89** had moderate dog clearance, whereas the *S*-2-methyloxetane **90** had high clearance. Both **12** and **89** were profiled further using the in house eXP and BROMOScan^{®91} assays (Figure 55). Gratifyingly the overall profile of **89** was superior to that of **12** (Figure 56), and exceeded target values for progression to the 14-day dog safety study.

A six step synthetic route that employed a Corey-Chaykovsky step to the chiral oxetane tailgroup, and improved boronylation conditions, was developed. With the help of colleagues,^{14,19} 11 g of **89** of greater than 97% purity was secured for use in the dog safety study; this development work led to an improvement in overall yield of **89** (12%) by three-fold relative to an existing route (4%).

The dog safety study aimed to determine whether selective BET BRD BD1 inhibition could be beneficial for the chronic treatment of autoimmune diseases without the toxic effects seen with *pan*-BET inhibitors. The study showed sufficient exposure to the selective BET BD1 inhibitor **89** had been achieved, and while no conclusive cardiovascular issues were observed, testicular changes in a number of animals were attributed to BET BRD BD1 inhibition. The testicular changes were milder in severity than those seen with *pan*-BET inhibitors, which suggested a greater benefit to risk ratio could be potentially achieved with another generation of BET BRD BD1 inhibitors with an improved profile, for example, with even higher selectivity for BD1 *versus* BD2.^{7,21,22} The Epinova DPU has used learnings from this work to inform the BET inhibitor franchise and has since refocussed efforts on the development of highly selective BET BRD BD2 inhibitors, with the aim of identifying treatments for immunoinflammatory diseases.

2.7. Future Work

This work successfully delivered the first potent and highly selective BET BRD BD1 inhibitor, **89** (Table 51), which had a suitable PK profile to progress to a dog safety study. The study showed at least some of the BET-related toxicity previously observed with *pan*-BET inhibitors such as **iBET762** (Figure 27), could be attributed to BET BRD BD1 inhibition. The roles of individual BET BRD binding domains in biological processes are still being elucidated, but their likely therapeutic applications are expected to be wide reaching, from cancer to RA. The challenge remains to develop more selective inhibitors to probe the role of each BET BRD binding domain; for example, eight different selective inhibitors would be required to probe the roles of each BET bromodomain (BRD2 BD1, BRD2 BD2, BRD3 BD1, BRD3 BD2, BRD4 BD1, BRD4 BD2, BRDT BD1 and BRDT BD2) in isolation. The binding site of bromodomains that recognises AcK and AcK-mimetics is highly conserved, and although a small number of residue differences exist that could be exploited to obtain selectivity with a small molecule inhibitor,⁴¹ selectivity between bromodomains is still to be achieved; further research towards this goal is therefore required.

Meteor®⁶⁰ and MetaSite®⁶¹ software was used to identify⁶² likely points of metabolic vulnerability on the two templates that could be removed or replaced to improve clearance using a knowledge- and CYP450 docking-based approach respectively. However, when point changes were made to increase metabolic stability, for example replacement of an *N*-Me with *N*-CD₃ (compounds **12** and **18** respectively, Table 37) to take advantage of the KIE effect,⁶⁷ no improvement in IVC_{rat} was observed possibly because **18** was subject to metabolic switching to another part of the molecule that was metabolically more vulnerable.⁷⁵ The chance of lowering clearance on any template could potentially be increased by the introduction of deuterium into *all* the positions that had the highest metabolic liability, which was an approach that was used successfully by Auspex to improve the human PK profile of Wyeth's blockbuster anti-depression drug venlafaxine to give SD-254 (Figure 44).^{73,74} By extrapolation the poly-deuteration approach could be applied retrospectively to any compound that has failed in the drug development process due to poor PK. Similarly compounds that were more potent and selective than **89** but had IVC too high to progress to the dog safety study could be

poly-deuterated to improve clearance and offer alternatives to **89**; two such compounds are **68** and **78** (Table 50) which could be poly-deuterated to **92** and **93** respectively (Figure 59). Potential drawbacks to this approach would be high cost of goods, and metabolic switching to other points of the molecule.

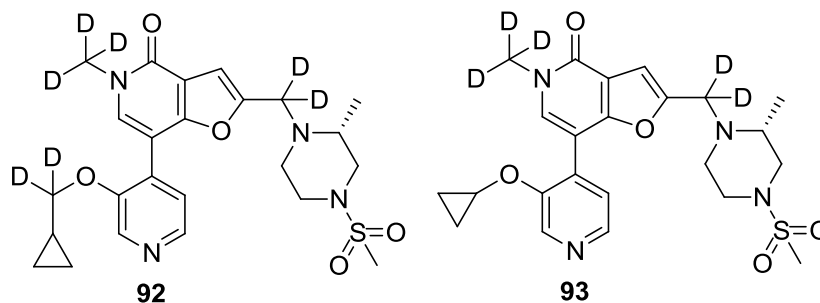


Figure 59. Structures of proposed deuterated analogues **92** and **93** that could have a lower clearance than the parent analogues **68** and **78** respectively.

The inhouse BioDig software was used to mine IVC data in the GSK database to identify alternative substituents to the cyclopropylmethyl ether of **68** that were likely to enable a reduction in IVC. Data for IVC_{dog} could not be included in the MMP searches, so IVC_{human} was used as a surrogate which led to the successful identification of compounds **74-77** (Table 49) that had lower IVC_{dog} than **68**. The software could be made more powerful if IVC_{dog} data was integrated into the searches because these data are likely to be more relevant in instances where a template's dog PK profile is being improved. This approach could be made more powerful still if the size of IVC datasets for each species could be increased; although this will happen with time as more and more compounds are tested for IVC, the process could be accelerated with the pooling of knowledge from other pharmaceutical companies and academic institutions. This proposal would have a number of obstacles to overcome before it could become reality, in particular the standardisation of assays and methods, and concerns with the potential disclosure of intellectual property to other parties. However, such a comprehensive database could have a huge positive impact on accelerating the drug discovery process.

2.8. General Methods

All animal studies performed as part of this research were ethically reviewed and carried out in accordance with Animals (Scientific Procedures) Act 1986 and the GSK Policy on the Care, Welfare and Treatment of Animals. Human biological samples were sourced ethically and their research use was in accord with the terms of the informed consents.

2.8.1. Analytical Methods

2.8.1.1. Nuclear Magnetic Resonance Methods

^1H , ^{13}C and ^{15}N Nuclear Magnetic Resonance (NMR) spectra were recorded using Bruker AVI or AVII NMR instruments. ^1H NMR spectra were recorded at 300 MHz, 400 MHz or 600 MHz, referenced to tetramethylsilane and internally referenced to the residual solvent peak. ^{13}C NMR spectra were recorded at 101 MHz, 126 MHz or 151 MHz, referenced to the residual solvent peak. ^{15}N NMR spectra were recorded at 60 MHz referenced to the ^{15}N chemical shift of liquid ammonia.

2.8.1.2. Infra-red Spectrometry Methods

Infrared (IR) spectra were generated using a Perkin Elmer Spectrum One FT-IR spectrometer with an Attenuated Total Reflectance (ATR) accessory.

2.8.1.3. Melting Points

Melting points were generated using Stuart SMP10 Bibby Scientific Ltd. melting point apparatus.

2.8.1.4. Liquid Chromatography Mass Spectrometry Methods

Method A

Liquid Chromatography Mass Spectrometry (LCMS) was conducted on an Acquity ultra performance liquid chromatography (UPLC) ethylene bridged hybrid (BEH) C18 column (50 mm x 2.1 mm in dimensions, 1.7 μm packing diameter) at 40 degrees centigrade, eluting with 0.1% v/v solution of formic acid in water (Solvent A) and 0.1% volume to volume (v/v) solution of formic acid in acetonitrile (Solvent B) using the

following elution gradient 0 to 1.5 min 3 to 100% B, 1.5 to 1.9 min 100% B, 1.9 to 2.1 min 3% B at a flow rate of 1 ml/min. The ultraviolet (UV) detection was a summed signal from wavelength of 210 nm to 350 nm. The mass spectra were recorded on a Waters ZQ Mass Spectrometer using Alternate-scan Positive and Negative Electrospray.

Method B

LCMS was conducted on an Halo C18 column (150 mm x 50 mm in dimensions, 5 µm packing diameter) at ambient temperature, then elution with 0.1% v/v solution of formic acid in water (Solvent A) and 0.1% v/v solution of formic acid in acetonitrile (Solvent B) using an elution gradient of between 5 and 95% Solvent B over over 2.5 min using a flow rate of 1.8 mL/min. The UV detection was an averaged signal from wavelength of 210 nm to 350 nm. The mass spectra were recorded on an Agilent 1200-6110 Mass Spectrometer.

Method C

Liquid Chromatography Mass Spectrometry (LCMS) was conducted on an Acquity ultra performance liquid chromatography (UPLC) ethylene bridged hybrid (BEH) C18 column (50 mm x 2.1 mm in dimensions, 1.7 µm packing diameter) at 40 degrees centigrade, eluting with 10 mM ammonium hydrogen carbonate in water adjusted to pH 10 with ammonia solution (Solvent A) and acetonitrile (Solvent B) using the following elution gradient 0 to 1.5 min 1 to 97% B, 1.5 to 1.9 min 97% B, 1.9 to 2.0 min 100% B at a flow rate of 1 ml/min. The ultraviolet (UV) detection was a summed signal from wavelength of 210 nm to 350 nm. The mass spectra were recorded on a Waters ZQ Mass Spectrometer using Alternate-scan Positive and Negative Electrospray.

2.8.1.5. Mass Directed Autopreparative Spectrometry Methods

Method A

Mass directed autopreparative spectrometry (MDAP) involved purification by HPLC using a Sunfire C18 column (150 mm x 30 mm in dimensions, 5 µm packing diameter) at ambient temperature, then elution with 0.1% formic acid in water (Solvent A) and 0.1% formic acid in acetonitrile (Solvent B) using an elution gradient of between 0 and 100% Solvent B over 15 or 25 minutes. The UV detection was an averaged signal from

wavelength of 210 nm to 350 nm. The mass spectra were recorded on a Waters ZQ Mass Spectrometer using Alternate-scan Positive and Negative Electrospray.

Method B

An Agilent 1100 Liquid Chromatograph equipped with a model G1367A autosampler, a model G1312A binary pump and an HP1100 model G1315B diode array detector was used. All separations were achieved using a Phenomenex Luna C18(2) reversed phase column (100 x 2.1 mm, 3 µm particle size). Gradient elution was carried out with the mobile phases as (Solvent A) water containing 0.1% (v/v) formic acid and (Solvent B) acetonitrile containing 0.1% (v/v) formic acid. The conditions for the gradient elution were initially 5% B, increasing linearly to 100% B over 6 minutes, remaining at 100% B for 2.5 minutes then decreasing linearly to 5% B over 1 minute followed by an equilibration period of 2.5 minutes prior to the next injection. The flow rate was 0.5 mL/min, temperature controlled at 35 °C with an injection volume of between 2 to 5 µL. All samples were diluted with DMSO (99.9%) prior to LC/MS analysis.

Method C

Mass directed autopreparative spectrometry (MDAP) involved purification by HPLC using either an XBridge C18 column (150 mm x 30 mm in dimensions, 5 µm packing diameter), or a Sunfire C18 column (150 mm x 30 mm in dimensions, 5 µm packing diameter), at ambient temperature, then elution with 10 mM ammonium bicarbonate in water adjusted to pH 10 with ammonia solution (Solvent A) and acetonitrile (Solvent B) using an elution gradient of between 0 and 100% Solvent B over 15 or 25 minutes. The UV detection was an averaged signal from wavelength of 210 nm to 350 nm. The mass spectra were recorded on a Waters ZQ Mass Spectrometer using Alternate-scan Positive and Negative Electrospray.

Method D

Mass directed autopreparative spectrometry (MDAP) involved purification by HPLC using a Sunfire C18 column (150 mm x 30 mm in dimensions, 5 µm packing diameter) at ambient temperature, then elution with 0.1% v/v solution of TFA in water (Solvent A) and 0.1% v/v solution of TFA in acetonitrile (Solvent B) using an elution gradient of

between 0 and 100% Solvent B over 15, 25 or 32 minutes. The UV detection was an averaged signal from wavelength of 210 nm to 350 nm. The mass spectra were recorded on a Waters ZQ Mass Spectrometer using Alternate-scan Positive and Negative Electrospray.

Method E

Mass directed autopreparative spectrometry (MDAP) involved purification by HPLC using a Waters CSH C18 column (150 mm x 30 mm in dimensions, 5 µm packing diameter) at ambient temperature, then elution with 10 mM ammonium bicarbonate in water adjusted to pH 10 with ammonia solution (Solvent A) and acetonitrile (Solvent B) using an elution gradient of between 0 and 100% Solvent B at a flowrate of 40 mL/min. The UV detection was an averaged signal from wavelength of 210 nm to 400 nm. The mass spectra were recorded on a Waters ZQ Mass Spectrometer using Alternate-scan Positive and Negative Electrospray

2.8.1.6. Preparative HPLC Method

Preparative HPLC involved purification by HPLC using a Gilson Gemini column (150 mm x 21 mm in dimensions, 5 µm packing diameter) at a flow rate of 20 mL per minute at ambient temperature, then elution with 0.1% formic acid in water (Solvent A) and 0.1% formic acid in acetonitrile (Solvent B) with an elution gradient of between 0 and 100% Solvent B over up to 20 minutes. The UV detection was 214 nm.

2.8.1.7. Chiral HPLC Analysis

Chiral HPLC analysis was performed using a Chiralpak IA column (4.6 mm x 25 cm). The sample was injected onto the column and eluted with 40% EtOH/hexane at a flowrate of 1 mL/min. The UV detection was 215 nm.

2.8.1.8. Chiral HPLC Purification

Method A

Chiral HPLC involved purification by HPLC using a Chiralpak IA column (20 mm 5 x 20 cm). The sample was injected onto the column and eluted with MeOH at a flowrate of 118 mL/min. The UV detection was 230 nm.

Method B

Chiral HPLC involved purification by HPLC using a Chiralpak IA column (30 mm x 25 cm). The sample was injected onto the column and eluted with 40% EtOH/hexane at a flowrate of 30 mL/min. The UV detection was 215 nm.

2.8.1.9. High Resolution Mass Spectrometry

Positive ion mass spectra were acquired as accurate mass centroided data using a Micromass Q-ToF Ultima hybrid quadrupole time-of-flight mass spectrometer, equipped with a Z-spray (ESI) interface, over a mass range of 100 to 1100 Da, with a scan time of 0.9 s and an interscan delay of 0.1 s. Reserpine was used as the external mass calibrant ($[M+H]^+ = 609.2812$ Da). The Q-ToF Ultima mass spectrometer was operated in W reflectron mode to give a resolution (FWHM) of 16,000 to 20,000. Ionisation was achieved with a spray voltage of 3.2 kV, a cone voltage of 100 V, with cone and desolvation gas flows of 10 to 20 and 600 L/h respectively. The source block and desolvation temperatures were maintained at 120 °C and 250 °C respectively. The elemental composition was calculated using MassLynx v4.1 for the $[M+H]^+$ and the mass error quoted as ppm.

2.8.2. Assay Methods

2.8.2.1. BRD2/3/4/T Time Resolved Fluorescence Resonance Energy Transfer (TR-FRET) Assay⁴³

Binding to BRD2/3/4/T BD1 and BD2 was assessed using a time resolved fluorescent resonance energy transfer binding assay. This utilises a 6-His purification tag at the *N*-terminus of the proteins as an epitope for an anti-6-His antibody labeled with Europium chelate (PerkinElmer AD0111) allowing binding of the Europium to the proteins which acts as the donor fluorophore. A small molecule, high affinity binder of the bromodomains BRD2, BRD3, BRD4 and BRDT, compound **iBET762** (**Figure 27**) was labeled with Alexa Fluor647 to give **1a** (**Figure 38**), which acted as the acceptor in the FRET pair.

Assay Principle

In the absence of a competing compound, excitation of the Europium causes the donor to emit at 615 nm which excites the Alexa labelled bromodomain binding compound leading to an increased energy transfer that is measurable at 665 nm. In the presence of a sufficient concentration of a compound that can bind these proteins, the interaction is disrupted leading to a quantifiable drop in fluorescent resonance energy transfer.

The binding of the compounds to bromodomains BRD2, BRD3, BRD4 and BRDT was assessed using mutated proteins to detect differential binding to either Binding Domain 1 (BD1) or Binding Domain 2 (BD2) on the bromodomain. These single residue mutations in the acetyl lysine binding pocket greatly lower the affinity of the fluoroligand **1a** for the mutated domain (>1000 fold selective for the non-mutated domain). Therefore in the final assay conditions, binding of the fluoroligand to the mutated domain cannot be detected and subsequently the assay is suitable to determine the binding of compounds to the single non-mutated bromodomain.

Protein Production

Recombinant Human Bromodomains [(BRD2 (1-473) (Y113A) and (Y386A), BRD3 (1-435) (Y73A) and (Y348A) BRD4 (1-477) (Y97A) and (Y390A) and BRDT (1-397) (Y66A) and (Y309A)] were expressed in *E. coli* cells (in pET15b vector for BRD2/3/4 and in pET28a vector for BRDT) with a 6-His tag at the *N*-terminal. The His-tagged Bromodomain pellet was resuspended in 50 mM HEPES (pH 7.5), 300 mM NaCl, 10 mM imidazole and 1 µL/mL protease inhibitor cocktail and extracted from the *E. coli* cells using sonication and purified using a nickel sepharose high performance column, the proteins were washed and then eluted with a linear gradient of 0 to 500 mM imidazole with buffer 50 mM HEPES (pH 7.5), 150 mM NaCl, 500 mM imidazole, over 20 column volumes. Final purification was completed by Superdex 200 preparative grade size exclusion column. Purified protein was stored at -80°C in 20 mM HEPES pH 7.5 and 100 mM NaCl. Protein identity was confirmed by peptide mass fingerprinting and predicted molecular weight confirmed by mass spectrometry.

Protocol for Bromodomain BRD2, 3, 4 and T, BD1 + BD2 Mutant Assays

All assay components were dissolved in buffer composition of 50 mM HEPES pH7.4, 50 mM NaCl, 5% glycerol, 1 mM DTT and 1 mM CHAPS. The final concentration of bromodomain proteins were 10 nM and the Alexa Fluor647 ligand was at K_d . These components were premixed and 5 μ L of this reaction mixture was added to all wells containing 50 nL of various concentrations of test compound or DMSO vehicle (0.5% DMSO final) in Greiner 384 well black low volume microtitre plates and incubated in dark for 30 minutes at room temperature. 5 μ L of detection mixture containing 1.5 nM final concentration anti-6-His Europium chelate was added to all wells and a further dark incubation of at least 30 minutes was performed. Plates were then read on the Envision platereader, ($\lambda_{ex} = 317$ nm, donor $\lambda_{em} = 615$ nm; acceptor $\lambda_{em} = 665$ nm; Dichroic LANCE dual). Time resolved fluorescent intensity measurements were made at both emission wavelengths and the ratio of acceptor/donor was calculated and used for data analysis. All data was normalised to the mean of 16 high (inhibitor control, Example 11 of WO2011/054846A1) and 16 low (DMSO) control wells on each plate. A four parameter curve fit of the following form was then applied:

$$y = \frac{a - d}{1 + (x/c)^b} + d$$

Where 'a' is the minimum, 'b' is the Hill slope, 'c' is the pIC₅₀ and 'd' is the maximum.

2.8.2.2. BRD9 Time Resolved Fluorescence Resonance Energy Transfer (TR-FRET) Assay⁴³

Binding to BRD9 was assessed using a time resolved fluorescent resonance energy transfer binding assay. This utilises a 6-His purification tag at the *N*-terminal of the proteins as an epitope for an anti-6-His antibody labeled with Europium chelate (PerkinElmer AD0111) allowing binding of the Europium to the proteins which acts as the donor fluorophore. A small molecule, high affinity binder of the BRD9, was labeled with Alexa Fluor647 to give **91 (Figure 60)** which acted as the acceptor in the FRET pair.

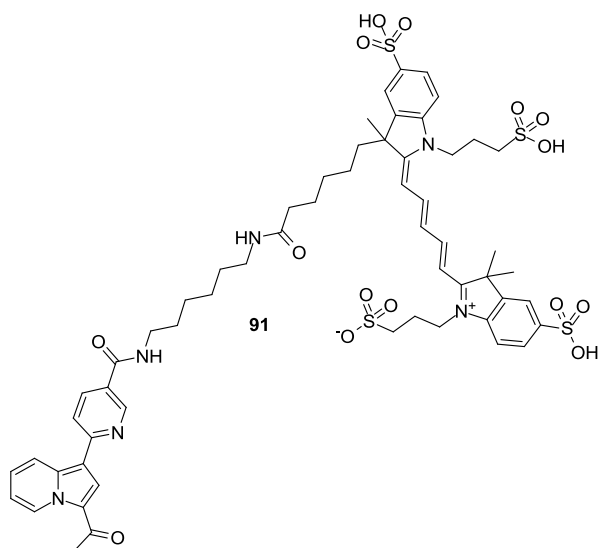


Figure 60. Compound **91** which acts as the acceptor in the FRET pair for the BRD9 TR-FRET assay.

Protocol for BRD9 TR-FRET Assay

All assay components were dissolved in buffer composition of 50 mM HEPES pH 7.4, 50 mM NaCl, 5% Glycerol, 1 mM DTT and 1 mM CHAPS. The final concentration of BRD9 protein was at 10 nM and the Alexa Fluor647 ligand was at K_d (~100 nM for BRD9). These components were premixed and 5 μ L of this reaction mixture was added to all wells containing 50 nl of various concentrations of test compound or DMSO vehicle (0.5% DMSO final) in Greiner 384 well black low volume microtitre plates and incubated in dark for 30 min at room temperature. Detection reagents were prepared in assay buffer by diluting Eu-W1024 Anti-6xHis Antibody (AD0111 PerkinElmer) to 1.5 nM FAC. 5 μ L of this solution was then added to all wells. The plates were read on the Envision reader and the donor and acceptor counts were determined. From this, the ratio of acceptor/donor was calculated ($\lambda_{ex} = 337$ nm, $\lambda_{em} = \text{donor} = 615$ nm, $\lambda_{em} = \text{acceptor} = 665$ nm) and used for data analysis. All data was normalized to the robust mean of 16 high and 16 low control wells on each plate. A four parameter curve fit of the following form was then applied.

$$y = \frac{a - d}{1 + (x/c)^b} + d$$

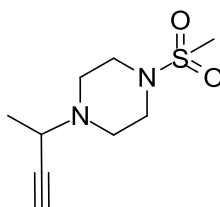
Where 'a' is the minimum, 'b' is the Hill slope, 'c' is the pIC₅₀ and 'd' is the maximum.

2.9. Experimental

Compound purity is assumed to be $\geq 95\%$ purity by LC-MS and ^1H NMR, unless otherwise stated.

2.9.1. Synthesis of Intermediates and Final Compounds

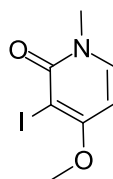
1-(But-3-yn-2-yl)-4-(methylsulfonyl)piperazine, **93**



A mixture of **91** (1.0 g, 11.3 mmol), **92** (3.7 g, 22.6 mmol), copper (0.014 g, 0.2 mmol, 2 mol%), and copper(I) chloride (0.022 g, 0.2 mmol, 2 mol%), in a mixture of diethyl ether (15 mL) and water (5 mL) was stirred at room temperature under nitrogen for 16 h. The reaction mixture was diluted with further water (40 mL) and diethyl ether (40 mL). The organic layer was isolated and the aqueous layer was re-extracted with diethyl ether (2 x 40 mL). The combined organic extracts were passed through a hydrophobic frit and concentrated under reduced pressure. The crude material was purified using a silica column (80 to 100% cyclohexane/EtOAc) to give **93** as a waxy white solid (1.6 g, 66% yield). IR (cm^{-1}) 3238, 2968, 2898, 2818, 1677, 1430, 1367, 1250, 1162, 1140, 1125, 1031, 684; ^1H NMR (400 MHz, DMSO- d_6 δ): 3.62-3.56 (m, 1H), 3.21 (s, 1H), 3.15-3.09 (m, 4H), 2.86 (s, 3H), 2.64-2.60 (m, 2H), 2.51-2.44 (m, 2H), 1.25 (d, $J = 7$ Hz, 3H); ^{13}C NMR (126 MHz, DMSO- d_6 , δ): 82.0, 78.7, 75.6, 50.8, 48.2, 28.0, 18.9; mp 67 - 69 °C.

General Iodination Procedure 1

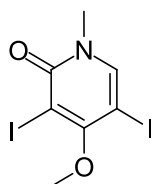
3-Iodo-4-methoxy-1-methylpyridin-2(1H)-one, **95**



A solution of **94** (1.2 g, 5.5 mmol) in acetonitrile (20 mL) was treated with 1-iodopyrrolidine-2,5-dione (0.8 g, 5.5 mmol). The reaction mixture stirred at room temperature for 16 h. The reaction mixture was concentrated under reduced pressure to give crude **95**. The crude product was purified using a silica column (80 to 100% cyclohexane/EtOAc) give **95** as a yellow solid (1.7 g, >99% yield). ^1H NMR (400 MHz, DMSO- d_6 δ): 7.79 (d, $J = 8$ Hz, 1H), 6.26 (d, $J = 8$ Hz, 1H), 3.88 (s, 3H), 3.48 (s, 3H); LC-MS (Method A) $m/z = [\text{M} + \text{H}]^+$ 266.1, t_R 0.53 mins.

General Iodination Procedure 2

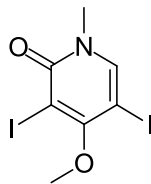
3,5-Iodo-4-methoxy-1-methylpyridin-2(1H)-one, **96**



A solution of **95** (150 mg, 0.57 mmol) in acetonitrile (3 mL) was treated with 1-iodopyrrolidine-2,5-dione (191 mg, 0.85 mmol) and TFA (44 μL , 0.60 mmol) and the reaction was stirred under nitrogen for 16 h. The reaction mixture was concentrated under reduced pressure to give crude **96**. The crude product was purified using a silica column (0 to 80% cyclohexane/EtOAc) give **96** as a white solid (190 mg, 86% yield). IR (cm^{-1}) 3054, 2936, 1628, 1580, 1390, 1146, 958, 749, 675; ^1H NMR (400 MHz, DMSO- d_6 δ): 8.22 (s, 1H), 3.78 (s, 3H), 3.46 (s, 3H); ^{13}C NMR (126 MHz, DMSO- d_6 δ): 167.8, 160.7, 145.4, 84.8, 64.2, 59.9, 37.6; HRMS-FAB (m/z): $[\text{M} + \text{H}]^+$ calcd for $\text{C}_7\text{H}_7\text{I}_2\text{NO}_2$, 391.8639; found, 391.8632; LC-MS (Method A) $m/z = [\text{M} + \text{H}]^+$ 392.0, t_R 0.79 mins; mp 132 - 135 $^\circ\text{C}$.

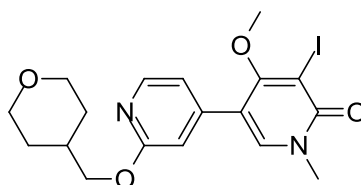
General Iodination Procedure 3

3,5-Iodo-4-methoxy-1-methylpyridin-2(1H)-one, **96**



A solution of **94** (1.8 g, 12.9 mmol) in acetonitrile (50 mL) was treated with 1-iodopyrrolidine-2,5-dione (2.9 g, 12.9 mmol) and the reaction mixture stirred at room temperature for 2 h. Further 1-iodopyrrolidine-2,5-dione (4.4 g, 19.4 mmol) was added to the reaction mixture, followed by TFA (1.0 mL, 12.9 mmol) and the reaction was stirred under nitrogen for 16 h. The reaction mixture was concentrated under reduced pressure to give crude **96**. The crude product was purified using a silica column (0 to 80% cyclohexane/EtOAc) give **96** as a yellow solid (5.1 g, >99% yield). ¹H NMR (400 MHz, DMSO-*d*₆ δ): 8.22 (s, 1H), 3.78 (s, 3H), 3.46 (s, 3H); LC-MS (Method A) *m/z* = [M + H]⁺ 391.9, *t*_R 0.79 mins.

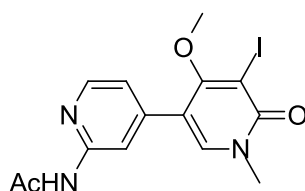
5-Iodo-4-methoxy-1-methyl-2'-((tetrahydro-2H-pyran-4-yl)methoxy)-[3,4'-bipyridin]-6(1H)-one, **98a**



A solution of TPPTS (20 mg, 0.035 mmol, 8 mol%), **96** (180 mg, 0.46 mmol), **97a** (BoroPharm Inc) (191 mg, 0.60 mmol), and diacetoxypalladium (3 mg, 0.013 mmol, 3 mol%) in acetonitrile (4 mL) and water (1 mL) was treated with DIPEA (0.105 mL, 0.60 mmol). The reaction mixture was heated at 60 °C under nitrogen for 16 h. Further diacetoxypalladium (3 mg, 0.013 mmol, 3 mol%) was added, followed by further **97a** (55 mg, 0.29 mmol) and the reaction stirred for 4 h at 60 °C under nitrogen. The reaction mixture was concentrated under reduced pressure and the crude material partitioned between DCM (20 mL) and water (20 mL). The aqueous layer was reextracted with DCM (2 x 20 mL). The combined organic extracts was passed through

a hydrophobic frit and concentrated under reduced pressure. The crude material was purified by silica chromatography (0 to 100 % EtOAc/cyclohexane) to give **98a** as a white solid (90 mg, 43%). ¹H NMR (400 MHz, DMSO-d₆ δ): 8.17 (d, *J* = 6 Hz, 1H), 8.07 (s, 1H), 7.10 (d, *J* = 5 Hz, 1H), 6.90 (s, 1H), 4.15 (d, *J* = 7 Hz, 2H), 3.88 (dd, *J* = 11, 4 Hz, 2H), 3.54 (s, 3H), 3.46 (s, 3H), 3.33 (t, *J* = 11 Hz, 2H), 2.07-1.99 (m, 1H), 1.66 (d, *J* = 12 Hz, 2H), 1.34 (qd, *J* = 12, 4 Hz, 2H); LC-MS (Method A) *m/z* = [M + H]⁺ 457.2, *t_R* 0.89 mins.

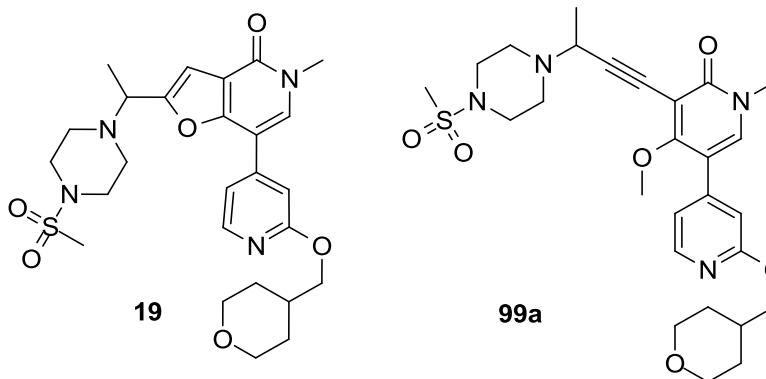
***N*-(5-Iodo-4-methoxy-1-methyl-6-oxo-1,6-dihydro-[3,4'-bipyridin]-2'-yl)acetamide, 98b**



A solution of TPPTS (22 mg, 0.039 mmol, 8 mol%), **96** (20 mg, 0.51 mmol), **97b** (Milestone Pharma Tech) (174 mg, 0.67 mmol), and diacetoxypalladium (7 mg, 0.031 mmol, 6 mol%) in acetonitrile (2 mL) and water (0.7 mL) was treated with DIPEA (0.116 mL, 0.67 mmol). The reaction mixture was heated at 60 °C under nitrogen for 16 h, then concentrated under reduced pressure, then purified using a silica column (0 to 20% solution of 2 N ammonia in MeOH dissolved in DCM) to give crude **98b**. The crude material was dissolved in MeOH and loaded onto a 10 g SCX-II SPE column which was washed with MeOH followed by a 2 N solution of ammonia in MeOH to give **98b** as a clear, colourless gum (80 mg, 39%). IR (cm⁻¹) 3243, 1640, 1591, 1552, 1526, 1502, 1428, 1399, 1135, 751; ¹H NMR (400 MHz, CD₃OD δ): 8.34 (d, *J* = 6 Hz, 1H), 8.26 (s, 1H), 7.93 (s, 1H), 7.27 (d, *J* = 6 Hz, 1H), 3.69 (s, 3H), 3.58 (s, 3H), 2.21 (s, 3H), *the amide proton underwent exchange in wet deuterated solvent and was not observed*; ¹³C NMR (126 MHz, DMSO-d₆, δ): 169.3, 167.0, 160.7, 152.5, 148.0, 143.5, 141.0, 118.5, 113.1, 112.3, 60.0, 57.1, 37.5, 23.9; HRMS-FAB (*m/z*): [M + H]⁺ calcd for C₁₄H₁₄IN₃O₃, 400.0153; found, 400.0152; LC-MS (Method C) *m/z* = [M + H]⁺ 400.1, *t_R* 0.67 mins; mp 119 – 202 °C.

5-Methyl-2-(1-(4-(methylsulfonyl)piperazin-1-yl)ethyl)-7-(2-((tetrahydro-2H-pyran-4-yl)methoxy)pyridin-4-yl)furo[3,2-*c*]pyridin-4(5H)-one, formate salt, 19

and 4-methoxy-1-methyl-5-(3-(4-(methylsulfonyl)piperazin-1-yl)but-1-yn-1-yl)-2'-((tetrahydro-2H-pyran-4-yl)methoxy)-[3,4'-bipyridin]-6(1H)-one, **99a**, formate salt



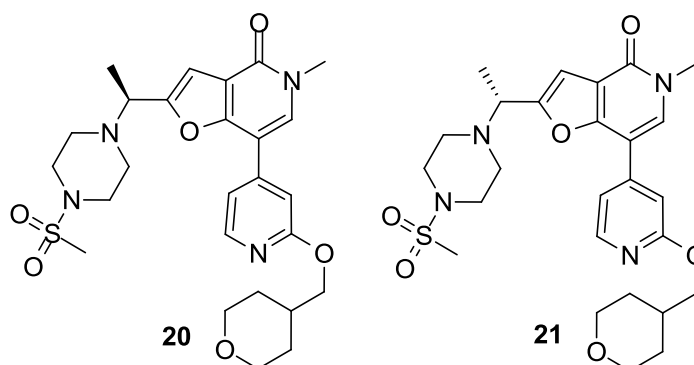
Bis(triphenylphosphino)palladium(II) dichloride (7 mg, 0.010 mmol, 5 mol%) was added to a mixture of **98a** (90 mg, 0.20 mmol), **93** (68 mg, 0.24 mmol at 75% purity), copper(I) iodide (4 mg, 0.021 mmol, 11 mol%), and triethylamine (4.0 mL, 28.7 mmol) in acetonitrile (4 mL). The reaction mixture was heated at 80 °C under nitrogen for four days, by which time the mixture had evaporated to dryness to form a brown gum that hardened on cooling to room temperature. The mixture was partitioned between EtOAc (30 mL) and water (30 mL). The organic layer was isolated and the aqueous layer re-extracted with EtOAc (2 x 30 mL). The combined organic extracts were passed through a hydrophobic frit then concentrated under reduced pressure to give a crude mixture of **19** and **99a**. The crude product was purified by MDAP (Method A).

The fraction containing **19** was concentrated under reduced pressure to give the formate salt as a clear, yellow gum (6 mg, 5%). ¹H NMR (600 MHz, DMSO-d₆ δ): 8.28 (s, 1H), 8.22 (d, *J* = 6 Hz, 1H), 8.20 (br. s, 1H), 7.42 (dd, *J* = 6, 2 Hz, 1H), 7.24 (s, 1H), 6.85 (s, 1H), 4.16 (d, *J* = 6 Hz, 2H), 4.09-4.04 (m, 1H), 3.88 (dd, *J* = 11, 3 Hz, 2H), 3.59 (s, 3H), 3.33 (td, *J* = 12, 2 Hz, 2H), 3.14-3.06 (m, 4H), 2.84 (s, 3H), 2.67-2.60 (m, 2H), 2.51-2.46 (m, 2H), 2.05-1.99 (m, 1H), 1.70-1.61 (m, 2H), 1.43 (d, *J* = 7 Hz, 3H), 1.34 (qd, *J* = 12, 4 Hz, 2H); LC-MS (Method A) *m/z* = [M + H]⁺ 531.3, *t_R* 0.67 mins.

The fraction containing **99a** was concentrated under reduced pressure to give the formate salt as a clear, yellow gum (9 mg). The ¹H NMR spectrum of crude material contained the following significant peaks: ¹H NMR (400 MHz, CD₃OD δ): 8.19 (br. s, 1H), 8.12 (d, *J* = 5 Hz, 1H), 7.82 (s, 1H), 7.06 (d, *J* = 5 Hz, 1H), 6.90 (s, 1H), 4.17 (d, *J* = 6 Hz, 2H), 3.99 (dd, *J* = 3, 11 Hz, 2H), 3.93 (q, *J* = 7 Hz, 1H), 3.79-3.70 (m, 2H), 3.60

(s, 3H), 3.53-3.43 (m, 2H), 3.40-3.25 (m, 5H, *obscured by residual solvent peak*), 3.00-2.91 (m, 2H), 2.87 (s, 3H), 2.81-2.70 (m, 2H), 2.17-2.01 (m, 1H), 1.77 (d, $J = 13$ Hz, 2H), 1.49 (d, $J = 7$ Hz, 3H), 1.47 (qd, $J = 11, 4$ Hz, 2H); LC-MS (Method A) $m/z = [M + H]^+$ 545.4, t_R 0.71 mins, *estimated 50% purity*.

(S)-5-methyl-2-(1-(4-(methylsulfonyl)piperazin-1-yl)ethyl)-7-(2-((tetrahydro-2H-pyran-4-yl)methoxy)pyridin-4-yl)furo[3,2-c]pyridin-4(5H)-one, 20, and (R)-5-methyl-2-(1-(4-(methylsulfonyl)piperazin-1-yl)ethyl)-7-(2-((tetrahydro-2H-pyran-4-yl)methoxy)pyridin-4-yl)furo[3,2-c]pyridin-4(5H)-one, 21



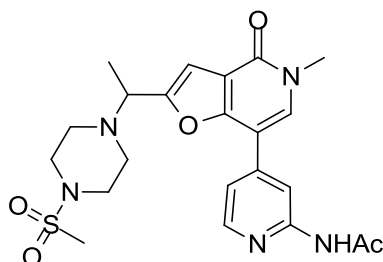
Bis(triphenylphosphino)palladium(II) dichloride (15 mg, 0.021 mmol, 4 mol%) was added to a mixture of **98a** (250 mg, 0.55 mmol), **93** (356 mg, 1.64 mmol) and copper(I) iodide (25 mg, 0.13 mmol, 24 mol%) in DMF (0.5 mL). The mixture was heated at 120 °C for 6 h using a microwave. The reaction was repeated as above with a second batch of reagents, and the two reaction mixtures were combined and concentrated under reduced pressure. The crude material was purified by silica chromatography (0 to 1% v/v of a solution of 2M ammonia in MeOH, in EtOAc, followed by a 0 to 10% v/v solution of 2M ammonia in MeOH, in EtOAc) to give crude product which was further purified by MDAP (Method C) to give **19** (60 mg, 10%) as a pale yellow gum. LC-MS (Method A) $m/z = [M + H]^+$ 531.3, t_R 0.67 mins. No NMR was taken as material was taken forward for chiral purification to afford **20** and **21**.

Compound **19** (60 mg, 0.11 mmol) was dissolved in EtOH (1 mL) and heptanes (2 mL), then portions of the solution (1 mL) were injected onto a 30 mm x 25 cm Chiralpak AD-H column.¹⁰ The column was eluted with 50 % EtOH/Heptane to give:

Compound **20**, eluted between 21 and 24 min, and on isolation was a white solid 20 mg (67%, assuming **19** was a 1:1 ratio of enantiomers); ^1H NMR (400 MHz, CD_3OD δ): 8.20 (d, $J = 5$ Hz, 1H), 8.08 (s, 1H), 7.39 (d, $J = 5$ Hz, 1H), 7.29 (s, 1H), 6.90 (s, 1H), 4.21 (d, $J = 6$ Hz, 2H), 4.09 (q, $J = 7$ Hz, 1H), 4.04-3.97 (m, 2H), 3.74 (s, 3H), 3.54-3.45 (m, 2H), 3.28-3.22 (m, 4H), 2.87-2.73 (m, 5H), 2.68-2.59 (m, 2H), 2.19-2.08 (m, 1H), 1.83-1.75 (m, 2H), 1.58-1.48 (m, 5H); LC-MS (Method A) $m/z = [\text{M} + \text{H}]^+$ 531.4, t_{R} 0.67 mins. Enantiomeric purity by chiral HPLC ≥ 99 % e.e.

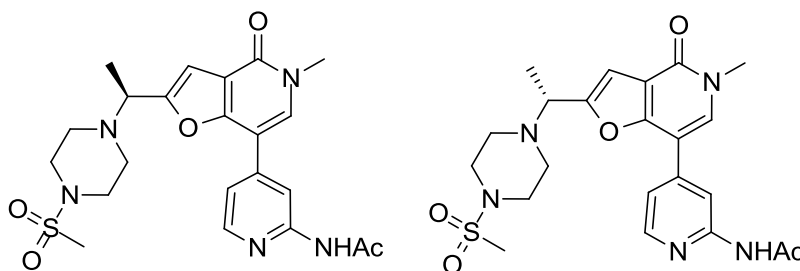
Compound **21**, eluted between 28 and 35 min, and on isolation was a white solid 20 mg (67%, assuming **19** was a 1:1 ratio of enantiomers); ^1H NMR (400 MHz, CD_3OD δ): 8.20 (d, $J = 6$ Hz, 1H), 8.08 (s, 1H), 7.39 (d, $J = 6$ Hz, 1H), 7.29 (s, 1H), 6.90 (s, 1H), 4.21 (d, $J = 6$ Hz, 2H), 4.09 (q, $J = 7$ Hz, 1H), 4.04-3.97 (m, 2H), 3.74 (s, 3H), 3.49 (s, 2H), 3.29-3.22 (m, 4H), 2.85-2.74 (m, 5H), 2.68-2.59 (m, 2H), 2.21-2.07 (m, 1H), 1.83-1.75 (m, 2H), 1.58-1.48 (m, 5H); LC-MS (Method A) $m/z = [\text{M} + \text{H}]^+$ 531.3, t_{R} 0.67 mins. Enantiomeric purity by chiral HPLC = 98 % e.e.

N*-(4-(5-Methyl-2-(1-(4-(methylsulfonyl)piperazin-1-yl)ethyl)-4-oxo-4,5-dihydrofuro[3,2-*c*]pyridin-7-yl)pyridin-2-yl)acetamide, formic acid salt, **22*



Bis(triphenylphosphino)palladium(II) dichloride (26 mg, 0.037 mmol, 6 mol%) was added to a mixture of **93** (406 mg, 1.88 mmol), **98b** (250 mg, 0.63 mmol), copper(I) iodide (29 mg, 0.15 mmol, 24 mol%) and triethylamine (1.5 mL, 10.8 mmol) in DMF (0.5 mL). The reaction mixture was heated at 120 °C for 6 h using a microwave. The reaction was repeated and combined with the first reaction and purified by MDAP (Method C) to give **22** (39 mg, 13%) which was purified by chiral chromatography. LC-MS (Method C) $m/z = [\text{M} + \text{H}]^+$ 474.2, t_{R} 1.64 mins. No NMR was taken as material was taken forward for chiral purification to access **23** and **24**.

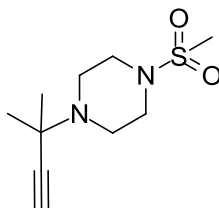
Stereoisomers **1** and **2** of **22**, *N*-(4-(5-methyl-2-(1-(4-(methylsulfonyl)piperazin-1-yl)ethyl)-4-oxo-4,5-dihydrofuro[3,2-*c*]pyridin-7-yl)pyridin-2-yl)acetamide, **23** and **24**



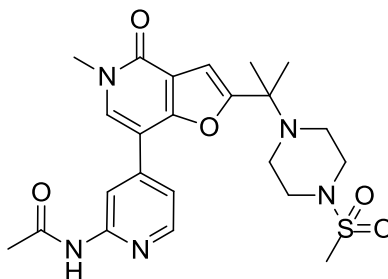
Compound **22** (39 mg, 0.082 mmol) was purified by chiral column chromatography using a Chiralpak ID 250 mm x 30 mm, 5 micron column, eluting with a 0.2 % v/v solution of isopropylamine in methanol at a flow rate of 55 mL/min over 45 min, to give the two enantiomers, **23** and **24**.¹¹

Compound **24** eluted at between 6 and 9 min, and on isolation was a gum (18 mg, 92%, assuming **22** was a 1:1 ratio of enantiomers), 99.6% e.e. by chiral analytical HPLC. ¹H NMR (400 MHz, DMSO-*d*₆ δ): 8.70 (s, 1H), 8.36 (d, *J* = 5 Hz, 1H), 8.23 (s, 1H), 7.45 (d, *J* = 5 Hz, 1H), 6.86 (s, 1H), 4.03 (q, *J* = 7 Hz, 1H), 3.61 (s, 3H), 3.20-3.05 (m, 4H), 2.84 (s, 3H), 2.72-2.62 (m, 2H), 2.47-2.41 (m, 2H), 2.12 (s, 3H), 1.47 (d, *J* = 7 Hz, 3H), amide proton underwent exchange in the wet deuterated solvent and was not observed; LC-MS (Method A) *m/z* = [M + H]⁺ 474.2, *t_R* 0.49 mins.

Compound **23** was the second eluting isomer at between 29 and 43 mins, and on isolation was a gum (19 mg, 97%, assuming **22** was a 1:1 ratio of enantiomers), 99.2% e.e. by chiral analytical HPLC. ¹H NMR (400 MHz, DMSO-*d*₆ δ): 10.51 (br. s, 1H), 8.70 (s, 1H), 8.36 (d, *J* = 5 Hz, 1H), 8.23 (s, 1H), 7.45 (d, *J* = 5 Hz, 1H), 6.86 (s, 1H), 4.03 (q, *J* = 7 Hz, 1H), 3.61 (s, 3H), 3.17-3.04 (m, 4H), 2.84 (s, 3H), 2.74-2.61 (m, 2H), 2.50-2.42 (m, 2H), 2.11 (s, 3H), 1.47 (d, *J* = 7 Hz, 3H); LC-MS (Method A) *m/z* = [M + H]⁺ 474.2, *t_R* 0.48 mins.

1-(2-Methylbut-3-yn-2-yl)-4-(methylsulfonyl)piperazine, 101

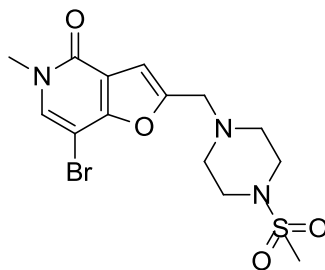
A mixture of **100** (1.0 g, 9.75 mmol), copper (0.012 g, 0.20 mmol, 2 mol%) and copper (I) chloride (19 mg, 0.20 mmol, 2 mol%) and **92** (4.3 g, 26.3 mmol) in diethylether (15 mL) and water (5 mL) was stirred at room temperature under nitrogen for 16 h. The reaction mixture was diluted with water (150 mL) and diethyl ether (150 mL) and the organic layer was isolated. The aqueous layer was re-extracted with diethyl ether (2 x 150 mL). The combined organic extracts were passed through a hydrophobic frit then concentrated under reduced pressure. The crude material was purified using a silica column (80 to 100% cyclohexane/EtOAc) to give **101** as a white solid (1.8 g, 78%). IR (cm⁻¹) 3266, 3003, 2833, 2855, 1343, 1327, 1274, 1156, 971, 959, 941, 782, 687, 661; ¹H NMR (400 MHz, DMSO-d₆ δ): 3.22 (s, 1H), 3.14-3.09 (m, 4H), 2.86 (s, 3H), 2.66-2.58 (m, 4H), 1.31 (s, 6H); ¹³C NMR (126 MHz, DMSO-d₆, δ): 85.2, 74.2, 53.2, 45.9, 45.7, 33.5, 27.4; mp 121 – 122 °C.

N-(4-(5-Methyl-2-(2-(4-(methylsulfonyl)piperazin-1-yl)propan-2-yl)-4-oxo-4,5-dihydrofuro[3,2-c]pyridin-7-yl)pyridin-2-yl)acetamide, 25

Bis(triphenylphosphino)palladium(II) dichloride (26 mg, 0.037 mmol, 6 mol%) was added to a mixture of **101** (455 mg, 2.0 mmol), **98b** (263 mg, 0.66 mmol), copper(I) iodide (30 mg, 0.16 mmol, 24 mol%) and triethylamine (3.0 mL, 21.5 mmol) in DMF (1.0 mL). The reaction mixture was heated at 120 °C for 6 h using a microwave. The reaction mixture was concentrated under reduced pressure to give crude **25**. The crude

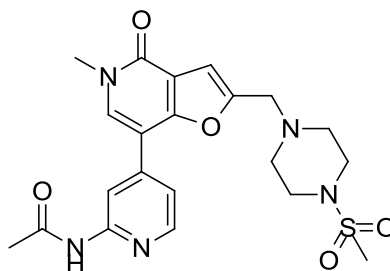
product was purified using a silica column (0 to 10% of a 2 M solution of ammonia in MeOH and EtOAc) followed by MDAP (Method C) to give **25** (25 mg, 8%). ¹H NMR (400 MHz, CD₃OD δ): 8.70 (s, 1H), 8.36 (d, *J* = 5 Hz, 1H), 8.08 (s, 1H), 7.48 (d, *J* = 5 Hz, 1H), 6.88 (s, 1H), 3.75 (s, 3H), 3.26-3.17 (m, 4H), 2.82 (s, 3H), 2.75-2.68 (m, 4H), 2.22 (s, 3H), 1.61 (s, 6H), *amide proton underwent exchange in the wet deuterated solvent and was not observed*; LC-MS (Method A) *m/z* = [M + H]⁺ 488.2, *t_R* 0.50 mins.

7-Bromo-5-methyl-2-((4-(methylsulfonyl)piperazin-1-yl)methyl)furo[3,2-*c*]pyridin-4(5*H*)-one, 106



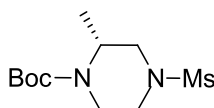
A solution of **105** (250 mg, 0.98 mmol) in a mixture of AcOH (2.5 mL) and MeOH (25.0 mL) was treated with **92** (241 mg, 1.47 mmol) followed by 2-picoline borane complex (115 mg, 1.07 mmol) then the reaction mixture was stirred at room temperature for 1.5 h. The mixture was concentrated under reduced pressure then partitioned between sodium bicarbonate (40 mL of a saturated aqueous solution) and DCM (40 mL). The organic layer was isolated then the aqueous layer was re-extracted with DCM (2 x 40 mL). The combined organic extracts were dried over MgSO₄ then concentrated under reduced pressure to give crude **106**. The crude product was purified using a silica column (0 to 5% MeOH/DCM) to give **106** (309 mg, 78%). ¹H NMR (400 MHz, CDCl₃ δ): 7.37 (s, 1H), 6.90 (s, 1H), 3.76 (s, 2H), 3.63 (s, 3H), 3.36-3.22 (m, 4H), 2.80 (s, 3H), 2.73-2.60 (m, 4H); LC-MS (Method C) *m/z* = [M + H]⁺ 404.1/406.1, *t_R* 0.74 mins.

***N*-(4-(5-Methyl-2-((4-(methylsulfonyl)piperazin-1-yl)methyl)-4-oxo-4,5-dihydrofuro[3,2-*c*]pyridin-7-yl)pyridin-2-yl)acetamide, 26**



A stirred suspension of **106** (100 mg, 0.25 mmol) in 1,2-DME (3 mL) was treated with **108** (104 mg, 0.40 mmol), potassium carbonate (103 mg, 0.74 mmol), followed by *tetrakis*(triphenylphosphino)palladium(0) (14 mg, 0.012 mmol, 5 mol%). The reaction mixture was heated at 120 °C for 2 h by microwave irradiation, then taken up in MeOH and concentrated under reduced pressure. Crude **26** was then dissolved in the minimum volume of MeOH then loaded onto a 1 g SCX SPE column. The column was eluted with MeOH (approximately 12 mL), then a solution of ammonia in MeOH (2 M, approximately 12 mL), the solution concentrated under reduced pressure, then crude material purified by MDAP (Method C) to give **26** as a white solid (45 mg, 40%). IR (cm⁻¹) 3389, 2836, 1650, 1589, 1566, 1538, 1425, 1375, 1340, 1325, 1163, 1118, 964, 933, 777, 704, 664; ¹H NMR (400 MHz, CDCl₃ δ): 8.56 (s, 1H), 8.34 (d, *J* = 5 Hz, 1H), 8.01 (br. s., 1H), 7.60 (s, 1H), 7.43 (d, *J* = 5 Hz, 1H), 6.91 (s, 1H), 3.80 (s, 2H), 3.73 (s, 3H), 3.37-3.25 (m, 4H), 2.80 (s, 3H), 2.76-2.67 (m, 4H), 2.26 (s, 3H); ¹³C NMR (126 MHz, DMSO-*d*₆, δ): 169.2, 157.9, 156.1, 153.5, 152.8, 148.2, 142.0, 135.4, 116.5, 115.7, 110.8, 106.3, 105.9, 53.2, 51.3, 45.4, 36.5, 33.7, 24.0; HRMS–FAB (*m/z*): [M + H]⁺ calcd for C₂₁H₂₅N₅O₅S, 460.1649; found, 460.1645; LC-MS (Method C) *m/z* = [M + H]⁺ 460.2, *t*_R 0.64 mins; mp 141 – 144 °C.

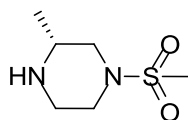
(*R*)-*Tert*-butyl 2-methyl-4-(methylsulfonyl)piperazine-1-carboxylate, 110



A stirred solution of **109** (4.93 g, 24.6 mmol) in THF (15 mL) was treated with NaOH (20 mL of a 2 M aqueous solution, 40.0 mmol), then cooled using an ice bath. The

reaction mixture was treated with a solution of methanesulfonyl chloride (2.1 mL, 24.6 mmol) in THF (15 mL) and stirred for 2 h. The reaction mixture was poured into HCl (20 mL of a 2 N aqueous solution) and partitioned with EtOAc (40 mL). The organic layer was isolated and the aqueous layer re-extracted with EtOAc (2 x 40 mL). The combined organic extracts were passed through a hydrophobic frit then concentrated under reduced pressure to afford **110** as a white solid (5.41 g, 79%). ¹H NMR (400 MHz, DMSO-d₆ δ): 4.34-4.21 (m, 1H), 3.83 (d, *J* = 13 Hz, 1H), 3.48 (d, *J* = 12 Hz, 1H), 3.30 (t, *J* = 4 Hz, 1H), 3.03 (t, *J* = 13 Hz, 1H), 2.86 (s, 3H), 2.84-2.79 (m, 1H), 2.67 (t, *J* = 12 Hz, 1H), 1.42 (s, 9H), 1.13 (d, *J* = 7 Hz, 3H).

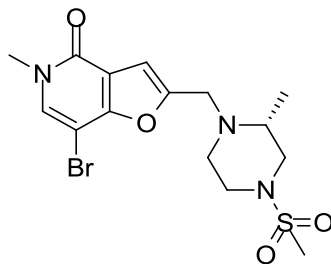
(R)-3-Methyl-1-(methylsulfonyl)piperazine, 111



A solution of **110** (4.73 g, 17.0 mmol) was dissolved in dioxane (20 mL), cooled using an ice-bath, and treated with HCl (20 mL of a 4 M solution in dioxane, 80.0 mmol). The reaction mixture was allowed to warm to room temperature overnight and concentrated under reduced pressure. The residue was dissolved in MeOH then passed through an aminopropyl SPE column (50 g) to give **111** as a white solid 2.96 g (98%). ¹H NMR (400 MHz, DMSO-d₆ δ): 3.37-3.30 (m, 3H), 2.95-2.89 (m, 1H), 2.83 (s, 3H), 2.70-2.53 (m, 3H), 0.97 (d, *J* = 6 Hz, 3H), *the piperazine proton underwent exchange in the wet deuterated solvent and was not observed.*

General Reductive Amination Procedure 1

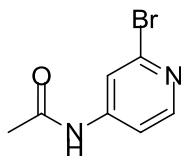
(R)-7-Bromo-5-methyl-2-((2-methyl-4-(methylsulfonyl)piperazin-1-yl)methyl)furo[3,2-*c*]pyridin-4(5*H*)-one, 115



A suspension of **112** (750 mg, 2.93 mmol) in AcOH (3 mL) and MeOH (27 mL) was treated with **111** (743 mg, 4.17 mmol). The reaction mixture was stirred for 1 h at room temperature then treated with 2-picoline borane complex (470 mg, 4.39 mmol) and stirred at room temperature overnight. The reaction mixture heated at 40 °C for 16 h. The reaction mixture was concentrated under reduced pressure and partitioned between saturated sodium bicarbonate solution (40 mL) and DCM (20 mL). The organic layer was isolated and the aqueous layer re-extracted with DCM (2 x 20 mL). The combined organic extracts were passed through a hydrophobic frit then concentrated under reduced pressure. The crude product was purified using a silica column (1 to 5% MeOH/DCM) to give **115** as a yellow solid (716 mg, 58%). ¹H NMR (400 MHz, CD₃OD δ): 7.84 (s, 1H), 6.95 (s, 1H), 4.09-3.85 (m, 2H), 3.64 (s, 3H), 3.52-3.43 (m, 2H), 3.04-2.93 (m, 2H), 2.84 (s, 3H), 2.76-2.68 (m, 1H), 2.64-2.50 (m, 2H), 1.28 (d, *J* = 6 Hz, 3H); LC-MS (Method A) *m/z* = [M + H]⁺ 418.1/420.1, *t_R* 0.53 mins.

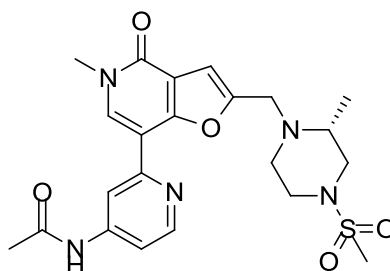
General Formation of an Amide from an Acid Chloride Procedure 1

N-(2-Bromopyridin-4-yl)acetamide, **114**



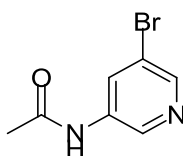
A suspension of **113** (800 mg, 4.62 mmol) in DCM (20 mL) was treated with pyridine (0.748 mL, 9.25 mmol) and acetyl chloride (0.417 mL, 5.32 mmol). The reaction mixture was stirred for 3 h, diluted with DCM (20 mL) and washed with water (20 mL). The organic layer was isolated then concentrated under reduced pressure to afford **114** as an orange solid (920 mg, 93%). ¹H NMR (400 MHz, CD₃OD δ): 9.61 (br. s, 1H), 8.19 (d, *J* = 5 Hz, 1H), 8.03 (d, *J* = 8 Hz, 1H), 7.45 (dd, *J* = 5, 8 Hz, 1H), 2.12 (s, 3H); LC-MS (Method A) *m/z* = [M + H]⁺ 215.0/217.0, *t_R* 0.46 mins.

Attempted preparation of (*R*)-*N*-(2-(5-Methyl-2-((2-methyl-4-(methylsulfonyl)piperazin-1-yl)methyl)-4-oxo-4,5-dihydrofuro[3,2-*c*]pyridin-7-yl)pyridin-4-yl)acetamide, **56**



A solution of **114** (278 mg, 1.3 mmol) in THF (8 mL) under a nitrogen atmosphere was cooled using an ice bath and treated dropwise with isopropylmagnesium chloride (1.8 mL of a 2 M solution in THF, 3.5 mmol). The reaction mixture was stirred for 2 h then treated with more of isopropylmagnesium chloride (0.3 mL of a 2 M solution in THF, 0.6 mmol). The reaction mixture was stirred for 1 h and cooled with an ice bath then treated with ZnCl_2 (4.3 mL of a 1 M solution in ether, 4.3 mmol). The reaction mixture was treated with **115** (264 mg, 0.6 mmol), *tetrakis*(triphenylphosphino)palladium(0) (149 mg, 0.1 mmol, 17 mol%) and refluxed overnight. *Compound 56 was not evident by LCMS analysis.*

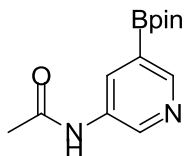
N-(5-Bromopyridin-3-yl)acetamide, **57b**



Prepared using the general formation of an amide from an acid chloride procedure 1 using **57a** (500 mg, 2.89 mmol) and acetyl chloride (0.236 mL, 3.32 mmol) to afford **57b** as an orange solid (563 mg, 91%). ^1H NMR (400 MHz, DMSO-d_6 δ): 10.38 (br. s, 1H), 8.63 (s, 1H), 8.39-8.36 (m, 2H), 2.10 (s, 3H); LC-MS (Method A) $m/z = [\text{M} + \text{H}]^+$ 215.0/217.0, t_R 0.59 mins.

General Boronylation Procedure 1

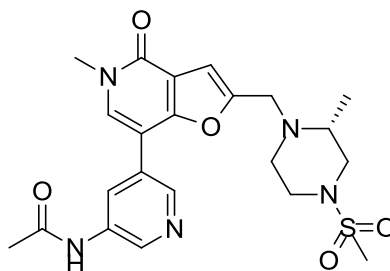
N-(5-(4,4,5,5-Tetramethyl-1,3,2-dioxaborolan-2-yl)pyridin-3-yl)acetamide, **116**



A suspension of **57b** (563 mg, 2.62 mmol) in 1,4-dioxane (8 mL) was treated with 4,4,4',4',5,5,5',5'-octamethyl-2,2'-bi(1,3,2-dioxaborolane) (1330 mg, 5.24 mmol), potassium acetate (771 mg, 7.85 mmol) and Pd(dppf)Cl₂ (192 mg, 0.262 mmol, 10 mol%). The reaction mixture was heated using microwave irradiation at 100 °C for 1 h. The reaction mixture was treated with EtOAc (approximately 10 mL) and filtered through a 10 g Celite^(R) cartridge (10 g). The solvent was removed under reduced pressure to give **116** as a brown oil (1770 mg, *maximum possible theoretical yield is 686 mg, so material is estimated to be a maximum of 686/1770 x 100 = 39% purity by weight*). The crude material was used in the next step to **57** without purification, so no yield is given; the ¹H NMR spectrum of crude material contained the following significant peaks: (400 MHz, CD₃OD δ): 9.06 (s, 1H), 8.87 (s, 1H), 8.49 (s, 1H), 8.14 (s, 1H), 2.18 (s, 3H), 1.35 (s, 12H); LC-MS (Method C) *m/z* = [M + H]⁺ 263.0, *t_R* 0.47 mins.

General Suzuki Coupling Procedure 1

(R)-*N*-(5-(5-Methyl-2-((2-methyl-4-(methylsulfonyl)piperazin-1-yl)methyl)-4-oxo-4,5-dihydrofuro[3,2-*c*]pyridin-7-yl)pyridin-3-yl)acetamide, **57**

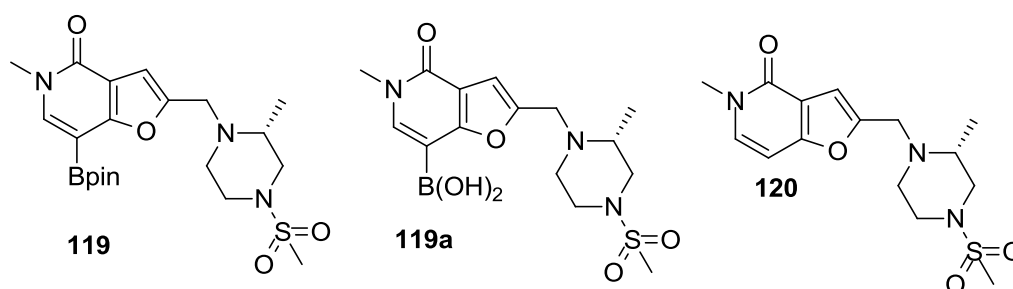


A stirred suspension of **115** (100 mg, 0.24 mmol) in 1,2-DME (3 mL) was treated with **116** (258 mg, *assumed 0.38 mmol at 39% purity by weight*), potassium carbonate (99

mg, 0.72 mmol) and *tetrakis*(triphenylphosphino)palladium(0) (14 mg, 0.012 mmol, 5 mol%). The reaction mixture was heated using microwave irradiation at 120 °C for 2 h. The reaction mixture was treated with EtOAc then filtered through a Celite^(R) cartridge. The solvent was removed under reduced pressure and the crude product purified by MDAP (Method A). The residue was dissolved in methanol and passed through an amino propyl SPE cartridge (500 mg) then concentrated under reduced pressure. The resulting residue was re-purified by MDAP (Method C) to give **57** as a white gum (6 mg, 5% over two steps, the boronylation and Suzuki steps). ¹H NMR (400 MHz, CD₃OD δ): 8.66-8.63 (m, 2H), 8.60 (s, 1H), 7.94 (s, 1H), 6.95 (s, 1H), 4.08-3.93 (m, 2H), 3.74 (s, 3H), 3.54-3.43 (m, 2H), 3.04-2.94 (m, 2H), 2.83 (s, 3H), 2.73-2.65 (m, 1H), 2.65-2.50 (m, 2H), 2.21 (s, 3H), 1.26 (d, *J* = 6 Hz, 3H), the amide proton underwent exchange in wet deuterated solvent and was not observed; LC-MS (Method C) *m/z* = [M + H]⁺ 474.2, *t_R* 0.62 mins.

General Boronylation Procedure 2

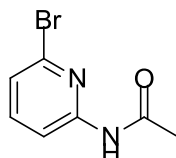
(R)-5-Methyl-2-((2-methyl-4-(methylsulfonyl)piperazin-1-yl)methyl)-7-(4,4,5,5-tetramethyl-1,3,2-dioxaborolan-2-yl)furo[3,2-*c*]pyridin-4(5*H*)-one, **119**, **(R)-(5-methyl-2-((2-methyl-4-(methylsulfonyl)piperazin-1-yl)methyl)-4-oxo-4,5-dihydrofuro[3,2-*c*]pyridin-7-yl)boronic acid**, **119a** and **(R)-5-methyl-2-((2-methyl-4-(methylsulfonyl)piperazin-1-yl)methyl)furo[3,2-*c*]pyridin-4(5*H*)-one**, **120**



A solution of **115** (100 mg, 0.24 mmol) in 1,4-dioxane (3 mL) was treated with triethylamine (0.133 mL, 0.96 mmol), PEPPSITM-SiPr^(R) (17 mg, 0.025 mmol, 10 mol%) and 4,4,5,5-tetramethyl-1,3,2-dioxaborolane (0.208 mL, 1.43 mmol). The reaction mixture was heated at 100 °C for 3 h using microwave irradiation, then diluted with EtOAc and filtered through Celite^(R) then concentrated under reduced pressure to afford a mixture of **119**, **119a** and **120** as a yellow solid (373 mg, maximum possible

theoretical yield is 111 mg, so material is estimated to be a maximum of $111/373 \times 100 = 30\%$ purity by weight with respect to **119**). LC-MS (Method A) $m/z = [M + H]^+$ 466.2, t_R 0.70 mins (**119**, 12% by peak area); $m/z = [M + H]^+$ 340.1, t_R 0.40 mins (**120**, 27% by area); $m/z = [M + H]^+$ 384.2, t_R 0.38 mins (**119a**, 57% by area). No NMR was taken, and material was taken forward without purification in the next synthetic step, so no yield is given.

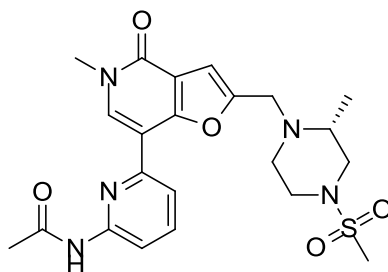
N-(6-Bromopyridin-2-yl)acetamide, **118**



Prepared using the general formation of an amide from an acid chloride procedure 1 using **117** (500 mg, 2.89 mmol) and acetyl chloride (0.236 mL, 3.32 mmol) to afford **118** as a white solid (597 mg, 96%) after trituration with ether then drying under vacuum. IR (cm⁻¹) 3229, 3043, 1658, 1564, 1533, 1435, 1387, 1309, 1152, 1128, 777, 725; ¹H NMR (400 MHz, CDCl₃ δ): 8.17 (d, $J = 8$ Hz, 1H), 7.93 (br. s., 1H), 7.57 (t, $J = 8$ Hz, 1H), 7.23 (d, $J = 8$ Hz, 1H), 2.21 (s, 3H); ¹³C NMR (126 MHz, DMSO-d₆, δ): 169.4, 152.3, 141.3, 138.7, 122.6, 112.1, 23.8; HRMS–FAB (m/z): $[M + H]^+$ calcd for C₇H₇BrN₂O, 214.9815; found, 214.9815; LC-MS (Method A) $m/z = [M + H]^+$ 215.0/217.0, t_R 0.70 mins; mp 90 – 91 °C.

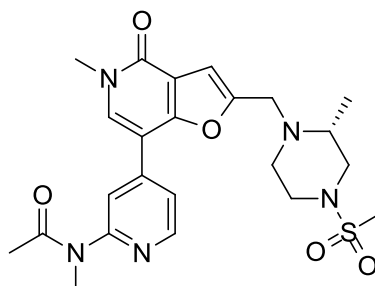
General Suzuki Coupling Procedure 2

(R)-*N*-(6-(5-Methyl-2-((2-methyl-4-(methylsulfonyl)piperazin-1-yl)methyl)-4-oxo-4,5-dihydrofuro[3,2-*c*]pyridin-7-yl)pyridin-2-yl)acetamide, **58**

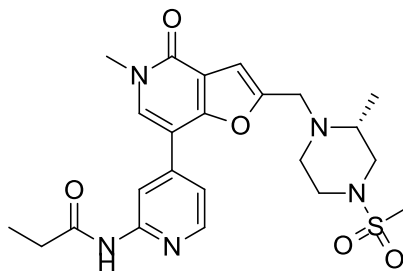


A mixture of **119**, **119a** and **120** (373 mg, assumed 30% maximum purity by weight with respect to **119**) in 1,2-DME (3 mL) was treated with **118** (35 mg, 0.16 mmol), a 2 M solution of sodium carbonate in water (0.65 mL, 1.26 mmol) and tetrakis(triphenylphosphino)palladium(0) (10 mg, 0.087 mmol, 5 mol%). The reaction mixture was heated using microwave irradiation at 120 °C for 2 h. The reaction mixture was treated with EtOAc then concentrated under reduce pressure. The crude material was purified by MDAP (Method C) to give **58** as a pale yellow solid (18 mg, 23%, over two steps). ¹H NMR (400 MHz, CD₃OD δ): 8.44 (s, 1H), 8.11-8.01 (m, 1H), 7.93-7.82 (m, 2H), 6.95 (s, 1H), 4.13-3.96 (m, 2H), 3.76 (s, 3H), 3.54-3.44 (m, 2H), 3.06-2.96 (m, 2H), 2.84 (s, 3H), 2.76-2.52 (m, 3H), 2.23 (s, 3H), 1.32 (d, *J* = 6 Hz, 3H), amide proton underwent exchange in wet deuterated solvent and was not seen; LC-MS (Method A) *m/z* = [M + H]⁺ 474.2, *t_R* 0.55 mins.

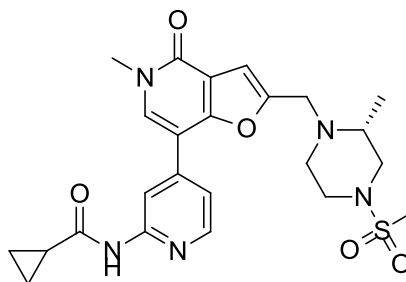
(R)-N-Methyl-N-(4-(5-methyl-2-((2-methyl-4-(methylsulfonyl)piperazin-1-yl)methyl)-4-oxo-4,5-dihydrofuro[3,2-c]pyridin-7-yl)pyridin-2-yl)acetamide, 59



Prepared using the general Suzuki coupling procedure 2 from **115** (95 mg, 0.23 mmol) and crude **126** (71 mg, 0.26 mmol) to afford **59** as a brown solid (34 mg, 31%). IR (cm⁻¹) 2932, 2826, 1655, 1593, 1321, 1152, 1118, 985, 795, 774; ¹H NMR (400 MHz, DMSO-d₆ δ): 8.56 (d, *J* = 5 Hz, 1H), 8.36 (s, 1H), 7.90 (s, 1H), 7.73 (d, *J* = 5 Hz, 1H), 6.93 (s, 1H), 3.99-3.87 (m, 2H), 3.62 (s, 3H), 3.36-3.27 (s, 3H, obscured by residual solvent peak), 2.95-2.81 (m, 5H), 2.63-2.53 (m, 3H), 2.48-2.36 (m, 2H), 2.07 (s, 3H), 1.18 (d, *J* = 6 Hz, 3H); ¹³C NMR (126 MHz, DMSO-d₆, δ): 169.7, 157.9, 156.6, 156.0, 153.6, 149.0, 142.5, 135.9, 118.6, 117.2, 115.6, 106.0, 105.2, 53.1, 51.6, 50.0, 48.5, 45.5, 36.5, 34.9, 33.7, 23.0, 15.6; HRMS-FAB (*m/z*): [M + H]⁺ calcd for C₂₃H₂₉N₅O₅S, 488.1962; found, 488.1964; LC-MS (Method A) *m/z* = [M + H]⁺ 488.3, *t_R* 0.51 mins; mp 131 – 135 °C.

4,5-dihydrofuro[3,2-*c*]pyridin-7-yl)pyridin-2-yl)propionamide, 60

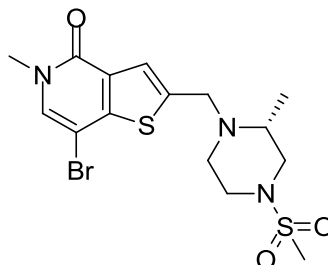
Prepared using the general Suzuki coupling procedure 2 from **115** (100 mg, 0.24 mmol) and crude **127** (80 mg, 0.29 mmol, *at a maximum of 87% purity by weight*) to afford **60** as a brown solid (28 mg, 24%). IR (cm⁻¹) 3257, 2983, 1659, 1598, 1561, 1539, 1429, 1321, 1154, 790, 773; ¹H NMR (400 MHz, DMSO-d₆ δ): 10.47 (s, 1H), 8.63 (s, 1H), 8.37 (d, *J* = 5 Hz, 1H), 8.19 (s, 1H), 7.44 (d, 5 Hz, 1H), 6.92 (s, 1H), 3.91 (s, 2H), 3.62 (s, 3H), 3.44-3.33 (m, 2H), 3.00-2.80 (m, 5H), 2.62-2.52 (m, 1H), 2.48-2.36 (m, 4H), 1.17 (d, *J* = 6 Hz, 3H), 1.09 (t, *J* = 8 Hz, 3H); ¹³C NMR (126 MHz, DMSO-d₆, δ): 172.8, 158.0, 156.1, 153.5, 152.8, 148.2, 142.0, 135.4, 116.3, 115.6, 110.8, 106.3, 106.1, 53.0, 51.6, 50.3, 48.4, 45.5, 36.5, 33.8, 29.3, 15.7, 9.4; HRMS–FAB (*m/z*): [M + H]⁺ calcd for C₂₃H₂₉N₅O₅S, 488.1962; found, 488.1965; LC-MS (Method A) *m/z* = [M + H]⁺ 488.3, *t*_R 0.53 mins; mp 145 – 147 °C.

(R)-N-(4-(5-Methyl-2-((2-methyl-4-(methylsulfonyl)piperazin-1-yl)methyl)-4-oxo-4,5-dihydrofuro[3,2-*c*]pyridin-7-yl)pyridin-2-yl)cyclopropanecarboxamide, 61

Prepared using the general Suzuki coupling procedure 2 from **115** (100 mg, 0.24 mmol) and crude **128** (85 mg, 0.29 mmol) to afford **61** as a brown solid (80 mg, 67%). ¹H NMR (400 MHz, CD₃OD δ): 8.62 (s, 1H), 8.36 (d, *J* = 5 Hz, 1H), 8.06 (s, 1H), 7.49 (d, *J* = 5 Hz, 1H), 6.95 (s, 1H), 4.08-3.96 (m, 2H), 3.74 (s, 3H), 3.58-3.46 (m, 2H), 3.08-2.93 (m, 2H), 2.83 (s, 3H), 2.72-2.52 (m, 3H), 1.97-1.85 (m, 1H), 1.27 (d, *J* = 6 Hz,

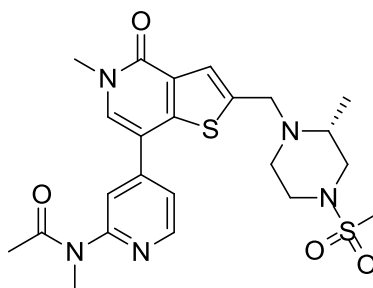
3H), 1.07-0.99 (m, 2H), 0.97-0.89 (m, 2H), *amide proton underwent exchange in wet deuterated solvent and was not seen*; LC-MS (Method A) $m/z = [M + H]^+$ 500.3, t_R 0.56 mins.

(R)-7-Bromo-5-methyl-2-((2-methyl-4-(methylsulfonyl)piperazin-1-yl)methyl)thieno[3,2-c]pyridin-4(5H)-one, 130



Prepared using general reductive amination procedure 1 from **129** (2.70 g, 9.9 mmol) and **111** (2.00 g, 11.2 mmol), heating at 50 °C overnight instead of room temperature, to afford **130** as a yellow solid (1.26 g, 29%). 1H NMR (400 MHz, DMSO- d_6 δ): 7.93 (s, 1H), 7.50 (s, 1H), 4.15-4.05 (m, 2H), 3.49 (s, 3H), 3.30-3.19 (m, 2H), 3.01-2.92 (m, 1H), 2.87 (s, 3H), 2.84-2.62 (m, 3H), 2.40-2.30 (m, 1H), 1.11 (d, $J = 6$ Hz, 3H); LC-MS (Method A) $m/z = [M + H]^+$ 434.1/436.1, t_R 0.62 mins.

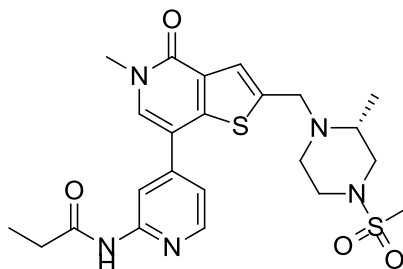
(R)-N-Methyl-N-(4-(5-methyl-2-((2-methyl-4-(methylsulfonyl)piperazin-1-yl)methyl)-4-oxo-4,5-dihydrothieno[3,2-c]pyridin-7-yl)pyridin-2-yl)acetamide, 62



Prepared using the general Suzuki coupling procedure 2 from **130** (115 mg, 0.27 mmol) and crude **126** (85 mg, 0.31 mmol) to afford **62** as a white solid (12 mg, 9%). 1H NMR (400 MHz, DMSO- d_6 δ): 8.58 (d, $J = 5$ Hz, 1H), 8.02 (s, 1H), 7.76 (s, 1H), 7.58 (d, $J = 5$ Hz, 1H), 7.50 (s, 1H), 4.20-3.69 (m, 2H), 3.60 (s, 3H), 3.39-3.31 (m, 3H, *obscured by residual solvent peak*), 3.29-3.16 (m, 2H), 2.98-2.88 (m, 1H), 2.86 (s, 3H), 2.83-2.75

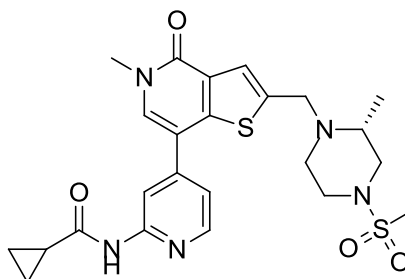
(m, 1H), 2.74-2.59 (m, 2H), 2.39-2.27 (m, 1H), 2.11 (s, 3H), 1.12 (d, $J = 6$ Hz, 3H); LC-MS (Method C) $m/z = [M + H]^+$ 504.3, t_R 0.75 mins.

(R)-N-(4-(5-Methyl-2-((2-methyl-4-(methylsulfonyl)piperazin-1-yl)methyl)-4-oxo-4,5-dihydrothieno[3,2-c]pyridin-7-yl)pyridin-2-yl)propionamide, 63



Prepared using the general Suzuki coupling procedure 2 from **130** (115 mg, 0.27 mmol) and crude **127** (80 mg, 0.25 mmol, *at a maximum of 87% purity by weight*) to afford **63** (23 mg, 17%). IR (cm^{-1}) 3229, 2979, 1646, 1588, 1553, 1528, 1425, 1332, 1317, 1149, 772; ^1H NMR (400 MHz, DMSO- d_6 δ): 10.56 (s, 1H), 8.45 (s, 1H), 8.40 (d, $J = 5$ Hz, 1H), 7.91 (s, 1H), 7.48 (s, 1H), 7.33 (d, $J = 5$ Hz, 1H), 4.23-3.70 (m, 2H), 3.60 (s, 3H), 3.28-3.15 (m, 2H), 3.00-2.90 (m, 1H), 2.84 (s, 3H), 2.82-2.62 (m, 3H), 2.43 (q, $J = 8$ Hz, 2H), 2.38-2.29 (m, 1H), 1.14-1.04 (m, 6H); ^{13}C NMR (126 MHz, DMSO- d_6 , δ): 173.1, 157.5, 152.9, 148.6, 145.3, 145.1, 142.8, 133.7, 139.5, 123.0, 117.2, 112.9, 110.8, 59.7, 53.4, 51.4 (2C), 45.5, 36.4, 33.6, 29.8, 14.1, 9.4; HRMS-FAB (m/z): $[M + H]^+$ calcd for $\text{C}_{23}\text{H}_{29}\text{N}_5\text{O}_4\text{S}_2$, 504.1734; found, 504.175; LC-MS (Method A) $m/z = [M + H]^+$ 504.3, t_R 0.58 mins; mp 270 – 272 °C.

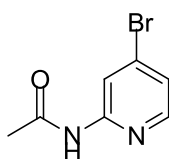
(R)-N-(4-(5-Methyl-2-((2-methyl-4-(methylsulfonyl)piperazin-1-yl)methyl)-4-oxo-4,5-dihydrothieno[3,2-c]pyridin-7-yl)pyridin-2-yl)cyclopropanecarboxamide, 64



Prepared using the general Suzuki coupling procedure 2 from **130** (120 mg, 0.28 mmol) and crude **128** (93 mg, 0.32 mmol) to afford **64** as a white solid (25 mg, 18%). ¹H NMR (400 MHz, DMSO-d₆ δ): 10.92 (s, 1H), 8.44-8.39 (m, 2H), 7.90 (s, 1H), 7.48 (s, 1H), 7.34 (d, *J* = 5 Hz, 1H), 4.12-3.73 (m, 2H), 3.59 (s, 3H), 3.28-3.14 (m, 2H), 2.99-2.89 (m, 1H), 2.85 (s, 3H), 2.81-2.60 (m, 3H), 2.38-2.26 (m, 1H), 2.10-2.00 (m, 1H), 1.11 (d, *J* = 6 Hz, 3H), 0.83 (d, *J*=6 Hz, 4H); LC-MS (Method C) *m/z* = [M + H]⁺ 516.3, *t_R* 0.84 mins.

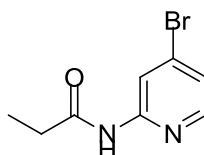
General Formation of an Amide from an Acid Chloride Procedure 2

N-(4-Bromopyridin-2-yl)acetamide, **122**



A solution of **121** (400 mg, 2.31 mmol) in DCM (10 mL) was treated with pyridine (0.374 mL, 4.62 mmol) then stirred at room temperature for 20 min. The reaction mixture was treated with acetyl chloride (0.190 mL, 2.66 mmol) and the mixture was stirred at room temperature overnight. The reaction mixture was partitioned with water and the organic extract was isolated then washed with brine and passed through a hydrophobic frit and concentrated under reduced pressure. The resulting residue was dissolved in MeOH then passed through a 10 g aminopropyl SPE column to give **122** as a white solid (404 mg, 81%). ¹H NMR (400 MHz, DMSO-d₆ δ): 10.71 (br. s., 1H), 8.32 (d, *J* = 2 Hz, 1H), 8.21 (d, *J* = 6 Hz, 1H), 7.35 (dd, *J* = 6, 2 Hz, 1H), 2.10 (s, 3H); LC-MS (Method A) *m/z* = [M + H]⁺ 215.0/217.1, *t_R* 0.65 mins.

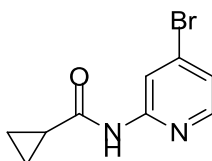
N-(4-Bromopyridin-2-yl)propionamide, **123**



Prepared using the general formation of an amide from an acid chloride procedure 2 from **121** (400 mg, 2.31 mmol) and propionyl chloride (0.232 mL, 2.66 mmol) to afford

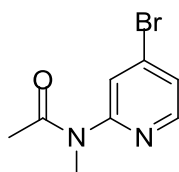
123 as a white solid (464 mg, 88%). IR (cm⁻¹) 3234, 2982, 1673, 1561, 1514, 1393, 1250, 1191, 875, 808, 771, 679; ¹H NMR (400 MHz, DMSO-d₆ δ): 10.66 (br. s, 1H), 8.35 (d, *J* = 2 Hz, 1H), 8.21 (d, *J* = 5 Hz, 1H), 7.34 (dd, *J* = 5, 2 Hz, 1H), 2.41 (q, *J* = 8 Hz, 2H), 1.06 (t, *J* = 8 Hz, 3H); ¹³C NMR (126 MHz, DMSO-d₆, δ): 173.4, 153.0, 149.2, 133.0, 122.0, 115.7, 29.3, 9.2; HRMS–FAB (*m/z*): [M + H]⁺ calcd for C₈H₉BrN₂O, 228.9971; found, 228.997; LC-MS (Method C) *m/z* = [M + H]⁺ 229.1/231.1, *t_R* 0.84 mins; mp 101 – 104 °C.

***N*-(4-Bromopyridin-2-yl)cyclopropanecarboxamide, 124**



Prepared using the general formation of an amide from an acid chloride procedure 2 from **121** (500 mg, 2.89 mmol) and cyclopropanecarbonyl chloride (0.60 mL, 6.64 mmol) to afford **124** as a white solid (610 mg, 88%). IR (cm⁻¹) 3236, 1667, 1559, 1515, 1396, 1254, 1185, 959, 813, 689, 673; ¹H NMR (400 MHz, DMSO-d₆ δ): 11.02 (br. s, 1H), 8.33 (d, *J* = 2 Hz, 1H), 8.22 (d, *J* = 5 Hz, 1H), 7.34 (dd, *J* = 5, 2 Hz, 1H), 2.01 (quin, *J* = 6 Hz, 1H), 0.89-0.77 (d, *J* = 6 Hz, 4H); ¹³C NMR (126 MHz, DMSO-d₆, δ): 173.1, 152.9, 149.2, 133.0, 122.0, 115.8, 14.2, 7.9; HRMS–FAB (*m/z*): [M + H]⁺ calcd for C₉H₉BrN₂O, 240.9971; found, 240.9974; LC-MS (Method A) *m/z* = [M + H]⁺ 241.1/243.1, *t_R* 0.84 mins; mp 127 – 129 °C.

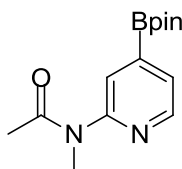
***N*-(4-Bromopyridin-2-yl)-*N*-methylacetamide, 125**



A solution of **122** (406 mg, 1.89 mmol) in DMF (10 mL) was cooled to 0 °C using an iced water bath. The solution was treated with sodium hydride (91 mg of a 60% w/w dispersion in mineral oils, 2.27 mmol) then stirred for 15 min. The reaction mixture was treated with iodomethane (0.142 mL, 2.27 mmol) then stirred for 2 h. The reaction

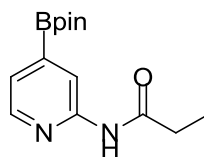
mixture was partitioned with water and diethyl ether (approximately 10 mL each), the organic extract isolated, and the aqueous layer re-extracted with diethyl ether (approximately 10 mL). The combined organic extracts were concentrated under reduced pressure then purified by silica column chromatography (50 to 100% cyclohexane/EtOAc) to afford **125** as a colourless oil (252 mg, 58%). ¹H NMR (400 MHz, DMSO-d₆ δ): 8.36 (d, *J* = 5 Hz, 1H), 7.90 (d, *J* = 2 Hz, 1H), 7.54 (dd, *J* = 5, 2 Hz, 1H), 3.30 (s, 3H), 2.11 (s, 3H); LC-MS (Method C) *m/z* = [M + H]⁺ 229.0/231.1, *t_R* 0.69 mins.

***N*-Methyl-*N*-(4-(4,4,5,5-tetramethyl-1,3,2-dioxaborolan-2-yl)pyridin-2-yl)acetamide, 126**



Prepared using the general boronylation procedure 1 from **125** (248 mg, 1.08 mmol) and bis(pinacolato)diboron (779 mg, 3.07 mmol), heating for 30 min rather than 1 h, to afford **126** as a brown residue (299 mg, *maximum possible theoretical yield is 299 mg, so material estimated to be a maximum of 299/299 x 100 = >99% purity by weight*). Material was taken forward without purification. LC-MS (Method A) *m/z* = [M + H]⁺ 195.1, *t_R* 0.37 mins (*observed mass ion is consistent with hydrolysis to boronic acid under LC-MS conditions; no NMR was taken*).

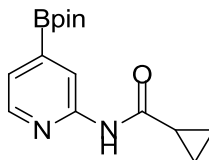
***N*-(4-(4,4,5,5-tetramethyl-1,3,2-dioxaborolan-2-yl)pyridin-2-yl)propionamide, 127**



Prepared using the general boronylation procedure 1 from **123** (200 mg, 0.87 mmol) and bis(pinacolato)diboron (665 mg, 2.62 mmol), heating for 30 min rather than 1 h, to afford **127** as a brown residue (276 mg, *maximum possible theoretical yield is 241 mg, so material estimated to be a maximum of 241/276 x 100 = 87% purity by weight*). Material was taken forward without purification, so no yield is given. LC-MS (Method

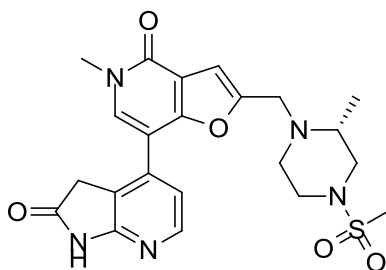
A) $m/z = [M + H]^+ 195.2$, t_R 0.34 mins (*observed mass ion is consistent with hydrolysis to boronic acid under LC-MS conditions; no NMR was taken*).

***N*-(4-(4,4,5,5-Tetramethyl-1,3,2-dioxaborolan-2-yl)pyridin-2-yl)cyclopropanecarboxamide, 128**

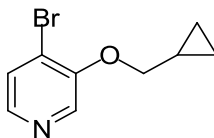


Prepared using the general boronylation procedure 1 from **124** (504 mg, 2.09 mmol) and *bis*(pinacolato)diboron (1062 mg, 4.18 mmol), heating for 30 min rather than 1 h, to afford **128** as a brown residue (602 mg, *maximum possible theoretical yield is 602 mg, so material estimated to be a maximum of 602/602 x 100 = >99% purity by weight*). Material was taken forward without purification, and no yield is given. LC-MS (Method A) $m/z = [M + H]^+ 207.2$, t_R 0.37 mins (*observed mass ion is consistent with hydrolysis to boronic acid under LC-MS conditions; no NMR was taken*).

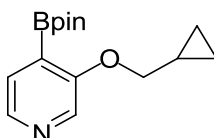
***(R)*-5-Methyl-2-((2-methyl-4-(methylsulfonyl)piperazin-1-yl)methyl)-7-(2-oxo-2,3-dihydro-1*H*-pyrrolo[2,3-*b*]pyridin-4-yl)furo[3,2-*c*]pyridin-4(5*H*)-one, 65**



A mixture of **119**, **119a** and **120** was prepared using the general boronylation procedure 2 from **115** (190 mg, 0.45 mmol). The general Suzuki coupling procedure 2 was used to couple the crude mixture with **131** (86 mg, 0.41 mmol), heating at 120 °C for 30 mins instead of 2 h, to give **65** as a brown solid (9 mg, 4%, *over two steps*). 1H NMR (400 MHz, DMSO- d_6 δ): 11.12 (s, 1H), 8.16 (d, $J = 6$ Hz, 1H), 8.01 (s, 1H), 7.18 (d, $J = 6$ Hz, 1H), 6.92 (s, 1H), 3.98-3.68 (m, 4H), 3.60 (s, 3H), 3.29-3.22 (m, 2H), 3.01-2.91 (m, 1H), 2.90-2.76 (m, 4H), 2.70-2.61 (m, 1H), 2.54 (d, $J = 5$ Hz, 1H), 2.42-2.29 (m, 1H), 1.12 (d, $J = 6$ Hz, 3H); LC-MS (Method A) $m/z = [M + H]^+ 472.2$, t_R 0.46 mins.

4-Bromo-3-(cyclopropylmethoxy)pyridine, 133

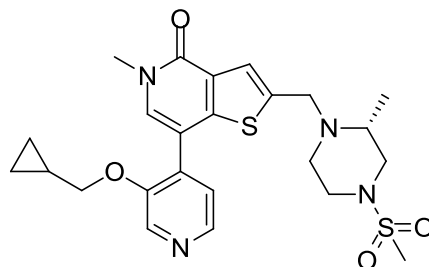
A solution of **132** (400 mg, 2.30 mmol) in DMF (15 mL) was cooled to 0 °C and was treated with sodium hydride (110 mg, 2.76 mmol, 60% w/w dispersion in mineral oils). The reaction mixture was stirred for 30 min then treated with (bromomethyl)cyclopropane (0.268 mL, 2.76 mmol) and allowed to warm to room temperature overnight. The reaction mixture was partitioned with water (40 mL) and EtOAc (40 mL). The organic extract was isolated, washed with brine then passed through a hydrophobic frit and concentrated under reduced pressure. The crude product was purified by silica column chromatography (0 to 5% of a solution of ammonia in MeOH/DCM) to afford **133** as a brown oil (234 mg, 45%). ¹H NMR (400 MHz, DMSO-d₆ δ): 8.37 (s, 1H), 8.05 (d, *J* = 5 Hz, 1H), 7.67 (d, *J* = 5 Hz, 1H), 4.06 (d, *J* = 7 Hz, 2H), 1.32-1.21 (m, 1H), 0.63-0.56 (m, 2H), 0.40-0.34 (m, 2H); LC-MS (Method A) *m/z* = [M + H]⁺ 228.0/230.1, *t_R* 0.87 mins.

3-(Cyclopropylmethoxy)-4-(4,4,5,5-tetramethyl-1,3,2-dioxaborolan-2-yl)pyridine, 134

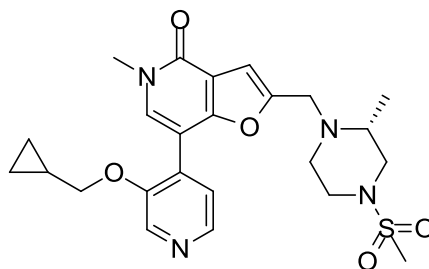
A mixture of **133** (228 mg, 1.00 mmol), *bis*(pinacolato)diboron (508 mg, 2.00 mmol), Pd (dppf)Cl₂ (73 mg, 0.10 mmol, 10 mol%) and potassium acetate (294 mg, 3.00 mmol) in 1,4-dioxane (5 mL) was heated at 100 °C for 30 min using microwave irradiation. The reaction mixture was diluted with ethyl acetate (approximately 10 mL) and filtered through Celite^(R) then concentrated under reduced pressure to give **134** as a brown residue (275 mg, *maximum possible theoretical yield is 275 mg, so material estimated to be a maximum of 275/275 x 100 = >99% purity by weight*). The compound was taken forward without purification, so no yield is given. LC-MS (Method A) *m/z* = [M + H]⁺

194.1, t_R 0.36 mins (observed mass ion is consistent with hydrolysis to boronic acid under LC-MS conditions; no NMR was taken).

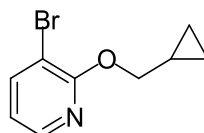
(R)-7-(3-(Cyclopropylmethoxy)pyridin-4-yl)-5-methyl-2-((2-methyl-4-(methylsulfonyl)piperazin-1-yl)methyl)thieno[3,2-c]pyridin-4(5H)-one, 67



A solution of **115** (100 mg, 0.23 mmol) in 1,2-DME (3 mL) was treated with crude **134** (74 mg, 0.27 mmol), *tetrakis*(triphenylphosphino)palladium(0) (13 mg, 0.012 mmol, 5 mol%) and sodium carbonate (0.921 mL of a 2 M aqueous solution, 1.84 mmol) was heated at 120 °C for 2 hours using microwave irradiation. The reaction mixture was diluted with ethyl acetate and water and filtered. The organic extract was isolated then concentrated under reduced pressure. The crude product was purified by MDAP (Method C) then re-purified by MDAP (Method D). The purified product was dissolved in MeOH and passed through an aminopropyl SPE cartridge (10 g) using MeOH to afford **67** as a beige solid (58 mg, 50%). IR (cm⁻¹) 2926, 1643, 1581, 1325, 1298, 1157, 985, 790, 771; ¹H NMR (400 MHz, DMSO-d₆ δ): 8.48 (s, 1H), 8.30 (d, *J* = 5 Hz, 1H), 7.74 (s, 1H), 7.45-7.39 (m, 2H), 4.15-3.65 (m, 4H), 3.57 (s, 3H), 3.28-3.13 (m, 2H), 2.93-2.86 (m., 1H), 2.84 (s, 3H), 2.82-2.74 (m, 1H), 2.72-2.56 (m, 2H), 2.36-2.27 (m, 1H), 1.18-1.05 (m, 4H), 0.51-0.44 (m, 2H), 0.29-0.23 (m, 2H); ¹³C NMR (126 MHz, DMSO-d₆, δ): 157.5, 151.8, 146.7, 142.5, 142.4, 135.7, 134.2, 131.7, 128.7, 124.3, 122.4, 109.7, 73.0, 53.4, 51.4 (2C), 49.1, 45.5, 36.3, 33.6, 14.7, 9.9, 3.1; HRMS–FAB (*m/z*): [M + H]⁺ calcd for C₂₄H₃₀N₄O₄S₂, 503.1781; found, 503.1768; LC-MS (Method A) *m/z* = [M + H]⁺ 503.2, t_R 0.59 mins; mp 118 – 120 °C.

(R)-7-(3-(Cyclopropylmethoxy)pyridin-4-yl)-5-methyl-2-((2-methyl-4-(methylsulfonyl)piperazin-1-yl)methyl)furo[3,2-c]pyridin-4(5H)-one, 68

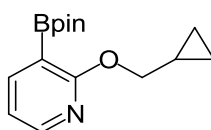
A solution of **115** (95 mg, 0.2 mmol) in 1,2-DME (3 mL) was treated with crude **134** (73 mg, 0.27 mmol), *tetrakis*(triphenylphosphino)palladium(0) (13 mg, 0.011 mmol, 5 mol%) and 2 M aqueous sodium carbonate (0.908 mL, 1.82 mmol) was heated at 120 °C for 2 hours using microwave irradiation. The reaction mixture was diluted with ethyl acetate (2 mL) and water (2 mL) and filtered through cotton wool. The organic extract was isolated then concentrated under reduced pressure. The crude product was purified by MDAP (Method A) then dissolved in MeOH and passed through an aminopropyl SPE cartridge (5 g) using MeOH to afford **68** as a white solid (54 mg, 55%). ¹H NMR (400 MHz, CD₃OD δ): 8.33 (s, 1H), 8.21 (d, *J* = 5 Hz, 1H), 7.91 (s, 1H), 7.57 (d, *J* = 5 Hz, 1H), 6.87 (s, 1H), 4.08-3.89 (m, 4H), 3.66 (s, 3H), 3.44-3.35 (m, 2H), 2.93-2.85 (m, 2H), 2.75 (s, 3H), 2.63-2.57 (m, 1H), 2.55-2.51 (m, 1H), 2.51-2.46 (m, 1H), 1.17 (d, *J* = 6 Hz, 3H), 1.17-1.12 (m, 1H), 0.54-0.47 (m, 2H), 0.27-0.20 (m, 2H); LC-MS (Method A) *m/z* = [M + H]⁺ 487.3, *t_R* 0.55 mins.

General Nucleophilic Substitution Procedure**3-bromo-2-(Cyclopropylmethoxy)pyridine, 136**

A solution of cyclopropylmethanol (0.388 mL, 5.20 mmol) in DMF (10 mL) was treated with sodium hydride (208 mg, 5.20 mmol, 60% w/w dispersion in mineral oils). The reaction mixture was stirred for 30 min and was treated with **135** (500 mg, 2.60 mmol) and stirred at room temperature overnight. The reaction mixture was partitioned

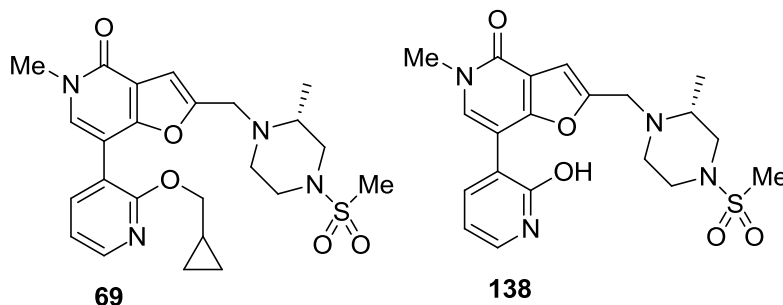
between water (20 mL) and EtOAc (20 mL) and the organic extract isolated. The aqueous layer was re-extracted with EtOAc (2 x 20 mL) and the combined organic extracts passed through a hydrophobic frit then concentrated under reduced pressure to afford **136** as an orange oil (528 mg, 36% at 80% purity by LCMS and NMR). ¹H NMR (400 MHz, DMSO-d₆ δ): 8.14 (dd, *J* = 5, 2 Hz, 1H), 8.02 (dd, *J* = 8, 2 Hz, 1H), 6.93 (dd, *J* = 8, 5 Hz, 1H), 4.18 (d, *J* = 7 Hz, 2H), 1.34-1.20 (m, 1H), 0.61-0.51 (m, 2H), 0.40-0.31 (m, 2H); LC-MS (Method A) *m/z* = [M + H]⁺ 228.0/230.0, *t_R* 1.18 mins.

2-(Cyclopropylmethoxy)-3-(4,4,5,5-tetramethyl-1,3,2-dioxaborolan-2-yl)pyridine, 137



A suspension of **136** (525 mg, 1.84 mmol, at 80% purity) in 1,4-dioxane (5 mL) was treated with 4,4,4',4',5,5,5',5'-octamethyl-2,2'-bi(1,3,2-dioxaborolane) (935 mg, 3.68 mmol), potassium acetate (542 mg, 5.52 mmol) and Pd(dppf)Cl₂ (135 mg, 0.18 mmol, 10 mol%). The reaction mixture was heated using microwave irradiation at 100 °C for 30 min then at 120 °C for 1 h. The reaction mixture was treated with EtOAc (approximately 5 mL) and filtered through a Celite^(R) cartridge. The solvent was removed under reduced pressure to give **137** as a brown oil (2430 mg, maximum possible theoretical yield is 495 mg, so material estimated to be a maximum of 495/2430 x 100 = 20% purity by weight). This crude material was used in the next step without purification, so no yield is given. The ¹H NMR spectrum of crude material contained the following significant peaks: ¹H NMR (400 MHz, DMSO-d₆ δ): 8.20 (dd, *J* = 5, 2 Hz, 1H), 7.85 (dd, *J* = 7, 2 Hz, 1H), 6.93 (dd, *J* = 7, 5 Hz, 1H), 4.16 (d, *J* = 6 Hz, 2H), 1.29 (s, 12H), 0.89-0.78 (m, 1H), 0.53-0.46 (m, 2H), 0.42-0.35 (m, 2H); LC-MS (Method A) *m/z* = [M + H]⁺ 194.0, *t_R* 0.79 mins (observed mass ion is consistent with hydrolysis to boronic acid under LC-MS conditions).

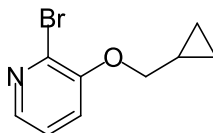
(*R*)-7-(2-(Cyclopropylmethoxy)pyridin-3-yl)-5-methyl-2-((2-methyl-4-(methylsulfonyl)piperazin-1-yl)methyl)furo[3,2-*c*]pyridin-4(5*H*)-one, **69**, and (*R*)-7-(2-hydroxypyridin-3-yl)-5-methyl-2-((2-methyl-4-(methylsulfonyl)piperazin-1-yl)methyl)furo[3,2-*c*]pyridin-4(5*H*)-one, **138**



The general Suzuki coupling procedure 2 was used in an attempt to prepare **69** from **115** (85 mg, 0.20 mmol) and **137** (311 mg, 0.24 mmol, at 20% purity by weight). The material was purified by MDAP (Method D); LC-MS (Method A) **69**: $m/z = [M + H]^+$ 487.2, t_R 0.76 mins (86% by area); **138**: $m/z = [M + H]^+$ 433.2, t_R 0.43 mins (14% by area).

General Alkylation Procedure 1

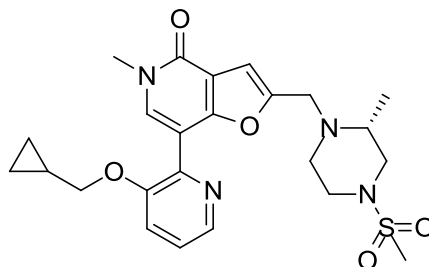
2-Bromo-3-(cyclopropylmethoxy)pyridine, **140**



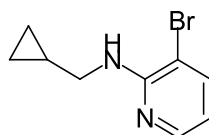
A solution of **132** (400 mg, 2.30 mmol) in DMF (15 mL) was cooled to 0 °C and treated with sodium hydride (110 mg, 2.76 mmol, 60% w/w dispersion in mineral oils). The reaction mixture was stirred for 30 min and treated with (bromomethyl)cyclopropane (0.268 mL, 2.76 mmol). The mixture was stirred overnight then partitioned between water and EtOAc (20 mL). The organic extract was isolated and washed with brine then concentrated under reduced pressure. The crude product was dissolved in MeOH and loaded onto a 10 g aminopropyl SPE column and eluted with MeOH to afford **140** as a yellow oil (455 mg, 87%). 1H NMR (400 MHz, DMSO- d_6 δ): 7.95 (dd, $J = 5, 2$ Hz, 1H), 7.49 (dd, $J = 8, 2$ Hz, 1H), 7.38 (dd, $J = 8, 5$ Hz, 1H), 3.97 (d, $J = 7$ Hz, 2H), 1.33-1.18

(m, 1H), 0.66-0.55 (m, 2H), 0.41-0.34 (m, 2H); LC-MS (Method A): $m/z = [M + H]^+$ 228.0/230.1, t_R 0.98 mins.

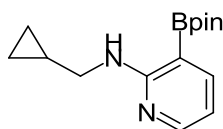
(R)-7-(3-(Cyclopropylmethoxy)pyridin-2-yl)-5-methyl-2-((2-methyl-4-(methylsulfonyl)piperazin-1-yl)methyl)furo[3,2-c]pyridin-4(5H)-one, 71



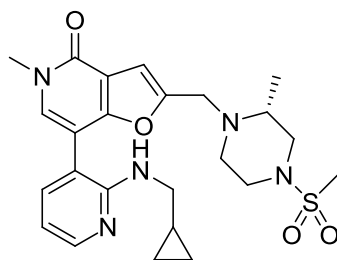
A solution of **140** (201 mg, 0.88 mmol) in THF (5 mL) was cooled under nitrogen using an iced water bath. The reaction mixture was treated with a solution of *i*PrMgCl (1.76 mL of a 2 M solution in ether, 3.52 mmol) and warmed to room temperature for 4 h. The reaction mixture was cooled using an iced water bath and treated dropwise with a solution of 1 M ZnCl₂ in ether (2.91 mL, 2.91 mmol). The reaction mixture was warmed to room temperature and stirred for 4 h to afford **141**. The reaction mixture was treated with **115** (221 mg, 0.53 mmol) followed by *tetrakis*(triphenylphosphino)palladium(0) (102 mg, 0.088 mmol, 17 mol%) then heated at 80 °C overnight. The reaction mixture was partitioned between water (20 mL) and EtOAc (20 mL) and the organic extract isolated. The aqueous layer was re-extracted with EtOAc (20 mL) and the combined extracts were passed through a hydrophobic frit and concentrated under reduced pressure. The crude product was purified by MDAP (Method C) to afford **71** as a white solid (65 mg, 25%). IR (cm⁻¹) 3431, 1661, 1327, 1279, 1159, 984, 790, 776; ¹H NMR (600 MHz, CD₃OD δ): 8.24 (d, *J* = 5 Hz, 1H), 7.83 (s, 1H), 7.60 (d, *J* = 8 Hz, 1H), 7.46 (dd, *J* = 8, 5 Hz, 1H), 6.94 (s, 1H), 4.00-3.83 (m, 4H), 3.74 (s, 3H), 3.51-3.41 (m, 2H), 2.99-2.91 (m, 2H), 2.82 (s, 3H), 2.69-2.64 (m, 1H), 2.63-2.52 (m, 2H), 1.21 (d, *J* = 6 Hz, 3H), 1.20-1.13 (m, 1H), 0.57-0.52 (m, 2H), 0.30-0.25 (m, 2H); ¹³C NMR (126 MHz, DMSO-d₆, δ): 158.0, 157.1, 153.2, 153.0, 141.4, 140.9, 136.1, 123.9, 120.1, 114.8, 107.0, 105.8, 72.4, 53.2, 51.5, 49.7, 48.9, 45.4, 36.3, 33.6, 15.2, 9.8, 2.9; HRMS–FAB (m/z): [M + H]⁺ calcd for C₂₄H₃₀N₄O₅S, 487.201; found, 487.2005; LC-MS (Method A): $m/z = [M + H]^+$ 487.2, t_R 0.67 mins; mp 101 – 103 °C.

3-Bromo-N-(cyclopropylmethyl)pyridin-2-amine, 72b

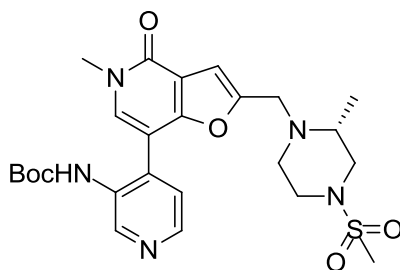
A solution of **72a** (250 mg, 1.30 mmol) in IPA (3 mL) was treated with DIPEA (0.454 mL, 2.60 mmol) and cyclopropylmethanamine (0.445 mL, 5.20 mmol). The reaction mixture was heated using microwave irradiation at 120 °C for 1 h then 180 °C for 4 h then partitioned with water (10 mL) and EtOAc (10 mL). The organic extract was isolated and the aqueous layer re-extracted with EtOAc (10 mL). Combined organic extracts were concentrated under reduced pressure then purified by silica chromatography using EtOAc to give **72b** as a colourless oil (232 mg, 79%). ¹H NMR (400 MHz, DMSO-d₆ δ): 8.01 (dd, *J* = 5, 2 Hz, 1H), 7.72 (dd, *J* = 8, 2 Hz, 1H), 6.47 (dd, *J* = 8, 5 Hz, 1H), 6.25-6.18 (m, 1H), 3.27-3.18 (m, 2H), 1.21-1.07 (m, 1H), 0.46-0.36 (m, 2H), 0.28-0.20 (m, 2H); LC-MS (Method A): *m/z* = [M + H]⁺ 227.0/229.0, *t_R* 0.74 mins.

N-(Cyclopropylmethyl)-3-(4,4,5,5-tetramethyl-1,3,2-dioxaborolan-2-yl)pyridin-2-amine, 72c

Prepared using the general boronylation procedure 1 from **72b** (228 mg, 1.00 mmol) to give **72c** as a brown gum (551 mg, *maximum possible theoretical yield is 275 mg, so material estimated to be a maximum of 275/551 x 100 = 50% purity by weight*). The compound was taken forward without purification, so no yield is given. The ¹H NMR spectrum of crude material contained the following significant peaks: ¹H NMR (400 MHz, DMSO-d₆ δ): 8.10 (dd, *J* = 5, 2 Hz, 1H), 7.67 (dd, *J* = 7, 2 Hz, 1H), 6.48 (dd, *J* = 7, 5 Hz, 1H), 6.40-6.31 (m, 1H), 3.28-3.16 (m, 2H), 1.32 (s, 12H), 1.07-0.99 (m, 1H), 0.50-0.40 (m, 2H), 0.26-0.16 (m, 2H); LC-MS (Method A) *m/z* = [M + H]⁺ 193.1, *t_R* 0.44 mins (*observed mass ion is consistent with hydrolysis to boronic acid under LCMS conditions*).

(R)-7-(2-((Cyclopropylmethyl)amino)pyridin-3-yl)-5-methyl-2-((2-methyl-4-(methylsulfonyl)piperazin-1-yl)methyl)furo[3,2-c]pyridin-4(5H)-one, 72

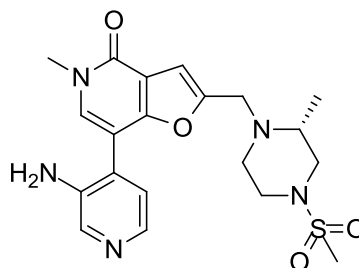
Prepared using the general Suzuki coupling procedure 2 from **115** (90 mg, 0.22 mmol) and **72b** (172 mg, 0.31 mmol, *at a maximum 50% purity by weight*) to afford **72** as a brown solid (35 mg, 34%). IR (cm⁻¹) 3348, 1662, 1587, 1506, 1323, 1157, 1014, 983, 927, 789, 771; ¹H NMR (600 MHz, CD₃OD δ): 8.05 (dd, *J* = 5, 2 Hz, 1H), 7.59 (s, 1H), 7.43 (dd, *J* = 7, 2 Hz, 1H), 6.93 (s, 1H), 6.67 (dd, *J* = 7, 5 Hz, 1H), 4.00-3.86 (m, 2H), 3.70 (s, 3H), 3.52-3.33 (m, 5H), 2.99-2.87 (m, 2H), 2.81 (s, 3H), 2.67-2.60 (m, 1H), 2.60-2.44 (m, 2H), 1.19 (d, *J* = 6 Hz, 3H), 1.14-1.02 (m, 1H), 0.48-0.34 (m, 2H), 0.24-0.13 (m, 2H); ¹³C NMR (126 MHz, DMSO-*d*₆, δ): 158.3, 157.4, 156.6, 153.0, 147.5, 138.1, 135.5, 115.4, 112.3, 111.0, 106.2, 105.4, 52.9, 51.5, 49.6, 48.7, 45.5, 44.9, 36.2, 33.6, 15.3, 11.0, 3.2; HRMS-FAB (*m/z*): [M + H]⁺ calcd for C₂₄H₃₁N₅O₄S, 486.217; found, 486.216; LC-MS (Method A) *m/z* = [M + H]⁺ 486.3, *t*_R 0.46 mins; mp 119 – 120 °C.

(R)-tert-Butyl (4-(5-methyl-2-((2-methyl-4-(methylsulfonyl)piperazin-1-yl)methyl)-4-oxo-4,5-dihydrofuro[3,2-c]pyridin-7-yl)pyridin-3-yl)carbamate, 73b

Prepared using the general Suzuki coupling procedure 2 from **115** (176 mg, 0.42 mmol) and **73a** (100 mg, 0.42 mmol). Crude product was purified by silica chromatography (0 to 5% of MeOH in DCM), instead of MDAP, to afford **73b** as a white solid (87 mg,

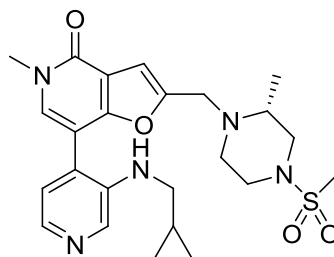
39%). ^1H NMR (400 MHz, CD_3OD δ): 8.75 (s, 1H), 8.43 (d, $J = 5$ Hz, 1H), 7.72 (s, 1H), 7.53 (d, $J = 5$ Hz, 1H), 6.95 (s, 1H), 4.01-3.78 (m, 2H), 3.71 (s, 3H), 3.49-3.40 (m, 2H), 3.01-2.88 (m, 2H), 2.82 (s, 3H), 2.72-2.63 (m, 1H), 2.60-2.43 (m, 2H), 1.36 (s, 9H), 1.21 (d, $J = 6$ Hz, 3H), *amide proton underwent exchange in the wet deuterated solvent and was not seen*; LC-MS (Method A) $m/z = [\text{M} + \text{H}]^+ 532.3$, t_R 0.57 mins.

(R)-7-(3-Aminopyridin-4-yl)-5-methyl-2-((2-methyl-4-(methylsulfonyl)piperazin-1-yl)methyl)furo[3,2-c]pyridin-4(5H)-one, 73c



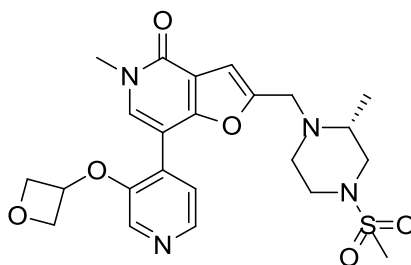
A suspension of **73b** (87 mg, 0.16 mmol) in DCM (2 mL) was treated with TFA (2 mL). The reaction mixture was stirred at room temperature for 30 min then concentrated under reduced pressure. The crude product was loaded onto an aminopropyl SPE column and eluted with MeOH to afford **73c** as a yellow solid (81 mg, 97% at 85% purity by LCMS and NMR). The ^1H NMR spectrum of crude material contained the following significant peaks: (400 MHz, CD_3OD δ): 8.12 (s, 1H), 7.88 (d, $J = 5$ Hz, 1H), 7.71 (s, 1H), 7.22 (d, $J = 5$ Hz, 1H), 6.94 (s, 1H), 4.02-3.87 (m, 2H), 3.70 (s, 3H), 3.53-3.40 (m, 2H), 3.38-3.34 (m, 1H), 3.02-2.88 (m, 2H), 2.82 (s, 3H), 2.70-2.49 (m, 3H), 1.22 (d, $J = 5$ Hz, 3H), *anilinic proton underwent exchange in the wet deuterated solvent and were not observed*; LC-MS (Method A) $m/z = [\text{M} + \text{H}]^+ 432.2$, t_R 0.34 mins.

(R)-7-(3-((Cyclopropylmethyl)amino)pyridin-4-yl)-5-methyl-2-((2-methyl-4-(methylsulfonyl)piperazin-1-yl)methyl)furo[3,2-c]pyridin-4(5H)-one, 73



A suspension of cyclopropanecarbaldehyde (0.012 mL, 0.16 mmol) in a solution of AcOH and MeOH (1 : 9 v/v, 10 mL) was treated with **73c** (81 mg, 0.16 mmol *at 85% purity by weight*). The reaction mixture was stirred at room temperature for 30 min. The reaction mixture was treated with 2-picoline borane complex (26 mg, 0.24 mmol) and stirred at room temperature overnight then concentrated under reduced pressure. The reaction mixture was partitioned with saturated sodium bicarbonate solution (20 mL) and DCM (10 mL). The organic extract was isolated and the aqueous layer re-extracted with DCM (10 mL). The combined organic extracts were passed through a hydrophobic frit then concentrated under reduced pressure. The crude product was purified by MDAP (Method C) and re-purified by MDAP (Method A). The purified product was loaded onto an aminopropyl SPE column and eluted with MeOH to afford **73** as a white solid (22 mg, 28%). ¹H NMR (400 MHz, CD₃OD δ): 8.08 (s, 1H), 7.91 (d, *J* = 5 Hz, 1H), 7.68 (s, 1H), 7.19 (d, *J* = 5 Hz, 1H), 6.94 (s, 1H), 3.99-3.88 (m, 2H), 3.71 (s, 3H), 3.51-3.40 (m, 2H), 3.09 (d, *J* = 7 Hz, 2H), 2.97-2.89 (m, 2H), 2.81 (s, 3H), 2.67-2.60 (m, 1H), 2.60-2.48 (m, 2H), 1.20 (d, *J* = 6 Hz, 3H), 1.12-1.01 (m, 1H), 0.54-0.46 (m, 2H), 0.27-0.19 (m, 2H), *aniline proton underwent exchange in the wet deuterated solvent and was not observed*; LC-MS (Method A) *m/z* = [M + H]⁺ 486.3, *t_R* 0.48 mins.

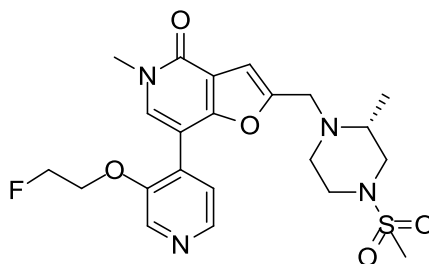
(R)-5-methyl-2-((2-methyl-4-(methylsulfonyl)piperazin-1-yl)methyl)-7-(3-(oxetan-3-yloxy)pyridin-4-yl)furo[3,2-c]pyridin-4(5H)-one, 88



A solution of **115** (200 mg, 0.48 mmol) in 1,4-dioxane (4 mL) was treated with triethylamine (0.265 mL, 1.91 mmol), PEPPSITM-SiPr^(R) (33 mg, 0.048 mmol, 10 mol%) and 4,4,5,5-tetramethyl-1,3,2-dioxaborolane (0.416 mL, 2.87 mmol). The reaction mixture was heated at 100 °C for 3 h. The reaction mixture was treated. The reaction mixture was treated with IPA (4 mL) and washed through Celite^(R) using IPA (10 mL) to afford a mixture of **119**, **119a** and **120**.

The solution was treated with **88b** (197 mg, 0.40 mmol, at a maximum of 47% purity by weight), PEPPSI-SiPr^(R) (16 mg, 0.02 mmol, 5 mol%), potassium carbonate (33 mg, 0.24 mmol) and water (3 mL). The reaction mixture was heated at reflux under nitrogen for 1 h. The reaction mixture was partitioned with water (10 mL) and DCM (20 mL). The organic extract was isolated and the aqueous layer re-extracted with DCM (3 x 20 mL). The combined organic extracts were concentrated under reduced pressure. Crude product was purified by silica chromatography (0 to 75% MeOH/acetone) to afford crude **88**. The crude product was purified by MDAP (Method A) then loaded in MeOH onto an aminopropyl SPE column (1 g) and eluted with MeOH to afford **88** as a yellow oil (40 mg, 20%). IR (cm⁻¹) 3420, 2943, 1659, 1586, 1323, 1299, 1247, 1157, 1117, 973, 790, 774; ¹H NMR (400 MHz, CDCl₃ δ): 8.38 (d, *J* = 5 Hz, 1H), 7.95 (s, 1H), 7.58 (s, 1H), 7.49 (d, *J* = 5 Hz, 1H), 6.88 (s, 1H), 5.41-5.32 (m, 1H), 5.05-4.97 (m, 2H), 4.74-4.65 (m, 2H), 3.96-3.79 (m, 2H), 3.70 (s, 3H), 3.54-3.44 (m, 2H), 2.96-2.86 (m, 2H), 2.74 (s, 3H), 2.65-2.49 (m, 3H), 1.19 (d, *J* = 6 Hz, 3H); ¹³C NMR (126 MHz, DMSO-d₆, δ): 158.0, 156.5, 153.4, 149.8, 143.1, 136.0, 134.5, 129.1, 124.7, 115.0, 106.0, 103.5, 76.5, 70.6, 53.3, 51.5, 49.8, 48.6, 45.4, 36.4, 33.5, 15.4; HRMS–FAB (*m/z*): [M + H]⁺ calcd for C₂₃H₂₈N₄O₆S, 489.1802; found, 489.1805; LC-MS (Method A) *m/z* = [M + H]⁺ 489.3, *t_R* 0.44 mins, mp 124 – 126 °C.

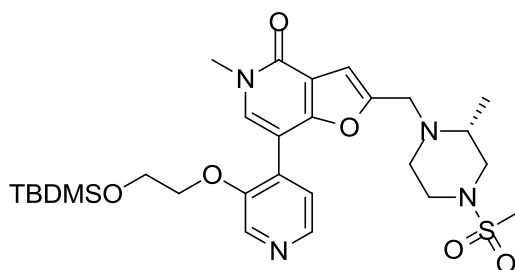
(R)-7-(3-(2-Fluoroethoxy)pyridin-4-yl)-5-methyl-2-((2-methyl-4-(methylsulfonyl)piperazin-1-yl)methyl)furo[3,2-*c*]pyridin-4(5*H*)-one, 75



A solution of **115** (179 mg, 0.43 mmol) in 1,4-dioxane (3 mL) was treated with triethylamine (0.239 mL, 1.71 mmol), PEPPSITM-SiPr^(R) (29 mg, 0.04 mmol, 10 mol%) and 4,4,5,5-tetramethyl-1,3,2-dioxaborolane (0.373 mL, 2.57 mmol). The reaction mixture was heated at 100 °C for 2.5 h by microwave irradiation. The reaction mixture was diluted with EtOAc and filtered through Celite^(R) then concentrated under reduced pressure to give a mixture of **119**, **119a** and **120**. The residue was dissolved in DME (3

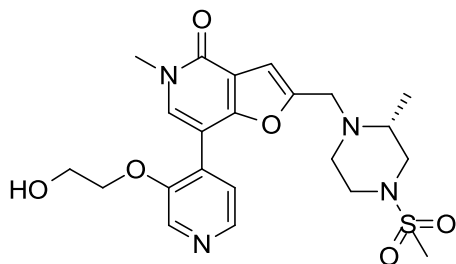
mL) and the reaction mixture treated with **75a** (92 mg, 0.42 mmol) *tetrakis*(triphenylphosphino)palladium(0) (24 mg, 0.021 mmol, 5 mol%), a 2 M aqueous solution of sodium bicarbonate (0.844 mL, 1.69 mmol). The reaction mixture was heated at 120 °C for 30 min using microwave irradiation then diluted with water and EtOAc. The organic extract was isolated and the aqueous layer re-extracted with EtOAc (3 x 20 mL). The combined organic extracts were passed through a hydrophobic frit then concentrated under reduced pressure. The crude product was purified by MDAP (Method C) to afford **75** as a beige solid (20 mg, 10% over two steps). ¹H NMR (400 MHz, CD₃OD δ): 8.46 (s, 1H), 8.33 (d, *J* = 5 Hz, 1H), 7.95 (s, 1H), 7.66 (d, *J* = 5 Hz, 1H), 6.93 (s, 1H), 4.70 (dt, ²*J*_{H-F} = 48, *J* = 4 Hz, 2H), 4.44 (dt, *J*_{H-F} = 29, *J* = 4 Hz, 2H), 4.05-3.85 (m, 2H), 3.71 (s, 3H), 3.52-3.40 (m, 2H), 3.01-2.90 (m, 2H), 2.82 (s, 3H), 2.71-2.63 (m, 1H), 2.63-2.48 (m, 2H), 1.23 (d, *J* = 6 Hz, 3H); LC-MS (Method A) *m/z* = [M + H]⁺ 479.3, *t*_R 0.70 mins.

(R)-7-(3-(2-((*tert*-Butyldimethylsilyl)oxy)ethoxy)pyridin-4-yl)-5-methyl-2-((2-methyl-4-(methylsulfonyl)piperazin-1-yl)methyl)furo[3,2-*c*]pyridin-4(5*H*)-one, 76b



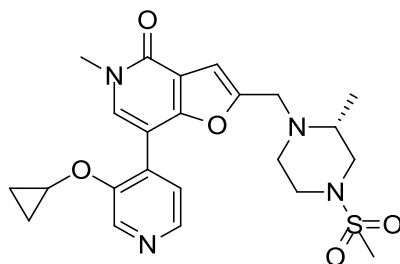
A crude mixture of **119**, **119a** and **120** was prepared using the general boronylation procedure 2 from **115** (170 mg, 0.41 mmol) and 4,4,5,5-tetramethyl-1,3,2-dioxaborolane (0.354 mL, 2.44 mmol). The crude material was used in the general Suzuki coupling procedure 2 using **76a** (118 mg, 0.36 mmol), using 5 mol% of *tetrakis*(triphenylphosphino)palladium(0) instead of 10 mol%, and heating for 30 min instead of 2 h, and material was purified by silica chromatography (12% MeOH/EtOAc), to afford **76b** as an orange oil (34 mg, 16% over two steps); *no NMR was obtained*; LC-MS (Method A) *m/z* = [M + H]⁺ 591.4, *t*_R 0.87 mins.

(R)-7-(3-(2-Hydroxyethoxy)pyridin-4-yl)-5-methyl-2-((2-methyl-4-(methylsulfonyl)piperazin-1-yl)methyl)furo[3,2-c]pyridin-4(5H)-one, 76



A stirred solution of **76b** (34 mg, 0.058 mmol) in THF (5 mL) was treated with a 1M solution of TBAF in THF (0.230 mL, 0.23 mmol). The reaction mixture was stirred for 2 h then concentrated under reduced pressure. Crude produce was purified by MDAP (Method C) to afford **76** as a (20 mg, 72%). IR (cm⁻¹) 3700 - 3100 (br.), 1654, 1586, 1323, 1300, 1156, 790, 774; ¹H NMR (400 MHz, CD₃OD δ): 8.45 (s, 1H), 8.30 (d, *J* = 5 Hz, 1H), 8.11 (s, 1H), 7.69 (d, *J* = 5 Hz, 1H), 6.93 (s, 1H), 4.28 (t, *J* = 4 Hz, 2H), 4.04-3.82 (m, 4H), 3.72 (s, 3H), 3.52-3.42 (m, 2H), 3.01-2.92 (m, 2H), 2.83 (s, 3H), 2.71-2.50 (m, 4H), 1.24 (d, *J* = 6 Hz, 3H); ¹³C NMR (126 MHz, DMSO-d₆, δ): 157.9, 156.6, 153.3, 151.9, 142.4, 136.6, 135.9, 128.6, 123.9, 115.1, 105.9, 103.2, 70.9, 60.0, 53.2, 51.5, 49.8, 48.7, 45.4, 36.4, 33.6, 15.3; HRMS-FAB (*m/z*): [M + H]⁺ calcd for C₂₂H₂₈N₄O₆S, 477.1802; found, 477.1795; LC-MS (Method A) *m/z* = [M + H]⁺ 477.3, *t_R* 0.38 mins; mp 118 – 120 °C.

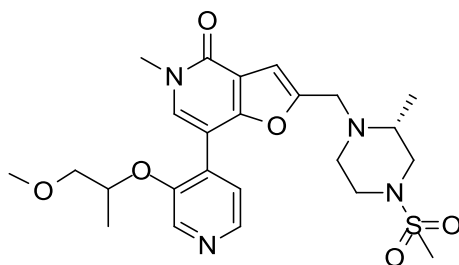
(R)-7-(3-Cyclopropoxy)pyridin-4-yl)-5-methyl-2-((2-methyl-4-(methylsulfonyl)piperazin-1-yl)methyl)furo[3,2-c]pyridin-4(5H)-one, 78



A crude mixture of **119**, **119a** and **120** was prepared using the general boronylation procedure 2 from **115** (200 mg, 0.48 mmol) and 4,4,5,5-tetramethyl-1,3,2-dioxaborolane (0.555 mL, 3.82 mmol). The crude material was used in the general

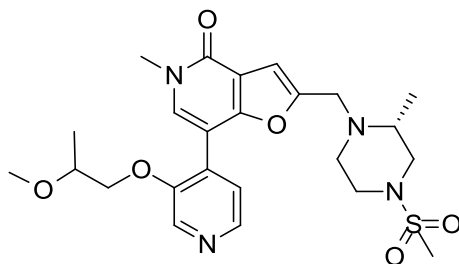
Suzuki coupling procedure 2 using **78a** (70 mg, 0.33 mmol), using 5 mol% of *tetrakis*(triphenylphosphino)palladium(0) instead of 10 mol%, and heating for 30 min instead of 2 h. Crude product was purified by MDAP (Method D) and loaded onto an SCX SPE column then eluted with a 2 M solution of ammonia in MeOH to afford **78** as a white solid (21 mg, 14% over two steps). ¹H NMR (400 MHz, CD₃OD δ): 8.73 (s, 1H), 8.31 (d, *J* = 5 Hz, 1H), 7.78 (s, 1H), 7.55 (d, *J* = 5 Hz, 1H), 6.93 (s, 1H), 4.08-4.02 (m, 1H), 3.99-3.94 (m, 2H), 3.70 (s, 3H), 3.54-3.44 (m, 2H), 3.02-2.91 (m, 2H), 2.83 (s, 3H), 2.71-2.53 (m, 3H), 1.24 (d, *J* = 6 Hz, 3H), 0.94-0.86 (m, 2H), 0.76-0.66 (m, 2H); LC-MS (Method A) *m/z* = [M + H]⁺ 473.2, *t_R* 0.49 mins.

7-(3-((1-Methoxypropan-2-yl)oxy)pyridin-4-yl)-5-methyl-2-(((*R*)-2-methyl-4-(methylsulfonyl)piperazin-1-yl)methyl)furo[3,2-*c*]pyridin-4(5*H*)-one, 79



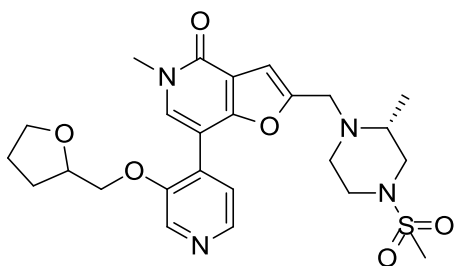
A crude mixture of **119**, **119a** and **120** was prepared using the general boronylation procedure 2 from **115** (200 mg, 0.48 mmol) and 4,4,5,5-tetramethyl-1,3,2-dioxaborolane (0.555 mL, 3.82 mmol). The crude material was used in the general Suzuki coupling procedure 2 using **79b** (83 mg, 0.34 mmol), using 5 mol% of *tetrakis*(triphenylphosphino)palladium(0) instead of 10 mol%, and heating for 30 min instead of 2 h, to afford **79** as a brown solid (36 mg, 20% over two steps). ¹H NMR (400 MHz, CD₃OD δ): 8.47 (s, 1H), 8.28 (d, *J* = 5 Hz, 1H), 8.03 (s, 1H), 7.67 (d, *J* = 5 Hz, 1H), 6.94 (s, 1H), 4.79-4.69 (m, 1H), 4.05-3.85 (m, 2H), 3.72 (s, 3H), 3.55-3.42 (m, 4H), 3.31-3.27 (s, 3H, *obscured by residual solvent peak*), 3.01-2.90 (m, 2H), 2.82 (s, 3H), 2.72-2.64 (m, 1H), 2.63-2.49 (m, 2H), 1.31 (d, *J* = 6 Hz, 3H), 1.24 (d, *J* = 6 Hz, 3H); LC-MS (Method A) *m/z* = [M + H]⁺ 505.3, *t_R* 0.50 mins.

7-(3-(2-Methoxypropoxy)pyridin-4-yl)-5-methyl-2-(((R)-2-methyl-4-(methylsulfonyl)piperazin-1-yl)methyl)furo[3,2-c]pyridin-4(5H)-one, 80



A crude mixture of **119**, **119a** and **120** was prepared using the general boronylation procedure 2 from **115** (225 mg, 0.54 mmol) and 4,4,5,5-tetramethyl-1,3,2-dioxaborolane (0.624 mL, 4.30 mmol). The crude material was used in the general Suzuki coupling procedure 2 using **80b** (106 mg, 0.43 mmol), using 5 mol% of *tetrakis*(triphenylphosphino)palladium(0) instead of 10 mol%, and heating for 30 min instead of 2 h, to afford **80** as a brown solid (28 mg, 13% over two steps). ¹H NMR (400 MHz, CD₃OD δ): 8.44 (s, 1H), 8.30 (d, *J* = 5 Hz, 1H), 8.04 (s, 1H), 7.68 (d, *J* = 5 Hz, 1H), 6.94 (s, 1H), 4.29-4.06 (m, 2H), 4.04-3.88 (m, 2H), 3.72 (s, 3H), 3.71-3.64 (m, 1H), 3.52-3.41 (m, 2H), 3.30 (s, 3H), 3.01-2.91 (m, 2H), 2.82 (s, 3H), 2.71-2.64 (m, 1H), 2.62-2.49 (m, 2H), 1.24 (d, *J* = 6 Hz, 3H), 1.18 (d, *J* = 6 Hz, 3H); LC-MS (Method A) *m/z* = [M + H]⁺ 505.3, *t_R* 0.50 mins.

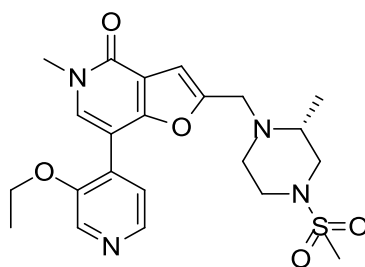
5-Methyl-2-(((R)-2-methyl-4-(methylsulfonyl)piperazin-1-yl)methyl)-7-(3-((tetrahydrofuran-2-yl)methoxy)pyridin-4-yl)furo[3,2-c]pyridin-4(5H)-one, 81



A crude mixture of **119**, **119a** and **120** was prepared using the general boronylation procedure 2 from **115** (200 mg, 0.48 mmol) and 4,4,5,5-tetramethyl-1,3,2-dioxaborolane (0.416 mL, 2.87 mmol). The crude material was used in the general Suzuki coupling procedure 2 using **81a** (98 mg, 0.38 mmol), using 5 mol% of *tetrakis*(triphenylphosphino)palladium(0) instead of 10 mol%, and heating for 30 min

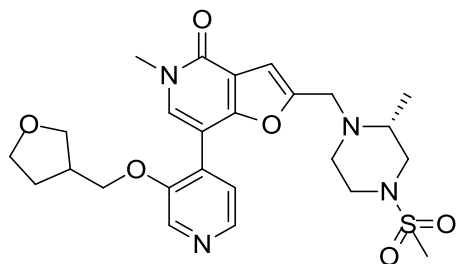
instead of 2 h, to afford **80** as a brown solid (33 mg, 17% over two steps). ¹H NMR (400 MHz, CD₃OD δ): 8.45 (s, 1H), 8.30 (d, *J* = 5 Hz, 1H), 8.05 (s, 1H), 7.66 (d, *J* = 5 Hz, 1H), 6.93 (s, 1H), 4.30-4.18 (m, 2H), 4.16-4.09 (m, 1H), 4.04-3.89 (m, 2H), 3.75 (t, *J* = 7 Hz, 2H), 3.72 (s, 3H), 3.53-3.41 (m, 2H), 3.00-2.92 (m, 2H), 2.82 (s, 3H), 2.71-2.63 (m, 1H), 2.62-2.48 (m, 2H), 2.09-1.96 (m, 1H), 1.92-1.77 (m, 2H), 1.76-1.63 (m, 1H), 1.23 (d, *J* = 6 Hz, 3H); LC-MS (Method A) *m/z* = [M + H]⁺ 517.1, *t_R* 0.50 mins.

(R)-7-(3-Ethoxypyridin-4-yl)-5-methyl-2-((2-methyl-4-(methylsulfonyl)piperazin-1-yl)methyl)furo[3,2-*c*]pyridin-4(5*H*)-one, 82



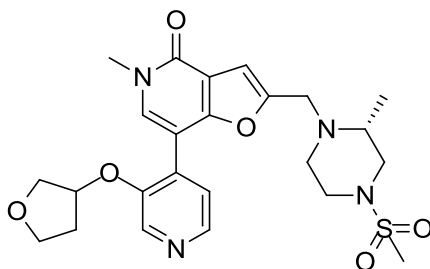
A crude mixture of **119**, **119a** and **120** was prepared using the general boronylation procedure 2 from **115** (200 mg, 0.48 mmol) and 4,4,5,5-tetramethyl-1,3,2-dioxaborolane (0.416 mL, 4.16 mmol). The crude material was used in the general Suzuki coupling procedure 2 using **82a** (40 mg, 0.20 mmol), using 5 mol% of *tetrakis*(triphenylphosphino)palladium(0) instead of 10 mol%, and heating for 30 min instead of 2 h, to afford **82** as a white solid (38 mg, 42%). ¹H NMR (400 MHz, CD₃OD δ): 8.41 (s, 1H), 8.28 (d, *J* = 5 Hz, 1H), 7.88 (s, 1H), 7.59 (d, *J* = 5 Hz, 1H), 6.93 (s, 1H), 4.25 (q, *J* = 7 Hz, 2H), 4.01-3.90 (m, 2H), 3.72 (s, 3H), 3.52-3.42 (m, 2H), 3.00-2.91 (m, 2H), 2.82 (s, 3H), 2.70-2.62 (m, 1H), 2.61-2.52 (m, 2H), 1.36 (t, *J* = 7 Hz, 3H), 1.22 (d, *J* = 6 Hz, 3H); LC-MS (Method A) *m/z* = [M + H]⁺ 461.2, *t_R* 0.47 mins.

5-Methyl-2-(((R)-2-methyl-4-(methylsulfonyl)piperazin-1-yl)methyl)-7-(3-((tetrahydrofuran-3-yl)methoxy)pyridin-4-yl)furo[3,2-c]pyridin-4(5H)-one, 84



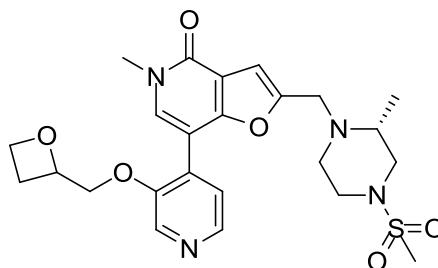
A crude mixture of **119**, **119a** and **120** was prepared using the general boronylation procedure 2 from **115** (230 mg, 0.55 mmol) and 4,4,5,5-tetramethyl-1,3,2-dioxaborolane (0.479 mL, 3.30 mmol). The crude material was used in the general Suzuki coupling procedure 2 using **84a** (224 mg, 0.52 mmol, at 60% purity by NMR), using 5 mol% of *tetrakis*(triphenylphosphino)palladium(0) instead of 10 mol%, and heating for 30 min instead of 2 h, to afford **84** as a white solid (30 mg, 11% over two steps). IR (cm⁻¹) 3447, 2855, 1660, 1586, 1324, 1300, 1157, 1013, 982, 790, 774; ¹H NMR (400 MHz, CD₃OD δ): 8.45 (s, 1H), 8.30 (d, *J* = 5 Hz, 1H), 7.87 (s, 1H), 7.60 (d, *J* = 5 Hz, 1H), 6.94 (s, 1H), 4.25-4.17 (m, 1H), 4.14-4.07 (m, 1H), 4.04-3.87 (m, 2H), 3.79-3.65 (m, 6H), 3.60-3.52 (m, 1H), 3.51-3.40 (m, 2H), 3.01-2.91 (m, 2H), 2.82 (s, 3H), 2.73-2.63 (m, 2H), 2.63-2.48 (m, 2H), 2.08-1.96 (m, 1H), 1.73-1.62 (m, 1H), 1.22 (d, *J* = 6 Hz, 3H); ¹³C NMR (126 MHz, DMSO-*d*₆, δ): 157.9, 156.6, 153.4, 151.8, 142.5, 136.1, 135.4, 128.7, 124.3, 115.0, 106.0, 103.4, 70.5, 69.5, 66.9, 53.2, 51.5, 49.7, 48.7, 45.4, 38.2, 36.3, 33.6, 28.3, 15.3; HRMS–FAB (*m/z*): [M + H]⁺ calcd for C₂₅H₃₂N₄O₆S, 517.2115; found, 517.2101; LC-MS (Method A) *m/z* = [M + H]⁺ 517.2, *t*_R 0.48 mins; mp 117 – 118 °C.

5-Methyl-2-(((R)-2-methyl-4-(methylsulfonyl)piperazin-1-yl)methyl)-7-(3-((tetrahydrofuran-3-yl)oxy)pyridin-4-yl)furo[3,2-c]pyridin-4(5H)-one, 86



A crude mixture of **119**, **119a** and **120** was prepared using the general boronylation procedure 2 from **115** (200 mg, 0.48 mmol) and 4,4,5,5-tetramethyl-1,3,2-dioxaborolane (0.416 mL, 2.87 mmol). The crude material was treated with **86b** (130 mg, 0.30 mmol, *at maximum of 57% purity by weight*), potassium carbonate (26 mg, 0.19 mmol), and PEPPSITM-SiPr^(R) (13 mg, 0.019 mmol, 6 mol%). The reaction mixture was suspended in DME (3 mL) and water (1 mL) and heated using microwave irradiation at 120 °C for 30 min. The reaction mixture was treated with further potassium carbonate (26 mg, 0.19 mmol), and PEPPSITM-SiPr^(R) (13 mg, 0.019 mmol, 6 mol%) and heated using microwave irradiation at 140 °C for 1 h. The reaction mixture was concentrated under reduced pressure, suspended in IPA (5 mL) and water (1 mL), and treated with potassium carbonate (26 mg, 0.19 mmol), and PEPPSITM-SiPr^(R) (13 mg, 0.019 mmol, 6 mol%), and heated to reflux for 1.5 h. The reaction mixture was partitioned with water (10 mL) and DCM (20 mL) and the organic layer separated. The aqueous layer was extracted twice more with DCM (20 mL) and the combined organic extracts were concentrated under reduced pressure. Crude material was purified by MDAP (Method A) then loaded in MeOH onto an aminopropyl SPE cartridge and eluted with MeOH to afford **86** as a yellow oil (19 mg, 12% over two steps). ¹H NMR (600 MHz, CD₃OD δ): 8.42 (s, 1H), 8.32 (d, *J* = 5 Hz, 1H), 7.87 (d, *J* = 3 Hz, 1H), 7.62 (t, *J* = 5 Hz, 1H), 6.94 (s, 1H), 5.27 (q, *J* = 6 Hz, 1H), 4.11-3.74 (m, 6H), 3.72 (s, 3H), 3.52-3.41 (m, 2H), 3.02-2.90 (m, 2H), 2.83 (d, *J* = 3 Hz, 3H), 2.73-2.63 (m, 1H), 2.62-2.48 (m, 2H), 2.36-2.22 (m, 1H), 2.13-1.99 (m, 1H), 1.23 (d, *J* = 6 Hz, 3H). LC-MS (Method A) *m/z* = [M + H]⁺ 503.3, *t_R* 0.42 mins.

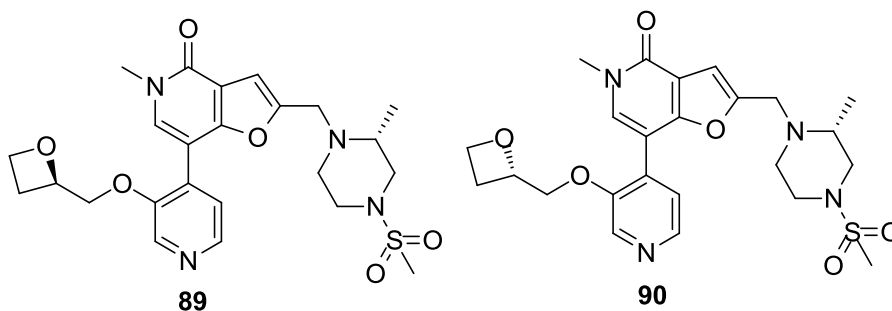
5-Methyl-2-(((R)-2-methyl-4-(methylsulfonyl)piperazin-1-yl)methyl)-7-(3-(oxetan-2-ylmethoxy)pyridin-4-yl)furo[3,2-c]pyridin-4(5H)-one, **87**



A crude mixture of **119**, **119a** and **120** was prepared using the general boronylation procedure 2 from **115** (120 mg, 0.29 mmol) and 4,4,5,5-tetramethyl-1,3,2-

dioxaborolane (0.250 mL, 1.72 mmol). The crude material was used in the general Suzuki coupling procedure 2 using **87b** (80 mg, 0.20 mmol, *at a maximum of 59% purity by weight*), using 5 mol% of *tetrakis*(triphenylphosphino)palladium(0) instead of 10 mol%, and heating for 30 min instead of 2 h, to afford **87** as a yellow oil (32 mg, 33% over two steps). ¹H NMR (400 MHz, DMSO-*d*₆ δ): 8.48 (s, 1H), 8.30 (d, *J* = 5 Hz, 1H), 7.96 (s, 1H), 7.63 (d, *J* = 5 Hz, 1H), 6.91 (s, 1H), 5.11-5.05 (m, 1H), 4.64-4.53 (m, 1H), 4.37-4.32 (m, 1H), 4.32-4.26 (m, 2H), 4.01-3.84 (m, 2H), 3.69 (s, 3H), 3.49-3.44 (m, 1H), 3.44-3.40 (m, 1H), 2.97-2.90 (m, 2H), 2.80 (s, 3H), 2.75-2.67 (m, 1H), 2.65-2.62 (m, 1H), 2.69-2.54 (m, 1H), 2.54-2.48 (m, 2H), 1.20 (d, *J* = 6 Hz, 3H); LC-MS (Method A) *m/z* = [M + H]⁺ 503.2, *t*_R 0.44 mins.

5-Methyl-2-(((*R*)-2-methyl-4-(methylsulfonyl)piperazin-1-yl)methyl)-7-(3-((*R*)-oxetan-2-ylmethoxy)pyridin-4-yl)furo[3,2-*c*]pyridin-4(5*H*)-one, **89, and 5-Methyl-2-(((*R*)-2-methyl-4-(methylsulfonyl)piperazin-1-yl)methyl)-7-(3-((*S*)-oxetan-2-ylmethoxy)pyridin-4-yl)furo[3,2-*c*]pyridin-4(5*H*)-one, **90****



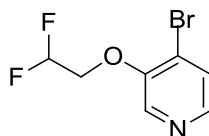
Racemate **87** (121 mg, 0.24 mmol) was purified by chiral HPLC method A to afford **89** (32 mg, 53% yield, *assuming the racemate was a 1:1 mixture of diastereomers, which would yield a maximum of 61 mg of each*), 98.8% by chiral HPLC analysis);¹² ¹H NMR (400 MHz, CD₃OD δ): 8.50 (s, 1H), 8.32 (d, *J* = 5 Hz, 1H), 7.98 (s, 1H), 7.65 (d, *J* = 5 Hz, 1H), 6.93 (s, 1H), 5.14-5.06 (m, 1H), 4.64-4.56 (m, 1H), 4.39-4.27 (m, 3H), 4.02-3.84 (m, 2H), 3.71 (s, 3H), 3.52-3.40 (m, 2H), 3.00-2.91 (m, 2H), 2.82 (s, 3H), 2.77-2.48 (m, 5H), 1.22 (d, *J* = 6 Hz, 3H); LC-MS (Method A) *m/z* = [M + H]⁺ 503.2, *t*_R 0.42 mins; mp 166 - 168 °C.

Compound **90** (36 mg, 60% yield, *assuming the racemate was a 1:1 mixture of diastereomers, which would yield a maximum of 61 mg of each*), 98.4% by chiral HPLC

analysis);¹² ¹H NMR (400 MHz, CD₃OD δ): 8.50 (s, 1H), 8.32 (d, *J* = 5 Hz, 1H), 7.98 (s, 1H), 7.64 (d, *J* = 5 Hz, 1H), 6.93 (s, 1H), 5.16-5.04 (m, 1H), 4.65-4.53 (m, 1H), 4.40-4.25 (m, 3H), 4.02-3.85 (m, 2H), 3.71 (s, 3H), 3.52-3.40 (m, 2H), 3.02-2.89 (m, 2H), 2.82 (s, 3H), 2.78-2.48 (m, 5H), 1.22 (d, *J* = 6 Hz, 3H); LC-MS (Method A) *m/z* = [M + H]⁺ 503.1, *t_R* 0.42 mins.

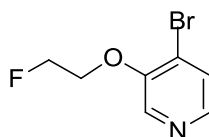
General Alkylation Procedure 2

4-Bromo-3-(2,2-difluoroethoxy)pyridine, 74a



A solution of **132** (100 mg, 0.58 mmol) in DMF (1.8 mL) was treated with caesium carbonate (206 mg, 0.63 mmol) and a solution of 2-bromo-1,1-difluoroethane (92 mg, 0.63 mmol) in DMF (0.3 mL). The reaction mixture was stirred overnight then was treated with caesium carbonate (412 mg, 1.27 mmol) and 2-bromo-1,1-difluoroethane (280 mg, 1.9 mmol). The reaction mixture was stirred at room temperature overnight and partitioned between water (5 mL) and EtOAc (5 mL). The organic extract was isolated and the aqueous layer re-extracted with EtOAc (2 x 5 mL). The combined organic extracts were dried over MgSO₄ and concentrated under reduced pressure to afford **74a** as a brown oil (73 mg, 53%). ¹H NMR (400 MHz, CDCl₃ δ): 8.28 (s, 1H), 8.17 (d, *J* = 5 Hz, 1H), 7.55 (d, *J* = 5 Hz, 1H), 6.13 (tt, ²*J*_{H-F} = 55, *J* = 4 Hz, 1H), 4.36 (dt, *J*_{H-F} = 13, *J* = 4 Hz, 2H); LC-MS (Method A) *m/z* = [M + H]⁺ 238.0/240.0, *t_R* 0.77 mins.

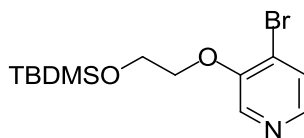
4-Bromo-3-(2-fluoroethoxy)pyridine, 75a



Prepared using the general alkylation procedure 2 from **132** (300 mg, 1.72 mmol) and 1-bromo-2-fluoroethane (0.141 mL, 1.90 mmol) to afford **75a** (277 mg, 73%). ¹H NMR (400 MHz, DMSO-d₆ δ): 8.43 (s, 1H), 8.10 (d, *J* = 5 Hz, 1H), 7.70 (d, *J* = 5 Hz, 1H),

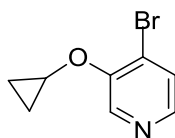
4.79 (dt, $^2J_{\text{H-F}} = 48$, $J = 4$ Hz, 2H), 4.49 (dt, $J_{\text{H-F}} = 30$, $J = 4$ Hz, 2H); LC-MS (Method A) $m/z = [\text{M} + \text{H}]^+$ 220.0/222.0, t_{R} 0.66 mins.

4-Bromo-3-(2-((*tert*-butyldimethylsilyl)oxy)ethoxy)pyridine, **76a**

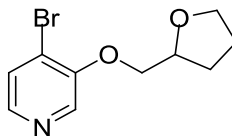


Prepared using the general alkylation procedure 2 from **132** (300 mg, 1.72 mmol) and (2-bromoethoxy)(*tert*-butyl)dimethylsilane (0.888 mL, 4.14 mmol). Crude product was purified by silica chromatography (0 to 25%, cyclohexane/EtOAc) to afford **76a** as an orange oil (363 mg, 63%). ^1H NMR (400 MHz, DMSO- d_6 δ): 8.42 (s, 1H), 8.05 (d, $J = 5$ Hz, 1H), 7.67 (d, $J = 5$ Hz, 1H), 4.28 (t, $J = 4$ Hz, 2H), 3.96 (t, $J = 4$ Hz, 2H), 0.86 (s, 9H), 0.07 (s, 6H); LC-MS (Method A) $m/z = [\text{M} + \text{H}]^+$ 332.1/334.1, t_{R} 1.36 mins.

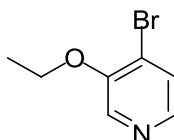
4-Bromo-3-cyclopropoxy pyridine, **78a**



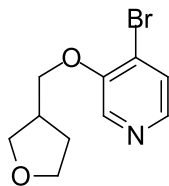
A solution of **132** (600 mg, 3.45 mmol) in DMF (15 mL) was treated with caesium carbonate (1124 mg, 3.45 mmol), bromocyclopropane (0.608 mL, 7.59 mmol) and NaI (284 mg, 1.90 mmol). The reaction mixture was heated at 150 °C for a total of 48 h then concentrated under reduced pressure. The reaction mixture was re-suspended in DMF (15 mL) and treated with bromocyclopropane (1.2 mL, 15.2 mmol) then heated at 150 °C for 60 h. The reaction mixture was partitioned between water and EtOAc (20 mL). The organic extract was isolated and the aqueous layer re-extracted with EtOAc (2 x 20 mL). The combined organic extracts were concentrated under reduced pressure to afford **78a** as a brown oil (70 mg, 9%). ^1H NMR (400 MHz, DMSO- d_6 δ): 8.64 (s, 1H), 8.10 (d, $J = 5$ Hz, 1H), 7.67 (d, $J = 5$ Hz, 1H), 4.19-4.07 (m, 1H), 0.91-0.84 (m, 2H), 0.79-0.71 (m, 2H); LC-MS (Method A) $m/z = [\text{M} + \text{H}]^+$ 214.0/216.0, t_{R} 0.77 mins.

4-Bromo-2-((tetrahydrofuran-3-yl)methoxy)pyridine, 81a

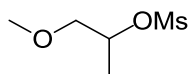
A solution of **132** (300 mg, 1.72 mmol) in DMF (15 mL) was treated with sodium hydride (76 mg, 1.90 mmol, 60% w/w dispersion in mineral oils). The reaction mixture was stirred for 1 h and treated with 2-(bromomethyl)tetrahydrofuran (0.216 mL, 1.90 mmol). The mixture was stirred overnight and treated sodium hydride (76 mg, 1.90 mmol, 60% w/w dispersion in mineral oils). The reaction mixture was heated at 60 °C for 24 then quenched with water and partitioned with EtOAc (20 mL). The organic extract was isolated and washed and the aqueous layer re-extracted with EtOAc (2 x 20 mL). The combined organic extracts were concentrated under reduced pressure to afford **81a** as a brown oil (197 mg, 44%). ¹H NMR (400 MHz, DMSO-d₆ δ): 8.41 (s, 1H), 8.06 (d, *J* = 5 Hz, 1H), 7.67 (d, *J* = 5 Hz, 1H), 4.26-4.11 (m, 3H), 3.85-3.76 (m, 1H), 3.75-3.64 (m, 1H), 2.08-1.90 (m, 2H), 1.89-1.72 (m, 2H); LC-MS (Method A): *m/z* = [M + H]⁺ 258.0/260.0, *t_R* 0.71 mins.

4-Bromo-3-ethoxy pyridine, 82a

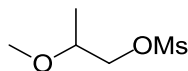
Prepared from **132** (500 mg, 2.87 mmol) and bromoethane (0.236 mL, 3.16 mmol) using the general alkylation procedure 1 to afford **82a** (367 mg, 63%). ¹H NMR (400 MHz, DMSO-d₆ δ): 8.39 (s, 1H), 8.06 (d, *J* = 5 Hz, 1H), 7.67 (d, *J* = 5 Hz, 1H), 4.25 (q, *J* = 7 Hz, 2H), 1.38 (t, *J* = 7 Hz, 3H); LC-MS (Method A): *m/z* = [M + H]⁺ 202.0/204.0, *t_R* 0.70 mins.

4-Bromo-3-((tetrahydrofuran-3-yl)methoxy)pyridine, 84a

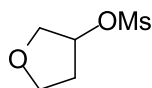
Prepared using the general alkylation procedure 1 from **132** (300 mg, 1.72 mmol) and 3-(bromomethyl)tetrahydrofuran (0.209 mL, 1.90 mmol) to afford **84a** as a yellow oil (224 mg, 30% at 60% purity by NMR). The compound was taken forward without purification. The ^1H NMR spectrum of crude material contained the following significant peaks: ^1H NMR (400 MHz, DMSO- d_6 δ): 8.42 (s, 1H), 8.07 (d, $J = 5$ Hz, 1H), 7.68 (d, $J = 5$ Hz, 1H), 4.22-4.15 (m, 1H), 4.15-4.07 (m, 1H), 3.86-3.74 (m, 2H), 3.72-3.64 (m, 1H), 3.61-3.54 (m, 1H), 2.73-2.63 (m, 1H), 2.09-1.97 (m, 1H), 1.78-1.65 (m, 1H); LC-MS (Method A) $m/z = [\text{M} + \text{H}]^+$ 258.0/260.0, t_R 0.69 mins.

General Mesylation Procedure**1-Methoxypropan-2-yl methanesulfonate, 79a**

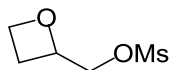
A solution of 1-methoxypropan-2-ol (500 mg, 5.55 mmol) in DCM (15 mL) was cooled using an ice water bath and treated with triethylamine (2.32 mL, 16.64 mmol) and methanesulfonyl chloride (0.473 mL, 6.10 mmol). The reaction mixture was stirred for 1 h then partitioned between water (20 mL) and EtOAc (20 mL). The organic phase was separated and the aqueous layer re-extracted with EtOAc (2 x 20 mL). The combined organic extracts were concentrated under reduced pressure to afford **79a** as a colourless oil (920 mg, 99%). The compound was taken on without purification. The ^1H NMR spectrum of crude material contained the following significant peaks: ^1H NMR (400 MHz, DMSO- d_6 δ): 4.87-4.76 (m, 1H), 3.44 (d, $J = 5$ Hz, 2H), 3.31 (s, 3H), 3.15 (s, 3H), 1.29 (d, $J = 6$ Hz, 3H).

2-Methoxypropyl methanesulfonate, 80a

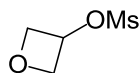
Prepared using the general mesylation procedure from 2-methoxypropan-1-ol (500 mg, 5.55 mmol) and methanesulfonyl chloride (0.473 mL, 6.10 mmol) to afford **80a** as a gum (849 mg, 91%). ^1H NMR (400 MHz, DMSO- d_6 δ): 4.26-4.17 (m, 1H), 4.14-4.04 (m, 1H), 3.65-3.54 (m, 1H), 3.29 (s, 3H), 3.18 (s, 3H), 1.11 (d, J = 6 Hz, 3H).

Tetrahydrofuran-3-yl methanesulfonate, 86a

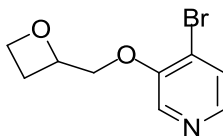
Prepared using the general mesylation procedure from tetrahydrofuran-3-ol (0.370 mL, 4.54 mmol) and methanesulfonyl chloride (0.387 mL, 5.00 mmol) to afford **86a** as a yellow oil (580 mg, 77%). ^1H NMR (400 MHz, DMSO- d_6 δ): 5.34-5.28 (m, 1H), 3.90-3.70 (m, 4H), 3.22 (s, 3H), 2.28-2.16 (m, 1H), 2.14-2.03 (m, 1H).

Oxetan-2-ylmethyl methanesulfonate, 87a

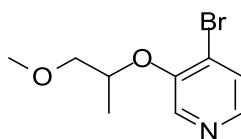
Prepared using the general mesylation procedure from oxetan-2-ylmethanol (0.370 mL, 4.54 mmol) and methanesulfonyl chloride (0.387 mL, 4.99 mmol) to afford **87a** as a yellow oil (572 mg, 76%). ^1H NMR (400 MHz, DMSO- d_6 δ): 5.00-4.86 (m, 1H), 4.57-4.41 (m, 2H), 4.40-4.24 (m, 2H), 3.22 (s, 3H), 2.75-2.61 (m, 1H), 2.56-2.41 (m, 1H).

Oxetan-3-yl methanesulfonate, 88a

Prepared using the general mesylation procedure from oxetan-3-ol (0.370 mL, 5.40 mmol) and methanesulfonyl chloride (0.461 mL, 5.94 mmol) to afford **88a** as a yellow oil (665 mg, 81%). ^1H NMR (400 MHz, DMSO- d_6 δ): 5.60-5.52 (m, 1H), 4.81 (dd, J = 8, 6 Hz, 2H), 4.63 (dd, J = 8, 6 Hz, 2H), 3.23 (s, 3H).

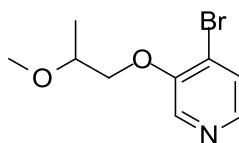
4-Bromo-3-(oxetan-2-ylmethoxy)pyridine, 87b

A suspension of **132** (300 mg, 1.72 mmol) in DMF (11 mL) was cooled to 0 °C and treated with sodium hydride (83 mg, 2.07 mmol) and stirred for 30 min. The reaction mixture was treated with **87a** (344 mg, 2.07 mmol) and stirred at room temperature for 4 h. The reaction mixture was treated with sodium hydride (83 mg, 2.07 mmol, 60% by weight dispersion in mineral oils) and stirred for 30 min. The reaction mixture was treated with **87a** (228 mg, 1.37 mmol) and stirred overnight. The reaction mixture was heated at 60 °C overnight and partitioned with EtOAc (20 mL) and water (20 mL). The organic extract was isolated and the aqueous layer re-extracted with EtOAc (3 x 20 mL). The combined organic extracts were passed through a hydrophobic frit and concentrated under reduced pressure. The crude product was partitioned between EtOAc (20 mL) and at 10% by weight solution of LiCl in water. The organic extract was isolated and the aqueous layer extracted with EtOAc (20 mL). The organic layer was isolated and the aqueous layer re-extracted with EtOAc (3 x 20 mL). The combined organic extracts were passed through a hydrophobic frit and concentrated under reduced pressure to afford **87b** as a yellow oil (708 mg, *maximum possible theoretical yield is 421 mg, so material estimated to be a maximum of $421/708 \times 100 = 59\%$ purity by weight*). The compound was taken forward without purification, so no yield is given. The ¹H NMR spectrum of crude material contained the following significant peaks: ¹H NMR (400 MHz, DMSO-d₆ δ): 8.45 (s, 1H), 8.08 (d, *J* = 5 Hz, 1H), 7.70 (d, *J* = 5 Hz, 1H), 5.09-4.99 (m, 1H), 4.96-4.87 (m, 1H), 4.57-4.51 (m, 1H), 4.37-4.32 (m, 2H), 2.67 (s, 1H), 2.49-2.43 (m, 1H); LC-MS (Method A) *m/z* = [M + H]⁺ 244.0/246.0, *t_R* 0.60 mins.

4-Bromo-3-((1-methoxypropan-2-yl)oxy)pyridine, 79b

A solution of **132** (300 mg, 1.72 mmol) in DMF (15 mL) was treated with caesium carbonate (618 mg, 1.90 mmol) and **79a** (319 mg, 1.90 mmol). The reaction mixture was heated at 50 °C overnight then partitioned between water and EtOAc (20 mL). The organic layer was isolated and the aqueous layer re-extracted with EtOAc (2 x 20 mL). The combined organic extracts were concentrated under reduced pressure. The reaction mixture was re-dissolved in DMF (15 mL) and treated with **132** (150 mg, 0.86 mmol) and caesium carbonate (309 mg, 0.95 mmol). The reaction mixture was heated at 50 °C for 2 d then partitioned between water (20 mL) and EtOAc (20 mL). The organic phase was separated and then aqueous layer re-extracted with EtOAc (2 x 20 mL). The combined organic extracts were concentrated under reduced pressure. The crude material was dissolved in IPA then loaded onto an aminopropyl SPE cartridge and eluted with IPA to afford **79b** as a colourless oil (318 mg, 68%). ¹H NMR (400 MHz, DMSO-d₆ δ): 8.46 (s, 1H), 8.05 (d, *J* = 5 Hz, 1H), 7.67 (d, *J* = 5 Hz, 1H), 4.89-4.78 (m, 1H), 3.56-3.50 (m, 2H), 3.33-3.29 (m, 3H), 1.27 (d, *J* = 6 Hz, 3H); LC-MS (Method A) *m/z* = [M + H]⁺ 246.0/248.0, *t_R* 0.73 mins.

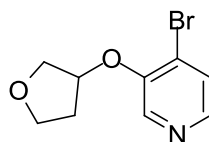
4-Bromo-3-(2-methoxypropoxy)pyridine, **80b**



A solution of **132** (300 mg, 1.72 mmol) in DMF (15 mL) was treated with caesium carbonate (618 mg, 1.90 mmol) and **80a** (319 mg, 1.90 mmol). The reaction mixture was heated at 50 °C overnight then partitioned between water (20 mL) and EtOAc (20 mL). The organic phase was separated and the aqueous layer re-extracted with EtOAc (2 x 20 mL). The combined organic extracts were concentrated under reduced pressure. The reaction mixture was re-dissolved in DMF (15 mL) and treated with **132** (150 mg, 0.9 mmol) and caesium carbonate (309 mg, 0.9 mmol). The reaction mixture was heated at 50 °C for 1 d then partitioned between water (20 mL) and EtOAc (20 mL). The organic phase was separated and the aqueous layer re-extracted with EtOAc (2 x 20 mL). The combined organic extracts were concentrated under reduced pressure. The crude material was dissolved in IPA then loaded onto an aminopropyl SPE cartridge and eluted with IPA to afford **80b** as an orange oil (322 mg, 69%). ¹H NMR (400 MHz,

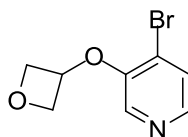
DMSO- d_6 δ): 8.41 (s, 1H), 8.07 (d, $J = 5$ Hz, 1H), 7.68 (d, $J = 5$ Hz, 1H), 4.21-4.13 (m, 2H), 3.76-3.65 (m, 1H), 3.35 (s, 3H), 1.21 (d, $J = 6$ Hz, 3H); LC-MS (Method A) $m/z = [M + H]^+$ 246.0/248.0, t_R 0.73 mins.

4-Bromo-3-((tetrahydrofuran-3-yl)oxy)pyridine, **86b**



A suspension of **132** (300 mg, 1.72 mmol) in DMF (7 mL) was treated with caesium carbonate (674 mg, 2.07 mmol) and **86a** (236 mg, 1.72 mmol). The reaction mixture was stirred overnight and was treated with caesium carbonate (674 mg, 2.07 mmol) and **86a** (236 mg, 1.72 mmol). The reaction mixture was stirred at room temperature for 3 h then heated at 60 °C overnight. The reaction mixture was diluted with water (25 mL) and partitioned with ether (25 mL). The organic layer was isolated and the aqueous layer re-extracted with ether (4 x 20 mL). The combined organic extracts passed through a hydrophobic frit and concentrated under reduced pressure to afford **86b** as a yellow liquid (734 mg, *maximum possible theoretical yield is 421 mg, so material estimated to be a maximum of $421/734 \times 100 = 57\%$ purity by weight*). The compound was taken forward without purification, so no yield is given. LC-MS (Method A) $m/z = [M + H]^+$ 194.1, t_R 0.36 mins. The 1H NMR spectrum of crude material contained the following significant peaks: 1H NMR (400 MHz, DMSO- d_6 δ): 8.40 (s, 1H), 8.08 (d, $J = 5$ Hz, 1H), 7.69 (d, $J = 5$ Hz, 1H), 3.97-3.69 (m, 3H), 2.34-2.15 (m, 2H), 2.13 - 1.96 (m, 2H); LC-MS (Method A) $m/z = [M + H]^+$ 244.0/246.0, t_R 0.63 mins.

4-Bromo-3-(oxetan-3-yloxy)pyridine, **88b**

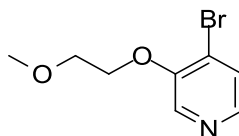


A suspension of **132** (300 mg, 1.72 mmol) in DMF (7 mL) was treated with caesium carbonate (674 mg, 2.07 mmol) and **88a** (350 mg, 1.72 mmol). The reaction mixture was stirred overnight and was treated with **88a** (350 mg, 1.72 mmol). The reaction

mixture was stirred overnight and was treated with caesium carbonate (674 mg, 2.07 mmol) and **88a** (350 mg, 1.72 mmol). The reaction mixture was heated at 60 °C for 4 h, 70 °C overnight then at 90 °C for 6 h. The reaction mixture was treated with caesium carbonate (337 mg, 1.72 mmol) and heated at 120 °C overnight.

The reaction mixture was diluted with water (25 mL) and partitioned with ether (25 mL). The organic layer was isolated and the aqueous layer re-extracted with ether (3 x 25 mL). The combined organic extracts passed through a hydrophobic frit and concentrated under reduced pressure to afford **88b** as a yellow oil (852 mg, *maximum possible theoretical yield is 397 mg, so material estimated to be a maximum of 397/852x 100 = 47% purity by weight*). The compound was taken forward without purification. The ¹H NMR spectrum of crude material contained the following significant peaks: ¹H NMR (400 MHz, DMSO-d₆ δ): 8.11 (d, *J* = 5 Hz, 1H), 8.04 (s, 1H), 7.73 (d, *J* = 5 Hz, 1H), 5.61-5.52 (m, 1H), 4.69-4.57 (m, 4H); LC-MS (Method A) *m/z* = [M + H]⁺ 230.0/232.0, *t_R* 0.63 mins.

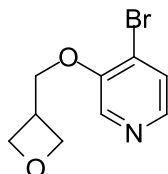
4-Bromo-3-(2-methoxyethoxy)pyridine, **83a**



A solution of **132** (500 mg, 2.87 mmol) in DMF (10 mL) was treated with sodium hydride (138 mg of a 60% w/w dispersion in mineral oils, 3.45 mmol). The reaction mixture was stirred for 30 min then treated with 1-bromo-2-methoxyethane (0.284 mL, 3.02 mmol). The reaction mixture was stirred overnight and treated with sodium hydride (138 mg, 3.45 mmol, 60% w/w dispersion in mineral oils) then stirred for 20 min. The reaction mixture was treated with 1-bromo-2-methoxyethane (0.284 mL, 3.02 mmol) and stirred for 3 h. The mixture was diluted with EtOAc (25 mL) and water (25 mL). The organic extract was separated and the aqueous layer re-extracted with EtOAc (3 x 25 mL). The combined organic extracts were concentrated under reduced pressure to afford **83a** as an orange oil (168 mg, 25%). The compound was taken forward without purification. The ¹H NMR spectrum of crude material contained the following significant peaks: ¹H NMR (400 MHz, CDCl₃ δ): 8.29 (s, 1H), 8.09 (d, *J* = 5 Hz, 1H),

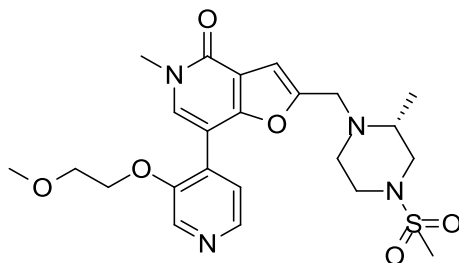
7.51 (d, $J = 5$ Hz, 1H), 4.31 (t, $J = 5$ Hz, 2H), 3.84 (t, $J = 5$ Hz, 2H), 3.50 (s, 3H); LC-MS (Method A): $m/z = [M + H]^+$ 232.0/234.0, t_R 0.61 mins.

4-Bromo-3-(oxetan-3-ylmethoxy)pyridine, **85a**



Prepared using the general alkylation procedure 1 from **132** (400 mg, 2.30 mmol) and 3-(bromomethyl)oxetane (417 mg, 2.76 mmol) to afford **85a** as an orange oil (332 mg, 59%). The compound was taken forward without purification. The ^1H NMR spectrum of crude material contained the following significant peaks: ^1H NMR (400 MHz, CDCl_3 δ): 8.26 (s, 1H), 8.08 (d, $J = 5$ Hz, 1H), 7.50 (d, $J = 5$ Hz, 1H), 4.89 (dd, $J = 8, 6$ Hz, 2H), 4.63 (t, $J = 6$ Hz, 2H), 4.36 (d, $J = 6$ Hz, 2H), 3.57-3.45 (m, 1H); LC-MS (Method A) $m/z = [M + H]^+$ 244.0/246.0, t_R 0.57 mins.

(*R*)-7-(3-(2-Methoxyethoxy)pyridin-4-yl)-5-methyl-2-((2-methyl-4-(methylsulfonyl)piperazin-1-yl)methyl)furo[3,2-*c*]pyridin-4(5*H*)-one, **83**

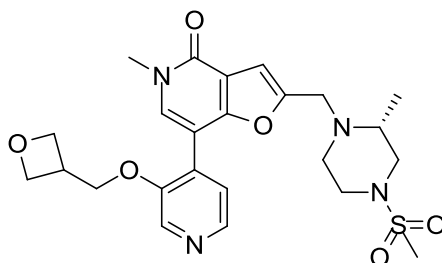


A suspension of **83a** (168 mg, 0.61 mmol) in 1,4-dioxane (10 mL) was treated with 4,4,4',4',5,5,5',5'-octamethyl-2,2'-bi(1,3,2-dioxaborolane) (309 mg, 1.22 mmol), potassium acetate (179 mg, 1.82 mmol) and $\text{Pd}(\text{dppf})\text{Cl}_2$ (45 mg, 0.061 mmol, 10 mol%). The reaction mixture was refluxed for 2 h and was treated with 4,4,4',4',5,5,5',5'-octamethyl-2,2'-bi(1,3,2-dioxaborolane) (309 mg, 1.22 mmol), potassium acetate (179 mg, 1.82 mmol) and $\text{Pd}(\text{dppf})\text{Cl}_2$ (45 mg, 0.061 mmol, 10 mol%). The reaction mixture was heated at 100 °C for 18 h and diluted with EtOAc then filtered through a 5 g Celite^(R) cartridge. The solvent was removed under reduced

pressure to afford crude **83b** as a brown oil (734 mg, *maximum possible yield 170 mg, so maximum purity was $170/734 \times 100 = 23\%$*).

Crude **83b** (416 mg, 0.34 mmol, *at a maximum 23% purity*) was used in the general Suzuki coupling procedure 1 with **115** (90 mg, 0.22 mmol) to afford **83** as a white solid (19 mg, 18%). ¹H NMR (400 MHz, CDCl₃ δ): 8.42 (s, 1H), 8.36 (d, *J* = 5 Hz, 1H), 7.99 (s, 1H), 7.63 (d, *J* = 5 Hz, 1H), 6.87 (s, 1H), 4.30 (t, *J* = 4 Hz, 2H), 3.91 (s, 2H), 3.74 (t, *J* = 4 Hz, 2H), 3.69 (s, 3H), 3.57-3.45 (m, 2H), 3.42 (s, 3H), 2.99-2.86 (m, 2H), 2.76 (s, 3H), 2.67-2.50 (m, 3H), 1.23 (d, *J* = 5 Hz, 3H); LC-MS (Method A) *m/z* = [M + H]⁺ 491.2, *t_R* 0.45 mins.

(R)-5-methyl-2-((2-methyl-4-(methylsulfonyl)piperazin-1-yl)methyl)-7-(3-(oxetan-3-ylmethoxy)pyridin-4-yl)furo[3,2-c]pyridin-4(5H)-one, 85



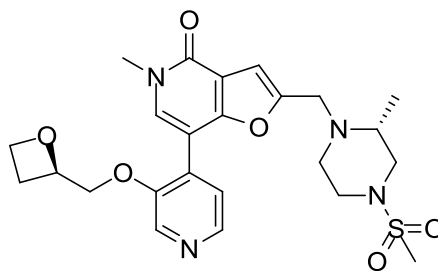
A suspension of **85a** (300 mg, 1.23 mmol) in 1,4-dioxane (10 mL) was treated with 4,4,4',4',5,5,5',5'-octamethyl-2,2'-bi(1,3,2-dioxaborolane) (624 mg, 2.46 mmol), potassium acetate (362 mg, 3.69 mmol), Pd(dppf)Cl₂ (90 mg, 0.12 mmol, 10 mol%). The reaction mixture was heated at 100 °C for 1 h using microwave irradiation. The reaction mixture was treated with 4,4,4',4',5,5,5',5'-octamethyl-2,2'-bi(1,3,2-dioxaborolane) (624 mg, 2.46 mmol), potassium acetate (362 mg, 3.69 mmol) and Pd(dppf)Cl₂ (90 mg, 0.12 mmol, 10 mol%). The reaction mixture was heated at 100 °C for 1 h using microwave irradiation then diluted with ethyl acetate and filtered through a 5 g Celite^(R) cartridge. The reaction mixture was concentrated under reduced pressure to afford **85b** as a brown oil (1.72 g, *maximum yield was 358 mg, so material was a maximum $358 / 1720 \times 100 = 21\%$ purity by weight*).

Crude **85b** (589 mg, 0.42 mmol, *at a maximum 21% purity by weight*) was used in the general Suzuki coupling procedure 1 with **115** (110 mg, 0.26 mmol) to afford **85** as a yellow oil (18 mg, 14%). LC-MS (Method A) *m/z* = [M + H]⁺ 503.2, *t_R* 0.44 mins. ¹H

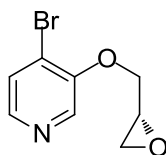
NMR (600 MHz, CD₃OD δ): 8.47 (s, 1H), 8.30 (d, $J = 5$ Hz, 1H), 7.97 (s, 1H), 7.65 (d, $J = 5$ Hz, 1H), 6.91 (s, 1H), 4.76 (ddd, $J = 8, 6, 3$ Hz, 2H), 4.48 (dt, $J = 6, 3$ Hz, 2H), 4.36 (d, $J = 6$ Hz, 2H), 4.05-3.86 (m, 2H), 3.68 (s, 3H), 3.48-3.44 (m, 1H), 3.44-3.40 (m, 1H), 3.40-3.35 (m, 1H), 2.97-2.90 (m, 1H), 2.96-2.89 (m, 1H), 2.79 (s, 3H), 2.67-2.61 (m, 1H), 2.59-2.52 (m, 1H), 2.54-2.48 (m, 1H), 1.20 (d, $J = 6$ Hz, 3H); LC-MS (2 min, Method A): $m/z = [M + H]^+$ 503.2, t_R 0.44 mins.

2.9.2. Large Scale Preparation of BET BD1 Selective Chemical Probe, **89**

Method development was performed on a small scale to confirm the chemistry delivered moderate to high yields for each step before increasing the scale. Intermediates and **89** were then prepared in larger amounts by colleagues Mitchell and Watson.^{14,19} Experimentals are shown for the preferred conditions that were developed as a result of the smaller scale investigations.



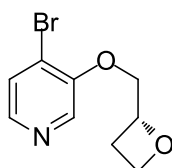
(*R*)-4-Bromo-3-(oxiran-2-ylmethoxy)pyridine, **143**¹⁴



A solution of **132** (36.9 g, 212 mmol) in DMF (667 mL) under nitrogen was treated with cesium carbonate (189.0 g, 579 mmol) and **142** (50.0 g, 193 mmol). The reaction mixture was stirred overnight at room temperature. The reaction mixture was cooled using an ice-water bath and treated with water (1 L). The reaction mixture was extracted with EtOAc (500 mL) and the organic extract isolated. The aqueous layer was re-extracted with EtOAc (500 mL). The aqueous layer was treated with brine (1 L) and partitioned with EtOAc (1 L). The organic extract was isolated and the aqueous layer re-extracted with EtOAc (1 L). The combined organic extracts were washed with water (2

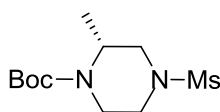
x 2 L) and a 5% w/v aqueous solution of LiCl in water (2 L). The combined organic extracts were dried over Na₂SO₄ to afford **143** as an orange oil (39.4 g, 80% at 90% purity by LCMS and NMR). Material was taken forward without purification. The ¹H NMR spectrum of crude material contained the following significant peaks: ¹H NMR (400 MHz, CDCl₃ δ): 8.27 (s, 1H), 8.10 (d, *J* = 5 Hz, 1H), 7.51 (d, *J* = 5 Hz, 1H), 4.44 (dd, *J* = 11, 3 Hz, 1H), 4.14 (dd, *J* = 11, 6 Hz, 1H), 3.46-3.39 (m, 1H), 2.98-2.93 (m, 1H), 2.89-2.85 (m, 1H); LC-MS (Method A) *m/z* = [M + H]⁺ 230.1/232.0, *t_R* 0.60 mins.

(R)-4-Bromo-3-(oxetan-2-ylmethoxy)pyridine, 87d¹⁴



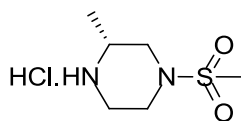
A suspension of potassium *tert*-butoxide (26.2 g, 234 mmol) in *t*BuOH (450 mL) under nitrogen was treated with trimethylsulfoxonium iodide (34.3 g, 156 mmol). The reaction mixture was heated at 80 °C for 10 min and cooled to room temperature. The reaction mixture was treated with a suspension of **143** (39.4 g, 154 mmol, at 90% purity) in *t*BuOH (100 mL) and heated at 60 °C for 6 h. The reaction mixture was allowed to cool to room temperature then concentrated under reduced pressure to ~1/3 volume and partitioned between water (500 mL) and EtOAc (500 mL). The organic extract was isolated and the aqueous layer re-extracted with EtOAc (3 x 500 mL). The combined organic extracts were washed with water (1 L) and brine (1 L) and dried with MgSO₄ to afford **87d** as an orange oil (18.8 g, 42% at 85% purity by LCMS and NMR). Material was taken forward without purification. The ¹H NMR spectrum of crude material contained the following significant peaks: ¹H NMR (400 MHz, CDCl₃ δ): 8.30 (s, 1H), 8.09 (d, *J* = 5 Hz, 1H), 7.52 (d, *J* = 5 Hz, 1H), 5.22-5.11 (m, 1H), 4.81-4.67 (m, 2H), 4.34 (dd, *J* = 11, 4 Hz, 1H), 4.24 (dd, *J* = 11, 4 Hz, 1H), 2.89-2.78 (m, 2H); LC-MS (Method A) *m/z* = [M + H]⁺ 244.0/246.0, *t_R* 0.62 mins.

(R)-Tert-butyl 2-methyl-4-(methylsulfonyl)piperazine-1-carboxylate, 110¹⁴

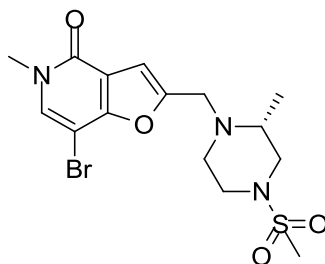


A vigorously stirred solution of **109** (49.0 g, 245 mmol) in THF (150 mL) was treated with NaOH (220 mL of a 2 M aqueous solution, 440 mmol), then cooled using an ice bath. The reaction mixture was cautiously treated with a solution of methanesulfonyl chloride (21.0 mL, 269 mmol) in THF (150 mL) and stirred overnight. The reaction mixture was treated with methanesulfonyl chloride (2 mL) and the reaction was stirred for 4 h. The reaction mixture was poured into HCl (400 mL of a 2 N aqueous solution) and ice (~200 mL) and partitioned with EtOAc (500 mL). The organic layer was isolated and the aqueous layer re-extracted with EtOAc (500 mL). The combined organic extracts were washed with NaOH (400 mL of a 2 N aqueous solution) and brine (500 mL) then dried over Na₂SO₄ and concentrated under reduced pressure to afford **110** as a white solid (62.7 g, 214 mmol, 87%, *at 95% purity by LCMS and NMR*). ¹H NMR (400 MHz, DMSO-d₆ δ): 4.32-4.21 (m, 1H), 3.83 (d, 1H, *J* = 14 Hz), 3.48 (d, 1H, *J* = 12 Hz), 3.30 (t, *J* = 6 Hz, 1H), 3.03 (t, *J* = 13 Hz, 1H), 2.86 (s, 3H), 2.84-2.79 (m, 1H), 2.67 (t, *J* = 9 Hz, 1H), 1.41 (s, 9H), 1.13 (d, *J* = 7 Hz, 3H).

(R)-3-Methyl-1-(methanesulfonyl)piperazine hydrochloride, 111¹⁴



A solution of **110** (58.5 g, 210 mmol) was dissolved in DCM, cooled using an ice-bath, and treated with a 4 M solution of HCl in dioxane (400 mL, 1600 mmol). The reaction mixture was allowed to warm to room temperature over 48 h and concentrated under reduced pressure. The residue was azeotroped with ether to give **111** as a white solid (49.8 g, >99%). IR (cm⁻¹) 2937, 2699, 2659, 2468, 1326, 1300, 1185, 1159, 1135, 1002, 921, 783; ¹H NMR (400 MHz, DMSO-d₆ δ): 9.29 (br. s, 2H), 3.69-3.60 (m, 2H), 3.42-3.33 (m, 2H), 3.13-3.02 (m, 2H), 3.00 (s, 3H), 2.91-2.81 (m, 1H), 1.26 (d, *J* = 7 Hz, 3H); ¹³C NMR (126 MHz, DMSO-d₆, δ): 50.1, 47.9, 42.0, 41.7, 35.1, 15.2; mp 216 - 218 °C.

(R)-7-Bromo-5-methyl-2-((2-methyl-4-(methylsulfonyl)piperazin-1-yl)methyl)furo[3,2-*c*]pyridin-4(5H)-one, 115¹⁹

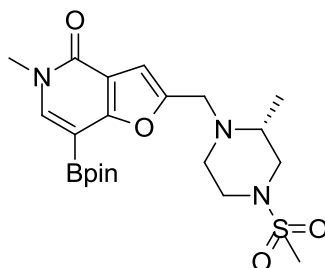
A suspension of **112** (5.0 g, 19.5 mmol) in 2-methyltetrahydrofuran (250 mL) under an atmosphere of nitrogen was treated with **111** (8.0 g, 37.1 mmol) and Et₃N (6.8 mL, 48.8 mmol). The reaction mixture was stirred for 10 min then treated with STAB (8.3 g, 39.1 mmol) over 10 min. The reaction mixture was stirred at room temperature for 4 h and concentrated under reduced pressure. The reaction mixture was treated with a saturated solution of sodium hydrogen carbonate (100 mL) and partitioned with DCM (200 mL). The organic layer was isolated and the aqueous layer re-extracted with DCM (200 mL). The combined organic extracts were dried over Na₂SO₄ and concentrated under reduced pressure.

Separately a suspension of **112** (45.0 g, 176.0 mmol) in 2-methyltetrahydrofuran (2.2 L) under an atmosphere of nitrogen was treated with **111** (71.7 g, 334.0 mmol) and Et₃N (61.2 mL, 439.0 mmol). The reaction mixture was stirred for 10 min then treated with STAB (74.5 g, 351.0 mmol) over 10 min. The reaction mixture was stirred at room temperature for 2 h and concentrated under reduced pressure. The reaction mixture was treated with a saturated solution of sodium hydrogen carbonate (1 L) and partitioned with DCM (1 L). The organic layer was isolated and the aqueous layer re-extracted with DCM (1 L). The combined organic extracts were dried over Na₂SO₄ and concentrated under reduced pressure.

The crude product from the 45.0 g scale reaction was combined with the crude product from the 5.0 g scale reaction and purified using a silica column (0 to 5% of a 2 M solution of ammonia in MeOH) to give crude **115** as a cream solid (64.1 g, 75% at 95% purity). IR (cm⁻¹) 3094, 1677, 1317, 1145, 1014, 971, 794, 769; ¹H NMR (400 MHz, CDCl₃ δ): 7.37 (s, 1H), 6.88 (s, 1H), 3.98-3.84 (m, 2H), 3.63 (s, 3H), 3.60-3.47 (m, 2H),

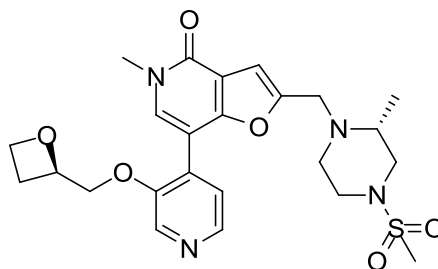
3.01-2.91 (m, 2H), 2.78 (s, 3H), 2.70-2.55 (m, 3H), 1.26 (d, $J = 6$ Hz, 3H); ^{13}C NMR (126 MHz, DMSO- d_6 , δ): 157.5, 155.6, 154.2, 135.6, 116.8, 106.9, 84.3, 53.3, 51.5, 49.8, 48.7, 45.5, 36.2, 33.7, 15.2; HRMS-FAB (m/z): $[\text{M} + \text{H}]^+$ calcd for $\text{C}_{15}\text{H}_{20}\text{BrN}_3\text{O}_4\text{S}$, 418.0431; found, 418.0436; LC-MS (Method C) $m/z = [\text{M} + \text{H}]^+$ 418.2/420.3, t_{R} 0.77 mins; mpt 169 - 171 °C.

(R)-5-Methyl-2-((2-methyl-4-(methylsulfonyl)piperazin-1-yl)methyl)-7-(4,4,5,5-tetramethyl-1,3,2-dioxaborolan-2-yl)furo[3,2-*c*]pyridin-4(5*H*)-one, **119¹⁹**



A solution of **115** (30.0 g, 71.7 mmol) in 1,4-dioxane (100 mL) was treated with triethylamine (60.1 mL, 430.0 mmol), 4,4,5,5-tetramethyl-1,3,2-dioxaborolane (62.4 mL, 430.0 mmol) and $\text{Pd}(\text{PPh}_3)_4$ (8.3 g, 7.2 mmol, 10 mol%) and the mixture was flushed with nitrogen, then heated at 100 °C for 18 h. The reaction mixture was cooled using an ice bath then quenched with IPA (30 mL), which was cautiously added dropwise. The resulting suspension was concentrated under reduced pressure then treated with IPA (100 mL). The resulting brown solution was stirred for 30 min to give a dense beige precipitate which was isolated by filtration, washed with IPA (30 mL) then dried under vacuum to give crude **119**. The crude material was re-suspended in IPA (100 mL) and stirred for 30 min, filtered and the isolated solid was washed with IPA to afford **119** as a grey solid (32.0 g, 96%). The ^1H NMR spectrum of crude material contained the following significant peaks: ^1H NMR (400 MHz, CDCl_3 δ): 7.67 (s, 1H), 6.77 (s, 1H), 3.99-3.86 (m, 2H), 3.65 (s, 3H), 3.59-3.49 (m, 2H), 3.02-2.90 (m, 2H), 2.78 (s, 3H), 2.70-2.60 (m, 3H), 1.38 (s, 12H), 1.29 (d, $J = 6$ Hz, 3H); LC-MS (Method C) $m/z = [\text{M} + \text{H}]^+$ 466.4, t_{R} 0.61 mins (**119**, 20% by peak area, *observed mass ion is consistent with boronate ester*); $m/z = [\text{M} - \text{H}]^-$ 382.4, t_{R} 0.38 mins (70% by area, *observed mass ion is consistent with hydrolysis to boronic acid under LC-MS conditions, 119a*).

5-Methyl-2-(((R)-2-methyl-4-(methylsulfonyl)piperazin-1-yl)methyl)-7-(3-((R)-oxetan-2-ylmethoxy)pyridin-4-yl)furo[3,2-*c*]pyridin-4(5*H*)-one, **89¹⁹**



A solution of **87d** (19.8 g, 81.0 mmol) in toluene (200 mL) and MeOH (60 mL) was treated with caesium carbonate (37.8 g, 116.0 mmol) and degassed with nitrogen. The reaction mixture was treated with *tetrakis*(triphenylphosphino)palladium(0) (6.7 g, 5.8 mmol, 10 mol%) and **119** (30 g, 58.0 mmol). The reaction mixture was heated at 100 °C and concentrated under reduced pressure. The reaction mixture was partitioned with DCM (300 mL) and water (500 mL). The organic extract was isolated and the aqueous layer re-extracted with DCM (300 mL). The combined organic extracts were concentrated under reduced pressure. Crude product was purified by silica column chromatography (0 to 30% of a solution of MeOH in acetone). A solution of the purified product was dissolved in DCM (300 mL) and treated with thioureidopropyl silica (30 g). The mixture was stirred for 30 min then filtered and the silica washed with DCM (200 mL) and concentrated under reduced pressure to afford **89** as a beige foam (11.1 g, 38%).

The batch of **89** was combined with a second batch of **89** that had been similarly prepared (11.2 g) and purified by chiral HPLC method B to afford **89** as a yellow solid. (10.9 g, 49%, >99% purity by chiral HPLC analysis). IR (cm⁻¹) 2887, 2850, 1664, 1587, 1326, 1157, 947, 794, 775; ¹H NMR (400 MHz, DMSO-d₆ δ): 8.55 (s, 1H), 8.32 (d, *J* = 5 Hz, 1H), 7.96 (s, 1H), 7.52 (d, *J* = 5 Hz, 1H), 6.86 (s, 1H), 5.00-4.91 (m, 1H), 4.51-4.40 (m, 1H), 4.38-4.26 (m, 2H), 4.24-4.15 (m, 1H), 3.92-3.69 (m, 2H), 3.57 (s, 3H), 3.29-3.23 (m, 1H), 2.93-2.78 (m, 5H), 2.67-2.53 (m, 3H), 2.47-2.30 (m, 3H), 1.10 (d, *J* = 6 Hz, 3H); ¹³C NMR (151 MHz, DMSO-d₆ δ): 157.9, 156.6, 153.4, 151.9, 142.6, 136.1, 135.8, 128.8, 124.2, 115.0, 105.8, 103.4, 79.1, 72.0, 67.7, 53.1, 51.5, 49.7, 48.7, 45.4, 36.3, 33.6, 22.7, 15.2; HRMS-FAB (*m/z*): [M + H]⁺ calcd for C₂₄H₃₀N₄O₆S,

503.1964; found, 503.1978; LC-MS (Method A) $m/z = [M + H]^+$ 503.1, t_R 0.44 mins;
mp 166 - 168 °C.

2.10. References

- (1) Kouzarides, T. *Cell* **2007**, *128*, 693-705.
- (2) Chung, C.-w.; Tough, D. F. *Drug Discov. Today: Ther. Strateg.* **2011**, *9*, e111-120.
- (3) GlaxoSmithKline. A Study to Investigate the Safety, Pharmacodynamics, and Clinical Activity of **GSK525762** in Subjects With NUT Midline Carcinoma (NMC) and Other Cancers. In: ClinicalTrials.gov [Internet]. Bethesda (MD): National Library of Medicine (US). 2000- [cited 2015 Nov 9th]. Available from: <https://clinicaltrials.gov/ct2/show/NCT01587703> NLM Identifier: NCT01587703.
- (4) Nicodeme, E.; Jeffrey, K. L.; Schaefer, U.; Beinke, S.; Dewell, S.; Chung, C.-w.; Chandwani, R.; Marazzi, I.; Wilson, P.; Coste, H.; White, J.; Kirilovsky, J.; Rice, C. M.; Lora, J. M.; Prinjha, R. K.; Lee, K.; Tarakhovsky, A. *Nature* **2010**, *468*, 1119-1123.
- (5) Mirguet, O.; Gosmini, R.; Toum, J. r. m.; Clément, C. A.; Barnathan, M. l.; Brusq, J.-M.; Mordaunt, J. E.; Grimes, R. M.; Crowe, M.; Pineau, O.; Ajakane, M.; Daugan, A.; Jeffrey, P.; Cutler, L.; Haynes, A. C.; Smithers, N. N.; Chung, C.-w.; Bamborough, P.; Uings, I. J.; Lewis, A.; Witherington, J.; Parr, N.; Prinjha, R. K.; Nicodème, E. *J. Med. Chem.* **2013**, *56*, 7501–7515.
- (6) Arrowsmith, C. H.; Bountra, C.; Fish, P. V.; Lee, K.; Schapira, M. *Nat. Rev. Drug Discov.* **2012**, *11*, 384-400.
- (7) GSK Quantitative Pharmacology group, *GSK colleagues responsible for PK studies, unpublished results*.
- (8) GlaxoSmithKline. A Dose Escalation Study to Investigate the Safety, Pharmacokinetics (PK), Pharmacodynamics (PD) and Clinical Activity of **GSK525762** in Subjects With Relapsed, Refractory Hematologic Malignancies. In: ClinicalTrials.gov [Internet]. Bethesda (MD): National Library of Medicine (US). 2000- [cited 2015 Nov 9th]. Available from: <https://clinicaltrials.gov/ct2/show/NCT01943851> NLM Identifier: NCT01943851.
- (9) GlaxoSmithKline. A Study to Investigate the Safety, Pharmacokinetics, Pharmacodynamics, and Clinical Activity of **GSK525762** in Subjects With NUT

- Midline Carcinoma (NMC) and Other Cancers. In: ClinicalTrials.gov [Internet]. Bethesda (MD): National Library of Medicine (US). 2000- [cited 2015 Nov 9th]. Available from: <https://clinicaltrials.gov/ct2/show/NCT01587703> NLM Identifier: NCT01587703.
- (10) Jackson, S. *GSK colleague responsible for chiral HPLC separation, unpublished results.*
 - (11) Knaggs, A. *GSK colleague responsible for chiral HPLC separation, unpublished results.*
 - (12) Hortense, E. *GSK colleague responsible for chiral HPLC analysis and separation, unpublished results.*
 - (13) Blake, P.; Thickett, C. *GSK colleagues responsible for chiral HPLC purification, unpublished results.*
 - (14) Mitchell, D. *GSK colleague responsible for synthesis, unpublished results.*
 - (15) Amans, D. *GSK colleague responsible for synthesis, unpublished results.*
 - (16) Barnett, H. *GSK colleague responsible for synthesis, unpublished results.*
 - (17) Bit, R. *GSK colleague responsible for synthesis, unpublished results.*
 - (18) Garton, N. S. *GSK colleague responsible for synthesis, unpublished results.*
 - (19) Watson, R. *GSK colleague responsible for synthesis, unpublished results.*
 - (20) Westaway, S. *GSK colleague responsible for synthesis, unpublished results.*
 - (21) Chowdhury, P. *GSK colleague responsible for dog safety studies, using Marshall Beagle® dogs from Marshall UK, Hull, HU11 4QE; unpublished results.*
 - (22) Lovatt, C. *GSK colleague responsible for designing and coordinating dog safety study, unpublished results.*
 - (23) Haynes, S. R.; Dollard, C.; Winston, F.; Beck, S.; Trowsdale, J.; B., Dawid, I. *Nucleic Acids Res.* **1992**, *20*, 2603.
 - (24) Sanchez, R.; Zhou, M.-M. *Curr. Opin. Drug Discov. Devel.* **2009**, *12*, 659-665.
 - (25) Prinjha, R. K.; Witherington, J.; Lee, K. *Trends in Pharmacol. Sci.* **2012**, *33*, 146-153. **Figure 29** is reprinted from this publication entitled Place your BETs: the therapeutic potential of bromodomains, © 2012 with permission from Elsevier.
 - (26) Chiang, C.-M. *F1000 Biol. Rep.* **2009**, *1*, 1-7. **Figure 30** and **Figure 32** are reprinted from this open-access article distributed under the terms of the Creative

Commons Attribution-Non Commercial License, which permits unrestricted use, distribution, and reproduction in any medium, provided the original work is properly cited.

- (27) Filippakopoulos, P.; Qi, J.; Picaud, S.; Shen, Y.; Smith, W. B.; Fedorov, O.; Morse, E. M.; Keates, T.; Hickman, T. T.; Felletar, I.; Philpott, M.; Munro, S.; McKeown, M. R.; Wang, Y.; Christie, A. L.; West, N.; Cameron, M. J.; Schwartz, B.; Heightman, T. D.; Thangue, N. L.; French, C. A.; Wiest, O.; Kung, A. L.; Knapp, S.; Bradner, J. E. *Nature* **2010**, *468*, 1067-1073.
- (28) Oncoethix. A Trial With Dose Optimization of **OTX015** in Recurrent Glioblastoma Multiforme (GBM) Patients (OTX015_107). In: ClinicalTrials.gov [Internet]. Bethesda (MD): National Library of Medicine (US). 2000- [cited 2015 Nov 9th]. Available from: <https://clinicaltrials.gov/ct2/show/NCT02296476> Identifier: NCT02296476.
- (29) Boi, M.; Gaudio, E.; Bonetti, P.; Kwee, I.; Bernasconi, E.; Tarantelli, C.; Rinaldi, A.; Testoni, M.; Cascione, L.; Ponzoni, M.; Mensah, A. A.; Stathis, A.; Stussi, G.; Riveiro, M. E.; Herait, P.; Inghirami, G.; Cvitkovic; Zucca, E.; Bertoni, F.; *Clin. Cancer Res.* **2015**, *21*, 1628-1638.
- (30) Oncoethix. A Phase I, Dose-finding Study of the Bromodomain (Brd) Inhibitor OTX015/MK-8628 in Hematologic Malignancies (MK-8628-001). 2000- [cited 2015 Nov 9th]. Available from: <https://clinicaltrials.gov/ct2/show/NCT01713582> Identifier: NCT01713582.
- (31) Oncoethix. A Phase IB Trial With **OTX015**, a Small Molecule Inhibitor of the Bromodomain and Extra-Terminal (BET) Proteins, in Patients With Selected Advanced Solid Tumors. 2000- [cited 2015 Nov 9th]. Available from: <https://clinicaltrials.gov/ct2/show/NCT02259114> Identifier: NCT02259114.
- (32) Mirguet, O. A., M.; Boullay, A. M.; Boursier, E.; Brusq, J.-M.; Clément, C.; Costaz, A.; Daugan, A.; Dudit, Y.; Gosmini, R.; Huet, P.; Martin, S.; Pineau, O.; Riou, A.; Toum, J.; Trottet, L.; Nicodème, E. Discovery of benzodiazepine derivatives as Apo A-1 upregulators. *Abstracts of Papers, 241st ACS National Meeting & Exposition, Anaheim, CA, United States, March 27-31, 2011*; American Chemical Society: Washington DC, 2011; MEDI-76.

- (33) Chung, C.-w.; Coste, H.; White, J. H.; Mirguet, O.; Wilde, J.; Gosmini, R. L.; Delves, C.; Magny, S. M.; Woodward, R.; Hughes, S. A.; Boursier, E. V.; Flynn, H.; Bouillot, A. M.; Bamborough, P.; Brusq, J.-M. G.; Gellibert, F. o. J.; Jones, E. J.; Riou, A. M.; Homes, P.; Martin, S. L.; Uings, I. J.; Toum, J. r. m.; Clément, C. A.; Boullay, A.-B. n. d.; Grimley, R. L.; Blandel, F. M.; Prinjha, R. K.; Lee, K.; Kirilovsky, J.; Nicodeme, E. *J. Med. Chem.* **2011**, *54*, 3827-3838.
- (34) GlaxoSmithKline. A Dose Escalation Study to Investigate the Safety, P. P., Pharmacodynamics (PD) and Clinical Activity of **GSK525762** in Subjects With Relapsed, Refractory Hematologic Malignancies. In: ClinicalTrials.gov [Internet]. Bethesda (MD): National Library of Medicine (US). 2000- [cited 2015 Nov 9th]. Available from: <https://clinicaltrials.gov/ct2/show/NCT01943851> NLM Identifier: NCT01943851.
- (35) French, C. A. *Head and Neck Path.* **2013**, *7*, 11-16.
- (36) French, C. A. *J. Clinical Pathol.* **2010**, *63*, 492-496.
- (37) Böhm, H.-J. *J. Comput.--Aided Mol. Des.* **1994**, *8*, 243-256.
- (38) Dawson, M. A.; Prinjha, R. K.; Dittmann, A.; Giotopoulos, G.; Bantscheff, M.; Chan, W.-I.; Robson, S. C.; Chung, C.-w.; Hopf, C.; Savitski, M. M.; Huthmacher, C.; Gudgin, E.; Lugo, D.; Beinke, S.; Chapman, T. D.; Roberts, E. J.; Soden, P. E.; Auger, K. R.; Mirguet, O.; Doehner, K.; Delwel, R.; Burnett, A. K.; Jeffrey, P.; Drewes, G.; Lee, K.; Huntly, B. J. P.; Kouzarides, T. *Nature* **2011**, *478*, 529-533.
- (39) Atkinson, S. J.; Soden, P. E.; Angell, D. C.; Bantscheff, M.; Chung, C.-w.; Giblin, K. A.; Smithers, N.; Furze, R. C.; Gordon, L.; Drewes, G.; Rioja, I.; Witherington, J.; Parr, N. J.; Prinjha, R. K. *MedChemComm* **2014**, *5*, 342-351.
- (40) Ito, T.; Umehara, T.; Sasaki, K.; Nakamura, Y.; Nishino, N.; Terada, T.; Shirouzu, M.; Padmanabhan, B.; Yokoyama, S.; Ito, A.; Yoshida, M. *Chem. Biol.* **2011**, *18*, 495-507.
- (41) Vidler, L. R.; Brown, N.; Knapp, S.; Hoelder, S. *J. Med. Chem.* **2012**, *55*, 7346-7359.
- (42) Amans, D.; Bamborough, P.; Bit, R. A.; Brown, J. A.; Campbell, M.; Lindon, M. J.; Shipley, T. J.; Theodoulou, N. H.; Wellaway, C. R.; Westaway, S. M.; WO2014/078257A1: 2014.

- (43) Gordon, L.; Karamshi, B. *GSK colleague responsible for running TR-FRET assays, unpublished results.*
- (44) Chung, C.-w. *GSK colleague responsible for X-ray crystallography, unpublished results.*
- (45) Young, R. J.; Green, D. V. S.; Luscombe, C. N.; Hill, A. P. *Drug Discov. Today* **2011**, *16*, 822-830.
- (46) Amans, D.; Bamborough, P.; Barker, M. D.; Bit, R. A.; Brown, J. A.; Campbell, M.; Garton, N. S.; Lindon, M. J.; Shipley, T. J.; Theodoulou, N. H.; Wellaway, C. R.; Westaway, S. M.; WO2014/140077A1: 2014.
- (47) Ishikawa, M.; Hashimoto, Y. *J. Med. Chem.* **2011**, *54*, 1539-1554.
- (48) Sridhar, J.; Liu, J.; Foroozesh, M.; Stevens, C. L. K. *Molecules* **2012**, *17*, 9283-9305.
- (49) Zanger, U. M.; Schwab, M. *Pharmacol. Ther.* **2013**, *138*, 103-141.
- (50) Amans, D. B., R. A.; Lindon, M. J.; Wellaway, C. R. *GSK colleagues responsible for med. chem. lead optimisation, unpublished results.*
- (51) Hallifax, D.; Rawden, H. C.; Hakooz, N.; Houston, J. B. *Drug Metab. Dispos.* **2005**, *33*, 1852-1858.
- (52) Diwaker, A. K.; Jadon, G. *IJARPB* **2011**, *1*, 9-11.
- (53) GSK; The 3Rs in medicine research, <http://www.gsk.com/en-gb/research/our-use-of-animals/the-3rs-in-medicine-research/>: accessed 9th November 2014.
- (54) Cyprotex, 15 Beech Lane, Macclesfield, Cheshire, SK10 2DR, UK.
- (55) Obach, R. S. *Drug Metab. Dispos.* **1999**, *27*, 1350-1359.
- (56) Lu, C.; Li, P.; Gallegos, R.; Uttamsingh, V.; Xia, C. Q.; Miwa, G. T.; Balani, S. K.; Gan, L.-S. *Drug Metab. Dispos.* **2006**, *34*, 1600-1605.
- (57) McGinnity, D. F.; Soars, M. G.; Urbanowicz, R. A.; Riley, R. J. *Drug Metab. Dispos.* **2004**, *32*, 1247-1253.
- (58) In *GSK DMPK Council communication, unpublished results, June 13th 2014.*
- (59) Chiba, M.; Ishii, Y.; Sugiyama, Y. *AAPS J.* **2009**, *11*, 262-276.
- (60) Meteor; Lhasa Ltd., Leeds, UK.
- (61) Metasite; Molecular Discovery Ltd., Middlesex, UK.
- (62) Gray, J. *GSK colleague responsible for running Meteor and Metasite predictions.*

- (63) T'jollyn H., B. K., Mortishire-Smith R. J., Coe K., De Boeck B., Van Bocxlaer J. F., Mannens G. *Drug Metab. Dispos.* **2011**, *39*, 2066-2075.
- (64) Bussy, U.; Boujtita, M. *Chem. Res. Toxicol.* **2014**, *27*, 1652-1668.
- (65) Timbrell, J. A. *Principles of Biochemical Toxicology*; Taylor and Francis Ltd.: London, 1991.
- (66) Theodoulou, N. H.; Bamborough, P.; Bannister, A. J.; Becher, I.; Bit, R. A.; Che, K. H.; Chung, C.-w.; Dittmann, A.; Drewes, G.; Drewry, D. H.; Gordon, L.; Grandi, P.; Leveridge, M.; Lindon, M.; Michon, A.-M.; Molnar, J.; Robson, S. C.; Tomkinson, N. C. O.; Kouzarides, T.; Prinjha, R. K.; Humphreys, P. G. *J. Med. Chem.* **2015**, *59*, 1425-1439.
- (67) Hjelmeland, L. M.; Aronow, L.; Trudell, J. R. *Biochem. Biophys. Res. Commun.* **1976**, *76*, 541-549.
- (68) Buncl, E., Lee, C. C., Eds.; *Isotopes in Organic Chemistry*; Vol. 5; Elsevier: Amsterdam, 1977.
- (69) Jones, R. A. Y. *Physical and Mechanistic Organic Chemistry*; Cambridge University Press, 1979.
- (70) Nelson, S. D.; Trager, W. F. *Drug Metab. Dispos.* **2003**, *31*, 1481-1497.
- (71) Karki, S. B.; Dinnocenzo, J. P.; Jones, J. P.; Korzekwa, K. R. *J. Am. Chem. Soc.* **1995**, *117*, 3657-3664.
- (72) Di Costanzo, L.; Moulin, M.; Haertlein, M.; Meilleur, F.; Christianson, D. W. *Arch. Biochem. Biophys.* **2007**, *465*, 82-89.
- (73) Barratt, M. J.; Frail, D. E., Eds. *Drug Repositioning: Bringing New Life to Shelved Assets and Existing Drugs*; John Wiley & Sons, 2012.
- (74) Gant, T. G.; Sarshar, S.; WO2010/120797A2: 2010.
- (75) Miwa, G. T.; Lu, A. Y. *BioEssays* **1987**, *7*, 215-219.
- (76) Patrick, G. L. *An Introduction to Medicinal Chemistry*; 5th ed.; Oxford University Press, 2013.
- (77) Evans, D. C.; Baillie, T. A. *Curr. Opin. Drug Discov. Devel.* **2005**, *8*, 44-50.
- (78) Log D suite version 6. Advanced Chemistry Development, I. T., Ontario, Canada (<http://www.acdlabs.com/>).
- (79) Wilke, T. J.; Jondorf, W. R.; Powis, G. *Xenobiotica* **1989**, *19*, 1013-1022.

- (80) Kaufman, F. C., *Conjugation—Deconjugation Reactions in Drug Metabolism and Toxicity Handbook of Experimental Pharmacology: Microsomal Amidases and Carboxylesterases*; Ed.; Springer-Verlag: Berlin, Heidelberg, 1994.
- (81) Patrick, G. L. *An Introduction to Medicinal Chemistry*; 4th ed.; Oxford University Press, 2009.
- (82) Alder, R. W., Baker, R., Brown, J. M. *Mechanism in Organic Chemistry*; Eds.; Wiley-Interscience, 1971.
- (83) Meijere, A. d. *Angew. Chem. Int. Ed.* **1979**, *18*, 809-886.
- (84) Chung, C.-w. *GSK colleague responsible for SPR experiments, unpublished results.*
- (85) Nassar, A.-E. F.; Talaat, R. E. *Drug Discov. Today* **2004**, *9*, 317-327.
- (86) Hussain, J.; Rea, C., GSK internal poster: "BioDig ADME – "Standing on the shoulders of giants".
- (87) TIBCO™, 281 Summer Street, 3rd Floor, Boston, MA 02210.
- (88) Cumming, J. G.; Davis, A. M.; Muresan, S.; Haeberlein, M.; Chen, H. *Nat. Rev. Drug Discov.* **2013**, *12*, 948-962.
- (89) Hortense, E. *GSK colleague responsible for chiral HPLC separation, unpublished results.*
- (90) Olbe, L.; Carlsson, E.; Lindberg, P. *Nat. Rev. Drug Discov.* **2003**, *2*, 132-139.
- (91) DiscoverRx Corporation, A. S., Suite 100 Fremont, CA 94538, United States.
- (92) Ashley, E. A.; Niebauer, J. *Cardiology Explained*; Remedica: London, 2004.
- (93) Eric Rossman; Wu, X. *GSK Internal Communication.*
- (94) Van de Water, A.; Verheyen, J.; Xhonneux, R.; Reneman, R. S. *J. Pharmacol. Methods* **1989**, *22*, 207-217.
- (95) Hanton, G.; Rabemampianina, Y. *Lab. Anim.* **2006**, *40*, 123-136
- (96) Conreaux, D.; Belot, S.; Desbordes, P.; Monteiro, N.; Balme, G. *J. Org. Chem.* **2008**, *73*, 8619-8622.
- (97) Messina, F.; Botta, M.; Corelli, F.; Villani, C. *Tetrahedron: Asymmetry* **2000**, *11*, 1681-1685.
- (98) Tata, J. R.; Chapman, K. T.; Duffy, J. L.; Kevin, N. J.; Cheng, Y.; Rano, T. A.; Zhang, F.; Huening, T.; Kirk, B. A.; Lu, Z.; Raghavan, S.; Fleitz, F. J.; Petrillo,

- D. E.; Armstrong, J. D. I.; Varsolona, R. J.; Askin, D.; Hoerner, R. S.; Purick, R.; WO 2001/038332A1: 2001.
- (99) Hennion, G. F.; Hanzel, R. S. *J. Am. Chem. Soc.* **1960**, *82*, 4908-4912.
- (100) Devadas, B.; Rogers, T. E.; Gray, S. H. *Synth. Commun.* **1995**, *25*, 3199-3210.
- (101) Conreaux, D.; Bossharth, E.; Monteiro, N.; Desbordes, P.; Vors, J.-P.; Balme, G. *Org. Lett.* **2007**, *9*, 271-274.
- (102) Castanet, A.-S.; Colobert, F.; Broutin, P.-E. *Tetrahedron Lett.* **2002**, *43*, 5047-5048.
- (103) Harisha, A. S.; Nayak, S. P.; Nagarajan, K.; Guru Row, T. N.; Hosamani, A. A. *Tetrahedron Lett.* **2015**, *56*, 1427-1431.
- (104) Smith, M. B.; March, J. *March's Advanced Organic Chemistry: Reactions, Mechanisms, and Structure*; 6th ed.; Wiley-Interscience, 2007.
- (105) Sato, S.; Sakamoto, T.; Miyazawa, E.; Kikugawa, Y. *Tetrahedron* **2004**, *60*, 7899-7906.
- (106) Miyaura, N.; Suzuki, A. *Chem. Rev.* **1995**, *95*, 2457-2483.
- (107) Coleridge, B. M.; Bello, C. S.; Ellenberger, D. H.; Leitner, A. *Tetrahedron Lett.* **2010**, *51*, 357-359.
- (108) Colombe, J. R.; Bernhardt, S.; Stathakis, C.; Buchwald, S. L.; Knochel, P. *Org. Lett.* **2013**, *15*, 5754-5757.
- (109) Molander, G. A.; Biolatto, B. *J. Org. Chem.* **2003**, *68*, 4302-4314.
- (110) Molander, G. A.; Canturk, B.; Kennedy, L. E. *J. Org. Chem.* **2009**, *74*, 973-980.
- (111) Jensen, A. E.; Dohle, W.; Sapountzis, I.; Lindsay, D. M.; Vu, V. A.; Knochel, P. *Synthesis* **2002**, *4*, 565-569.
- (112) Luzung, M. R.; Patel, J. S.; Yin, J. *J. Org. Chem.* **2010**, *75*, 8330-8332.
- (113) Kosar, W., *Handbook of Grignard Reagents*; Ed.; CRC Press, 1996.
- (114) ChemAxon software, ChemAxon Kft., Záhony u. 7, Building HX 1031, Budapest, Hungary.
- (115) Kim, S.-H.; Rieke, R. D. *Tetrahedron Lett.* **2010**, *51*, 2657-2659.
- (116) Qian, D.; Han, A. Q.; Hamilton, M.; Wang, E.; WO2009/155527: 2009.
- (117) Ishiyama, T.; Murata, M.; Miyaura, N. *J. Org. Chem.* **1995**, *60*, 7508-7510.
- (118) Ghosh, A. K.; Cheng, X.; Zhou, B. *Org. Lett.* **2012**, *14*, 5046-5049.

- (119) Organ, M. G.; Avola, S.; Dubovyk, I.; Hadei, N.; Kantchev, E. A. B.; O'Brien, C. J.; Valente, C. *Chem. Eur. J.* **2006**, *12*, 4749-4755.
- (120) Kantchev, E. A. B.; O'Brien, C. J.; Organ, M. G. *Angew. Chem. Int. Ed.* **2007**, *46*, 2768-2813.
- (121) Organ, M. G.; Abdel-Hadi, M.; Avola, S.; Dubovyk, I.; Hadei, N.; Kantchev, E. A. B.; O'Brien, C. J.; Sayah, M.; Valente, C. *Chem. Eur. J.* **2008**, *14*, 2443-2452.
- (122) Organ, M. G.; Abdel-Hadi, M.; Avola, S.; Hadei, N.; Nasielski, J.; O'Brien, C. J.; Valente, C. *Chem. Eur. J.* **2007**, *13*, 150-157.
- (123) Dowlut, M.; Mallik, D.; Organ, M. G. *Chem. Eur. J.* **2010**, *16*, 4279-4283.
- (124) Wada, A.; Kanamoto, S.; Nagai, S. *Chem. Pharm. Bull.* **1985**, *33*, 1016-1022.
- (125) Asada, M.; Obitsu, T.; Kinoshita, A.; Nakai, Y.; Nagase, T.; Sugimoto, I.; Tanaka, M.; Takizawa, H.; Yoshikawa, K.; Sato, K.; Narita, M.; Ohuchida, S.; Nakai, H.; Toda, M. *Bioorg. Med. Chem. Letters* **2010**, *20*, 2639-2643.
- (126) Smith, M. B.; March, J. *March's Advanced Organic Chemistry: Reactions, Mechanisms, and Structure*; Sixth ed.; John Wiley and Sons, 2007.
- (127) Barker, M. D.; Campbell, M.; Diallo, H.; Douault, C.; Humphreys, P.; Liddle, J.; Sheppard, R. J.; Thomas, P. J.; Wilson, D. M.; WO2013/143597A1: 2013.
- (128) Scott, J. D.; Stamford, A. W.; Gilbert, E. J.; Cumming, J. N.; Iserloh, U.; Misiaszek, J. A.; Li, G.; WO2011/044181: 2011.
- (129) Roberts, J. D. *J. Am. Chem. Soc.* **1951**, *73*, 5034-5040.
- (130) Walsh, A. D. *J. Chem. Soc. Faraday Trans.* **1949**, *45*, 179-190.
- (131) Butova, E. D.; Barabash, A. V.; Petrova, A. A.; Kleiner, C. M.; Schreiner, P. R.; Fokin, A. A. *J. Org. Chem.* **2010**, *75*, 6229-6235.
- (132) Feast, W. J.; Tsibouklis, J. *Polym. Int.* **1994**, *35*, 67-74.
- (133) Berdini, V.; Besong, G. E.; Callaghan, O.; Carr, M. G.; Congreve, M. S.; Gill, A. L.; Griffiths-Jones, C. M.; Madin, A.; Murray, C. W.; Nijjar, R. K.; O'Brien, M. A.; Pike, A.; Saxty, G.; Taylor, R. D.; Vickerstaffe, E.; WO2008/078091A1: 2008.
- (134) Murata, M.; Watanabe, S.; Masuda, Y. *J. Org. Chem.* **1997**, *62*, 6458-6459.
- (135) Murata, M.; Oyama, T.; Watanabe, S.; Masuda, Y. *J. Org. Chem.* **2000**, *65*, 164-168.
- (136) Matos, K.; Burkhardt, E. R. *Chim. Oggi* **2005**, *23*, 12-16.

Chapter 3: Future Work and Overall Conclusions

3.1. Future Considerations for Epigenetic Therapies

In the last decade significant progress has been made towards the characterisation of disease-associated cell phenotypes and their related epigenomes. The first generation of epigenetic-based treatments has reached the clinic, including the DNA methyltransferase inhibitor Decogen^(R) and the HDAC inhibitor Zolinza^(R). Clinical trials are currently underway to assess the potential of a number of other HDAC inhibitors in the treatment of indications such as cancer. Furthermore, small molecules that can selectively inhibit writers, readers and erasers in addition to HDAC inhibitors have been reported, which provides further evidence that these epigenetic targets should be druggable. However, all small molecule inhibitors reported to date tend to target proteins on the same branch of the phylogenetic tree due to structural similarities between the proteins. Given the complexity and dynamism of the epigenome, inhibitors with increased selectivity need to be identified in order to determine what combinations of epigenetic marks can affect cell phenotypes involved in development and progression of different diseases. A number of high resolution X-ray crystal structures of inhibitors bound to the proteins have been determined; these should prove invaluable in designing in selectivity and potency in subsequent iterations of optimisation.

A clear benefit in the treatment of a given disease with an acceptable safety and tolerability profile, or therapeutic index, will need to be demonstrated with therapies that act *via* mechanisms of epigenetic modification. Although this is the case with all new drug therapies, the wider role of epigenetics in the regulation of global gene expression patterns increases the chance of adverse events. This puts more of an emphasis on the development of highly selective inhibitors of epigenetic writers, readers and erasers which was a similar issue seen with NOS inhibitors that are still to be made completely NOS subtype selective even after decades of research. The use of the first generation of DNA-methyltransferase and HDAC inhibitors has proven beneficial in the treatment of various cancers with acceptable adverse event profiles and there are ongoing studies of therapeutic potential of HDAC inhibitors for non-oncology indications. However, for chronic indications that, although debilitating, are not immediately life-threatening like RA or SLE, any new treatment will need to exhibit a minimal number of adverse events, if any. Long-term effects on stem cells and germ

cells, especially potential trans-generational effects, also need to be determined, particularly for non-oncology indications. Similarly to NOS inhibitors, the vast potential for epigenetics-based treatments to manage or even cure a wide range of diseases that are currently poorly understood and poorly managed may be tempered by safety issues that may be associated with such a treatment.

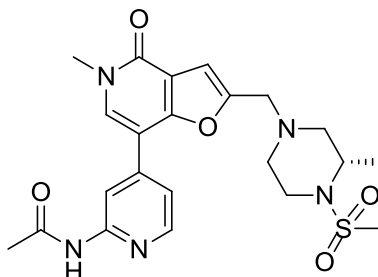
3.2. Thesis Conclusions

The dysregulation of the activity of an enzyme that affects the erasure of methyl epigenetic modifications by citrullination, PAD4, and separately a family of proteins that affects the reading of acetyl-lysine epigenetic modifications, the BET family, has been strongly associated with the development and progression of autoimmune diseases such as SLE and RA. Existing therapies cannot halt or reverse the development of these debilitating and potentially life-threatening diseases; the absence of appropriate treatments stimulated research by the Epinova DPU to increase understanding of the biological mechanisms underlying the disease states. The work herein describes the medicinal chemistry approaches used to successfully identify a set of novel potent pyridazine PAD4 inhibitors, and a novel potent selective furanopyridone BET BD1 inhibitor. The research lays the foundations to support the development of medicines to treat patients' unmet needs, so that they can do more, feel better and live longer.

Appendix: Experimental for Compounds
Prepared by Colleagues

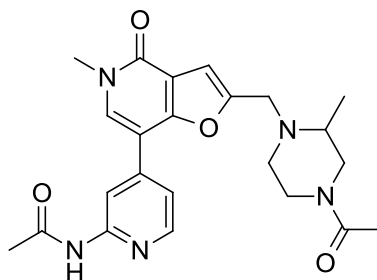
General Alkylation Procedure 1

(S)-N-(4-(5-Methyl-2-((3-methyl-4-(methylsulfonyl)piperazin-1-yl)methyl)-4-oxo-4,5-dihydrofuro[3,2-c]pyridin-7-yl)pyridin-2-yl)acetamide, **34**¹⁹



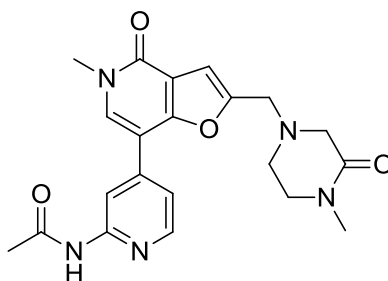
A solution of **103** (50 mg, 0.15 mmol) in DMF (5 mL) was treated with potassium carbonate (63 mg, 0.45 mmol) followed by (S)-2-methyl-1-(methylsulfonyl)piperazine (27 mg, 0.15 mmol), then stirred at room temperature for 3 h. The reaction mixture was partitioned between water (10 mL) and a solution of MeOH (3 mL) in DCM (15 mL). The organic layer was isolated, then concentrated under reduced pressure to give crude **34**. The crude produce was purified by MDAP (Method C) to afford **34** (45 mg, 63%). IR (cm⁻¹) 3263, 1657, 1599, 1562, 1533, 1428, 1318, 1144, 1117, 771; ¹H NMR (400 MHz, CDCl₃ δ): 8.55 (s, 1H), 8.34 (d, *J* = 5 Hz, 1H), 8.05 (br. s, 1H), 7.60 (s, 1H), 7.44 (d, *J* = 5 Hz, 1H), 6.89 (s, 1H), 4.15-4.05 (m, 1H), 3.81-3.69 (m, 5H), 3.58 (d, *J* = 15 Hz, 1H), 3.33 (td, *J* = 12, 4 Hz, 1H), 2.94-2.84 (m, 4H), 2.75 (d, *J* = 11 Hz, 1H), 2.47 (dd, *J* = 11, 4 Hz, 1H), 2.33 (td, *J* = 12, 3 Hz, 1H), 2.26 (s, 3H), 1.39 (d, *J* = 7 Hz, 3H); ¹³C NMR (126 MHz, DMSO-d₆, δ): 169.2, 157.9, 156.0, 153.6, 152.8, 148.2, 141.9, 135.3, 116.4, 115.7, 110.8, 106.3, 105.7, 57.2, 53.6, 51.9, 48.7, 40.0, 36.5, 23.9, 15.8; a piperidine ¹³C was not observed due to obscuration by the residual DMSO solvent peak; HRMS–FAB (*m/z*): [M + H]⁺ calcd for C₂₂H₂₇N₅O₅S, 474.1806; found, 474.1789; LC-MS (Method C) *m/z* = [M + H]⁺ 474.3, *t_R* 0.68 mins; mp 139 – 141 °C.

***N*-(4-(2-((4-Acetyl-2-methylpiperazin-1-yl)methyl)-5-methyl-4-oxo-4,5-dihydrofuro[3,2-*c*]pyridin-7-yl)pyridin-2-yl)acetamide, **41**¹⁹**



Prepared from **103** (50 mg, 0.15 mmol) and 1-(3-methylpiperazin-1-yl)ethanone (21 mg, 0.15 mmol) using the general alkylation procedure 1 to afford **41** (25 mg, 38%). ¹H NMR (400 MHz, CDCl₃ δ): 8.55 (br. s, 1H), 8.42 (s, 1H), 8.33 (d, *J* = 5 Hz, 1H), 7.59 (s, 1H), 7.42 (d, *J* = 5 Hz, 1H), 6.88 (s, 1H), 4.34-4.21 (m, 1H), 4.03-3.87 (m, 2H), 3.76-3.54 (m, 3H), 3.35-3.25 (m, 1H), 3.06-2.95 (m, 1H), 2.94-2.84 (m, 1H), 2.65-2.55 (m, 1H), 2.52-2.34 (m, 2H), 2.25 (s, 3H), 2.06 (s, 3H), 1.26-1.19 (m, 3H); LC-MS (Method C) *m/z* = [M + H]⁺ 438.4, *t_R* 0.61 mins.

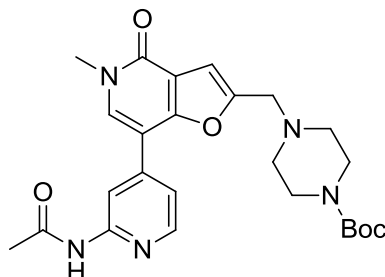
***N*-(4-(5-Methyl-2-((4-methyl-3-oxopiperazin-1-yl)methyl)-4-oxo-4,5-dihydrofuro[3,2-*c*]pyridin-7-yl)pyridin-2-yl)acetamide, **43**¹⁹**



Prepared from **103** (50 mg, 0.15 mmol) and 1-methylpiperazin-2-one (17 mg, 0.15 mmol) using the general alkylation procedure 1 to afford **43** (25 mg, 41%). ¹H NMR (400 MHz, CDCl₃ δ): 8.53 (s, 1H), 8.35 (d, *J* = 5 Hz, 1H), 8.09 (s, 1H), 7.60 (s, 1H), 7.45 (d, *J* = 5 Hz, 1H), 6.93 (s, 1H), 3.81 (s, 2H), 3.73 (s, 3H), 3.38-3.32 (m, 2H), 3.29 (s, 2H), 2.96 (s, 3H), 2.86 - 2.80 (m, 2H), 2.26 (s, 3H); LC-MS (Method C) *m/z* = [M + H]⁺ 410.3, *t_R* 0.58 mins.

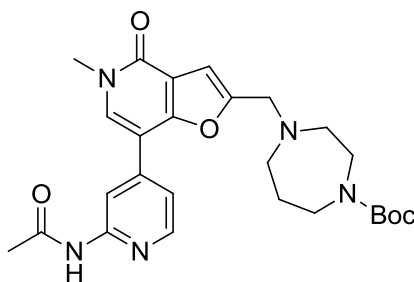
General Alkylation Procedure 2

tert-Butyl 4-((7-(2-acetamidopyridin-4-yl)-5-methyl-4-oxo-4,5-dihydrofuro[3,2-*c*]pyridin-2-yl)methyl)piperazine-1-carboxylate, **27a**¹⁶



A solution of **104** (50 mg, 0.133 mmol) and *tert*-butyl piperazine-1-carboxylate (30 mg, 0.159 mmol) in DMF (0.5 mL) was treated with DIPEA (0.070 mL, 0.400 mmol). The reaction mixture was heated at 110 °C for 30 min by microwave irradiation, then diluted with DMF (0.5 mL) and purified by MDAP (Method E) to afford **27a** (26 mg, 40%). ¹H NMR (600 MHz, DMSO-*d*₆ δ): 10.51 (s, 1H), 8.56 (s, 1H), 8.36 (d, *J* = 5 Hz, 1H), 8.15 (s, 1H), 7.43 (d, *J* = 5 Hz, 1H), 6.87 (s, 1H), 3.71 (s, 2H), 3.60 (s, 3H), 3.33-3.25 (m, 4H), 2.48-2.39 (m, 4H), 2.12 (s, 3H), 1.36 (s, 9H); LC-MS (Method A) *m/z* = [M + H]⁺ 482.3, *t*_R 0.58 mins.

tert-Butyl 4-((7-(2-acetamidopyridin-4-yl)-5-methyl-4-oxo-4,5-dihydrofuro[3,2-*c*]pyridin-2-yl)methyl)-1,4-diazepane-1-carboxylate, **31a**¹⁶

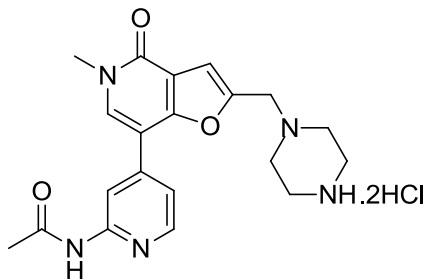


Prepared from **104** (50 mg, 0.133 mmol) and *tert*-butyl 1,4-diazepane-1-carboxylate (32 mg, 0.159 mmol) using the general alkylation procedure 2 to afford **31a** (15 mg, 21%). ¹H NMR (600 MHz, DMSO-*d*₆ δ): 10.51 (br. s, 1H), 8.58 (s, 1H), 8.35 (d, *J* = 5 Hz, 1H), 8.16 (s, 1H), 7.44 (d, *J* = 6 Hz, 1H), 6.85 (s, 1H), 3.83 (s, 2H), 3.60 (s, 3H), 3.54-

3.46 (m, 4H), 2.73-2.58 (m, 4H), 2.11 (s, 3H), 1.78-1.68 (m, 2H), 1.41-1.29 (m, 9H);
LC-MS (Method A) $m/z = [M + H]^+$ 496.0.3, t_R 0.59 mins.

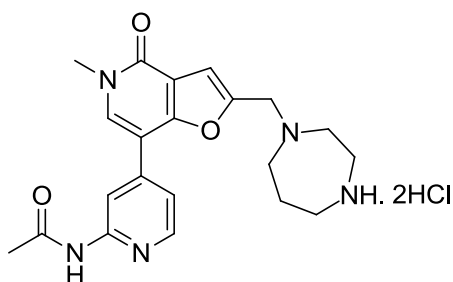
General Boc Deprotection Procedure 1

***N*-(4-(5-Methyl-4-oxo-2-(piperazin-1-ylmethyl)-4,5-dihydrofuro[3,2-*c*]pyridin-7-yl)pyridin-2-yl)acetamide dihydrochloride salt, **27**¹⁶**



A suspension of **27a** (26 mg, 0.053 mmol) in DCM (0.2 mL) was treated with HCl (0.2 mL of a 4 M solution in dioxane) then left to stand at room temperature for 18 h to give **27** (26 mg, 97% at 90% purity). ¹H NMR (400 MHz, DMSO-*d*₆ δ): 11.13 (br. s, 1H), 9.31 (br. s, 2H), 8.62 (s, 1H), 8.46-8.35 (m, 2H), 7.71-7.61 (m, 1H), 7.31-7.15 (m, 1H), 3.65 (s, 2H), 3.58 (s, 3H), 3.55-3.40 (m, 8H), 2.19 (s, 3H), *a hydrochloride underwent exchange in wet deuterated solvent and was not observed*; LC-MS (Method A) $m/z = [M + H]^+$ 382.1, t_R 0.41 mins.

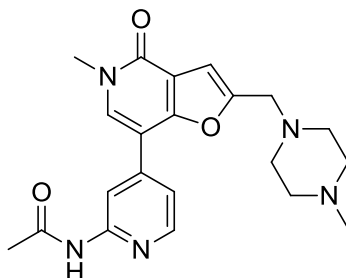
***N*-(4-(2-((1,4-Diazepan-1-yl)methyl)-5-methyl-4-oxo-4,5-dihydrofuro[3,2-*c*]pyridin-7-yl)pyridin-2-yl)acetamide dihydrochloride salt, **31**¹⁶**



Prepared from **55** (15 mg, 0.030 mmol) using the general Boc deprotection procedure 1, leaving to stand for 2 h rather than 18 h, to afford **31** (15 mg, >99% at 90% purity). ¹H NMR (400 MHz, DMSO-*d*₆ δ): 12.01 (br. s, 1H), 11.25 (br. s, 1H), 9.44 (br. s, 2H), 8.66 (s, 1H), 8.48 (s, 1H), 8.38 (d, $J = 6$ Hz, 1H), 7.69 (d, $J = 6$ Hz, 1H), 7.35 (s, 1H), 4.67

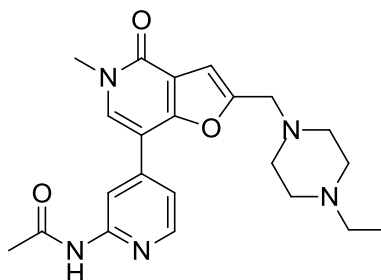
(br. s, 2H), 3.95-3.37 (m, 11H, *obscured by residual solvent peak*), 2.30-2.14 (m, 5H); LC-MS (Method A) $m/z = [M + H]^+$ 396.1, t_R 0.37 mins.

***N*-(4-(5-Methyl-2-((4-methylpiperazin-1-yl)methyl)-4-oxo-4,5-dihydrofuro[3,2-*c*]pyridin-7-yl)pyridin-2-yl)acetamide, **28**¹⁶**



Prepared from **104** (50 mg, 0.133 mmol) and 1-methylpiperazine (16 mg, 0.159 mmol) using the general alkylation procedure 2 to afford **28** (17 mg, 30% *at 90% purity*). IR (cm^{-1}) 3700 - 2500 (m), 1676, 1654, 1598, 1564, 1536, 1426, 1374, 1339, 1277, 1131, 1119, 1006, 838, 815, 775; ^1H NMR (600 MHz, DMSO- d_6 δ): 10.51 (br. s, 1H), 8.55 (s, 1H), 8.36 (d, $J = 5$ Hz, 1H), 8.14 (s, 1H), 7.44 (d, $J = 5$ Hz, 1H), 6.84 (s, 1H), 3.67 (s, 2H), 3.60 (s, 3H), 3.56-3.43 (m, 4H), 2.46-2.22 (m, 4H), 2.17-2.09 (m, 6H); ^{13}C NMR (126 MHz, DMSO- d_6 , δ): 169.2, 157.9, 155.9, 154.0, 152.8, 148.2, 142.0, 135.3, 116.5, 115.7, 110.8, 106.3, 105.6, 54.6, 53.7, 52.0, 45.7, 36.5, 24.0; HRMS-FAB (m/z): $[M + H]^+$ calcd for $\text{C}_{21}\text{H}_{25}\text{N}_5\text{O}_3$, 396.2030; found, 396.2047; LC-MS (Method A) $m/z = [M + H]^+$ 396.3, t_R 0.42 mins; mp 178 – 179 °C.

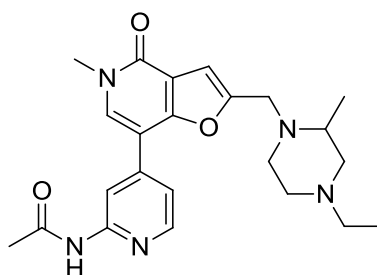
***N*-(4-(2-((4-ethylpiperazin-1-yl)methyl)-5-methyl-4-oxo-4,5-dihydrofuro[3,2-*c*]pyridin-7-yl)pyridin-2-yl)acetamide, **29**¹⁶**



Prepared from **104** (50 mg, 0.133 mmol) and 1-ethylpiperazine (18 mg, 0.159 mmol) using the general alkylation procedure 2 to afford **29** (24 mg, 40% *at 90% purity*). IR (cm^{-1}) 3247, 2803, 1656, 1602, 1566, 1539, 1429, 773; ^1H NMR (600 MHz, DMSO- d_6

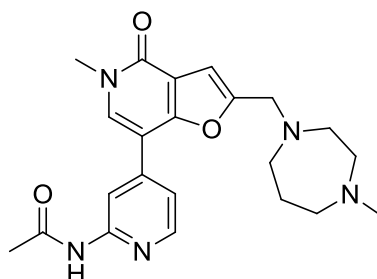
δ): 10.51 (s, 1H), 8.55 (s, 1H), 8.36 (d, $J = 5$ Hz, 1H), 8.13 (s, 1H), 7.43 (d, $J = 5$ Hz, 1H), 6.83 (s, 1H), 3.66 (s, 2H), 3.60 (s, 3H), 3.53 - 3.41 (m, 2H), 3.17 (s, 2H), 2.47 - 2.31 (m, 4H), 2.26 (q, $J = 7$ Hz, 2H), 2.12 (s, 3H), 0.94 (t, $J = 7$ Hz, 3H); ^{13}C NMR (126 MHz, DMSO- d_6 , δ): 169.2, 157.9, 155.9, 154.0, 152.8, 148.2, 142.0, 135.2, 116.5, 115.7, 110.8, 106.3, 105.6, 53.7, 52.3, 52.2, 51.5, 36.4, 24.0, 12.0; HRMS-FAB (m/z): $[\text{M} + \text{H}]^+$ calcd for $\text{C}_{22}\text{H}_{27}\text{N}_5\text{O}_3$, 410.2187; found, 410.2204; LC-MS (Method A) $m/z = [\text{M} + \text{H}]^+$ 410.2, t_{R} 0.42 mins; mp 120 – 121 $^{\circ}\text{C}$.

***N*-(4-(2-((4-Ethyl-2-methylpiperazin-1-yl)methyl)-5-methyl-4-oxo-4,5-dihydrofuro[3,2-*c*]pyridin-7-yl)pyridin-2-yl)acetamide, 30¹⁶**



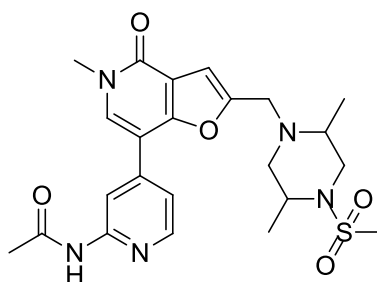
Prepared from **104** (50 mg, 0.133 mmol) and 1-ethyl-3-methylpiperazine (20 mg, 0.159 mmol) using the general alkylation procedure 2 to afford **30** (15 mg, 27% at 90% purity). ^1H NMR (600 MHz, DMSO- d_6 δ): 10.50 (s, 1H), 8.55 (s, 1H), 8.36 (d, $J = 5$ Hz, 1H), 8.15 (s, 1H), 7.45 (d, $J = 5$ Hz, 1H), 6.85 (s, 1H), 3.84 (s, 2H), 3.61 (s, 4H), 2.79-2.73 (m, 1H), 2.71-2.60 (m, 2H), 2.40-2.28 (m, 1H), 2.26-2.17 (m, 2H), 2.11 (s, 3H), 2.01-1.93 (m, 1H), 1.75-1.66 (m, 1H), 1.09 (d, $J = 6$ Hz, 3H), 0.92 (t, $J = 7$ Hz, 3H); LC-MS (Method A) $m/z = [\text{M} + \text{H}]^+$ 424.3, t_{R} 0.46 mins.

***N*-(4-(5-Methyl-2-((4-methyl-1,4-diazepan-1-yl)methyl)-4-oxo-4,5-dihydrofuro[3,2-*c*]pyridin-7-yl)pyridin-2-yl)acetamide, 32¹⁶**

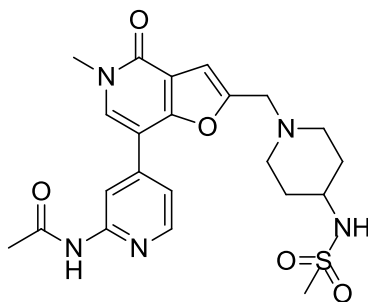


Prepared from **104** (50 mg, 0.133 mmol) and 1-methyl-1,4-diazepane (18 mg, 0.159 mmol) using the general alkylation procedure 2 to afford **32** (8 mg, 14% *at 90% purity*). ¹H NMR (600 MHz, DMSO-d₆ δ): 10.51 (br. s, 1H), 8.57 (s, 1H), 8.36 (d, *J* = 6 Hz, 1H), 8.15 (s, 1H), 7.44 (d, *J* = 6 Hz, 1H), 6.82 (s, 1H), 3.80 (s, 2H), 3.60 (s, 3H), 3.52-3.42 (m, 4H), 2.78-2.70 (m, 4H), 2.21 (s, 3H), 2.11 (s, 3H), 1.73-1.65 (m, 2H); LC-MS (Method A) *m/z* = [M + H]⁺ 410.2, *t_R* 0.40 mins.

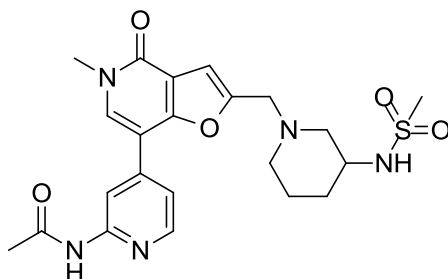
***N*-(4-(2-((2,5-Dimethyl-4-(methylsulfonyl)piperazin-1-yl)methyl)-5-methyl-4-oxo-4,5-dihydrofuro[3,2-*c*]pyridin-7-yl)pyridin-2-yl)acetamide, 33¹⁶**



Prepared from **104** (50 mg, 0.133 mmol) and 2,5-dimethyl-1-(methylsulfonyl)piperazine (31 mg, 0.159 mmol) using the general alkylation procedure 2 to afford **33** (30 mg, 42% *at 90% purity*). IR (cm⁻¹) 3208, 1669, 1608, 1570, 1433, 1316, 1143, 1002, 773; ¹H NMR (600 MHz, DMSO-d₆ δ): 10.51 (s, 1H), 8.55 (s, 1H), 8.36 (d, *J* = 5 Hz, 1H), 8.15 (s, 1H), 7.44 (d, *J* = 5 Hz, 1H), 6.87 (s, 1H), 3.75-3.66 (m, 3H), 3.63-3.54 (m, 4H), 3.04-2.96 (m, 1H), 2.92-2.81 (m, 5H), 2.37-2.30 (m, 1H), 2.11 (s, 3H), 1.24 (d, *J* = 6 Hz, 3H), 1.04 (d, *J* = 6 Hz, 3H); ¹³C NMR (126 MHz, DMSO-d₆ δ): 169.2, 157.9, 156.0, 154.5, 152.8, 148.2, 142.0, 135.2, 116.6, 115.7, 110.8, 106.3, 105.1, 52.3, 51.8, 50.0, 49.9, 47.4, 38.0, 36.5, 23.9, 15.7, 9.7; HRMS-FAB (*m/z*): [M + H]⁺ calcd for C₂₃H₂₉N₅O₅S, 488.1962; found, 488.1964; LC-MS (Method A) *m/z* = [M + H]⁺ 488.2, *t_R* 0.49 mins; mp 229 – 230 °C.

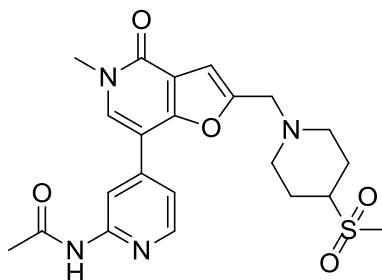
***N*-(4-(5-Methyl-2-((4-(methylsulfonamido)piperidin-1-yl)methyl)-4-oxo-4,5-dihydrofuro[3,2-*c*]pyridin-7-yl)pyridin-2-yl)acetamide, 35¹⁶**

Prepared from **104** (50 mg, 0.133 mmol) and *N*-(piperidin-4-yl)methanesulfonamide (34 mg, 0.159 mmol) using the general alkylation procedure 2 to afford **35** (22 mg, 31% at 90% purity). ¹H NMR (600 MHz, DMSO-*d*₆ δ): 10.51 (s, 1H), 8.56 (s, 1H), 8.36 (d, 1H, *J* = 5 Hz), 8.14 (s, 1H), 7.44 (d, 1H, *J* = 5 Hz), 7.00 (d, 1H, *J* = 7 Hz), 6.84 (s, 1H), 3.68 (s, 2H), 3.61 (s, 3H), 3.11-3.03 (m, 1H), 2.88 (s, 3H), 2.86-2.79 (m, 2H), 2.20-2.08 (m, 5H), 1.86-1.77 (m, 2H), 1.51-1.39 (m, 2H); LC-MS (Method A) *m/z* = [M + H]⁺ 474.2, *t*_R 0.42 mins.

***N*-(4-(5-Methyl-2-((3-(methylsulfonamido)piperidin-1-yl)methyl)-4-oxo-4,5-dihydrofuro[3,2-*c*]pyridin-7-yl)pyridin-2-yl)acetamide, 36¹⁶**

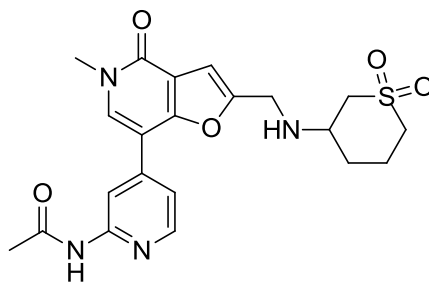
Prepared from **104** (50 mg, 0.133 mmol) and *N*-(piperidin-3-yl)methanesulfonamide (28 mg, 0.159 mmol) using the general alkylation procedure 2 to afford **36** (26 mg, 37% at 90% purity). ¹H NMR (600 MHz, DMSO-*d*₆ δ): 10.53 (s, 1H), 8.58 (s, 1H), 8.36 (d, *J* = 5 Hz, 1H), 8.15 (s, 1H), 7.45 (d, *J* = 5 Hz, 1H), 6.99 (d, *J* = 8 Hz, 1H), 6.87 (s, 1H), 3.78-3.69 (m, 2H), 3.60 (s, 3H), 3.30-3.22 (m, 1H), 2.97-2.86 (m, 4H), 2.74-2.65 (m, 1H), 2.13 (s, 3H), 2.08-1.98 (m, 2H), 1.82-1.73 (m, 1H), 1.69-1.60 (m, 1H), 1.53-1.39 (m, 1H), 1.20-1.04 (m, 1H); LC-MS (Method A) *m/z* = [M + H]⁺ 474.2, *t*_R 0.42 mins.

***N*-4-(5-Methyl-2-((4-(methylsulfonyl)piperidin-1-yl)methyl)-4-oxo-4,5-dihydrofuro[3,2-*c*]pyridin-7-yl)pyridin-2-yl)acetamide, **37**¹⁶**



Prepared from **104** (50 mg, 0.133 mmol) and 4-(methylsulfonyl)piperidine (26 mg, 0.159 mmol) using the general alkylation procedure 2 to afford **37** (22 mg, 32% *at 90% purity*). IR (cm⁻¹) 3003, 1672, 1609, 1434, 1335, 1276, 1261, 1117, 1109, 792, 775; ¹H NMR (600 MHz, DMSO-*d*₆ δ): 10.51 (s, 1H), 8.58 (s, 1H), 8.36 (d, *J* = 5 Hz, 1H), 8.14 (s, 1H), 7.43 (d, *J* = 5 Hz, 1H), 6.87 (s, 1H), 3.74 (s, 2H), 3.60 (s, 3H), 3.07-2.97 (m, 3H), 2.88 (s, 3H), 2.12 (s, 5H), 2.02-1.94 (m, 2H), 1.67-1.57 (m, 2H); ¹³C NMR (126 MHz, DMSO-*d*₆, δ): 169.3, 157.9, 156.0, 153.8, 152.8, 148.3, 142.0, 135.3, 116.5, 115.7, 110.8, 106.3, 105.8, 58.5, 53.3, 50.9, 37.3, 36.5, 24.5, 23.9; HRMS–FAB (*m/z*): [M + H]⁺ calcd for C₂₂H₂₆N₄O₅S, 459.1697; found, 459.1712; LC-MS (Method A) *m/z* = [M + H]⁺ 459.2, *t*_R 0.41 mins; mp 246 – 247 °C.

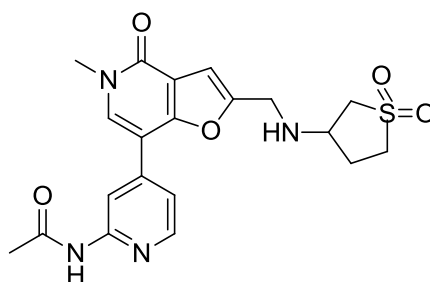
***N*-4-(2-(((1,1-Dioxidotetrahydro-2*H*-thiopyran-3-yl)amino)methyl)-5-methyl-4-oxo-4,5-dihydrofuro[3,2-*c*]pyridin-7-yl)pyridin-2-yl)acetamide, **38**¹⁶**



Prepared from **104** (50 mg, 0.133 mmol) and 3-aminotetrahydro-2*H*-thiopyran 1,1-dioxide (24 mg, 0.159 mmol) using the general alkylation procedure 2 to afford **38** (15 mg, 23% *at 90% purity*); IR (cm⁻¹) 3600 - 2650 (m), 1656, 1600, 1566, 1542, 1432, 1281, 1120, 867, 826, 769, 683, 661; ¹H NMR (600 MHz, DMSO-*d*₆ δ): 10.54 (s, 1H), 8.65 (br. s, 1H), 8.35 (d, *J* = 5 Hz, 1H), 8.18 (s, 1H), 7.48 (d, *J* = 5 Hz, 1H), 6.83 (s,

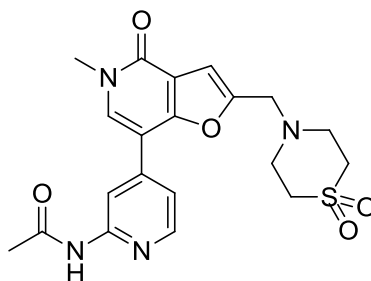
1H), 4.10 (br. s, 1H), 3.91 (d, $J = 6$ Hz, 2H), 3.60 (s, 3H), 3.03-2.92 (m, 3H), 2.92-2.83 (m, 1H), 2.55-2.52 (m, 1H), 2.13 (s, 3H), 2.04-1.93 (m, 2H), 1.76-1.62 (m, 1H), 1.37 - 1.26 (m, 1H); ^{13}C NMR (126 MHz, DMSO- d_6 , δ): 169.5, 158.0, 156.4, 155.8, 152.8, 148.2, 141.9, 135.1, 116.3, 115.7, 110.7, 106.2, 103.6, 55.8, 53.5, 50.0, 42.1, 36.5, 30.0, 24.0, 20.7; HRMS-FAB (m/z): $[\text{M} + \text{H}]^+$ calcd for $\text{C}_{21}\text{H}_{24}\text{N}_4\text{O}_5\text{S}$, 445.154; found, 445.1567; LC-MS (Method A) $m/z = [\text{M} + \text{H}]^+$ 445.2, t_R 0.42 mins; mp 165 – 167 °C.

***N*-(4-(2-(((1,1-Dioxidotetrahydrothiophen-3-yl)amino)methyl)-5-methyl-4-oxo-4,5-dihydrofuro[3,2-*c*]pyridin-7-yl)pyridin-2-yl)acetamide, 39¹⁶**



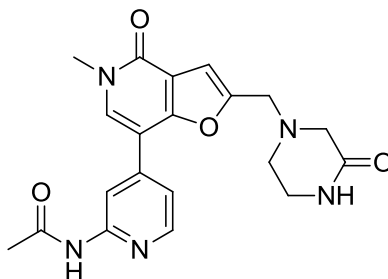
Prepared from **104** (50 mg, 0.133 mmol) and 3-aminotetrahydrothiophene 1,1-dioxide (21 mg, 0.159 mmol) using the general alkylation procedure 2 to afford **39** (17 mg, 26% at 90% purity). ^1H NMR (600 MHz, DMSO- d_6 δ): 10.55 (br. s, 1H), 8.68 (s, 1H), 8.35 (d, $J = 5$ Hz, 1H), 8.19 (s, 1H), 7.47 (d, $J = 5$ Hz, 1H), 6.86 (s, 1H), 4.20-4.04 (m, 1H), 3.95-3.83 (m, 2H), 3.60 (s, 3H), 3.49-3.41 (m, 1H), 3.27-3.20 (m, 1H), 3.10-2.99 (m, 1H), 2.97-2.87 (m, 1H), 2.86-2.75 (m, 1H), 2.32-2.23 (m, 1H), 2.13 (s, 3H), 2.08-1.98 (m, 1H); LC-MS (Method A) $m/z = [\text{M} + \text{H}]^+$ 431.2, t_R 0.42 mins.

***N*-(4-(2-(((1,1-Dioxothiomorpholino)methyl)-5-methyl-4-oxo-4,5-dihydrofuro[3,2-*c*]pyridin-7-yl)pyridin-2-yl)acetamide, 40¹⁶**



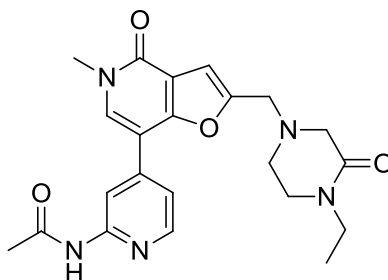
Prepared from **104** (50 mg, 0.133 mmol) and thiomorpholine 1,1-dioxide (21 mg, 0.159 mmol) using the general alkylation procedure 2 to afford **40** (19 mg, 30% at 90% purity). IR (cm⁻¹) 3466, 1655, 1563, 1539, 1428, 1323, 1291, 1268, 1182, 1120, 851, 830, 768; ¹H NMR (600 MHz, DMSO-d₆ δ): 10.52 (s, 1H), 8.62 (s, 1H), 8.36 (d, *J* = 5 Hz, 1H), 8.19 (s, 1H), 7.44 (d, *J* = 5 Hz, 1H), 6.94 (s, 1H), 3.90 (s, 2H), 3.61 (s, 3H), 3.56-3.43 (m, 4H), 3.02-2.95 (m, 4H), 2.12 (s, 3H); ¹³C NMR (126 MHz, DMSO-d₆, δ): 169.3, 157.9, 156.1, 153.2, 152.8, 148.2, 141.9, 135.6, 116.3, 115.6, 110.8, 106.2, 106.1, 52.2, 50.5, 50.0, 36.5, 24.0; HRMS–FAB (*m/z*): [M + H]⁺ calcd for C₂₀H₂₂N₄O₅S, 431.1384; found, 431.1377; LC-MS (Method A) *m/z* = [M + H]⁺ 431.2, *t_R* 0.50 mins; mp 240 – 243 °C.

***N*-(4-(5-Methyl-4-oxo-2-((3-oxopiperazin-1-yl)methyl)-4,5-dihydrofuro[3,2-*c*]pyridin-7-yl)pyridin-2-yl)acetamide, 42¹⁶**



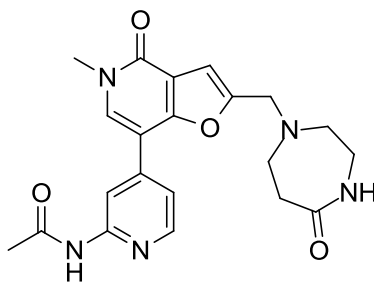
Prepared from **104** (50 mg, 0.133 mmol) and piperazin-2-one (16 mg, 0.159 mmol) using the general alkylation procedure 2 to afford **42** (5 mg, 9% at 90% purity). ¹H NMR (600 MHz, DMSO-d₆ δ): 10.52 (s, 1H), 8.56 (s, 1H), 8.36 (d, *J* = 5 Hz, 1H), 8.16 (s, 1H), 7.72 (s, 1H), 7.44 (d, *J* = 5 Hz, 1H), 6.93 (s, 1H), 3.78 (s, 2H), 3.61 (s, 3H), 3.56-3.46 (m, 2H), 3.01 (s, 2H), 2.73-2.64 (m, 2H), 2.12 (s, 3H); LC-MS (Method A) *m/z* = [M + H]⁺ 396.2, *t_R* 0.43 mins.

***N*-(4-(2-((4-ethyl-3-oxopiperazin-1-yl)methyl)-5-methyl-4-oxo-4,5-dihydrofuro[3,2-*c*]pyridin-7-yl)pyridin-2-yl)acetamide, **44**¹⁶**



Prepared from **104** (50 mg, 0.133 mmol) and 1-ethylpiperazin-2-one (20 mg, 0.159 mmol) using the general alkylation procedure 2 to afford **44** (22 mg, 35% *at 90% purity*). IR (cm⁻¹) 3397, 1659, 1638, 1598, 1563, 1538, 1412, 773.7; ¹H NMR (600 MHz, DMSO-d₆ δ): 10.51 (s, 1H), 8.56 (br. s., 1H), 8.35 (d, *J* = 5 Hz, 1H), 8.14 (s, 1H), 7.43 (d, *J* = 5 Hz, 1H), 6.92 (s, 1H), 3.76 (s, 2H), 3.60 (s, 3H), 3.31-3.23 (m, 4H), 3.05 (s, 2H), 2.80-2.71 (m, 2H), 2.12 (s, 3H), 0.99 (t, *J* = 7 Hz, 3H); ¹³C NMR (126 MHz, DMSO-d₆, δ): 169.2, 165.1, 157.9, 156.2, 152.9, 152.8, 148.2, 141.9, 135.5, 116.5, 115.7, 110.8, 106.3, 106.2, 56.1, 52.1, 48.6, 45.2, 40.0, 36.5, 23.1, 11.9; HRMS–FAB (*m/z*): [M + H]⁺ calcd for C₂₂H₂₅N₅O₄, 424.1979; found, 424.1972; LC-MS (Method A) *m/z* = [M + H]⁺ 424.2, *t_R* 0.49 mins| mp 206 – 208 °C.

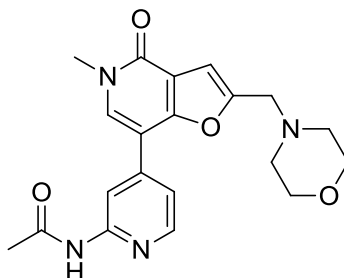
***N*-(4-(5-Methyl-4-oxo-2-((5-oxo-1,4-diazepan-1-yl)methyl)-4,5-dihydrofuro[3,2-*c*]pyridin-7-yl)pyridin-2-yl)acetamide, **45**¹⁶**



Prepared from **104** (50 mg, 0.133 mmol) and 1,4-diazepan-5-one (18 mg, 0.159 mmol) using the general alkylation procedure 2 to afford **45** (14 mg, 23% *at 90% purity*). ¹H NMR (600 MHz, DMSO-d₆ δ): 10.53 (s, 1H), 8.61 (s, 1H), 8.36 (d, *J* = 5 Hz, 1H), 8.18 (s, 1H), 7.54- 7.48 (m, 1H), 7.44 (d, *J* = 5 Hz, 1H), 6.87 (s, 1H), 3.81 (s, 2H), 3.60 (s,

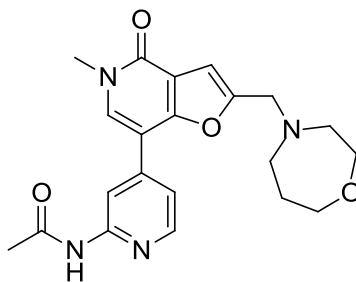
3H), 3.56-3.49 (m, 2H), 2.56-2.42 (m, 6H), 2.12 (s, 3H); LC-MS (Method A) m/z = [M + H]⁺ 410.2, t_R 0.39 mins.

N-4-(5-Methyl-2-(morpholinomethyl)-4-oxo-4,5-dihydrofuro[3,2-*c*]pyridin-7-yl)pyridin-2-yl)acetamide, **46**¹⁶

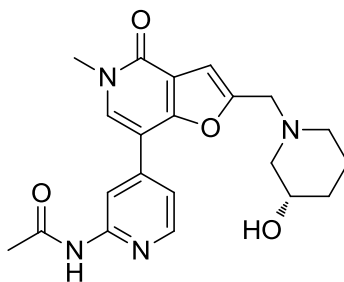


Prepared from **104** (50 mg, 0.133 mmol) and morpholine (14 mg, 0.159 mmol) using the general alkylation procedure 2 to afford **46** (26 mg, 46% at 90% purity). ¹H NMR (600 MHz, DMSO-*d*₆ δ): 10.51 (s, 1H), 8.56 (s, 1H), 8.36 (d, *J* = 5 Hz, 1H), 8.14 (s, 1H), 7.43 (d, *J* = 5 Hz, 1H), 6.87 (s, 1H), 3.68 (s, 2H), 3.60 (s, 3H), 3.59-3.55 (m, 4H), 2.49-2.43 (m, 4H), 2.12 (s, 3H); LC-MS (Method A) m/z = [M + H]⁺ 383.2, t_R 0.41 mins.

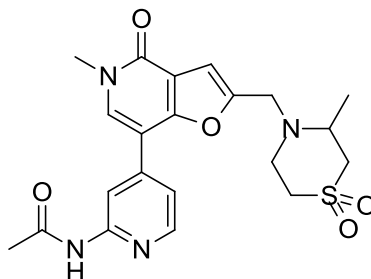
N-4-(2-((1,4-Oxazepan-4-yl)methyl)-5-methyl-4-oxo-4,5-dihydrofuro[3,2-*c*]pyridin-7-yl)pyridin-2-yl)acetamide, **47**¹⁶



Prepared from **104** (50 mg, 0.133 mmol) and 1,4-oxazepane (16 mg, 0.159 mmol) using the general alkylation procedure 2 to afford **47** (23 mg, 39% at 90% purity). ¹H NMR (600 MHz, DMSO-*d*₆ δ): 10.50 (s, 1H), 8.58 (s, 1H), 8.36 (d, *J* = 5 Hz, 1H), 8.15 (s, 1H), 7.44 (d, *J* = 5 Hz, 1H), 6.85 (s, 1H), 3.84 (s, 2H), 3.66 (t, *J* = 6 Hz, 2H), 3.63-3.59 (m, 5H), 2.74-2.70 (m, 4H), 2.11 (s, 3H), 1.83-1.78 (m, 2H); LC-MS (Method A) m/z = [M + H]⁺ 397.2, t_R 0.42 mins.

(S)-N-(4-(2-((3-Hydroxypiperidin-1-yl)methyl)-5-methyl-4-oxo-4,5-dihydrofuro[3,2-*c*]pyridin-7-yl)pyridin-2-yl)acetamide, 48¹⁶

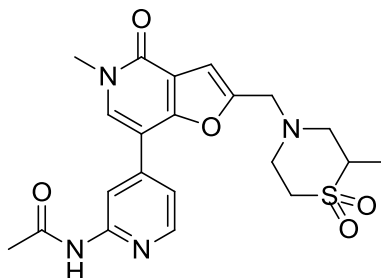
Prepared from **104** (50 mg, 0.133 mmol) and (*S*)-piperidin-3-ol (22 mg, 0.159 mmol) using the general alkylation procedure 2 to afford **48** (23 mg, 39% at 90% purity). ¹H NMR (600 MHz, DMSO-*d*₆ δ): 10.52 (s, 1H), 8.56 (s, 1H), 8.36 (d, *J* = 5 Hz, 1H), 8.14 (s, 1H), 7.44 (d, *J* = 5 Hz, 1H), 6.84 (s, 1H), 4.58 (d, *J* = 5 Hz, 1H), 3.73-3.64 (m, 2H), 3.60 (s, 3H), 3.50-3.45 (m, 1H), 2.88-2.82 (m, 1H), 2.73-2.67 (m, 1H), 2.12 (s, 3H), 2.03-1.95 (m, 1H), 1.87-1.80 (m, 1H), 1.77-1.71 (m, 1H), 1.65-1.57 (m, 1H), 1.45-1.36 (m, 1H), 1.07-0.98 (m, 1H); LC-MS (Method A) *m/z* = [M + H]⁺ 397.2, *t*_R 0.41 mins.

N-(4-(5-Methyl-2-((3-methyl-1,1-dioxithiomorpholino)methyl)-4-oxo-4,5-dihydrofuro[3,2-*c*]pyridin-7-yl)pyridin-2-yl)acetamide, 49¹⁶

Prepared from **104** (50 mg, 0.133 mmol) and 3-methylthiomorpholine 1,1-dioxide (24 mg, 0.159 mmol) using the general alkylation procedure 2 to afford **49** (18 mg, 28% at 90% purity). IR (cm⁻¹) 3285, 2978, 1656, 1600, 1563, 1532, 1430, 1290, 1255, 1123, 770; ¹H NMR (400 MHz, DMSO-*d*₆ δ): 10.52 (br. s, 1H), 8.60 (s, 1H), 8.37 (d, *J* = 5 Hz, 1H), 8.20 (s, 1H), 7.45 (d, *J* = 5 Hz, 1H), 6.96 (s, 1H), 4.11-3.89 (m, 2H), 3.62 (s, 3H), 3.23-3.03 (m, 4H), 3.02-2.82 (m, 3H), 2.13 (s, 3H), 1.30 (d, *J* = 6 Hz, 3H); ¹³C NMR (126 MHz, DMSO-*d*₆, δ): 169.3, 157.9, 156.0, 153.5, 152.8, 148.2, 141.9, 135.5, 116.4, 115.6, 110.7, 106.2, 106.0, 55.6, 53.5, 49.6, 48.9, 46.7, 36.5, 23.9, 18.6; HRMS–

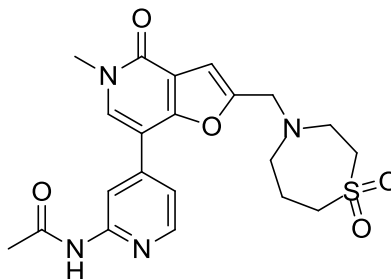
FAB (m/z): $[M + H]^+$ calcd for $C_{21}H_{24}N_4O_5S$, 445.154; found, 445.154; LC-MS (Method A) $m/z = [M + H]^+$ 445.1, t_R 0.55 mins; mp 211 – 213 °C.

***N*-(4-(5-Methyl-2-((2-methyl-1,1-dioxidothiomorpholino)methyl)-4-oxo-4,5-dihydrofuro[3,2-*c*]pyridin-7-yl)pyridin-2-yl)acetamide, 50¹⁶**



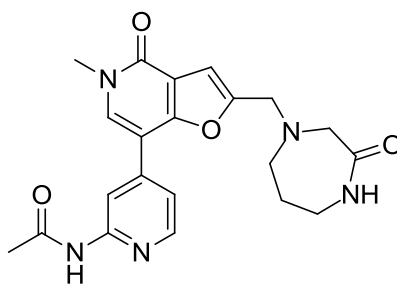
Prepared from **104** (50 mg, 0.133 mmol) and 2-methylthiomorpholine 1,1-dioxide (24 mg, 0.159 mmol) using the general alkylation procedure 2 to afford **50** (23 mg, 35% at 90% purity). IR (cm^{-1}) 3425, 1658, 1530, 1428, 1286, 1268, 1115; 1H NMR (400 MHz, DMSO- d_6 δ): 10.52 (s, 1H), 8.65 (s, 1H), 8.37 (d, $J = 5$ Hz, 1H), 8.21 (s, 1H), 7.45 (d, $J = 5$ Hz, 1H), 6.94 (s, 1H), 3.90 (s, 2H), 3.62 (s, 3H), 3.28-3.06 (m, 5H), 2.86-2.75 (m, 1H), 2.59-2.53 (m, 1H), 2.13 (s, 3H), 1.15 (d, $J = 7$ Hz, 3H); ^{13}C NMR (126 MHz, DMSO- d_6 , δ): 169.3, 157.9, 156.2, 153.2, 152.8, 148.2, 141.9, 135.5, 116.2, 115.6, 110.8, 106.2, 106.0, 56.4, 54.6, 52.4, 50.2, 49.6, 36.5, 24.0. The final carbon was obscured by residual DMSO; HRMS-FAB (m/z): $[M + H]^+$ calcd for $C_{21}H_{24}N_4O_5S$, 445.154; found, 445.1558; LC-MS (Method A) $m/z = [M + H]^+$ 445.1, t_R 0.56 mins; mp 231 – 233 °C.

***N*-(4-(2-((1,1-Dioxido-1,4-thiazepan-4-yl)methyl)-5-methyl-4-oxo-4,5-dihydrofuro[3,2-*c*]pyridin-7-yl)pyridin-2-yl)acetamide, 51¹⁶**



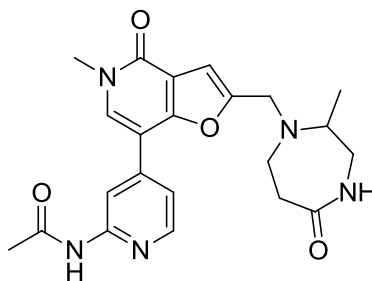
Prepared from **104** (50 mg, 0.133 mmol) and 1,4-thiazepane 1,1-dioxide (24 mg, 0.159 mmol) using the general alkylation procedure 2 to afford **51** (19 mg, 29% at 90% purity). ^1H NMR (400 MHz, DMSO- d_6 δ): 10.51 (br. s, 1H), 8.66 (s, 1H), 8.36 (d, $J = 5$ Hz, 1H), 8.20 (s, 1H), 7.46 (d, $J = 5$ Hz, 1H), 6.92 (s, 1H), 3.95 (s, 2H), 3.62 (s, 3H), 3.27-3.20 (m, 4H, *partially obscured by residual solvent peak*), 3.06-2.98 (m, 2H), 2.90 (t, $J = 6$ Hz, 2H), 2.13 (s, 3H), 2.00-1.91 (m, 2H); LC-MS (Method A) $m/z = [\text{M} + \text{H}]^+$ 445.1, t_R 0.48 mins.

***N*-(4-(5-Methyl-4-oxo-2-((3-oxo-1,4-diazepan-1-yl)methyl)-4,5-dihydrofuro[3,2-*c*]pyridin-7-yl)pyridin-2-yl)acetamide, 52¹⁶**



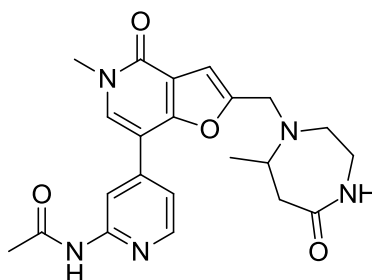
Prepared from **104** (50 mg, 0.133 mmol) and 1,4-diazepan-2-one (18 mg, 0.159 mmol) using the general alkylation procedure 2 to afford **52** (11 mg, 18% at 90% purity). NMR (400 MHz, DMSO- d_6 δ): 10.50 (s, 1H), 8.55 (s, 1H), 8.37 (d, $J = 5$ Hz, 1H), 8.15 (s, 1H), 7.58-7.53 (m, 1H), 7.46 (d, $J = 5$ Hz, 1H), 6.89 (s, 1H), 3.86 (s, 2H), 3.62 (s, 3H), 3.37-3.27 (m, 2H, *partially obscured by residual solvent peak*), 3.17-3.07 (m, 2H), 2.94-2.85 (m, 2H), 2.12 (s, 3H), 1.72-1.62 (m, 2H); LC-MS (Method A) $m/z = [\text{M} + \text{H}]^+$ 410.1, t_R 0.41 mins.

***N*-(4-(5-Methyl-2-((2-methyl-5-oxo-1,4-diazepan-1-yl)methyl)-4-oxo-4,5-dihydrofuro[3,2-*c*]pyridin-7-yl)pyridin-2-yl)acetamide, 53¹⁶**

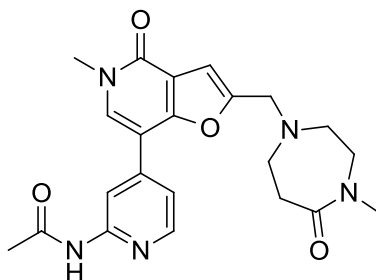


Prepared from **104** (50 mg, 0.133 mmol) and 2-methyl-1,4-diazepan-5-one (20 mg, 0.159 mmol) using the general alkylation procedure 2 to afford **53** (16 mg, 25% at 90% purity). IR (cm⁻¹) 3257, 1653, 1597, 1561, 1535, 1427, 1374, 772; NMR (400 MHz, DMSO-d₆ δ): 10.51 (br. s, 1H), 8.56 (s, 1H), 8.37 (d, *J* = 5 Hz, 1H), 8.15 (s, 1H), 7.44 (d, *J* = 5 Hz, 1H), 7.37-7.29 (m, 1H), 6.87 (s, 1H), 3.94-3.77 (m, 2H), 3.61 (s, 3H), 3.44-3.35 (m, 1H), 3.00-2.78 (m, 3H), 2.70-2.55 (m, 2H), 2.31-2.19 (m, 1H), 2.13 (s, 3H), 0.99 (d, *J* = 7 Hz, 3H); ¹³C NMR (126 MHz, DMSO-d₆, δ): 175.7, 169.2, 157.9, 155.9, 155.1, 152.8, 148.2, 142.0, 135.2, 116.6, 115.7, 110.8, 106.4, 105.0, 60.2, 55.0, 50.7, 46.0, 43.9, 36.8, 36.5, 23.9; HRMS–FAB (*m/z*): [M + H]⁺ calcd for C₂₂H₂₅N₅O₄, 424.1979; found, 424.1994; LC-MS (Method A) *m/z* = [M + H]⁺ 424.2, *t_R* 0.42 mins; mp 141 – 143 °C.

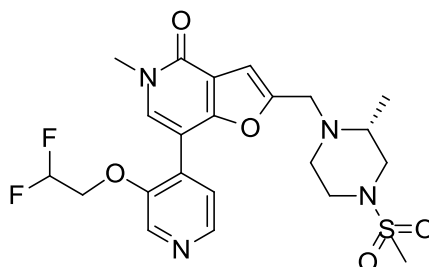
***N*-(4-(5-Methyl-2-((7-methyl-5-oxo-1,4-diazepan-1-yl)methyl)-4-oxo-4,5-dihydrofuro[3,2-*c*]pyridin-7-yl)pyridin-2-yl)acetamide, 54¹⁶**



Prepared from **104** (50 mg, 0.133 mmol) and 7-methyl-1,4-diazepan-5-one (20 mg, 0.159 mmol) using the general alkylation procedure 2 to afford **54** (9 mg, 14% at 90% purity). NMR (400 MHz, DMSO-d₆ δ): 10.51 (br. s, 1H), 8.57-8.54 (m, 1H), 8.37 (d, *J* = 5 Hz, 1H), 8.14 (s, 1H), 7.51-7.42 (m, 2H), 6.87 (s, 1H), 3.96-3.75 (m, 2H), 3.61 (s, 3H), 3.28-3.23 (m, 1H), 3.09-2.93 (m, 2H), 2.86-2.75 (m, 2H), 2.70-2.63 (m, 1H), 2.27-2.19 (m, 1H), 2.13 (s, 3H), 1.04 (d, *J* = 7 Hz, 3H); LC-MS (Method A) *m/z* = [M + H]⁺ 424.2, *t_R* 0.41 mins.

***N*-4-(5-Methyl-2-((4-methyl-5-oxo-1,4-diazepan-1-yl)methyl)-4-oxo-4,5-dihydrofuro[3,2-*c*]pyridin-7-yl)pyridin-2-yl)acetamide, **55**¹⁶**

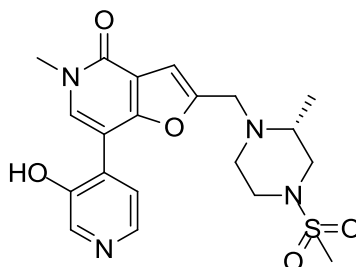
Prepared from **104** (50 mg, 0.133 mmol) and 4-methyl-1,4-diazepan-5-one (20 mg, 0.159 mmol) using the general alkylation procedure 2 to afford **55** (16 mg, 25% *at* 90% purity). ¹H NMR (500 MHz, DMSO-*d*₆ δ): 10.55 (br. s, 1H), 8.61 (s, 1H), 8.37 (d, *J* = 5 Hz, 1H), 8.19 (s, 1H), 7.44 (d, *J* = 5 Hz, 1H), 6.88 (s, 1H), 3.83 (s, 2H), 3.61 (s, 3H), 3.47-3.43 (m, 2H), 3.18 (s, 2H), 2.82 (s, 3H), 2.68-2.54 (m, 4H), 2.14 (s, 3H); LC-MS (Method A) *m/z* = [M + H]⁺ 424.1, *t*_R 0.41 mins.

***(R)*-7-(3-(2,2-Difluoroethoxy)pyridin-4-yl)-5-methyl-2-((2-methyl-4-(methylsulfonyl)piperazin-1-yl)methyl)furo[3,2-*c*]pyridin-4(5*H*)-one, **74**²⁰**

A solution of **115** (100 mg, 0.24 mmol) in 1,4-dioxane (2 mL) was treated with triethylamine (0.048 mL, 0.35 mmol), PEPPSITM-SiPr^(R) (10 mg, 0.014 mmol, 6 mol%) and 4,4,5,5-tetramethyl-1,3,2-dioxaborolane (0.046 mL, 0.32 mmol). The reaction mixture was heated at 60 °C for 2 h then at 100 °C for 3.5 h. The reaction mixture was treated with 4,4,5,5-tetramethyl-1,3,2-dioxaborolane (0.092 mL, 0.63 mmol) and triethylamine (0.048 mL, 0.35 mmol) then heated at 100 °C for 3.5 h. The reaction mixture was treated with IPA (2 mL) and washed through Celite^(R) using IPA (3 mL) to afford a mixture of **119**, **119a** and **120**.

The solution was treated with **74a** (17 mg, 0.07 mmol), PEPPSI-SiPr^(R) (5 mg, 0.007 mmol, 10 mol%), potassium carbonate (10 mg, 0.07 mmol) and water (1 mL). The reaction mixture was heated at reflux under nitrogen for 7 h. The reaction mixture was partitioned with water (10 mL) and DCM (20 mL). The organic extract was isolated and the aqueous layer re-extracted with DCM (20 mL). The combined organic extracts were passed through a hydrophobic frit then concentrated under reduced pressure. Crude product was purified by silica chromatography (0 to 20% MeOH/EtOAc) to afford **74** (16 mg, 45% over two steps). IR (cm⁻¹) 2856, 1662, 1588, 1322, 1302, 1156, 1127, 1080, 929, 792, 773; ¹H NMR (400 MHz, CDCl₃ δ): 8.47-8.38 (m, 2H), 7.68 (s, 1H), 7.57 (d, *J* = 5 Hz, 1H), 6.89 (s, 1H), 6.10 (tt, ²*J*_{H-F} = 55, *J* = 4 Hz, 1H), 4.38 (td, *J*_{H-F} = 13, *J* = 4 Hz, 2H), 3.95-3.80 (m, 2H), 3.70 (s, 3H), 3.58-3.45 (m, 2H), 2.94 (s, 2H), 2.77 (s, 3H), 2.70-2.48 (m, 3H), 1.24 - 1.18 (d, *J* = 6 Hz, 3H); ¹³C NMR (126 MHz, DMSO-d₆, δ): 157.9, 156.4, 153.4, 150.9, 143.4, 136.3, 136.0, 129.0, 124.3, 115.1, 114.9 (t, *J*_{C-F} = 239 Hz), 105.9, 103.0, 67.5 (t, ²*J*_{H-F} = 27 Hz), 53.3, 51.4, 49.7, 48.7, 45.4, 36.4, 33.6, 15.2; HRMS-FAB (*m/z*): [M + H]⁺ calcd for C₂₂H₂₆F₂N₄O₅S, 497.1665; found, 497.1688; LC-MS (Method A) *m/z* = [M + H]⁺ 497.3, *t*_R 0.49 mins; mp 158 – 161 °C.

(R)-7-(3-Hydroxypyridin-4-yl)-5-methyl-2-((2-methyl-4-(methylsulfonyl)piperazin-1-yl)methyl)furo[3,2-*c*]pyridin-4(5*H*)-one, 77²⁰



A solution of **115** (100 mg, 0.24 mmol) in 1,4-dioxane (1 mL) was treated with triethylamine (0.133 mL, 0.96 mmol), PEPPSI-SiPr^(R) (16 mg, 0.024 mmol, 10 mol%) and 4,4,5,5-tetramethyl-1,3,2-dioxaborolane (0.208 mL, 1.43 mmol). The reaction mixture was heated at 100 °C for 2.5 h then treated with IPA (2 mL) and washed through Celite^(R) using IPA (3 mL) to afford a mixture of **119**, **119a** and **120**.

The IPA solution was treated with PEPPSI-SiPr^(R) (7 mg, 0.01 mmol, 8 mol%), potassium carbonate (27 mg, 0.20 mmol), **132** (50 mg, 0.29 mmol) and water (1 mL).

The reaction mixture was heated at reflux under nitrogen for 1.3 h then concentrated under reduced pressure. The crude material was suspended in MeOH (5 mL) and filtered through Celite^(R) then concentrated under reduced pressure. The crude product was purified by MDAP (Method C) to afford **77** as a yellow solid (20 mg, 19%). ¹H NMR (400 MHz, CD₃OD δ): 8.20 (s, 1H), 8.07 (s, 1H), 8.04 (d, *J* = 5 Hz, 1H), 7.60 (d, *J* = 5 Hz, 1H), 6.92 (s, 1H), 4.03-3.89 (m, 2H), 3.71 (s, 3H), 3.51-3.42 (m, 2H), 3.02-2.92 (m, 2H), 2.82 (s, 3H), 2.71-2.63 (m, 1H), 2.62-2.50 (m, 2H), 1.25 (d, *J* = 6 Hz, 3H), *the phenolic proton underwent exchange in the wet deuterated solvent and was not observed*; LC-MS (Method C) *m/z* = [M + H]⁺ 433.3, *t_R* 0.55 mins.